WOODHEAD PUBLISHING SERIES IN CIVIL AND STRUCTURAL ENGINEERING

# Rehabilitation of Metallic Civil Infrastructure using Fiber-reinforced Polymer (FRP) Composites

Edited by Vistasp M. Karbhari

WP
WOODHEAD PUBLISHING

# Rehabilitation of Metallic Civil Infrastructure using Fiber-reinforced Polymer (FRP) Composites

**Related titles:**

*Eco-efficient construction and building materials*
(ISBN 978-0-85709-767-5)

*Advanced fibre-reinforced polymer (FRP) composites for structural applications*
(ISBN 978-0-85709-418-6)

*Developments in fiber-reinforced polymer (FRP) composites for civil engineering*
(ISBN 978-0-85709-234-2)

Woodhead Publishing Series in Civil and Structural Engineering:
Number 51

# Rehabilitation of Metallic Civil Infrastructure using Fiber-reinforced Polymer (FRP) Composites

Edited by
Vistasp M. Karbhari

AMSTERDAM • BOSTON • CAMBRIDGE • HEIDELBERG • LONDON
NEW YORK • OXFORD • PARIS • SAN DIEGO
SAN FRANCISCO • SINGAPORE • SYDNEY • TOKYO
Woodhead Publishing is an imprint of Elsevier

Woodhead Publishing is an imprint of Elsevier
80 High Street, Sawston, Cambridge, CB22 3HJ, UK
225 Wyman Street, Waltham, MA 02451, USA
Langford Lane, Kidlington, OX5 1GB, UK



**Notice**
No responsibility is assumed by the publisher for any injury and/or damage to persons or property as a matter of products liability, negligence or otherwise, or from any use or operation of any methods, products, instructions or ideas contained in the material herein. Because of rapid advances in the medical sciences, in particular, independent verification of diagnoses and drug dosages should be made.

**British Library Cataloguing-in-Publication Data**
A catalogue record for this book is available from the British Library.

**Library of Congress Control Number:** 2014931605

ISBN 978-0-85709-653-1 (print)
ISBN 978-0-85709-665-4 (online)



Typeset by Toppan Best-set Premedia Limited

Printed and bound in the United Kingdom

# Contents

*This book is dedicated to Professor Len Hollaway, a pioneer in the field, who sadly died before this book was completed.*

This page intentionally left blank

# Contributor contact details

(* = main contact)

## Editor and Chapter 1

Vistasp M. Karbhari
University of Texas at Arlington
Campus Box 19125
701 South Nedderman Drive
Arlington
TX 76019-0125, USA

E-mail: vkarbhari@uta.edu

## Chapter 2

Alan A. Baker
Advanced Composite Structures Australia Pty Ltd (ACS-A)
1/320 Lorimer St
Port Melbourne
Victoria 3207, Australia

and

Aerospace Division
Defence Science and Technology Organisation
506 Lorimer Street
Fishermans Bend
Victoria 3207, Australia

E-mail: alan.baker@dsto.defence.gov.au; a.baker@acs-aus.com

## Chapter 3

Reza Haghani
Department of Civil and Environmental Engineering
Chalmers University of Technology
Sven Hultinsgata 8
412 98 Gothenburg, Sweden

Email: reza.haghani@chalmers.se

## Chapter 4

Mina Dawood
Department of Civil and Environmental Engineering
University of Houston
N107 Engineering Bldg 1
Houston
TX 77204-4003, USA

Email: mmdawood@uh.edu

## Chapter 5

Kent A. Harries
Department of Civil and Environmental Engineering
University of Pittsburgh
742 Benedum Hall
Pittsburgh
PA 15261, USA

E-mail: kharries@pitt.edu

## Chapter 6

Mike R. Bambach
Transport and Road Safety Research (TARS)
Old Main Building (K15)
University of New South Wales
Sydney, NSW 2052, Australia

E-mail: m.bambach@unsw.edu.au

## Chapter 7

Fabio Matta*
Department of Civil and Environmental Engineering
University of South Carolina
300 Main Street
Room C210
Columbia
SC 29208, USA

E-mail: fmatta@sc.edu

Mina Dawood
Department of Civil and Environmental Engineering
University of Houston
N107 Engineering Bldg 1
Houston
TX 77204-4003, USA

Email: mmdawood@uh.edu

## Chapter 8

Chris P. Pantelides
Civil and Environmental Engineering Department
University of Utah
110 South Central Campus Drive
Room 2000
Salt Lake City
UT 84112, USA

E-mail: c.pantelides@utah.edu

## Chapter 9

Jun Deng*
School of Civil and Transportation Engineering
Guangdong University of Technology
No. 100 Waihuan Xi Road
Guangzhou Higher Education Mega Center
Guangzhou, 510006, China

Email: jdeng@gdut.edu.cn

Marcus M. K. Lee
Department of Civil and Construction Engineering
Curtin University Sarawak
CDT 250
98009 Miri, Sarawak, Malaysia

Email: marcus.lee@curtin.edu.my

## Chapter 10

Pierluigi Colombi* and G. Fava
Department of Architecture, Built Environment and Construction Engineering ABC
Technical University of Milan (Politecnico di Milano)
Pizza L. da Vinci, 32
20133 Milan, Italy

E-mail: pierluigi.colombi@polimi.it

## Chapter 11

Ron Barrett-Gonzalez*
Aerospace Engineering Department
2120 Learned Hall
The University of Kansas
Lawrence
KS 66045, USA

E-mail: adaptivebarrett@yahoo.com

Stanley Rolfe, Adolfo Matamoros and Caroline Bennett
Department of Civil, Architectural and Environmental Engineering
2150 Learned Hall
The University of Kansas
Lawrence
KS 66045, USA

E-mail: srolfe@ku.edu; amatamor@ku.edu; crb@ku.edu

## Chapter 13

Alessio Pipinato
University of Padova
Department of Civil and Environmental Engineering
via Marzolo 9
35131 Padova, Italy

E-mail: alessio.pipinato@dicea.unipd.it

## Chapter 14

Stuart Moy
Formerly of School of Civil Engineering and the Environment
University of Southampton
18 Leigh Road
Highfield
Southampton
SO17 1EF, UK

E-mail: ssjm@soton.ac.uk; S.S.Moy@soton.ac.uk

This page intentionally left blank

# Woodhead Publishing Series in Civil and Structural Engineering

1 **Finite element techniques in structural mechanics**
*C. T. F. Ross*
2 **Finite element programs in structural engineering and continuum mechanics**
*C. T. F. Ross*
3 **Macro-engineering**
*F. P. Davidson, E. G. Frankl and C. L. Meador*
4 **Macro-engineering and the earth**
*U. W. Kitzinger and E. G. Frankel*
5 **Strengthening of reinforced concrete structures**
*Edited by L. C. Hollaway and M. Leeming*
6 **Analysis of engineering structures**
*B. Bedenik and C. B. Besant*
7 **Mechanics of solids**
*C. T. F. Ross*
8 **Plasticity for engineers**
*C. R. Calladine*
9 **Elastic beams and frames**
*J. D. Renton*
10 **Introduction to structures**
*W. R. Spillers*
11 **Applied elasticity**
*J. D. Renton*
12 **Durability of engineering structures**
*J. Bijen*
13 **Advanced polymer composites for structural applications in construction**
*Edited by L. C. Hollaway*
14 **Corrosion in reinforced concrete structures**
*Edited by H. Böhni*
15 **The deformation and processing of structural materials**
*Edited by Z. X. Guo*
16 **Inspection and monitoring techniques for bridges and civil structures**
*Edited by G. Fu*
17 **Advanced civil infrastructure materials**
*Edited by H. Wu*

18 **Analysis and design of plated structures Volume 1: Stability**
*Edited by E. Shanmugam and C. M. Wang*
19 **Analysis and design of plated structures Volume 2: Dynamics**
*Edited by E. Shanmugam and C. M. Wang*
20 **Multiscale materials modelling**
*Edited by Z. X. Guo*
21 **Durability of concrete and cement composites**
*Edited by C. L. Page and M. M. Page*
22 **Durability of composites for civil structural applications**
*Edited by V. M. Karbhari*
23 **Design and optimization of metal structures**
*J. Farkas and K. Jarmai*
24 **Developments in the formulation and reinforcement of concrete**
*Edited by S. Mindess*
25 **Strengthening and rehabilitation of civil infrastructures using fibre-reinforced polymer (FRP) composites**
*Edited by L. C. Hollaway and J. C. Teng*
26 **Condition assessment of aged structures**
*Edited by J. K. Paik and R. M. Melchers*
27 **Sustainability of construction materials**
*J. Khatib*
28 **Structural dynamics of earthquake engineering**
*S. Rajasekaran*
29 **Geopolymers: Structures, processing, properties and industrial applications**
*Edited by J. L. Provis and J. S. J. van Deventer*
30 **Structural health monitoring of civil infrastructure systems**
*Edited by V. M. Karbhari and F. Ansari*
31 **Architectural glass to resist seismic and extreme climatic events**
*Edited by R. A. Behr*
32 **Failure, distress and repair of concrete structures**
*Edited by N. Delatte*
33 **Blast protection of civil infrastructures and vehicles using composites**
*Edited by N. Uddin*
34 **Non-destructive evaluation of reinforced concrete structures Volume 1: Deterioration processes**
*Edited by C. Maierhofer, H.-W. Reinhardt and G. Dobmann*
35 **Non-destructive evaluation of reinforced concrete structures Volume 2: Non-destructive testing methods**
*Edited by C. Maierhofer, H.-W. Reinhardt and G. Dobmann*
36 **Service life estimation and extension of civil engineering structures**
*Edited by V. M. Karbhari and L. S. Lee*
37 **Building decorative materials**
*Edited by Y. Li and S. Ren*
38 **Building materials in civil engineering**
*Edited by H. Zhang*
39 **Polymer modified bitumen**
*Edited by T. McNally*

40 **Understanding the rheology of concrete**
*Edited by N. Roussel*
41 **Toxicity of building materials**
*Edited by F. Pacheco-Torgal, S. Jalali and A. Fucic*
42 **Eco-efficient concrete**
*Edited by F. Pacheco-Torgal, S. Jalali, J. Labrincha and V. M. John*
43 **Nanotechnology in eco-efficient construction**
*Edited by F. Pacheco-Torgal, M. V. Diamanti, A. Nazari and C. Goran-Granqvist*
44 **Handbook of seismic risk analysis and management of civil infrastructure systems**
*Edited by F. Tesfamariam and K. Goda*
45 **Developments in fiber-reinforced polymer (FRP) composites for civil engineering**
*Edited by N. Uddin*
46 **Advanced fibre-reinforced polymer (FRP) composites for structural applications**
*Edited by J. Bai*
47 **Handbook of recycled concrete and demolition waste**
*Edited by F. Pacheco-Torgal, V. W. Y. Tam, J. A. Labrincha, Y. Ding and J. de Brito*
48 **Understanding the tensile properties of concrete**
*Edited by J. Weerheijm*
49 **Eco-efficient construction and building materials: Life cycle assessment (LCA), eco-labelling and case studies**
*Edited by F. Pacheco-Torgal, L. F. Cabeza, J. Labrincha and A. de Magalhães*
50 **Advanced composites in bridge construction and repair**
*Edited by J. Kim*
51 **Rehabilitation of metallic civil infrastructure using fiber-reinforced polymer (FRP) composites**
*Edited by V. M. Karbhari*
52 **Rehabilitation of pipelines using fiber-reinforced polymer (FRP) composites**
*Edited by V. Karbhari*
53 **Transport properties of concrete: Measurement and application**
*P. A. Claisse*

This page intentionally left blank

# Preface

Worldwide, civil infrastructure is facing challenges of critical dimensions. On the one hand, the demands placed on infrastructure components and systems are increasing due to higher densities of population in urban areas and greater need for the faster and more efficient conveyance of goods and service from one point to another while, on the other hand, our existing infrastructure is aging (with a significant portion either beyond its service life or close to it) or functionally deficient in that it is unable to meet the demands currently being placed on it because of design limitations. As with all structures, the materials used in construction also deteriorate over time further increasing the limitations and causing concerns not just in terms of functionality of use, but also in terms of safety.

Among all infrastructure systems, those related to transportation infrastructure, especially roadways and networks, have drawn significant attention over the past two decades. In the US alone, the American Society of Civil Engineers in its 2013 Report Card for America's Infrastructure[1] stated that 'Over two hundred million trips are taken daily across deficient bridges in the nation's 102 largest metropolitan regions. In total, one in nine of the nation's bridges is rated as structurally deficient, while the average age of the nation's 607 380 bridges is currently 42 years. The Federal Highway Administration (FHWA) estimates that to eliminate the nation's bridge backlog by 2028, we would need to invest $20.5 billion annually, while only $12.8 billion is being spent currently.' The state of bridges and allied transportation infrastructure in Europe is no different, and is perhaps worse in South East Asia where tremendous construction activity took place in the early part of the latter half of the last century.

While significant attention has been paid to the challenges related to the rehabilitation of structural concrete used in bridges and affiliated infrastructure components and systems, attention has not been as focused on metallic and steel components although in many cases these are both

[1]ASCE 2013 Report Card for America's Infrastructure, http://www.infrastructurereportcard.org/a/#p/home.

more prevalent and older in age. While traditional methods of repair, such as bolting and riveting of additional strengthening sections and welding of others, can be used, they all suffer from two primary deficiencies in that the rehabilitation itself adds significant weight to the already under-capacity component or system, and that the technique is either not as reliable as needed, or takes too long (resulting in elongated periods of closure) or in itself causes further distress albeit in terms of different performance metrics (such as the addition of deleterious residual stresses initiated by welding).

Fiber-reinforced polymer (FRP) composites provide significant opportunities for the rehabilitation of metallic infrastructure components and systems and have attracted significant attention recently due to the ease of use in the field, light weight and ability to match both configuration and performance characteristics. It should be noted that, although the application of FRP composites to civil infrastructure is relatively new, the materials have a long, and successful, history of use in the naval/marine and aerospace sectors, where they have been used extensively both for the purpose of rapid repair in the field and for the extension of service life. There is, thus, a significant body of knowledge that is available for use in civil infrastructure based on application in other areas and it behooves us to take advantage of this rather than 'reinventing the wheel.'

Based on the increasing need for the development of a rapid, low weight technique for the rehabilitation of metallic infrastructure, especially as related to bridge components and systems, there has been a significant interest in the fields of research and field application of FRP materials for the rehabilitation of metallic components and systems. In a large number of cases, the FRP composites have been based on carbon fiber reinforcements due to the need for stiffness matching but, in some cases, the use of glass fibers can provide significant advantages. This volume provides an introduction to the overall topic, focusing on specific areas of interest and application, and should thus be considered as providing a synopsis of the topic rather than a comprehensive overview. For ease of reference and use it is divided into four parts.

Part I consists of a general introduction to materials and systems aspects (Chapter 1), a summary of the use of FRP for rehabilitation in the aerospace sector (Chapter 2), adhesive bonding (Chapter 3), and issues related to durability (Chapter 4). Chapter 2, specifically, provides a broad overview of the use of FRP composites in repair of metallic airframe components, an area that is now considered mature with a long history of successful use in the field. It is hoped that the inclusion of this chapter will serve two primary purposes – first to show that the technique can be implemented successfully even in areas where factors of safety are significantly lower than those in civil infrastructure, and second to assist in cross-fertilization between areas

of application in the hope that this would accelerate advancements and adoption in civil infrastructure areas.

Part II focuses on the application of FRP composites to specific components, enabling a more in-depth treatment of the topic. Part III emphasizes the importance of consideration of fatigue loading and overall performance on design and application and provides examples at the component (Chapters 9 and 10) and system (Chapter 11) levels. Part IV concludes with case studies of application in the field.

It is hoped that this collection of chapters will prove to be both instructive and educational to the reader, and that it provides knowledge both to the student and the practitioner.

This page intentionally left blank

# Part I

Introduction and overview

This page intentionally left blank

# 1

# Rehabilitation of metallic civil infrastructure using fiber-reinforced polymer (FRP) composites: a materials and systems overview at the adhesive bond level

V. M. KARBHARI, University of Texas at Arlington, USA

**DOI**: 10.1533/9780857096654.1.3

**Abstract**: This chapter provides an overview at the materials and systems levels to the use of fiber-reinforced polymer (FRP) composites for the rehabilitation of metallic civil infrastructure. The focus of the chapter is the adhesive bond between the FRP composite and the metallic substrate, which is intrinsic to any rehabilitation scheme involving bonded elements. Factors considered include the types of adhesives, surface characteristics of the adherends, and characteristics of the bond between the adhesive and the adherend.

**Key words**: adhesive bond, metallic infrastructure, fiber-reinforced polymer (FRP) composites.

## 1.1 Introduction

Due to their high stiffness-to-weight and strength-to-weight ratios, light weight, potentially high durability and relative ease of use in the field, fiber-reinforced polymer (FRP) composites have seen increasing adoption since the 1990s for use in the rehabilitation of civil infrastructure. For the most part, this has been in conjunction with structural concrete, and numerous examples now exist of the successful use of FRP composites for the rehabilitation of concrete bridges and their components ranging from the flexural and shear strengthening of girders, and the strengthening of decks/slabs, to the strengthening and/or seismic retrofitting of columns. However, a significant percentage of the aging and deteriorating infrastructure has been fabricated from metals ranging from wrought and cast iron (such as used by the railways in the UK) to aluminum (used on road signposts and pylons) to steel (used in decks, girders, and columns).

Corrosion, and subsequent structural deterioration including cracking and loss of section, is a major reason for the structural deficiency in steel-based infrastructure components and can lead to progressive weakening and, in rare cases – sudden collapse. In addition, specific decks and other structural components can be rendered functionally deficient since they are not able, as designed, to support loads and traffic levels currently needed.

FRP composites strengthening components, both in the prefabricated form and fabricated on-site using the wet layup or pre-preg process, have been used to effect efficient strengthening of metallic structures. Irrespective of the method used, the efficacy of the process depends intrinsically on the integrity of the bond between the FRP composite and the metallic substrate. This chapter focuses on this critical feature. Subsequent chapters will provide further details on the FRP composite systems, design approaches and applications, as well as case studies.

## 1.2 Overall considerations

For the purposes of focus, the emphasis will be on the use of carbon fiber-reinforced polymer (CFRP) composites. While details may differ, these could in structural form be used in the field in the form of fabrics, prefabricated elements or pre-impregnated sheets (generally of the hot-melt variety). Irrespective of the type, the system must be considered to be made up of the adherends (FRP composite and metal substrate), the adhesive (which in the case of a wet layup process could be the impregnating resin itself or a modification thereof), and the interfaces. In general, one could consider that between the substrate and the bulk adhesive there will be a thin substrate surface (which in the case of the metallic adherend would include an oxide layer or remnants thereof), a coupling layer, and the interphase region to the bulk adhesive.

Several basic considerations need to be kept in mind. The composition of the metal (especially as related to the galvanic series), its surface morphology, the level of pre-treatment (or lack thereof), and the time period between pre-treatment and application of the primer/adhesive are basic considerations at the level of the metal substrate. In terms of the adhesive, due consideration needs to be given to the type (including chemical composition) and cure regime (which would include details such as environment, and the necessity for the application of pressure and temperature to effect cure). While the type of fiber reinforcement is important as related to stiffness mismatch and galvanic corrosion potential, aspects such as surface morphology (generically in the resin-rich surface layer), pre-treatment of the surface to which the adhesive would be applied, and the method of cure (in the event that the FRP composite were fabricated in the field) need to be considered.

While the process of adhesive bonding is extremely well established, it still has a number of aspects that often make it more of an art than a well-defined science. Since the material is actually formed during the process itself, the *in situ* properties are not measurable prior to cure. Local effects such as the ambient environment as well as the integrity of interfaces can have significant effects on the final performance characteristics. Also, since the adhesive is often the only means of attachment between the two

substrates (FRP composite and the metallic adherend), there is no redundancy. As with most field processes, there is still a lack of rapid, cost-effective, and reliable inspection methods, and this results in the application of high factors of safety. As an aside, there is very little that can be done in the field to accurately detect contamination, and this results in some level of uncertainty in assurance of load transfer capabilities at theoretically determined levels. Depending on the nature of the adherend surfaces the bond itself will be a combination of chemical and mechanical, and hence surface-related aspects such as surface preparation including the removal of contamination and the creation of chemically active surfaces are important.

## 1.3 Understanding adhesive bonds

In the best of circumstances, bonding is a chemical process rather than one of mechanical interlock. In this case, there are two potential failure modes: (i) cohesion wherein there is failure within the adhesive itself; and (ii) adhesion wherein failure is at an interface. The former takes place in cases where the overlap length between adherends is inadequate which leads to inadequate stress transfer, or if thermal stresses are present or due to the presence of gross defects such as air voids formed during fabrication. Adhesive failure is process dominated and is generally due to inadequate or ineffective surface preparation. In both cases, the presence of voids, especially micro voids, can lead to failure during fatigue loading.

At a systems level, failure of the bond can be due to a variety of reasons with the most common one being the presence of a weak oxide layer on the metallic adhered. This happens in cases where the metallic surface has not been adequately treated or too much time has been allowed between treatment and application of the adhesive resulting in the formation of the layer. The oxide layer becomes the surface to which the adhesive bonds and, since it has a weak bond to the metal adherend itself, failure occurs through peeling of the oxide layer away from the surface, or cracking of the layer, causing separation of the adhesive layer from the metallic substrate. Beyond reasons of poor substrate preparation, failure can also occur due to incomplete or under cure of the adhesive, degradation of the adhesive through environmental exposure or loading prior to cure. It should be noted that just like resin systems the adhesive can be attacked by moisture, oxygen, chemicals, and solvents depending on its chemical composition and degree of cure.

While a detailed description of surface energy is beyond the scope of this chapter, it is important that a basic understanding is provided since surface energy affects how the adhesive wets the surface of the prepared adherends and hence adhesion is directly dependent on it. Metals, polyamides, polyesters, acrylics, rigid polyurethanes, acrylonitrile butadiene styrenes (ABS), polycarbonates, and rigid polyvinyl chlorides (PVC) all have high

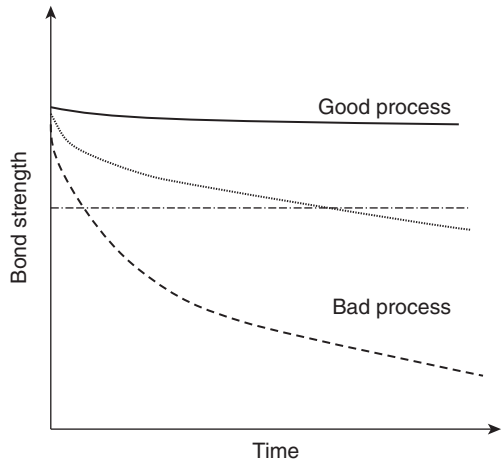


*1.1* The importance of surface preparation on bond strength over time.

surface energy resulting in good wet out and coverage, whereas polystyrenes, acetals, polyvinyl acetates, polyurethane elastomers, polypropylenes, polyvinyl fluorides (PVF), polytetrafluoroethylenes (PTFE), and ethylene propylene diene monomer (EPDM) rubbers have low surface energy which can result in incomplete wet out and the inclusion of voids between the adherend surface and the adhesive.

The condition of the surfaces themselves has a significant effect on the quality of the bond, and surface preparation is probably the most significant factor in ensuring long-term bond durability (Fig. 1.1). A clean, chemically active surface that is resistant to hydration is a prime requirement for bond reliability and integrity. Glassy surfaces are advantageous for ensuring wetting if the adhesive has a lower surface energy than the adherend, and a light level of abrasion is needed to increase contact area. In contrast, a rough surface can be advantageous for adhesives with high surface energy and enables significant mechanical interlock between the adherend substrate and the adhesive in addition to chemical bonding, thereby enhancing the overall bond performance. Care should, however, be taken to ensure that air is not entrapped in areas where the bond line is thicker, and sharp edges should be smoothened to decrease the potential for cracking due to the presence of local stress risers.

The use of grit blasting and/or sanding on the metal is often the most important step in the initial preparation of the adherend as it results in mechanical deoxidation. This not only removes the surface oxide layer exposing fresh metal for bonding but also provides a roughened surface with good mechanical interlock. Although initial adhesion is generally very good, failure can occur at the interface under hot–wet conditions through

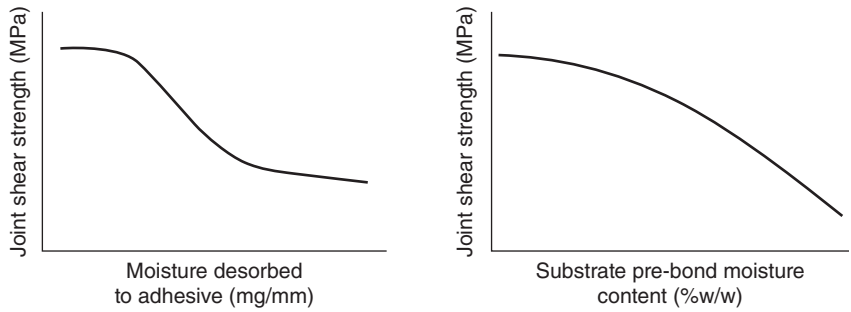


*1.2* Effect of pre-bond moisture on short-term joint performance.

post-fabrication formation of corrosion products within the interface region. Prebond humidity results in an increased level of moisture content on the surface and in the adhesive and can cause significant decreases in fracture energy and shear strength. It should be noted that many polymers (adhesives) absorb moisture from the operating environment which results in a reduction in glass transition temperature, modulus, and strength. The absorbed moisture can, however, cause plasticization of the polymer resulting in short-term gains in damage tolerance. Moisture uptake prior to bond formation is especially of concern in adhesives cured under elevated temperatures since it interferes with wetting of the surface, causes the cure itself to be retarded and can result in excessive formation of voids, all of which result in weaker adherend–adhesive interfaces. Figure 1.2 shows schematic effects of pre-bond adherend moisture content on short-term bond performance.

The use of anodizing addresses this to an extent through the creation of a microstructure that promotes better wetting, and hence coverage, of the adhesive which not only results in enhanced mechanical interlock but also in better control over inhibition of corrosion initiation. Chemical etching wherein the metal surface is deoxidized assists in the retardation of later corrosion but can cause embrittlement of the steel itself. In many cases, functional coatings such as silanes are sprayed or otherwise applied to the prepared surfaces to further enable chemical bonding of the adhesive to the surface of the adherend. A generic representation of the efficacy of silane treatment on bond strength is shown in Fig. 1.3.

## 1.4 Bond level considerations

In addition to the considerations related to surfaces and the chemistry of the adhesive itself, appropriate attention needs to be paid to aspects related to operating temperature, moisture, and chemicals present in the operating environment. As with most polymers, the presence of higher ambient

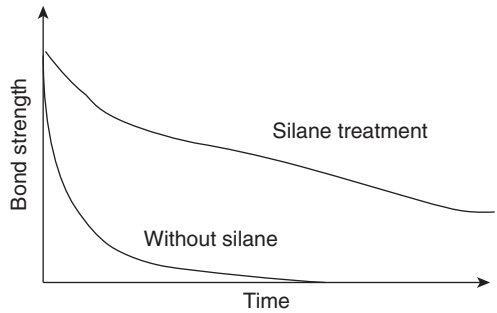


*1.3* Effect of silane treatment on bond strength in the presence of humidity.

temperatures in the operating environment can result in an increase in the rate of creep and stress relaxation of the adhesive itself. Further, if moisture uptake occurs in conjunction with higher temperatures, an increase in the rate of deterioration at the adhesive and interface levels may be expected. Exposure to sub-zero temperatures can result in both embrittlement of the adhesive and cracking in the adhesive and interphase regions. It is important to remember also that there are significant differences in the coefficients of thermal expansion between steel ($12 \times 10^{-6}$/K) and carbon fiber-reinforced composites (which can be as high as $0.52 \times 10^{-6}$/K for high strength unidirectional and as low as $-0.07 \times 10^{-6}$/K for high modulus unidirectional). This difference between the adherends can result in the build-up of thermal stresses leading to debonding.

As mentioned previously, moisture can have significant effects on the overall integrity of the bond. This is not just through moisture effects during cure but even through the life of the bonded component since moisture can diffuse through the bulk, be transported along the interfaces, absorbed through capillary action through cracks and crazes, or even diffused through the adherends if the FRP composite is permeable or the metal is cracked. Initial moisture uptake causes largely reversible plasticization which results in increased toughness and damage tolerance. However, over time the results are irreversible and can cause overall deterioration through hydrolysis, leaching, cracking and crazing. In addition, due consideration needs to be given to the potential for the attack of interfaces through displacement of the adhesive or hydration of the metal surfaces which causes the growth of an oxide film which in itself can result in debonding. A schematic of the effect of outdoor weathering is shown in Fig. 1.4 and the synergistic effect of moisture and temperature is shown in Fig. 1.5. It is noted that the curves are similar in shape, but the response of moisture uptake as shown in the 'wet joint' represents a shift to lower temperatures by an amount equal to the depression in glass transition temperature caused by the absorption of moisture.

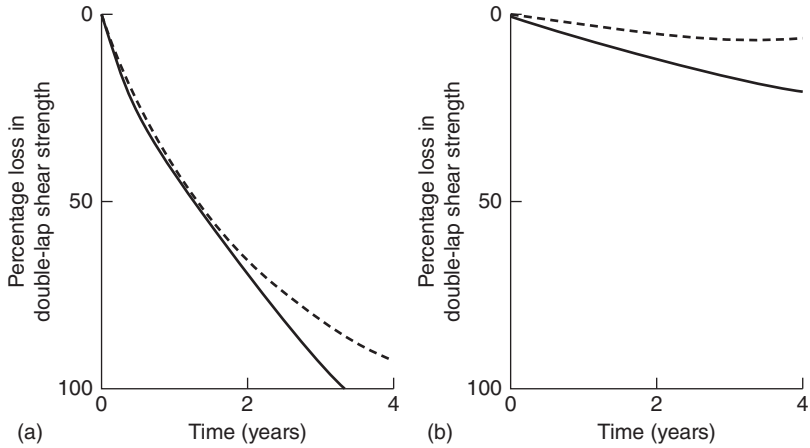


*1.4* Effects of outdoor weathering: (a) under 'hot-wet' tropical conditions; (b) under 'hot-dry' desert conditions. The dashed line represents the unstressed state and the solid line represents effects at 10% of the breaking stress.

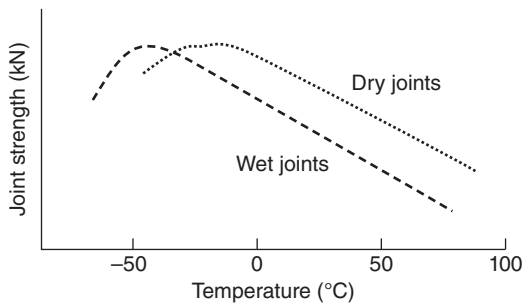


*1.5* Synergistic effects of moisture and temperature.

Due consideration also needs to be given to bondline thickness with thinner bondlines being preferred for strength and durability. Thicker bondlines are susceptible to greater occurrence of voids and defects and to failure in the adhesive itself, although the increase in thickness may offer greater tolerance of elastic mismatch between the steel adherend and the FRP composite, and to effects of vibration and impact. Figure 1.6 shows the effect of bondline thickness (described as gap thickness) on a number of performance characteristics.

While there are a number of design approaches, a relatively effective one is the load–capacity approach advocated by Hart-Smith wherein the bond is designed to be stronger than the adherends. For full efficacy the adhesive stresses in shear are necessarily very low in magnitude.

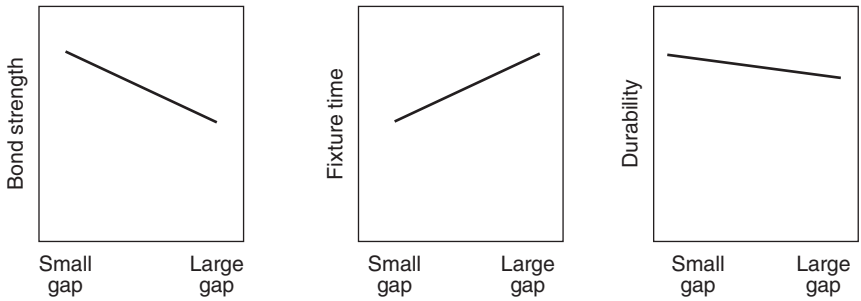


*1.6* Effect of gap thickness.

The issue of deterioration due to the formation of a galvanic cell between carbon fibers when used as a reinforcement in the FRP composite and the steel adherend cannot be neglected. This is, however, the subject of significant research and will not be considered in depth herein. Rather the issues are just pointed out as reference. The formation of a galvanic cell is largely misunderstood and neglected despite evidence from the aerospace and naval/marine areas. Galvanic corrosion occurs when a cell is formed between the carbon fibers and a less noble metal. The anodic metal corrodes faster in the presence of corroding mechanisms such as pitting and crevice corrosion which are generally not seen. The cathodic reaction in the FRP composite causes the formation of surface blisters and moisture-induced degradation of the adhesive itself. While the use of a layer of glass fabric decreases the potential of direct contact between a bare carbon fiber end or surface and the metallic adherend, galvanic cells can still be formed through moisture diffusion and, hence, the key to reducing the deleterious effect is the reduction of diffusion and the increase in toughness and encapsulation of the surfaces.

## 1.5 Summary and conclusion

This chapter reviews salient points related to adhesive bonds at the materials and systems levels. Although FRP composites, especially high modulus carbon fiber-reinforced composites, provide an efficient and generally reliable means of rehabilitating structurally and functionally deficient metallic components, due care has to be taken at the materials and systems level since the efficacy of the process depends intrinsically on the surfaces of the adherends, the type of adhesive used, and the bond between the adhesive and the adherends. Although this area is still in its infancy as related to civil infrastructure, there is a tremendous and rich body of research and application in the marine/naval and aerospace areas and the interested reader is urged to study these areas for best practices.

# 2

# Repair of metallic airframe components using fibre-reinforced polymer (FRP) composites

A. A. BAKER, Advanced Composite Structures, Australia and Defence Science and Technology Organisation, Australia

**DOI**: 10.1533/9780857096654.1.11

**Abstract**: This chapter discusses the repair of metallic aircraft structures with bonded composite patches or reinforcements. Aspects discussed include key materials aspects, including pre-bonding surface preparation and patch application procedures, and an analytical repair design approach, with experimental confirmation. The difficult issue of the certification of bonded repairs to critically damaged primary aircraft structures is discussed. This results from the inability of conventional non-destructive testing to detect weak adhesive bonds. Two approaches to alleviate this difficulty are proposed: structural health monitoring and proof testing. Finally, two applications, one from the United States and the other Australian, are described followed by a conclusion on limitations and lessons learned.

**Key words**: aircraft repairs, composite materials, adhesive bonding, certification.

## 2.1 Introduction

Airframe structures must be repaired or replaced when service damage results, or has the potential to result, in the residual strength being reduced below an acceptable level for flight safety. The most prevalent forms of service damage in aging metallic airframe components are cracks and corrosion. The availability of efficient, rapid and cost-effective means of making repairs is a very important economic requirement for both military and civil aircraft. Repairs to significant damage generally involve the attachment of a reinforcing metallic patch or doubler over the damaged region. The aim is to restore mechanical properties to the original design specifications, including: residual strength, stiffness, fatigue resistance and damage tolerance.[1] The method of attaching the repair patch prescribed in the Structural Repair Manual (SRM) for the aircraft uses bolts or rivets. Figure 2.1a is a schematic of a typical mechanically fastened repair, for example to a wing skin. Generally, prior to application of the reinforcement, the defect – typically a crack – is removed leaving a round or elliptical shaped smooth-edged cut-out.

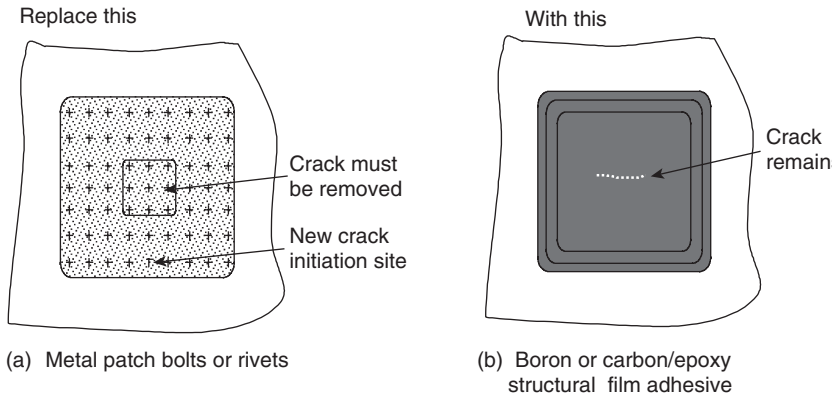


*2.1* Comparison of typical repair involving mechanically fastened patches (a) with one involving adhesively bonded fibre composite patches (b).

Although these SRM repair procedures are generally effective, they can have limited fatigue lives, especially for repairs to relatively thick, highly loaded primary structure; they are also damaging in that they require a large number of extra fastener holes. The purpose of this chapter is to show that application of a fibre composite patch by structural adhesive bonding over the defective region, as illustrated in Fig. 2.1b, can provide a far more efficient and cost-effective repair as well as being much less damaging, fatigue prone and intrusive to the structure.

This chapter discusses the repair of metallic aircraft structure with adhesively bonded fibre-reinforced composites, mainly from an Australian perspective. Firstly, a brief background is provided on the advantages and scope of bonded composite repairs for aircraft structure – including material choices. Details are then provided on the technology for applying the reinforcing patches to the structure, especially the critical issue of surface treatment for durable adhesive bonding. The design of patch repairs is then discussed, mainly from the perspective of estimation of stress intensity in the patched crack, including some experimental confirmation of an analytical model.

The future challenge in the certification of bonded repairs for flight-critical applications is discussed, and a proposal is made on how to meet this challenge. This is based on the testing of representative joints to obtain material allowables for the patch system and the use of proof testing or structural-health monitoring to validate the through-life integrity of the applied patch. Finally, two applications, one USAF and the other Australian, are briefly described followed by a conclusion on limitations and lessons learned.

## 2.2 Metallic airframe components

To minimise weight airframe structures were predominantly made of high-strength aluminium alloys.[2] Although these will continue to be used extensively, they are gradually being replaced in many key applications by polymer-matrix carbon fibre composites. Steel and titanium alloys are used where higher strength or temperature capabilities are required and the weight penalty can be accepted. The main aluminium alloys are the precipitation hardening 2### and 7### series. In the former, the main alloying addition is copper and in the latter zinc, copper and magnesium. There have been many significant improvements in these alloys over recent years; for example, special heat treatments have been developed to reduce the susceptibility to stress corrosion cracking.

Typically, the alloy 2024T3 was used for pressurised fuselage skins and lower (tension-dominated) wing skin because of its high fracture toughness and resistance to crack growth under service loading and 7075-T6, because of its high strength for the upper (compression-dominated) wing skins. In airframe structures, the alloy thickness can vary upwards, from ~ 1.5 mm for fuselage skins and light frames and longerons, to over 25 mm for heavy frames in civil transport aircraft. The wing skins and spars, which are generally the most highly stressed components, can range in thickness in large aircraft from 3 mm in the outer regions of the wing up to 25 mm near the wing root.

Wing skins with integral stiffeners may be machined from thick plate or (more recently) fabricated by advanced welding techniques. Thinner structures are made by fairly conventional sheet metal techniques and complex heavy frames may be made by machining, casting or forging or all of these. Adhesive bonding is used to manufacture thin-skin honeycomb panels used for control surfaces and, in some cases, fuselage panels. Crack stoppers (tear strips) are often adhesively bonded to the fuselage skins.

Fatigue cracking is often a significant problem in military aircraft, either because of more severe usage (higher spectrum loading) or use for lifetimes beyond those originally anticipated.[3] Corrosion is a problem with older military or civil aircraft because of the use of susceptible alloys and inadequate corrosion-protective processes.[1] Corrosion damage includes uniform section loss, pitting, exfoliation (grain boundary attack) and cracking. Other than stress corrosion cracking, considered later, exfoliation and pitting[4] are the most damaging to structural capability since they can result in extensive local loss of section and can initiate fatigue cracks.

Stress corrosion cracks arise in susceptible alloys (particularly thick forgings and machined integrally-stiffened plate) in the short-transverse grain direction from the combination of residual (internal) stress and

adverse environment. These cracks often lie parallel to loading direction so may not constitute a major threat to structural integrity unless they initiate transverse fatigue cracks; however, they can reduce buckling strength.

Even within the anticipated stress range, initiation and growth of fatigue cracks can occur in regions of localised high strain[5] resulting from faulty design, materials defects, (typically voids or inclusions), corrosion pits and scratches or cuts or from poor machining procedures. Fretting of faying surfaces is also a source of fatigue cracks.

Fatigue cracks pose the greatest threat to structural integrity since they grow perpendicular to the applied load direction and can sever the load path; consequently, they are especially a concern in single-load path structures. However, in multi-load path structure widespread damage in the form of extensive minor cracking[1] is also a major concern with aging aircraft. This is because of loss of the ability of the structure to maintain the required level of residual strength if one of the loading paths fails. Thus most significant repairs made to structural metallic airframe components are to repair fatigue cracks.

## 2.3 Key issues in repair

When structural degradation is detected, a decision must be made on the requirement for a repair. Essentially[6] one of the following decisions is required:

1. No-repair action required.
2. Cosmetic or sealing repair is sufficient.
3. Structural repair is required (if feasible), because strength has been reduced below the design limits or has the potential to be reduced in subsequent service.
4. Repair is not economical and the component must be replaced.

A major consideration in the choice of repairs is the level at which the repair can be implemented. Repair activities on military aircraft are performed at one of the following levels:

- *Field level*: Undertaken directly on the aircraft, in a situation where skilled personnel and/or adequate facilities are unavailable. Such activities will generally be limited to fairly minor repairs to non-primary structure or non-critical repairs to primary structure. However, aircraft battle-damage repair (ABDR) may be undertaken as quickly as feasible to make the aircraft operational or to allow it to be flown back to base. Since BDRs will subsequently be replaced with permanent repairs, they should cause minimum damage to the airframe.

- *Depot level*: Undertaken in a situation where skilled personnel and facilities are available (up to factory capability in some cases). However, if the component is too large or difficult to remove from the aircraft, repairs are implemented directly on the aircraft, using depot facilities, where feasible.

Generally, the repair scheme employed for structural restoration should be the simplest and least intrusive and damaging to the structure that can restore structural capability to the required level. The repair must be able to be implemented in the repair environment, without compromising other functions of the component or structure, such as clearance on moving parts, aerodynamic smoothness and balance (control surfaces).

For the purpose of airworthiness assessment, aircraft structures are often classified as follows:

- *Primary-structure*: Critical to the safety of the aircraft.
- *Secondary-structure*: If it were to fail, would affect the operation of the aircraft but not lead to its loss.
- *Tertiary-structure*: Failure would not significantly adversely affect operation of the aircraft.

In general, most structural repairs are made to secondary or tertiary structures or to primary structure where formal certification is not an issue. The issue of certification of bonded repairs to primary structure where the damage has reduced strength below the design allowables is discussed later.

Reinforcing patch repairs are aimed at restoring the load path in the parent structure removed by the damage, ideally without significantly changing the original strain distribution[7] or causing excessive extra damage to the external or internal structure. The following is a partial 'check list' of requirements for a significant structural repair:

- restoration of design strength;
- prevent or slow growth of residual damage – if remaining in the structure;
- minimum change in local stiffness or stress distribution;
- very low probability of failure (or high durability) in the stress, chemical and thermal environment experienced by the airframe;
- tolerance to potential mechanical or service damage;
- proof of satisfactory design and implementation – suitable quality control tracking procedures;
- no unforeseen consequences: aerodynamic, flutter or clearance.

Important additional requirements that the repair implementation should satisfy are:

- minimal down-time of the aircraft;
- use of readily available and easily storable materials;

- removal of as little sound material as possible;
- minimal degradation or damage to the surrounding region;
- simple procedures or tooling requirements.

## 2.4 The use of adhesively bonded patch repairs

As mentioned earlier, repairs based on metallic reinforcements or patches fastened with rivets or bolts are currently the recommended SRM approach; however, although mostly effective, compared with adhesively bonded repairs they are less efficient and can be more problematic. To demonstrate the advantages[8] of the use of bonded repairs for crack repair, fatigue tests were performed on patched edge-notched 2024 T3 aluminium alloy panels, with details as shown in the inset in Fig. 2.2.

The total thickness of the aluminium patches, both sides, was equal to the thickness of the metal. For reasons described in the next section, the composite unidirectional boron/epoxy was chosen for the bonded patch. As unidirectional boron/epoxy is three times the stiffness of the aluminium alloy, the thickness used was one-third of the thickness of the panel. Another very important advantage of the boron/epoxy is that since it is non-conductive, non-destructive inspection (NDI) techniques using eddy currents can be used to detect crack growth – as shown by the plotted points in Fig. 2.2.

It is seen that the mechanically attached metallic patch provides poor reinforcing efficiency since there is only a very slight reduction in crack growth rate. Also, as seen from the figure, once the crack emerges from under the patch it grows very rapidly. The metallic patch can appear to be effective in some cases if the crack arrests temporarily in a fastener hole. In contrast, the adhesively bonded boron/epoxy patch is shown to reduce the rate of crack growth significantly, even when it emerges from under the patch. The growth rate of the emerging crack with the boron/epoxy patch is similar to that expected for a crack of the emerged length, indicating that the patch is still effectively restraining crack opening. The advantages of bonded composite repairs for fatigue cracks are summarised in Fig. 2.3.

The reason for the poor patching efficiency in the mechanically fastened patch arises from its higher compliance when compared with a patch bonded with a structural adhesive. Mechanical joints transfer load primarily by compression on the internal faces of the fastener hole and by shear through friction on the contacting elements. The high compliance results mainly from:

- The requirement for a finite edge distance (generally 2 to 3 $\times$ hole diameter) for the fasteners results in a long fastener-free zone spanning or bridging the crack.

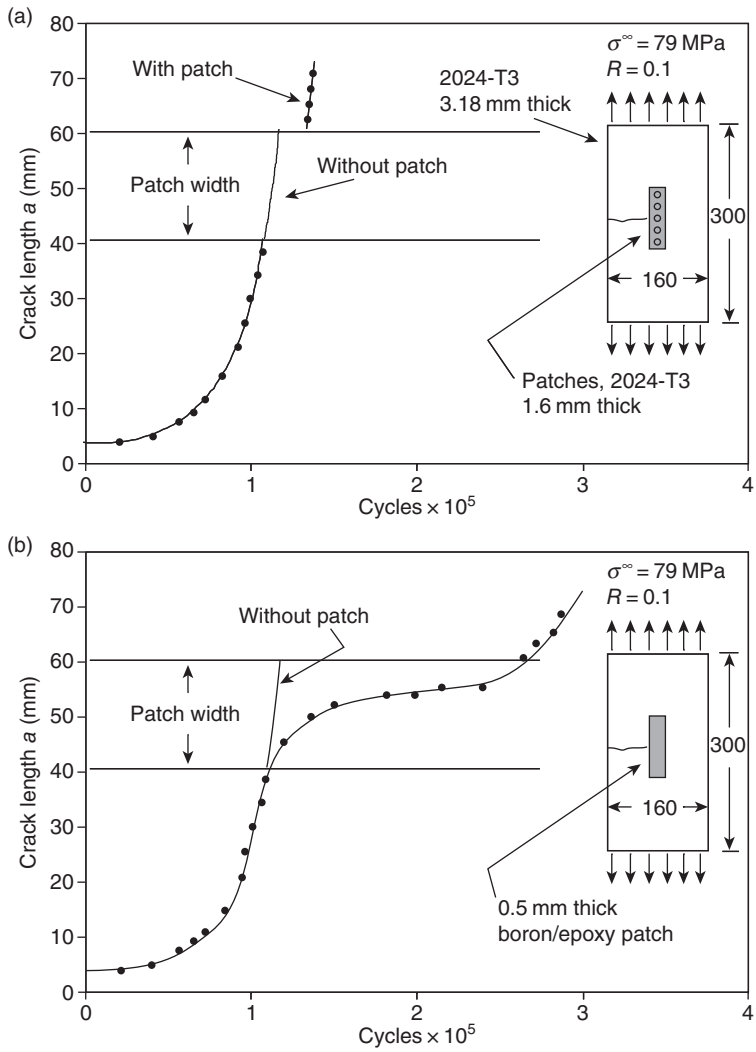


*2.2* Comparison of crack growth performance of patching efficiency between a mechanically fastened mechanical repair (a) and an adhesively bonded composite repair (b).

- Large hole tolerances, as may be expected in a repair situation (unless interference-fit fasteners are used), allow movement and rotation of fasteners
- The high stresses at the fasteners and fastener holes result in significant local displacements – and significant stress concentrations.
- The frictional shear component on the surfaces of the joint can relax under cyclic loading or due to the lubricating effect of water-displacing compounds and other aircraft fluids.

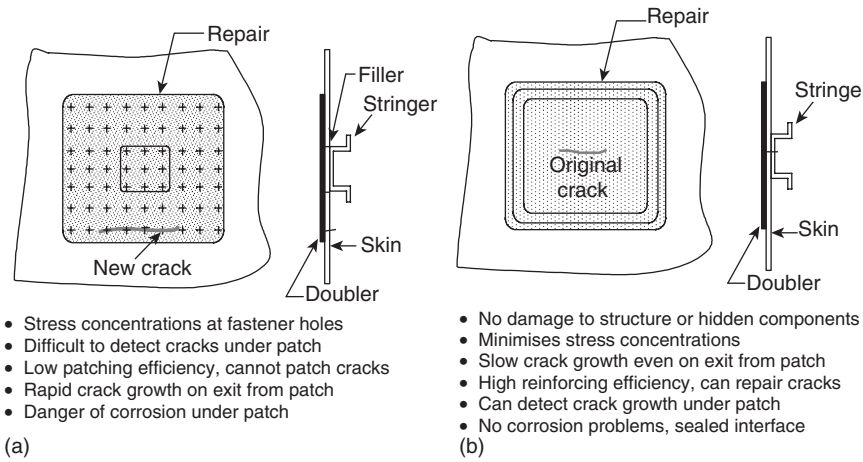


*2.3* (a) Some disadvantages of standard mechanically fastened repairs. (b) Some advantages of bonded composite repairs.

Because of the relatively low reinforcing efficiency in mechanical repairs, components having cracks generally cannot be satisfactorily reinforced and the cracked region must be removed prior to application of the repair; the resulting cut-out is filled with an insert before applying the reinforcing patch. In relatively thick-skinned components, crack removal is a costly, time-consuming requirement and may be impractical in many repair situations. Furthermore, *in situ* drilling of new fastener holes can cause internal damage (e.g. to hydraulic lines, electrical wires or optical fibres) as well as introducing swarf into the structure.

Mechanical repairs are often designed to restore static strength. However, Swift[9] shows that these repairs, if not well designed, can reduce fatigue life significantly. The main concern is the danger of initiation of a crack from a fastener hole in the reinforcing patch. The crack may initiate at quite low stresses because of high stress concentrations (usually at the first row of fasteners) or because of poor-quality hole drilling or riveting – common problems when applied under field conditions. There is also the danger of cracks initiating from hidden corrosion which can develop under a poorly sealed mechanical repair. Importantly, there is concern with the difficulty of detecting the crack by standard NDI procedures, until it emerges from under the metallic patch – when growth may be rapid because of low reinforcing efficiency.

In contrast, loads in bonded joints are transferred by shear over the surface area of the elements. Because of the large area for load transfer, which extends up to the crack, the bonded joint is intrinsically much stiffer than the mechanical joint, despite the very low stiffness of the adhesive

compared to the metal fasteners. The transfer length determines the rate of load transfer from the cracked region into the composite adherends, which is a function of the joint geometry and mechanical properties.[10] A low transfer length equates to high joint stiffness.

In a well-designed patch, one having optimally tapered ends to minimise shear and peel stresses in the adhesive, minor, but not insignificant, stress concentrations arise in the parent structure. These stresses can be a concern and must not be disregarded, as they can result in the initiation of fatigue cracks, especially if the patch terminates near another stress raiser – such as a fastener hole or a large inclusion or corrosion pit.

## 2.5 Composite materials and adhesives for bonded patch repairs

The advantages of high performance fibre carbon/epoxy and boron/epoxy materials for patches when compared with metallic alloys include:[6]

- high directional stiffness, which allows use of thin patches (important for external repairs) and allows reinforcement to be applied only in desired directions;
- high failure strain and durability under cyclic loading, which minimises danger of patch failure at even quite high strain levels in the parent metal structure;
- low weight, an important advantage where changes in the balance of a control surface must be minimised; and
- excellent formability that allows low cost manufacture of patches with complex contours.

Another important advantage of polymer-matrix composites with thermosetting matrices is that the pre-bonding surface treatment of composite patches for adhesive bonding is less demanding than for metals. This is because mechanical abrasion to produce a high energy uncontaminated surface is all that is required. Alternatively, the composite patch can be co-cured onto the metallic component with the adhesive, which obviates the need for any surface treatment of the patch and simplifies the patch fabrication procedure.

In most repair applications, use of unidirectional patches (all 0° plies) is optimal since this provides the highest reinforcement efficiency in the loading direction, and minimises undesirable stiffening in other directions. However, in some applications with high biaxial stress components, or where there is concern that the crack may change orientation, it may be desirable to provide transverse and/or shear reinforcement, for example repairs to a pressurised fuselage.[11] This can be achieved by using a laminate including ±20° or a smaller number of higher angle, e.g. ±45°, plies.

The main disadvantage of using carbon/epoxy or boron/epoxy results from a mismatch in thermal expansion coefficient between the composite and the metal.[8] Residual stresses are tensile in the parent metal structure and compressive in the composite patch. These stresses are particularly severe when elevated-temperature-curing adhesives are used to bond the patch and when operating temperatures are very low, typically –10 to –50 °C. The tensile residual stress could be expected, for example, to increase the growth rate of the patched crack by increasing the minimum to maximum stress ratio $R$, reducing patching efficiency. In severe situations, thermal cycling of the patched region causes cyclic stresses which could result in crack growth, independent of external stressing – however, no such problems have been found.[12]

The desire to avoid the residual stress problem is the major reason why[13] GLARE patches were used for repairs to thin-skin fuselage structure. GLARE is a glass-fibre/epoxy-reinforced aluminium alloy laminate. GLARE has a similar expansion coefficient to aluminium alloys, and excellent fatigue crack growth resistance compared to normal aluminium alloy materials; the glass fibres bridge any fatigue crack which may develop in the metal layers.

GLARE is less suited for repair of thick or highly contoured structure since it has a lower modulus than aluminium alloys and has limited formability (similar that of sheet aluminium alloy). Despite the residual stress concerns, the composites boron/epoxy and carbon/epoxy offer excellent properties for patches or reinforcements. Boron/epoxy is often considered to be the superior because of:

- better combination of strength and stiffness which provides the highest efficiency reinforcement;
- higher coefficient of thermal expansion, which reduces the severity of the residual stress problem;
- low electrical conductivity, which avoids the danger associated with carbon/epoxy of inducing galvanic corrosion of the metal and allows optimal use of eddy-current NDI to detect and monitor cracks under the patch.

However, carbon/epoxy is chosen if a patch with a small radius of curvature is required (less than 30 mm) or if the cost of boron/epoxy (very much higher than carbon/epoxy) or availability is a concern.

The choice for the adhesive for bonded repairs is generally a toughened structural epoxy film. The main adhesive used in Australian repairs is Cytec FM 73, a nominally 120 °C-curing epoxy–nitrile structural film. Reasons for this choice include the following:

- excellent strength fatigue resistance and toughness from low to moderate temperatures;

- resistance to aircraft fluids;
- ability to form strong durable bonds with appropriate pre-bond treatments;
- ability to cure (with some sacrifice in properties) at relatively low temperatures – as low as 80 °C (with extended times) compared with the standard one hour at 120 °C.[8]

The first three advantages are typical of most moderate-temperature-curing structural epoxy–nitrile film adhesives. However, the ability of FM 73 to cure and provide good properties at temperatures as low as 80 °C is both unusual and valuable for repairs where the higher temperatures cannot be achieved or where there is a need to minimise residual stresses. For higher temperature applications (above 80 °C) the adhesive FM 300-2, also by Cytec, is most often selected. This adhesive cures at a relatively low temperature (120 °C) while providing properties more typical of a 175 °C-curing adhesive.

Two-part epoxy paste adhesives are suitable when significantly elevated-temperature curing is impractical or undesirable or high bonding pressures can't be achieved. Current paste adhesives with very good properties for patching applications include toughened epoxy paste, such as Hysol EA 9395 as well as several others in this series. Finally, modified acrylic adhesives have been found to be highly effective for less demanding applications (temperatures not exceeding 60 °C or not below –10 °C, if peel stresses are high), especially where the use of elevated cure temperature is not feasible.

Bonded composite repairs are a versatile cost-effective method of repairing, strengthening or upgrading metallic structures. Potential applications can be summarised as follows:[14]

1. Reduce stress intensity:
   - in regions with fatigue cracks,
   - in regions with stress corrosion cracks,
   - to increase damage tolerance (provide slow crack-growth characteristics) in safe-life structure or structure with multi-site damage.
2. Restore strength and stiffness:
   - after removal of corrosion damage to below allowable SRM limits,
   - after removal of flaws,
   - after reshaping to minimise stress concentrations,
   - after heat damage,
   - after failure of a load path in multi-load path structure.
3. Stiffen under-designed regions:
   - to reduce strain at stress concentrations,
   - to reduce secondary bending,
   - to reduce vibration and prevent acoustic damage.

Applications have been developed in a number of these categories.[15] Studies related to the repair of corrosion damage are reported in references 16 and 17.

## 2.6 Application technologies and non-destructive inspection of bonded repairs

The processes by which the adhesive and patch material are installed critically affect the initial strength and long-term durability of the repair. These include surface preparation, both for the aircraft structure and patch material, as well as heating and pressurisation for bonding the patch to the parent structure.

### 2.6.1 Surface preparation

Preparation of adherend surfaces prior to bonding is the single most important process step for ensuring a successful repair.[18,19] Highly effective surface preparation is necessary to achieve initial bond strength and long-term durability in the service environment. Although the environment includes temperature extremes and exposure to many aircraft fluids and maintenance chemicals, moisture tends to be the biggest impediment to long-term durability.

The surface preparation process must firstly remove contaminants and naturally occurring oxide from the metal surface. It must also chemically and/or physically modify the surface to promote adhesion with the adhesive (or primer) and enable it to resist moisture attack. Cleaning and deoxidising alone can sometimes provide adequate initial adhesion but rarely result in bonded joints with long-term service durability. For repair applications, only very simple and non-hazardous treatments that can be applied on aircraft under field conditions are considered viable for most applications. Ideally, such a surface preparation will allow formation of highly durable bonded joints in a range of airframe metals, including aluminium alloys, steel, stainless steel and titanium alloys.

To satisfy these requirements, Australian work focused on the use of silane coupling agents. The coupling agent found most suitable for epoxy adhesives is the epoxy-terminated silane, $\gamma$-GPS.[18] This coupling agent can provide high strength durable bonds to aluminium alloys as well as stainless steel, nickel and titanium alloys. It is applied from an aqueous solution to the metal surface following mechanical abrasion by alumina grit blasting. The silane treatment is safe since it does not rely on noxious chemicals or electrical power. The process does not use acids, so it eliminates the corrosion concerns they cause if not properly rinsed and their potential to embrittle high strength steel fasteners.

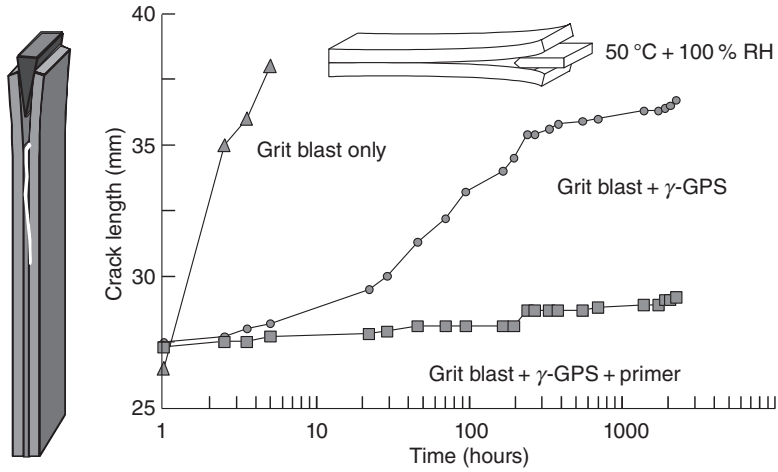


*2.4* Plots of crack growth versus time for wedge-test specimens (illustrated in inset) made of 2024-T3 aluminium and subjected to the surface treatments indicated, prior to bonding with FM 73 adhesive.

The resistance against moisture degradation provided by the silane can be further enhanced by use of a standard corrosion-inhibiting primer. Figure 2.4 shows typical results for crack growth in the wedge test[20] for 2024-T3 aluminium bonded with FM 73 adhesive following (i) grit blasting, (ii) grit blasting + silane and (iii) grit blasting + silane + primer. The wedge test can compare different surface preparations, with all other factors being equal, and relate the results to service experience. Minimal crack extension following exposure to hot/wet conditions and a crack that remains predominantly in the adhesive (rather than at a metal interface) indicate a good surface preparation. For FM 73 adhesive, conditioning at 50 °C and 100 % relative humidity (RH), crack growths of about 5 mm after seven days of exposure tend to indicate an adequate surface treatment. This behaviour is exhibited by system (iii) in the figure. However, despite the longer crack extension and interfacial failure modes, system (ii) has performed adequately in service for many applications.

Repairs in the US initially followed the Australian lead using the grit blast/silane (GBS) surface preparation,[18,21] including application of a corrosion-inhibiting adhesive bond primer, as a practical on-aircraft pre-bond treatment that yields good in-service environmental durability. More recently, a process based on sol–gel chemistry developed for the USAF by Boeing has emerged for applications on the same metal alloys currently treated using GBS.[22] This approach is similar chemically to GBS chemistry, but is a quicker process that performs as well as GBS in laboratory tests, including the wedge test.

For pre-cured (thermosetting) fibre composite patches, surface removal by light grit blasting with alumina is a highly effective treatment that provides excellent bond strength and durability.[23] Sometimes, in the Australian applications[24] a co-cured layer of adhesive is applied to the surface of the boron/epoxy patch to increase the toughness of the surface resin and to provide a layer more suitable for grit blasting without the danger of damaging the large boron fibres.

### 2.6.2 Heating and pressurisation

Heating and pressurisation are key installation issues since both have a direct impact on the quality of the repair. Controlled heating is required to cure adhesives and, if required, co-cure the composite patches to the aircraft structure. Heating may be required with certain surface preparations and for adhesive primer cure. It may also be necessary for drying structure prior to repair installation. Pressure application is needed to mate the patch to the aircraft structure. Adequate pressure must be applied to ensure proper bondline thickness and minimise bondline voids and porosity. It also causes the adhesive to flow and properly 'wet' the treated surfaces to achieve adequate adhesion. In the case of co-cured composite patches, pressure may be required to consolidate the composite in order to obtain the desired mechanical properties.

Heating may be conducted by any of a number of methods provided they are able to safely control the temperature in the repair area within prescribed tolerances without contaminating the repair. Typical on-aircraft heating methods include electric-resistance heat blankets, infrared heat lamps and hot-air devices. Application specifics determine the method best suited to a given repair. Heat blankets are typically used to cure adhesives, whereas heat lamps are usually the choice for silane drying and pre-curing primers. 'Hot bonders' that automatically control heating based on temperature feedback from the repair area are normally used with heat blankets. These units or similar means can be employed to control heat lamps and hot-air devices.

Attaining specified repair temperatures within desired tolerances can often be difficult on aircraft, since portions of the structure can act as 'heat sinks'. These regions conduct heat away from the repair site and become locally cooler, creating the possibility that the adhesive may not fully cure. Thermal surveys of the repair area are important to ensure proper heating will be attainable. The surveys should be conducted on the actual repair area using the equipment to be employed during the repair. They can determine the placement of insulation materials or the locations needed for supplemental heating, and they will reveal the required temperature readings for surrounding 'monitoring' locations that can be used to

determine the temperature in the repair area. Methods of obtaining a reasonable temperature distribution under these circumstances are provided in reference 25. Often the approach is to accept a significant temperature variation over the repair region and set the controller to control at the point of hottest temperature and to cure at a time sufficient to cure the coolest region.

Pressure application on aircraft may also be achieved by a variety of means. These include vacuum bag, inflated bladder or various forms of mechanical pressure. The use of a vacuum bag is the most common since it is almost always the most convenient. Vacuum bags are light, conform to almost any surface, apply uniform pressure, can remove volatiles from the repair area and can hold a heat blanket in place. To apply pressure this way, a bag is built over the repair area and air is extracted, allowing atmospheric pressure to be applied. In most cases, it is not desirable to achieve a full vacuum throughout the cure cycle since the vacuum allows volatiles in the adhesive, such as moisture or solvents, to volatilise more readily, and it allows entrapped air to expand more easily. Often, high vacuum levels are applied initially to remove volatiles from the repair, then vacuum levels are reduced before the adhesive gels in order to minimise porosity in the bondline. Bladders inflated with air can be used to apply positive pressure (as opposed to vacuum) on a repair area. This may be desirable to minimise void formation due to the evolution of volatiles. Mechanical pressure may also be applied by clamping or other means. As with bladders, these forces must be reacted, and it may be difficult to apply uniform pressure over a large area.

Fibre composite patches should be pre-cured under positive pressure per manufacturer's recommendations whenever possible. This is ideally done in an autoclave to minimise porosity and achieve the per ply thickness value envisioned by the design – however, where this is not feasible, cure in an oven under a vacuum bag can produce acceptable results, if pre-preg materials specially designed for cure under vacuum are used.[26] The approach here is to leave open channels in the pre-preg (for example, by applying the matrix resin to only one side) for removal of entrapped air and volatiles.

If use of this type of pre-preg is not feasible, the resulting patch may be highly porous However, using a combined pre-consolidation and de-gassing approach known as double-vacuum processing,[27] it is possible to reduce voids to less than 3 % and markedly increase fibre-volume fraction. This procedure, which reduces the pressure required during patch application and minimises porosity, involves placing the patch lay-up with the vacuum bag inside a sealed box to which a vacuum can be applied. Firstly, the vacuum is applied under the bag and to the box which allows the lay-up to de-gas under no external pressure, maximising the removal of trapped air

and volatiles. The vacuum in the box is then vented and normal vacuum allowed to consolidate the patch lay-up.

The cured patch can be non-destructively inspected prior to application on the aircraft. The knowledge that the patch has minimal porosity, typically a couple of percent or less, eases the on-aircraft inspection burden for the adhesive bondline. Alternatively, fibre composite patch materials are co-cured on the aircraft with the adhesive. This may be done to allow them to conform to a complex geometry where the alternative of secondarily bonding would require a tool to recreate the surface of the repair area. Prior to co-curing, fibre composite patches are often consolidated (de-bulked) at stages in a vacuum bag or in an autoclave to minimise porosity and achieve the desired fibre volume fraction.

### 2.6.3 Non-destructive inspection (NDI) of bonded repairs

Conventional NDI procedures, including ultrasonics and thermography, can readily detect fairly large defects in the patch system such as disbonds, delaminations (in the case of composite patches) and significant porosity. Eddy-current procedures and radiography can be used to detect crack growth under the patch – this technique performs optimally with non-conducting patches (see Fig. 2.2).

These NDI procedures specifically for patch repairs of metallic structures are evaluated in detail in reference 28 with several practical examples provided. However, a major concern with bonded repairs (and adhesive bonding generally) is that NDI techniques cannot detect weak bonds in situations where the adherend surfaces are in intimate contact or coupled by a thin layer of liquid. Nor can they provide any information on bonds weakened by degradation in service, providing no physical separation occurs. This limitation restricts the application of bonded repairs to primary structure, especially in situations where the failure of the repair can compromise safety in flight. A more detailed discussion on related certification issues is provided later.

## 2.7 Design and modelling of bonded composite repairs

The first requirement is to assess the defect, assumed here to be a crack, in terms of its length and depth, etc., and to determine the thickness and geometry of the cracked region as well as the local loading conditions. For example, of particular importance in adhesively bonded repairs is the available overlap length on either side of the crack. The thicker the structure and consequently the higher the loads, the thicker the patch and the longer

the overlap length needed to transfer the loads into the patch. The temperature and environment experienced by the region to be repaired must also be considered, since this will help determine the type of adhesive to be used.

It is unlikely, other than possibly for relatively simple cases such as fuselage repairs, that information on local loading will be available or easily estimated, unless there is access to detailed design data. Failing this, a good approximate estimate[29] (in the author's view, at least) of the stress at design limit load (DLL) is achieved by equating design ultimate load (DUL) with the material yield stress $\sigma_y$. The basis for this assumption is that at DLL = $\sigma_y/1.5$ yielding would not occur at a typical stress concentration $K_c$ of ~ 1.2. Then DLL is the yield stress divided by 1.5. This has proven to be a conservative estimate in all cases examined where the DLL was available. Reference 29 provides some data based on the F-111. Clearly, assumption of the ultimate strength $\sigma_u$ as equal to $\sigma_{DLL}$ is over conservative. A knowledge of the loading spectrum for the region is also unlikely to be available, so a reasonable approach, if such detail is required for design, is to assume one of the standard spectrums, FALSTAF or TWISS, according to whether the aircraft is a fighter or transport,[30] respectively.

Once sufficient information is available concerning the loading and other parameters and it is considered on the basis of the forgoing discussion that a bonded repair is feasible, a patch design can be undertaken. The patch must be designed to ensure that: (i) the stress intensity in the patched crack is reduced to an acceptable level and (ii) the patch system can initially transmit and subsequently survive the service loading. Although analytical procedures, as described in the next section, are available for simple configurations, design for complex repairs will be based on finite element (FE) approaches.[31,32]

### 2.7.1 Modelling bonded composite repairs

The analytical approach has the advantage that it provides a clear insight into the important patching parameters as well as providing a basis for design in geometrically simple repairs, so an analytical model is described in the next section followed by some experimental validation studies. Most analytical approaches to estimate stress intensity in the patched crack are based on the elegant model developed by Rose[33] and later further developed by Rose and Wang;[34] this has been further developed by many others, including Boeing under USAF funding in the 'Composite Repair of Metallic Structures' (CRMS) Program.[35,36]

Very briefly and considerably simplified, in the Rose models a two-step approach is used, as illustrated in Fig. 2.5. In step 1, the patch is modelled

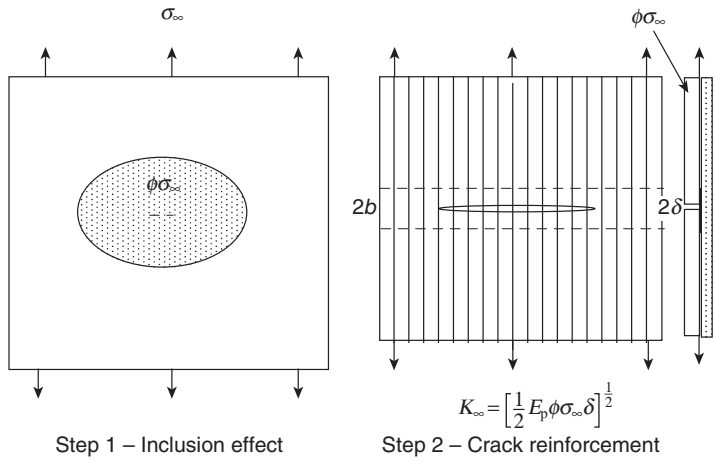


*2.5* Schematic illustration of the analytical approach to crack patching. The parallel lines represent a disbond, width 2*b*.

as an inclusion in a large panel and the presence of the crack (assumed to be relatively very small) is neglected. The stress in the metallic component in the prospective region of the crack is then given by $\phi\sigma_\infty$, where $\phi$ is a factor which accounts for the stiffness and shape of the patch. Because the patch attracts load, the stress reduction may be significantly less than predicted simply on the basis of the ratio of patch stiffness to plate stiffness. Calculation of $\phi$ is described in reference 33. For full-width reinforcement, $\phi$ is given by $(1 + E_R t_R / E_P t_P)^{-1}$. If $\phi$ for full-width reinforcement with equal stiffness patch and panel is 0.5 then, for an isotropic circular patch of the same nominal stiffness, it is 0.69.

In step 2, the crack is modelled as being semi-infinite and fully covered by the patch. The far-field stress in the region of the panel containing the crack is $\phi\sigma_\infty$. Based on considerations of the changes in potential energy for the growth of the crack under the patch, an estimate of the corresponding energy release rate and therefore the stress intensity is derived. From this analysis, the upper-bound estimate of stress intensity $K_\infty$ is given by:

$$K_\infty = \phi\sigma_\infty (\pi\lambda)^{\frac{1}{2}} \qquad [2.1a]$$

$\pi\lambda$ the characteristic crack length is given by

$$\pi\lambda = \left(1 + \frac{1}{S}\right)\beta^{-1} \qquad [2.1b]$$

where

$$S = E_R t_R / E_P t_P \qquad [2.1c]$$

$$\beta^2 = \frac{G_A}{t_A}\left[\frac{1}{E_P t_P} + \frac{1}{E_R t_R}\right] \quad [2.1d]$$

and where $E$ and $t$, respectively refer to modulus and thickness, subcripts P and R indicate the panel and the reinforcement, respectively, the subscript A indicates adhesive and $G_A$ represents the adhesive shear modulus. $\beta$ is the exponent of the elastic shear strain distribution ($\beta^{-1}$ is often called the characteristic load transfer length). The use of $K_\infty$ to assess the stress intensity in the cracked component allows considerable simplification in crack growth analysis since, as seen in Eq. (2.1a), $K_\infty$ is independent of crack length $a$.

Equation (2.1a) is applicable only for a relatively long crack and for linear behaviour (no yielding of the adhesive) but provides a reasonable estimate of $K_\infty$ with limited yielding of the adhesive. For the equivalent unpatched centre-notched panel

$$K = \sigma_\infty (\pi a)^{\frac{1}{2}} \quad [2.2]$$

where $2a$ is the crack length so the maximum patching efficiency in this case is given by:

$$\frac{K_\infty}{K} = \phi\left(\frac{\lambda}{a}\right)^{\frac{1}{2}} \quad [2.3]$$

For an edge-notched 3.14 mm thick 2024 T3 aluminium alloy panel (edge-notched) with a 7 ply (0.09 mm thick) unidirectional boron/epoxy patch used in experiments described in the next section, $\lambda = 3.5$ mm, $\phi = 0.68$, and, taking $a = 35$ mm, the ratio is ~0.2.

To justify use of $K_\infty$ for this case, Fig. 2.6 plots, $K_R$ the predicted stress intensity[37] versus $a$. The parameters used are those of the boron/epoxy patched panels just provided. This plot shows that $K_R$ asymptotes to $K_\infty$ for crack lengths above around 25 mm. Thus, at least to a good first approximation, the assumption that $K_R$ is equal to $K_\infty$ for $a$ above 25 mm is reasonable for these specimens.

For correlation with the fatigue studies described later, an alternative relationship[29] for $K_\infty$ was used, given by:

$$K_\infty = \left[\frac{1}{2} E_P \Phi \sigma_\infty \delta\right]^{\frac{1}{2}} \quad [2.4a]$$

where $\delta$ is the 'crack' mouth opening displacement; $\delta$ is estimated from the overlap joint that would be obtained by cutting a strip through the panel normal to the crack.

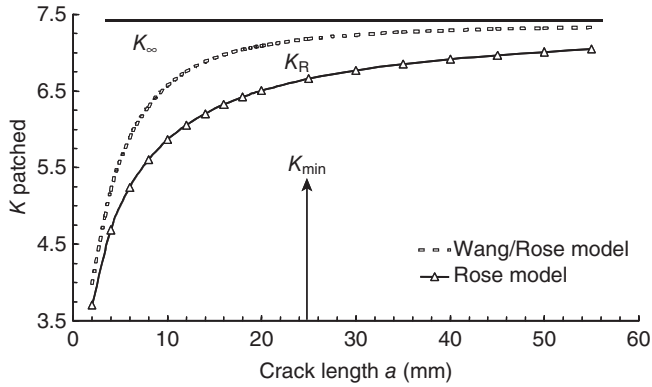


*2.6* Plot of predicted variation of stress intensity of the patched crack $K_R$ versus crack length, based on Rose's model and the more recent Rose/Wang model from reference 34. $K_\infty$ is the upper bound estimate used in these studies. The patching parameters are for the experimental studies described in Section 2.7.3, at a stress of 80 MPa.

The estimation of $\delta$ is as described in reference 8; for the elastic adhesive case, it is given by the following relationship:

$$\delta = 2\sigma_0 t_P / (\beta E_R t_R) \qquad [2.4b]$$

where $\sigma_0 = \phi\sigma_\infty$ is the effective stress under the patch in the vicinity of the crack.

For the case where the adhesive yields plastically we have:[33]

$$\delta = \frac{\tau_y t_A}{G_A}\left[1 + \left(\frac{\sigma_0}{\sigma_{0y}}\right)^2\right] \qquad [2.4c]$$

where $\tau_y$ is the shear yield stress of the adhesive and $\sigma_0 \geq \sigma_{0y}$ and where

$$\sigma_{0y} = \frac{\tau_y}{\beta t_P}$$

Under the cyclic stress range $\Delta\sigma_\infty$, the stress intensity range $\Delta K_\infty$ is given approximately by:

$$\Delta K_\infty = \left[\frac{1}{2} E_P \Phi \Delta\sigma_\infty \Delta\delta\right]^{\frac{1}{2}} \qquad [2.4d]$$

The displacement range $\Delta\delta$ is dependent on the thicknesses and stiffnesses of the patch and of the cracked component and on the thickness, shear modulus and effective shear yield stress of the adhesive.

$\Delta K_\infty$ is not constant if disbonding occurs in the patch over the crack region. Local disbonds often develop in the high shear stress regions at the edges of the crack in the parent structure. It is thus necessary to modify the model to account for this behaviour.

It was assumed for a simple extension to the basic model[38] that a parallel disbond, size $2b$, traverses the specimen, as illustrated in Fig. 2.5. Then the opening of the representative joint is increased by $2be$, where $e$ is the estimated strain in the reinforcement. Equation (2.4a) then becomes:

$$\Delta K_\infty = \left[\frac{1}{2} E_P \Phi \Delta\sigma_\infty (\delta + 2be)\right]^{\frac{1}{2}} \quad [2.5a]$$

If it is assumed as a first approximation (based on early fatigue tests on double-overlap joints[8,39]) that $db/dN$ is a constant which can be estimated for given stressing conditions, then

$$b = N\left[\frac{db}{dN}\right] \quad [2.5b]$$

Thus, the effect of disbond growth on crack growth behaviour can be estimated inserting Equation (2.5b) into (2.5a). $\Delta K_\infty$ then no longer remains constant but is a function of $N$.

### 2.7.2 Additional design issues

There are many other design issues that need to be considered, even for relatively simple repair configurations. The most important of these are secondary bending and residual stress effects which are briefly considered in this section (see the references for further details). Firstly, in many patching applications, because of accessibility limitations, the patch is applied only to the one surface, typically the outside skin of an aircraft. In this case, the displacement of the neutral axis by the patch will cause secondary bending to a degree depending on the constraint offered by the surrounding structure. Restraint may be expected to be relatively high in the case of a wing skin and relatively low in the case of a large fuselage panel.

Secondary bending causes considerable practical and analytical[33,34] complications. Where bending occurs, as shown in Fig. 2.7 three points of differing stress intensity through the panel thickness are identified: $K_{max}$ on the face opposite to the patch where $\delta$ is greatest; $K_{min}$ on the face under the patch where $\delta$ is minimum; and $K_m$, the membrane value – approximately the mean of $K_{min}$ and $K_{max}$.

As included in Fig. 2.6 for the 25 mm crack, taken as an example, $K_{min}$ is (as expected) significantly lower than $K_R \sim 5.5\,\text{MPa}\,\text{m}^{1/2}$ compared with

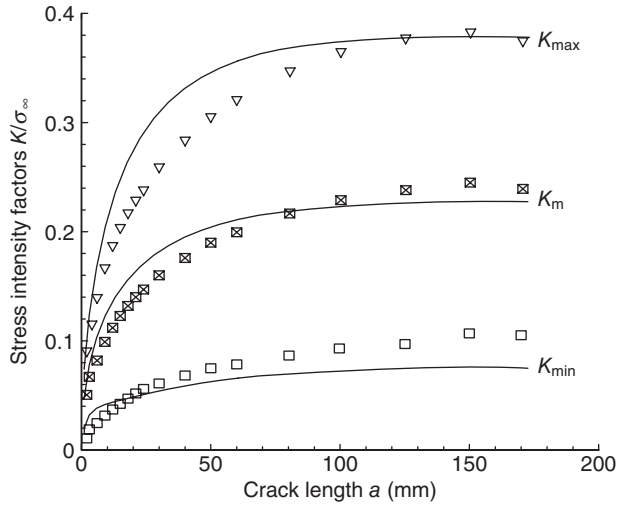


*2.7* Theoretical predictions and finite element results for a typical one-sided repair assuming geometrically linear deformation, taken from reference 34.

~6.6 MPa m$^{1/2}$; however, $K_{max}$ is very much greater at around 30 MPa m$^{1/2}$. Thus, a fatigue crack will grow more quickly on the outside face, although the growth rate is expected to be retarded by the reducing stress intensity though the thickness of the panel.

Secondly, a complication with composite patches that must be considered is the development of residual stress $\sigma_T$ caused by the mismatch between the thermal expansion of the patch and parent structure,[8] and dependent on $\Delta T$, the difference between the elevated cure temperature required for the adhesive and the service operation temperature. In a component under cyclic loading, $\sigma_T$ acts as a mean stress and, in the presence of a crack, it results in the development of a residual stress intensity $K_T$ which, in the simple case of a centre-cracked panel, is given as:

$$K_T = \sigma_T(\pi a)^{\frac{1}{2}} \qquad [2.6a]$$

This relationship for $K_T$ was shown experimentally[8] to apply up to a crack size of approximately 30 mm.

As a simple example, for a patch bonded to a metallic strip of similar width we have that:

$$\sigma_T = t_R E_R E_P \Delta T(\alpha'_P - \alpha_R)/(1/E_P t_P + 1/E_R t_R) \qquad [2.6b]$$

This equation illustrates some of the main parameters and provides a ball-park estimate of $\sigma_T$; for the more complicated situation of a circular

patch on a metal panel, see reference 37. The effective thermal expansion of the metallic plate $\alpha'_P$ depends on the length $L_P$ between mechanical constraints on the ends of the plate and the length $L_R$ of the reinforcement – which is assumed also to be the length of the hot zone. Then, assuming $\Delta T$ increases linearly from the constraint ends of the strip to the heated region, as expected for steady-state conditions:

$$\alpha'_P = (\alpha_P/2)(1 - L_R/L_P) \quad [2.6c]$$

Thus when $L_R/L_P \to 0$ $\alpha'_P \to \alpha_P/2$ and when $L_R/L_P \to 1$ $\alpha'_P \to 0$.

For aluminium $\alpha_P$, the unconstrained expansion coefficient, is $23 \times 10^{-6}\,°C^{-1}$ whereas for boron/epoxy in the fibre direction it is $4.5 \times 10^{-6}\,°C^{-1}$. For a clamped circular plate with a circular patch, it is shown[40] that for

$$L_R/L_P \to 0, \quad \alpha'_P \to (\alpha_P/2)(1 + \nu_P) \quad [2.6d]$$

where $\nu_P$ is the Poisson's ratio of the plate. The constrained expansion coefficient is then about 30 % larger than for the strip case.

### 2.7.3 Validation of the patching model to estimate fatigue crack growth

It is assumed for simplicity that, as for unpatched cracks, a Paris-type relationship holds with

$$da/dN = f(\Delta K, R) = A_R \Delta K^{n_R} \quad [2.7]$$

Assuming $\Delta K \cong \Delta K_\infty$, the relationship between crack length $a$ and the number of cycles $N$ can be obtained from:

$$a = A_R \int_0^N (\Delta K_\infty)^{n_R}\, dN \quad [2.8]$$

where $N$ is number of constant amplitude cycles and $A_R$ and $n_R$ are assumed to be constants for a given $R$ (ratio of minimum stress to maximum stress). As $\Delta K_\infty$ is a constant, providing disbonding does not occur, it can be moved outside of the integration sign. Thus $a$ should be linearly related to $N$.

Studies were undertaken to investigate patching behaviour using the specimen configurations and details depicted in Fig. 2.8. Two studies taken from reference 29 are briefly mentioned here: (i) influence of stress range on patched cracks and (ii) the influence of patch stiffness. To illustrate the influence of stress range, Figs 2.9a and 2.9b plot the results for $a$ versus $N$ for an edge-notched 3.14 mm thick 2024 T3 aluminium alloy panel with a 7

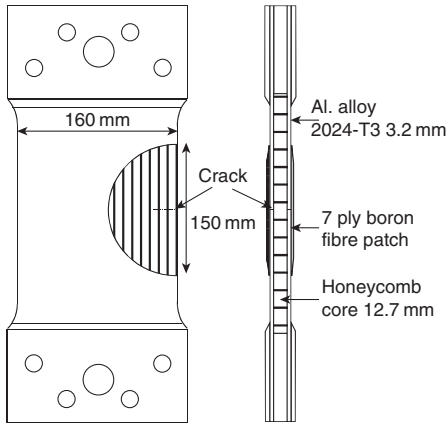


| Panel | Patch | Adhesive | Units |
|---|---|---|---|
| $E_P = 72$ | $E_R = 200$ | – | GPa |
| $G_P = 27$ | $G_R = 10$ | $G_A = 0.57$, 20 °C | GPa |
| | | $= 0.25$, 60 °C | |
| | | $= 0.17$, 80 °C | |
| | | $= 0.11$, 100 °C | |
| | | $\tau_y = 36$, 20 °C | MPa |
| | | $= 16$, 60 °C | |
| | | $= 12$, 80 °C | |
| | | $= 8$, 100 °C | |
| $t_P = 3.14$ | $t_R = 0.52$ | $t_A = 0.4$ | mm |
| | $= 0.90$ | | |
| | $= 1.30$ | | |
| $\alpha_P = 23E{-}6$ | $\alpha_R = 4E{-}6$ | – | °C$^{-1}$ |

*2.8* Illustration of the test configuration used to evaluate patching efficiency in patched panels. Note that two cracked-patched panels are tested simultaneously in this configuration. A 7 ply patch is standard but 4 and 10 ply patches were also evaluated. The table provides properties assumed in the calculations based on Cytec short-overlap shear data.

ply (0.9 mm thick) unidirectional boron/epoxy patch for a nominal stress ratio (minimum/maximum) $R = 0.1$ at $\sigma_{max}$ levels ranging from 80–244 MPa. The highest stress level corresponds to typical DLL capability for this alloy.

The relationships between crack length $a$ and cycles $N$ in Fig. 2.9a at the low stress levels are remarkably linear, suggesting that the experimental value of $K_R$ is indeed effectively constant even at $a$ values between 10 and 25 mm, where some non-linearity was expected (see Fig. 2.6). The change from an approximately linear relationship to a more parabolic relationship occurs above $\sigma_{max} = 138$ MPa and results from the development of disbond damage in the bond layer, indicated as a $2b$ value in the figure. At the 138 MPa stress level, damage in the adhesive system was found to be negligible.

Using these results, Fig. 2.10 plots log d$a$/d$N$ versus log $\Delta K_\infty$. A reasonable graphical fit is obtained for $da/dN = 7.9 \times 10^{-11} \Delta K_\infty^3$ m/cycle , showing that the influence of stress can be approximately accounted for with this approach. For test panels with 4, 7 or 10 ply thick patches, Fig. 2.10a plots d$a$/d$N$ versus stress and Fig. 2.10b plots log d$a$/d$N$ versus log $\Delta K_\infty$. The $R_R$ is based on both the applied and estimated residual stresses.[38] This plot shows that the log d$a$/d$N$ versus log $\Delta K_\infty$ relationship for the 7 ply panel would have given quite reasonable predictions for the 4 and 10 ply panels, again providing a limited validation of the model and approach. In general,

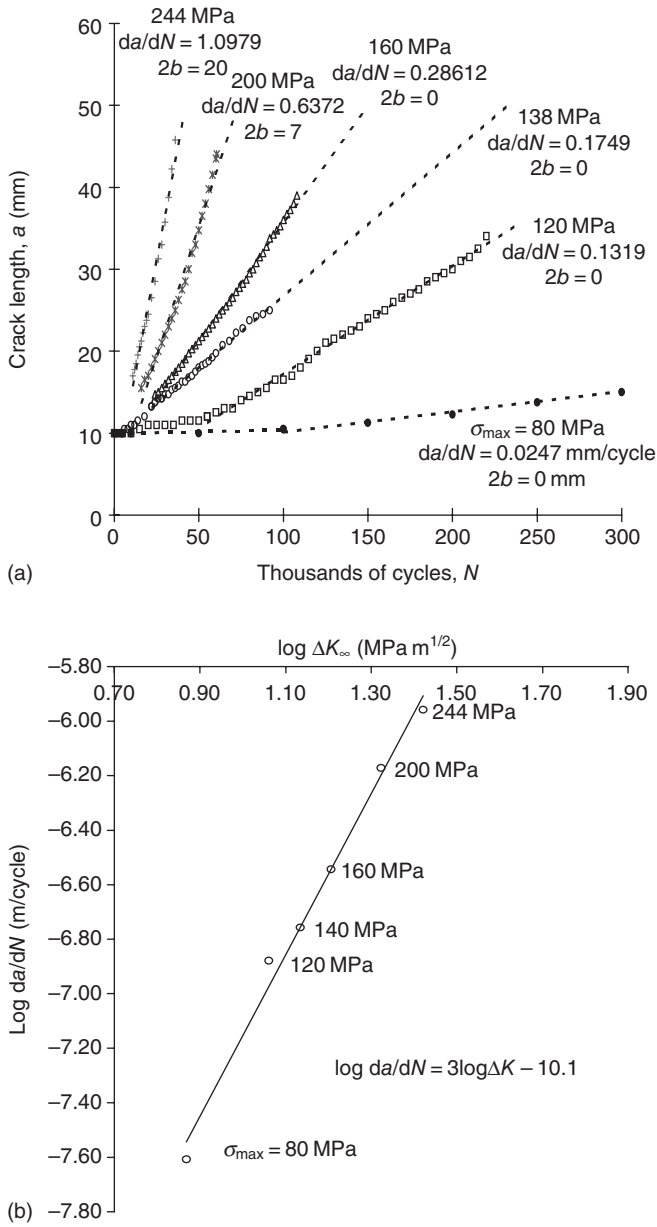


*2.9* (a) Plots of crack length *a* versus cycles *N* for a standard 7 ply patched specimen for applied $R = 0.1$. (b) Plot of log d*a*/d*N* versus log $\Delta K_\infty$ for the results in Fig. 2.6.

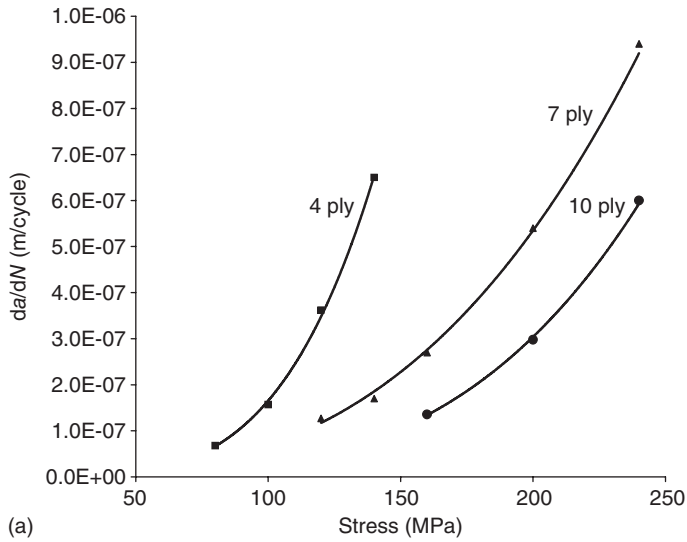


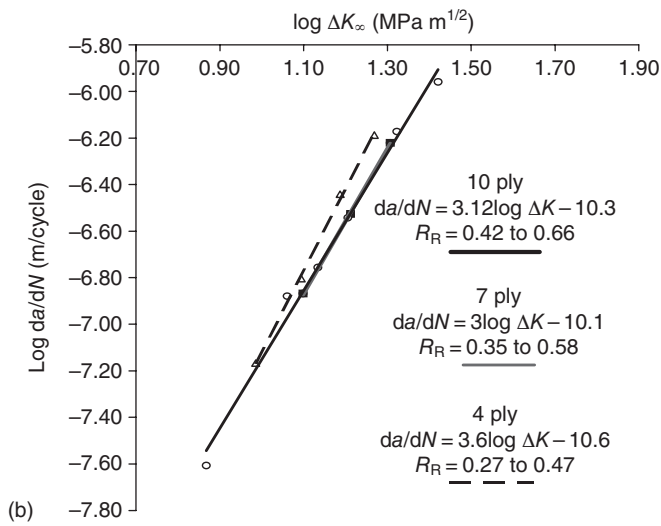


*2.10* Plots of (a) d*a*/d*N* versus maximum stress and (b) log d*a*/d*N* versus log $\Delta K_\infty$ for test panels having 4, 7 or 10 ply patches. *R* is 0.1, $R_R$ is as indicated on (b) and $t_A$ is about 0.5 mm.

from the above and other studies, it can be tentatively concluded that the analytical approach is suitable for the design of repairs under constant amplitude cyclic loading.

## 2.8 Certification of repairs to primary structures

There are two key issues that must be addressed as part of a certification process:

1. demonstrated use of validated patch design procedures;
2. assurance of initial strength and long-term durability (integrity) of the patch system.

Durability can be divided into two distinct topics: environmental durability and fatigue durability (given good environmental durability) – but not neglecting potential interaction between the two.[41]

Environmental durability is a critical inspection and quality control issue which does not lend itself to the provision of design data, equivalent, for example, to fatigue crack growth in metals. What is required is an assurance that large-scale failure of adhesion – gross disbonding at the patch or parent surface – will not occur either initially or over the required lifetime of the repair.

None of these issues is sufficiently well addressed at this time, especially that of environmental durability. Thus repairs to primary structure are currently only accepted on the basis that the structure in the *absence of the patch* has sufficient residual strength. This strength would be at some acceptable fraction of the DUL, which may vary from DUL to DUL/1.5 (the DLL). The bottom line is that if the residual strength in the absence of the patch falls below the chosen one of these levels, no credit is given to the patch for restoring strength.

To overcome this limitation, in reference 42 an approach is proposed by which credit could be given to the patch in restoring residual strength in situations where, in the absence of the repair, residual strength is reduced below an acceptable limit. An outline is provided in the following sections.

### 2.8.1 Proposed design procedures

The design approach must include two major aspects: (a) design of the patch or reinforcement to provide acceptable reduction in stress intensity and consequent rate of crack growth in the parent structure under the service loading; and (b) prediction of the life or fatigue durability of the patch system, based on estimated patch system stresses. The influence of the patch on raising local stresses in the parent structure (for example at the patch termination) must also be included in (a).

The assumption regarding (a) is that the available design models, based on analytical or FE procedures, can provide a reliable assessment of the key parameters, including: (i) reduction in stress intensity and (ii) stresses in the patch system. For (i), this has been validated to a limited extent by experimental studies on the analytical approach, examples of which were provided in Section 2.7.3.

All that is needed then is the materials database for the fatigue allowables for the patch system that can be input into the analysis. The main requirement is to provide a generic design allowables database which is valid over a range of geometries and environmental (moisture absorption and temperature) conditions similar to the specific repair. The downside of this approach is that to be cost-effective the number of repair systems would have to be severely restricted to minimise the number of databases that need to be acquired.

### 2.8.2 The representative joint specimen

As a first consideration, an attractive generic approach appears to be to base the static design on allowables obtained from adhesive shear-stress/shear-strain data, for example using the analytical approach developed by Hart-Smith.[10] The stress/strain data required can most easily be obtained from the thick adherend shear test.[43] However, this appealing design approach, proposed for example by Davis *et al*,[44] can be very misleading. This is because: (i) there are several potentially lower stress failure modes than failure in the adhesive layer (called cohesive failure), especially with composite patches; and (ii) even if failure occurs cohesively in the adhesive, typically at elevated temperature, the joint strength often does not correlate with shear-stress/shear-strain behaviour. Importantly, the approach based only on shear-stress/shear-strain behaviour ignores peel stresses at the ends of the joint which can have a major influence on failure locus and mode and is especially a concern when considering the effect of cyclic loading – even in the absence of peel stresses.

Composites have a significantly lower toughness than the structural adhesives used in repair, so failure, especially under cyclic loading, often occurs in the near-surface plies – a particularly prevalent mode when there are significant peel stresses. The tendency and level at which failure occurs depends on several factors, including the surface ply orientation, the temperature and (at elevated temperatures) the absorbed moisture level.

It is assumed here that the fatigue design allowables can be obtained from joints which represent the most severe loading conditions experienced by the repair. Obviously, there are significant differences between a simple joint and the repair – for example, the joint is single-load path element, whereas loads can bypass the repaired region in an actual repair. The joints

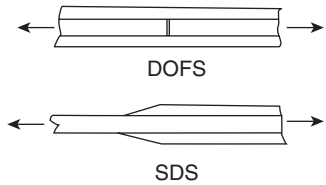


*2.11* Schematic illustrations of the representative joints proposed and studied.

must be representative of the materials, the application processes, the repair geometry, the loading conditions and the temperature and environment expected for the actual repairs.

Some representative joints suitable for developing the fatigue allowables[45] are shown in Fig. 2.11. These were designed for tests conducted under tension loading; however, using anti-buckling guides they should also be suitable for compression loading. The double-overlap fatigue specimen (DOFS) represents the stresses in the adhesive system over the crack. The skin-doubler specimen (SDS) represents the stressing conditions at the termination of the repair.

Essentially, the overall approach will be to use this generic data after assessing (for example using the appropriate FE model) the stress distribution in the proposed repair zone then, if required, design and test some extra details to check the influence of differences from the simple stress distribution in the generic specimen. For example, there may be significant through-thickness (peel) stresses that do not arise in the generic test specimen.

### 2.8.3 Double-overlap fatigue specimen (DOFS)

Previous work[8,39] conducted only at room temperature (RT)/dry conditions showed that the most promising damage parameter for fatigue in the DOFS is the measured or estimated shear strain range in the $\Delta\gamma$ adhesive. The damage response measured is the rate of disbond growth d$b$/d$N$. Fig 2.12 shows some results obtained from fatigue tests at ambient temperature conducted on a DOFS made of aluminium adherends with boron/epoxy outer adherends under constant load amplitude cycling. The damage growth was interpreted from the opening under load of the gap in the inner adherend.

These data were used to determine an allowable value $\Delta\gamma_A$ for acceptable damage growth just for ambient conditions. However, this conclusion was preliminary with no attempt to gain statistically valid data or include a hot/wet environment, thus much further confirmation is required. Several other

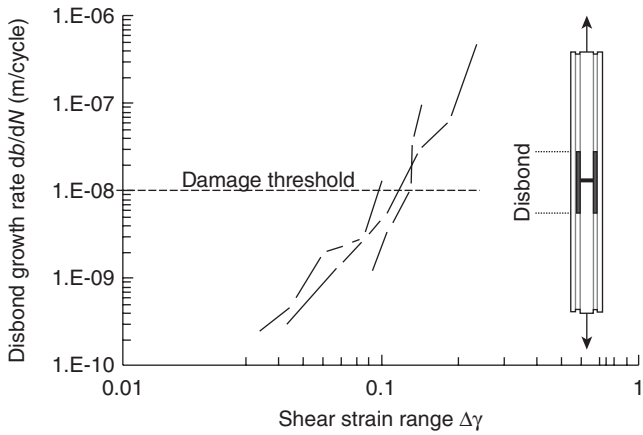


*2.12* Disbond growth versus measured shear strain range in the adhesive layer obtained from DOFS made of aluminium alloy adherends and boron/epoxy outer adherends.

correlating parameters, especially those based on fracture mechanics approaches, are also feasible although were not found to be useful in this study.

### 2.8.4 Skin-doubler specimen (SDS)

Studies were carried out using SDSs made of aluminium alloy inner adherends and boron/epoxy outer adherends tested under constant amplitude load cycling. The approach was to bond strain gauges at the ends of the taper region on the boron/epoxy patch and note the decrease in strain as an indicator of tip disbonding. As shown in Fig. 2.13, the load range was increased in steps after 5000 cycles until damage occurred. The Mode 1 energy release rate $\Delta G_1$ was considered to be a potentially useful damage correlation parameter.

A follow-up study[46] based on an all-aluminium alloy SDS showed much more clearly that indeed $\Delta G_1$ or $\Delta G_T$, the total energy release rate, are potentially suitable damage correlation parameters. The use of an all-metallic SDS considerably simplifies the behaviour and interpretation, especially as thermal stresses are relatively small compared to the metal/composite SDS and, unlike in composite patches, first-ply failure or shear lag through the composite laminate is not an issue. The energy release rate Mode1, Mode 2 or some combination of the two has also been shown to be a suitable parameter in other studies.[47] Under tension loading, especially under low temperature/dry conditions, it is anticipated that the lowest stress failure mode in the SDS will be peel in composite patch.

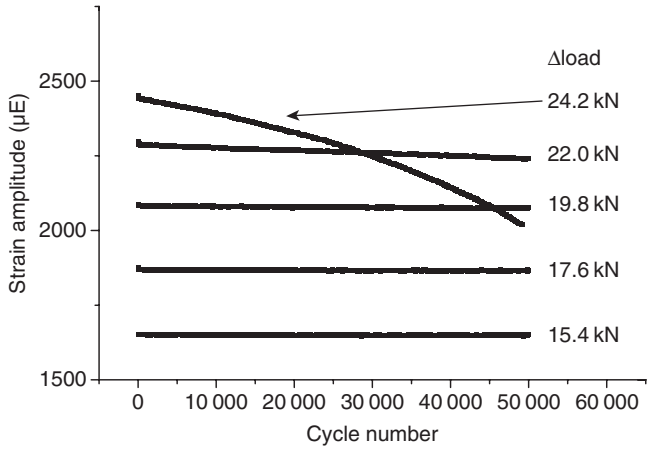


*2.13* Strain amplitude versus cycle number for SDS made of aluminium alloy adherends and boron/epoxy outer adherends stepped end, 4 mm/ply.

### 2.8.5 Design approach based on the analytical model

There are two basic approaches based on the Rose analysis: CalcuRep,[48] developed by the USAF Academy, an established software program for the analytical approach. Earlier, an iterative approach was developed by the author[8] to determine optimum patch dimensions. Based on this approach, Fig. 2.14 provides a simple decision design chart which also includes the other important parameters and part of the notional generic materials database.[42] This approach includes the important issue of patch transfer length and aims to design the minimum thickness patch to minimise residual stresses which arise from the mismatch in the coefficients of thermal expansion between the parent metallic structure and the composite patch. The analysis also allows for load attraction by the patch. The iterative approach is as follows. Patch thickness is increased one ply at a time then:

- The computed patch length $L_R$ is compared with the allowable $L^*$.
- The computed strain in the patch is compared with the allowable strain $e_R$.
- The computed shear strain range $\Delta\gamma^*$ is compared with experimentally determined allowable (from the DOFS) $\Delta\gamma_A$.
- *The allowable damage parameter at the patch termination, as determined, for example, from the SDS is not shown in this chart.*
- Check to see if $\Delta K$ reduction is acceptable.

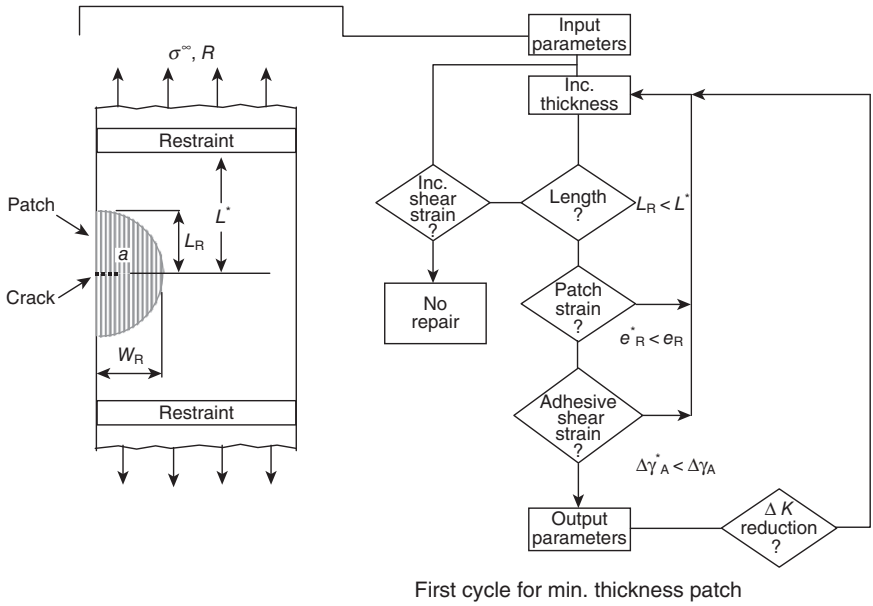


*2.14* Outline of algorithm for design of minimum thickness patch.

## 2.9 Validation of certified repairs

Given that the proposed generic approach to repair design is acceptable to the Certification Authority, i.e. a correctly implemented patch system will be durable for the required lifetime and will prevent or acceptably reduce the rate of crack growth in the parent structure, the issue is to qualify the actual repair as a materials system. The main requirement is to qualify patch application, including surface treatment, degree of cure, thickness of the adhesive and absence of physical defects.

In some bonded repairs, especially those applied in a factory or depot environment, it may be sufficient to base qualification solely on the use of appropriate processes and quality control; for example, pre-bond surface treatment and patch and adhesive cure conditions. However, generally it will not be feasible to ensure the required level of quality control in a practical repair situation so some form of *in situ* qualification will be required.

Firstly, any concerns with initial patch system integrity, that is the presence of physical defects (such as extensive voiding and disbonds) in the repair system after implementation, can be minimised by conventional NDI. Similarly, NDI can detect in-service damage to the patch system – e.g. delaminations or disbonding, provided the region continues to be accessible

and the required frequency of inspections is feasible. The proven techniques are ultrasonics for the patch system and, for repairs involving a cracked metallic parent structure, eddy current. Thermography has also been found to be an effective and reliable approach to detect defects in the patch system.

However, these NDI techniques cannot detect weak bonds or bonds that can become weak in service. A major concern is the detection of non-existent bonds where an intimate contact is formed between the patch adhesive and parent structure, but no actual bond is formed – contact may be by coupling through a liquid infiltrated by capillary action. This is the so called problem of 'kissing bonds'. Even this major defect cannot be detected by conventional NDI.

The degradation of bond strength with time due to environmental effects is mainly a concern with metallic structure since initially strong bonds to polymer–matrix composites do not generally deteriorate in moist conditions; however, degradation may occur from other service fluids.[49] The major cause of bond degradation with metals is the hydration of the surface metal oxide caused by the presence of moisture. This occurs only when the pre-bonding surface treatment to the parent metallic structure is either inappropriate or inadequately applied.[18]

### 2.9.1 The proof testing option

Because of the concern with the severe limitations of conventional NDI and the consequential need to provide clear assurance of the initial and subsequent through-life strength and structural integrity of repairs, studies were undertaken to develop a stress or proof test.[50] The implementation of the test is as follows: thin coupons of the patch material, called the bonded repair coupon (BRC), are bonded to the surface of the parent structure simultaneously with, and therefore under very similar conditions to, the repair patch. Using a removable (adhesively bonded) torque adaptor, the BRCs are proof tested periodically in shear using a manual torque wrench or similar automated device. Failure of the coupon below a pre-determined proof load provides an indication that the adhesive bond to the patch or (possibly) the patch itself has inadequate initial strength or has degraded in service and should be replaced. Clearly the BRCs are not the repair patch, which will itself be subject to internal variations of bonding conditions; however, they must provide a highly reliable representation.

Figure 2.15 provides a schematic of the test. The aim is to obtain a proof torque load below which with some chosen level of confidence, in this study 90 %, failure of sound BRCs would not occur. Figure 2.16 shows some experimental data for boron/epoxy BRCs bonded using adhesive FM73 to a 2024-T3 aluminium panel. Bond degradation was simulated in these tests

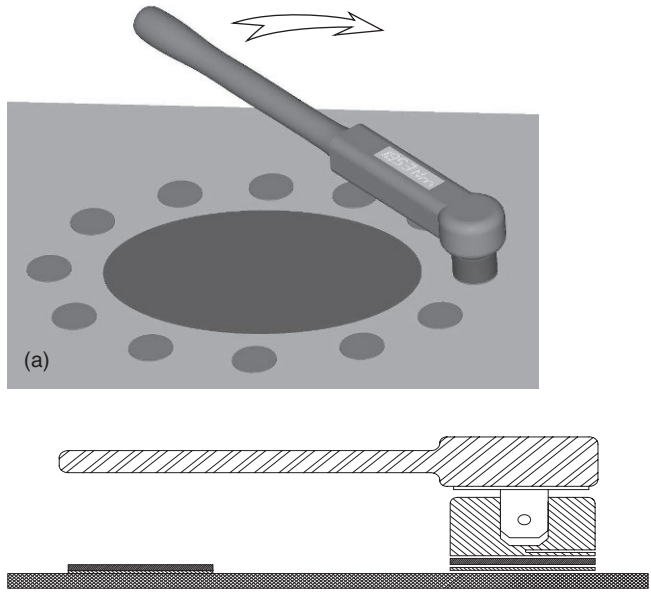


*2.15* (a) A repair patch and satellite BRCs, with one BRC under torsion test and (b) details of the BRC with adaptor required to apply the torsion loading.

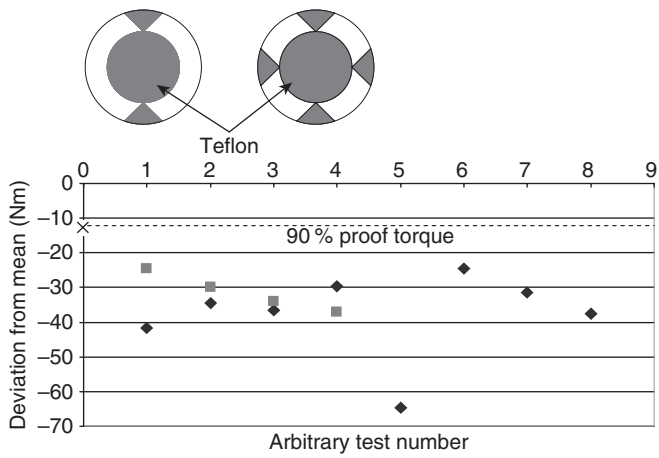


*2.16* Plot of deviation from the mean strength for boron/epoxy BRCs with two or four disbonds. Square and diamond points are, respectively, for two and four disbonds as shown schematically above.

by artificial disbonds, either two or four, as shown inset in Fig. 2.16. This demonstrates that the proof test can easily detect loss in bond area. Similarly, the test can detect poor bond strength, porosity and inadequate (under or over) cure.

### 2.9.2 The structural health monitoring (SHM) option

Where the proof test is considered inadequate for particularly critical repairs, some form of structural health monitoring (SHM) will be required.[51] It is expected that this requirement will be fairly rare and only for very high value critical repairs; for example, large monolithic composite or metallic structure where replacement is very costly or not an option, or hidden regions where the proof test cannot be applied without excessive disassembly of the component or structure.

To be viable, the SHM system must itself have a high reliability and probability of detection (POD), consistent with airworthiness standards, otherwise concern with the reliability of the adhesive bond simply extends also to the reliability of the SHM system. It must be rugged and able to survive in the aircraft environment, have minimum impact on the aircraft system and, as far as possible, be stand-alone and autonomous.

Ideally, the sensors should be embedded in the patch. Surface-mounted sensors will be exposed on the outside of the aircraft and will need to survive sunlight, moisture (and other aircraft fluids), erosion and severe mechanical contact. Polymer-matrix composites lend themselves very well to the embedded approach since sensors (and other elements of the SHM system) can be incorporated during manufacture of the patch.

There a several options for SHM of repairs to assess bond integrity, some of which are listed in Fig. 2.17. In the opinion of the author, the most reliable and direct approach is the measurement of strain transfer into the tapered ends of the external patch, any reduction being an indication of disbonding of the patch from the parent structure. The basic in-service measurement is

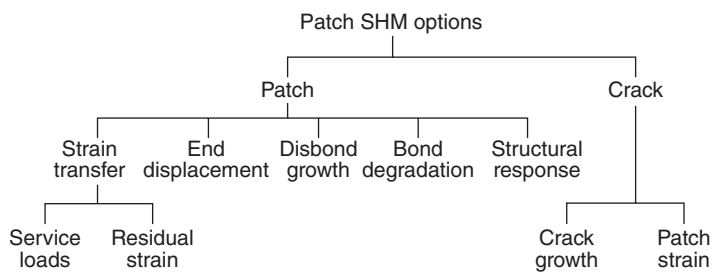


*2.17* An outline of some structural health monitoring (SHM) options.

generally simply the synchronous ratio between gauges on the patch and those in a similar stress field on the parent structure; this approach thus does not require knowledge of the service loads. An example of the use of this approach is provided in Section 2.10.2.

Figure 2.17 also includes the option of using SHM to measure crack growth in the parent structure. The use of this SHM approach is reported in reference 11; piezoelectric actuators and sensors were bonded to the surface of either boron/epoxy or aluminium alloy patches. The actuators produce guided ultrasonic waves that are detected by the sensors – forming an *in situ* ultrasonic NDI system. Using this SHM system, they were successfully able to measure crack length.

### 2.9.3 Compliance with Federal Aviation Administration (FAA) advisory circular based on proof testing and/or SHM

The FAA Advisory on Composite Aircraft Structure[52] includes guidance for bonded joints in primary composite structure and therefore critical repairs where failure of the joint (or repair) would result in failure of the structure. It should equally apply to bonded repair of metallic structure. This, paraphrased, implies that for any joint the failure of which would result in catastrophic loss of the aeroplane, the limit load capacity must be substantiated by one of the following methods:

(i) The maximum disbonds of each bonded joint consistent with the capability to withstand the loads in paragraph (a)(3)[52] [that is, limit loads] must be determined by analysis, tests or both. Disbonds of each bonded joint greater than this must be prevented by design features; or
(ii) Proof testing must be conducted on each production article that will apply the critical limit design load to each critical bonded joint; or
(iii) Repeatable and reliable non-destructive inspection techniques must be established that ensure the strength of each joint.

Method (i) alone would rule out bonded repairs if bond failure due to poor durability could result in loss of the reinforcement provided by the patch, reducing strength below the design limit – in other guidelines, the requirement may be set much higher, up to ultimate 1.5 times limit. This requirement is, however, not aimed at environmental or fatigue durability issues, but rather the occasional rogue flaw.

Method (ii) would in most cases not be feasible to conduct for repairs and, in any case, does not address long-term bond durability. Guidance in the advisory circular implies that this should be addressed in parallel by demonstrating the long-term environmental durability of the qualified

bonding processes and materials using appropriate tests. It is contended that Method (iii) which cannot be met by current NDI capability could be met using the proof test possibly, in more extreme circumstances, combined with SHM.

## 2.10 Case studies

Just two challenging applications are described here one of the US Air Force F16 and the other on an Australian F-111.

### 2.10.1 F-16 lower wing-skin 'vent hole' repair

Fatigue cracks, running forward and aft, initiated at fasteners around the vent holes in lower left wing skins in older F-16 aircraft[19] (Fig. 2.18). Some cracks extended to the second fastener row. Cracks extending beyond the vent tube flange would allow a direct path to the wing fuel tank and result

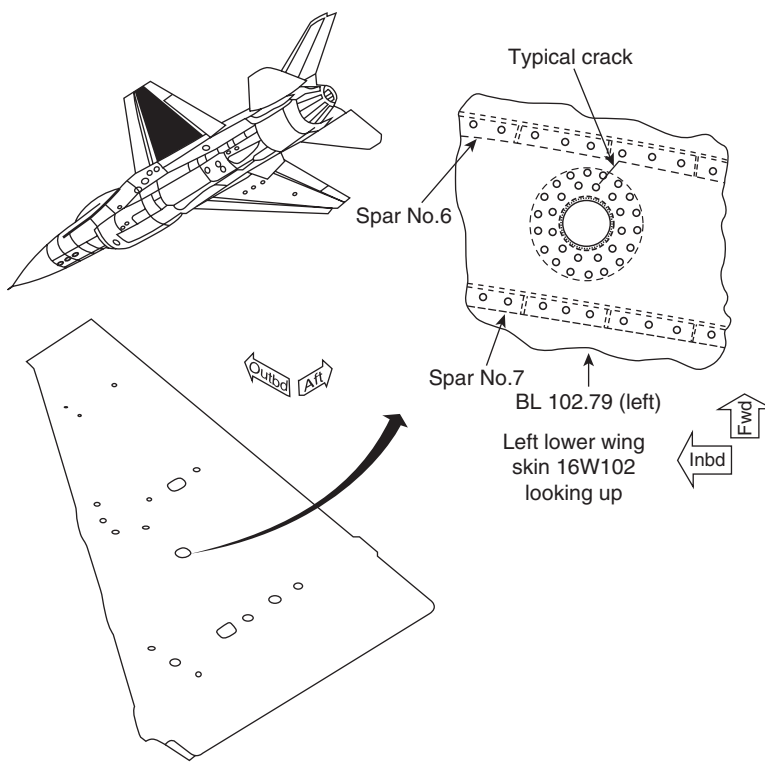


*2.18* Typical crack location in F-16.

in a fuel leak. This was considered the end of the service life for the lower wing skin.

A mechanically fastened aluminium patch repair was designed for the application. Analysis showed that this repair would not stop fatigue crack growth but would extend service life from about 3300 hours to about 5700 hours, but short of the 8000-hour goal. Installation of the mechanically fastened repair would have been time-consuming since the upper wing skin must be removed to permit access to the required fasteners in the lower wing skin. The need to drill new fastener holes in the skin was also a very significant disadvantage of this approach. A bonded boron/epoxy composite patch repair bonded with an epoxy–nitrile film adhesive was considered the best option since it could be performed without drilling additional holes or removing the upper wing skin.

FE analyses were conducted for both the wing and the patch. The pre-cured patch consisted of 14 unidirectional plies of boron/epoxy, aligned on the structure normal to the fatigue cracks, and ±45° plies on the top and bottom of the patch. The important metal surface preparation step was initially GBS followed by application of a corrosion-inhibiting primer which was cured prior to the application of the adhesive. Extensive thermal surveys on an F-16 wing were used to determine the heating methods and necessary insulation. Electric-resistance heat blankets were used to cure the adhesive, while infrared heat lamps were used for silane drying and primer cure. Pressure was applied using a vacuum bag. The first F-16 vent hole bonded repair installation was completed in early 1993. Twenty aircraft from three countries were successfully repaired.

### 2.10.2 Royal Australian Air Force (RAAF) F-111 lower wing-skin repair

Several F-111 aircraft in service with the Royal Australian Air Force (RAAF) were found to suffer from fatigue cracking in the outboard section of the aluminium alloy lower wing skin (Fig. 2.19). The cracking is caused by a stress concentration from a run-out in the forward auxiliary spar to create a fuel flow passage.[53] When the first (and largest) crack was discovered, fracture mechanics calculations indicated that it was beyond critical length at DLL. A conventional mechanically fastened metallic repair was considered, but this was unattractive (i) from an aerodynamic standpoint (excessive thickness) and (ii), more importantly, new fastener holes would have been unacceptable in this highly stressed primary structure, and (iii) the crack would have been uninspectable beneath such a repair. A bonded composite repair was considered the only alternative to scrapping the wing.

Extensive and detailed 2-D and 3-D FE analysis was conducted so that the stress distribution around the defect could be quantified. This revealed

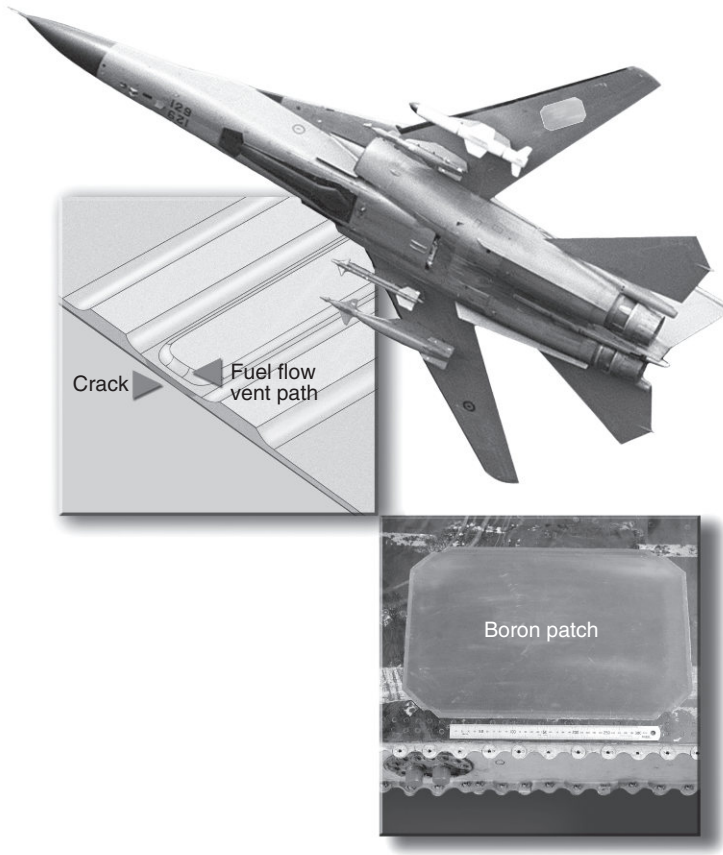


*2.19* Region of fatigue cracking in F-111 lower wing skin and, inset, a photograph of the boron/epoxy repair.

that the wing skin at this location was subject to secondary bending and this was the explanation for the observation that the crack had initiated on the inside surface of the wing skin. The model was validated with strain measurements from a full-scale wing test. In addition, three levels of specimen testing were undertaken:

- Small, inexpensive coupon-sized specimens were used to investigate the effects of impact damage, temperature and moisture and load spectrum truncation effects.
- Panel specimens with a full-scale representation of the local wing geometry were used as structural details in a fatigue and environmental study.

- Large box specimens were used to represent the wing as a quasi full-scale test article in testing static and fatigue strength and an examination of thermal residual stresses.

Boron/epoxy was chosen as the repair patch for the reasons provided in Section 2.5. The epoxy–nitrile film adhesive FM 73 was selected and cured at the comparatively low temperature of 80 °C to minimise the thermally-induced residual stresses. The surface treatment used was the GBS process. Advantage was taken of nearby hard-points on the wing to make use of positive pressure during the cure. An inflated bladder was used to apply pressure to the repair and the pressurisation loads were reacted out via a rigid plate to the hard-points. Initial static tests on representative panels depicted in Fig. 2.20 showed that, as predicted, the unpatched cracked panel failed at a stress well below DLL whilst all of the repaired panels exceeded the DUL. Similar encouraging results were obtained from spectrum fatigue tests on structural details panels and components.

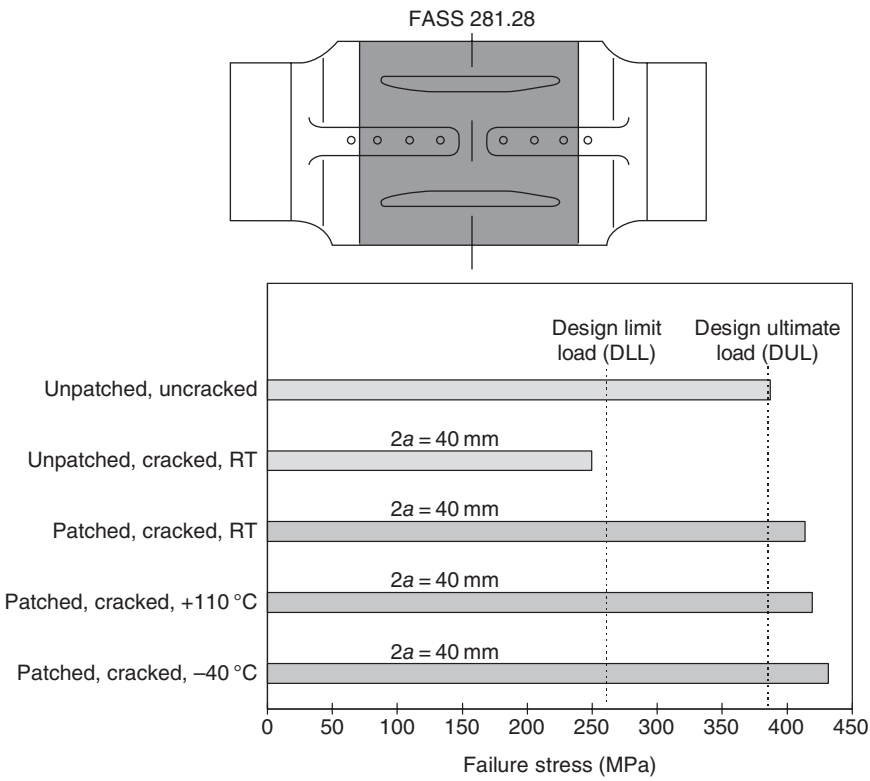


*2.20* Representative panel specimen and results of static strength tests.

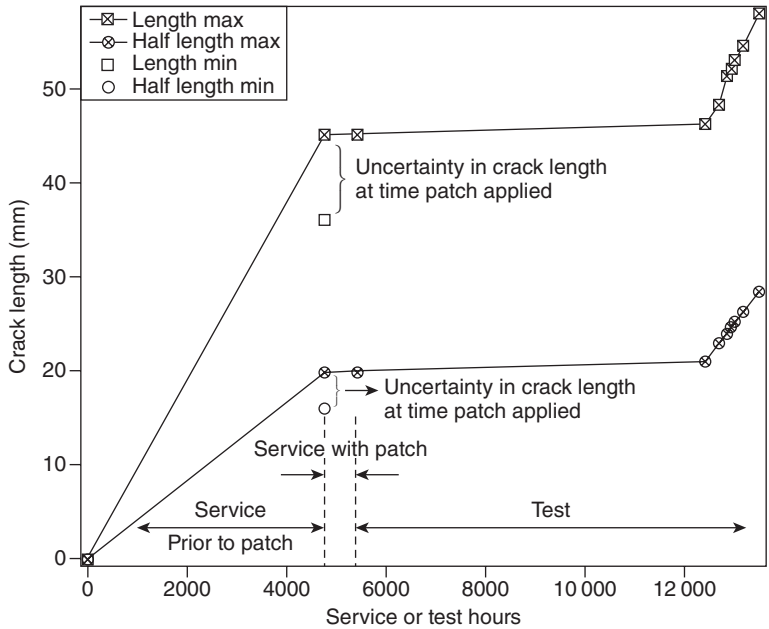


*2.21* Plot of crack size over the life of the wing measured from fractographic analysis of the patched crack region.

The history of the crack before and after repair is depicted in Fig. 2.21 (for more details see reference 54). This wing was later used as a fatigue test article for damage tolerance analysis and to assess the effectiveness and durability of the repair. As shown in Fig. 2.21, the patched crack did not grow during in-flight service of the wing or when the wing was used as a fatigue test article for over 7000 simulated flying hours. Then the aft auxiliary spar failed and the increased load caused the crack to propagate. Final failure of the wing occurred from a region approximately in line with but unrelated to the patched crack.

During the test, the patch was monitored for disbonds using the strain-transfer SHM approach, mentioned in Section 2.9.2, using standard resistance strain gauges. Figure 2.22 shows the location of the strip and single gauges. Plots of strain (at load-line 27 in the spectrum) versus blocks of spectrum loading are provided in Figs 2.23a and 2.23b. Because of the high reproducibility of the spectrum loading in the fatigue test, the strain at a specific load rather than strain ratio (patch/far-field) was measured; however, it would be necessary to use this strain ratio in an in-flight application.

The strain measurements shown in Figs 2.23a and 2.23b were taken respectively from a sound and small unsound region of the patch, showing

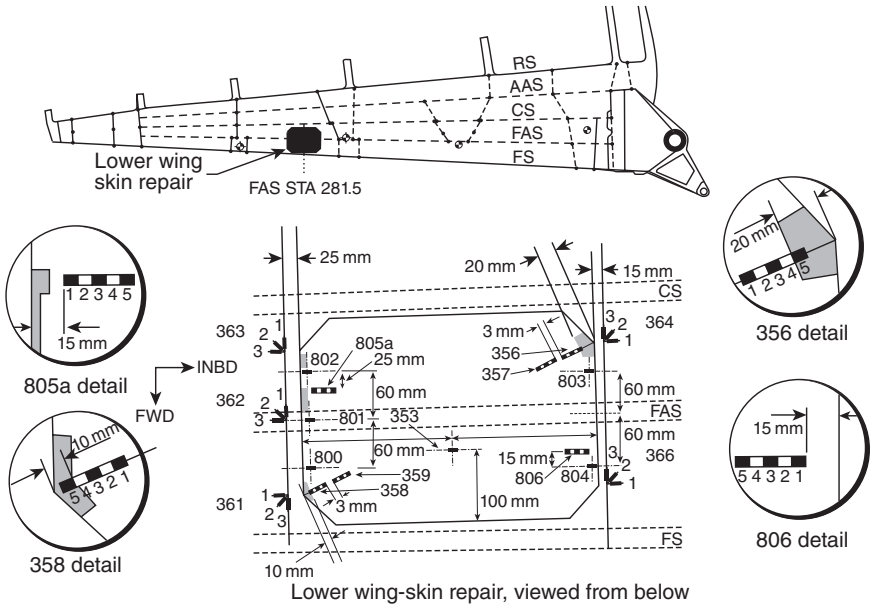


*2.22* Location of strain gauges used on the patch and parent structure from block 12; also showing, schematically, the position and nominal size of some of the disbonds detected by NDI.

that the strain-transfer approach was easily able to detect growth of disbond demonstrating that, with some further development, this SHM approach has good potential to be used to provide early warning against degradation or impending failure of a patch system. Reference 51 provides more details of this test program.

It must be emphasised that, because of its criticality, the F-111 wing-skin repair is far from a typical example, but rather represents the limit of what the bonded repair technology can achieve. In this case, an extensive program was required to certify the repair – however, acceptance of a generic methodology similar to that proposed in this chapter, including proof testing and/or SHM, would make certification of such a challenging repair much more cost-effective by avoiding the need for an extensive test program.

## 2.11 Conclusion: limitations and lessons learnt

An excellent overview of lessons learned is provided by Schweinberg *et al*. following extensive programs on repair of USAF C141 and C 130 aircraft;[55] the reader is strongly recommended to read this in conjunction with the following comments.

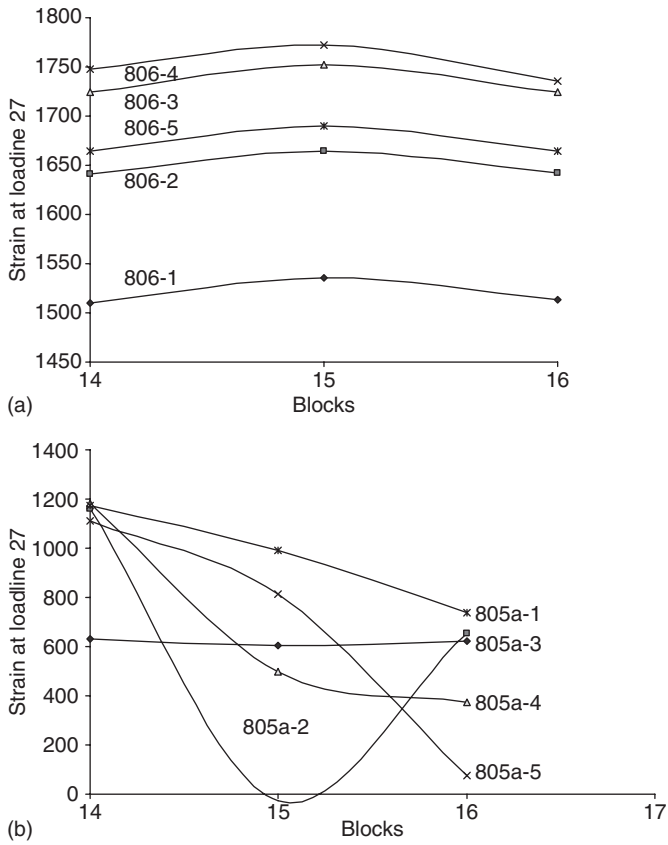


*2.23* Strain at loadline 27 versus blocks of spectrum fatigue loading for (a) a soundly bonded region and (b) a region where minor disbonds were growing.

## 2.11.1 Component thickness and bond area limitations

Bonded composite repairs are most suited to repair of cracks in relatively thin-skin components, <4 mm, with sufficient unobstructed surface area to obtain effective load transfer from the parent structure into the patch. They have more limited effectiveness for through cracks in thick-skin components, >4 mm; however, they are well suited to the repair of part-through cracks, deep scratches or corrosion pitting.

Bonded composite doublers are also far more suited than mechanical doublers for strain reduction in thin- or thick-skin components – providing the load-transfer requirements can be met. In some circumstances, e.g. the F-111, wing-skin bonded repairs were the only viable option,[53] since the formation of extra fastening holes in this highly stressed region would have been unacceptable.

### 2.11.2 Bond durability

Failure of the patch system by fatigue has proved to be an issue only in one Australian repair – the F-111 wing pivot fitting – most likely resulting from inadequate ply step length and thickness at the ends of the patch.[56] However, durability under service loading must be considered as a very important design consideration for demanding applications.

Disbond growth in the patch system over the damaged region in the parent structure caused by service loading can in principle be managed by damage tolerance approaches; however, for the tapered ends, a safe-life approach is more appropriate.[41]

The greatest concern in bonded repairs is disbonding caused by environmental degradation resulting from incorrect or inadequate surface treatment. In this case, the application of a damage tolerance approach is infeasible, as the rate of disbond growth is essentially unpredictable. The greatest risk is inadequate surface treatment or an adequate surface treatment applied by poorly trained (or negligent technicians). It is vital that technicians should be subjected to frequent requalification regarding bonding as well as other application processes.[57] Ideally, they should be qualified along similar lines to welding technicians.

### 2.11.3 Application technology

The main problem in bonding of the patch is how to obtain uniform temperature in components with varying and sometimes very large thermal masses. This requires the use of multi-zone heaters and controllers.[25,55] When applying patches inside or even on the outside of a wing fuel tank, great care must be taken to render the fuel tank inert. This can be done by gas or liquid purging.[55]

The use of vacuum bagging approaches, whilst versatile and attractive for many reasons, can result in contaminant leakage into the surface of the component and fluid and air into the uncured patch system through joints fastener holes, cracks and other flaws resulting in poor bond strength and severe porosity in the adhesive. Mechanical pressure using spring clamps, gas bags or (at least for horizontal surfaces) dead weights are safer in these respects but are very much less versatile and often difficult to apply.

### 2.11.4 Validation of the patch system

The standard NDI procedures, including ultrasonics and thermography, can detect excessive voids and disbonds in the adhesive after patch application and patch quality, especially in the case of preformed patches. However, most importantly, they are unable to assess bond strength or detect weak or even non-existent (kissing) bonds. Various pre-bond approaches have

been made to assess removal of contamination and the presence of the required surface chemistry after surface treatment, but will probably be unable to provide sufficient confidence in bond strength. These limitations cause considerable difficulties in certifying critical repairs – especially when flight safety depends on the continuing effectiveness of the patch system. In this situation, the main alternatives, are the use of proof testing[50] or structural health monitoring[51] (or both) for through-life monitoring of the patch system. These approaches are of course ancillary and not a replacement for adequate quality control.

### 2.11.5 Design issues

Experimental studies have generally validated analytical or FE design approaches for predicting fatigue crack propagation of patched cracks based on estimation of the stress intensity. However, whilst capable in terms of stress analysis or fracture mechanics, design approaches for predicting patch system durability under service loads are, in most cases, not validated since (at least to the author's knowledge) they are based on unrealistic materials allowables for failure modes in the patch system – for example, the shear stress or shear strain allowable for the adhesive. There is, thus, a need to develop patch system allowables appropriate for the temperature, humidity and cyclic stresses experienced by the adhesive and composite patch. These data are required to develop a generic approach to the design of repairs since, in most cases, especially for one-off repairs, a supporting experimental program will not be feasible.

## 2.12 Acknowledgement

The author would like to thank Dr Andrew Gunnion of ACS-A for helpful discussions and comments on the manuscript.

## 2.13 Sources of further information and advice

- *Advances in the Bonded Composite Repair of Aircraft Structure*, Baker A.A., Rose L.F.J. and Jones R. (eds) Elsevier 2002.
- *Composite Repair Theory and Design*, Duong C.N. and Wang C.H., Elsevier 2007.
- *Bonded Repair of Aircraft Structures*, Baker A.A. and Jones R. (eds), Martinis Nijoff 1988.
- *Joining and Repair of Composite Structures*, Kedward, K.T. and Kim H., STP 1455, ASTM 2004.
- *Recent Advances in Structural Joints and Repairs for Composite Materials*, Tong L. and Soutis C., Kluwer Academic Publishers 2003.

- *Care and Repair of Advanced Composites*, 2nd edn, Armstrong K., B., Cole W. and Bevan G., SAE International 2005.
- *Composites A*, Special Issue: Repair, A.A. Baker (ed.), 40 (2009).
- *International Journal of Adhesion and Adhesives*, Special Issue: Bonded Repairs, K. D. Armstrong (ed.), 19 (1999).
- *Eleventh International Conference on Composite Materials*, Australian Composites Structure Society, Woodhead Publishing Ltd 1997.
- *Composite Repair of Military Aircraft Structures*, AGARD-CP-550, AGARD 1995.
- *Aging of U.S. Air Force Aircraft*, Final Report Publication NMAB-488-2, National Academy Press, Washington D.C. 1997.
- *International Conference on Aircraft Damage Assessment and Repair: Melbourne 1991*, Jones R. and Miller N. J. (eds), National Conference Publication 91/17, The Institution of Engineers, Barton, ACT, pp. 92–99.
- *Proceedings of an International Workshop on Defence Applications for Advanced Repair Technology for Metal and Composite Structure*, Naval Research Labs, Washington D.C. 1981.
- Ratwani M.M., Repair options for airframes, *Aging Aircraft Fleets: Structural and Other Subsystem Aspects*, RTO-EN-015, paper 4-1, 2001, NATO Research and Technology Organization, Neuilly-sur-Seine.


## 2.14 References


1. Gorenson U.G., 'Damage Tolerance Facts and Fiction', *International Conference on Damage Tolerance of Aircraft Structures*, Technical University, Delft, 25th September 2007.
2. Niu M.C., *Airframe Structural Design*, Technical Book Company 1988.
3. *Aging of U.S. Air Force Aircraft*, Final Report Publication NMAB-488-2, National Academy Press, Washington, DC 1997.
4. Cole G., Clark G. and Sharp K., *The Implications of Corrosion With Respect to Aircraft Structural Integrity*, DSTO Research Report, DSTO-RR-0102, DSTO 1997.
5. Broek D., *The Practical Use of Fracture Mechanics*, Kluwer 1997.
6. Baker A.A. 'Introduction', Chapter 1 in Baker A.A., Rose L.F.J and Jones R. (eds) *Advances in the Bonded Composite Repair of Metallic Aircraft Structure*, Elsevier 2002.
7. Baker A.A. 'A proposed approach for certification of bonded composite repairs to flight-critical airframe structure', *Applied Composite Materials*, 2011, 18, pp. 337–369.
8. Baker A.A., 'Crack patching: experimental studies, practical applications', Chapter 6 in Baker A.A. and Jones R. (eds), *Bonded Repair of Aircraft Structures*, Martinus Nijhoff 1988.
9. Swift T., 'Repairs to damage tolerant aircraft,' *Proceedings International Symposium on Structural Integrity of Aging Airplanes*, FAA-AIR-01, Atlanta, GA, 20–22 Mach 1990.

10. Hart-Smith L.J., *Stress Analysis: A Continuum Mechanics Approach to Developments in Adhesives*, 2, Kinloch A.J. (ed.) Applied Science Publishers 1981.
11. Chalda R., Bakuckas J.G. Jr, Won I.Y., Westerman B., Keller K., McIver K., Hsu C., Awerbuch J. and Tan T., 'Characterization of adhesive bonded repairs to fuselage structure', *Proceedings of the Joint DoD/NASA/FAA Conference on Airworthiness Assurance and Sustainment*, Austin, TX, 10–13 May 2010.
12. Baker A.A, Hawks G.A. and Lumley E.J., *Proceedings of the 10th International Committee on Aeronautical Fatigue*, paper 4.3 1979.
13. Fredell R.S., van Barnveld W. and Vlot A., 'Analysis of composite crack patching of fuselage structures: high patch modulus isn't the whole story', *Proceedings of the 39th International SAMPE Symposium and Exhibition*, Anaheim, CA, 11–14 April, pp. 610–623.
14. Baker A.A., 'Bonded composite repair of metallic aircraft components', *Composite Repair of Military Aircraft Structures*, AGARD-CP-550, Paper 1, AGARD 1994.
15. Baker A.A. and Jones R. (eds), *Bonded Repair of Aircraft Structures*, Martinus Nijhoff 1988.
16. Oakafor A.C. and Bhogpurapu H., 'Design and analysis of adhesively bonded thick composite patch repair of corrosion grind out in 2024T3 clad aging aircraft structures', *Composite Structures*, 2006, 76 (1–2), pp. 138–150.
17. Baker A.A., 'Fatigue life recovery in corroded aluminium alloys using bonded composite reinforcements' *Applied Composite Materials*, 2006, 13, pp. 127–146.
18. Arnot D., Rider A. and Mazza J., 'Surface treatment and repair bonding', Chapter 3 in Baker A.A., Rose L.F.J. and Jones R. (eds), *Advances in the Bonded Composite Repair of Metallic Aircraft Structure*, Elsevier 2002.
19. A.A. Baker, R.J. Chester and J. Mazza, 'Bonded repair technology for aging aircraft', *Specialists Meeting on Life Management Techniques for Aging Air Vehicles 2001*, RTO-MP-079-11, NATO Science and Technology Organization, 2003.
20. ASTM D 3762, 'Standard Test Method for Adhesive-Bonded Surface Durability of Aluminum (Wedge Test)', *Annual Book of ASTM Standards, Volume 15.06: Adhesives*, pp. 254–257, ASTM 1997.
21. Kuhbander R.J. and Mazza J.J., 'Understanding the Australian silane surface preparation', *Proceedings of the 38th International SAMPE Symposium and Exhibition*, Anaheim, CA, 10–13 May 1993, pp. 1225–1234.
22. McCray D.B. and Mazza J.J., 'Optimization of sol–gel surface preparations for repair bonding of aluminum alloys', *Proceedings of the 45th International SAMPE Symposium and Exhibition*, Long Beach, CA, 22–25 May 2000, pp. 53–54.
23. Hart-Smith L.J., Ochsner R.W. and Radecky R.L., *Engineered Materials Handbook, Vol. 3 Adhesives and Sealants*, H.F. Brinson (technical chairman), ASM International, 1990, pp. 840–844.
24. Baker A.A., Chester R.J., Davis M.J., Retchford J.A. and Roberts J.D., 'The development of a boron/epoxy doubler system for the F111 wing pivot fitting – materials engineering aspects', *Composites*, 1993, 24, pp. 511–521.
25. Davis, M., 'Practical application technology for adhesive bonded repairs' Chapter 24 in Baker A.A., Rose L.F.J. and Jones R. (eds), *Advances in the Bonded Composite Repair of Metallic Aircraft Structure*, Elsevier 2002.

26. Campbell F.C., *Manufacturing Processes for Advanced Composites*, Elsevier 2004.
27. Diberardino M.F., Cochran R.C., Donnellan T.M., and Trabocco R.E., 'Materials for composite damage repair', *Proceedings of the 5th Australian Aeronautical Conference*, The Institution of Engineers Australia 1993.
28. Roach D.P. and Scala C.M., 'Nondestructive evaluation and quality control in bonded composite repair of aircraft structures', Chapter 23 in Baker A.A., Rose L.F.J and Jones R. (eds), *Advances in the Bonded Composite Repair of Metallic Aircraft Structure*, Elsevier 2002.
29. Baker A.A., 'Boron/epoxy efficiency studies', Chapter 13 in Baker A.A., Rose L.F.J and Jones R. (eds), *Advances in the Bonded Composite Repair of Metallic Aircraft Structure*, Elsevier 2002.
30. Broek D., *The Practical Use of Fracture Mechanics*, Kluwer Academic Publishers 1988.
31. Jones R. 'Numerical analysis and design', Chapter 9 in Baker A.A., Rose L.F.J and Jones R. (eds), *Advances in the Bonded Composite Repair of Metallic Aircraft Structure*, Elsevier 2002.
32. Okafor A.C., Singh N., Enemough V.E. and Rao S.V. 'Design analysis and performance of adhesively bonded composite patch repair of aluminium aircraft panels', *Composite Structures*, 2005, 71, pp. 258–270.
33. L.R.F. Rose, 'Theoretical analysis of crack patching', Chapter 6 in Baker A.A. and Jones R. (eds), *Bonded Repair of Aircraft Structures*, Martinus Nijhoff, 1988.
34. Rose L.R.F. and Wang C.H., 'Analytical methods for designing composite repairs', Chapter 7 in Baker A.A., Rose L.F.J and Jones R. (eds), *Advances in the Bonded Composite Repair of Metallic Aircraft Structure*, Elsevier 2002.
35. Hart-Smith L.J., 'Recent expansions in the capabilities of Rose's closed-form analysis for bonded crack patching', Chapter 8 in Baker A.A., Rose L.F.J, Jones R., (eds), *Advances in the Bonded Composite Repair of Metallic Aircraft Structure*, Elsevier 2002.
36. CRMS Guidelines for Composite Repair to Metallic Structure, AFRL-WP-TR-1998–4113, 1998.
37. Wang C.H. and Rose L.R.F., 'Bonded repair of cracks under mixed mode loading', *International Journal of Solids*, 1998, 35, pp. 2748–2773.
38. Baker A.A. 'Repair efficiency in fatigue-cracked panels reinforced with boron/epoxy patches', *Fatigue and Fracture of Engineering Materials and Structures*, 1993, 16, pp. 753–765.
39. Chalkley, P. D. and Baker, A. A., 'Development of a generic repair joint for certification of bonded composite repairs', *International Journal of Adhesion and Adhesives*, 1999, 19, pp. 121–132.
40. Rose L.R.F., 'A cracked plate repaired by bonded reinforcements', *International Journal of Fracture*, 1982, 18, pp. 135–44.
41. Baker A.A., 'Certification issues for bonded repairs' Chapter 22 in Baker A.A., Rose L.F.J. and Jones R. (eds), *Advances in the Bonded Composite Repair of Metallic Aircraft Structure*, Elsevier 2002.
42. Baker A.A., 'A proposed approach for certification of bonded composite repairs to flight-critical airframe structure', *Applied Composite Materials*, 2011, 18, pp. 337–369.

43. Kieger R.B., 'Stress analysis concepts for adhesive bonding of aircraft primary structure,' in Johnson W.S. (ed.), *Adhesively Bonded Joints: Testing Analysis, and Design*, ASTM STP 981, ASTM 1988.
44. Davis M.J., Janardhana M. and MacKenzie A., 'A rigorous approach to the certification of adhesive bonded repairs', *FAA Workshop on Certification of Adhesive Bonded Structures and Repairs*, Seattle, WA, 16–18 June 2004.
45. Chalkley P.D. Wang C.H. and Baker A.A. 'Fatigue testing of generic bonded joints', Chapter 5 in Baker A.A., Rose L.F.J. and Jones R. (eds), '*Advances in the Bonded Composite Repair of Metallic Aircraft Structure*', Elsevier 2002.
46. Wang J., Rider A.N., Heller M. and Kaye R. 'Theoretical and experimental research into optimal edge taper for bonded repair patches subject to fatigue loading', *International Journal of Adhesion and Adhesives*, 2005, 25, pp. 410–426.
47. Alderliesten R.C., 'Damage tolerance of bonded aircraft structures', *International Journal of Fatigue*, 2008, 31, pp. 1024–1030.
48. Vlot A., Vernhoeven S., Nijssen P.J.M., *Bonded Repairs for Aircraft Structures, Series 07: Aerospace Materials 11*, Delft University Press 1998.
49. Rider A. and Yeo E., *The Chemical Resistance of Epoxy Adhesive Bonds*, DSTO Report DSTO-TR-1650, DSTO 2005.
50. Baker A., Bitton D. and Wang J., 'Development of a proof test for through-life of bond integrity in adhesively bonded repairs to aircraft structure', *International Journal of Adhesion and Adhesives*, 2012, 36, pp. 65–76.
51. Baker A.A, Rajic N. and Davis C., 'Towards a practical health monitoring system for patched cracks in aircraft structure', *Composites Part A*, 2009, 40A, pp. 1340–1352.
52. FAA Advisory Circular on Composite Aircraft Structure, AC 20–107B, US Department of Transportation Federal Aviation Authority, 9/8/09.
53. Walker K.F. and Rose L.R.F., 'Case history: F-111 lower wing skin repair substantiation', Chapter 27 in Baker A.A., Rose L.F.J and Jones R. (eds), *Advances in the Bonded Composite Repair of Metallic Aircraft Structure*, Elsevier 2002.
54. Baker A.A, Rajic N. and Davis C., 'Towards a practical health monitoring system for patched cracks in aircraft structure', *Composites Part A*, 2009, 40A, pp. 1340–1352.
55. Schweinberg W. H. and Fiebig J.W., 'Case histories: advanced composite repairs of USAF C-141 and C-130 Aircraft', Chapter 41 in Baker A.A., Rose L.F.J. and Jones R. (eds), *Advances in the Bonded Composite Repair of Metallic Aircraft Structure*, Elsevier 2002.
56. Chester R., 'Case history: F-111 wing pivot fitting reinforcement', Chapter 29 in Baker A.A., Rose L.F.J. and Jones R. (eds), *Advances in the Bonded Composite Repair of Metallic Aircraft Structure*, Elsevier 2002.
57. Smith M.A. 'Standardized training and certification for bonded repair specialists', Chapter 26 in Baker A.A., Rose L.F.J. and Jones R. (eds), *Advances in the Bonded Composite Repair of Metallic Aircraft Structure*, Elsevier 2002.

# 3

# Finite element modelling of adhesive bonds joining fibre-reinforced polymer (FRP) composites to steel

R. HAGHANI, Chalmers University of Technology, Sweden

**DOI**: 10.1533/9780857096654.1.60

**Abstract**: This chapter explains some behavioural aspects of adhesive joints used to bond fibre-reinforced polymer (FRP) composites to steel substrates using the finite element method. The chapter aims to give the reader an overview of conventional stress/strain analysis techniques including analytical and numerical analyses as well as the applications, advantages and drawbacks of each technique.

**Key words**: adhesive joint, finite element modelling, fibre-reinforced polymer (FRP) composite.

## 3.1 Introduction

Stress analysis is one of the most important steps in any structural design practice. A suitable analysis technique should provide reasonably accurate, reliable results in terms of the magnitude and distribution of stresses or strains in the structure of interest which is subjected to a specific load and boundary condition. The information from the analysis will enable the engineer to predict the strength of the structure. This procedure also applies to adhesive joints. Stress analysis of adhesive joints is one of the most difficult engineering tasks due to the presence of bimaterial interfaces and geometrical discontinuities which might cause stress singularities and consequently uncertainty in evaluations of stresses or strains.

This chapter explains some behavioural aspects of adhesive joints used to bond FRP composites to steel substrates using the finite element (FE) method. The chapter aims to give the reader an overview of conventional stress/strain analysis techniques including analytical and numerical analyses as well as application, advantages and drawbacks of each technique. In Section 3.2 an introduction to the behaviour of adhesive joints in terms of force transfer mechanism and failure modes is presented. Section 3.3 introduces and compares different analysis methods. Section 3.4 addresses the stress singularity problem in adhesive joints and cautions regarding possible misleading results from FE method.

Section 3.5 explains the strain distribution in adhesive joints used to bond fibre-reinforced polymer (FRP), laminates to steel substrates. A

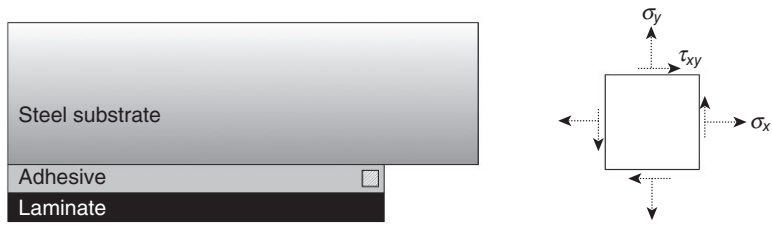


*3.1* Illustration of shear and normal stress components in adhesive layer.

comparison of the results obtained from FE analysis of an adhesive joint with those from analytical analysis and experimental tests is presented. Finally, Section 3.6 presents the contribution of the FE method in analysis of adhesive joints with complex geometries.

## 3.2 Behaviour of adhesive joints

When it comes to analysis of adhesive joints, it is important to have a picture of how these joints behave and what parameters affect their behaviour. It is also essential for designers to know the accuracy of the results obtained from analytical or numerical analyses, what the consequent effects of certain assumptions on which the modelling is based are, and how to interpret the results. In this section, some basic behavioural aspects of adhesive joints used to bond FRP composites to steel substrates are explained and, in the coming sections, the effects of different parameters on stress/strain distribution which influences the capacity and failure of such adhesive joints are elaborated.

### 3.2.1 Force transfer mechanism in adhesive joints

Irrespective of the load type applied on a joint, the stresses in an adhesive joint can be decomposed into two main stress components: shear stress ($\tau$) and normal stresses ($\sigma$) as illustrated in Fig. 3.1. Normal and shear stresses are caused by forces acting perpendicular and parallel to the element under consideration in the adhesive layer, respectively. Normal stresses result in tension or compression in the material, known as normal strain ($\varepsilon$) while shear stresses cause diagonal deformation in the material known as shear strain ($\gamma$). Stresses and strains are simply related to each other by the modulus of elasticity of the adhesive material.

In order to understand how these stresses are developed and interaction between them, it is helpful to consider Fig. 3.2. The load transfer in adhesive

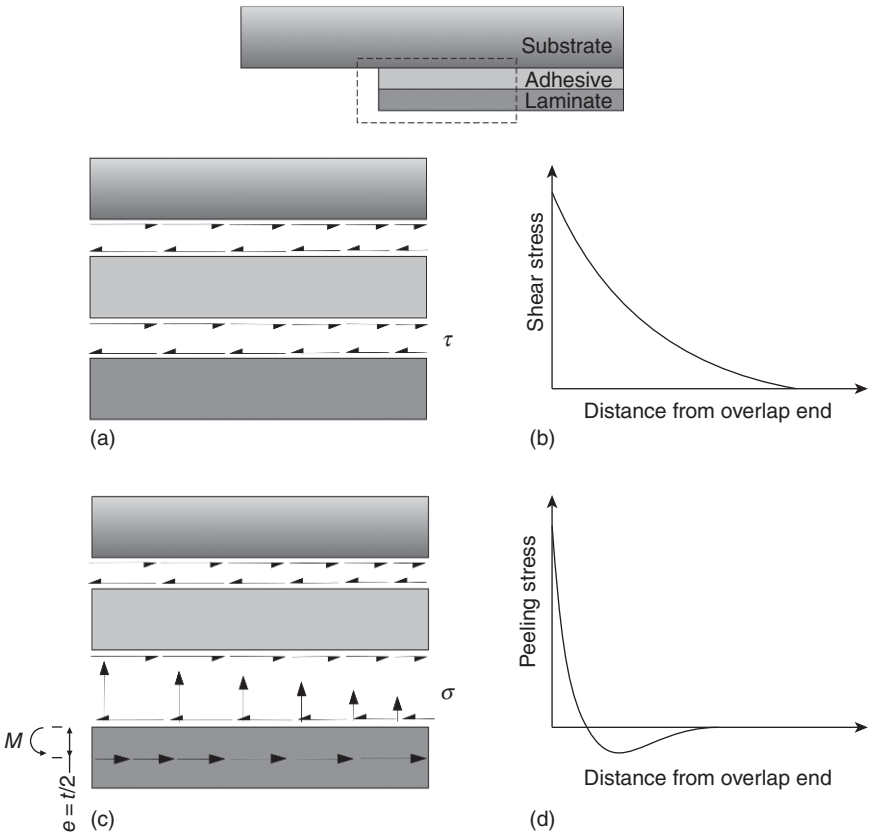


*3.2* Formation of (a) shear and (c) peeling stresses in adhesive joint and corresponding (b) shear and (d) peeling stress distributions.

joints from one adherent to another is achieved via shear action in the adhesive layer (Fig. 3.2a). As the load is transferred from the substrate to the composite laminate in the joint, shear deformation reduces in the adhesive layer. This results in stress distribution that decays with increasing distance from the end of the laminate as shown in Fig. 3.2b.

The shear action in the joint causes a secondary bending effect in the laminate as illustrated in Fig. 3.2c. The shear force acting on the laminate–adhesive interface is balanced with the axial force in the FRP laminate which acts through the laminate neutral axis position. This force couple has a lever arm which is the distance between the adhesive–laminate interface to the mid-thickness of the laminate. The bending moment in the laminate is the product of the shear force acting on this interface by the moment lever arm. The bending moment in the laminate is counteracted by

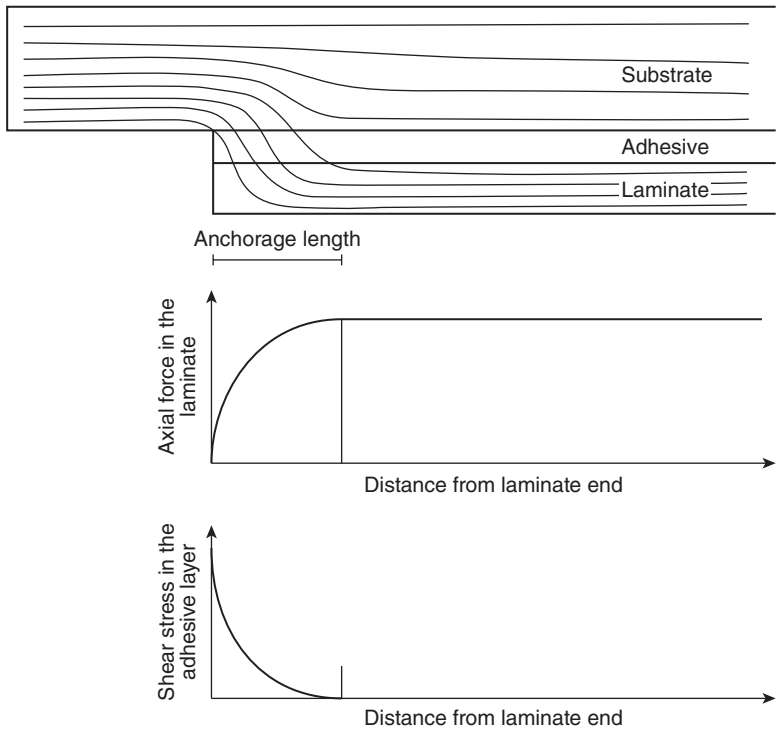


*3.3* Illustration of stress flow in joint and anchorage length.

through-thickness force in the adhesive layer, referred to as peeling force and which causes peeling stress in the adhesive layer (Fig. 3.2d). Considering the peeling stress distribution in the adhesive layer, it is seen that the direction of the stresses changes as the distance from laminate end is increased. This is due to the fact that peeling stresses are self-balancing since the total peeling force along the bond line is zero.

The anchorage length in adhesive joints is defined as the distance needed to obtain full composite action between the substrate and the FRP laminate. In other words, it is the distance at which the shear stress due to the lag effect becomes zero (Fig. 3.3). The anchorage length is a function of the ratio of the axial stiffness of the substrate to the axial stiffness of the laminate. The stiffness of the laminate $EA$ has a direct relationship with anchorage length, which means that the stiffer the laminate, the longer the anchorage length, as illustrated in an example in Fig. 3.4. Other parameters, such as the thickness of the adhesive layer or the E-modulus of the adhesive, do not significantly influence the anchorage length.

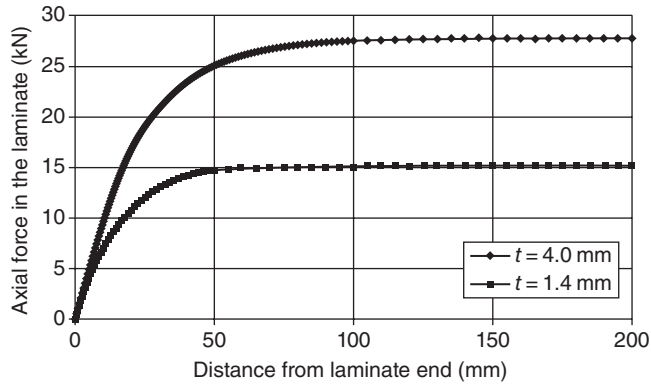


*3.4* Comparison of the anchorage length for laminates with different thicknesses (*t*).

### 3.2.2 Failure modes

It is known that one of the characteristics of adhesive joints is the stress concentration at the area close to the end of FRP laminate. The reason for stress concentration at this area is the abrupt change in the stiffness of the system and resulting shear lag effect (see Fig. 3.3). This stress concentration might govern the failure of the joint. The failure of adhesive joints in FRP-bonded steel members may take place in one, or a combination, of the following modes. Figure 3.5 depicts possible failure modes in a steel I girder bonded with a FRP laminate:

1. Cohesive failure, which is governed by the strength of the adhesive (mode B in Fig. 3.5).
2. Delamination in the composite laminate, which is characterised by the failure of the matrix in the laminate (mode C in Fig. 3.5).
3. Debonding along one of the two steel–adhesive or laminate–adhesive interfaces (mode A in Fig. 3.5) – a good bond at the steel–adhesive and laminate–adhesive interfaces is crucial to prevent this mode.

Needless to say, the rupture of the laminate can also occur if the aforementioned failure modes can be avoided.

## 3.3 Analysis of adhesive joints

There are two basic techniques for analysing adhesive joints: analytical methods and numerical methods. In the former, the state of stress/strain is predicted using analytical expressions, usually expressed as closed-form solutions. The solution is obtained by solving the differential equations

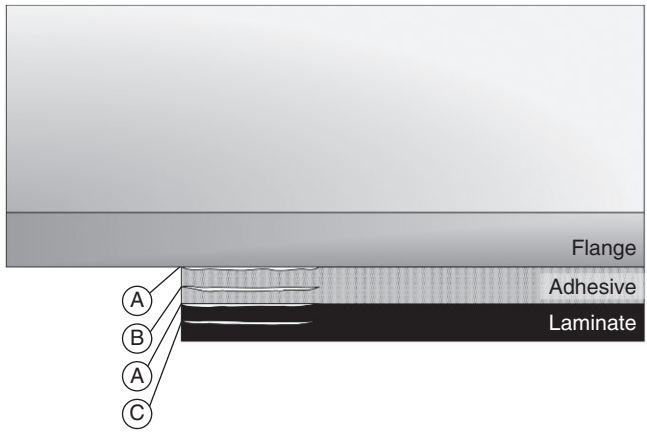


*3.5* Possible failure modes in steel members bonded with FRP laminates.

derived from force equilibrium and deformation compatibility conditions formed for the composite element. The latter method is mostly performed using a FE method. Numerical analyses are usually conducted using commercially available FE software and can provide more detailed results in terms of stress and strain distribution in different parts of adhesive joints.

The two methods usually complement one another for design purposes. Closed-form solutions can provide an estimation of maximum stress or strain which can be used in quick joint design or first guesses. They are also suitable for conducting parametric studies that serve in the selection of appropriate adhesives and fundamental geometry. Numerical analysis, on the other hand, can provide more accurate, detailed information about the stress field in joints. However, it is generally more time-consuming and requires more knowledge and modelling work. A comparison between these methods is presented in Table 3.1.

### 3.3.1 Analytical analysis of adhesive joints

The analytical analysis of adhesive joints has been studied by a number of researchers. The initial analyses were one-dimensional and solutions were presented in the form of explicit equations for different stress components. However, subsequent analysis models became more complex, through the introduction of generalised boundary conditions, non-linearity and the introduction of a second dimension (through the adhesive thickness). A brief review of analytical solutions to express the stress state in different adhesive joint configurations is presented in this section.

*Table 3.1* Comparison between analytical and numerical analyses

| Method | Advantages | Drawbacks |
|---|---|---|
| Analytical analysis | Simple<br>Fast | Developed for specific configuration<br>Considers ideal material response<br>Returns results at specific locations |
| Finite element analysis | Provides more detailed results<br>Treats complex geometries<br>Considers complex material behaviour | Time-consuming<br>Requires expertise for modelling and interpretation of results<br>Stress singularity and mesh dependency |

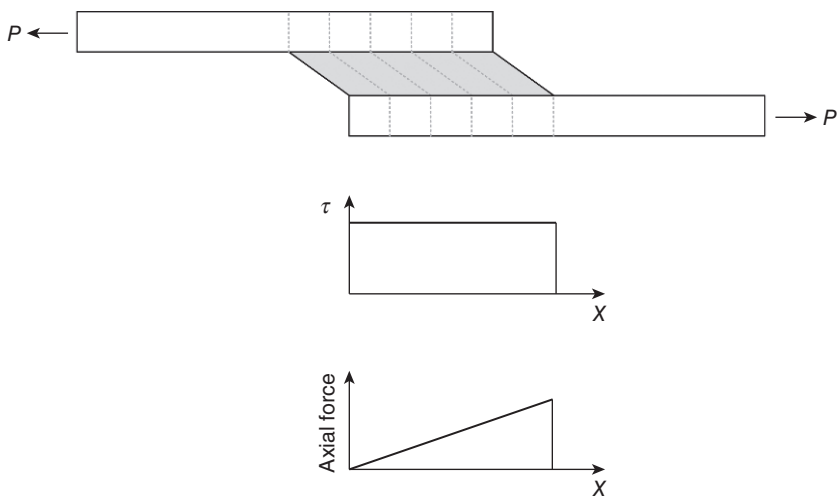


*3.6* Simple linear elastic analysis considering average shear stress.

*Analytical solutions for single- or double-lap joints*

The simplest analysis of single-lap joints considers the uniform distribution of shear stress along the bond line, as shown in Fig. 3.6. In this analysis, the adherents are assumed to be rigid, the adhesive is assumed to deform only in shear and the magnitude of shear stress $\tau$ is expressed by:

$$\tau = \frac{P}{bL} \qquad [3.1]$$

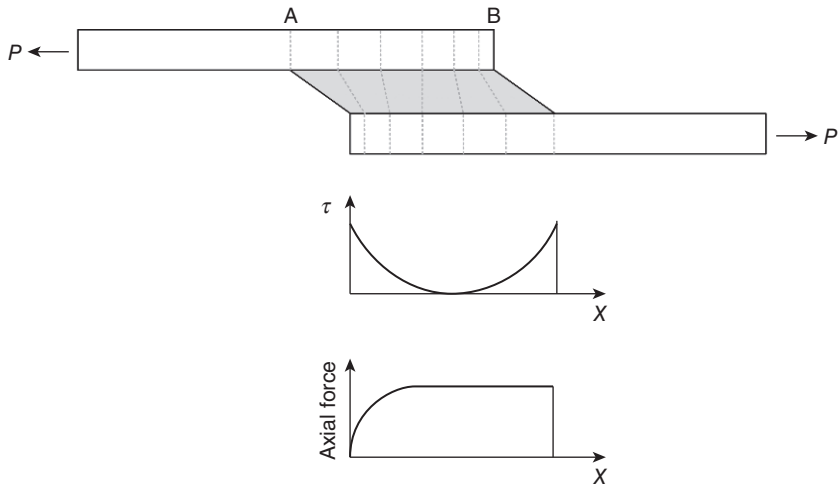


*3.7* Concept of differential shear proposed by Volkersen (1938).

where $P$ is the applied load on the joint, $b$ is the joint width and $L$ is the overlap length. In this kind of analysis, the calculated shear stress can be interpreted as the average stress. Needless to say, this analysis is not accurate since the adherents are elastic and the rigidity assumption is not realistic. This means that the adherents display axial deformations and the shear stress that arises from differentiation in the deformation of adherents is therefore not constant along the bond line. Volkersen (1938) introduced the concept of differential shear for the first time. In this analysis, it is assumed that the adhesive deforms only in shear, but adherents can display deformation. This concept is illustrated in Fig. 3.7. The axial stress in the top adherent gradually decreases from the maximum value to zero from point A to B. The progressive reduction in axial stress in the adherents causes a non-uniform shear strain in the adhesive layer, which results in a non-uniform shear stress distribution. Volkersen's solutions did not take account of the bending of the adherents due to load eccentricity.

The eccentricity in the load path in single-lap joints causes a bending moment and a transverse shear force in the joint. These additional forces should be applied to adherents at the end of overlap, in addition to the applied axial load. The extra bending moment causes rotation in the joint, which necessitates considering the large deformations in the joint. Goland and Reissner (1944) were the first to treat this problem by relating the additional bending moment and shear force to the axial force applied to the joint. They assumed that adherents are integrated with a very thin adhesive layer, thereby enabling them to neglect the adhesive layer when calculating for large deformations. Hart-Smith (1973a) considered the

individual deformation of each adherent, which made it possible to consider the adhesive layer as well. Oplinger (1994) developed another solution to take account of the deformation of adherents outside the overlap area, in addition to deformation in the overlap area. Other researchers followed these studies and developed solutions for shear and peeling stress distributions in the adhesive layer (see, for example, Tsai and Morton, 1994; Wu and Wardenier, 1997; Tsai *et al.*, 1998).

The aforementioned analyses or so-called 'classical analyses' involve three important drawbacks. (i) They do not account for variations in stress through the thickness of the adhesive layer. This means that these analyses are unable to predict the stresses at interface levels, which might be interesting when it comes to the design of joints. (ii) As a consequence of uniform stress assumption through the thickness of the adhesive layer, the maximum shear stress is found at the very end of the overlap, which violates the free-stress condition at this point. (iii) The adhesive material is assumed to be linear elastic. However, adhesives can display some non-linear behaviour which can result in stress redistribution in the adhesive layer. Such an assumption would result in conservative results in predictions of joint strength.

To overcome the first two problems, some researchers developed high-order analyses, such as those presented by Allman (1977) and Chen and Cheng (1983). However, high-order analyses do not usually produce explicit closed-form solutions and usually involve complicated mathematical calculations and are therefore not suitable for design purposes.

Analyses of adhesive joints with elasto-plastic adhesives were first carried out by Hart-Smith for single- (1973a) and double-lap (1973b) joints. The behavioural model for the adhesive in Hart-Smith's analysis is presented in Fig. 3.8. Figures 3.8a and 3.8b show shear stress and strain distribution patterns in joints with elasto-plastic adhesives. As in Fig. 3.8c, the shear stress–strain curve is modeled by a bilinear curve which ends up at the same shear stress ($\tau_P$) and shear strain $\gamma_{ult}$ as the real curve at failure. The two curves have the same strain energy. Hart-Smith showed that, irrespective of the shape of the stress–strain curves, if different curves contain the same amount of strain energy, they will result in the same predicted joint strength. Other researchers also tried to develop analytical solutions to describe the stress state in adhesive joints considering the non-linear behaviour of the adhesive. Bigwood and Crocombe (1990) further developed the elastic analysis they had previously developed (Bigwood and Crocombe, 1989) to take account of the non-linear behaviour of the adhesive. They assumed that the adhesive layer acts as a series of shear and tensile springs. A hyperbolic tangent approximation was used to describe the non-linear behaviour of the adhesive. Adams and Mallick (1993) also considered a non-linear behaviour for the adhesive in joints. They introduced the concept

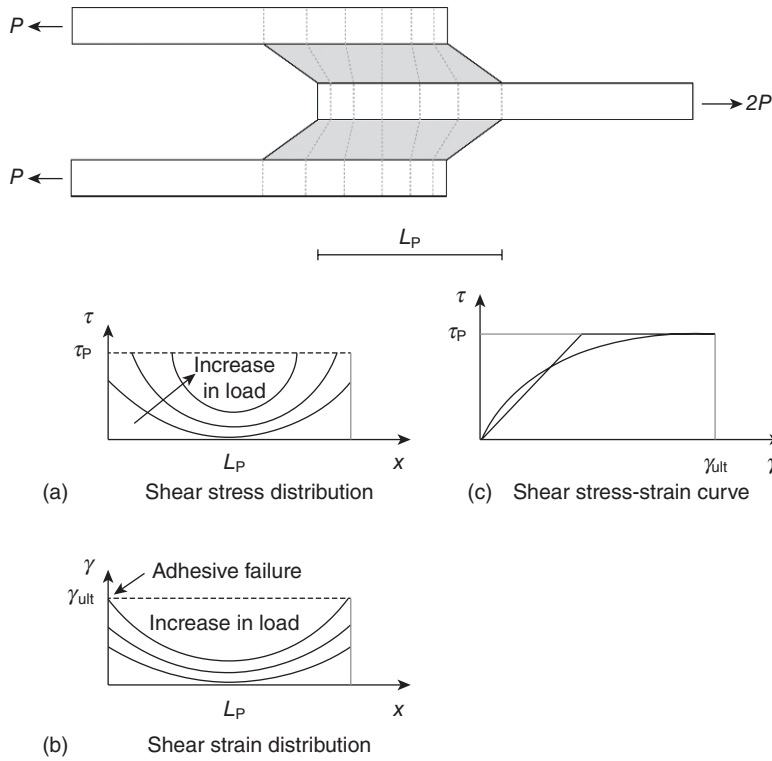


*3.8* Analysis of adhesive joints considering the non-linear behaviour of the adhesive (Hart-Smith 1973a, b).

of 'effective modulus' ($E_{eff}$) which is derived from equating the energy under the stress–strain curve for two cases and using the same strain at failure, as illustrated in Fig. 3.9. Using this concept, it was possible to avoid the bilinear stress–strain curves used by Hart-Smith and perform linear analysis.

*Analytical solutions for adhesive joints between fibre-reinforced polymer (FRP) laminates and steel beams*

Like single- and double-lap joints, solutions for shear and peeling stress distributions in steel beams bonded with FRP laminates have been developed by some researchers. These solutions are derived by solving the differential equations based on force equilibrium and deformation compatibility. To make it possible to find closed-form expressions, some assumptions and simplifications have been made. These assumptions usually include:

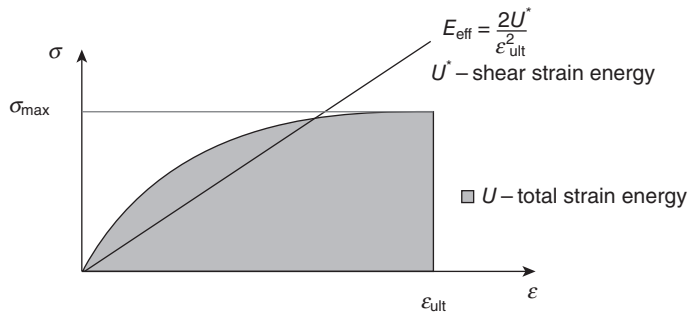


*3.9* Concept of effective modulus used by Adams and Mallick (1993).

- All materials are linear elastic.
- The shear and peeling stresses in the adhesive layer do not vary through the thickness of the adhesive.
- Shear deformations in the carbon fibre-reinforced polymer (CFRP) plate and steel beam are ignored.
- Bending deformation of the adhesive is ignored.
- When calculating the interfacial shear stress, bending of the CFRP plate is ignored.
- The beam is simply supported and shallow, and the St Venant theory is therefore used.

The derivation of interfacial stresses in the adhesive layer in beams bonded with FRP or steel plates has been carried out in number of studies (for example, Vilnay, 1988; Roberts, 1989; Roberts and Haji-Kazemi 1989; Malek *et al*., 1998). Smith and Teng (2001) gave a review of existing closed-form solutions for calculating the interfacial stresses in beams strengthened with adhesively bonded laminates. They identified the assumptions and limitations in the different existing solutions, thereby clarifying the differences between them. These existing solutions have been developed, focusing on the strengthening of reinforced concrete beams which, in turn, allowed for the omission of some terms in the solution. In their paper, Smith and Teng also presented a new solution for calculating the stresses in beams bonded with thin laminates, irrespective of the cross-section type or material of the beam. The derivation of these solutions was based on force equilibrium and deformation compatibility. Specific expressions for the interfacial stresses were given for three different and important load cases. However, all the solutions were only valid in the elastic phase. The key assumption for the derived solution was uniform stress distribution through the adhesive layer thickness. Deng *et al*. (2004) presented an analytical solution to calculate the interfacial stresses in a reinforced steel beam under mechanical

and thermal loads. They also presented a numerical solution for the joints in which normal-tapered FRP laminates were used.

All these analyses do not satisfy the zero shear stress at the very end of the bond line, as they do not consider the variation in stresses through the thickness of the adhesive layer. This drawback is assumed to have little effect at a very small distance at the end of the laminate (Roberts, 1989). For this condition to be satisfied, the variation in stresses through the thickness of the adhesive layer should be considered. Consideration of this variation does not allow for the formation of low-order differential equations, which means that that force and/or displacement compatibility should be carried out using high-order differential equations. Analyses of this kind can be seen in the work carried out by Rabinovich and Frostig (2000) and Yang *et al*. (2004). These high-order solutions do not, however, provide explicit solutions for stress distribution in the adhesive layer and, as a result, the use of these solutions for design purposes is not appealing. Moreover, the precision of high-order solutions has been questioned (Shen *et al*., 2001).

### 3.3.2 Finite element (FE) analysis of adhesive joints

Finite element (FE) analysis is a general analysis technique that can be applied to any engineering structure including adhesive joints. In this method, the structure to be analysed is divided into small regions referred to as finite elements. The technique is based on the stationary potential energy theory which states that the loaded structure takes the deformed shape that minimises the energy in the system. This deformation is found as the displacements of nodes which are located on the element boundaries. Using this technique, it is important to ensure that the type of elements and the number of used nodes provide a sufficiently accurate approximation for the deformation of nodes. Using the FE method, it is possible to model aspects of an adhesive joint that are very difficult to account for in closed-form analyses such as those discussed before. The main advantages of using FE methods in comparison to analytical analyses include (i) the opportunity to include complex geometries and (ii) the opportunity to include complex material responses.

As discussed earlier, closed-form solutions are usually developed for specific configurations. Most of the existing solutions have been derived for basic configurations, i.e. joints without adhesive fillets and tapered laminates. Accounting for different joint geometries complicates the differential equations and often makes it impossible to develop closed-form solutions. One of the most important contributions of the FE method in analyses of adhesive joints is the opportunity to take account of different, complex geometries. Some examples of complex geometries of adhesive joints are

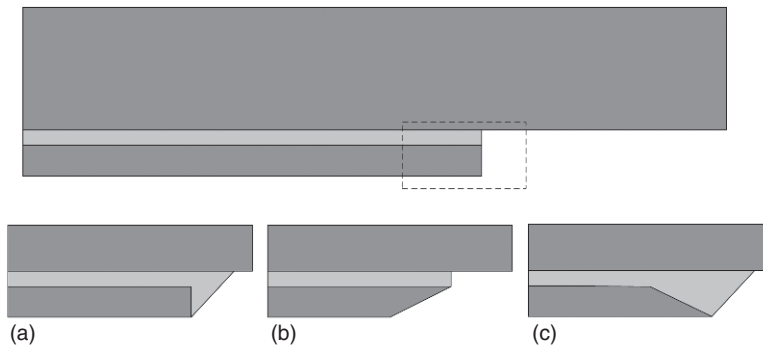


*3.10* Different details at the end of the laminate in adhesive joints: (a) adhesive fillet; (b) normal taper; and (c) reverse taper with adhesive fillet.

presented in Fig. 3.10. The FE method has also enabled the 3D modelling and analysis of adhesive joints by which it is possible to investigate the variation in the stresses/strains through the width of adhesive joints (Linghoff, 2009).

Most of the closed-form analyses discussed in Section 3.3.1 assume a linear elastic material response. More advanced solutions may include a simple representation of non-linear material behaviour. Most adhesives display a complex time- and temperature- dependent non-linear response. Sometimes, substrates also exhibit non-linearity. In order to simulate the actual response of a bonded structure, it is necessary to include such material behaviours in analyses. These responses can be included in FE analyses using material models, such as plasticity (irrecoverable deformation), hyper-elasticity (recoverable deformation) and viscoplasticity or elasticity (time-dependent irrecoverable or recoverable deformation). These models are now available in many FE packages. Another important contribution of the FE method in the field of analysis is damage modelling. This feature enables the modelling of the complete response of the joint up to the failure point (see for example Andre *et al.*, 2012).

## 3.4 Singular stress fields

One of the most important problems when using FE as a tool to analyse adhesive joints is the singular stress fields at geometrical and material discontinuities. In engineering, a singular point is defined as a position at which the stresses or other physical quantities become infinite or non-deterministic. Different sources might cause singular or infinite stresses in adhesive joints. They include fillers, micro-voids, cracks and bimaterial wedges due to strain incompatibility between the adjacent materials.

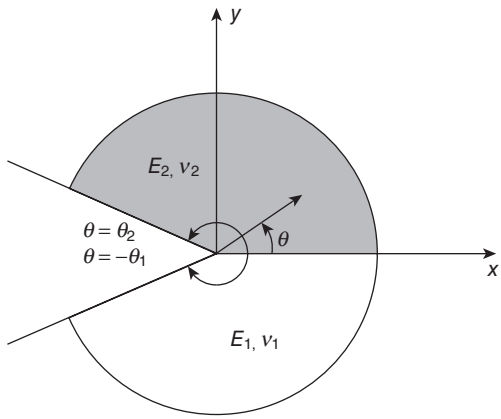


*3.11* Elastic bimaterial wedge.

In a laminate-strengthened steel beam, for example, each pair of adjacent materials, i.e. adhesive–steel and laminate–adhesive, can be regarded as a bimaterial wedge. According to the theory of elasticity, the point at the end of an interface in a wedge of this kind is a point of stress singularity, and the stresses approach infinity towards this point (Hein and Erdogan, 1971). The severity of the stress singularity is expressed by the 'strength of singularity', which shows how rapidly the stresses develop towards the singular point. The relationship between the magnitude of the stresses $\sigma_i$ and the strength of singularity $\lambda$ can be expressed as $\sigma_i \propto r^{-\lambda}$ (Hein and Erdogan, 1971), where $r$ is the distance from the singular point. The strength of singularity $\lambda$ is dependent on the elastic modulus of the two materials ($E_1$ and $E_2$), their Poisson's ratio ($\nu_1$ and $\nu_2$) and the geometrical shape ($\theta_1$ and $\theta_2$) of the wedge (Fig. 3.11).

The singularity problem at bimaterial edges has been investigated by a number of researchers – see, for example, Bogy (1971) and Hein and Erdogan (1971). The singular stress field in such location can be expressed as (Bogy 1971):

$$\sigma_{ij}(r,\theta) = \sum_{k=1}^{N} \frac{K}{r^{\lambda_k}} f_{ijk}(\theta) + \sigma_{ij0}(\theta) \qquad [3.2]$$

where $r$, $\theta$ are the polar co-ordinates, $N$ is the number of $r$-dependent stress terms, $\lambda_k$ is the strength of singularity, which is dependent on the elastic constants of the two materials, ($E_1$, $\nu_1$, $E_2$, $\nu_2$) and the angles $\theta_1$, $\theta_2$, $f_{ijk}$ is a function dependent on the angle $\theta$ and, $\sigma_{ij0}(\theta)$ and the constant $k$ depend on loading and global geometry. Possible singularity points in adhesive joints with different end configurations are shown in Fig. 3.12. The


*3.12* Possible positions of stress singularity denoted as dots in adhesive joints with different configurations.

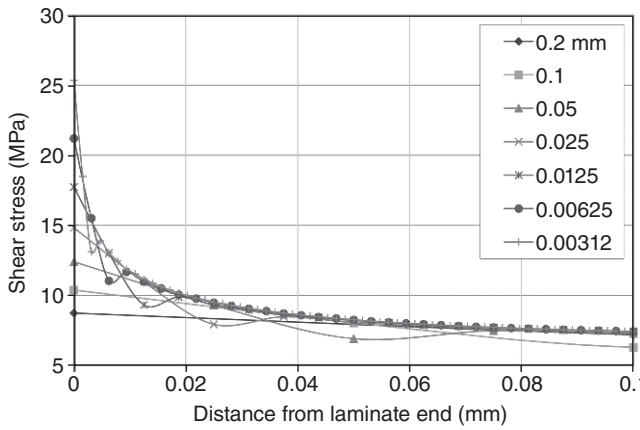


*3.13* Effect of mesh refinement on shear stress at steel–adhesive interface.

stress field along the steel–adhesive interface in adhesive joints with different end configurations has been investigated by many researchers; see, for example, Haghani *et al*. (2009).

Singularity at these points can lead to misleading results for stresses and strains obtained from FE analysis, and therefore designers should be aware of the unrealistic values. The magnitude of stresses and strains at singularity points is dependent on the size of the finite elements used in the model. In order to illustrate this, consider the sharp corner of the steel–adhesive in a joint shown in Fig. 3.12. Figures 3.13 and 3.14, show how mesh refinements influence the shear and peeling stress in the vicinity of the singularity point, i.e. the end of the laminate. The element size in this parametric study changes from 0.2 to 0.003 mm in a small region close to the singular point. It is observed that with mesh refinements, the values for the shear and peeling stresses tend to approach the theoretical value of infinity at the end point of the bond line. As a result of mesh refinement, the size of this

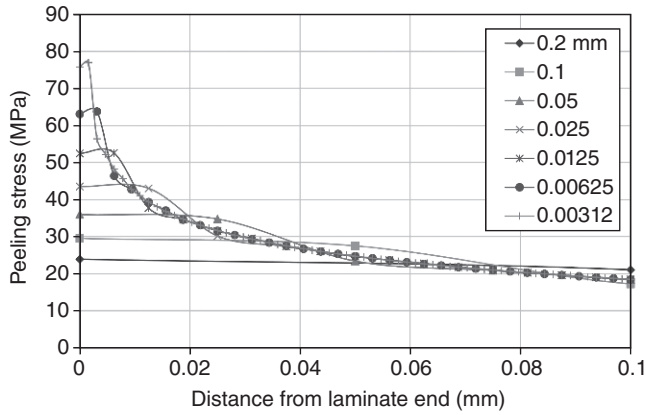


*3.14* Effect of mesh refinement on peeling stress at steel–adhesive interface.

'inconsistent' result area is reduced and pushed close to the end of the interface.

It goes without saying that an infinite stress does not exist in reality. In reality, extreme stress values at points of severe stress concentration points are levelled out due to plasticity (i.e. the non-linear behaviour of the materials in the joint). In addition, ideal sharp corners like those incorporated in FE models do not exist in reality due to various geometrical imperfections and irregularities. This issue was addressed by Adams and Harris (1987). Nevertheless, it is important to point out here that the points of stress singularity clearly indicate spots of local stress raisers which might be critical in terms of the strength of the joint. When focusing on adhesively bonded composite laminates, the presence of these local stress raisers is particularly important for the strength of the joint in relation to the poor strength of the composite laminates in the transverse (through-thickness) direction.

## 3.5 Strain distribution in adhesive joints

In order to investigate the difference between different stress analysis techniques and evaluate their precision in predicting the bond stress/strain, a comparison between the results obtained from analytical and FE analyses in terms of bond strain with experimental results is presented in this section. The original work was carried out by the author (Haghani, 2010). The configuration under consideration for this investigation included a steel plate bonded with CFRP laminates on both sides subjected to tensile load. The configuration and nominal dimensions of the specimen are presented

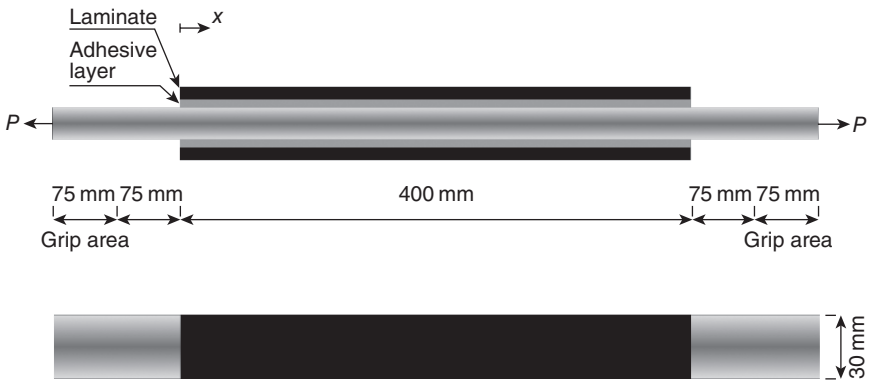


*3.15* Configuration and nominal dimensions of the modelled specimen equipped with strain gauges.

*Table 3.2* Material properties used to manufacture specimens and thickness of constituents

| Material | *E*-modulus (GPa) | Poisson's ratio | Tensile strength (MPa) | Thickness (mm) |
|---|---|---|---|---|
| Sikadur® 330 | 4.5 | 0.3 | 32 | 3.4 |
| StoBPE lim 567 | 7 | 0.3 | 26 | 2 |
| Sika® carbodur® | 165 | 0.3 | 3100 | 2.4 |
| BPE 4014 UHM | 383 | 0.3 | 1100 | 4 |
| Steel (S355) | 210 | 0.29 | 510 | 10 |

*Note*: The yield strength of steel is 430 MPa.

in Fig. 3.15. The strain in the specimen has been measured using an optic measurement system which will be explained in this section.

Two different strengthening systems provided by Sika® and STO® were used in this study. The STO system included StoBPE primer 50 super, BPE 4014 UHM laminate and StoBPE lim 567 epoxy, and the Sika system included Sika carbodur S624 laminate and Sikadur 330 epoxy. The material properties used in each system are summarised in Table 3.2. Comparison of the stress–strain curves for epoxy adhesives used in this investigation showed that the adhesive developed by STO had more pronounced non-linear characteristics in comparison to the one from Sika (Fig. 3.16). This gave the opportunity to investigate the effect of non-linear behaviour of the adhesive on strain distribution in the joint. Numerical models of specimens were developed using the commercial FE package, ABAQUS 6.7.2. Every part of the specimens was modelled using 8-node linear solid elements with reduced integration (C3D8R) (see Fig. 3.17). Due to symmetry, only a quarter of each specimen was modelled. An isotropic

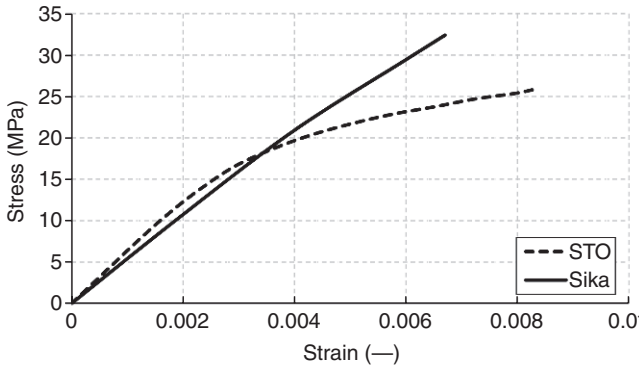


*3.16* Behaviour of adhesives used in the investigation.

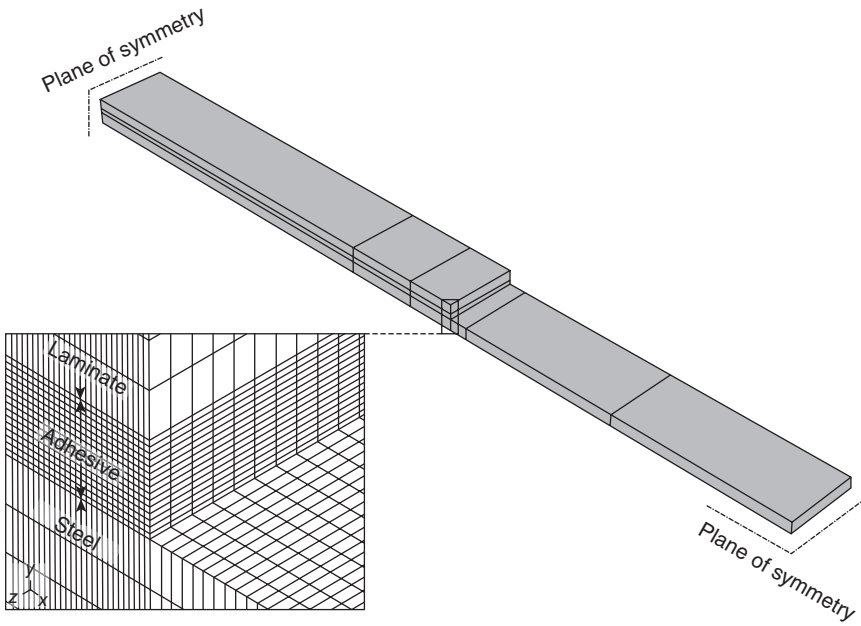


*3.17* FE model of the investigated configuration.

and linear elastic material model was considered for steel and adhesive. To investigate the effect of laminate properties on stress/strain distribution in the adhesive layer, both isotropic and orthotropic material models were adopted for laminates.

The measurement of strain in the adhesive layer, especially in the through-thickness direction, has been one of the challenges in experimental studies of adhesive joints. Recent advances in optical measurement techniques

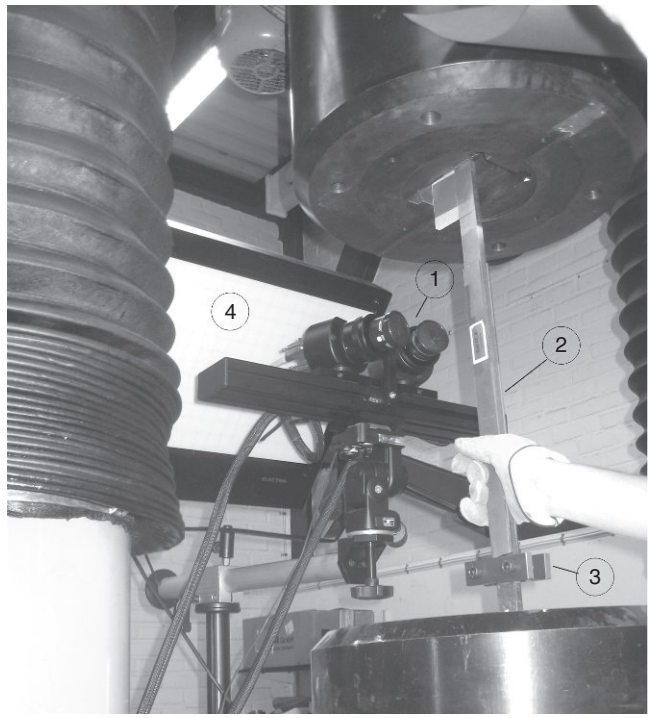


*3.18* Set-up of optical measurement system. 1, digital cameras; 2, specimen; 3, clamp; 4, source of light.

have opened up a new horizon in high-precision strain measurements for research and industrial purposes. In this investigation, a full-field, commercial, non-contact, optical deformation measurement system, ARAMIS™ 4M by GOM, is used. This system uses a measurement technique based on digital image correlation (DIC) with a stereoscopic camera set-up, consisting of two CCD cameras with a resolution of four megapixels (2048×2048 pixels). The basic idea behind DIC is to measure the displacement of the specimen during testing by tracking the deformation of a naturally-occurring or applied surface speckle pattern in a series of digital images acquired during loading.

The experimental set-up of the system is fairly simple (see Fig. 3.18). The cameras are placed in front of the specimen. The surface of the specimen should have a characteristic speckle pattern with high contrast which can deform together with the specimen during loading. This pattern is usually achieved by first applying white retro-reflective paint as the background and then applying black stains on top of the white paint, as shown in Fig. 3.19. Image pairs at a sampling rate of one per second are taken by digital cameras. In addition, the signals of the load and displacements obtained

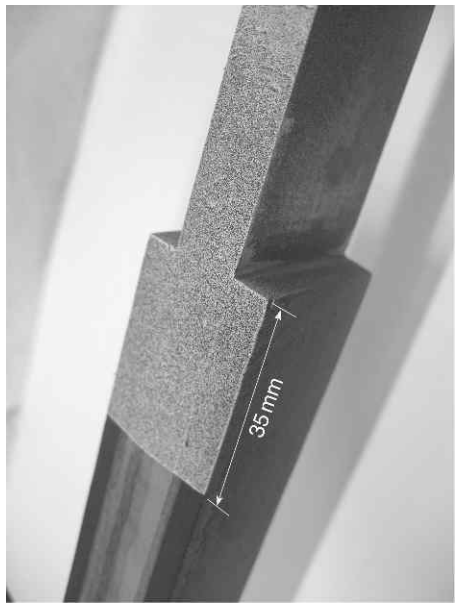


*3.19* Painted specimen.

from the testing machine are also recorded in the ARAMIS system at the time the images are recorded, and it would be therefore possible to synchronise the images and the corresponding post-processed results with the load history of the specimen. The system used in this investigation is capable of measuring strains in the range of 0.01 to 100 % with an accuracy of 0.01 %.

### 3.5.1 Effect of material properties on strain distribution

*Laminate material model*

Laminates used for strengthening and repair purposes usually consist of unidirectional fibres embedded in a resin epoxy matrix. One clear characteristic of a structure of this kind is the orthotropy of the material. Unidirectional laminates have better mechanical properties in the direction of the fibres in comparison to those in the transverse direction. Through-thickness properties are mostly dependent on the properties of the matrix, since the load is only transferred by the matrix. However, when analysing the adhesive joints using analytical or numerical approaches, composite laminates are usually assumed to be isotropic materials.

Having the opportunity to study the strain distribution in the adhesive layer using an optical measurement technique makes it possible to

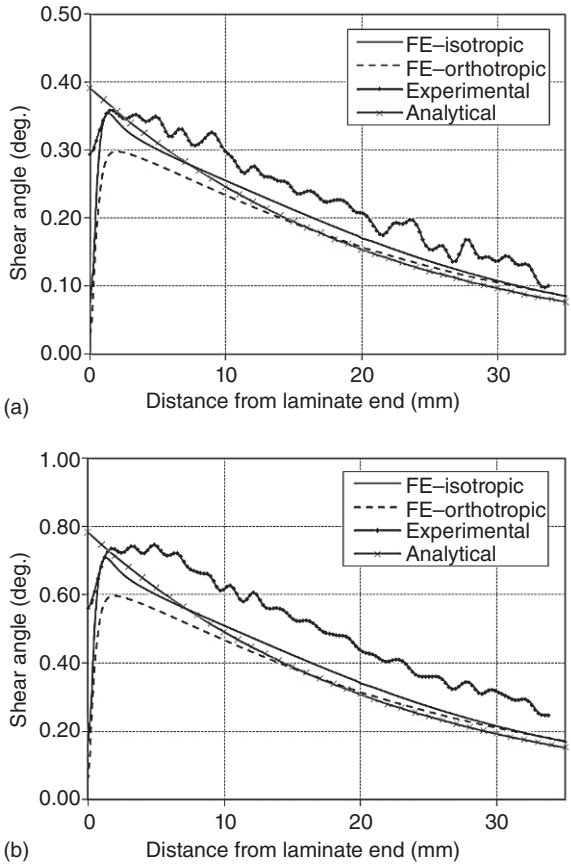


*3.20* Comparison of FE with isotropic and orthotropic material assumption for laminates and experimental results for shear angle at (a) 40 kN and (b) 80 kN for STO specimen.

investigate the influence of this assumption on the magnitude and distribution of strain in adhesive joints. For this purpose, the FE results for the STO specimen with isotropic and orthotropic material assumptions for the laminates were compared to those from analytical and experimental results. Figures 3.20 and 3.21 present a comparison between the calculated and measured shear and peeling strain at the mid-thickness of the adhesive layer. Comparisons are made at two load levels: at 40 kN, at which linear behaviour is presumed in the adhesive layer; and at 80 kN, at which the adhesive is expected to be in the non-linear phase.

Generally, it can be seen that the orthotropic material model for laminate results in a lower approximation of shear strain and a higher approximation

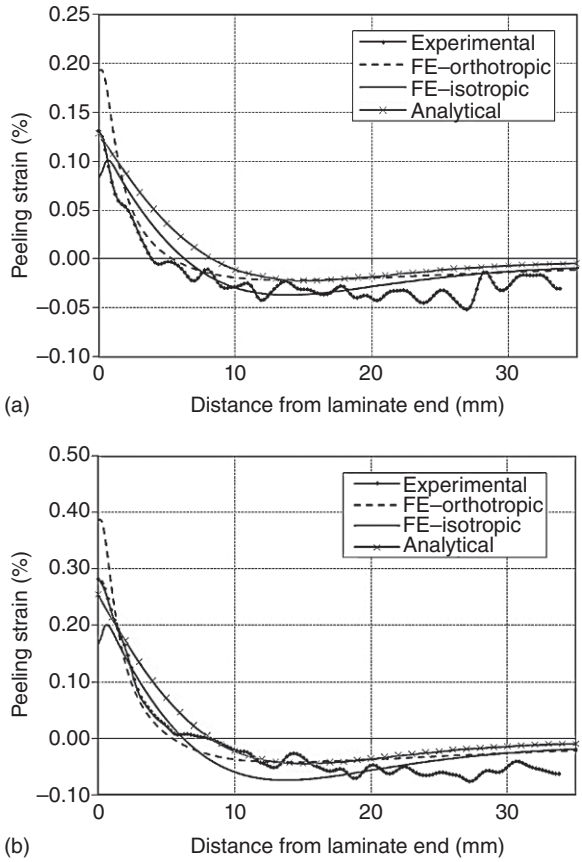


*3.21* Comparison of FE with isotropic and orthotropic material assumption for laminates and experimental results for peeling strain at (a) 40 kN and (b) 80 kN for STO specimen.

of peeling strain compared with the results obtained from the isotropic model. A comparison of the results from the two material models with experimental results reveals that the isotropic model provides better approximations for both shear and peeling strain. It might be concluded that the strain distribution in the adhesive layer is not significantly affected by the transverse properties of the composite laminate. This observation provides a concrete basis for numerical and analytical studies based on the isotropic material model for laminates. To complete the comparison, the results from analytical solutions proposed by Bocciarelli *et al.* (2009) are included in the plots and reasonably good agreement with the experimental results can be observed.

*Adhesive properties*

Structural epoxy adhesives used to bond composite laminates to existing structures are usually classified as brittle adhesives. Unlike toughened adhesives (failure strain up to 50 %), structural epoxies usually fail at strain levels below 1 %. Structural epoxies are therefore modelled as linear elastic materials. However, even within this range, they can display some degree of non-linearity (see Fig. 3.16). Non-linearity can lead to strain redistribution in the adhesive layer and therefore affects the capacity of the joint. Figures 3.22 and 3.23 show a comparison for the Sika specimen in which the adhesive behaves more linearly. One interesting point that should be noted when it

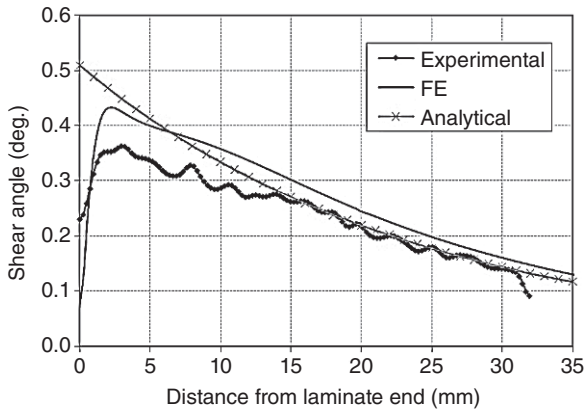


*3.22* Comparison of FE, experimental and analytical results for shear angle at 80 kN for Sika specimen.

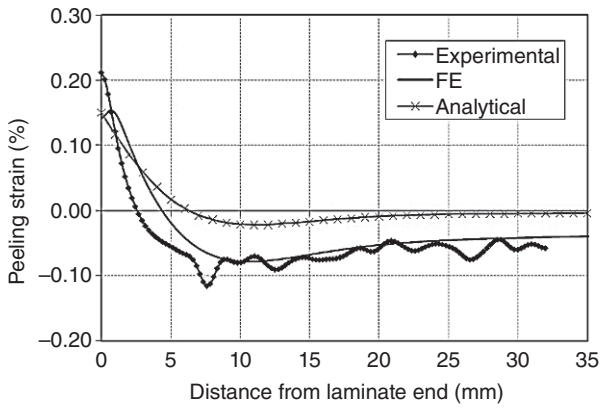


*3.23* Comparison of FE, experimental and analytical results for peeling strain at 80 kN for Sika specimen.

comes to Figs 3.20–3.23 is that, irrespective of the non-linearity of the adhesive, the linear model is capable of providing a good estimate of the maximum strain at different load levels.

### 3.5.2 Strain distribution through the thickness of the adhesive layer

One important issue when studying the force-transfer mechanism in adhesive joints is the distribution of the stresses/strains through the thickness of the adhesive layer. This is extremely important, since most of the analytical solutions developed to approximate the state of stresses/strains are based on a uniform strain distribution assumption over the thickness of the adhesive layer – see, for example, Goland and Reissner (1944) and Smith and Teng (2001). The most interesting location along the bond line at which to consider strain distribution is the area close to the end of the laminate where the shear lag effect is observed and failure of the joint is usually initiated. Experimental results in terms of shear and peeling strain distributions through the thickness of the adhesive layer are plotted in Figs 3.24 and 3.25 along the thickness of the adhesive at a distance of 0.5 mm from the end of the laminate for STO specimen. The first point to be noted when it comes to the shear distribution is that the shear strain at the adhesive–laminate interface is higher than that at the steel–adhesive interface. This is mainly due to the more restrained condition of the adhesive close to the steel interface compared to the adhesive–laminate interface. The next point is the difference between the shear and peeling strain patterns. The shear strain distribution pattern has almost a constant shape when the load is increased (maximum value at almost mid-height), while a

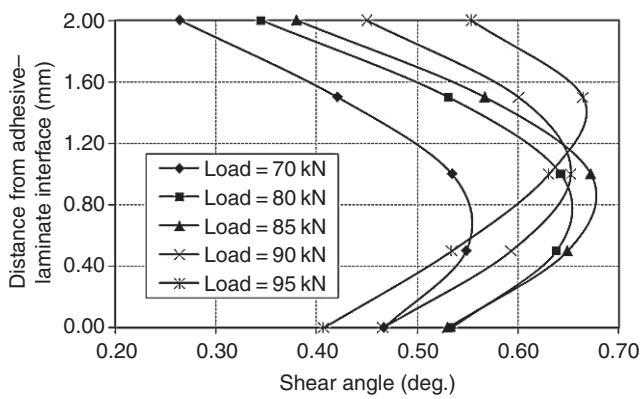


*3.24* Distribution of shear strain through the thickness at different load levels in STO specimen.

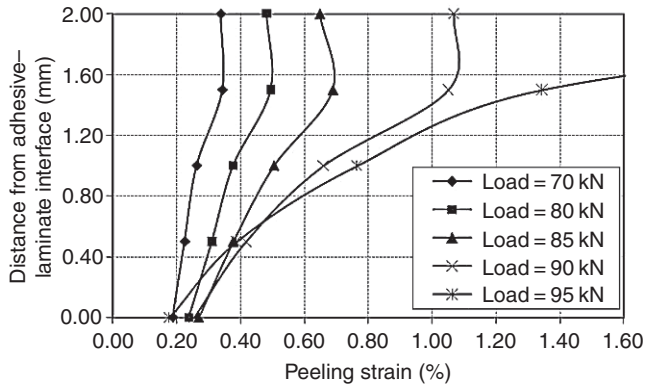


*3.25* Distribution of peeling strain through the thickness at different load levels in STO specimen.

strain concentration close to the steel–adhesive interface can be seen in the peeling strain distribution. This behaviour was also observed for the Sika specimen.

This observation, in fact, questions the 'uniform stress distribution' assumption made in the development of mathematical closed-form models to calculate stresses in the adhesive layer. However, referring to Figs 3.22 and 3.23, it can be seen that the analytical solution proposed by Bocciarelli *et al*. (2009) provides fairly good approximations of strain.

Increasing the distance from the end of the laminate reduces the shear lag effect, and distribution tends to be more uniform. Figures 3.26 and 3.27 show the experimental results for shear and peeling strain distribution through the thickness of the adhesive layer along the adhesive joint at a load level of 80 kN for the STO specimen. It can be seen that increasing the distance from the end of the laminate tends to make the strain distribution for both shear and peeling components more uniform. This rate for peeling strain is higher than that for shear, due to the more local nature of the peeling stresses.

Considering the distribution of principal strain just before failure can also provide useful information about the failure mechanism. Figure 3.28 shows the principal strain distributions in Sika and STO specimens. The vertical axis represents the normalised distance from the laminate–adhesive interface, i.e. laminate–adhesive interface at 0 and adhesive–steel interface at 1. One important observation is that the maximum strain takes place at a distance of almost 20 % of the adhesive layer thickness, away from the adhesive–steel interface, and this is independent of the adhesive layer thickness. The other point is the distribution pattern in the two specimens. In the Sika specimen, the strain is more uniformly distributed in comparison

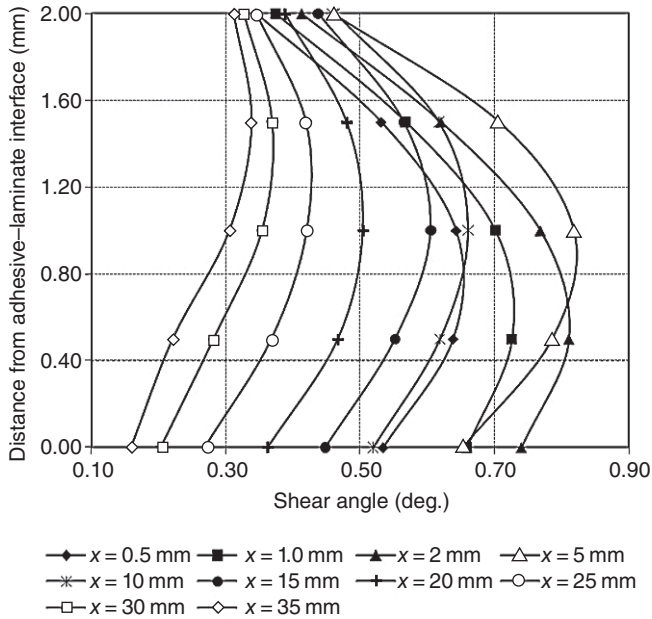


*3.26* Distribution of shear strain through the thickness at different locations at 80 kN for STO specimen.

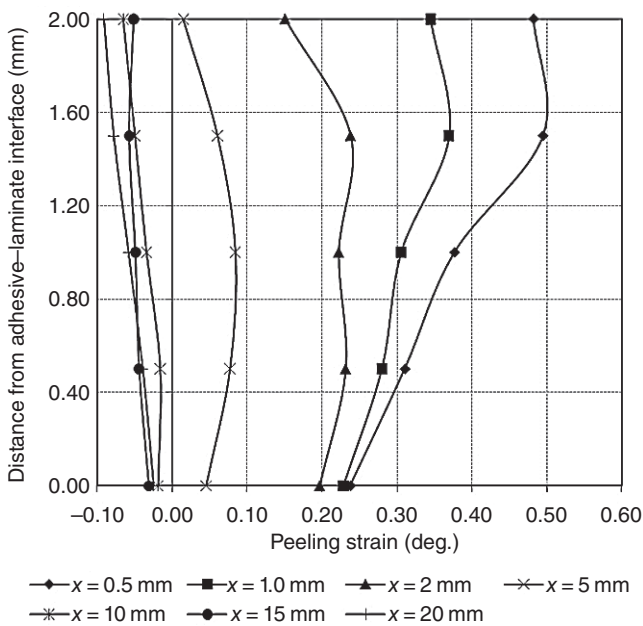


*3.27* Distribution of peeling strain through the thickness at different locations at 80 kN for STO specimen.

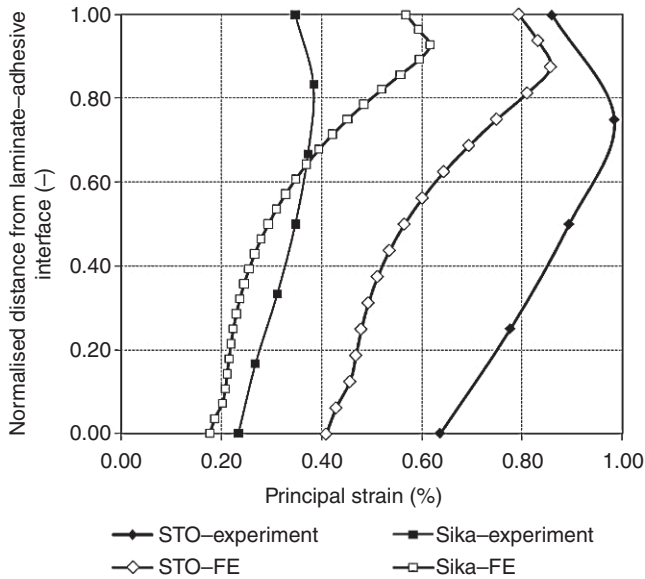


*3.28* Distribution of principal strain through the thickness of the adhesive layer at failure for STO and Sika specimens.

to the STO specimen. The reason for this difference could be explained by the more non-linear behaviour of the STO adhesive.

In existing practice when it comes to the design of adhesive joints (see, for example, Cadei *et al*., 2004), the maximum stress or strain at the mid-thickness of the adhesive layer is compared with the characteristic strength of the adhesive material used in the joint. The latter observation gives rise to the accuracy of this approach for joints made from adhesives with somewhat non-linear behaviour. The difference between the measured and calculated strain from elastic analysis (FE) reveals that the non-linearity of the adhesive layer will most probably produce conservative results.

## 3.6 The contribution of the finite element method in the analysis of geometrically modified adhesive joints

One of the most important areas that the FE method contributes in design of joints is the analysis of adhesive joints with complex geometries. An example of these complexities is adhesive joints with tapered laminates. One of the methods which has been suggested to reduce the stress concentration in adhesive joints is to modify the geometry of the laminate by tapering (Cadei *et al*., 2004). The idea is to obtain a more gradual force

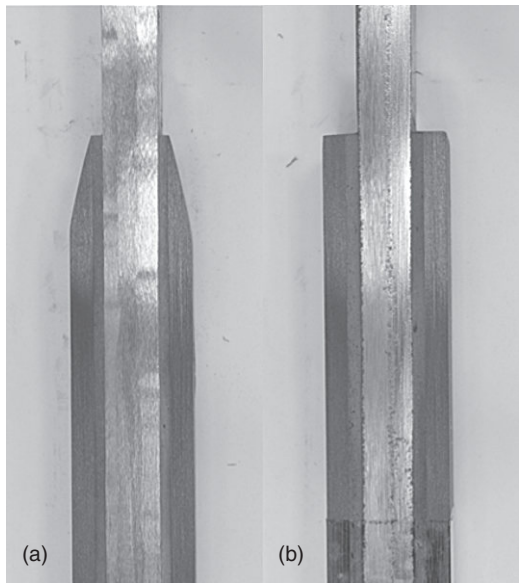


*3.29* Adhesive joint with (a) tapered and (b) untapered laminate.

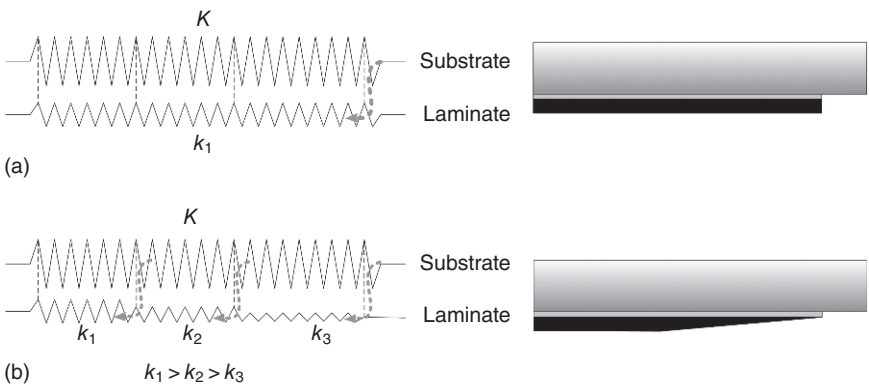


*3.30* Force transfer in adhesive joints with tapered (b) and untapered laminates (a) where $K$ and $k_i$ represent the axial stiffness of the substrate and laminate, respectively.

transfer from the substrate to the laminate by modifying the stiffness of the laminate. Obviously, more gradual force transfer will produce lower peak stress in the adhesive layer. The configuration and the idea are illustrated in Figs 3.29 and 3.30.

This method is widely used in other areas of adhesive bonding applications, such as the aerospace and automotive industries. Based on the experience

obtained from these fields, this modification is also recommended by some design guidelines in order to reduce the stress concentration and enhance the strength of adhesive joints used in structural engineering applications (see, for example, Cadei *et al*., 2004). The effect of tapering on the interfacial stresses in adhesive joints has been the focus of several investigations (see, for example, Hildebrand, 1994; Tsai and Morton, 1995; Belingardi *et al*., 2002; Teng *et al*., 2002; da Silva and Adams, 2007; Haghani, 2010). Most of the studies cited in the literature indicate the favourable effects of tapering in reducing stress concentrations in adhesive joints. However, there are a few experimental studies presenting controversial results that indicate that laminate tapering might actually result in a reduction in joint strength.

A numerical and experimental study was conducted by Vallee and Keller (2006) to investigate the effect of tapering on the strength of double-lap adhesive joints made of glass fibre-reinforced polymer (GFRP) laminates. One interesting conclusion following their experimental results was that tapering did not improve the strength of joints, even though it reduced the peak interfacial stresses along the joint. The authors' explanation of this observation was that the favourable effect of tapering in reducing the interfacial stresses was counteracted by the reductive effect of tapering on the through-thickness shear strength of the laminate.

An experimental investigation of the behaviour of steel beams strengthened with bonded CFRP laminates by Deng and Lee (2007) also indicated that tapering of the CFRP laminate might reduce the strength of joints. The load-carrying capacity of a strengthened beam with a tapered laminate was found to be lower in comparison with the beam with an untapered laminate. The authors attributed this observation to the smaller thickness of the adhesive layer in the specimen with a tapered laminate in comparison with that in the control specimen. This would have caused a higher stress concentration and thereby less strength in the former case.

Wendel and Luke (2007) carried out a study in which the behaviour of steel members strengthened with tapered and untapered composite strips was investigated. They used the vacuum resin infusion technique to manufacture specimens, which made it possible to obtain a uniform adhesive thickness with good precision. It was found that the load-bearing capacity of the specimen with tapered laminate was less than that of the specimen with an untapered laminate. The authors attributed this observation to bond defects in the joint.

In another study carried out by the author (Haghani *et al*., 2010), it was observed that the tapering of the laminate resulted in 14 % reduction in the capacity of the tested joints. The above-mentioned contradictory results encouraged the author to investigate the effect of tapering on the behaviour of adhesive joints in more detail using an experimental and numerical approach. In this study, 3D finite element models of both configurations

were prepared as illustrated in Fig. 3.31. The specimens have the same configuration as shown in Fig. 3.15. In order to investigate the effect of tapering length, different models with different tapering lengths were developed.

Monitoring of the strains in the adhesive layer along the bond line revealed that even though the tapering has a favourable effect in reducing the shear stress/strain in the joint, it significantly increased the peeling stress/strain component. Figure 3.32 shows the variation of peak shear and peeling stresses along the bond line, normalised with respect to corresponding

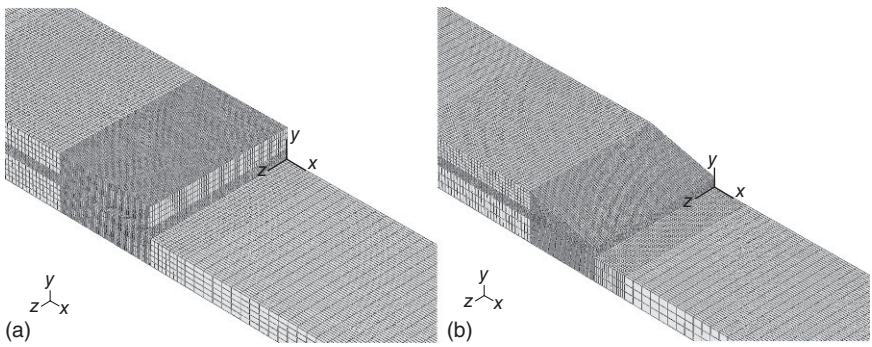


*3.31* 3D FE models of adhesive joints with (a) untapered and (b) tapered laminates.

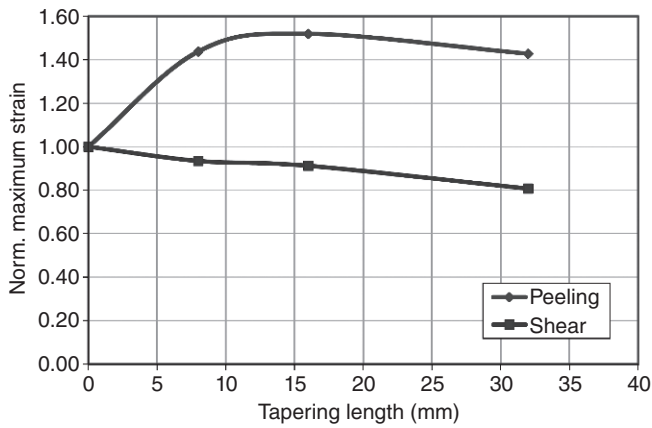


*3.32* Maximum shear and peeling strains along the bond line in the joint with tapered laminate, normalised with regard to untapered laminate.

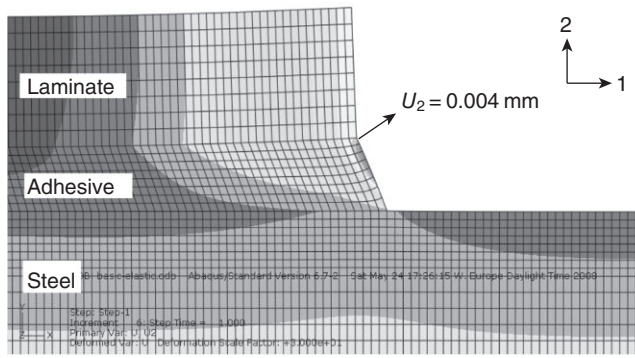


(a)

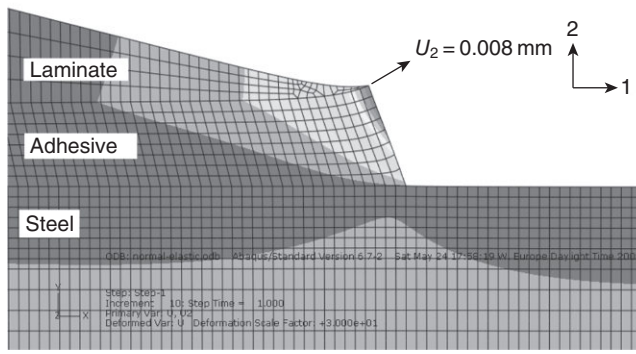


(b)

*3.33* Deformation at the laminate tip in joints with (a) untapered and (b) tapered laminate.

values in the joint with untapered laminate. It was observed that the increase in peeling stress component, for a certain length, could be up to 50 %. Figure 3.33 shows a comparison between the vertical deformations of the laminate tip in tapered and untapered laminate.

These results and conclusions were verified by experimental results in which the strain field was monitored using an optical measurement system. Figures 3.34 and 3.35 show a comparison of peeling and shear strains in joints with tapered and untapered laminates. It is observed that tapering increases the peeling strain in the joint while it does not influence the shear strains significantly.

Sensitivity of the bond between the steel and the adhesive to peeling stresses explains the reason for lower capacity of the joints with tapered laminates. Further investigations by the author showed that the effect of tapering has a direct relationship with the ratio of modulus of elasticity of

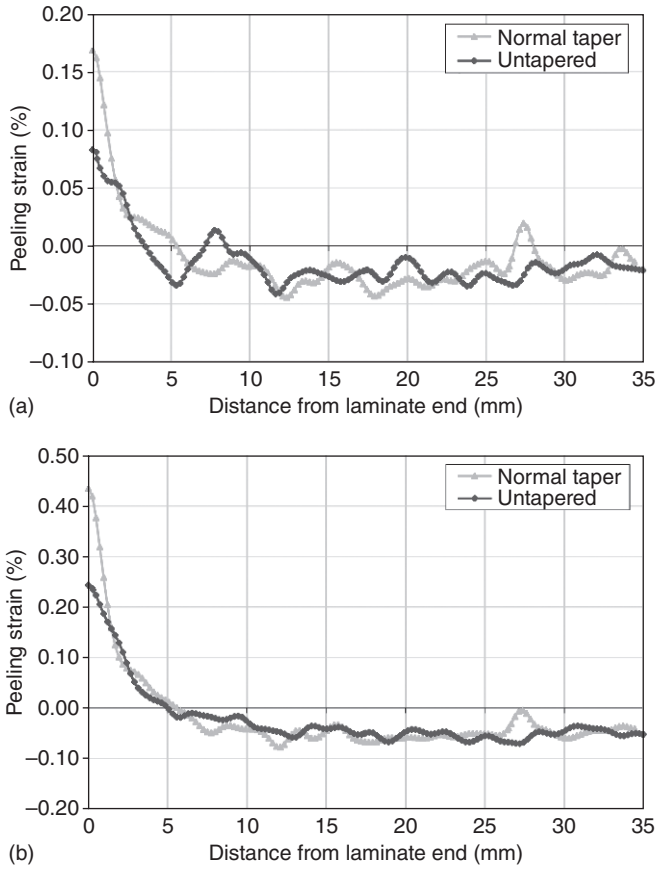


*3.34* Comparison of peeling strains in joints with tapered and untapered laminates at (a) 30 kN and (b) 70 kN.

the laminate material to adhesive material. It was shown that the higher this ratio, the more unfavourable the effect from the tapering. The fact that the effect of tapering has to do with this ratio explains the favourable effect of tapering of the adherents on the joint strength in the aerospace industry where the adherents are usually made of aluminium and the above-mentioned ratio is rather small.

## 3.7 Conclusion

The FE method is a powerful tool for analysis of adhesive joints. It is a useful aid when it comes to designing such joints, especially for adhesive joints with complex geometries or constituents' material responses. However, the method involves several shortcomings. It needs calculation

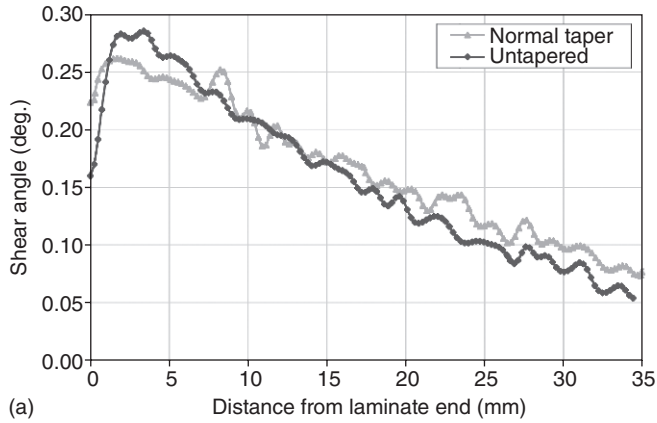


(a)

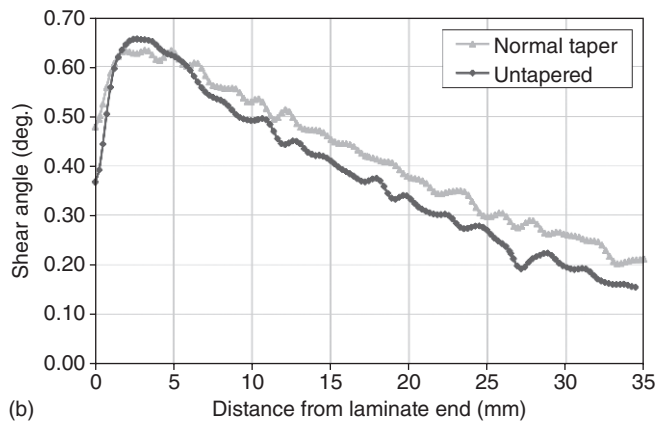


(b)

*3.35* Comparison of shear strains in joints with tapered and untapered laminates at (a) 30 kN and (b) 70 kN.

resources, it is time-consuming and it usually needs experience to interpret the results. It might also provide misleading results around singular stress fields which should be dealt with carefully. Numerical errors and convergence problems, where geometrical and non-linear materials are used, are just examples of problems which might be involved when using the FE method. Therefore, it is important for engineers, using this tool, to have a clear picture of the reliability of the results that they obtain from their analyses.

## 3.8 References

Adams, R. D., Harris, J. A. (1987) The influence of local geometry on the strength of adhesive joints, *International Journal of Adhesion and Adhesives*, V. 7, No. 2, 69–80.

Adams, R. D., Mallick, V. (1993) The effect of temperature on the strength of adhesively-bonded composite-aluminium joints, *The Journal of Adhesion*, V. 43, No. 1–2, 17–33.

Allman, D. J. (1977) A theory for elastic stresses in adhesive bonded lap joints, *The Quarterly Journal of Mechanics and Applied Mathematics*, V. 30, No. 4, 415–436.

Andre, A., Haghani, R., Biel, A. (2012) Application of fracture mechanics to predict the failure load of adhesive joints used to bond CFRP laminates to steel members, *Construction and Building Materials*, V. 24, No. 1, 331–340.

Belingardi, G., Goglio, L., Tarditi, A. (2002) Investigating the effect of spew and chamfer size on the stresses in metal/plastic adhesive joints, *International Journal of Adhesion and Adhesives*, V. 22, 273–282.

Bigwood, D. A., Crocombe, A. D. (1989) Elastic analysis and engineering design formulae for bonded joints, *International Journal of Adhesion and Adhesives*, V. 9, No. 4, 229–242.

Bigwood, D. A., Crocombe, A. D. (1990) Non-linear adhesive bonded joint design analyses, *International Journal of Adhesion and Adhesives*, V. 10, No. 1, 31–41.

Bocciarelli, M., Colombi, P., Fava, G., Poggi, C. (2009) Prediction of debonding strength of tensile steel/CFRP joints using fracture mechanics and stress based criteria, *Engineering Fracture Mechanics*, V. 76, 299–313.

Bogy, D. B. (1971) Two-edge bonded elastic wedges of different materials and wedge angles under surface tractions, *Journal of Applied Mechanics*, V. 38, 377–386.

Cadei, J. M. C., Statford, T. J., Hollaway, L. C., Duckett, W. G. (2004) *Strengthening Metallic Structures Using Externally Bonded Fiber-reinforced Polymers*, C595, London, CIRIA.

Chen, D., Cheng, S. (1983) An analysis of adhesive-bonded single-lap joints, *Journal of Applied Mechanics*, V. 50, No.1, 109–115.

da Silva, L. F. M., Adams, R. D. (2007) Techniques to reduce the peel stresses in adhesive joints with composites, *International Journal of Adhesion and Adhesives*, V. 27, 227–235.

Deng, J., Lee, M. M. K. (2007) Behaviour under static loading of metallic beams reinforced with a bonded CFRP plate, *Composite Structures*, V. 78, 232–242.

Deng, J., Lee, M. M. K., Moy, S. S. J. (2004) Stress analysis of steel beams reinforced with a bonded CFRP plate, *Composite Structures*, V. 65, 205–215.

Goland, M., Reissner, E. (1944) Stresses in cemented joints, *Journal of Applied Mechanics*, V. 11, 17–27.

Haghani, R. (2010) *Behaviour and design of adhesive joints in flexural steel members bonded with FRP laminates*, PhD Thesis, Chalmers University of Technology, Sweden.

Haghani, R., Al-Emrani, M., Kliger, R. (2009) Interfacial stress analysis of geometrically modified adhesive joints in steel beams strengthened with FRP laminates, *Construction and Building Materials*, V.23, No. 3, 1413–1422.

Haghani, R., Al-Emrani, M., Kliger, R. (2010) Effect of laminate tapering on strain distribution in adhesive joints: Experimental investigation, *Journal of Reinforced Plastics and Composites*, Vol. 29, No.7, 972–985.

Hart-Smith L. J. (1973a) *Adhesive-bonded Double-lap joints*, NASA Langley Research Center Technical Report NASA-CR-112235, Washington, DC, National Aeronautics and Space Administration.

Hart-Smith L. J. (1973b) *Adhesive-bonded Single-lap joints*, NASA Langley Research Center Technical Report NASA-CR-112236, Washington, DC, National Aeronautics and Space Administration.

Hein, V. L., Erdogan, F. (1971) Stress singularities in a two-material wedge, *International Journal of Fracture Mechanics*, V. 7, No. 3, 317–330.

Hildebrand, M. (1994) Non-linear analysis and optimization of adhesively bonded single lap joints between fibre-reinforced plastics and metals, *International Journal of Adhesion and Adhesives*, V. 14, No. 4, 261–267.

Linghoff, D. (2009) *Steel members strengthened with carbon fibre reinforced polymers*, PhD thesis, Chalmers University of Technology, Sweden.

Malek, A. M., Saadatmanesh, H., Ehsani, M. R. (1998) Prediction of failure load of R/C beams strengthened with FRP plate due to stress concentration at the plate end, *ACI Structural Journal*, V. 95, No. 1, 142–152.

Oplinger, D. W. (1994) Effects of adherend deflections in single lap joints, *International Journal of Solids and Structures*, V. 31, No. 18, 2565–2587.

Rabinovich, O., Frostig, Y. (2000) Closed-form high-order analysis of RC beams strengthened with FRP strips, *ASCE Journal of Composites for Construction*, V. 4, No. 2, 65–74.

Roberts, T. M. (1989) Approximate analysis of shear and normal stress concentrations in the adhesive layer of plated RC beams, *The Structural Engineer*, V. 67, No. 12, 229–233.

Roberts, T. M., Haji-Kazemi, H. (1989) Theoretical study of the behaviour of reinforced concrete beams strengthened by externally bonded steel plates, *Proceedings of Institution of Civil Engineers*, V. 87, Part 2, 39–55.

Shen, H. S., Teng, J. G., Yang, J. (2001) Interfacial stresses in beams and slabs bonded with a thin plate, *Journal of Engineering Mechanics*, V. 127, No. 4, 399–406.

Smith, S. T., Teng, J. G. (2001) Interfacial stresses in plated beams, *Engineering Structures*, V. 23, 857–871.

Teng, J. G, Zhang, J. W., Smith, S. T. (2002) Interfacial stresses in reinforced concrete beams bonded with a soffit plate: a finite element study, *Construction and Building Materials*, V. 16, 1–14.

Tsai, M. Y., Morton, J. (1994) An evaluation of analytical and numerical solutions to the single-lap joint, *International Journal of Solids and Structures*, V. 31, No. 18, 2537–2563.

Tsai, M. Y, Morton, J. (1995) The effect of a spew fillet on adhesive stress distribution in laminated composite single-lap joints, *Composite Structures*, V. 32, 123–131.

Tsai, M. Y., Oplinger, D. W., Morton, J. (1998) Improved theoretical solutions for adhesive lap joints, *International Journal of Solids and Structures*, V. 35, No. 12, 1163–1185.

Vallee, T., Keller, T. (2006) Adhesively bonded lap joints from pultruded GFRP profiles Part 3: Effects of chamfers, *Composites part B: Engineering*, V. 37, 328–336.

Vilnay, O. (1988) The analysis of reinforced concrete beams strengthened by epoxy bonded steel plates, *International Journal of Cement Composites and Lightweight Concrete*, V. 10, No. 2, 73–78.

Volkersen, O. (1938) Die Nietkraftverteilung in zugbeanspruchten Niet verbindungen mit konstanten Laschenquerschnitten. *Luftfahrtforschung*, V. 15, 41–47.

Wendel, S., Luke, S. (2007) Interface failure mechanics of elastically (advanced composite) reinforced steel members, *Journal of Structural Engineering*, ASCE, May, 683–694.

Wu, Z. J., Wardenier, J. (1997) Stress expressions of single-lap adhesive joints of dissimilar adherends, *Composite Structures*, V. 38, No. 1–4, 273–280.

Yang, J., Teng, G. J., Chen, J. F. (2004) Interfacial stresses in soffit-plated reinforced concrete beams, *Proceedings of Institution of Civil Engineers*, V. 157, No. 1, 77–89.

# 4

# Durability of steel components strengthened with fiber-reinforced polymer (FRP) composites

M. DAWOOD, University of Houston, USA

**DOI**: 10.1533/9780857096654.1.96

**Abstract**: Fiber-reinforced polymer (FRP) materials are gaining prominence as an alternative to traditional materials and methods for repair and rehabilitation of existing steel structures. This chapter describes the primary environmental degradation mechanisms of steel structures that are strengthened with externally bonded FRP materials with an emphasis on carbon FRP (CFRP). Specifically, galvanic corrosion, degradation of the steel–adhesive interface and degradation of the bulk adhesive are discussed in detail. The effects of thermally-induced stresses and exposure to moisture are summarized. Best practices to enhance the environmental durability of FRP-strengthened steel members are also presented. Overall, this chapter indicates that, based on an understanding of the predominant environmental degradation mechanisms, FRP systems can be designed and detailed to provide an effective long-term system for the repair and rehabilitation of existing steel structures.

**Key words**: galvanic corrosion, moisture diffusion, thermal stresses, organosilanes, bond.

## 4.1 Introduction

The effectiveness of using externally bonded fiber-reinforced polymer (FRP) materials to enhance the strength and stiffness of flexural members has been well documented (Colombi and Poggi, 2006; Dawood *et al*., 2007; Miller *et al*., 2001; Schnerch and Rizkalla, 2008; Sen *et al*., 2001; Tavakkolizadeh and Saadatmanesh, 2003). Recent research findings also indicate that externally bonded FRP can be used to stabilize slender compression members such as columns (Shaat and Fam, 2007) and plate elements (Okeil *et al*., 2009) thereby increasing their strength, and/or their post-buckling displacement capacity. All of these applications depend on the integrity of the bonded interface to transmit forces between the steel member and the FRP repair materials. In addition, when carbon fiber-reinforced polymers (CFRP) are used, the possibility for galvanic corrosion must also be considered. Therefore, the long-term durability of FRP-strengthened steel members should be carefully considered. The need to consider durability is

particularly critical for applications in which the repaired members will be exposed to environmental factors in service such as in bridge or marine applications.

This chapter summarizes the primary environmental degradation mechanisms that affect steel members rehabilitated with externally bonded FRP materials. The mechanisms of degradation are presented and the implications on the serviceability and ultimate capacity of strengthened structures are discussed. Techniques to enhance the durability of the repaired members are presented based on the findings of the published research and the generally accepted best practice.

The chemical and physical mechanisms that cause the environmental degradation of steel members reinforced with externally bonded FRP are quite complex. As such, the specific degradation rates, and in many cases the predominant mechanisms of corrosion, are sensitive to many factors including the specific formulation of the adhesive used, the surface preparation techniques, the fabrication method used to produce the FRP reinforcements and the exposure conditions. Therefore, the discussion presented herein is general in nature and is not intended to be universally applicable to all types of strengthening materials, adhesives, surface preparation techniques or environmental exposure conditions. In fact, some mechanisms which may be particularly severe for a specific strengthening system in one application may have little or no effect on the durability of another type of system in another application. For a more detailed discussion, the interested reader is directed to the references cited in this chapter and to other references available in the published technical or commercial literature on the topic.

## 4.2 Basic degradation mechanisms

Steel structures that are strengthened with externally bonded FRP materials are susceptible to three primary degradation mechanisms: galvanic corrosion, interfacial degradation and degradation of the bulk adhesive. Since steel and carbon have significantly different electrical potentials, early studies on environmental durability focused specifically on the possibility of accelerated corrosion of the steel member due to galvanic coupling with the carbon fibers. The primary concern in this case was that bonding CFRP directly to the steel member would induce a galvanic current thereby accelerating the degradation of the competent structural steel. Consequently, galvanic corrosion could potentially decrease the serviceable life of the structure. Therefore, considerable research effort was expended to characterize the corrosion behavior of steel bonded to CFRP. The research indicates that CFRP-based strengthening systems, when properly detailed, exhibit a minimal risk for inducing galvanic corrosion.

The adhesives that are used to bond FRP materials to steel structures are susceptible to degradation of their mechanical properties due to exposure to environmental conditions. Adhesive degradation can occur due to absorption of moisture, or exposure to elevated temperatures. A reduction in the strength of the adhesive could reduce the load-carrying capacity of the strengthened member. Similarly, thermally-induced bond stresses could reduce the load-carrying capacity of the strengthened member since less of the strength of the adhesive is available to resist mechanically-applied loads. Further, softening of the adhesive could reduce the effectiveness of the adhesive in transmitting stresses to the FRP strengthening materials. All of these factors should be considered when selecting a suitable adhesive for a proposed strengthening application.

In repair applications, FRP reinforcing materials are typically bonded to steel surfaces using organic polymers, epoxies being most common. However, steel surfaces are inorganic. Consequently, the organic adhesives do not typically form primary chemical bonds with the inorganic steel surface. Rather, bond is achieved by secondary forces such as van der Waals forces, or by adsorption or by mechanical interlock. Therefore, the interface between FRP strengthening materials and steel surfaces is susceptible to moisture ingress which displaces these weaker bonding forces and could compromise the integrity of the bonded interface. Proper surface preparation and pre-treatment is an important factor in maintaining the long-term durability of FRP-strengthened steel structures.

## 4.3 Galvanic corrosion

### 4.3.1 Fundamental principles

Galvanic corrosion is an electrochemical process that occurs when electrons can flow freely between two different materials with sufficiently different electrical potentials. In order for galvanic corrosion to occur, four factors must be present as illustrated in Fig. 4.1:

1. two metals (or semi metals) with sufficiently different electrical potentials to drive a current;
2. an electrical connection between the two materials;
3. an electrolyte bridging the two materials;
4. a sustained reaction at the cathode (in structural applications this typically requires the presence of dissolved oxygen in the electrolyte).

Electrical half-cell potential can be defined as the voltage difference between a given material and a standard reference electrode, such as hydrogen or calomel. The potential difference between two materials is, thus, the difference between their respective half-cell potentials. Some

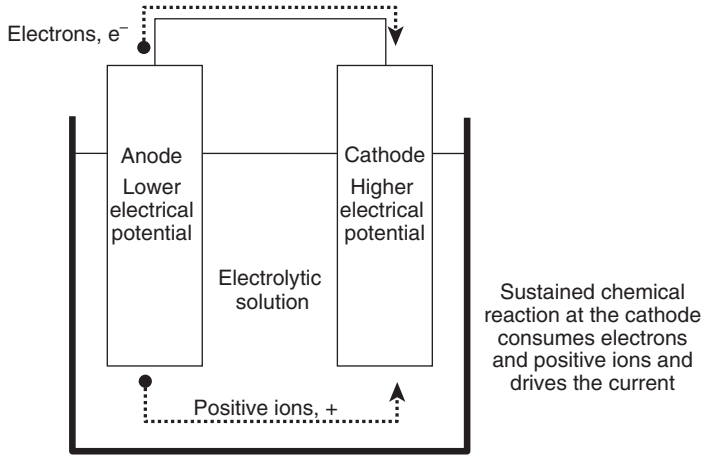


*4.1* Schematic representation of a galvanic couple.

references indicate that in order for two materials to drive a galvanic current, the electrical potential difference between them should be at least 100 mV (Vargel, 2004). In the presence of the other three factors, the material with the lower (more negative) electrical potential becomes the anode and the material with the higher (more positive) electrical potential becomes the cathode. When the two materials are coupled, the anode loses electrons to the cathode and releases positive ions into the electrolyte. This coupling accelerates the corrosion rate of the anode and reduces the corrosion rate, or halts corrosion altogether, of the cathode. Research indicates that the potential difference between carbon (coated with a thin layer of epoxy) and steel submerged in different electrolytes is between 500 and 700 mV with the steel being more electronegative (anode) and the carbon being less electronegative (cathode) (Tavakkolizadeh and Saadatmanesh, 2001). This electrical potential difference is sufficient to drive a galvanic current which could accelerate the corrosion of the steel if the remaining three conditions are met.

For steel structures strengthened with CFRP that are exposed to environmental factors, the presence of an electrolyte which bridges the two materials can reasonably be expected. For example, in marine applications, or for partially submerged structures, the presence of seawater or fresh water containing dissolved salts or minerals could provide an appropriate medium for the necessary ion exchange between the steel and CFRP to occur. Similarly, in bridge applications, the use of de-icing solutions could provide an electrolytic medium that would facilitate galvanic corrosion of the steel. In exposed structures, rainwater ponded on or around structural

steel members or surface moisture could also act as an electrolyte. Therefore, for CFRP-strengthened structures exposed to environmental factors, particular care should be taken to minimize the possibility of galvanic corrosion. Similarly, in some industrial or commercial structures, such as chemical plants and food-processing plants, exposure to electrolytes is likely. In contrast, in many interior applications, such as in schools, office buildings or hospitals, exposure to electrolytes is minimal and intermittent, if any. As such, in these applications, the likelihood of galvanic corrosion is inherently low.

When electrolytes are present, a sustained cathodic reaction must proceed in order to sustain the high rate of corrosion of the anodic material. If a cathodic reaction cannot be sustained, the positive ions and the electrons that are released from the anode cannot be consumed at the cathode. Consequently, the rate of corrosion gradually decreases. In structural applications, the sustained cathodic reaction typically involves consumption of dissolved oxygen. Consequently, the likelihood of galvanic corrosion is higher for structures that are exposed to repeated cycles of wetting and drying such as in splash zones, around bridges or in structures exposed to rainwater or melt runoff. In contrast, structures that are permanently submerged are less likely to experience galvanic corrosion since the dissolved oxygen necessary to drive the cathodic reaction can be quickly consumed. Often the structures that are most in need of repair are those structures that are most susceptible to galvanic corrosion due to repeated wetting and drying. In these applications, care must be taken to minimize the likelihood of galvanic corrosion, for example by preventing an electrical connection between the steel and the CFRP or by coating the structure, to maximize the longevity of the intervention.

### 4.3.2 Preventing galvanic corrosion

In order to prevent galvanic corrosion from occurring in steel structures that are reinforced with externally bonded CFRP, it is necessary to eliminate one or more of the factors that are necessary for galvanic corrosion to occur. Due to their stiffness, steel structures should be repaired or strengthened with stiff repair materials. As such, when considering repair with FRP materials, the use of CFRP materials, with their higher moduli, is typically preferred from the perspective of structural efficiency. Since CFRP composites are preferred for strengthening steel structures, little can be done to reduce the electrical potential difference between the existing steel and the repair materials. One notable difference is in applications where FRP materials are used to increase the stability of slender plate elements. In these applications, research indicates that pultruded GFRP elements can be bonded to the structure to delay plate buckling (Okeil *et al.*, 2009).

Further, in most typical outdoor exposure conditions the presence of an electrolyte, and the presence of dissolved oxygen in the electrolyte, can reasonably be expected. It is, therefore, difficult to reliably eliminate the possibility of a sustained cathodic reaction in the presence of an electrolyte. This leaves two options to minimize the possibility of galvanic corrosion: (i) electrically isolating the steel and CFRP materials; or (ii) preventing exposure to an electrolyte by coating the repaired structure.

Determining an effective method of electrically isolating CFRP materials that are bonded to steel structures has been the topic of considerable research attention. Some researchers suggest that the presence of the adhesive layer between the steel and the CFRP provides adequate electrical insulation to prevent galvanic coupling of the two materials. On the other hand, some other researchers recommend embedding a non-structural layer of glass fibers in the adhesive to provide a more reliable barrier against electrical contact.

In an early research study, the potential for galvanic corrosion between carbon fibers and structural steel in different electrolytes was studied (Tavakkolizadeh and Saadatmanesh, 2001). In that study, small samples of carbon fibers were prepared by coating them with different thicknesses of an adhesive resin. The fibers were coupled to A36 steel plates and submerged in two different electrolytes: simulated seawater with a salt concentration of 3.5 % by weight and a de-icing solution with a salt concentration of 7 % by weight. The possibility for galvanic corrosion was evaluated by measuring the current density of the steel–CFRP couples with different thicknesses of adhesive coatings ranging from 0.1 to 0.25 mm as shown in Fig. 4.2. The results indicate that the current densities of steel coupled to uncoated carbon fibers were significantly higher than that of uncoupled steel in both electrolyte solutions. However, the presence of a relatively thin layer of epoxy adhesive on the surface of the carbon fibers (0.25 mm thick) reduced the galvanic current density of the couple by 95 % to $0.2 \times 10^{-6}$ A/mm$^2$ in both electrolytes as illustrated in Fig. 4.2. This is comparable to the current densities of plain steel which were measured as $0.04 \times 10^{-6}$ A/mm$^2$ and $0.09 \times 10^{-6}$ A/mm$^2$ in simulated seawater and de-icing solution respectively.

In a similar study, the galvanic current of CFRP composites with and without multiwalled carbon nanotubes (MWCNT) embedded in the resin matrix was evaluated (Arronche *et al.*, 2013). The CFRP composites were fabricated using a hand layup technique similar to that used for many structural strengthening applications. This fabrication technique typically results in complete encapsulation of the carbon fibers in a thin layer of epoxy resin, although the thickness of the resin coating was not reported. The CFRP composites with and without MWCNT were coupled to steel and submerged in a 2 % by weight sodium chloride solution. The

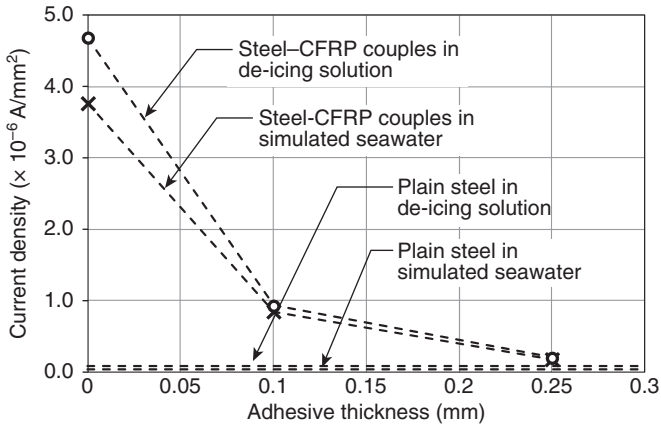


*4.2* Effect of adhesive thickness on galvanic current density (after Tavakkolizadeh and Saadatmanesh, 2001).

presence of the highly conductive MWCNT in the composite resin was expected to significantly increase the corrosion rates of the galvanically coupled steel. The average current densities of the steel coupled to CFRP with and without MWCNT were found to be $2.7 \times 10^{-9}$ A/mm$^2$ and $1.6 \times 10^{-9}$ A/mm$^2$, respectively. This confirms the findings of the previous study that suggest that a thin layer of epoxy resin can provide an effective electrical barrier between steel and CFRP materials.

Some researchers recommend embedding a layer of non-structural glass fibers within the adhesive between the steel and the CFRP to provide an added degree of protection against electrical contact between the two materials (West, 2001; Photiou *et al.*, 2006). This is particularly recommended for the case when air voids may form in the adhesive layer which could potentially increase the chance for direct contact between the carbon fibers and the steel surface. In a recent study, steel–CFRP double-lap shear coupons with and without an intermediate glass fiber layer were fabricated and exposed to a 5 % by weight sodium chloride solution at 100 °F (Dawood and Rizkalla, 2010). The exposure of the coupons was cycled, one week wet and one week dry, to sustain the cathodic reaction. At the conclusion of the environmental exposure program, the double-lap shear coupons were tested to determine the residual capacity of the bonded joints. Both sets of joints exhibited a reduction in the bond strength of 55–60 % compared to the original, unconditioned control joints regardless of the presence or absence of the intermediate glass fiber layer. This suggests that the glass fiber layer had little effect on the durability of the system. The results also suggested that moisture may have wicked along the

partially saturated glass fibers. This could potentially adversely affect the durability of the system under longer exposure times.

In addition to electrically isolating the steel and CFRP materials, coating the strengthened member with an impermeable coating could potentially prevent exposure to electrolytic solutions. An early study of the durability of aerospace metals bonded to carbon fiber composites indicated that steel specimens coated with an epoxy-based paint did not exhibit any notable corrosion after exposure to environmental conditioning (Brown, 1974). Practical experience indicates that protective coatings on exposed steel structures typically require significant maintenance and regular reapplication to maintain their integrity.

## 4.4 Degradation of the bulk adhesive

### 4.4.1 Susceptibility to moisture

It is widely recognized that polymeric adhesives absorb moisture from the surrounding environment. Research indicates that the moisture absorption rate of different types of polymeric adhesives can be described using a Fickian diffusion law (Hand *et al*., 1991; Lapique and Redford, 2002; Nguyen *et al*., 2012). These studies demonstrate that the diffusion coefficients and steady state moisture content generally depend on the exposure conditions, ambient temperature and type of polymer being considered. Other testing indicates that the initial Fickian diffusion stage is followed by an equilibrium state and a tertiary stage of accelerated diffusion (de Nève and Shanahan, 1992). The absorption of moisture has several effects on the mechanical characteristics of the adhesive. Absorption of moisture can lead to swelling of the adhesive which in turn can lead to a relaxation of the applied tensile stresses or an increase of the applied compressive stresses in a fixed strain condition. Further, the presence of moisture in the adhesive can lead to a reduction in the elastic modulus and ultimate strength and an increase in the plastic strain of the adhesives. These often competing effects can significantly influence the long-term performance of the bond between steel structures and FRP strengthening materials.

In one study, the effect of moisture absorption on the properties of six different adhesives was evaluated (Hand *et al*., 1991). Adhesive films with a thickness of 2.5 mm were submerged in water at room temperature and their weight gain was monitored. The films approached their steady-state moisture content within only a few days. After 21 days of exposure, the different adhesives tested exhibited weight gains due to moisture absorption ranging from 2 to 7 % of the dry film weights. Under 90 % relative humidity exposure conditions at 50 °C, a similar trend was observed; however, the equilibrium moisture content was approximately half that of

the fully submerged cases. In the same study, additional tests were conducted to evaluate the stress relaxation due to creep of the adhesive after saturation. For the adhesives tested, under a constant applied strain of 6 %, the reported stress relaxation due to creep was between 50 and 90 % of the initial stress level. Exposure to moisture also reduced the ultimate strength of the adhesives by up to 70 %. Thus, the strength reduction of an adhesive due to moisture absorption may be counteracted by the relaxation of stresses due to viscoplastic or creep effects. The testing indicated that adhesives with different formulations exhibited widely different performance under moisture exposure conditions. While exposure to moisture rendered some of the adhesives essentially unusable for structural purposes, others exhibited very good moisture resistance. Other researchers have observed a moderate reduction of adhesive strength and stiffness, in the range of 10–20 %, due to exposure to moist conditions (Knox and Cowling, 2000).

In contrast, some research indicates that moisture absorption has a minimal effect on the mechanical properties of some structural adhesives. In one study, four different adhesives, two acrylics and two epoxies, were exposed to different environmental conditions, including submersion in distilled water and dilute sodium chloride solutions for up to 500 hours (Horton *et al.*, 1992). Three of the tested adhesives exhibited a trend of increasing weight gain due to moisture absorption. The fourth adhesive exhibited an initial weight gain, attributed to moisture absorption, followed by a weight loss, attributed to leaching of soluble compounds out of the adhesive. Mechanical tests indicated that the mechanical properties of the adhesive were essentially unaffected by the exposure despite the apparent absorption of moisture. In another study, dynamic mechanical analysis of a structural epoxy indicated that environmental exposure to 100 % relative humidity at 70 °C for 1260 hours resulted in only a 5 % reduction of the elastic modulus of the adhesive, although the glass transition temperature decreased from 126 to 77 °C (de Nève and Shanahan, 1992).

A recent study indicates that, for a specific set of CFRP–steel double lap-joints, the degradation of bond strength can be attributed primarily to the degradation of the adhesive properties due to exposure to moisture for durations up to 12 months (Nguyen *et al.*, 2012). In that study, a Fickian diffusion law was proposed to represent the absorption of moisture by the adhesive and a power law was proposed to represent the degradation of the adhesive strength and modulus with exposure time. Testing of companion double-lap shear joints indicated that the magnitude of the bond strength degradation was comparable to the magnitude of deterioration of the tensile strength of the bulk adhesive under similar exposure conditions.

In contrast, tests by several other researchers suggest that the degradation of bonded joints cannot be attributed only to the degradation of the adhesive

properties (Horton *et al.*, 1992; Knox and Cowling, 2000; Dawood and Rizkalla, 2010). In all of these studies, bulk adhesive tensile specimens and companion bonded lap joints were fabricated, conditioned and tested to determine their residual strengths. In all cases, the percentage reduction of the bond strength of the lap joints was greater than that of the tensile strength of the bulk adhesive. This suggests that while degradation of the adhesive strength may have contributed to the degradation of the bonded joint, another mechanism must also have contributed to the measured reduction of the bond strength. Inspection of the failed bonded joints typically revealed the ingress of moisture into the interfacial region between the adhesive and the bonded substrate which was evidenced by the presence of physical moisture or corrosion products at the interface. A discussion of the mechanisms and effects of interfacial degradation is presented later in this chapter.

### 4.4.2 Thermally-induced stresses and degradation

In addition to the influence of moisture on the mechanical properties and overall durability of steel structures strengthened with FRP, thermal fluctuations can cause deterioration of the mechanical properties of structural adhesives. Additionally, the thermal mismatch between the adherends can result in thermally-induced stresses due to differential thermal expansion and contraction of the adherends with different coefficients of thermal expansion. It is well documented that the polymeric adhesives typically used in steel strengthening applications exhibit a glass transition temperature (Al-Shawaf, 2011; Stratford and Bisby, 2012). Below this transition temperature, the adhesives can be considered to demonstrate a 'glassy' behavior. In this state, the adhesives are stiff and typically exhibit minimal plastic deformation prior to brittle fracture. At temperatures above the glass transition temperature the adhesives can be said to be in a 'rubbery' state. In this state, the elastic modulus is significantly lower, often an order of magnitude less, than in the 'glassy' state. 'Rubbery' adhesives are also typically much weaker than 'glassy' adhesives and usually exhibit significant plastic strain prior to failure.

Analytical models have been proposed to predict the elastic bond stresses in steel beams strengthened with externally bonded FRP plates (Schnerch, 2005; Stratford and Cadei, 2006). These analyses indicate that the thermally-induced bond stresses in steel beams strengthened with externally bonded FRP plates can be comparable to the stresses induced by mechanical loading under service load conditions. However, these analyses are typically based on the room temperature elastic properties of the adhesive and do not account for the change in the mechanical properties of the adhesive due to the associated change in temperature.

More recently, the influence of the variation of adhesive properties at elevated temperatures on the bond behavior of CFRP–steel lap joints was investigated both experimentally and analytically (Nguyen *et al*., 2011). Experimental results clearly indicate that the strength and stiffness of bonded joints decrease dramatically with increased temperature. This trend was attributed to the degradation of the material properties of the adhesive at elevated temperatures. The measured reduction of the normalized stiffness of the bonded joints closely matched the reduction of the normalized elastic modulus of the adhesive (Nguyen *et al*., 2011). Further, the bond strength of the tested joints at 20 °C above the measured glass transition temperature dropped to only 20 % of the bond strength of the same specimen configurations measured at room temperature. This reduction in strength was attributed to the reduction in the adhesive strength at elevated temperatures but also to the reduction in the adhesive stiffness which results in a redistribution of the bond stresses for relatively short adhesive joints.

Another study demonstrated that the bond behavior of steel–CFRP bonded joints at elevated temperatures can be predicted using a coupled, non-linear, thermomechanical finite element analysis (Al-Shawaf, 2011). In that study, it was proposed that failure can be predicted using a maximum principal stress failure criterion for bonded joints tested below the adhesive's glass transition temperature for which the adhesive exhibited an essentially linear and elastic response. In contrast, for bonded joints tested above the adhesive's glass transition temperature, the von-Mises failure criterion is recommended since, at these temperatures, the adhesives typically fail in a ductile mode.

Recent tests of steel beams strengthened with CFRP plates and subjected to sustained loads at elevated temperatures demonstrate that this loading combination can lead to debonding failure of the strengthened members (Stratford and Bisby, 2012). Under the effect of sustained load, softening of the adhesive at elevated temperatures results in relative slip between the steel beam and the strengthening plate. Additionally, the thermal mismatch of the materials induces additional bond stresses in the adhesive layer. The reduction of the adhesive strength at elevated temperatures can lead to debonding of the FRP due to the combined thermally- and mechanically-induced bond stresses at temperatures near or above the glass transition temperature of the adhesive. Based on this testing, an analytical model was proposed to predict the distribution of shear stresses in the adhesive layer due to mechanical and thermal loads. The model implements a simplified elastic–perfectly plastic constitutive relationship to account for the change in the material properties of the adhesive at elevated temperatures.

Based on these experimental and analytic studies, it is generally recommended that the service temperature of strengthened structures

should remain well below the glass transition temperature of the adhesive used in the strengthening application. However, further research is needed in this area before broadly applicable design recommendations can be established.

## 4.5 Degradation of the steel/adhesive interface

### 4.5.1 Surface chemistry

Four main theories of adhesion have been proposed to describe the mechanisms of adhesion between different surfaces (Adams, 2005; Harries and Dawood, 2012):

- *Physical adsorption*. This mechanism is predominant when the adhesive used has sufficiently low surface energy to effectively 'wet' the mating surface. When the free energy of the surface to be bonded is sufficiently high, a fluid with a lower surface tension can spread out making intimate contact with the surface. The free energy of a metallic surface can be increased by proper surface preparation which includes removing weakly adhered oxide layers and chemical contaminants. Adhesive forces are achieved through secondary molecular forces, such as van der Waals forces, which act over a short distance away from the interface. Adhesive bonding to metallic surfaces is largely attributed to this mechanism which is discussed in more detail below.
- *Chemical bonding*. This mechanism is similar to physical adsorption but implies the formation of stronger primary chemical bonds. The organic polymers that are used in typical structural applications do not typically form primary chemical bonds with inorganic, metallic surfaces. However, primary chemical bonding can be achieved if a properly formulated primer is applied to the surface. This is the principle behind the use of organosilane coupling agents, discussed later.
- *Electrostatic attraction*. An electrostatic double layer forms when a surface is placed in a liquid. Two layers of molecules in the liquid with opposite charges arrange themselves preferentially at the interface due to the electrostatic charge at the surface. This bonding mechanism does not typically play a significant role in structural bonding, particularly after the adhesive has cured.
- *Mechanical interlocking*. Bond is achieved by transmission of force through friction along rough interfaces. Rougher surfaces, such as grit blasted metals, generally provide better interlock than smooth surfaces, such as polished metals. A low viscosity adhesive can flow into pores, crevices or cracks in the surface. The cured adhesive then provides a mechanical means to transmit forces across the interface, similar to a series of small shear keys.

The bond between epoxy adhesives and steel surfaces can be attributed to adsorption. The theory suggests that adhesion is due to van der Waals forces between molecules across the interface at two different materials (Owens, 1970). Van der Waals forces are weak, short-ranged intermolecular forces. According to the physical adsorption theory, the thermodynamic work of adhesion, $W_A$, between two materials, B and C, is the energy required to separate the interface into two separate surfaces. This work is given by:

$$W_A = \gamma_B + \gamma_C - \gamma_{BC}$$

where $\gamma_B$ = free energy of surface B, $\gamma_C$ = free energy of surface C and $\gamma_{BC}$ = interfacial free energy between the two adhered surfaces. If this energy is positive, the bonded surface is stable. If this energy is negative, the bonded surface is unstable which could lead to debonding. If the debonding occurs in the presence of a liquid, the values $\gamma_B$ and $\gamma_C$ should be replaced by corresponding values for the submerged surfaces, $\gamma_{BL}$ and $\gamma_{CL}$, respectively. These are typically less than their 'dry' counterparts. A series of tests was conducted to validate this theory (Owens, 1970). Polypropylene films were coated with different polymers. The cured samples were submerged in different liquid surfactants. When the calculated work of adhesion, $W_A$, was negative, the polymer debonded from the polypropylene film after submersion in the liquid.

Other sources indicate that, for epoxy/steel interfaces in the presence of water, the thermodynamic work of adhesion is negative (Adams, 2005). This suggests that the bond is unstable in the presence of water and, thus, exposure to moisture may lead to debonding. In order to achieve competent bond to steel surfaces, the surface must be adequately prepared. This typically involves degreasing and mechanically removing weakly adhered oxide layers (Davis and Bond, 1999). This surface preparation generates a surface with a high free energy that is suitable for bonding with epoxy adhesives. However, this approach also renders the surface hydrophilic. Therefore, a surface which is chemically active and suitable for bonding may also attract moisture into the bond interface thereby reducing the interfacial free energy. As such, application of a properly selected chemical pre-treatment or primer is also recommended to enhance the moist durability of the bonded interface (Davis and Bond, 1999).

### 4.5.2 Organosilane adhesion promoters

Organosilanes are monomeric silicone-based chemicals, similar to hydrocarbons, which have at least one direct bond between a silicon atom and a carbon atom in the molecule (de Buyl, n.d.). The structure of a typical

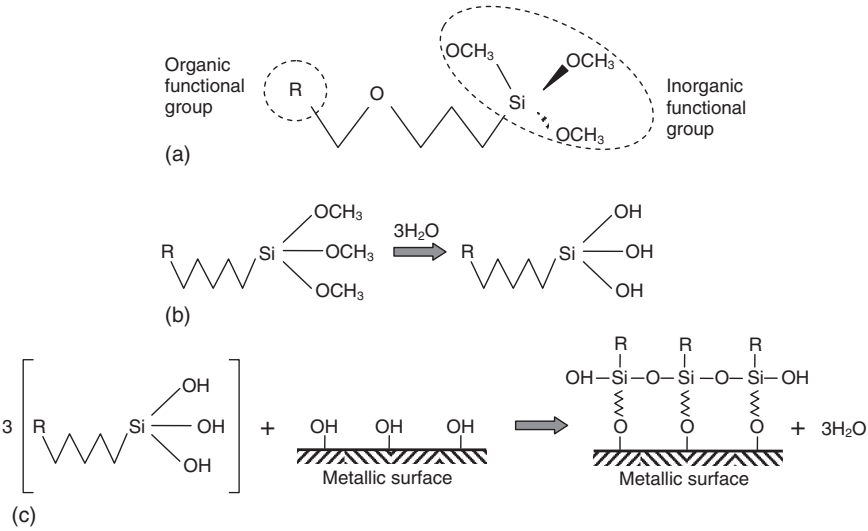


*4.3* (a) Schematic of an organosilane monomer. (b) Hydrolysis of silane monomer. (c) Condensation and covalent bonding to inorganic substrate (adapted from de Buyl, n.d.).

organosilane molecule is shown in Fig. 4.3a. Organosilane monomers consist of an organic functional group and an inorganic functional group that are both attached to a silicon atom. The inorganic functional group reacts with inorganic surfaces, such as metals or glass, by hydrolysis, condensation and covalent bonding as illustrated in Figs. 4.3b and 4.3c. This results in the formation of a stable polymeric siloxane network on the surface of the inorganic substrate. The organic functional group should be selected to match the reactivity of the organic adhesive being used. Consequently, the resin reacts with the organic functional groups forming a well-bonded interpenetrating network with the siloxane coupling agent. The resulting chemical interface is more stable, and therefore more resistant to moisture ingress, than the secondary van der Waals forces that would cause adhesion to the untreated steel surface. Therefore, properly selected organosilane primers can be used to significantly enhance the moist durability of steel structures retrofitted with externally bonded FRP materials.

Silanes can be used in several different ways: applied to a surface directly as a pre-treatment, as a part of a formulated primer, or as an additive to an adhesive (Walker, 1991). The optimum method of application depends on the type of silane being used, the nature of the substrate and the nature of the coating or adhesive. A comprehensive experimental study was conducted to investigate the effect of different silane chemistries and application methods on the bond strength and durability of different coatings bonded

to different substrates (Walker, 1991). The study included a total of eight different silanes, four different coatings (including two paints, one epoxy adhesive and one polyurethane adhesive) and four different substrates (steel, stainless steel, aluminum and glass). The silanes were applied using one of two methods, direct application to the surface in a dilute solution, or as an additive to the adhesives or coatings. For the specific case of epoxy adhesives bonded to stainless steel surfaces, the use of different organosilanes as a surface pre-treatment increased the bond durability when compared to the untreated case. Stainless steel samples were pre-treated with four different types of organosilanes and bonded with an epoxy adhesive. The specimens were exposed to 100 % relative humidity at 21 °C for 52 weeks. After exposure, the residual bond strength of the samples that were pre-treated with silane was four to six times greater than the residual bond strength of untreated samples. At this stage, the residual strength of the pre-treated specimens stabilized and similar residual strengths were measured after 150 weeks of exposure. In contrast, the trend of the data for the untreated specimens suggests that the bond strength had not yet stabilized after 52 weeks of exposure.

Research indicates that several factors can influence the effectiveness of an organosilane pre-treatment in improving the durability of a bonded joint to metallic substrates (Gledhill *et al*., 1990; Wang and Gupta, 2005; Abel *et al*., 2006). Specific factors that influence the effectiveness of the organosilane pre-treatment include the age of the silane solution at the time of application on the surface, the type of solvent used to prepare the silane solution, the drying time after application, the pH of the solution, silane concentration, drying temperature and the type of inorganic substrate being considered. In one study, a series of mild steel, butt joint specimens were tested to evaluate the effect of various parameters on the bond durability. The steel was grit blasted, solvent cleaned and pre-treated with one of five different organosilanes. Bonded joints were prepared and immersed in 60 °C water for 1500 hours and subsequently tested to determine their residual bond strengths. Specimens that were not treated with silane exhibited a degradation of the bond strength of 85 % after 1500 hours of environmental exposure. The greatest increase of durability was achieved when the silane was mixed in distilled water, applied to the steel surface 30–90 minutes after mixing and allowed to dry at 20 °C. Using this application procedure, the tested joints exhibited essentially no degradation of the bond strength. Specimens prepared with different application times or drying temperatures also exhibited better bond durability compared to the untreated case; however, the benefit was not as significant as that achieved using the optimum parameters. Specimens that were treated with silane that was prepared in an ethanol/water-based solution exhibited essentially no improvement of the durability compared to the untreated specimens.

Other test results indicate a complex interaction between the concentration of a specific type of organosilane, known as γ-glycidoxypropyltrimethoxy silane (γ-GPS), and solution pH (Abel *et al.*, 2006). The general trend indicated that with increased γ-GPS concentration, increasing the solution pH yielded interfaces with the best environmental durability. The results also indicated that better joint durability was achieved when the γ-GPS was mixed in distilled water as compared to solutions prepared with a methanol/water mixture. Alternatively, tests conducted using a different type of organosilane, known as γ-methacryloxypropyltrimethoxysilane (γ-MPS), on steel substrates suggested that increasing the methanol content of the solution enhanced the bond durability (Wang and Gupta, 2005).

In infrastructure applications, the use of γ-GPS applied in a dilute solution as a surface pre-treatment to grit blasted steel in conjunction with an epoxy-based adhesive has yielded an extremely durable interface (West, 2001; Dawood and Rizkalla, 2010). This combination of parameters exhibited the greatest bond durability under both hot–wet and freeze–thaw conditions in a study in which three different types of adhesives, paired with three different types of primers, were compared (West, 2001). In another study, steel–CFRP double-lap joints were prepared using a γ-GPS silane applied to a grit blasted steel surface, and bonded using an epoxy adhesive (Dawood and Rizkalla, 2010). These specimens exhibited essentially no degradation of bond strength after six months of wet/dry cycling in a 5 % NaCl solution at 100 °F. By comparison, specimens prepared using the same bonding technique, but without the silane pre-treatment, exhibited a 60 % reduction in bond strength on average.

In general, no single set of parameters can be universally recommended to maximize the durability for all types of bonded joints to metallic substrates. The type of organosilane and solvent used in the preparation, the concentration of the organosilane and the application technique must all be considered along with the type of adhesive being used and the application conditions. The selection of a suitably formulated organosilane, the mixture parameters and the application procedure should be conducted in consultation with the silane and adhesive manufacturers while considering the specific details of the particular application at hand (Petrie, 2007).

## 4.6 Conclusion and future trends

The extensive body of work that has been conducted related to durability of steel and metallic structures strengthened with FRP has led to a detailed understanding of the basic mechanisms of degradation that can lead to failure of these types of structures. However, these mechanisms, and their interactions, are complex and depend on a wide range of factors. This makes it difficult to reliably predict the behavior of strengthened structures

exposed to environmental factors. Further, the dominant mechanisms of degradation depend on several factors, further complicating the prediction of the long-term performance of strengthened members. While analytical models have been developed to predict the effect of individual degradation mechanisms on the long-term durability of FRP-strengthened metallic structures, reliable and comprehensive deterioration models which account for multiple degradation mechanisms have not yet been established. Additionally, existing models generally treat durability from a deterministic perspective. However, there is significant uncertainty in the long-term behavior of steel and metal structures strengthened with composites. Therefore, a stochastic approach may be more suitable in this case. This is consistent with the trend of code-writing bodies towards the use of reliability-based design methodologies such as the so-called Load and Resistance Factor (LRFD) design method that is widely adopted for civil infrastructure in the USA.

## 4.7 Sources of further information and advice

Strengthening of metal and steel structures with composites is a relatively new area of research in civil infrastructure. As such, it is continually evolving and new developments are being reported on a continual basis. New developments are generally published in internationally recognized technical journals in a timely manner. Additionally, the International Institute of FRP in Construction (IIFC) has an active working group that consists of academics from around the world whose primary research interest is rehabilitation of metallic structures with FRP composites. This group is active in all aspects of this field including the study of environmental durability. The working group compiles a comprehensive, categorized database of available relevant publications on an annual basis.

## 4.8 References

Abel, M., Allington, R. and Digby, R. (2006). Understanding the relationship between silane application conditions, bond durability and locus of failure. *International Journal of Adhesion and Adhesives*, 26(1–2), 2–15.

Adams, R. (2005). *Adhesive Bonding: Science, Technology and Applications*. London: Woodhead Publishing.

Al-Shawaf, A. (2011). Modelling wet lay-up CFRP–steel bond failures at extreme temperatures using stress-based approach. *International Journal of Adhesion and Adhesives*, 31(6), 416–428.

Arronche, L., Gordon, K., Donghyeon, R., La Saponara, V. and Cheng, L. (2013). Investigation of galvanic corrosion between AISI 1018 carbon steel and CFRPs modified with multi-walled carbon nanotubes. *Journal of Materials Science*, 48(3), 1315–1323.

Brown, A. (1974). The corrosion of CFRP-to-metal couples in saline environments. *Proceedings of the 2nd International Conference on Carbon Fibers*, London, 18–20 February, 230–241.

Colombi, P. and Poggi, C. (2006). An experimental, analytical and numerical study of the static behavior of steel beams reinforced by pultruded CFRP strips. *Composites Part B: Engineering*, 37(1), 64–73.

Davis, M. and Bond, D. (1999). Principles and practices of adhesive bonded structural joints and repairs. *International Journal of Adhesion and Adhesives*, 19, 91–105.

Dawood, M. and Rizkalla, S. (2010). Environmental durability of a CFRP system for strengthening steel structures. *Construction and Building Materials*, 24(9), 1682–1689.

Dawood, M, Rizkalla, S. and Sumner, E. (2007). Fatigue and overloading behavior of steel – concrete composite flexural members strengthened with high modulus CFRP materials, *Journal of Composites for Construction*, 11(6), 659–669.

de Buyl, F. (n.d.). Organo-functional silanes. Available at: http://www.dowcorning.com/content/publishedlit/Chapter19.pdf (accessed October 2013).

de Nève, B. and Shanahan, M. E. R. (1992). Effects of humidity on an epoxy adhesive. *International Journal of Adhesion and Adhesives*, 12(3), 191–196.

Gledhill, R., Shaw, S. and Tod, D. (1990). Durability of adhesive-bonded joints employing organosilane coupling agents. *International Journal of Adhesion and Adhesives*, 10(3), 192–198.

Hand, H., Arah, C., McNamara, D. K. and Mecklenburg, M. F. (1991). Effects of environmental exposure on adhesively bonded joints. *International Journal of Adhesion and Adhesives*, 11(1).

Harries, K. A. and Dawood, M. (2012). Behavior and performance of fiber-reinforced polymer-to-steel bond. *Transportation Research Record*, 2313, 181–188.

Horton, T., Spinks, G. and Isles, N. (1992). Structural adhesive performance in marine environments. *Polymer International*, 28(1), 9–17.

Knox, E. and Cowling, M. (2000). Durability aspects of adhesively bonded thick adherend lap shear joints. *International Journal of Adhesion and Adhesives*, 20(4), 323–331.

Lapique, F. and Redford, K. (2002). Curing effects on viscosity and mechanical properties of a commercial epoxy resin adhesive. *International Journal of Adhesion and Adhesives*, 22(4), 337–346.

Miller, T. C., Chajes, M. J., Mertz, D. R. and Hastings, J. N. (2001). Strengthening of a steel bridge girder using CFRP plates. *Journal of Bridge Engineering*, 6(6), 514–522.

Nguyen, T.-C., Bai, Y., Zhao, X.-L. and Al-Mahaidi, R. (2011). Mechanical characterization of steel/CFRP double strap joints at elevated temperatures. *Composite Structures*, 93(6), 1604–1612.

Nguyen, T.-C., Bai, Y., Zhao, X.-L. and Al-Mahaidi, R. (2012). Durability of steel/CFRP double strap joints exposed to sea water, cyclic temperature and humidity. *Composite Structures*, 94(5), 1834–1845.

Okeil, A., Bingol, Y. and Ferdous, M. (2009). Novel technique for inhibiting buckling of thin-walled steel structures using pultruded glass FRP sections. *Journal of Composites for Construction*, 13(6), 547–557.

Owens, D. K. (1970). Some thermodynamic aspects of polymer adhesion. *Journal of Applied Polymer Science*, 14(7), 1725–1730.

Petrie, E. M. (2007). Silanes as primers and adhesion promotors for metal substrates. *Metal Finishing*, 105(7), 85–93.

Photiou, N., Hollaway, L. and Chryssanthopoulos, M. K. (2006). Selection of carbon-fiber-reinforced polymer systems for steelwork upgrading. *Journal of Materials in Civil Engineering*, 18(5), 641–649.

Schnerch, D. A. (2005). *Strengthening of steel structures with high modulus carbon fiber reinforced polymer (CFRP) materials*. PhD Thesis North Carolina State University, Raleigh, NC.

Schnerch, D. and Rizkalla, S. (2008). Flexural strengthening of steel bridges with high modulus CFRP strips. *Journal of Bridge Engineering*, 13(2), 192–201.

Sen, R., Liby, L. and Mullins, G. (2001). Strengthening steel bridge sections using CFRP laminates. *Composites Part B: Engineering*, 32(4), 309–322.

Shaat, A. and Fam, A. (2007). Fiber-element model for slender HSS columns retrofitted with bonded high-modulus composites. *Journal of Structural Engineering*, 133(1), 85–95.

Stratford, T. J. and Bisby, L. A. (2012). Effect of warm temperatures on externally bonded FRP strengthening. *Journal of Composites for Construction*, 16(3), 235–244.

Stratford, T. and Cadei, J. (2006). Elastic analysis of adhesion stresses for the design of a strengthening plate bonded to a beam. *Construction and Building Materials*, 20(1–2), 34–45.

Tavakkolizadeh, M. and Saadatmanesh, H. (2001). Galvanic corrosion of carbon and steel in aggressive environments. *Journal of Composites for Construction*, 5(3), 200–210.

Tavakkolizadeh, M. and Saadatmanesh, H. (2003). Repair of damaged steel-concrete composite girders using carbon fiber-reinforced polymer sheets. *Journal of Composites for Construction*, 5(3), 311–322.

Vargel, C. (2004). *Corrosion of Aluminium*. (M. P. Schmidt, Trans.). Oxford: Elsevier.

Walker, P. (1991). Organosilanes as adhesion promoters. *Journal of Adhesion Science and Technology*, 5(4), 279–305.

Wang, X. and Gupta, V. (2005). Construction and characterization of chemically joined stainless steel/E-glass composite sections. *Mechanics of Materials*, 37(12), 1198–1209.

West, T. (2001). *Enhancement to the bond between advanced composite materials and steel for bridge rehabilitation*, CCM report 2001–04. Newark, DE: University of Delaware Center for Composite Materials, University of Delaware.

# Part II

Application to components

This page intentionally left blank

# 5

# Enhancing the stability of structural steel components using fibre-reinforced polymer (FRP) composites

K. A. HARRIES, University of Pittsburgh, USA

**DOI**: 10.1533/9780857096654.2.117

**Abstract**: The innovative use of fibre-reinforced polymer (FRP) composite materials to control the manifestation of buckling in steel sections is described. The high stiffness and linear behaviour of FRP materials are utilised to provide 'bracing' against local buckling in a way that strategically leverages the unique mechanical properties of each material in an efficient application domain. Such an approach is not aimed at increasing the load-carrying capacity of the steel section, *per se*, although this may certainly be accomplished if desired. Rather, the approach is aimed at providing stability (in the sense of bracing) to the steel section through the use of FRP application to enforce nodal lines in a plate element for the purposes of increasing its critical load and constraining plastic flow in the plate element. The member becomes, in effect, an *FRP-stabilised steel section*.

**Key words**: fibre-reinforced polymer (FRP), elastic buckling, inelastic buckling, stability.

## 5.1 Introduction

The use of fibre-reinforced polymer (FRP) composite materials has become relatively common in infrastructure applications. Most existing applications involve concrete–FRP composite members or FRP-repaired concrete. Nonetheless, a relatively small and innovative body of work is developing focusing on steel–FRP composite structural systems (Teng *et al.*, 2012, Harries and El-Tawil, 2008 and Zhao and Zhang, 2006 all provide overviews of the state-of-the-art). Steel–FRP composite systems are almost exclusively aimed at retrofit methods for the underlying steel material or structure. Applications include strengthening flexural (examples include Sen *et al.*, 2001; Tavakkolizadeh and Saadatmanesh, 2003a; Chacon *et al.*, 2004; Miller *et al.*, 2001; Patnaik and Bauer, 2004; Lenwari *et al.*, 2005, 2006; Colombi and Poggi, 2006a, Photiou *et al.*, 2006) and tension (Jiao and Zhao, 2004; Colombi and Poggi, 2006b) members, repairing fractures and relieving stress to enhance fatigue performance (Jones and Civjan, 2003; Tavakkolizadeh and Saadatmanesh, 2003b; Liu *et al.*, 2005; Nozaka *et al.*, 2005) and enhancing local or member stability. In each application, steel–FRP systems leverage the unique material properties of each material in

establishing a composite member or structure. The present work focuses on applications in which the strategic application of unidirectional or 0/90° bidirectional FRP to a steel compression member results in a degree of buckling restraint, thereby affecting member behaviour and capacity.

FRP composite materials have recently been demonstrated to enhance the stability of steel members. In this application, the high stiffness and linear material behaviour of the unidirectional FRP materials used are utilised to provide 'bracing' that improves the buckling and post-buckling behaviour of steel components. Recent research has demonstrated that the application of FRP reinforcement can lead to improvements in the flange local buckling (FLB), web local buckling (WLB) and flexural torsional buckling (FTB) behaviours of steel members. This application is not aimed at increasing the load-carrying capacity of the steel section, *per se*, although this may certainly be accomplished if desired. Rather, the approach is aimed at providing stability (in the sense of bracing) to the steel section through the use of FRP application to enforce nodal lines in a plate element for the purposes of increasing its critical load and constraining plastic flow in the plate element. The member becomes, in effect, an *FRP-stabilised steel section*.

Stability can refer to local (flange or web) or global (sectional) buckling; both will be addressed in this chapter, the former at great length. Global buckling restraint for structural shapes, although extensively studied, is not viewed as a significant application. Stability enhancement through the application of FRP to steel members is primarily a 'research' topic at this time, with few known applications in practice. The following sections focus on different types of buckling behaviour followed by a discussion of some potential 'design spaces' for FRP-stabilised steel members.

## 5.2 Inelastic section (local) buckling

Current design specifications for steel structures promulgate an approach in which local buckling effects on structural behaviour are considered through the prescription of limiting plate slenderness parameters. In the case of US specifications (AISC, 2010b), plate slenderness limits, $\lambda_p$, for cross-sectional plate components are identified such that satisfaction of these limits will result in an overall flexural cross-section able to accommodate sufficient plastic hinge rotation to support system-wide moment redistribution as required for the development of a global collapse mechanism. In pursuit of this condition, and as a general guiding principle, compactness limits have historically been formulated to loosely accommodate strains approaching strain hardening values within an individual plate component prior to the attenuation of post-buckling strength due to effects of material non-linearity.

The nature of inelastic local buckling effects involves a complex interrelationship between local plate element proportions and overall member geometry (Earls, 2000a) as well as critical aspects of the underlying mechanical response of the steel grade used (Earls, 1999, 2000b). Research clearly points to the fact that complexities associated with garnering well-behaved and ductile plastic hinge response increase dramatically as non-conventional grades (i.e., those having a yield strength greater than 480 MPa) of steel are employed (Greco and Earls, 2003; Thomas and Earls, 2003). It is also noted that, even with the use of conventional structural steel grades (i.e., those having a yield strength between 250 and 480 MPa), control of the manifestation of localised buckling effects leads to dramatic improvements in overall member ductility as needed for well-defined system-wide response.

The interesting point to be made in this context is that the force required to 'brace' plate elements sufficiently against a particular mode is small. As with any classical bracing problem, a small bracing force goes a long way to improving overall structural efficiency and load-carrying capacity. The mismatch in elastic moduli that has scuttled many efforts to employ FRP as a practical strengthening option for structural steel elements is in fact leveraged as being advantageous in providing the necessary bracing force. The fact that the lower-modulus FRP materials being bonded to the plate elements in a steel section are only modestly stressed at the condition of incipient local buckling of the steel plate substrate is a benefit since very little of the FRP material's ability to resist loading is consumed by membrane effects. Thus, essentially the entire FRP flexural capacity remains available for use in effectively bracing the steel plate against local buckling. In this way, FRP strips bonded to steel section plate elements may be notionally viewed as a 'piggy-back' system; they ride along with the steel essentially unstressed until flexural deformations present themselves at incipient buckling.

El-Tawil *et al*. (2011) demonstrated the use of carbon fibre-reinforced polymer (CFRP) wraps to enhance the plastic hinge behaviour of double-channel members subjected to reversed cyclic flexural loads (Fig. 5.1). The specimens were modelled on chord members of a special truss moment frame. Two cases are considered, one in which the entire gross cross-section is wrapped, the second where only the extending flanges are wrapped; both methods exhibited improved behaviour of the hinge as compared to unwrapped specimens. El-Tawil *et al*. report that the presence of the CFRP wrap increased the size of the yielded plastic hinge region, inhibited the occurrence of local buckling and delayed the onset of lateral torsional buckling. These effects resulted in reduced strain demands, increased rotational capacity and improved energy dissipation capacity in the plastic hinge region.

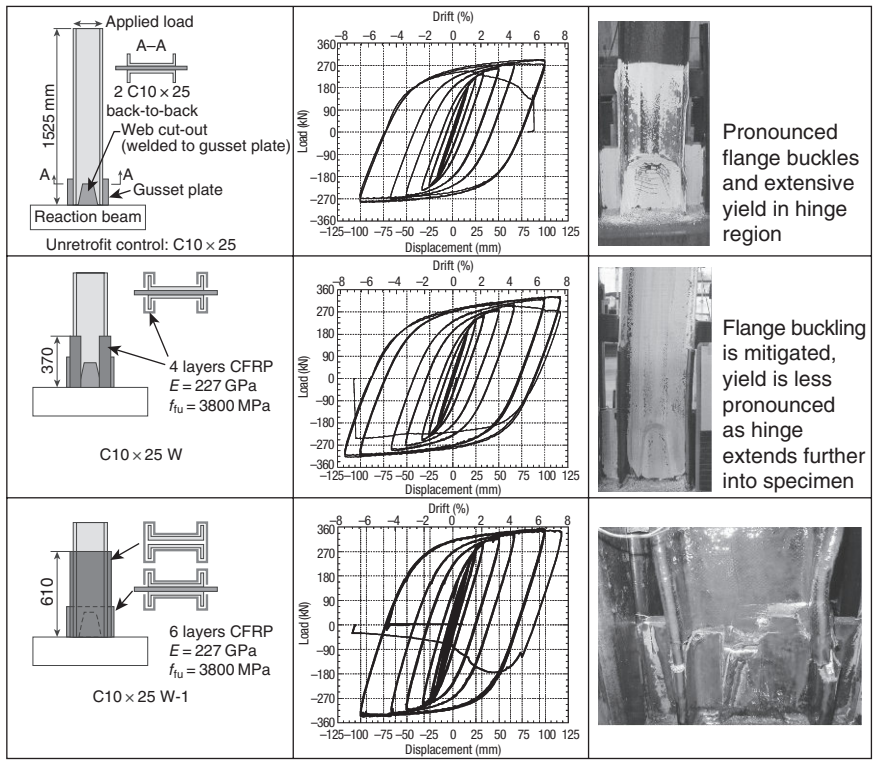


*5.1* Restraint of local buckling using CFRP: (a) specimen schematic; (b) load–displacement response; (c) specimen at approximately 6.5% drift (adapted from El-Tawil *et al.*, 2011).

Accord and Earls (2006) present an analytical study wherein non-linear finite element modelling strategies were employed to examine the effects that bonded low modulus glass fibre-reinforced polymer (GFRP) strips have on the inelastic cross-sectional response of I-shaped sections developing plastic hinges under a moment-gradient loading. The modelling involved the discretisation of the I-section by shell finite elements and the modelling of the GFRP, and the flexible adhesive located along the steel–GFRP interface, using continuum elements. Both geometric and material non-linearity were considered. This work demonstrated that the presence of the GFRP strips enhanced the structural ductility of the cross-section as a result of providing effective bracing of the flange outstands, and thus inhibiting the formation of the local buckles in the compression flange of the cross-section (Fig. 5.2). As the location of the GFRP strips was adjusted to increase their efficacy as bracing elements, a concomitant increase in

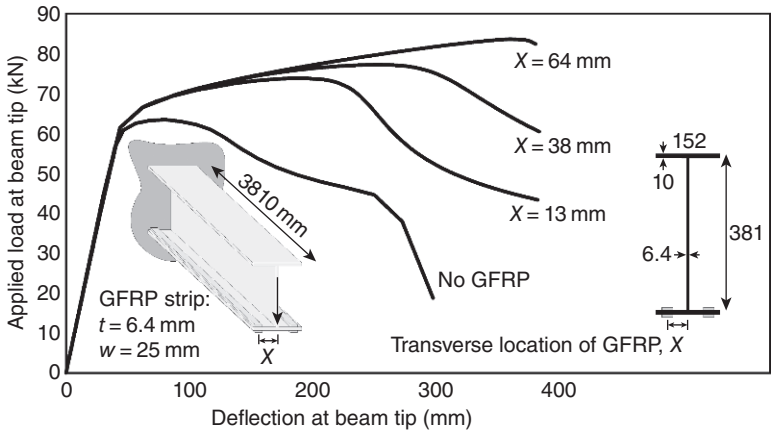


*5.2* Analytical load-deflection behaviour of GFRP-stabilised steel cantilever (after Accord and Earls, 2006). *t* and *w* are the thickness and width of the GFRP strips applied to the bottom flange as shown.

structural ductility was noted (Fig. 5.2), thus supporting the notion that GFRP employed in this fashion enhances the overall performance of the steel member through the bracing that it provides against dominant plate buckling modes.

In a study investigating the use of CFRP to strengthen hollow structural square (HSS) columns, Shaat and Fam (2006) report on concentric axial load tests of squat HSS sections wrapped with both longitudinal and transversely oriented CFRP sheets. Axial compression strength increases on the order of 8–18 % are reported and axial stiffness increases (resulting from the longitudinally oriented CFRP) of between 4 and 28 % are reported. The authors suggested that the transverse CFRP helps to restrain outward directed local buckling of the HSS walls, affecting the improved behaviour observed. Tests on longer specimens, expected to be dominated by FTB, demonstrated no effect from CFRP wrapping. In this case, long column behaviour was dominated by initial imperfections and FTB.

Harries *et al*. (2009) reported an experimental study demonstrating the premise of an FRP-stabilised steel section. Concentric axial compression tests of both long and 'stub' WT 155 × 10.5 (US designation WT 6 × 7) sections were carried out to investigate the ability of an FRP retrofit to affect FTB and WLB behaviour, respectively. Since WT sections were used, warping is not considered in the sectional behaviour. Unretrofit control specimens and four retrofit scenarios were investigated using either high-strength (HS) CFRP strips or ultra-high modulus (UHM) GFRP strips. For each material, two cases were considered: a single 50.8 mm wide by 1.4 mm thick strip applied to the WT stem; and two 25.4 mm wide strips placed on

top of each other at the same location. The average adhesive thickness was measured to be 0.58 mm. Specimens are designated as CFRP or GFRP and the width (in inches) of the FRP application. The two FRP configurations used result in the same area of FRP materials having the same centroid applied to the steel section. Table 5.1 provides a summary of the five specimen geometries and material properties.

Three specimens of each type, each 356 mm long, were tested in concentric compression to failure. The specimen length was selected to ensure local buckling of the WT stem with no FTB of the section. The stem slenderness, $d/t_w = 29.8$, is more than three times that of the flanges, $b/2_{tf} = 8.8$, while the member slenderness, $L/r_y = 18.6$. Specimen length was also selected to provide a bonded length of FRP both above and below the mid-height of the specimen greater than the effective bond length of the FRP, calculated as falling between 60–75 mm and 30–40 mm for the CFRP and GFRP, respectively (Nozaka *et al.*, 2005).

Each specimen was dominated by web (stem) local buckling (WLB). No evidence of FLB or FTB was observed. A summary of average test results is given in Table 5.1. The bifurcation load given in Table 5.1 is the applied load at which WLB at the tip of the stem initiated and was defined as the apparent eccentricity of the axial load resultant on the stem falling outside the stem thickness (i.e., $e > t_w/2$). This value was determined using strain gauges on either side of the stem tip to determine the apparent through-stem eccentricity of the axial load. This value is initially zero and increases as buckling-induced bending of the web initiates (Peck, 2007). The presence of the FRP increased the axial load-carrying capacity between 4 and 14 %. The bifurcation loads were increased as much as 17 %. In these tests, the CFRP specimens exhibited a more pronounced improvement in behaviour. Similarly, the specimens having two 25.4 mm wide FRP strips (C/GFRP-1) performed better that those with one 50.8 mm strip (C/GFRP-2). In all specimens, the presence of the FRP served to mitigate the 'kink' associated with inelastic buckling (Bruneau *et al.*, 1998). This improved behaviour is evident in Table 5.1 where all FRP specimens exhibit a smooth curvature over their 356 mm length whereas the control specimen exhibits a pronounced kink having a 'wavelength' of approximately 260 mm. In no case was FRP debonding observed until the post-peak applied load had fallen below 80 % of the peak load attained and the lateral deflections of the stem tip exceeded 16 mm.

The slenderness of a compression member is a function of member length and radius of gyration. In Harries *et al.* (2009), the stem of the WT section is locally very slender and presents a specific region at which to concentrate the FRP retrofit application. Considering only the WT stem (defined as the entire distance from the flange to the stem tip, $d–t_f$), the increase in weak-axis radius gyration due the application of the FRP ranged from 12 to 35 %

(Table 5.1). This suggests the prospect of increasing stability on a local level. However, a negligible increase in $r_y$ is determined when the entire WT cross-section is considered (Table 5.1); thus there is a negligible effect on the global brace behaviour as will be discussed below. The FRP-retrofitted WT sections tested mirror this predicted behaviour where the increases in radius of gyration are proportional to, although approximately three times greater than, the observed increases in axial load-carrying capacity and bifurcation load in the inelastic sub column tests.

Ekiz and El-Tawil (2008) demonstrated the use of a hybrid FRP system to inhibit inelastic buckling of a steel plate. In this study, the plate is first 'built out' with mortar, PVC or honeycomb core materials and then wrapped with CFRP. Cores ranging from 6.4 to 19 mm thick were used, effectively increasing the 6.4 mm steel plate thickness between three and seven times. The performance of the strengthening scheme depended upon the strength and stiffness of the core material. Mortar performed best as it is less compressible than the PVC and honeycomb materials used. Provided the steel did not crush into the core material, improved performance was obtained when there was no bond between the core material and steel plate, allowing a strain discontinuity at this interface. This behaviour is analogous to a buckling restrained brace (BRB) in which the brace is debonded from the restraining shell (Black *et al*., 2004; Xie, 2004).

## 5.3 Buckling (crippling) induced by high local stresses

FRP 'patches' have been demonstrated to reinforce thin-walled (thin-webbed) steel structures against the crippling effects of concentrated transverse and axial loads (Zhao *et al*., 2006; Fernando *et al*., 2009). Zhao *et al*. investigated the use of CFRP wraps and plates to improve the web crippling behaviour of cold-formed rectangular steel sections subject to end crushing (Fig. 5.3a). The specimens had 100 mm tall webs having thicknesses of 2, 3 and 5 mm resulting in web slenderness ratios ranging from 50 to 20. The CFRP plates used had a thickness of 1.2 mm and a modulus of 165 MPa. Thus the effect of the bonded CFRP on the slenderness was equivalent to adding 1 mm of steel per CFRP plate. The presence of the CFRP plates increased the crippling loads but not, however, to the same extent as simply increasing the steel web thickness. Importantly, Zhao *et al*. concluded that the presence of CFRP sufficiently mitigated web buckling to permit web yield and, in some cases, strain hardening behaviour. Based on the limited available research and the related research on inelastic buckling (above), it is felt that the effectiveness of such 'in-plane' FRP patches is limited, most likely to cold-formed steel applications where the addition of the FRP represents a significant effect on local slenderness.

*Table 5.1* Inelastic and elastic buckling of FRP-stabilised non-compact WT sections. Values in brackets are ratios with respect to control specimen

| | | Control | CFRP-1 | GFRP-1 | CFRP-2 | GFRP-2 |
|---|---|---|---|---|---|---|
| Steel:<br>$f_y$ = 345 MPa; $E$ = 200 GPa<br>1.4 mm CFRP strip:<br>$f_u$ = 2.8 GPa; $E$ = 155 GPa<br>1.4 mm GFRP strip:<br>$f_u$ = 895 MPa; $E$ = 41.4 GPa<br>≈ 0.6 mm adhesive layer:<br>$f_u$ = 31 MPa; $E$ = 3.9 GPa | | 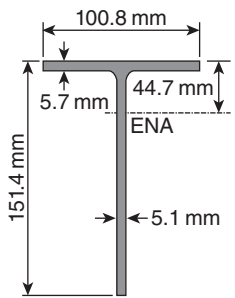 | 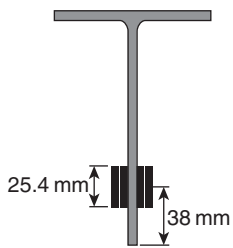 | | 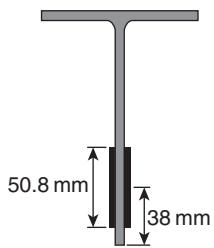 | |
| Equivalent radius of gyration, mm | WT section | 19.12 | 19.15 | 19.13 | 19.14 | 19.13 |
| | Web only | 1.47 | 1.99 (1.35) | 1.77 (1.20) | 1.80 (1.22) | 1.64 (1.12) |
| *Inelastic buckling specimens* | | | | | | |
| Representative photograph taken during post-peak response at axial load of 80% of peak load | |  |  |  |  |  |
| Max. capacity (kN) | | 345 | 392 (1.14) | 377 (1.09) | 370 (1.07) | 358 (1.04) |
| WLB bifurcation (kN) | | 320 | 375 (1.17) | 371 (1.16) | 348 (1.09) | 327 (1.02) |

*Elastic buckling specimens*

| | | | | | | |
|---|---|---|---|---|---|---|
| Photograph of specimen at end of testing |  | $L = 1664$ mm<br>$L/r_y = 87$ |  |  |  |  |
| Max. capacity (kN) | 219 | | 213 (0.97) | 239 (1.09) | 217 (0.99) | 232 (1.06) |
| Weak axis bifurcation (kN) | 132 | | 138 (1.05) | 145 (1.10) | 140 (1.06) | 149 (1.13) |
| Strong axis bifurcation (kN) | 148 | | 210 (1.42) | 217 (1.47) | 206 (1.39) | 205 (1.38) |

*Source*: Adopted from Harries *et al*. (2009).

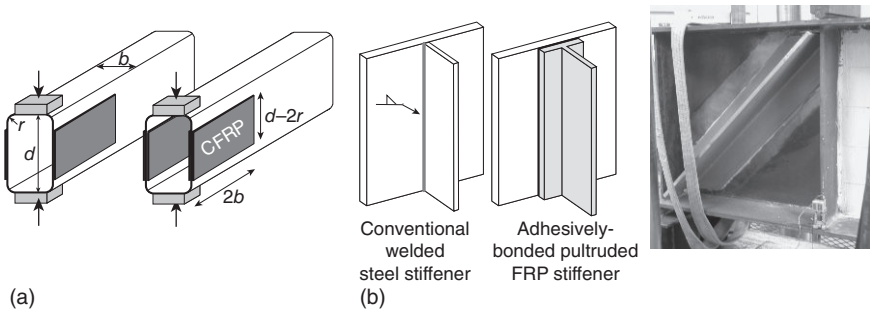


*5.3* Use of FRP to mitigate crippling associated with local loads and stress fields: (a) methods for mitigating crippling in thin-walled rectangular sections (after Zhao *et al.*, 2006); (b) adhesively bonded FRP stiffeners (adapted from Okeil *et al.*, 2010) (photo courtesy of Dr Ayman Okeil).

Okeil *et al*. (2009) proposed the use of adhesively bonded pultruded FRP sections as stiffeners for slender plate elements (Fig. 5.3b). Okeil *et al*. focus on stiffeners for thin-webbed built-up steel sections and demonstrate that these may be designed in a manner similar to conventional steel stiffeners to control tension field action in such sections. Such adhesively bonded FRP stiffeners are common in both new design and repair applications in both aerospace and marine applications.

Thin-walled circular steel tubes and structures such as tanks subject to transient axial load, often resulting from seismic effects, are susceptible to so-called 'elephant-foot buckling'. Recent studies (Nishino and Furukawa, 2004; Teng and Hu, 2007; Haedir and Zhao, 2011; Bhetwal and Yamada, 2012) have demonstrated that external FRP wraps can mitigate this mode of failure and enhance the ductility of the structure. Batikha *et al*. (2009) propose a method of reinforcing thin-walled cylindrical structures using adhesively bonded FRP 'rib' stiffeners. Similar to the work of Okeil *et al*. (2009), such an approach is aimed at controlling tension field action.

## 5.4 Elastic global (Euler) buckling

Application of thin sections of FRP directly to a steel substrate is not expected to affect global buckling behaviour to a large extent since this behaviour is a function of section stiffness and radius of gyration, both of which remain largely unaffected by small amounts of surface-bonded FRP. Harries *et al*. (2009) demonstrated this behaviour. In addition to the stub column tests described above, Harries *et al*. report tests on the same WT sections having a length of 1664 mm and weak-axis slenderness ratio of $L/r_y$ = 87 (Table 5.1). End conditions for these tests consisted of a double angle

connection engaging only the stem of the WT. This connection was designed to (i) reflect an AISC-compliant (2010b) brace connection; and (ii) result in a transfer of forces coincident with the neutral axis of the WT section. All specimens were heavily instrumented and tested under concentric cyclic compressive loading to failure. Each brace was initially subjected to a small tensile force of approximately 8.9 kN to allow the loading sequence to pass through zero in each cycle. The first loading cycle imposed a maximum 22.2 kN compressive load and then returned to the initial 8.9 kN tensile load. The following cycles incrementally increased the maximum compressive load by 22.2 kN each cycle and each returned to the initial 8.9 kN tensile load upon cycle completion. Each specimen reached at least a 200 kN compression load (Table 5.1) in this manner, and cyclic loading was continued until failure occurred as defined by either excessive lateral deflection or FRP strip debonding. Details of the test set-up, protocol and results are reported by Abraham (2006). A summary of test results and images of each specimen are shown in Table 5.1.

Each specimen exhibited elastic FTB typical of a slender WT section. This behaviour is characterised by large lateral translations of the stem tip, twist about the centroid and nominal strong axis translation. For the slender stem WT tested ($d/t_w = 29.8$), plastic 'kinking' of the stem was observed with increased axial load and coincident lateral displacement. This behaviour is particularly obvious in the unretrofit control specimen (Table 5.1). The presence of FRP on subsequent specimens helped to mitigate this post-buckling crippling.

The FRP retrofit specimens did not provide a significant increase in axial capacity. The GFRP-2 and GFRP-1 retrofit specimens exhibited 6 and 9 % increases in axial capacity, respectively. Specimens CFRP-2 and CFRP-1 exhibited a slight decrease in axial capacity as compared with the control specimen, possibly resulting from misalignment of the specimens in the test frame. Despite little effect on axial capacity, the retrofit specimens did exhibit greater control over weak-axis lateral displacement as well as the weak- and strong-axis bifurcation loads (Table 5.1).

While not generally efficient for improving global buckling behaviour as a conventional surface-bonded system, hybrid FRP systems, modelled on BRB (Black *et al.*, 2004; Xie, 2004) have been demonstrated to improve global buckling behaviour. Examples of proposed systems are shown in Fig. 5.4a. El-Tawil and Ekiz (2009) report on an analytical and experimental research program conducted to investigate the buckling behaviour of compressive steel braces strengthened with CFRP laminates. To improve the effectiveness of the CFRP wraps, the steel member is first sandwiched within a core comprising mortar or PVC blocks prior to attaching the external CFRP sheets (Fig. 5.4). The authors derived expressions for requirements to prevent buckling of the steel braces from equilibrium

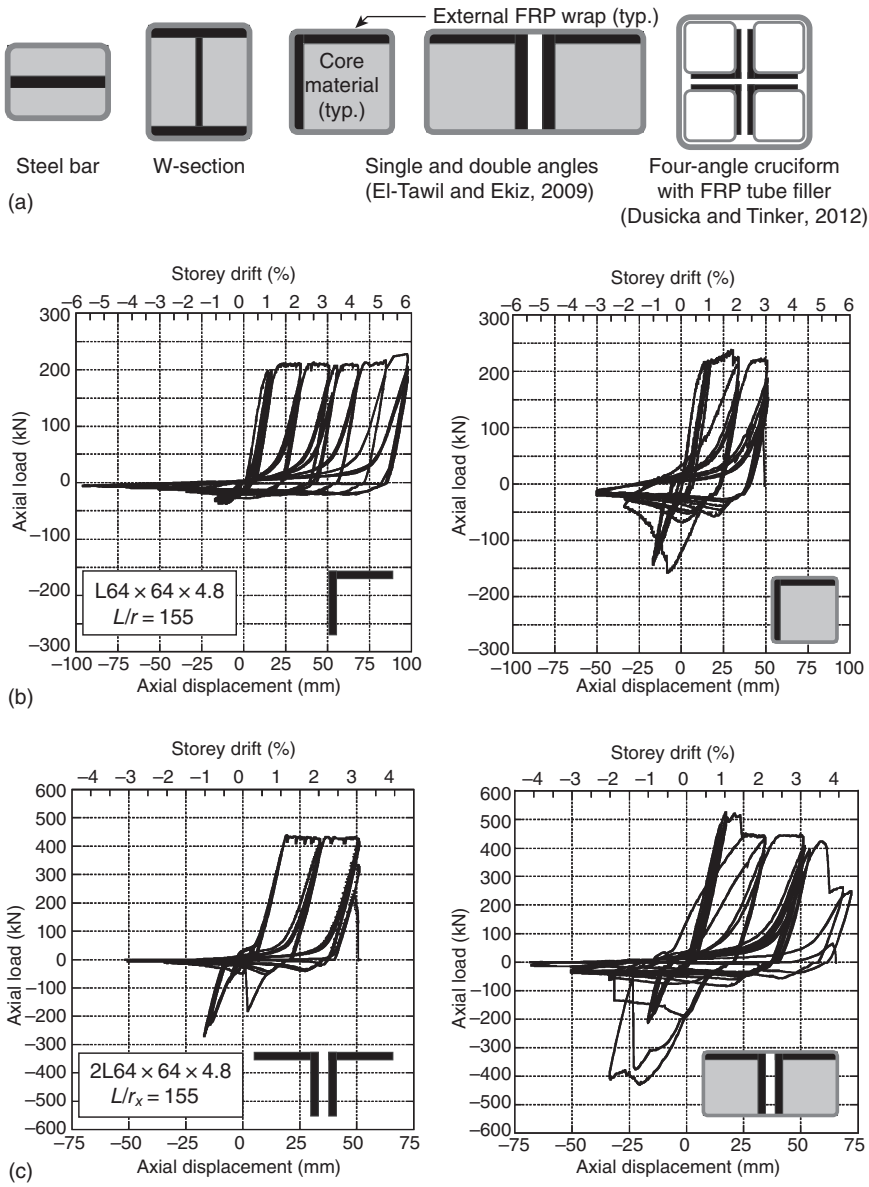


*5.4* Hybrid FRP-stabilised brace geometry and behaviour. (a) Hybrid FRP methods of affecting buckling restraint; (b) load deflection behaviour of hybrid FRP-stabilised single angle braces (El-Tawil and Ekiz, 2009); (c) load deflection behaviour of hybrid FRP-stabilised double angle braces (El-Tawil and Ekiz, 2009).

considerations and verified the expressions with test results. As shown in Fig. 5.4b, El-Tawil and Ekiz demonstrated significant improvements in the buckling and post-buckling response of 3 m long double (2L64 × 64 × 4.8; US designation 2L2.5 × 2.5 × 3/16) and single angle (L64 × 64 × 4.8) brace members subjected to reversed cyclic loading. The authors proposed that CFRP wrapping could be used to make steel braces behave in a buckling-restrained manner for seismic retrofit purposes. In an entirely analytical study, Dusicka and Tinker (2012) demonstrated the improved behaviour for aluminum four-angle cruciform braces having FRP tubular sections as filler wrapped with GFRP fabric (Fig. 5.4a). These braces were modelled to closely resemble conventional BRBs.

## 5.5 Field applications of fibre-reinforced polymer (FRP)-stabilised steel sections

To date, there are no known field applications of FRP specifically to address local or global buckling stability of a steel structure. Nonetheless, there are a limited number of cases of FRP repairs being deployed to address steel-section loss in compression members (Moy, 2003; Chacon *et al*., 2004; Ehsani and Croarkin, 2011). Regardless of specific need, such repairs will also enhance the stability of the repaired section.

### 5.5.1 Potential application space for FRP-stabilised steel

The linear behaviour, high strength and high stiffness of FRP materials can be applied to a steel section to increase member stability. More specifically, it is proposed that small amounts of FRP can be utilised to increase resistance to flange (FLB) and/or web (WLB) local buckling. The purpose of such an application is not necessarily to increase load-carrying capacity but rather to restrict plastic flow of the plate member. Previous work (reported above) has focused on enhancing the stability of compression members. Limit states requiring the control of local instability are relatively rare in structural engineering. Nonetheless, the following application in seismic retrofit is proposed, indicating a potentially large application space.

### 5.5.2 Ensuring ductility in seismic moment connections

The premise of conventional seismic lateral force design of steel frames is to assure ductile behaviour and sufficient redundancy to permit adequate redistribution of force in the event of loss of capacity of members. To achieve frame ductility, connections (connection regions) must be designed to prevent or delay fracture or instability until the prescribed storey drift

has been achieved. The widespread damage to welded moment frame connections observed in the Northridge (EERI, 1995) and Kobe (Cromartin *et al*., 1995) earthquakes led to extensive research aimed at improving the performance of these connections (FEMA, 2000). The outcome of this effort is reflected in the *AISC Seismic Provisions for Structural Steel Buildings* (AISC, 2010a). The performance requirement prescribed by these provisions is that moment connections in special moment frames (SMF) must sustain an inter-storey drift angle of at least 0.04 rad without 'significant loss of strength', defined as the moment capacity falling below 80 % of the nominal plastic moment capacity, $0.8M_p$. Intermediate moment frames (IMF) must sustain a drift angle of at least 0.02 rad. and ordinary moment frames (OMF) have no such performance requirement.

The primary form of damage observed in moment frame connections in the Northridge and Kobe events was fracture of the flange welds. Thus, the provisions developed from the subsequent research aimed to mitigate such fractures. Ductility was assured by (variations on the theme of) moving the plastic hinge region away from the critical welded connection as is done through the use of reduced beam section (RBS) members (AISC, 2010a). However, once fracture has been mitigated, instabilities are observed to become the critical behaviour limiting capacity and ductility. Little attention has been paid to potential instabilities beyond conventional limitations to beam slenderness ($L/r_y$) and width-to-thickness ratios of webs and flanges ($h/t_w$ and $b_f/2t_f$, respectively). These limits were largely established based on *monotonic* tests (ASCE, 1971) and are formulated to accommodate strains approaching strain hardening values within an individual plate component prior to the onset of local buckling (Haaijer, 1957; Haaijer and Thurlimann, 1958; Lay, 1965). Nakashima *et al*. (2003) demonstrated two critical aspects of moment frame behaviour, both related to stability:

- The interaction of the three buckling modes: FTB, WLB and FLB. Significantly, they demonstrated the hierarchy of buckling is dominated by either: (i) FLB followed by simultaneous WLB and FTB; or (ii) FLB and FTB occurring simultaneously, followed by WLB. Furthermore, they demonstrated the relative influence of FLB, FTB, and WLB based on beam, flange and web slenderness. These findings will be discussed further below.
- The degradation of capacity under conditions of cyclic loading may be significantly more severe than observed under monotonic loading. This is attributed to the accumulation of residual plastic deformations associated with FTB and FLB. More stringent lateral bracing and flange and web width-to-thickness ratios are recommended to address the strength reduction associated with cyclic loading.

In an analytical study, Okazaki *et al*. (2006) studied the effects of web and flange slenderness and proposed an alternative basis for prescribing such slenderness limits based on inter-storey drift demand. More relevant to the present discussion, Okazaki *et al*. conclude:

> *The current stability requirements for SMFs are adequate to maintain strength of 0.8*$M_p$ *at a storey drift of 0.04 rad. However, the same requirements are not sufficient to maintain strength of* $M_p$ *at a storey drift of 0.04 rad. This suggests that improved performance of SMF beams can be achieved by choosing beam sections having width–thickness ratios somewhat smaller than the current code limits.*

An essentially identical conclusion was drawn with respect to IMFs.

Nakashima *et al*. (2003) generated flange versus web slenderness limit curves for the performance objective that $M/M_p > 1.0$ at a rotation capacity of 0.045 rad. (Fig. 5.5a). These curves are additionally coupled with the requirement that $L/r_y < 80$, also to ensure $M/M_p > 1.0$. Beams having geometric properties falling to the right of the curves are unable to attain this specified performance. Similar curves may be generated for the AISC (2010a) requirements ($M/M_p > 0.8$ at 0.04 or 0.02 rad) or any other performance objective desired. The limit curves describe four distinct 'regions' of behaviour (Fig. 5.5a).

- *Region A*: Slender flanges and stocky webs result in beam behaviour controlled by FLB followed by FTB.
- *Region B*: Intermediate flange and web slenderness results in beam behaviour controlled by FTB followed typically by FLB.
- *Region C*: Stocky flanges and slender webs result in beam behaviour controlled by WLB followed by almost simultaneous FLB and FTB.
- *Region D*: For very slender flanges having $d/t_w > 100$, beam behaviour is controlled by web shear buckling (WSB) resulting in rapid loss of capacity due to reduction in beam depth, $d$.

Lateral buckling can be largely mitigated by improving bracing. As the slenderness ($L/r_y$) approaches zero, the limit curve shifts to encompass a greater range of beam geometries. Additionally, as FTB is mitigated, Region B is minimised and there is a more abrupt transition between Regions A and C as shown in Fig. 5.5a.

The ranges of geometric properties of typical US rolled wide flange beam shapes (W-sections) are shown in Fig. 5.5b. Only 114 of 273 (42 %) of W-sections satisfy the performance objective shown ($L/r_y = 80$; $M/M_p > 1.0$ at a rotation capacity of 0.045 rad). Additionally, most behaviour is predicted to be in Regions A and B. Mitigating FTB will shift the limit curve to the right and 'sharpen' the Region B transition. In such a case, more sections will satisfy the performance criteria, but those remaining will be

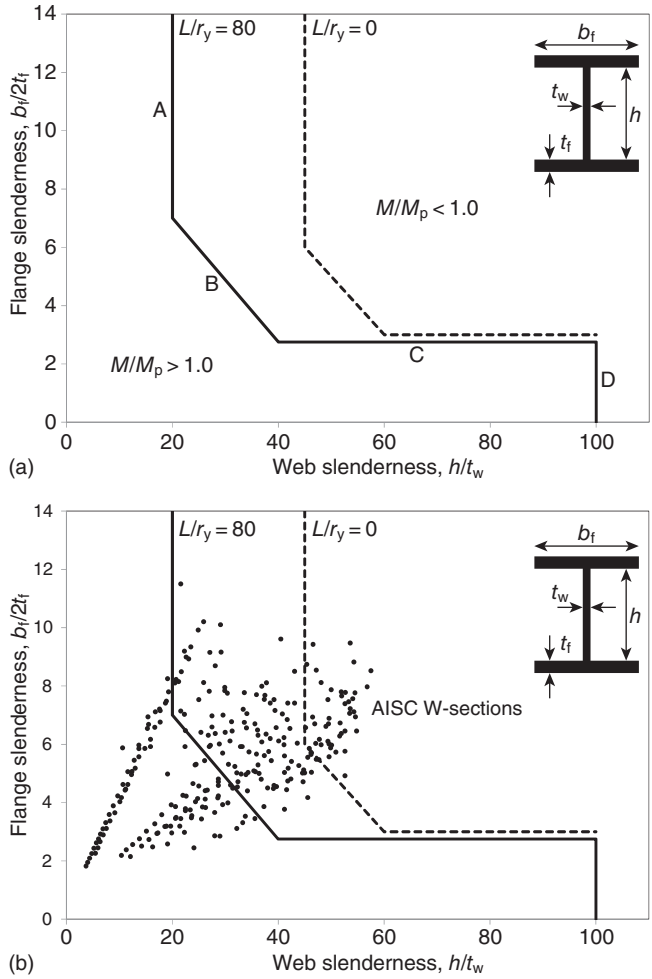


*5.5* Slenderness limits associated with beam instabilities (after Nakashima *et al.*, 2003): (a) example of limiting curves for 0.045 rad; (b) geometries for US rolled W-sections.

dominated by Region A behaviour. Thus it is demonstrated that there is a considerable design space for FLB stabilisation.

Uang and Fan (2002) quantify the interaction between FTB, FLB and WLB through a regression analysis of a relatively small database of 55 test results. The relationship between beam rotation capacity and flange, web and beam slenderness ratios highlighted the interaction between buckling behaviours and demonstrated (i) that behaviour is more sensitive to WLB behaviour where it is critical and (ii) that there is a relatively weak interaction

with FTB in any case. More stringent equations for flange, web and beam slenderness limits based on a desired rotation capacity are proposed.

The independent results of Nakashima *et al*. (2003) and Uang and Fan (2002), proposing more stringent slenderness ratios, would result in fewer rolled shapes being considered 'compact for flexure' (AISC, 2010a, b) which introduces a need for stability retrofit of existing sections. Additionally, the current performance criteria for special moment frames ($0.8M_p$ at 0.04 rad) may arguably be improved, again introducing a need for stability retrofit to ensure beam capacity at greater rotational demands. Significantly, increasing the capacity of the member is not desirable in a moment frame application as this must be echoed in the connection region itself and will accumulate through the structure as increased column and eventually foundation demands.

### 5.5.3 Partial buckling-restrained braces

The concept of FRP-stabilised steel sections is analogous to that of BRB which display significantly increased compressive capacity due to restraint to local and lateral buckling of the steel bracing members (Black *et al*., 2004; Xie, 2004). Properly detailed BRB (AISC, 2010a) display full, symmetric hysteretic behaviour, dissipating a considerable amount of energy. However, these systems may not always be ideal, especially in retrofitted structures because they are expensive, difficult to install, may result in different load distributions than originally intended, and may also be over-designed for structures in low to moderate seismic regions. The concept of partially buckling restrained braces (PBRB) whose behaviour lies between that of a BRB and a conventional brace has been proposed (Abraham and Harries, 2007). In a PBRB, FRP composite materials are applied to the steel brace in an attempt to enhance the member's buckling capacity and hysteretic behaviour. The FRP material is elastic to failure and thus is able to provide a 'bracing' force to a steel plate that has achieved plasticity.

As has been discussed, a typical FRP retrofit is unable to significantly affect the axial load-carrying capacity of typical brace members. Nonetheless, in these applications, FRP was observed to help stabilise slender elements of the brace section and increase the bifurcation load at which elastic buckling initiates (see Table 5.1, for instance). Significantly, a softer GFRP retrofit provided sufficient restraining forces to mitigate residual deflections following significant buckling. Mitigating residual displacement also mitigates the formation of the plastic 'kink' which forms in the member and ultimately contributes to the degradation of the compressive capacity of the brace (Bruneau *et al*., 1998). Thus, reduced residual displacements lead to reduced degradation of capacity resulting in greater compressive capacity for subsequent load cycles. The potentially improved brace performance is

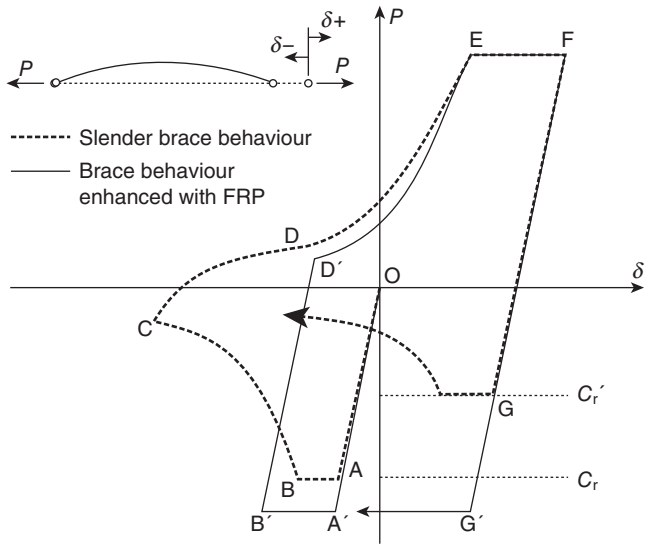


*5.6* Brace hysteresis modified to reflect reduced 'kinking' behaviour (after Bruneau *et al.* 1998).

shown schematically in Fig. 5.6 (Bruneau *et al.*, 1998) as having: (i) an elongated compression 'plateau' A–B; (ii) an increased residual compressive load $C_r'$; (iii) the 'negative stiffness' region (B–C) minimised or mitigated altogether; (iv) in increased reloading tensile stiffness (C–D–E); (v) a less significant transition in stiffness during tension reloading (D–E), reducing the possibility of an 'impact' effect (CISC, 2007); and (vi) an increased number of cycles to eventual fracture of the section due to low cycle since plastic deformation demand is reduced. Each of these effects results in an increase in energy that may be dissipated by the brace as illustrated by a greater area contained under the hysteresis in Fig. 5.6. This behaviour is also seen in the experimental results shown in Figs 5.4b and c.

The concept of strategically applying FRP materials to a steel brace to create a PBRB may not hold great promise as a viable retrofit option *per se*. The nominal effect of the addition of small amounts of FRP has little effect on the elastic buckling behaviour of long brace sections typically found in building structures. Nonetheless, the FRP retrofit is able to affect local behaviour and enhance brace behaviour to a degree, particularly under conditions of repeated loading. Application to shorter brace members, such as those used for cross frames between bridge girders (Carden *et al.*, 2006), where global behaviour is not as critical appears to present a more appropriate application of an FRP-stabilised steel member.

## 5.6 Conclusion and future trends

The concept of strategically applying FRP material to a steel compression member in order improve global and local buckling behaviour has been described. This application is not aimed at increasing the load-carrying capacity of the steel section, *per se*, although this may be accomplished if desired. Rather, the approach is aimed at providing stability (in the sense of bracing) to the steel section through the use of FRP application to enforce nodal lines in a plate element for the purposes of increasing its critical load and constraining plastic flow in the plate element. The member becomes, in effect, an FRP-stabilised steel section. The effect of the addition of small amounts of FRP has little effect on the elastic buckling behaviour of long sections typical of braces found in building structures. The FRP retrofit is, however, able to affect local behaviour. Improvement in load-carrying capacity is proportional to the increase in effective radius of gyration ($r$) of the plate element affected by the presence of the FRP. For elastic buckling, the entire section is considered, in which case the increase in $r$ is nominal. For inelastic buckling, only the outstanding plate element is considered, in which case the proportional improvement in capacity is greater. Prior to FRP debonding, the presence of the FRP controls inelastic buckling and delays the formation of the plastic 'kink'. The formation of this kink affects the cyclic compressive capacity of the section upon subsequent reloading and the tensile stiffness of the section, and can lead to section fracture in relatively few loading cycles. Thus the application of FRP may represent a method of improving the energy absorption and ultimate cyclic ductility of elements susceptible to inelastic buckling in a seismic lateral force resisting system.

The application space for FRP-stabilised steel is likely limited in scope. The ability of FRP repair methods to improve the capacity of corrosion damaged steel members remains an application requiring significant study. The effect of section loss on slenderness of compression elements has generally been neglected despite the easily demonstrable fact that thinning of steel plates due to corrosion may affect local buckling capacity more significantly than axial capacity. Further study is necessary to identify not only cases in which local stability is affected but also a method of effectively repairing these deteriorated regions using FRP systems. A significant challenge is to establish likely bond relationships for corrosion damaged steel and protocols for preparation of such regions prior to FRP application.

## 5.7 References

Abraham, E.J. (2006) *Conceptual Investigation of Partially Buckling Restrained Braces*. MSCE Thesis, University of Pittsburgh, Pittsburgh, PA, December.

Abraham, E.J. and Harries, K.A. (2007) Development of 'partial buckling-restrained braces' using FRP, *Proceedings of the ASCE Structures '07 Congress*, Long Beach CA, 16–19 May.

Accord, N.B. and Earls, C.J. (2006) Use of fiber reinforced polymer composite elements to enhance structural steel member ductility, *ASCE Journal of Composites for Construction*, **10**(4), 337–344.

AISC (2010a) *ANSI/AISC 341-05 – Seismic provisions for structural steel buildings*, American Institute of Steel Construction, Chicago, IL.

AISC (2010b) *ANSI/AISC 360-10 – Specifications for Structural Steel Buildings*, American Institute of Steel Construction, Chicago, IL.

ASCE (1971) *Plastic design in steel: A guide and commentary*, 2nd edn, ASCE Manuals and Reports on Engineering Practice No. 41, American Society of Civil Engineers, New York.

Batikha, M., Chen, J., Rotter, J. and Teng, J. (2009) Strengthening metallic cylindrical shells against elephant's foot buckling with FRP, *Thin-Walled Structures*, **47**(10), 1078–1091.

Bhetwal, K.K. and Yamada, S. (2012) Effects of CFRP reinforcements on the buckling behavior of thin-walled steel cylinders under compression, *International Journal of Structural Stability and Dynamics*, **12**(1), 131–151.

Black, C.J., Makris, N. and Aiken, I.D. (2004) Component testing, seismic evaluation and characterization of buckling-restrained braces, *ASCE Journal of Structural Engineering*, **130**(6), 880–894.

Bruneau, M., Uang, C. M. and Whittaker, A. (1998) *Ductile Design of Steel Structures*, McGraw-Hill, Boston, MA.

Carden, L.P., Ahmad, M.I. and Buckle, I.G. (2006) Seismic performance of steel girder bridges with ductile cross frames using buckling-restrained braces, *ASCE Journal of Structural Engineering*, **132**(3), 338–345.

Chacon, A., Chajes, M., Swinehart, M., Richardson, D. and Wenczel, G. (2004) Applications of advanced composites to steel bridges: a case study on the Ashland Bridge, *Proceedings of the 4th Advanced Composites for Bridges and Structures Conference*, Calgary, 20–23 July.

CISC (2007) *Handbook of Steel Construction*, 9th edn, Canadian Institute of Steel Construction, Markham, ON.

Colombi, P. and Poggi, C. (2006a) An experimental, analytical and numerical study of the static behavior of steel beams reinforced by pultruded CFRP strips, *Composites: Part B*, **37**, 64–73.

Colombi, P. and Poggi, C. (2006b) Strengthening of tensile steel members and bolted joints using adhesively bonded CFRP plates, *Construction and Building Materials*, **20**, 22–33.

Cromartin, C.D., Greene, M. and Tubbesing, S.K. (technical editors) (1995) *Hyogo-ken Nanbu (Kobe) Earthquake, January 17, 1995: Preliminary Reconnaissance Report*, Earthquake Engineering Research Institute.

Dusicka, P. and Tinker, J. (2012) Global restraint in ultra-lightweight buckling-restrained braces, *ASCE Journal of Composites for Construction*, **17**(1), 139–150.

Earls, C.J. (1999) On the inelastic failure of high strength steel I-shaped beams, *Journal of Constructional Steel Research*, **49**(1), 1–24.

Earls, C.J. (2000a) On geometric factors influencing the structural ductility of compact I-shaped beams, *ASCE Journal of Structural Engineering*, **126**(7), 780–789.

Earls, C.J. (2000b) The influence of material effects on the structural ductility of compact I-shaped beams, *ASCE Journal of Structural Engineering*, **126**(11), 1268–1278.

EERI (1995) Northridge, California, 1994 Earthquake: Reconnaissance Report, Part 1, *Earthquake Spectra*, Vol. 11 (Supplement C), April.

Ehsani, M. and Croarkin, M. (2011) Restoration of deteriorated piles, *Government Engineering*, March–April, 14–15.

Ekiz, E. and El-Tawil, S. (2008) Restraining steel brace buckling using a carbon fiber-reinforced polymer composite system: experiments and computational simulation. *ASCE Journal of Composites for Construction*, **12**(5), 562–569.

El-Tawil, S. and Ekiz, E. (2009) Inhibiting steel brace buckling using carbon fiber-reinforced polymers: large-scale tests, *ASCE Journal of Structural Engineering*, **135**(5), 530–538.

El-Tawil, S., Ekiz, E., Goel, S. and Chao, S.-H. (2011) Restraining local and global buckling behavior of steel plastic hinges using CFRP, *Journal of Constructional Steel Research*, **67**, 261–269.

FEMA (2000) *FEMA 350 Recommended Seismic Design Provisions Criteria for New Steel Moment-Frame Buildings*, Federal Emergency Management Agency, Washington DC.

Fernando D., Yu T., Teng J.G. and Zhao X.-L. (2009) CFRP strengthening of rectangular steel tubes subjected to end bearing loads: effect of adhesive properties and finite element modelling, *Thin-Walled Structures*, **47**(10), 1020–1028.

Greco, N. and Earls, C.J. (2003) Structural ductility in hybrid high performance steel beams, *ASCE Journal of Structural Engineering*, **129**(12), 1584–1595.

Haaijer, G. (1957) Plate buckling in the strain-hardening range, *Journal of the Engineering Mechanics Division*, ASCE, **83**, EM2, Paper Number 1212.

Haaijer, G. and Thürlimann, B. (1958) On inelastic buckling in steel, *Journal of the Engineering Mechanics Division*, ASCE, **84**, EM2, Paper Number 1581.

Haedir, J. and Zhao, X.-L. (2011) Design of short CFRP-reinforced steel tubular columns, *Journal of Constructional Steel Research*, **67**, 497–509.

Harries, K.A. and El-Tawil, S. (2008) Review of steel-FRP composite structural systems, *Proceedings of the 5th International Conference on Composite Construction*, Tabernash, CO, 20–24 July.

Harries, K.A., Peck, A. and Abraham, E.J. (2009) Enhancing stability of structural steel sections using FRP, *Thin-Walled Structures*, **47**(10), 1092–1101.

Jiao, H. and Zhao, X.L. (2004) CFRP strengthened butt-welded very high strength circular steel tubes, *Thin-Walled Structures*, **42**, 963–978.

Jones, S.C. and Civjan, S.A. (2003) Application of fiber reinforced polymer overlays to extend steel fatigue life, *ASCE Journal of Composites for Construction*, **7**(4), 331–338.

Lay, M.G. (1965) Flange local buckling in wide-flange shapes, *Journal of the Structural Division*, ASCE, **91**, ST6, 95–116.

Lenwari, A., Thepchatri, T. and Albrecht, P. (2005) Flexural response of steel beams strengthened with partial-length CFRP plates. *ASCE Journal of Composites for Construction*, **9**(4), 296–303.

Lenwari, A., Thepchatri, T. and Albrecht, P. (2006) Debonding strength of steel beams strengthened with CFRP plates. *ASCE Journal of Composites for Construction*, **10**(1), 69–78.

Liu, H.B., Zhao, X.L. and Al-Mahaidi, R. (2005) The effect of fatigue loading on bond strength of CFRP bonded steel plate joints, in Chen, J.F. and Teng, J.G. (eds), *Proceedings of the International Symposium on Bond Behavior of FRP in Structures*, International Institute for FRP in Construction, Hong Kong, 459–464.

Miller, T.C., Chajes, M.J., Mertz, D.R. and Hastings, J.N. (2001) Strengthening of a steel bridge girder using CFRP plates, *ASCE Journal of Bridge Engineering*, **6**(6), 514–522.

Moy, S.S.J. (2003) Three case studies of carbon fibre composite strengthening of metallic structures on the London Underground, *Proceedings of Advancing with Composites 2003*, Milan, 3–5 May.

Nakashima, M., Liu, D. and Kanao, I. (2003) Lateral–torsional and local instability of steel beams subjected to large cyclic loading, *International Journal of Steel Structures*, **3**(3), 179–189.

Nishino, T. and Furukawa, T. (2004) Strength and deformation capacities of circular hollow section steel member reinforced with carbon fiber. *Proceedings of the Seventh Pacific Structural Steel Conference*. American Institute of Steel Construction, Chicago, IL.

Nozaka, K., Shield, C.K. and Hajjar, J.F. (2005) Effective bond length of carbon fiber reinforced polymer strips bonded to fatigued steel bridge I-girders, *ASCE Journal of Bridge Engineering*, **10**(2), 195–205.

Okazaki, T., Liu, D., Nakashima, M. and Engelhardt, M.D. (2006) Stability requirements for beams in seismic steel moment frames, *ASCE Journal of Structural Engineering*, **132**(9), 1334–1342.

Okeil, A., Bingol, Y. and Ferdous, M. (2009) Novel technique for inhibiting buckling of thin-walled steel structures using pultruded glass FRP sections, *ASCE Journal of Composites for Construction*, **13**(6), 547–557.

Okeil, A., Bingol, Y. and Chorkey, M. (2010) Stiffening thin-walled structures using pultruded FRP sections, *2010 FHWA Bridge Engineering Conference: Highways for LIFE and Accelerated Bridge Construction*, Orlando, FL, 8–9 April.

Patnaik, A.K. and Bauer, C.L. (2004) Strengthening of steel beams with carbon FRP laminates, *Proceedings of the 4th Advanced Composites for Bridges and Structures Conference*, Calgary, 20–23 July.

Peck, A. (2007) *Investigation of FRP Stabilization of Plastic Buckling Behavior of Slender Steel Sections*. MSCE Thesis, University of Pittsburgh, Pittsburgh, PA, December 2007.

Photiou, N.K., Hollaway, L.C. and Chryssanthopoulos, M.K. (2006) Strengthening of an artificially degraded steel beam utilizing a carbon/glass composite system, *Construction and Building Materials*, **20**, 11–21.

Sen, R. Liby, L. and Mullins, G. (2001) Strengthening steel bridge sections using CFRP laminates, *Composites: Part B*, **32**, 309–322.

Shaat, A. and Fam, A. (2006) Axial loading test on short and long hollow structural steel columns retrofitted using carbon fibre reinforced polymers, *Canadian Journal of Civil Engineering*, **33**(4), 458–470.

Tavakkolizadeh, M. and Saadatmanesh, H. (2003a) Strengthening of steel–concrete composite girders using carbon fiber reinforced polymers sheets, *ASCE Journal of Structural Engineering*, **129**(1), 30–40.

Tavakkolizadeh, M. and Saadatmanesh, H. (2003b) Fatigue strength of steel girders strengthened with carbon fiber reinforced polymer patch, *ASCE Journal of Structural Engineering*, **129**(1), 186–196.

Teng, J. and Hu, Y.M. (2007) Behaviour of FRP-jacketed circular steel tubes and cylindrical shells under axial compression, *Construction and Building Materials*, **21**(4), 827–838.

Teng, J.G., Yu, T. and Fernando, D. (2012) Strengthening of steel structures with fiber-reinforced polymer composites, *Journal of Constructional Steel Research*, **78**, 131–143.

Thomas, S. and Earls, C.J. (2003) Cross sectional compactness and bracing requirements for HPS483W girders, *ASCE Journal of Structural Engineering*, **129**(12), 1569–1583.

Uang, C.M and Fan, C.C. (2002) Cyclic stability criteria for steel moment connections with reduced beam section, *ASCE Journal of Structural Engineering*, **127**(9) 1021–1027.

Xie, Q. (2004) State of the art of buckling-restrained braces in Asia, *Journal of Constructional Steel Research*, **61**, 727–748.

Zhao, X.-L. and Zhang, L. (2006) Sate-of-the-art review on FRP strengthened steel structures, *Engineering Structures*, **29**, 1808–1823.

Zhao, X.-L., Fernando, D. and Al-Mahaidi, R. (2006) CFRP strengthened RHS subjected to transverse end bearing force, *Engineering Structures*, **28**(11), 1555–1565.

# 6

# Strengthening of thin-walled (hollow) steel sections using fibre-reinforced polymer (FRP) composites

M. R. BAMBACH, University of New South Wales, Australia

**DOI**: 10.1533/9780857096654.2.140

**Abstract**: This chapter summarises recent research on the strengthening of thin-walled steel structures with fibre-reinforced polymers. The focus is on steel square hollow sections strengthened with carbon fibre-reinforced polymer. An extensive series of experiments with a wide range of thin-walled steel section geometries where the exterior surfaces of the tube walls were strengthened with bonded carbon fibres, is discussed. Experiments were performed under quasi-static axial compression to investigate strengthening with regards to elastic buckling and compression strength, and under axial impact to investigate strengthening with regards to dynamic axial crushing and associated crashworthiness indicators. Design models are developed and compared with the experimental results, and optimisation is discussed.

**Key words**: thin-walled steel, carbon fibre-reinforced polymer, compression strength, axial crushing, impact.

## 6.1 Introduction

Thin-walled plates and tubes made from metals or fibre-reinforced polymers (FRP) are used extensively in many different applications, including the construction, infrastructure, aeronautical, aerospace, automotive, marine and sporting industries. In strength applications, the advantage of using thin elements is the high strength- and stiffness-to-weight ratios. In energy-absorbing applications, the advantage is the high energy absorption-to-weight ratios (specific energies). A relatively recent advent to compression members is the combination of metal and FRP tubes produced by externally bonding fibres to the metal section (Hanefi and Wierzbicki, 1996; Song *et al*., 2000; Wang and Lu, 2002; Shaat and Fam, 2006; Teng and Hu, 2007).

In axial compression applications, the motivation for strengthening thin-walled steel structures with FRP is to control buckling deformations and/or provide increased compression capacity. For these types of sections, strengthening by welding steel plates, for example, may exacerbate buckling deformations and lead to residual stress issues that are well known to result from the welding of thin plate elements. Site conditions may also provide complications for welding, and the application of additional steel elements

(either welded or bolted) may result in undesirable mass increases. In such cases, the use of externally bonded FRP may provide an economical and reliable strengthening solution.

In axial impact applications, the motivation for strengthening thin-walled steel structures with FRP is to produce structures that provide the desired stiffness, strength or energy absorption properties for the minimum structural mass. Minimising structural mass in the transportation industries can reduce fuel consumption and associated pollutants, and may result in follow-on mass reductions in associated mechanical systems (such as engine capacities, gearing and braking systems, etc.). While a minimum mass solution is sought, the structure must continue to satisfy the energy dissipation and crash characteristics required to maintain appropriate safety for the occupants and cargo. A key advantage of metal components is that they provide ductile, stable plastic collapse mechanisms as they progressively deform axially, thus absorbing the energy of a collision in a controlled and stable manner. This has been shown to be the case both for seam-welded tubes (Johnson *et al*., 1977; Meng *et al*., 1983; Wierzbicki and Abramowicz, 1983; Abramowicz and Jones, 1984, 1986) and spot-welded tubes (White and Jones, 1999; White *et al*., 1999; Schneider and Jones, 2003, 2004; Tarigopula *et al*., 2006; Fyllingen *et al*., 2008, 2009). FRP composite energy absorbers have high compression strength-to-weight ratios; however, they typically undergo brittle, unstable crushing modes that involve extensive micro-cracking development, delamination, fibre breakage, etc., instead of plastic deformation (Thornton, 1986; Mamalis *et al*., 1989, 1991, 1996, 1997a, b, 2005; Czaplicki and Robertson, 1991; Farley and Jones, 1992; Chiu *et al*., 1997; Park *et al*., 2000). Metal–FRP composites take advantage of the favourable characteristics of each material, these being the stable, ductile plastic collapse mechanism of the metal and the high strength-to-weight ratio of the fibre/resin composite.

The aim of this chapter is to summarise recent research by the author (Bambach and Elchalakani, 2007; Bambach *et al*., 2009a, b, c; Bambach, 2010a, b) on the development of thin-walled steel tubes strengthened with carbon fibre-reinforced polymer (CFRP), for axial compression (buckling and strength) and axial impact (quasi-static and dynamic axial crushing) applications. Section 6.2 summarises experimental programs conducted on thin-walled steel square hollow sections (SHS) strengthened with CFRP. Sections 6.3 and 6.4 discuss the experimental results with respect to axial compression buckling and strength, and quasi-static and dynamic axial crushing behaviour. Design models are presented and compared with the experimental results, and optimisation is discussed. Section 6.5 discusses the role of the bond in the behaviour of the steel SHS strengthened with CFRP, and Section 6.6 discusses future trends in the field of thin-walled steel structures strengthened with FRP.

## 6.2 Testing thin-walled steel square hollow sections (SHS) and spot-welded (SW) SHS strengthened with carbon fibre-reinforced polymer (CFRP) composites

This section summarises experimental programs conducted by the author on thin-walled steel SHS strengthened with CFRP (Bambach and Elchalakani, 2007; Bambach *et al.*, 2009a, b, c; Bambach, 2010a, b). Two different types of sections were investigated: commercially produced seam-welded steel SHS (hereafter referred to as 'SHS'); and manually produced spot-welded steel SHS (hereafter referred to as 'SW SHS'). The two different types were investigated in order to produce a wide variety of plate width-to-thickness ratios, and section types typical of both static strength and dynamic axial crushing applications.

The section dimensions of the SHS and SW SHS ranged from 20 to 200 mm with wall thicknesses between 1.6 and 2 mm. The SHS were produced from steel with nominal yield stress and ductility (strain at failure) values of 350 MPa and 32 %. The SW SHS were produced from steel with nominal yield stress and ductility values of 450 MPa and 9 %. The SW sections were fabricated with constant lip dimensions ($b_{lip}$) of 15 mm, with the lips being placed in opposing corners (Fig. 6.1) and spot-welded every 20 mm along the length. The section and material properties are tabulated in Tables 6.1 to 6.4.

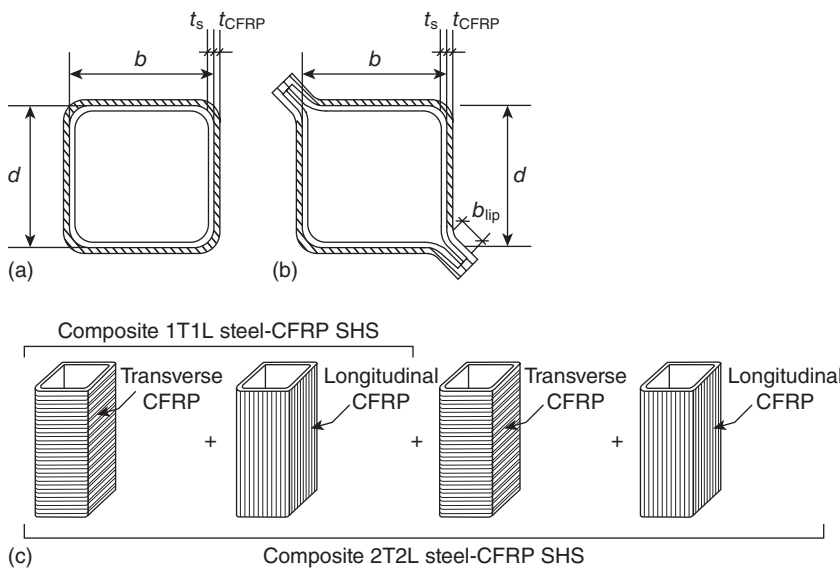


*6.1* SHS with externally bonded CFRP: (a) SHS (commercially produced); (b) SW SHS (spot-welded); and (c) preparation method for 1T1L and 2T2L specimens (Bambach *et al.*, 2009b).

*Table 6.1* Experimental and theoretical quasi-static axial compression buckling results for the slender SHS and SW SHS specimens – commercially produced SHS (SHS) and spot-welded SHS (SW SHS)

| Square hollow section | Steel section ($b \times d \times t$) + CFRP matrix (mm) | (Ave.) Exp. buckling stress, $f_{crtest}$ (MPa) | (Ave.) Exp. slenderness, $\lambda_{test}$ | Increase in buckling stress compared with steel | Theory composite buckling stress, $f_{crc}$ (MPa) | Theory composite slenderness, $\lambda_c$ | $\lambda_{test}/\lambda_c$ |
|---|---|---|---|---|---|---|---|
| SHS | $100 \times 100 \times 2.0$ | 290 | 1.36 | | 314 | 1.31 | 1.04 |
| SHS | 1T1L | 410 | 1.15 | 1.41 | 447 | 1.10 | 1.04 |
| SHS | 2T2L | 517 | 1.02 | 1.78 | 650 | 0.91 | 1.12 |
| SW SHS | $100 \times 100 \times 1.66$ | 224 | 1.54 | | 213 | 1.57 | 0.97 |
| SW SHS | 1T1L | 328 | 1.27 | 1.46 | 329 | 1.27 | 1.00 |
| SW SHS | 2T2L | 501 | 1.03 | 2.24 | 509 | 1.02 | 1.01 |
| SW SHS | $150 \times 150 \times 1.66$ | 96 | 2.34 | | 93 | 2.39 | 0.98 |
| SW SHS | 1T1L | 187 | 1.68 | 1.94 | 143 | 1.92 | 0.87 |
| SW SHS | 2T2L | 435 | 1.10 | 4.52 | 221 | 1.54 | 0.71 |
| SW SHS | $200 \times 200 \times 1.66$ | 41 | 3.57 | | 51 | 3.20 | 1.11 |
| SW SHS | 1T1L | 131 | 2.01 | 3.15 | 80 | 2.58 | 0.78 |
| SW SHS | 2T2L | 176 | 1.73 | 4.24 | 123 | 2.07 | 0.84 |
| | | | | | | Mean: | 0.96 |
| | | | | | | COV: | 0.13 |

COV, coefficient of variation.
*Source*: Bambach *et al*. (2009b).

*Table 6.2* Experimental and theoretical quasi-static axial compression strength results – commercially produced SHS (SHS) and spot-welded SHS (SW SHS)

| Square hollow section | Steel section ($b \times d \times t$) + CFRP matrix (mm) | Steel yield stress, $f_{ys}$ (MPa) | Steel plate slenderness, $\lambda_s$ | Exp. compression capacity, $P_{test}$ (kN) | Capacity increase compared with steel | Exp. capacity/ yield capacity, $P_{test}/P_y$ | Strength/ weight ($s/w$) ratio (kN/kg) | Increase in $s/w$ ratio compared with steel | Theory capacity $P_{uc}$ (kN) | $P_{test}/P_{uc}$ |
|---|---|---|---|---|---|---|---|---|---|---|
| SHS | 20 × 20 × 1.6 | 485 | 0.27 | 57 | | 1.06 | 707 | | 60 | 1.06 |
| SHS | 1T1L | 485 | 0.27 | 66 | 1.16 | 1.22 | 672 | 0.95 | 60 | 0.91 |
| SHS | 1T1L | 485 | 0.27 | 66 | 1.15 | 1.22 | 665 | 0.94 | 60 | 0.91 |
| SHS | 2T2L | 485 | 0.27 | 75 | 1.32 | 1.39 | 677 | 0.96 | 60 | 0.80 |
| SHS | 2T2L | 485 | 0.27 | 69 | 1.21 | 1.28 | 633 | 0.90 | 60 | 0.87 |
| SHS | 50 × 50 × 2.0 | 484 | 0.60 | 182 | | 1.00 | 414 | | 190 | 1.05 |
| SHS | 1T1L | 484 | 0.60 | 201 | 1.11 | 1.11 | 424 | 1.02 | 190 | 0.95 |
| SHS | 1T1L | 484 | 0.60 | 191 | 1.05 | 1.06 | 396 | 0.96 | 190 | 1.00 |
| SHS | 2T2L | 484 | 0.60 | 221 | 1.22 | 1.22 | 414 | 1.00 | 190 | 0.86 |
| SHS | 2T2L | 484 | 0.60 | 213 | 1.17 | 1.18 | 398 | 0.96 | 190 | 0.89 |
| SHS | 65 × 65 × 2.0 | 405 | 0.72 | 177 | | 0.85 | 257 | | 200 | 1.14 |
| SHS | 1T1L | 405 | 0.72 | 183 | 1.04 | 0.88 | 234 | 0.91 | 208 | 1.14 |
| SHS | 1T1L | 405 | 0.72 | 209 | 1.18 | 1.01 | 264 | 1.03 | 208 | 0.99 |
| SHS | 2T2L | 405 | 0.72 | 235 | 1.33 | 1.13 | 267 | 1.04 | 208 | 0.88 |
| SHS | 2T2L | 405 | 0.72 | 214 | 1.21 | 1.03 | 248 | 0.97 | 208 | 0.97 |
| SHS | 75 × 75 × 2.0 | 417 | 0.85 | 198 | | 0.80 | 205 | | 217 | 1.09 |
| SHS | 1T1L | 417 | 0.85 | 247 | 1.25 | 1.00 | 220 | 1.07 | 247 | 1.00 |
| SHS | 1T1L | 417 | 0.85 | 243 | 1.22 | 0.98 | 218 | 1.06 | 247 | 1.02 |
| SHS | 2T2L | 417 | 0.85 | 297 | 1.49 | 1.20 | 231 | 1.13 | 247 | 0.83 |
| SHS | 2T2L | 417 | 0.85 | 267 | 1.35 | 1.08 | 213 | 1.04 | 247 | 0.93 |
| SHS | 100 × 100 × 2.0 | 539 | 1.31 | 238 | | 0.56 | 127 | | 276 | 1.16 |
| SHS | 1T1L | 539 | 1.31 | 337 | 1.41 | 0.79 | 160 | 1.26 | 315 | 0.94 |
| SHS | 1T1L | 539 | 1.31 | 354 | 1.49 | 0.83 | 169 | 1.33 | 315 | 0.89 |
| SHS | 2T2L | 539 | 1.31 | 425 | 1.78 | 0.99 | 179 | 1.40 | 358 | 0.84 |

| | | | | | | | | | | |
|---|---|---|---|---|---|---|---|---|---|---|
| SHS | 2T2L | 539 | 1.31 | 481 | 2.02 | 1.12 | 202 | 1.58 | 358 | 0.74 |
| SW SHS | 70 × 70 × 1.66 | 528 | 1.09 | 211 | | 0.71 | 236 | | 233 | 1.11 |
| SW SHS | 1T1L | 528 | 1.09 | 310 | 1.47 | 1.05 | 290 | 1.23 | 262 | 0.85 |
| SW SHS | 1T1L | 528 | 1.09 | 305 | 1.45 | 1.03 | 284 | 1.20 | 262 | 0.86 |
| SW SHS | 2T2L | 528 | 1.09 | 328 | 1.56 | 1.11 | 279 | 1.18 | 296 | 0.90 |
| SW SHS | 2T2L | 528 | 1.09 | 315 | 1.50 | 1.07 | 272 | 1.15 | 296 | 0.94 |
| SW SHS | 100 × 100 × 1.66 | 528 | 1.57 | 236 | | 0.59 | 136 | | 247 | 1.05 |
| SW SHS | 1T1L | 528 | 1.57 | 295 | 1.25 | 0.74 | 147 | 1.08 | 283 | 0.96 |
| SW SHS | 1T1L | 528 | 1.57 | 286 | 1.21 | 0.71 | 143 | 1.05 | 283 | 0.99 |
| SW SHS | 2T2L | 528 | 1.57 | 398 | 1.68 | 0.99 | 177 | 1.30 | 323 | 0.81 |
| SW SHS | 2T2L | 528 | 1.57 | 407 | 1.72 | 1.02 | 177 | 1.31 | 323 | 0.79 |
| SW SHS | 150 × 150 × 1.66 | 528 | 2.39 | 204 | | 0.35 | 54 | | 257 | 1.26 |
| SW SHS | 1T1L | 528 | 2.39 | 334 | 1.64 | 0.58 | 73 | 1.36 | 299 | 0.89 |
| SW SHS | 1T1L | 528 | 2.39 | 382 | 1.87 | 0.66 | 85 | 1.58 | 299 | 0.78 |
| SW SHS | 2T2L | 528 | 2.39 | 574 | 2.81 | 1.00 | 106 | 1.98 | 347 | 0.60 |
| SW SHS | 2T2L | 528 | 2.39 | 446 | 2.19 | 0.77 | 82 | 1.54 | 347 | 0.78 |
| SW SHS | 200 × 200 × 1.66 | 528 | 3.20 | 249 | | 0.33 | 37 | | 262 | 1.06 |
| SW SHS | 1T1L | 528 | 3.20 | 356 | 1.43 | 0.47 | 43 | 1.16 | 307 | 0.86 |
| SW SHS | 1T1L | 528 | 3.20 | 366 | 1.47 | 0.49 | 45 | 1.20 | 307 | 0.84 |
| SW SHS | 2T2L | 528 | 3.20 | 366 | 1.47 | 0.49 | 39 | 1.04 | 359 | 0.98 |
| SW SHS | 2T2L | 528 | 3.20 | 356 | 1.43 | 0.42 | 33 | 0.88 | 359 | 1.14 |
| | | | | Mean 1T1L: | 1.32 | | | | Mean: | 1.08 |
| | | | | Mean 2T2L: | 1.57 | | | | COV: | 0.14 |

*Source*: Bambach *et al*. (2009b).

*Table 6.3* Experimental and theoretical quasi-static axial crushing results – commercially produced SHS (SHS) and spot-welded SHS (SW SHS)

| Square hollow section | Steel section ($b \times d \times t$) + CFRP matrix (mm) | Crush displ., $\Delta L$ (mm) | Yield stress, $f_y$ (MPa) | Mass/ length, $\mu$ (kg/m) | Static mean crush load, $P_{ms}$ (kN) | Increase in $P_{ms}$ compared with steel | Static specific energy, $E_{ss}$ (kJ/kg) | Increase in $E_{ss}$ compared with steel | *nf, nc* | Test/ exact* theory, $P_{mexact}$ |
|---|---|---|---|---|---|---|---|---|---|---|
| SHS | 50 × 50 × 2.0 | 42 | 484 | 2.80 | 72.3 | | 25.8 | | 4,4 | 1.02 |
| SHS | 1T1L | 42 | 484 | 3.09 | 102.0 | 1.41 | 33.0 | 1.28 | 4,4 | 1.03 |
| SHS | 1T1L | 42 | 484 | 3.10 | 105.0 | 1.45 | 33.9 | 1.31 | 4,4 | 1.06 |
| SHS | 2T2L | 42 | 484 | 3.37 | 132.9 | 1.84 | 39.4 | 1.53 | 4,4 | 1.25 |
| SHS | 2T2L | 42 | 484 | 3.36 | 125.9 | 1.74 | 37.5 | 1.45 | 4,4 | 1.19 |
| SHS | 65 × 65 × 2.0 | 94 | 405 | 3.64 | 71.9 | | 19.8 | | 4,4 | 1.09 |
| SHS | 1T1L | 94 | 405 | 4.03 | 96.9 | 1.35 | 24.0 | 1.22 | 4,4 | 0.97 |
| SHS | 1T1L | 94 | 405 | 4.05 | 106.3 | 1.48 | 26.2 | 1.33 | 4,4 | 1.06 |
| SHS | 2T2L | 94 | 405 | 4.42 | 130.8 | 1.82 | 29.6 | 1.50 | 4,4 | 1.27 |
| SHS | 2T2L | 94 | 405 | 4.41 | 110.1 | 1.53 | 25.0 | 1.26 | 4,4 | 1.06 |
| SHS | 75 × 75 × 2.0 | 79 | 417 | 4.21 | 73.5 | | 17.5 | | 4,4 | 1.00 |
| SHS | 1T1L | 79 | 417 | 4.68 | 107.9 | 1.47 | 23.1 | 1.32 | 4,4 | 0.97 |
| SHS | 1T1L | 79 | 417 | 4.66 | 107.8 | 1.47 | 23.1 | 1.33 | 4,4 | 0.97 |
| SHS | 2T2L | 79 | 417 | 5.05 | 130.0 | 1.77 | 25.7 | 1.47 | 4,4 | 1.11 |
| SHS | 2T2L | 79 | 417 | 5.07 | 143.7 | 1.96 | 28.3 | 1.62 | 4,4 | 1.23 |
| SHS | 100 × 100 × 2.0 | 108 | 539 | 6.54 | 97.1 | | 14.8 | | 4,4 | 0.88 |
| SHS | 1T1L | 108 | 539 | 7.22 | 123.5 | 1.27 | 17.1 | 1.15 | 4,4 | 0.77 |
| SHS | 1T1L | 108 | 539 | 7.26 | 138.1 | 1.42 | 19.0 | 1.28 | 4,4 | 0.86 |
| SHS | 2T2L | 108 | 539 | 7.75 | – | – | – | – | – | – |
| SHS | 2T2L | 108 | 539 | 7.79 | – | – | – | – | – | – |
| SW SHS | 70 × 70 × 1.66 | 69.5 | 528 | 4.25 | 63.6 | | 15.0 | | 4,4 | 1.13 |
| SW SHS | 1T1L | 69.5 | 528 | 5.10 | 89.8 | 1.41 | 17.6 | 1.18 | 4,4 | 1.01 |
| SW SHS | 1T1L | 69.5 | 528 | 5.12 | 96.8 | 1.52 | 18.9 | 1.26 | 4,4 | 1.09 |
| SW SHS | 2T2L | 69.5 | 528 | 5.59 | 123.7 | 1.95 | 22.1 | 1.48 | 4,4 | 0.97 |

| | | | | | | | | | | |
|---|---|---|---|---|---|---|---|---|---|---|
| SW SHS | 2T2L | 69.5 | 528 | 5.51 | 120.7 | 1.90 | 21.9 | 1.46 | 4,4 | 0.95 |
| SW SHS | 100 × 100 × 1.66 | 93 | 528 | 5.80 | 61.8 | | 10.7 | | 4,3 | 1.18 |
| SW SHS | 1T1L | 93 | 528 | 6.70 | 87.2 | 1.41 | 13.0 | 1.22 | 4,3 | 1.01 |
| SW SHS | 1T1L | 93 | 528 | 6.69 | 88.9 | 1.44 | 13.3 | 1.25 | 4,3 | 1.02 |
| SW SHS | 2T2L | 93 | 528 | 7.50 | 133.8 | 2.16 | 17.8 | 1.68 | 4,3 | 1.12 |
| SW SHS | 2T2L | 93 | 528 | 7.65 | 139.8 | 2.26 | 18.3 | 1.72 | 4,3 | 1.17 |
| SW SHS | 150 × 150 × 1.66 | 175 | 528 | 8.45 | 43.2 | | 5.1 | | 4,2 | 0.92 |
| SW SHS | 1T1L | 175 | 528 | 10.18 | 87.9 | 2.03 | 8.6 | 1.69 | 4,2 | 1.08 |
| SW SHS | 1T1L | 175 | 528 | 9.99 | 92.6 | 2.14 | 9.3 | 1.81 | 4,2 | 1.14 |
| SW SHS | 2T2L | 175 | 528 | 11.98 | 144.0 | 3.33 | 12.0 | 2.35 | 4,2 | 1.33 |
| SW SHS | 2T2L | 175 | 528 | 12.02 | 121.2 | 2.80 | 10.1 | 1.97 | 4,2 | 1.12 |
| SW SHS | 200 × 200 × 1.66 | 300 | 528 | 11.10 | 64.6 | | 5.8 | | 4,2 | 1.16 |
| SW SHS | 1T1L | 300 | 528 | 13.68 | 100.5 | 1.55 | 7.3 | 1.26 | 4,2 | 1.02 |
| SW SHS | 1T1L | 300 | 528 | 13.58 | 100.9 | 1.56 | 7.4 | 1.28 | 4,2 | 1.02 |
| SW SHS | 2T2L | 300 | 528 | 15.75 | 127.7 | 1.98 | 8.1 | 1.39 | 4,2 | 0.99 |
| SW SHS | 2T2L | 300 | 528 | 16.04 | 145.7 | 2.25 | 9.1 | 1.56 | 4,2 | 1.13 |
| | | | | Mean 1T1L: | | 1.52 | | 1.32 | Mean: | 1.06 |
| | | | | Mean 2T2L: | | 2.09 | | 1.60 | COV: | 0.11 |

* Includes the observed effects of corner splitting and curling indicated by *nf* and *nc*, where *nf* = number of faces engaged in folding, *nc* = number of corners engaged in corner yielding and corner restraint (i.e. corners that have not fractured and split).

*Table 6.4* Experimental and theoretical dynamic impact axial crushing results – commercially produced SHS (SHS) and spot-welded SHS (SW SHS)

| Square hollow section | Steel section ($b \times d \times t$) + CFRP matrix (mm) | Crush displ, $\Delta L$ (mm) | Dyn. peak force, $P_{maxd}$ (kN) | Incr. in $P_{maxd}$ c/w steel | Dyn. mean crush load, $P_{md}$ (kN) | Incr. in $P_{md}$ compared with steel | Dynamic specific energy, $E_{sd}$ (kJ/kg) | Incr. in $E_{sd}$ compared with steel | Dynamic/ static structural effective, $\eta_d/\eta_s$ | Dynamic structural effective, $\eta_d$ | Test/lower bound theory, $P_{mlower}$ $nf = nc = 2$ for SW SHS | Test/ exact* theory, $P_{mexact}$ (*nf,nc*,d) |
|---|---|---|---|---|---|---|---|---|---|---|---|---|
| SHS | 50 × 50 × 2.0 | 136 | 205 | | 76 | | 27.2 | | 1.41 | 0.53 | 1.14 | 1.14 (4,4) |
| SHS | 1T1L | 123 | 227 | 1.10 | 84 | 1.11 | 27.2 | 1.00 | 1.11 | 0.58 | 0.90 | 0.90 (4,4) |
| SHS | 1T1L | 114 | 209 | 1.02 | 91 | 1.19 | 29.2 | 1.08 | 1.16 | 0.63 | 0.97 | 0.97 (4,4) |
| SHS | 2T2L | 79 | 267 | 1.30 | 131 | 1.72 | 38.8 | 1.43 | 1.32 | 0.91 | 1.30 | 1.30 (4,4) |
| SHS | 2T2L | 96 | 244 | 1.19 | 108 | 1.42 | 32.1 | 1.18 | 1.15 | 0.75 | 1.08 | 1.08 (4,4) |
| SHS | 65 × 65 × 2.0 | 151 | 190 | | 68 | | 18.8 | | 1.26 | 0.36 | 1.10 | 1.10 (4,4) |
| SHS | 1T1L | 111 | 273 | 1.44 | 93 | 1.36 | 23.1 | 1.23 | 1.27 | 0.49 | 0.99 | 0.99 (4,4) |
| SHS | 1T1L | 109 | 253 | 1.33 | 95 | 1.39 | 23.4 | 1.24 | 1.18 | 0.50 | 1.01 | 1.01 (4,4) |
| SHS | 2T2L | 86 | 327 | 1.72 | 120 | 1.76 | 27.2 | 1.45 | 1.22 | 0.63 | 1.23 | 1.23 (4,4) |
| SHS | 2T2L | 66 | 340 | 1.79 | 157 | 2.29 | 35.5 | 1.89 | 1.88 | 0.82 | 1.60 | 1.60 (4,4) |
| SHS | 75 × 75 × 2.0 | 115 | 232 | | 90 | | 21.4 | | 1.42 | 0.42 | 1.14 | 1.14 (4,4) |
| SHS | 1T1L | 93 | 318 | 1.37 | 111 | 1.24 | 23.8 | 1.11 | 1.19 | 0.51 | 0.93 | 0.93 (4,4) |
| SHS | 1T1L | 90 | 330 | 1.42 | 115 | 1.28 | 24.7 | 1.15 | 1.23 | 0.53 | 0.96 | 0.96 (4,4) |
| SHS | 2T2L | 67 | 432 | 1.86 | 154 | 1.72 | 30.5 | 1.43 | 1.37 | 0.71 | 1.23 | 1.23 (4,4) |
| SHS | 2T2L | 64 | 389 | 1.67 | 161 | 1.80 | 31.9 | 1.49 | 1.30 | 0.75 | 1.29 | 1.29 (4,4) |
| SHS | 100 × 100 × 2.0 | 89 | 309 | | 116 | | 17.7 | | 1.50 | 0.34 | 1.08 | 1.08 (4,4) |
| SHS | 1T1L | 51 | 438 | 1.42 | 203 | 1.75 | 28.1 | 1.58 | 2.05 | 0.59 | 1.29 | 1.29 (4,4) |
| SHS | 1T1L | 55 | 460 | 1.49 | 188 | 1.62 | 25.9 | 1.46 | 1.70 | 0.54 | 1.20 | 1.20 (4,4) |
| SHS | 2T2L | 50 | 624 | 2.02 | 207 | 1.78 | 26.7 | 1.50 | – | 0.60 | 1.20 | 1.20 (4,4) |
| SHS | 2T2L | 50 | 552 | 1.79 | 245 | 2.11 | 31.4 | 1.77 | – | 0.71 | 1.43 | 1.43 (4,4) |
| SW SHS | 70 × 70 × 1.66 | 114 | 221 | | 100.9 | | 23.8 | | 1.59 | 0.41 | 1.86 | 0.93 (4,4) |
| SW SHS | 1T1L | 117 | 290 | 1.23 | 98.3 | 0.97 | 19.3 | 0.81 | 1.09 | 0.40 | 1.15 | 1.32 (2,2,d) |

| | | | | | | | | | | | | |
|---|---|---|---|---|---|---|---|---|---|---|---|---|
| SW SHS | 1T1L | 109 | 297 | 1.26 | 105.5 | 1.05 | 20.6 | 0.87 | 1.09 | 0.43 | 1.23 | 1.42 (2,2,d) |
| SW SHS | 2T2L | 88 | 434 | 1.84 | 130.7 | 1.30 | 23.4 | 0.98 | 1.06 | 0.53 | 1.06 | 1.22 (2,2,d) |
| SW SHS | 2T2L | 89 | 448 | 1.94 | 129.2 | 1.28 | 23.4 | 0.99 | 1.07 | 0.53 | 1.05 | 1.21 (2,2,d) |
| SW SHS | 100 × 100 × 1.66 | 151 | 259 | | 76.2 | | 13.1 | | 1.23 | 0.22 | 1.23 | 1.23 (2,2) |
| SW SHS | 1T1L | 82 | 357 | 1.38 | 140.2 | 1.84 | 20.9 | 1.59 | 1.61 | 0.40 | 1.38 | 0.99 (4,3,d) |
| SW SHS | 1T1L | 102 | 352 | 1.36 | 112.7 | 1.48 | 16.9 | 1.28 | 1.27 | 0.32 | 1.11 | 1.24 (2,2,d) |
| SW SHS | 2T2L | 92 | 415 | 1.60 | 125.0 | 1.64 | 16.7 | 1.27 | 0.93 | 0.36 | 0.88 | 0.98 (2,2,d) |
| SW SHS | 2T2L | 91 | 433 | 1.79 | 126.4 | 1.66 | 16.5 | 1.26 | 0.90 | 0.36 | 0.89 | 1.00 (2,2,d) |
| SW SHS | 150 × 150 × 1.66 | 93 | 336 | | 123.7 | | 14.6 | | 2.86 | 0.24 | 1.63 | 1.46 (4,2) |
| SW SHS | 1T1L | 109 | 401 | 1.23 | 105.5 | 0.85 | 10.4 | 0.71 | 1.20 | 0.20 | 0.82 | 0.89 (2,2,d) |
| SW SHS | 1T1L | 80 | 434 | 1.33 | 143.8 | 1.16 | 14.4 | 0.98 | 1.55 | 0.27 | 1.12 | 0.98 (4,2) |
| SW SHS | 2T2L | 60 | 593 | 1.82 | 191.7 | 1.55 | 16.0 | 1.09 | 1.33 | 0.36 | 1.10 | 0.98 (4,2) |
| SW SHS | 2T2L | 58 | 557 | 1.74 | 198.3 | 1.60 | 16.5 | 1.13 | 1.64 | 0.38 | 1.14 | 1.02 (4,2) |
| SW SHS | 200 × 200 × 1.66 | 88 | 357 | | 130.7 | | 11.8 | | 2.02 | 0.19 | 1.46 | 1.33 (4,2) |
| SW SHS | 1T1L | 86 | 406 | 1.14 | 133.7 | 1.02 | 9.8 | 0.83 | 1.33 | 0.19 | 0.86 | 0.91 (2,2,d) |
| SW SHS | 1T1L | 61 | 386 | 1.08 | 188.5 | 1.44 | 13.9 | 1.18 | 1.87 | 0.27 | 1.21 | 1.09 (4,2) |
| SW SHS | 2T2L | 55 | 413 | 1.16 | 209.1 | 1.60 | 13.3 | 1.13 | 1.64 | 0.30 | 1.01 | 1.08 (2,2,d) |
| SW SHS | 2T2L | 56 | 397 | 1.11 | 205.4 | 1.57 | 12.8 | 1.09 | 1.41 | 0.29 | 0.99 | 1.06 (2,2,d) |
| | | Mean 1T1L: | | 1.29 | | 1.30 | | 1.13 | 1.37 | Mean: | 1.16 | 1.14 |
| | | Mean 2T2L: | | 1.65 | | 1.68 | | 1.32 | 1.30 | COV: | 0.19 | 0.15 |

*Includes the observed effects of corner splitting, curling and debonding indicated by *nf*, *nc* and d, where *nf* = number of faces engaged in folding, *nc* = number of corners engaged in corner yielding and corner restraint (i.e. corners that have not fractured and split) and d = debonding of the CFRP from one or more faces of the SHS.

All compression members had a nominal length ($L$) of three times the section dimension ($b$, $d$).

High strength unidirectional carbon fibre was used and applied to the exterior of the SHS and SW SHS with epoxy. The high strength carbon fibre (termed MBrace® CF-130) was nominally 3790 MPa ultimate tensile strength and 230 GPa elastic modulus fibre. The fibre was nominally 0.176 mm thick. Two different fibre layouts were investigated: one layer laid transversely (i.e. around the section perpendicular to the direction of axial load) with one layer longitudinally (i.e. in the direction of axial load), hereafter termed '1T1L'; and two layers transversely with two layers longitudinally, hereafter termed '2T2L' (Fig. 6.1). The transverse layer was laid first, bonded directly to the steel, and the longitudinal layer second, then, for the 2T2L specimens, another transverse layer followed with the final layer longitudinal (Fig. 6.1). The resulting carbon fibre to steel ratios for the 1.6 mm thick specimens were 0.21 and 0.42 for 1T1L and 2T2L, respectively and, for the 2 mm thick specimens 0.18 and 0.35 for 1T1L and 2T2L, respectively.

Epoxy was used between the steel and first carbon fibre layer and each layer thereafter, Araldite® 420 for the SHS and Mbrace Part A and B saturant epoxy for the SW SHS. The sheets were overlapped by 20 mm such that premature failure at the overlaps was avoided. Prior to laying the carbon fibre, the metal surfaces were prepared by hand grinding (SHS) or sand blasting (SW SHS) to roughen the surface, then cleaned with acetone. All specimens were cured for at least 10 days at room temperature as per the manufacturer's instructions. After curing, the specimen ends were ground square and the CFRP was minimally hand ground at the ends such that only the steel was in contact with the loading platens of the testing machine. The purpose of this is that in some applications where CFRP might be retrofitted to an existing structure, access restrictions may preclude the application of the CFRP to the end of the member. Photos of a prepared SW SHS with CFRP are presented in Fig. 6.2.

The quasi-static compression specimens were tested in pure axial compression (0.2 mm/min), and were crushed to around one half of the member length. The dynamic compression specimens were tested axially in a drop-mass rig. The rig dropped a mass of 574 kg (SHS) or 639 kg (SW SHS) from a height of 1.835 m, resulting in a nominal impact velocity of 6 m/s and impact energy of 10.3 kJ (SHS) or 11.5 kJ (SW SHS).

## 6.3 Strengthening of thin-walled steel sections for axial compression

### 6.3.1 Buckling

Steel SHS may be considered as four stiffened plates, simply supported along both longitudinal edges, whose plate slenderness ratio ($\lambda$) is given by

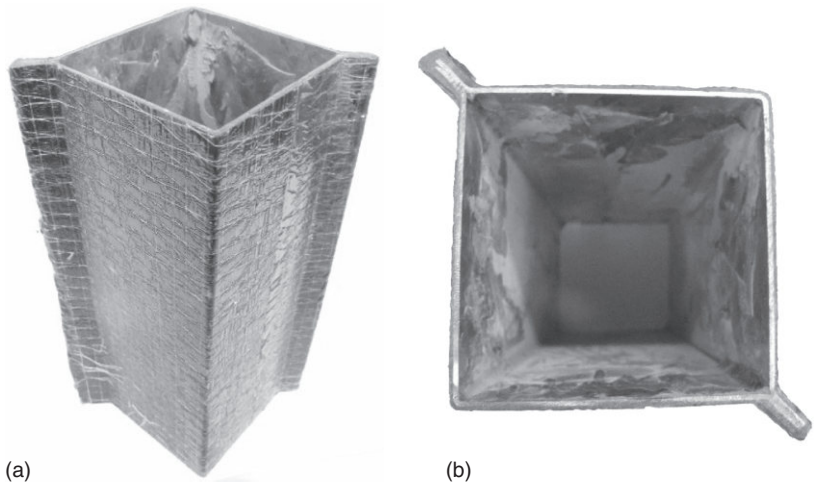


*6.2* Photographs of prepared 100 × 100 × 1.66 mm steel-CFRP 1T1L SW SHS (Bambach *et al.*, 2009b).

Eqs (6.1) and (6.2). The theoretical elastic buckling coefficient ($k$) is 4.0 for stiffened elements. In Eqs (6.1) and (6.2), $f_{cr}$ is the theoretical elastic buckling stress, $f_y$ is the yield stress, $E$ is Young's modulus, $t$ is the plate thickness, $b$ is the plate width and $\upsilon$ is Poisson's ratio.

$$\lambda = \sqrt{\frac{f_y}{f_{cr}}} \qquad [6.1]$$

$$f_{cr} = \frac{k\pi^2 E}{12(1-\upsilon^2)}\left(\frac{t}{b}\right)^2 \qquad [6.2]$$

The experimental elastic buckling loads were determined from the tests, and the experimental slenderness ($\lambda_{test}$) of the specimens was determined from Eq. (6.1) using the experimental buckling stress ($f_{crtest}$).

The (average) experimental buckling stress and slenderness results are presented in Table 6.1 for the slender sections, where it is shown that the increase in the buckling stress provided by externally bonding CFRP increases with the plate slenderness ratio and varies between 1.4 and 3.2 for the 1T1L specimens and between 1.8 and 4.2 for the 2T2L specimens. This is because more slender plates undergo greater buckling deformations, and correspondingly larger increases in buckling load result from the restriction of elastic buckling deformations that the CFRP provides. It was for this reason that both longitudinal and transverse layers of carbon fibre were provided, since membrane strains will be activated in both directions

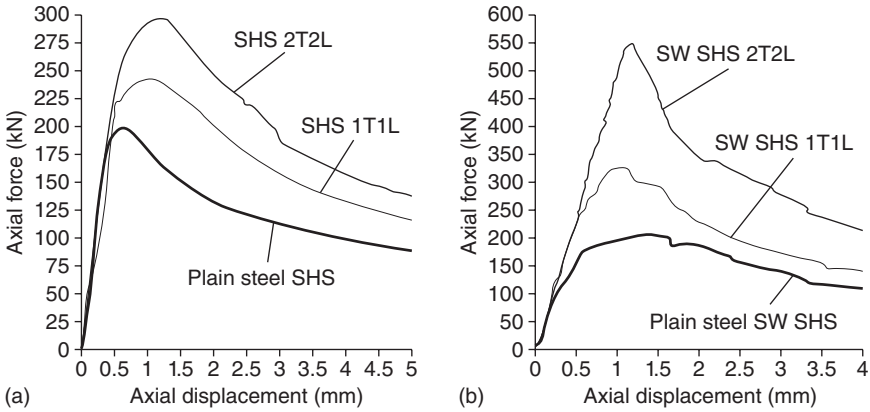


*6.3* Typical axial force–axial displacement results for quasi-static axial compression: (a) 75 × 75 × 2 mm SHS; (b) 150 × 150 × 1.66 mm SW SHS (Bambach and Elchalakani, 2007; Bambach *et al.*, 2009b).

when the section elastically buckles, whereas the carbon fibre is a unidirectional material. The increase in the buckling load provided by the CFRP is also evident in a sample of force–displacement plots shown in Fig. 6.3, where the change in axial stiffness that results from elastic buckling occurs at considerably higher loads in the CFRP-strengthened specimens. It is also evident that additional layers of CFRP provide additional increases in the elastic buckling load.

### 6.3.2 Post-buckling and strength

The experimental axial compression capacities ($P_{test}$) are presented in Table 6.2, along with the capacity increases resulting from the bonding of 1T1L and 2T2L CFRP matrix layouts, compared with the plain steel specimens. It is clear in Table 6.2 and Fig. 6.3 that significant increases in axial capacity result from the CFRP strengthening, 1.04–1.87 times the plain steel capacity for CFRP 1T1L (mean of 1.32) and 1.17–2.81 times for CFRP 2T2L (mean of 1.57). The addition of extra layers of CFRP further increases the capacity, and the capacity increases generally increase with plate slenderness as a result of the restriction of the elastic buckling deformations of slender sections.

### 6.3.3 Design

In this section, a generalised approach is derived, such that the buckling stress and axial capacity of composite SHS and SW SHS with any steel

geometry and carbon fibre matrix layout may be determined from the strength equation for steel plates (Winter equation) and the composite plate slenderness ratio ($\lambda_c$).

The slenderness of the composite plate is determined by assuming that the steel and CFRP are individual homogeneous layers that are perfectly bonded to form a two-layered plate, which was found to be the case in the experiments (up to the ultimate load). The CFRP layer may be treated as an isotropic layer in the present case, since the carbon fibres are distributed in the epoxy adhesive in orthogonal pairs (1T1L or 2T2L). The thickness of the carbon fibres used was 0.176 mm, and the thickness of the adhesive was assumed to be on average 0.1 mm per layer of carbon fibre which provides a lower bound to the measured dimensions. The thickness of the CFRP ($t_{CFRP}$) is the sum of the thickness of each of the carbon fibre ($t_{cf}$) and adhesive layers ($t_a$), and the total thickness of the two-layered plate ($t_t$) is given by Eq. (6.3) (where $t_s$ is the thickness of the steel).

The elastic modulus of the CFRP was determined from the modular ratio concept and given by Eq. (6.4), where the nominal values of the carbon fibre modulus ($E_{cf}$) and the adhesive modulus ($E_a$), 230 GPa and 1.9 GPa respectively, were used. The elastic buckling stress of the composite plate ($f_{crc}$) is given by Eq. (6.5), where the solution for the transformed flexural rigidity ($D_t$) of the perfectly bonded two-layered plate where each layer is isotropic was taken from Pister and Dong (1959). Nominal values of Poisson's ratio for the steel and CFRP of 0.3 and 0.25, respectively, were used. The theoretical composite plate slenderness ($\lambda_c$) is then given by Eq. (6.6), where the elastic buckling stress of the composite plate is non-dimensionalised to the yield stress of the steel plate ($f_{ys}$).

The theoretical composite plate slenderness is compared with the measured experimental composite plate slenderness (determined from the experimental buckling stress) in Table 6.1. Good correlation is shown in Table 6.1 with a mean test to predicted ratio of 0.96 and coefficient of variation of 0.13. The reasonably high variability is not uncommon due to the scatter that is typically found in experimental elastic buckling results, which is largely a result of geometric and material imperfections.

$$t_t = t_s + t_{CFRP} = t_s + (t_{cf} + t_a) \quad [6.3]$$

$$E_{CFRP} = \frac{E_a t_a + E_{cf} t_{cf}}{t_a + t_{cf}} \quad [6.4]$$

$$f_{crc} = \frac{k\pi^2}{t_t b^2} D_t \quad [6.5a]$$

$$D_t = \frac{AC - B^2}{A} \quad [6.5b]$$

$$A = \frac{E_s}{1-\upsilon_s^2} t_s + \frac{E_{CFRP}}{1-\upsilon_{CFRP}^2}(t_t - t_s) \quad [6.5c]$$

$$B = \frac{E_s}{1-\upsilon_s^2} \frac{t_s^2}{2} + \frac{E_{CFRP}}{1-\upsilon_{CFRP}^2} \frac{(t_t^2 - t_s^2)}{2} \quad [6.5d]$$

$$C = \frac{E_s}{1-\upsilon_s^2} \frac{t_s^3}{3} + \frac{E_{CFRP}}{1-\upsilon_{CFRP}^2} \frac{(t_t^3 - t_s^3)}{3} \quad [6.5e]$$

$$\lambda_c = \sqrt{\frac{f_{ys}}{f_{crc}}} \quad [6.6]$$

The experimental non-dimensionalised strengths are plotted against the experimental and theoretical composite plate slenderness values in Fig. 6.4a for the slender sections. Good agreement is found between the results, since the theoretical plate slenderness is reasonably accurate (Table 6.1). The Winter Eq. (6.7) for the strength of stiffened plates is plotted in Fig. 6.4a, and is shown to provide good correlation to the experimental strengths. Thus, having calculated the composite plate slenderness of the steel–CFRP sections, the Winter equation may be used to adequately determine the non-dimensionalised strength of the section. The properties

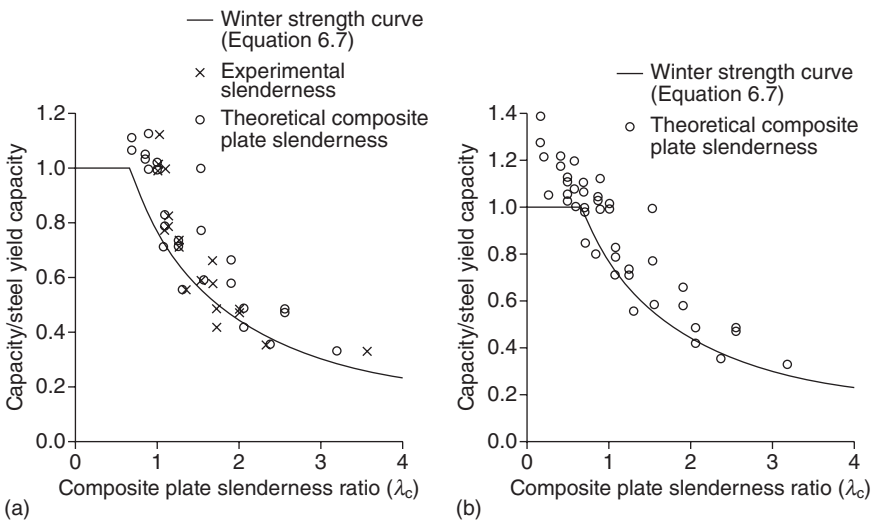


*6.4* Strength curves of the experimental capacity compared with the Winter strength curve (Eq. (6.7)) for SHS and SW SHS, against the plate slenderness ratio of the composite section: (a) experimental and theoretical slenderness for the slender sections; (b) theoretical slenderness for all sections (Bambach *et al.*, 2009b).

of the plain steel section were used to determine the axial capacity ($P_{uc}$), as shown by Eq. (6.8). An example calculation is presented in Bambach *et al*. (2009b).

$$\rho_c = \frac{1 - \frac{0.22}{\lambda_c}}{\lambda_c} \quad [6.7]$$

$$P_{uc} = \rho_c A_s f_{ys} \quad [6.8]$$

In qualitative terms, the design follows a procedure whereby the CFRP is included in the (geometric) calculation of the buckling stress and thereby the slenderness; however, only the steel section is used to calculate the strength. That is, the CFRP is assumed to play an important role in elastic buckling but not strength. This is congruent with the fact that the CFRP is not extended to the end of the specimens and is not in contact with the loading platens of the machine, and is thus not directly carrying axial load. This is also congruent with consideration of the axial strains in the composite section, where the axial strain in the steel at ultimate was approximately 0.003, whereas the ultimate stress of the carbon fibres is reached at an axial (tensile) strain of 0.015. Indeed, if the strain in the steel is 0.003 then the strain in the fibres will be considerably less due to shear lag (and will decrease across additional layers of carbon fibre). The assumption that the carbon fibres have minimal longitudinal compressive strain and may be ignored as a load-carrying element is only applicable to axial compression loading. This is certainly not the case in other applications, for example under axial crushing where the carbon fibres are engaged in the tension zone of the localised folds of the crushing process, as discussed in Section 6.4.2.

The experimental and theoretical results for all specimens are compared in Fig. 6.4b and Table 6.2. It is shown in Table 6.2 that good agreement with the experiments is provided by the design method, with a mean test to predicted ratio of 1.08 and coefficient of variation of 0.14. The design method is directly applicable to thin-walled steel hollow sections with flat plate elements of any geometry (within practical limits), strengthened with unidirectional carbon fibre layers laid in orthogonal directions. The method should only be applied to matrix layouts that consist of orthogonal fibre layer pairs, since the theory assumes that both the steel and CFRP are isotropic layers.

### 6.3.4 Optimisation

It is clear in Tables 6.1 and 6.2 that, as the steel section slenderness increases, the increase in the buckling stress and compressive strength of the

CFRP-strengthened sections compared to the steel sections also increases. The application of CFRP to sections with low slenderness ratios, or sections that are fully effective at ultimate (plate slenderness ratios of less than 0.673), may not be expected to provide appreciable benefit. Such sections do not suffer from elastic buckling, thus the application of CFRP provides minimal increases in strength.

It is also clear in Table 6.2 that there is a limit to the strength increase provided by the CFRP. Beyond a slenderness of 2.4 it appears that the 1T1L and 2T2L matrix layouts do not provide greater strength increases than around 1.5 times the plain steel capacity. This is similar behaviour to plain steel plates where, for very large slenderness values, changes in the buckling stress and therefore slenderness value produce only small changes in strength. Thus increasing benefit may be achieved by the application of CFRP to thin-walled steel sections with plate slenderness values from 0.673 to 2.4, with the optimum benefit at a steel plate slenderness of approximately 2.4.

## 6.4 Strengthening of thin-walled steel sections for axial impact

### 6.4.1 Quasi-static and dynamic axial crushing

A number of crashworthiness indicators are typically determined for crush components in order to assess their performance and to compare with other types of energy absorbing systems. The energy absorbed by a component under axial deformation ($E$) is determined as the area beneath the load–displacement curve. The mean crush load ($P_m$) is defined as the energy absorbed divided by the crushing distance ($\Delta L$):

$$P_m = \frac{E}{\Delta L} \qquad [6.9]$$

The specific energy ($E_s$) is an important parameter with regard to energy absorption capability, and is defined as the energy dissipated per crushed specimen weight, where $\mu$ is the mass/unit length of the specimen:

$$E_s = \frac{P_m}{\mu} = \frac{E}{\mu \Delta L} \qquad [6.10]$$

The structural effectiveness parameter ($\eta$) allows comparisons of the mean dynamic load to be made between structures having different material properties. The mean crush load is non-dimensionalised to the yield load of the steel specimens, where $A_s$ is the cross-sectional area of the steel and $\sigma_{ys}$ is the yield stress of the steel:


*6.5* Typical quasi-static axial crushing mechanisms: (a) 75 × 75 × 2 SHS; (b) 100 × 100 × 1.66 mm SW SHS (Bambach and Elchalakani, 2007; Bambach *et al.*, 2009c).

$$\eta = \frac{P_{\mathrm{m}}}{A_{\mathrm{s}}\sigma_{\mathrm{ys}}} \qquad [6.11]$$

The quasi-static and dynamic steel SHS specimens failed in an axi-symmetric ductile, stable plastic collapse mode where the flat faces formed a roof mechanism and progressively folded axially. The 1T1L and 2T2L steel–CFRP SHS generally failed in the same axi-symmetric ductile, stable plastic collapse mode as the steel SHS. Figure 6.5a shows typical failure modes for steel SHS and steel–CFRP SHS. The CFRP generally folded in the crushing mechanism with the steel, without debonding from the steel; however, at the corners some crushing and fibre breakage of the CFRP was evident (Fig. 6.5a). In many cases, the steel–CFRP specimens also displayed some minor debonding of the CFRP away from the steel at the ends of the specimens at the first fold (Fig. 6.5a). The quasi-static and dynamic axial crushing test results are tabulated in Tables 6.3 and 6.4, and the crushing

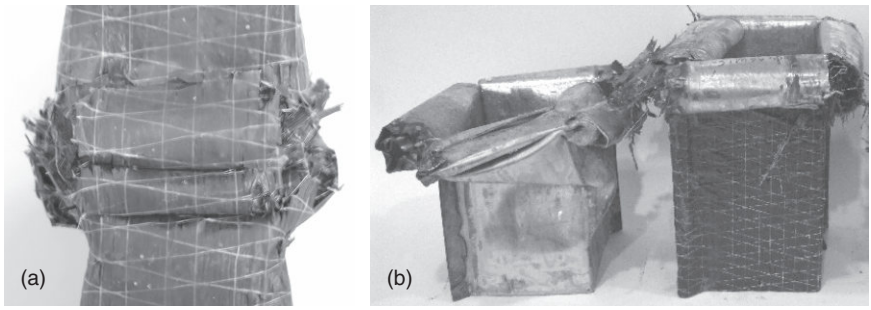


*6.6* Typical dynamic impact axial crushing mechanisms: (a) 75 × 75 × 2 SHS; (b) 100 × 100 × 1.66 mm SW SHS (Bambach *et al.*, 2009a, b).

behaviours were nominally identical between quasi-static (Fig. 6.5a) and dynamic (Fig. 6.6a) conditions for the steel–CFRP SHS.

The quasi-static steel SW SHS specimens failed in a similar manner to the SHS; however, they underwent a substantial amount of material fracturing, either along the spot-welded corners or the cold-formed corners. At the spot-welded corners, the failure occurred by fracture of the spot-weld and/or fracture of the parent material around the spot-weld (Fig. 6.5b). Such pull-out failure was due to mechanical overloading of the spot-weld and/or parent material, not interfacial failure due to inadequate spot-weld quality. Such failure modes are related to the limited ductility of the steel (only 9 % for the SW SHS), and the effect of the heat-affected zone around the spot-weld on the ductility of the steel. At the cold-formed corner material fracture was also evident in many quasi-static tests (Fig. 6.5b). Such failure modes were related to the limited ductility of the steel and the residual plastic strain induced in the corner material as a result of the cold-forming process. All quasi-statically loaded specimens exhibited spot-weld and material fracture to some degree and, in many cases, the effect was so extensive as to cause corner splitting. The term 'corner splitting' describes when fracture at either the spot-welded or cold-formed corner occurs completely, such that no steel remains connected between the two adjoining faces of the SW SHS (Fig. 6.5b). This process occurred longitudinally along the length of the corner in conjunction with the face folding crushing process. That is, the corner opened up progressively as the crushing process developed progressively. The corner splitting process necessarily also involves fibre breakage of the CFRP fibres in the transverse direction (Fig. 6.5b). Additionally, in many instances one or two of the flat faces of the SW SHS underwent curling rather than folding. Curling is the process by which the face curls outwards and rolls up, in conjunction with corner splitting along both edges (Fig. 6.5b). In most cases, the CFRP remained bonded to the steel face during curling.

The extent of corner splitting in the quasi-static SW SHS tests is indicated in Table 6.3, where the number of corners that did not undergo corner splitting (*nc*) is documented for each specimen. It is clear in Table 6.3 that the extent of corner splitting tended to increase as the face width of the SW SHS increased, and the extent of corner splitting was found to be dependent upon the material ductility and the steel section geometry. The extent of curling is also indicated in Table 6.3, where the number of faces that underwent folding is documented (*nf*) (i.e. the number of faces that did not undergo curling).

Similar to the quasi-static SW SHS tests, the dynamic SW SHS axial impact tests exhibited extensive material fracturing, either along the spot-welded corners or the cold-formed corners. Fracturing occurred to such a degree that in all dynamic tests corner splitting occurred in at least two of the four corners of the section, and in some cases more (Fig. 6.6b). In many impact tests, the specimens also exhibited some debonding of the CFRP from the face(s) of the SW SHS. This is sometimes referred to as 'laminar splaying', and the CFRP debonds and moves away from the steel as a sheet of CFRP (Fig. 6.6b). In most cases, only one or two of the faces involved debonding, and in some cases partial debonding occurred whereby the CFRP folded into the first fold then debonded away from additional folds. In cases where debonding occurred, the folding mechanism of the steel face beneath occurred in the usual manner. Additionally, in many instances one or two of the flat faces of the SW SHS underwent curling (Fig. 6.6b). The extent of corner splitting, face curling and face debonding in the impact tests is indicated in Table 6.4.

The increase in the crashworthiness indicators resulting from the bonding of CFRP to steel SHS and SW SHS is tabulated in Tables 6.3 and 6.4 for quasi-static and dynamic axial crushing, respectively. Sample force–displacement plots for dynamic axial crushing are presented in Fig. 6.7. It is clear that substantial increases in peak force, mean crush load and specific energy absorption may be achieved with the application of externally bonded CFRP. The quasi-static crush load was increased from 1.27 to 2.14 times with CFRP 1T1L (mean of 1.52), and from 1.53 to 3.33 times with CFRP 2T2L (mean of 2.09). The dynamic crush load was increased from 1.02 to 1.84 times with CFRP 1T1L (mean of 1.30), and from 1.30 to 2.29 times with CFRP 2T2L (mean of 1.68).

The strengthening effect of the CFRP was less pronounced for the SW SHS than for the SHS sections, and less pronounced for the SW SHS dynamic tests than the SW SHS quasi-static tests. The result is that the strengthening effect of bonded CFRP is generally less pronounced for dynamic crushing than quasi-static crushing (as evidenced by the mean crush loads above). This was due to the extensive fracturing, curling and debonding that occurred, where such a change in crushing mechanism

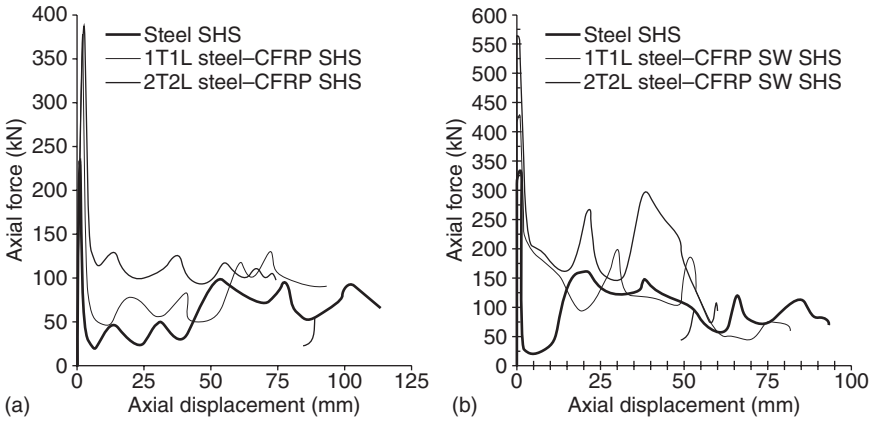


*6.7* Typical axial force–axial displacement results for dynamic impact axial crushing: (a) 75 × 75 × 2 mm SHS; (b) 150 × 150 × 1.66 mm SW SHS (Bambach *et al.*, 2009a, c).

reduces the ability of the specimens to absorb energy, and the members become less efficient. However, while many of the failure mechanisms associated with the SW SHS tests involved brittle modes such as material fracture, splitting, curling and debonding, all tests displayed ductile, stable plastic collapse under large axial deformation. This is due to the fact that while some brittle processes occurred on some faces of the SW SHS, the remaining faces continued to deform in stable plastic folding mechanisms. Where debonding occurred, in some cases it was partial debonding such that the CFRP remained engaged in some of the folds and, when debonding did occur, the steel face beneath continued to deform in the stable face folding mechanism. These processes also absorb energy, as the steel tears and spot-welds deform and fracture.

## 6.4.2 Design

In Bambach and Elchalakani (2007) a theoretical method was derived to calculate the quasi-static mean crushing load for steel–CFRP SHS, which explicitly accounts for the contributions of the face folding mechanism ($P_f$), the (compression) yielding of the corners ($P_{cy}$) and the corner membrane restraint ($P_{cr}$). The reader is referred to Bambach and Elchalakani (2007) for the full derivation and details. The formulae for the mean crushing load are summarised in Fig. 6.8, where $A_c$ is the corner area, $t_s$ and $t_f$ are the steel and CFRP thickness, $\alpha$ was found to be 0.84, $\sigma_{ys}$ and $\sigma_{yf}$ are the steel yield stress and CFRP ultimate tensile stress, respectively, and $\sigma_{yc}$ is the corner yield stress which was taken as $1.25\sigma_{ys}$. The theory determines an effective

| | |
|---|---|
| $M_p = \sigma'_{yf} \frac{t_s^2}{4}$<br>$P_f = \frac{2\pi M_p}{\alpha}$<br>$P_{cy} = \sigma_{yc} A_c$<br>$P_{cr} = \frac{\pi \sigma'_{yc} t_s \lambda}{4\beta}$<br>$P_m = \sum_1^{nf} P_f + \sum_1^{nc} P_{cy} + \sum_1^{nc} P_{cr}$ | $\sigma'_{yf} = \frac{1 + 2k_f t_r + 2k_f t_r^2 - k_f^2 t_r^2}{(1 + t_r^2)} \cdot \sigma_{ys}$<br>$\sigma'_{yc} = \frac{1 + 2k_c t_r + 2k_c t_r^2 - k_c^2 t_r^2}{(1 + t_r^2)} \cdot \sigma_{yc}$<br>$k_f = \frac{\sigma_{yf}}{\sigma_{ys}} \quad k_c = \frac{\sigma_{yf}}{\sigma_{yc}} \quad t_r = \frac{t_f}{t_s}$<br>$b_2 = b - 2r_{ext} \quad \lambda = \frac{\alpha b_2}{2} \quad r_{ext} = \beta t_s$ |
| *nf* = number of faces engaged in face folding<br>*nc* = number of corners engaged in corner yielding and corner restraint | |
| Strain-rate effects may be incorporated by increasing the flow-stress according to:<br>$\frac{\sigma_d}{\sigma_s} = 1 + \left(\frac{\dot{\varepsilon}}{D}\right)^{\frac{1}{p}} \quad \dot{\varepsilon} = 0.33 \frac{v_0}{b}$ | |
| For exact calculations, *nf* and *nc* correspond to observed failure mechanisms.<br>For design calculations, the following values may be assumed:<br>Seam-welded or spot-welded steel with good ductility: $nf = nc = 4$<br>Spot-welded steel with limited ductility < 10 % (lower bound): $nf = nc = 2$ | |

*6.8* Summary of theory for predicting the quasi-static and dynamic impact mean crush load (Bambach *et al.*, 2009c).

yield stress for the composite steel–CFRP, given by $\sigma_{ys}'$ and $\sigma_{yf}'$. The theory assumes that the longitudinal layers of carbon fibre (L) are fully engaged in the face folding process of the crushing mechanism, the transverse layers (T) are fully engaged in the corner membrane restraint, and the carbon fibres are not engaged in the corner (compression) yielding mechanism.

Modifications were required in order to account for the failure mechanisms observed in the steel–CFRP SW SHS tests. The corner splitting process reduces the energy absorbed from the corner yielding and corner membrane restraint components of the mean crush load, and the theory may be modified accordingly by excluding the corner yielding and corner restraint components for the split corners. The curling mechanism may be accounted for by excluding the contribution to the mean crush load of face folding, for the faces that exhibited curling. The energy involved in the curling process was comparatively small and was neglected. The debonding mechanism may be accounted for by excluding the contribution of the CFRP in the face folding mechanism, and was achieved by replacing the effective yield stress for the composite steel–CFRP face folding with the steel yield stress, for the faces on which debonding occurred. Additionally, the steel and CFRP lips (Fig. 6.1) were included in the theoretical mean crush load by incorporating the extra material in the face folding and corner yielding contributions.

The quasi-static theory was modified to account for strain-rate effects by increasing the effective yield stress of the steel according to the well-known Cowper–Symonds Equation (6.12). An equation for estimating the strain-rate from the impact velocity ($\upsilon_0$) was derived by Abramowicz and Jones (1984) and is given by Eq. (6.13). The strain-rate parameters $D$, $p$ in Eq. 6.12 are typically taken as $40.4\,s^{-1}$ and 5 respectively, which corresponds to the increase in the yield stress of mild steel (Jones, 1983).

$$\frac{\sigma_d}{\sigma_s} = 1 + \left(\frac{\dot{\varepsilon}}{D}\right)^{\frac{1}{p}} \qquad [6.12]$$

$$\dot{\varepsilon} = 0.33\frac{v_0}{b} \qquad [6.13]$$

The corner splitting, curling and debonding mechanisms were explicitly included in the theoretical mean crush load calculations for the SW SHS, according to the values of *nf*, *nc* and *d* in Tables 6.3 and 6.4. Additionally, accounting for strain-rate effects for the impact tests, theoretical mean crush loads ($P_{mexact}$) were calculated and are compared with the experimental results in Tables 6.3 and 6.4. The results compare well with the test results, with means and coefficients of variation of test to predicted ratios for quasi-static and dynamic axial crushing of (1.06, 0.11) and (1.14, 0.15), respectively.

While the theory for standard axial crushing of thin-walled seam-welded SHS may be appropriately modified to account for the effects of corner splitting, curling and debonding, the specimens must first be tested and the failure mechanisms observed and accounted for. In a design situation, such failure mechanisms will not be known *a priori*; therefore, a lower bound theory was developed that may conservatively be used for design. Due to the extent of corner splitting, curling and debonding in the dynamic tests, one should assume that only two faces will be engaged in steel–CFRP face folding, and only two corners will be engaged in corner yielding and corner restraint. Thus the standard axial crushing theory was applied to one half of the specimen, and increased for strain-rate effects according to Eqs (6.12) and (6.13). This approach was recommended for steels with ductility less than 10 % (Fig. 6.8), and was thus applied only to the SW SHS specimens. The resulting lower bound is designated $P_{mlower}$ in Table 6.4 and provides a slightly more conservative prediction, with a mean test to predicted ratio of 1.16 and coefficient of variation of 0.19.

### 6.4.3 Optimisation

The quasi-static axial crushing results indicated an optimum increase in mean crush load of around three times for the specimens of slenderness 2.4

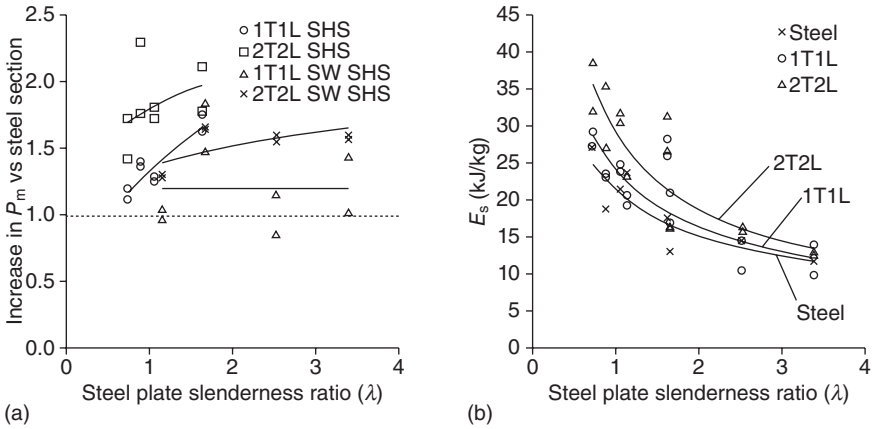


*6.9* Comparisons of (a) the increase in mean crush force with bonded CFRP, (b) the specific energy magnitudes, for SHS and SW SHS under dynamic impact axial crushing.

with 2T2L CFRP (Table 6.3). In order to investigate the effect of section geometry and bonding CFRP for dynamic impact axial crushing, comparison figures are presented in Fig. 6.9. It is clear in Fig. 6.9a that the bonding of CFRP generally has increasing benefit to the dynamic mean crush load with increasing slenderness; however, there is a substantial difference between the SHS and SW SHS. The increase in the dynamic mean crush load is less pronounced for the SW SHS, due to the fracturing, curling and debonding as discussed previously. It is clear in Fig. 6.9b that the dynamic specific energy of 2T2L steel–CFRP sections is superior to that for 1T1L steel–CFRP sections, which in turn is superior to that for steel-only sections. As the ratio of the tube wall width to thickness increases, the dynamic specific energy decreases, which is a well-known result for thin-walled tubes. Thus, while more slender sections will benefit more from the application of bonded CFRP, the optimum section for dynamic specific energy absorption is steel sections with low width to thickness ratios strengthened with 2T2L CFRP.

## 6.5 The role of the steel–CFRP bond

In the composite steel–CFRP SHS sections, a strong bond was achieved by preparing the surface of the steel, then a layer of epoxy adhesive was used between the steel and the first layer of carbon fibres. The strong bond was evidenced in the experiments, where it was shown that no debonding occurred prior to the ultimate condition being attained; however, some debonding occurred during the crushing process at the specimen ends. In

Bambach (2010b) CFRP-only SHS, identical to those bonded to the steel SHS previously, were fabricated by using the steel SHS as a mandrel. Using a barrier material, the CFRP-only SHS were slid off the steel SHS mandrel after curing. The strengths of the CFRP-only SHS were then determined independently under quasi-static compression and crushing, and were compared with the steel-only SHS and composite steel–CFRP SHS in order to determine the extent of composite action occurring in the composite SHS.

The axial compression strength of the composite steel–CFRP SHS was significantly greater than the sum of the capacities of the individual components (the CFRP-only SHS strength plus the steel-only SHS strength), with a mean of 1.26 and maximum of 1.83. In all cases, this value exceeded 1.0, which indicated that the composite action provided by the bond was always beneficial, regardless of the steel geometry. An example comparison force–displacement plot of the steel-only SHS, CFRP-only SHS, composite steel–CFRP SHS and the (numerical) addition of the steel-only and CFRP-only SHS is shown in Fig. 6.10a for the SHS with highest strength ratio, which demonstrates the benefit of the composite action. Similarly, the quasi-static crush loads of the composite steel–CFRP SHS were significantly greater than those of the individual components, with a mean of 1.44 and maximum of 1.82. An example comparison plot is shown in Fig. 6.10b for the SHS with highest crush load ratio.

The mechanism by which the strength ratio and crush load ratio exceed one was composite action provided by the bond. As discussed previously,

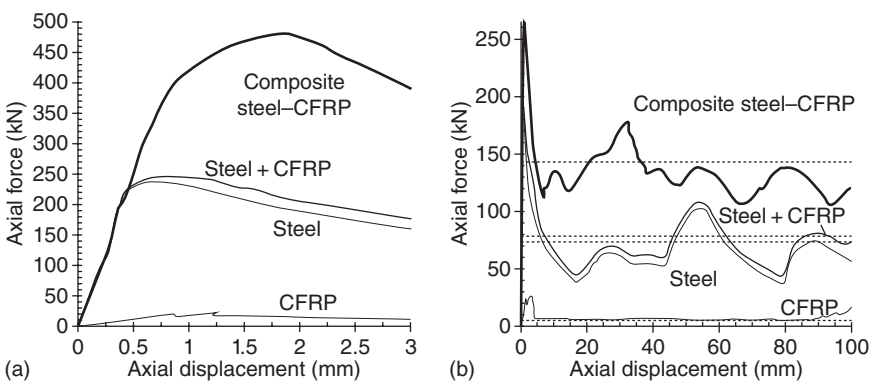


*6.10* Comparison of the axial load–axial displacement results for (a) 100 × 100 × 2 mm SHS, (b) 75 × 75 × 2 mm SHS. Plots are for CFRP-only SHS (CFRP), steel-only SHS (Steel), CFRP-only + steel-only SHS (Steel + CFRP) and steel with bonded CFRP SHS (Composite steel–CFRP) (Bambach *et al.*, 2010b).

the axial compression strength increases with the application of CFRP due to the increase in the buckling stress and, for this to occur, the steel and CFRP require a strong bond in order for them to behave as a perfectly bonded two-layered plate. The mean crush load increases with the application of CFRP, primarily due to the bond enforcing tension strains in the carbon fibres in the exterior of the folding lobes during the crushing process. Without being bonded to the steel, the CFRP tubes crushed with bending and/or fracture of the CFRP walls, both of which provided limited load resistance and corresponding small mean crush loads. The bonding of the carbon fibres to steel and subsequent tension straining in the folding lobes is a more efficient utilisation of the fibres than in the wall bending/fracturing of the CFRP SHS independently.

## 6.6 Conclusion and future trends

The experimental and design results summarised in this chapter were for thin-walled square steel sections with externally bonded carbon fibres. However, the behaviours are generally applicable to other metals and FRP materials, so long as the bond between the metal and FRP may be achieved. This has been shown to be the case with a variety of metals by Song *et al.* (2000) for example, where aluminium, steel and copper circular hollow sections were strengthened with externally epoxy bonded glass fibres. Similarly, in Bambach (2010a), aluminium and stainless steel SHS were successfully strengthened with CFRP in a similar manner to the steel sections discussed in this chapter. Indicative strength design could be achieved using the design equations presented in this chapter, using the material properties for the particular metal and FRP. With future advances in metal alloys, fibre materials and polymer adhesives, high performance composite metal-fibre structures could be manufactured. Fibre orientations could also be varied (already commonplace in FRP structures), producing metal–fibre composites with advanced properties tailored to particular applications. Similarly, metal–fibre composites could be developed for loading conditions other than the axial compression conditions discussed in this chapter. Studies of thin-walled steel circular sections strengthened with CFRP under pure bending have shown significant strength improvements (Haedir *et al.*, 2009), and fibre layouts may again be tailored to the particular application.

With the practical application of such structures will come the necessity of maintaining a strong bond throughout the service life of the metal–fibre composite structure. As discussed in Section 6.5, the strengthening mechanism relies on the bond between the metal and the fibres. Environmental conditions will need to be considered for some applications, and further research is required into the environmental degradation of

metal–fibre adhesives over time, some preliminary studies of which are presented by Nguyen (2012a, b).

## 6.7 References

Abramowicz W. and Jones N. (1984). 'Dynamic axial crushing of square tubes'. *International Journal of Impact Engineering*, 2(2), pp. 179–208.

Abramowicz W. and Jones N. (1986). 'Dynamic progressive buckling of circular and square tubes'. *International Journal of Impact Engineering*, 4(4), pp. 243–270.

Bambach M.R. (2010a). 'Axial capacity and crushing behaviour of metal-fibre square tubes – steel, stainless steel and aluminium with CFRP'. *Composites Part B: Engineering*, 41(7), pp. 550–559.

Bambach M.R. (2010b). 'Axial capacity and crushing of thin-walled metal, fibre-epoxy and composite metal-fibre tubes'. *Thin-Walled Structures*, 48(6), pp. 440–452.

Bambach M.R. and Elchalakani M. (2007). 'Plastic mechanism analysis of steel SHS strengthened with CFRP under large axial deformation'. *Thin-Walled Structures*, 45(2), pp. 159–170.

Bambach M.R., Elchalakani M. and Zhao X.L. (2009a). 'Composite steel-CFRP SHS tubes under axial impact'. *Journal of Composite Structures*, 87(3), pp. 282–292.

Bambach M.R., Jama H.H. and Elchalakani M. (2009b). 'Axial capacity and design of thin-walled steel SHS strengthened with CFRP'. *Thin-Walled Structures*, 47(10), pp. 1112–1121.

Bambach M.R., Jama H.H. and Elchalakani M. (2009c). 'Static and dynamic axial crushing of spot-welded thin-walled composite steel-CFRP square tubes'. *International Journal of Impact Engineering*, 36(9), pp. 1083–1094.

Chiu C.H., Lu C.K. and Wu C.M. (1997). 'Crushing characteristics of 3D braided composite square tubes'. *Journal of Composite Materials*, 31, pp. 2309–2327.

Czaplicki M.J. and Robertson R.E. (1991). 'Comparison of bevel and tulip triggered pultruded tubes for energy absorption'. *Composites Science and Technology*, 40, pp. 31–46.

Farley G. and Jones R. (1992). 'Crushing characteristics of continuous fibre-reinforced composite tubes'. *Journal Composite Materials*, 26, pp. 37–50.

Fyllingen Ø., Hopperstad O.S. and Langseth M. (2008). 'Simulations of a top-hat section subjected to axial crushing taking into account material and geometry variations'. *International Journal of Solids and Structures*, 45, pp. 6205–6219.

Fyllingen Ø., Hopperstad O.S. and Langseth M. (2009). 'Robustness study on the behaviour of top-hat thin-walled high-strength steel sections subjected to axial crushing'. *International Journal of Impact Engineering*, 36(1), pp. 12–24.

Haedir J., Bambach M.R., Zhao X.-L. and Grzebieta R. (2009). 'Strength of circular hollow sections (CHS) tubular beams externally reinforced by carbon FRP sheets in pure bending'. *Thin-Walled Structures*, 47(10), pp. 1136–1147.

Hanefi E.H. and Wierzbicki T. (1996). 'Axial resistance and energy absorption of externally reinforced metal tubes'. *Composites Part B*, 27B, pp. 387–394.

Johnson W., Soden P.D. and Al-Hassani S.T.S. (1977). 'Inextensional collapse of thin-walled tubes under axial compression'. *Journal of Strain Analysis*, 12(4), pp. 317–330.

Jones N. (1983). Structural aspects of ship collisions, in Jones N. and Wierzbicki T. (eds), *Structural Crashworthiness*. Butterworths, London, pp. 308–337.

Mamalis A.G., Manolakas D.E. and Viegelahn G.L. (1989). 'Axial crushing of thin PVC tubes and frusta of square cross section'. *International Journal of Impact Engineering*, 8(3), pp. 241–264.

Mamalis A., Manolakos D., Viegelahn G., Yap S. and Demosthenous G. (1991). 'Microscopic failure of thin-walled fibre-reinforced composite frusta under static axial collapse'. *International Journal of Vehicle Design*, 12, p. 557.

Mamalis A., Manolakos D., Demosthenous G.A. and Ioannidis M. (1996). 'Analysis of failure mechanisms observed in axial collapse of thin-walled circular fibreglass composite tubes'. *Thin-walled Structures*, 24, pp. 335–352.

Mamalis A., Manolakos D., Demosthenous G. and Ioannidis M. (1997a). 'The static and dynamic axial crumbling of thin-walled fibreglass composite square tubes'. *Composites Part B*, 28B, pp. 439–551.

Mamalis A., Robinson M., Manolakos D., Demosthenous G., Ioannidis M. and Carruthers J. (1997b). 'Review: crashworthy capability of composite material structures'. *Composite Structures*, 37, pp. 109–134.

Mamalis A., Manolakos D., Ioannidis M. and Papapostolou D. (2005). 'On the response of thin-walled CFRP composite tubular components subjected to static and dynamic axial compressive loading: experimental'. *Composite Structures*, 69, pp. 407–420.

Meng Q., Al-Hassani S.T.S. and Soden P.D. (1983). 'Axial crushing of square tubes'. *International Journal of Mechanical Science*, 25(9–10), pp. 747–773.

Nguyen T.C., Bai Y., Zhao X.L. and Al-Mahaidi R. (2012a). 'Durability of steel/CFRP double strap joints exposed to sea water, cyclic temperature and humidity'. *Composite Structures*, 94(5), pp. 1826–1833.

Nguyen T.C., Bai Y., Al-Mahaidi R. and Zhao X.L. (2012b). 'Time-dependent behaviour of steel/CFRP double strap joints subjected to combined thermal and mechanical loading'. *Composite Structures*, 94(5), pp. 1834–1845.

Park H.C., Choi Y. and Yoon K.J. (2000). 'Crush energy absorbing characteristics of graphite/epoxy square tubes'. *Key Engineering Materials*, 183–187, pp. 1099–1104.

Pister K.S. and Dong S.B. (1959). 'Elastic bending of layered plates'. *Journal of the Engineering Mechanics Division, ASCE*, 85(EM4).

Schneider F. and Jones N. (2003). 'Influence of spot-weld failure on crushing of thin-walled structural sections'. *International Journal of Mechanical Science*, 45, pp. 2061–2081.

Schneider F. and Jones N. (2004). 'Impact of thin-walled high-strength steel structural sections'. *Proceedings of the Institution of Mechanical Engineers D: Journal of Automobile Engineering*, 218, pp. 131–158.

Shaat A. and Fam A. (2006). 'Axial loading tests on short and long hollow structural steel columns retrofitted using carbon fibre reinforced polymers'. *Canadian Journal of Civil Engineering*, 33, pp. 458–470.

Song H.W., Wan Z.M., Xie Z.M. and Du X.W. (2000). 'Axial impact behavior and energy absorption effciency of composite wrapped metal tubes'. *International Journal of Impact Engineering*, 24, pp. 385–401.

Tarigopula V., Langseth M., Hopperstad O.S. and Clausen A.H. (2006). 'Axial crushing of thin-walled high-strength steel sections'. *International Journal of Impact Engineering*, 32, pp. 847–882.

Teng J.G. and Hu Y.M. (2007). 'Behaviour of FRP-jacketed circular steel tubes and cylindrical shells under axial compression'. *Construction and Building Materials*, 21(4), pp. 827–838.

Thornton P.H. (1986). 'The crush behaviour of glass fiber reinforced plastic sections'. *Composites Science and Technology*, 27, pp. 199–223.

Wang X.G. and Lu G. (2002). 'Axial crushing force of externally fibre-reinforced metal tubes'. *Proceedings of the Institute of Mechanical Engineers*, 216, pp. 863–873.

White M.D. and Jones N. (1999). 'Experimental quasi-static axial crushing of top-hat and double-hat thin-walled sections'. *International Journal of Mechanical Science*, 41, pp. 179–208.

White M.D., Jones N. and Abramowicz W. (1999). 'A theoretical analysis for the quasi-static axial crushing of top-hat and double-hat thin-walled sections'. *International Journal of Mechanical Science*, 41, pp. 209–233.

Wierzbicki T. and Abramowicz W. (1983). 'On the crushing mechanics of thin-walled structures'. *Journal of Applied Mechanics*, 50, pp. 727–734.

# 7

# Rehabilitation of steel tension members using fiber-reinforced polymer (FRP) composites

F. MATTA, University of South Carolina, USA and
M. DAWOOD, University of Houston, USA

**DOI**: 10.1533/9780857096654.2.169

**Abstract**: This chapter discusses the repair of steel tension members using adhesively bonded FRP laminates. The chapter first outlines conventional repair methods and introduces the alternative of bonded FRP laminates, discussing the key issue of surface preparation for durability. The chapter then covers the fundamentals of design and analysis with an emphasis on detailing and stress, and comments on future trends fostered by the latest advances in material science.

**Key words**: adhesive bonding, corrosion, fatigue, repair, steel.

## 7.1 Introduction

This chapter reviews the repair of damaged tension members using adhesively bonded fiber-reinforced polymer (FRP) composite laminates. Representative tension members include truss elements, eye bars, flanges in flexural members and portions of hollow core members subjected to tensile stresses. Repair responds to the need to restore the original or an enhanced structural capacity as prompted by structural deficiencies in the main members or connections, either welded or mechanically fastened (see Fig. 7.1). Typical damage conditions may accrue from fatigue and fracture phenomena (Fisher, 1984; Nishikawa *et al*., 1998; Marianos *et al*., 2006), corrosion (Zoccola, 1976; Albrecht and Hall, 2003) and accidental overloads. These conditions are encountered especially in steel structures that operate in sometimes aggressive environments (e.g., proximity to seawater, industrial site, cold regions where de-icing salts are routinely used) and that are subjected to fatigue loads (e.g., traffic including rails, wind), such as steel bridges and overhead transmission line structures.

Section 7.2 outlines conventional repair methods together with the idea of using of adhesively bonded steel plates as a means to avoid the stress raisers and fatigue-sensitive details introduced by bolting and welding, while Section 7.3 introduces the use of adhesively bonded FRP laminates as a rational means to overcome limitations in the constructability and structural efficiency offered by traditional methods. Section 7.4 outlines the

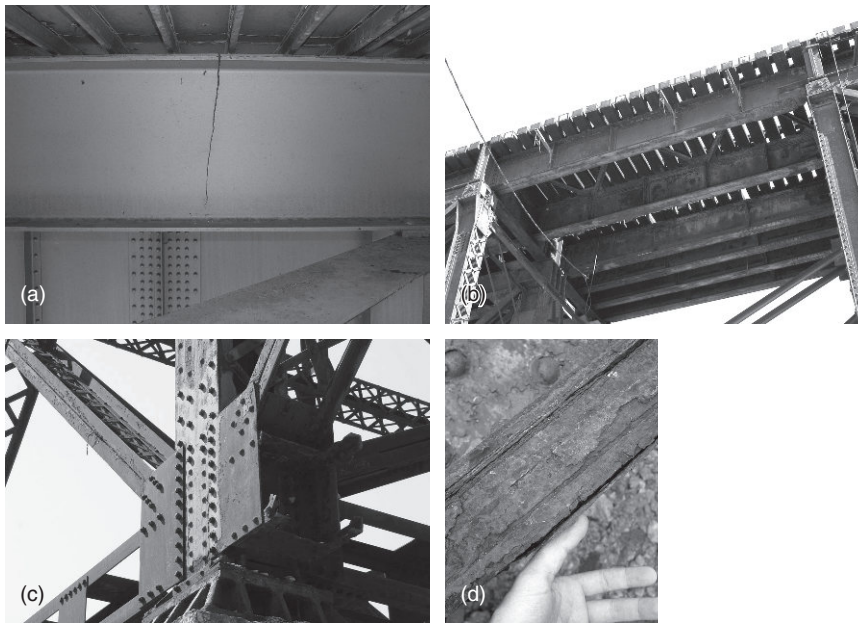


*7.1* Damage in steel tension members: (a) stringer with crack initiated at open butt joint between fillet welded shim plates on top flange subjected to tensile fatigue stresses; (b) railroad bridge superstructure to be replaced showing diffuse corrosion; (c) corroded steel truss members with riveted connections partially replaced with bolted connections; and (d) close-up photograph of through-thickness corrosion in riveted steel members of railroad bridge structure.

materials used in bonded FRP repairs and Section 7.5 discusses enhancements to the steel–FRP bond, ranging from the critical aspect of surface preparation and its implications for durability, to the mitigation of galvanic and crevice corrosion phenomena. Section 7.6 outlines the fundamentals of design and analysis of adhesively bonded FRP repairs with an emphasis on best practices for detailing and stress analysis, while Section 7.7 offers a brief commentary on likely future trends that stem primarily from advances in material science. The chapter concludes with a short descriptive section of sources of further information and advice.

## 7.2 Repair methods

### 7.2.1 Conventional methods

Structural repair may be preferable to partial or complete replacement when a structure or structural member is damaged or fails to meet applicable serviceability requirements. It is important to note that the choice often

depends on considerations related to structural efficiency and durability as much as constructability and workers' safety. For example, the overall cost of removing lead paint in an old steel member to be repaired may render a repair impractical in the absence of other relevant constraints. Klaiber *et al*. (1987) compiled a comprehensive literature review on methods for repairing steel bridge members, including tension members that are also representative of those in other steel structures. The review had the objective to serve as a best practice manual for engineers. Traditional repair methods that have been successfully implemented include the following.

When repairing a cracked tension member, drilling a hole in front of the crack tip is the most common and immediate strategy to blunt crack propagation by eliminating stress singularities. This may be the only action required in the case of secondary members. However, this method is typically deployed when the crack has grown enough to be visually detected; in the case of primary members, such as bridge girders, crack blunting only serves to limit the damage and prevent rapid crack growth due to fracture phenomena, and must be complemented with more extensive repairs to restore or increase the original stiffness and strength.

The load resisting area of steel can be increased where needed by attaching a cover plate onto the deficient or damaged member by means of bolted or welded connections, thereby increasing the load resisting area of steel where needed. Splice plates can be used to repair cracked members by enabling the load to be transferred across the crack. In general, heavy equipment is required to lift and position the steel plates due to their relatively high weight. This may be an issue in overhead applications, such as the repair of portions of beams and girders subjected primarily to tensile stresses that are produced by positive bending moments. Welds and, to a lesser extent, mechanically fastened connections inevitably generate fatigue-sensitive details (Fisher, 1984), especially when they are executed in the field where it is more challenging to ensure quality compared with shop conditions. Another concern is the potential for galvanic and crevice corrosion (Fontana, 1986) when dissimilar metals are joined by means of mechanical fasteners or welds.

### 7.2.2 Adhesively bonded steel plates

Instead of being welded or bolted onto the damaged steel tension member, steel cover plates can be adhesively bonded using structural adhesives without introducing stress raisers and fatigue-sensitive details as can be the case with welding and bolting. In fact, adhesive bonding was originally investigated as a successful means to connect bridge girders to secondary members (e.g., transverse stringers and stiffeners) in lieu of welds, which proved to be prone to fatigue failure (Nara and Gasparini, 1981; Gasparini

*et al.*, 1990). Adhesive bonding of cover plates may also be used in conjunction with bolting the plate ends to prevent debonding; Albrecht (1987) demonstrated through laboratory tests that the use of hybrid bolted/adhesive joints can result in an increase in fatigue life by a factor of 20 over that of welded cover plates. In addition to constructability concerns because of the need for heavy equipment posed by the weight of steel plates, the appeal of this method was offset by the lack of knowledge of long-term environmental and fatigue bond durability. However, this method served as the precursor to the use of adhesively bonded light weight FRP laminates in lieu of steel cover plates, both in terms of idea and dissemination of empirical evidence in support thereof.

## 7.3 Adhesive bonding of fiber-reinforced polymer (FRP) laminates

The use of adhesively bonded FRP laminates pairs the concept of enlisting structural adhesives instead of mechanical fasteners and welds that may introduce fatigue-sensitive details, with the peculiar advantages offered by FRP laminates instead of steel plates, including:

- *High strength-to-weight and stiffness-to-weight ratio*, which makes it possible to design repairs to achieve the target reduction in stress and deformations, or increase in strength, with a much smaller increase in dead loads compared with steel cover plates. In addition, the bonding of relatively thin laminates may not pose issues related to clearance, when applicable, and may have more acceptable aesthetic impacts, making it attractive for the restoration of historical structures.
- *Light weight*, which becomes a constructability advantage as it facilitates the bonding operations without the need for heavy equipment and relatively large numbers of workers, especially in overhead applications.
- *Tailorability in terms of shape and physical and mechanical properties*, which enables one to design and manufacture FRP laminates with shape and ply stacking sequence to meet specific design requirements. In addition, commercially available pultruded FRP laminates can be supplied as coils, making the need to join them unlikely.
- *Superior fatigue life to that of structural steel*, which is an important attribute in structures subjected to live loads; and,
- *Corrosion resistance*, which offsets durability concerns in the case of structures that operate in aggressive environments and contributes to minimizing the life-cycle costs.

By capitalizing on these advantages, relatively time-consuming and expensive repair operations may be avoided, thereby minimizing the period of interruption to the use of a given structure. The effectiveness of an

adhesive bond depends on the correct selection of the bonding method (and implementation thereof) and materials; quality control is critical, since the effective non-destructive inspection and evaluation of adhesive bonds remains a challenge (Roach and Scala, 2002). Different methods may be employed when bonding FRP laminates onto steel tension members. The most representative methods are introduced as follows, while the materials are introduced in the next section.

- *Adhesive bonding of prefabricated laminates*: Prefabricated FRP laminates are cut into strips (Miller *et al*., 2001) or larger plates (Luke, 2001) and adhesively bonded under pressure, for example by clamping, to facilitate adhesion. Compelling advantages are the ease and speed of application, and the consistency of the adhesive layer in terms of homogeneity and gap filling, resulting in relatively stiff and strong repair systems. The main drawbacks are related to the adhesives used (which are typically based on thermoset polymeric resins that cure under ambient temperature), ranging from the brittleness of the adhesive to the difficulty of the replacement operations, and the sustainability features, including toxicity and non-recyclability. In addition, only applications on flat surfaces without major geometric discontinuities other than cracks to be repaired are feasible.
- *Wet layup*: Fabrics made of reinforcing fibers are impregnated and bonded with a polymeric resin (e.g., Jones and Civjan, 2003; Xiao *et al*., 2011), typically using rollers to maximize compaction and eliminate voids. New layers are added until the required thickness is achieved. As an alternative, pre-impregnated plies may be used in lieu of dry fabrics (Photiou *et al*., 2006). The main advantage is the ability to bond onto steel surfaces that are curved (e.g., tubular members) or with geometric discontinuities (e.g., mechanically fastened connections). However, this procedure may be slow and complex, and requires extreme care since it is susceptible to introducing defects as the reinforcing fabrics may wave and wrinkle during installation, resulting in weaker areas. This problem may be offset if a vacuum bagging procedure is used, which would also increase costs. It is noted that wet layup FRP laminates generally exhibit lower fiber volume fraction and stiffness than prefabricated FRP laminates; consequently, wet layup applications may require thicker laminates to achieve the structural enhancement sought.
- *Hot-melt bonding*: Prefabricated FRP laminates that use a thermoplastic resin are bonded to the steel substrate via hot-melting without the need for an external adhesive (Bourban *et al*., 1994; Love and Karbhari, 2006). This solution makes it possible to take advantage of the higher toughness of thermoplastic FRP laminates compared to thermoset counterparts. Hot-melt bonded thermoplastic FRP laminates can accommodate

relatively large deformations when subjected to mechanical or thermal stresses without compromising the steel–FRP bond.

- *In situ resin infusion*: Dry fabrics made of reinforcing fibers are secured onto the area to be repaired, which is then fully encapsulated in a vacuum bag. A suitable low viscosity polymeric resin is then infused into the preform and cured while vacuum is drawn to compact the FRP patch (Mertz and Gillespie, 1996; Rajagopalan *et al*., 1996). Similar to the wet layup method, the main advantage is the ability to bond onto steel surfaces that are curved or with geometric discontinuities. However, FRP bonding may require complex and time-consuming operations.

Heating methods may be enlisted to accelerate the curing of the adhesive. In particular, induction heating is especially suitable for steel members, since the temperature can be uniformly raised along the steel–adhesive interface through magnetic induction (Bourban *et al*., 1994; Wetzel, 1995).

## 7.4 Materials

### 7.4.1 Carbon fiber-reinforced polymer laminates

Carbon FRP (CFRP) laminates are the advanced composite material of choice to repair steel members due to the more compatible stiffness of CFRP materials compared to steel, whereas glass FRP (GFRP) laminates having lower stiffness may be considered for the repair of aluminum members (Fam *et al*., 2006). CFRP laminates are made up primarily by two constituents, namely reinforcing carbon fibers and polymeric matrix. Sizing agents are applied to the surface of the fibers to protect them during handling and to improve the adhesion with the polymeric matrix. The carbon fibers contribute to the specific (i.e., per unit weight) strength and stiffness properties, while the resin matrix binds the fibers together and provides toughness and environmental resistance. A review of the salient properties can be found in Walsh (2001). Representative properties of carbon fibers for use in structural CFRP composites are summarized in Table 7.1, including high strength (HS), high modulus (HM) and ultra-high modulus (UHM) fibers. The tensile strength is one order of magnitude greater than that of structural steel and, in the case of the UHM fibers, the modulus of elasticity may be more than four times that of structural steel. However, a major limitation is posed by the inability to undergo plastic deformations and the relatively low strain to failure.

The polymeric matrix typically consists of thermoset resins, in particular epoxy and vinyl ester-based systems. Thermoset matrices offer advantages including relatively high tensile strength and elastic modulus (typically in the range 27–90 MPa and 700–3500 MPa, respectively), low level of volatiles, low shrinkage and good chemical resistance; in addition, they lend

*Table 7.1* Representative engineering properties of carbon fibers for structural CFRP laminates

| Property | High strength (HS) | High modulus (HM) | Ultra-high modulus (UHM) |
|---|---|---|---|
| Density (g/cm$^3$) | 1.8 | 1.9 | 2.1 |
| Modulus of elasticity (GPa) | 230 | 390 | 620–930 |
| Tensile strength (MPa) | 3400 | 2900 | 2600–2700 |
| Strain to failure (%) | 1.50 | 0.75 | 0.60 |
| Coefficient of thermal expansion (1/°C) | –1 to 0.4 | –1 to 0.4 | –1 to 0.4 |

*Table 7.2* Representative properties of precured carbon–epoxy CFRP laminates

| Property | High strength (HS) | High modulus (HM) | Ultra-high modulus (UHM) |
|---|---|---|---|
| Density (g/cm$^3$) | 1.6 | 1.6 | 1.6 |
| Modulus of elasticity* (GPa) | 165 | 210 | 300 |
| Tensile strength* (MPa) | 3100 | 3200 | 1500 |
| Strain to failure* (%) | >1.70 | >1.35 | >0.45 |

*In the longitudinal direction (mean value showed).

themselves to use in different processes of CFRP manufacturing. The main shortcomings are the relative brittleness and sensitivity to moisture, together with high costs and the sustainability concerns introduced previously.

Representative properties of HS, HM and UHM carbon–epoxy CFRP laminates (Sika, 2009) are summarized in Table 7.2. The fatigue resistance of unidirectional CFRP laminates is highlighted by an endurance limit that ranges between 60 and 70 % of the monotonic tensile strength (National Research Council, 1991), compared with 50 % for structural steels. CFRP laminates are also nearly insensitive to creep (Yamaguchi *et al.*, 1997; Malvar, 1998). Table 7.3 also presents a comparison between the density, tensile strength and elastic modulus of CFRP laminates and low-carbon structural steel, which is commonly encountered in steel repair applications. It is noted that the mechanical properties of the composite material reflect the contribution of the polymeric matrix, which has significantly lower strength and stiffness properties compared to those contributed by the fibers. The main implication is perhaps the reduction in elastic modulus to a level that lies below that of structural steel for the case of HS CFRP laminates. It is important to maximize the elastic modulus of the CFRP to develop a structurally efficient repair. In fact, higher elastic moduli increase

*Table 7.3* Representative property ratios between CFRP pultruded laminates and Fe 250 steel

| Property | HS CFRP/steel | HM CFRP/steel | UHM CFRP/steel |
|---|---|---|---|
| Density ratio | 0.2 | 0.2 | 0.2 |
| Elastic modulus* ratio | 0.8 | 1.0 | 1.4 |
| Tensile strength* ratio | 5.1–7.0 | 4.4–6.0 | 2.4–3.2 |

*In the longitudinal direction.

the portion of load that can be transferred from the steel to the CFRP prior to and after yielding of the steel unless relatively thick composite laminates are used. This is relevant for repair applications that target service loads, such as in response to the need to transfer tensile stresses from the steel to the CFRP across a fatigue crack. Conversely, the ratio of tensile strength of CFRP to steel is not a concern for repair cases where CFRP rupture is considered even when using applicable strain limitations to account for the brittleness of the composite material.

Given the relatively high elastic modulus of steel of about 200 GPa, the use of externally bonded pultruded unidirectional HM or UHM CFRP laminates is the most attractive option for repairs where stress transfer along a specific direction is sought. In fact, pultrusion manufacturing results in high quality unidirectional and continuous CFRP plates with constant cross-section (Sumerak and Martin, 2001), and with an elastic modulus that is maximized by ensuring a fiber volume fraction of 65 % or more. Pultruded CFRP plates or strips can also be supplied with a pre-treated (e.g., roughened) bonding surface. A review of manufacturing techniques can be found in Mazumdar (2001).

### 7.4.2 Structural adhesives

The correct selection of a structural adhesive is a key task in the design of an FRP repair system. Different bonding strategies must be evaluated on a case-by-case basis considering the main variables that play a role in meeting structural demand (Bonk *et al.*, 1996; Rajagopalan *et al.*, 1996; West, 2001). Besides cost considerations, the following attributes should be considered:

- *Shear strength and ductility*, in order to provide the necessary load transfer capabilities, deformability and toughness;
- *Fatigue resistance*, which is critical in tension members subjected to cyclic loads such as bridge trusses or transmission line poles in windy areas;

- *Creep resistance*, especially when the repaired member is expected to carry sustained loads;
- *Environmental durability*, especially when repairing structures that operate in aggressive environments;
- *Sensitivity to changes in the bond line thickness*, which is relevant when repairing geometrically discontinuous parts and heavily corroded members;
- *Curing time and temperature*, in order to attain the design strength rapidly and preferably without the need of artificial heating;
- *Workability*, as adhesives must be viscous enough to remain in place during bonding;
- *Consolidation pressure*, where lower requirements benefit constructability by reducing the need for special equipment; and
- *Pot life*, where higher values benefit constructability by facilitating installation over large areas.

One-component epoxy resins tend to have a longer pot life, making them suitable for installations over large areas, but typically require elevated temperatures for curing (Rajagopalan *et al*., 1996). Two-part, HS epoxy resins are often considered to bond precured CFRP laminates (Mertz and Gillespie, 1996; Miller *et al*., 2001; Sen *et al*., 2001; Lenwari *et al*., 2002; Dawood and Rizkalla, 2010). Table 7.4 lists representative properties of a two-part epoxy adhesive (Sika, 2011) that is suitable for steel–CFRP applications (e.g., Matta *et al*., 2005). Together with being specifically developed to ensure good adhesion to metal substrates, two-part epoxy adhesives cure at ambient temperature, typically achieving 70 % or more

*Table 7.4* Representative properties of two-part epoxy structural adhesive*

| Property | Test standard | Value |
|---|---|---|
| Specific weight (g/cm$^3$) | After mixing of the components | 2.0 |
| Pot life (min) | – | ~70 |
| Tensile strength (MPa) | After 7 days, ASTM D 638 | 24.8 |
| Tensile modulus of elasticity (MPa) | After 7 days, ASTM D 638 | 4482 |
| Strain to failure (%) | After 7 days, ASTM D 638 | 1.0 |
| Compressive strength (MPa) | After 7 days, ASTM D 695 | 59.3 |
| Compressive modulus of elasticity (MPa) | After 7 days, ASTM D 695 | 2689 |
| Shear strength (MPa) | After 14 days, ASTM D 732 | 24.8 |
| Moisture absorption (%) | After 24 h, ASTM D 570 | 0.03 |

* Determined at a temperature of 23 °C and relative humidity of 50 %.

of the specified strength within 24 hours (Campbell, 2001). In this regard, it was reported that it is feasible to bond CFRP laminates to the tension flange of steel beams that are subjected to cyclic loading during curing of the two-part epoxy adhesive, provided that the maximum shear stress in the adhesive is limited (Moy, 2007). However, brittleness remains an issue, together with the difficulties associated with removal and replacement operations and sustainability concerns. Epoxy-based adhesives that cure at ambient temperature may also be post-cured at elevated temperature; in fact, post-curing can elevate the glass transition temperature, which may be desirable for applications where relatively high service temperatures are expected.

Methacrylate adhesives may also be considered with the intent of offsetting the lower shear strength (compared to that of two-part epoxy adhesives) with a reduced sensitivity to changes in the bond line thickness, and a shorter curing time where about 75 % of the specified shear strength can be achieved in two hours at ambient temperature (Mertz and Gillespie, 1996).

Hot-melt adhesives based on thermoplastic resins are suitable for wet layup applications, together with thermoset (e.g., epoxy and vinyl ester) resins (Rajagopalan *et al*., 1996). The toxicity of the resins used in wet layup applications is generally an issue, and the bonding operations must be carefully performed to reduce the risk of accidents and release of hazardous chemicals into the surrounding environment. For example, a vinyl ester-based resin was used in a CFRP laminate bonded to the substrate of an aluminum ship structure in need of strengthening, with the aid of vacuum bagging (Grabovac, 2003). Some vinyl ester resins are suitable for *in situ* infusion due to their low viscosity prior to curing (Rajagopalan *et al*., 1996). Thermoplastic resins are also a valid option for fusion bonding applications aimed at repairing structural members with irregular geometries or whose substrates are difficult to access (Rajagopalan *et al*., 1996; Clifford and Manger, 2002; Love and Karbhari, 2006); in this case, a shear strength comparable to that of two-part epoxy adhesives may be attained (Bourban *et al*., 1994), but heat sources and pressure are required, thus raising costs. A comprehensive review of fusion bonding techniques can be found in Ageorges and Ye (2002).

## 7.5 Bond enhancement

### 7.5.1 Surface preparation

The surface preparation of the steel and FRP adherends is critical to ensure the strength and durability of an adhesively bonded repair. In general, it is expected that a correct selection of materials and bonding method will

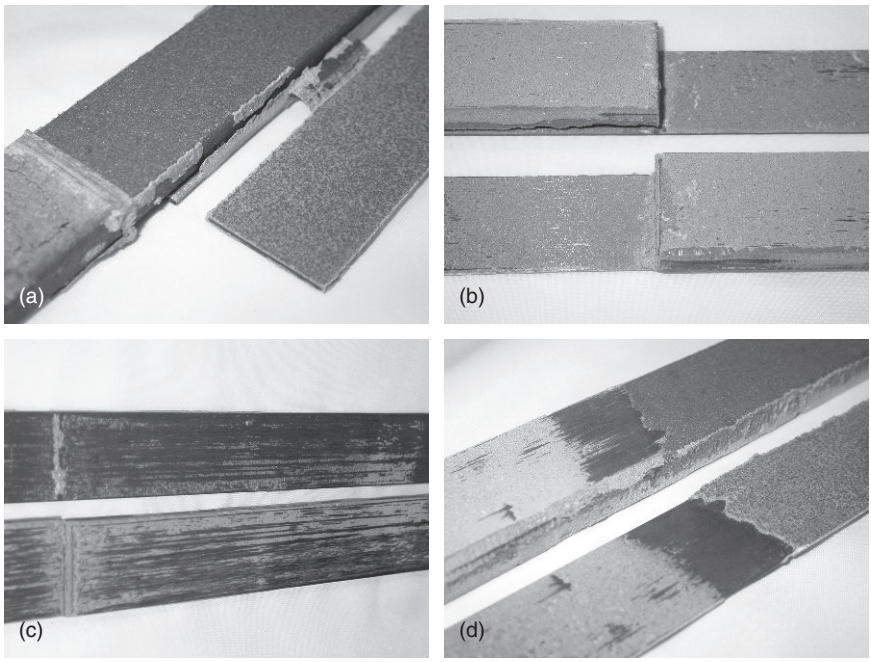


*7.2* Failure mode of steel–CFRP adhesive joints in steel plates tested in tension: (a) interface fracture between steel and adhesive; (b) cohesive failure in adhesive layer; (c) interlaminar failure in composite; and (d) mixed cohesive–interlaminar–interface failure.

result in cohesive failure in the adhesive layer rather than disbonding along the steel–FRP interface or interlaminar failure in the FRP laminate, as illustrated in the photographs in Fig. 7.2. A review of surface preparation techniques can be found in Arnott *et al*. (2002). Surface preparation may entail the following three basic steps.

- *Solvent degreasing*: This process aims at removing surface contaminants such as oil, rust and coatings. The selection of the solvent depends on the substrate material; for example, acetone is suitable for steel while methyl ethyl ketone (MEK) or methanol are suitable for CFRP when precured laminates are used. The solvents may be applied using a damp cloth. It is important that the cloth be free of contaminants such as dyes and lanoline; for example, MEK can dissolve the organic material in certain cloths, leaving the contaminants on the FRP substrate after it evaporates.
- *Chemical etching or surface abrasion*: This process aims at exposing a chemically active surface to enable the formation of strong and durable chemical bonds between the adhesive and the substrates. For steel

substrates including corroded ones, the procedure may entail grit blasting followed by removal of debris by dry wiping. Light grit blasting and dry wiping may also be applied on CFRP substrates, paying attention to avoiding damaging the composite. For the case of precured CFRP laminates whose substrate has been roughened to make it 'bond ready', solvent degreasing may be sufficient, although light sand blasting may contribute to providing a more chemically active surface.

- *Priming of the steel substrate*: This process aims at enhancing the chemical affinity between the hydroxyl terminations of the steel oxide layer and the adhesive, thereby yielding a more stable and durable interface. Silane-based primers are particularly attractive (Gettings and Kinloch, 1977). The chemical composition of (trioxy) silane-based primers is typically R–Si(OR')$_3$, where R is a functional group with chemical affinity with the polymeric adhesive, and R' is usually methyl or ethyl. The primer is generally diluted in aqueous solutions; the hydrolysis to trisilanols –Si(OH)$_3$ is followed by the condensation with the –OH groups on the steel substrate, and results in the formation of a covalently bonded siloxane where the R groups can react with the adhesive (Adams *et al.*, 1997). This process is illustrated in Fig. 7.3. The chemical modification of the FRP substrate is not generally recommended since the interface between the composite and the adhesive is not as susceptible to hydration as that between the steel and the adhesive. Chapter 4 of this book presents a detailed discussion of the functionality of silane coupling agents and the selection of a compatible silane-based primer.

The comparative experimental evaluation of alternative solutions may rely on simple single-lap-bond tensile tests (for example, per ASTM D 1002). The most appropriate test method to assess surface preparation and durability is perhaps a modified wedge test (for example, based on ASTM

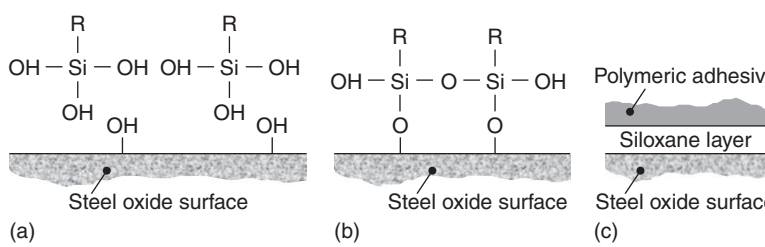


*7.3* Schematic of formation of siloxane layer on silane-primed steel substrate: (a) silane absorption from aqueous solution; (b) silane condensation and formation of covalent bonds with oxide layer; and (c) application of polymeric adhesive and cross-linking with siloxane layer.

D 3762). The standard procedure consists of forcing a 3.2 mm thick steel wedge in the adhesive layer between two flat 25 × 200 mm aluminum strips, which are replaced by a steel and a FRP strip. The initial crack is measured after the introduction of the wedge following the exposure of the specimens to different environments (e.g., ambient conditions, salt water, freeze–thaw cycles). Then, the specimens are returned to the original exposure environment, measuring the progressive crack growth resulting from the concurrent action of stress concentration due to the wedge and environmental conditioning. The relative effectiveness of different bonding strategies is evaluated by comparing the measured crack lengths. While this technique is useful in comparing different bonding methods and materials, it does not provide quantitative information to estimate service life.

Evidence from wedge tests was used in a number of investigations. Bourban *et al*. (1994) reported that silane-based primers do not necessarily improve the shear strength of steel-CFRP adhesive bonds, but contribute to enhancing the durability of epoxy bonded and fusion bonded (through thermoplastic resins) joints. Experimental evidence reported by West (2001) suggested that the use of a silane-based primer can aid in ensuring a more desirable cohesive failure in the adhesive layer when epoxy bonded pultruded CFRP strips are used. A similar case study was also reported by McKnight *et al*. (1994). In addition, Karbhari and Shulley (1995) noted that epoxy bonds between steel and glass FRP laminates may be more durable than those with CFRP laminates; thus, the use of a hybrid carbon and S-glass composite was proposed for rehabilitation purposes, with the glass layer being in contact with the adhesive. It was also noted that such arrangement may aid in reducing the risk of galvanic corrosion.

An alternative test method to study the long term durability of adhesive bonds was investigated by Pitrone and Brown (1988); the method makes use of a 'cyclic stress durability' apparatus to subject single lap joints to the concurrent effect of sustained or cyclic shear stresses and hygrothermal exposure to simulate severe service environments. Dawood and Rizkalla (2010) reported that silane coupling significantly enhances bond durability while inserting a fiberglass scrim in the adhesive layer only contributes to bond strength, based on empirical evidence from steel–CFRP double-lap shear specimens exposed to different environmental conditions, with and without sustained tensile load. A comprehensive insight into the experimental methods to study the environmental durability of adhesive joints is provided in Kinloch (1983) and Adams *et al*. (1997).

### 7.5.2 Mitigation of galvanic and crevice corrosion

Enhancement of steel–CFRP adhesive bonds in repair applications also entails mitigating the risk of galvanic and crevice corrosion. Corrosion may

accrue from the coupling of steel with more noble (cathodic) carbon fibers in presence of an electrolyte (e.g., humidity in the environment). For bonded CFRP repairs of steel tension members in civil structures, the following important factors contribute to making corrosion an issue of concern.

- *Exposure to corrosive environments*: Civil structures in need of repair often operate in aggressive environments, such as in presence of seawater (coastal regions), de-icing salts (used routinely on bridges in cold regions) and industrial settings. Under these circumstances, the increase in dissolved ions makes water more electrically conductive, which may exacerbate the effects of corrosion including weakening the adhesive bond between steel and CFRP repair patches.
- *Localized direct contact between steel and CFRP*: The adhesive bonding of CFRP patches to repair heavily corroded steel members may result in a significant irregularity of the thickness of the adhesive layer. Localized direct contact between the steel and the composite may occur as the steel pokes through the adhesive layer in the areas where the mass loss is smaller. This condition is akin to a low resistance connection between the electrodes of a galvanic cell, which may facilitate corrosion in the presence of moisture acting as the electrolyte.
- *Presence of geometric discontinuities*: The occurrence of galvanic and crevice corrosion may be greatly facilitated at the sites of geometric discontinuities, such as at the ends of the CFRP patch and at the repaired cracked steel sections. Crevices may form as the water partially penetrates the interface between the steel and the adhesive. The local damage that may be produced is of special concern since most of the load transfer to the CFRP patch occurs in the vicinity of these areas; in addition, the peel stress in adhesive joints in a repaired tension member reaches its peak in the patch ends.

Corrosion in coupled steel and carbon fiber composites has been extensively studied, and the salient findings are summarized in this section. If the realistic experimental investigation of specific case studies is to take place, it is necessary to closely replicate the actual service conditions, since the complex interaction of the materials, specimen configurations, exposure conditions and electrolytes will affect the results; nonetheless, the outcomes of the research reviewed herein offer relevant insight and practical recommendations. Bellucci (1991, 1992) investigated the galvanic corrosion between two graphite/epoxy composites having a fiber volume fraction of 60 % and aluminum alloys, a nickel aluminum bronze (NAB) alloy and AISI 4340 steel. The corrosion intensity of galvanic couples was monitored for 24 hours; in addition, weight loss and potentiodynamic polarization measurements were taken in a neutral and an air-saturated aqueous 3.5 % NaCl solution. The use of aluminum, steel and NAB alloys coupled with

graphite/epoxy composites was discouraged due to the high galvanic currents measured.

Aylor (1993) studied the galvanic compatibility between a graphite/epoxy composite having a fiber volume fraction of 62 % coupled to HY80 steel and a NAB alloy. Galvanic corrosion tests and accelerated electrochemical tests were performed over 180 days in filtered natural seawater at room temperature. The corrosion tests were conducted using metallic specimens that were individually connected to composite specimens, where the amount of graphite fibers exposed ranged between 0 (i.e., as received) and about 68 % (i.e., with one machine sanded face). Corrosion of the metals was documented also when no graphite fibers were initially exposed due to moisture absorption by the polymeric matrix.

Tavakkolizadeh and Saadatmanesh (2001) performed accelerated electrochemical tests and 1000-second galvanic corrosion tests on a carbon/two-part epoxy composite and A36 steel coupons. The corrosion current density and the half-cell potential of galvanic couples were studied, including two artificial aggressive environments (seawater and a de-icing salt solution), four CFRP specimen configurations having different amounts of fibers initially exposed (no epoxy, epoxy on back, thin and standard epoxy coatings) and three solvents used to remove sizing agents (acetone, isopropyl alcohol and carbon tetrachloride) except for the specimens with the standard epoxy coating thickness. It was shown that the presence of thin films of epoxy coating on the fibers significantly decreases the corrosion rate; specifically, up to seven and 23 times for a 0.1 and 0.25 mm thickness, respectively. It was also shown that sizing agents act as protective films, decreasing the corrosion rate of steel–CFRP couples by over 30 %. Both sizing agents and polymeric matrix typically protect the reinforcing fibers in undamaged CFRP repair patches, thereby contributing to mitigating corrosion effects.

West (2001) conducted a comprehensive investigation aimed at experimentally characterizing the galvanic corrosion in steel members with two-part epoxy bonded precured CFRP strips having a fiber volume fraction of 51 %. This work was part of an extensive program developed at the University of Delaware, USA, starting in the early 1990s, which culminated with a field demonstration (Miller *et al.*, 2001). It was noted that, although the adhesive layer between steel and CFRP acts as an insulating medium, discontinuities such as surface pits may result in the direct contact between the two adherends; therefore, it was proposed to insert a fiberglass scrim between the steel and the CFRP strips as an additional non-conductive barrier, as illustrated in Fig. 7.4(a), which is a common practice in aircraft applications (Poole, 2002). Eight different couples representing a variety of bond configurations, including possible defects, were cyclically exposed to a corrosive wet/dry environment for over seven months to assess corrosion

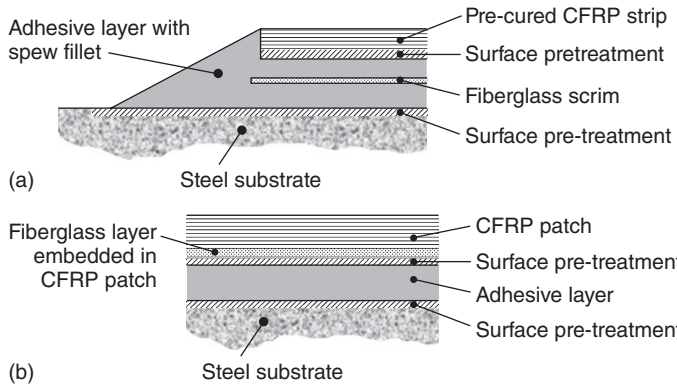


*7.4* Schematic of steel–CFRP adhesive bond configuration to mitigate galvanic and crevice corrosion: (a) West (2001); and (b) Karbhari and Shulley (1995).

in the steel substrate and around the edges of the CFRP strips. A 10 % NaCl aqueous solution representative of a de-icing salt solution served as the electrolyte. The combination of materials and adhesive bonding strategy proved to be effective in preventing corrosion phenomena without reducing the joint strength. It was also found that placing an adhesive spew fillet around the exposed edges of the CFRP plates, as shown in Fig. 7.4(a), prevented any physical contact between water and steel–adhesive and CFRP–adhesive interface, virtually eliminating the risk of crevice corrosion.

Karbhari and Shulley (1995) proposed to use hybrid carbon and S-glass composites as repair patches, having the non-conductive fiberglass in direct contact with the steel substrate in the worst case scenario (i.e., localized absence of protective matrix and adhesive layer). The concept is illustrated in Fig. 7.4(b). High quality hybrid carbon and S-glass composite patches may be prefabricated as unidirectional pultruded laminates, possibly having a roughened substrate.

## 7.6 Fundamentals of analysis and design

### 7.6.1 General considerations

In steel tension members that are repaired with adhesively bonded FRP laminates as illustrated in Fig. 7.5, the tensile force is transferred between the adherends primarily through shear stresses that act throughout the adhesive interface. The shear stress distribution along the overlap length is non-uniform as originally established through elastic shear lag analysis (Volkersen, 1938). The load is transferred primarily in the end zones of the FRP overlaps and at the section changes in the joint (e.g., at cracked steel

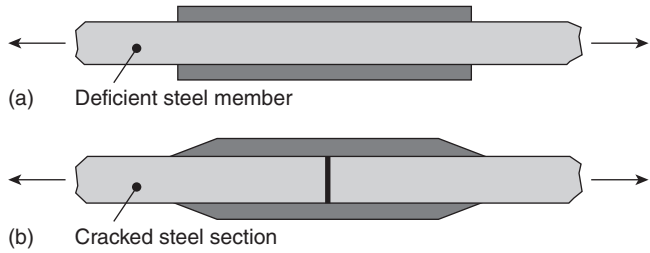


*7.5* Schematic of bonded FRP repairs of steel tension members: (a) two-side skin doubler joint to repair deficient member (e.g. severely corroded eyebar); and (b) double strap joint to repair cracked member.

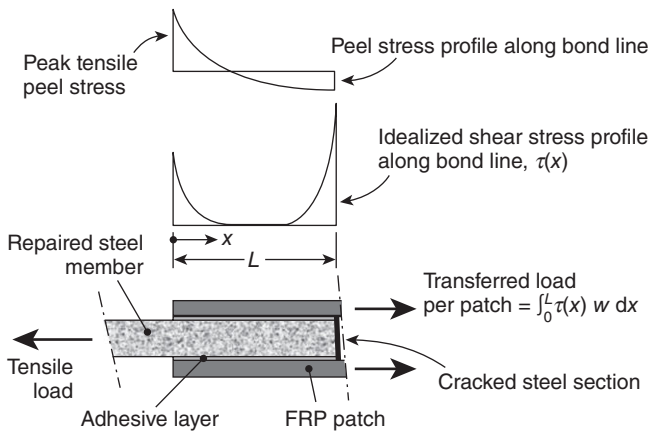


*7.6* Idealized shear and peel stress distribution along overlap length in double strap joint ($w$ = width of FRP patch).

sections with bonded FRP patches), with a lightly loaded elastic trough in between. From a design perspective, the main implication is that increasing the overlap length does not necessarily result in an increase in the tensile load capacity of the bonded system; in fact, the length of the bond zones where most of the load is transferred, sometimes referred to as 'anchorage length' or 'development length', is not a function of the overlap length (Hart-Smith, 1973a). The schematic in Fig. 7.6 illustrates the load transfer mechanism across a cracked section in a steel tension member by means of symmetrically bonded FRP patches. It is noted that the idealized elastic shear stress profiles along the development length do not reflect the fact that the shear stress is zero at the load-free edges of the adhesive layer; however, the resulting error negligibly affects the shear stress profile (Teodosiadis, 1969). As a result of secondary bending effects on the

adherends due to eccentricities in the loads carried, peel stresses acting in the thickness direction of the adhesive layer form at the overlap ends (Fig. 7.6), as first analyzed by Goland and Reissner (1944) for the case of single lap joints.

A correct design practice aims at configuring the adhesive joint to minimize peel stresses and ensure that the bond strength is greater or equal to that of the adherends, thereby providing sufficient damage tolerance for the joint to not be the weak structural link. Aside from adherend failure, cohesive failure modes either in the adhesive or in the adherends are desirable. Adhesive (i.e., interface) failures are typically associated with poor surface preparation, material selection and processing and are not acceptable. The fundamentals of the analysis and design of adhesively bonded joints that are representative of repairs in steel tension members are based on the work done by Hart-Smith (1973a, b) in the early 1970s, followed by the research conducted in the mid-1970s under the aegis of the US Air Force Primary Adhesively Bonded Structures Technology (PABST) program (Hart-Smith, 2001). The methodologies developed introduced relatively simple and accurate algorithms that account for the influence of relevant parameters that are briefly reviewed as follows.

## 7.6.2 Effects of joint geometry

The influence of joint geometry is illustrated in Fig. 7.7. The schematic summarizes the strength cut-off for representative bonded FRP repair

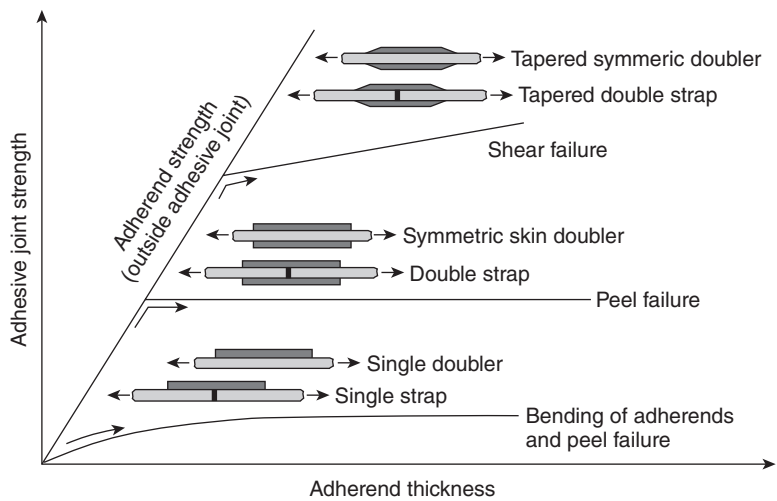


*7.7* Influence of joint geometry on adhesive bond strength and failure mode (adapted from Hart-Smith, 1974).

scenarios, including uncracked but deficient members and cracked members, with respect to the tensile strength of the adherends outside the adhesive joint. Single doubler and single strap joints with untapered FRP patches have the lowest strength cut-off because of the sensitivity to the bending effects induced by the eccentricities in the load paths resulting in relatively high peel stress peaks; thus, these configurations are more suitable for the repair of thin steel members. As the adherend thickness increases, greater cut-off levels are attained using symmetric doubler and double strap joint configurations; however, peel stresses are still present due to their sensitivity to eccentricities in the load paths, and peel failures may still govern.

This drawback can be offset by tapering the FRP patches near the overlap ends, similar to Fig. 7.5(b), forming adhesive spew fillets as the adhesive is squeezed out under pressure during installation and cutting the ends of the FRP patches to form chamfers (Adams, 1989; Hildebrand, 1994; Tsai and Morton, 1995; Wang and Rose, 2000; Belingardi *et al*., 2002). Alternatively, a reverse-tapered detail may be implemented in which the FRP thickness is reduced while the adhesive thickness is simultaneously increased near the plate end. This type of detail has been found to reduce, and possibly eliminate, the peel stress concentrations that form near the patch end (Dawood *et al*., 2009). The shape optimization for adherends in bonded joints, including tapering and chamfering, has been discussed in detail by Kaye and Heller (2002).

### 7.6.3 Effects of adherend thickness

The reliability of a bonded repair improves when it is designed to ensure that failure occurs in the adherends instead of in the adhesive layer, whose performance may be affected by the presence of voids and other defects, thickness variations, environmental effects, faulty bonding procedure and other factors that are difficult to control. For a given adhesive joint, the load that can be transferred must exceed that associated with the tensile failure of the unnotched adherends outside the joint up to a determinable thickness, which should be restricted within an appropriate range. It is good practice to design for a joint strength that is at least 50 % greater than that of the adherends, thereby providing an acceptable tolerance against the loss of bond due to defects and damage (Hart-Smith, 2001).

### 7.6.4 Effects of adherend stiffness imbalance and thermal mismatch

The axial stiffness imbalance between a repaired steel member and the adhesively bonded FRP laminates adversely affects the structural efficiency

of a given joint configuration. For example, in the case of a double strap joint where the inner (steel) adherend is stiffer than the outer (FRP) adherends (Fig. 7.6), failure takes place at the unloaded end where the shear strain is greater than that at the loaded end. As a result of the unbalanced design, the bond strength at the end of the FRP overlap cannot be fully utilized. A correct design aims at relying on balanced joints to the extent possible to maximize efficiency (Hart-Smith, 1973a). The effect of the mismatch in the coefficients of thermal expansion between steel member and bonded FRP laminates should also be accounted for, especially when relatively high curing temperatures are used in the bonding process, thereby producing locked-in stresses in the adhesive layer, or in applications where large thermal fluctuations are expected in service.

### 7.6.5 Effects of FRP adherend matrix properties

The in-plane shear modulus of FRP adherends such as unidirectional CFRP laminates is governed by that of the polymeric matrix, and thus reaches values that are an order of magnitude smaller than that of steel. When using relatively thick FRP laminates to approach adherend stiffness balance in repaired steel tension members, through-thickness shear lag effects may become of concern. In fact, the reduced effectiveness in distributing the axial load to the reinforcing fibers or plies away from the bond line may result in a non-uniform axial stress in the FRP laminate, and in turn in a reduced load transfer capacity that may need to be accounted for in design (Renton and Vinson, 1973).

### 7.6.6 Effects of adhesive layer properties

*Ductility*

The ductility of the adhesive layer in shear is the key property affecting the joint strength; the reference parameter is the ultimate adhesive shear strain energy, which is proportional to the toughness given by the area under the stress–strain curve (Hart-Smith, 1973a). In addition, ductility offsets the effect of shear and peel stress peaks. The shear stress–strain response varies with the service temperature typically without significant changes in toughness, as illustrated in Fig. 7.8(a). Therefore, the strength of a realistically configured joint is not sensitive to the operating temperature below the glass transition limit.

*Fatigue resistance*

Bonded FRP repairs may need to be designed to withstand cyclic loads such as in bridge structures, highlighting the importance of the fatigue resistance

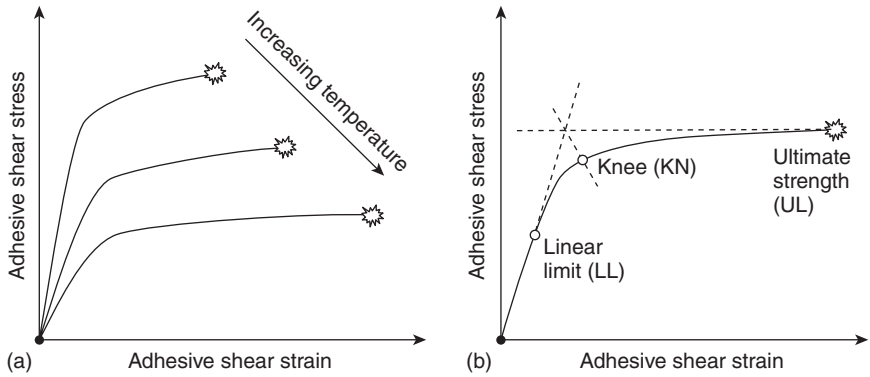


*7.8* Shear stress–strain constitutive model of structural adhesive: (a) effect of temperature; and (b) determination of knee point for fatigue design.

of the adhesive. Figure 7.8(b) illustrates a typical shear stress–strain constitutive model for an adhesive layer, where the three points proposed by Krieger (1988) to define the model are marked, namely the linear limit (LL), the knee (KN) and the ultimate strength (UL) point. The LL mark indicates the end of the linear portion of the curve, while KN marks the intersection between the stress–strain curve and the line that bisects the tangents to the linear portion and the plastic plateau in the constitutive model, pursuant to ASTM D 5656. It is best practice to limit the adhesive shear stress below the KN point to provide the damage tolerance needed for an effective fatigue design (Krieger, 1988; Hart-Smith, 2001). Evidence of the effectiveness of bonded CFRP patches in reducing the stress intensity factor in and extending the fatigue life of damaged steel tension members is discussed in Colombi *et al*. (2003a) and Jones and Civjan (2003). Matta *et al*. (2005, 2006) reported on the effectiveness of CFRP patches in relieving the fatigue stress in symmetric skin doubler and double strap joints (Fig. 7.7) representative of repairs in tension members with significant section loss and cracked sections, respectively; in particular, the former were subjected to periodic overloads at 80 % of the yield strength of the steel adherend, and the latter to constant amplitude fatigue loads where the upper limit was 70 % greater than that associated with the transition from elastic to plastic shear deformation in the adhesive.

*Creep resistance*

Damage or failure of the bond due to creep accumulation is best prevented by using sufficiently long overlaps. In short overlaps, the relatively small difference between maximum and minimum adhesive shear stress and

strain makes the bond layer more sensitive to creep effects. Based on evidence from load tests performed on both joint specimens and larger structural assemblies as part of the PABST program, it was recommended to design with overlap lengths that ensure a minimum value of shear stress equal to 10 % of the peak shear stress (Hart-Smith, 2001). Finally, it is noted that the combined effects of sustained and cyclic loads and the specific environmental exposure should be assessed on a case-by-case basis, especially with regard to durability in demanding operating environments.

*Thickness*

An increase in the thickness of the adhesive layer typically results in reduced shear and peel stress peaks (Adams, 1989; Hildebrand, 1994). It has been noted that an optimum bond line thickness exists, typically up to 0.5 mm, beyond which both the shear and peel stress peak in the adhesive increase (Gleich *et al*., 2001). This explains the empirical evidence where increasing the bond line thickness may negatively affect static strength (Kim *et al*., 1999) and fatigue life (Kim *et al*., 1992).

### 7.6.7 Stress analysis of bonded FRP repairs

The analysis and design of bonded FRP repairs of damaged steel tension members may rely on models from the relatively simple analytical to the more computationally demanding analytical and numerical. The latter option is best applicable to more complex scenarios such as:

- use of bonded CFRP patches (either unstressed or prestressed) to repair fatigue cracks, where it is important to estimate the reduction in stress intensity factor, as demonstrated by Colombi *et al*. (2003a, b) based on the work of Naboulsi and Mall (1996), and by Jones and Civjan (2003);
- use of joint configurations with geometric non-linearities (e.g., tapers, chamfers) aimed at reducing the peak shear and peel stress in the adhesive (Albat and Romilly, 1999; Wang and Rose, 2000; Kaye and Heller, 2002);
- assessment of triaxial stress states (Wang and Rose, 1997);
- assessment of response under dynamic loads (Al-Zubaidy *et al*., 2013).

For the preliminary design of structural repairs similar to skin doubler joints and double strap joints (Fig. 7.7), one may enlist simpler procedures based on the analytical algorithms that were developed by Hart-Smith (1973a, b, 1974) for the stress analysis and design of adhesive joints aimed at aircraft applications, which are extensively implemented in current practice and constitute the architecture of well-known computer programs. These algorithms are based on one-dimensional analysis that accounts for

plastic deformation in the adhesive layer, peeling effects, adherend stiffness imbalance and adherend thermal mismatch, neglecting through-thickness stress gradients in the adhesive and the adherends.

For the purpose of elastic stress analysis relevant to serviceability and fatigue design, the accuracy of one-dimensional analytical models for adhesive shear stress and FRP patch longitudinal stress distribution (Hart-Smith, 1973a; Albat and Romilly, 1999) has been demonstrated for skin doubler joints (Miller *et al*., 2001; Colombi and Poggi, 2006) and double strap joints (Colombi and Poggi, 2006). Shape optimization (e.g., tapering of the FRP laminate ends) may be dealt with using numerical simulations or based on empirical stress reduction coefficients (Dawood *et al*., 2009). In addition, shear lag coefficients may be used to account for the shear lag effects in FRP patches due to their relatively low shear modulus (Albat and Romilly, 1999), as demonstrated by (Miller *et al*., 2001). For the purpose of ultimate strength design, non-linear one-dimensional analysis is required (Hart-Smith, 1973a, b) as demonstrated by Matta *et al*. (2005) for both skin doubler joints and double strap joints, as illustrated in Fig. 7.9 and Fig. 7.10, respectively.

## 7.7 Conclusion and future trends

Research on strengthening and repair of metallic structures with adhesively bonded FRP composites is advancing relatively rapidly on several fronts. One of the main fronts is related to the integration between this technology and other emerging materials and technologies. These advancements are progressing notably in two areas: nano-enhanced and nano-engineered adhesives and composites, and integration with other new and advanced materials such as shape memory alloys (SMAs) to develop 'active patches'. Nanomodified FRP composites incorporate carbon nanotubes (CNTs) or carbon nanofibers (CNFs). Due to their promising properties, these materials have been gaining attention; specifically, CNTs or CNFs can increase the electrical conductivity of the composites making them promising as 'self-sensing' repair alternatives. The increased electrical conductivity of the composites has raised concerns about the potential for accelerated galvanic corrosion. However, early studies indicate that carbon nanocomposites do not exhibit any statistically significant increase of galvanic potential when coupled with steel relative to traditional carbon composites (Arronche *et al*., 2013).

Other researchers have focused on mixing small amounts of nanoparticles, including CNFs, CNTs and silicon carbide (SiC) nanopowder, into structural epoxy resins to enhance their mechanical and thermal properties (Faleh *et al*., 2012). Early studies suggest that the presence of nanoparticles within the adhesive resin can increase the elastic modulus of the adhesive by up

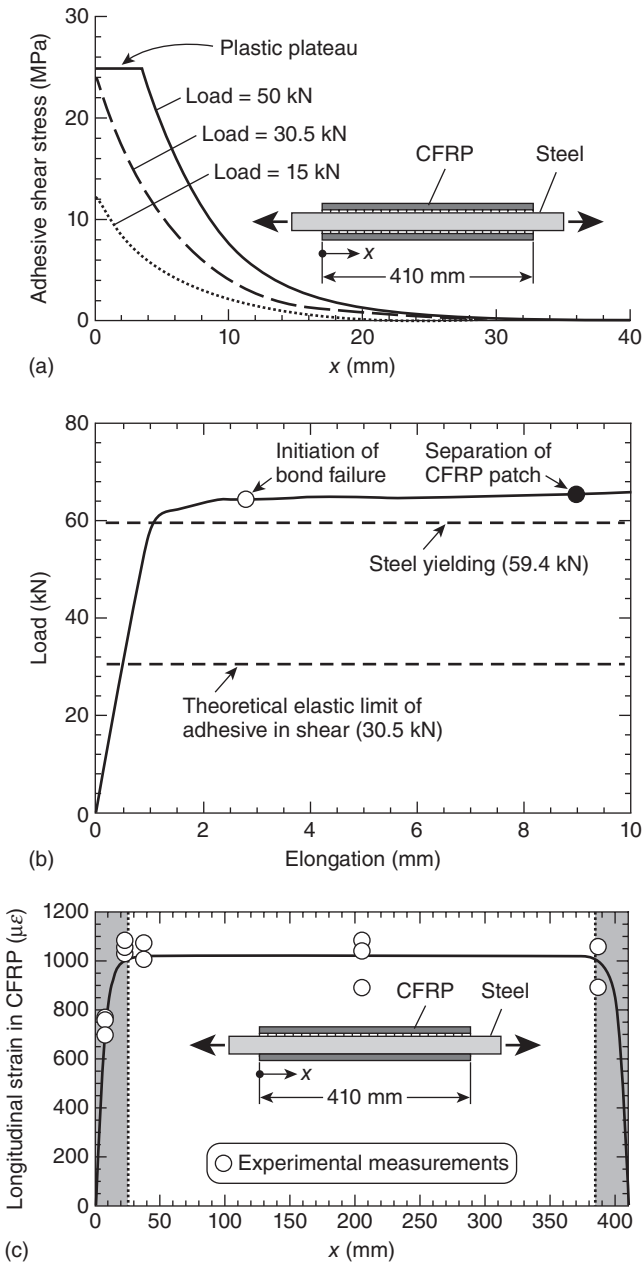


*7.9* Load transfer in steel–CFRP skin doubler joint: (a) theoretical adhesive elastic and plastic shear stress distribution; (b) monotonic load–elongation response; and (c) experimental and theoretical axial strain in CFRP past elastic limit of adhesive in shear (dashed lines and shaded areas indicate theoretical effective transfer length).

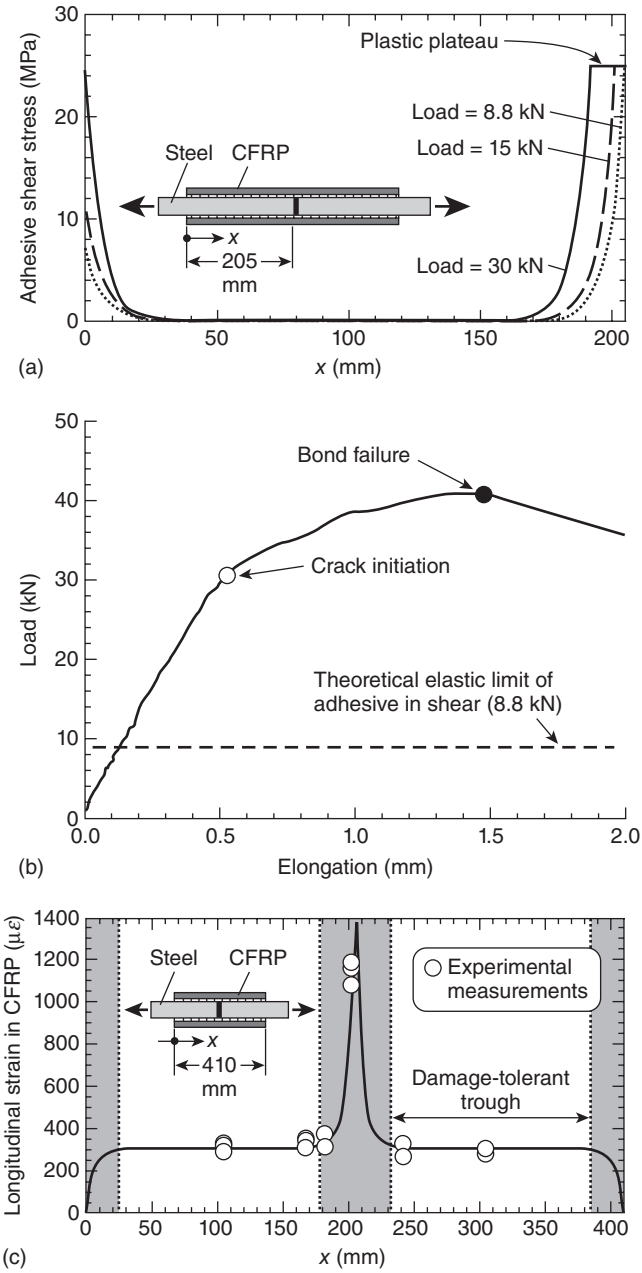


*7.10* Load transfer in steel–CFRP double strap joint: (a) theoretical adhesive elastic and plastic shear stress distribution; (b) monotonic load–elongation response; and (c) experimental and theoretical axial strain in CFRP past elastic limit of adhesive in shear (dashed lines and shaded areas indicate theoretical effective transfer length).

to 50 % compared to the non-nanomodified counterpart which may be advantageous in minimizing shear-lag effects. However, several other potential benefits can be envisioned including increasing adhesive toughness, providing a self-sensing mechanism to detect debonding or environmental degradation, or enhancing the thermal characteristics of commercially available adhesives.

Another recent trend looks at the integration of SMAs into traditional CFRP laminates for repair applications. The use of embedded SMAs has been investigated in the aerospace industry for energy dissipation and self-actuation applications. Recent trends have focused on adapting these promising properties for structural repair applications; specifically, the use of FRP patches with embedded SMAs for repair of cracked steel structures is currently under investigation. In this application, embedded SMA wires are intended to provide a sustained prestressing force to offset crack opening and reduce the stress intensity factor near the crack tip with the objective of eliminating the need for heavy prestressing fixtures on site.

## 7.8 Sources of further information and advice

Interested readers may find additional information and further guidance from a number of sources. The International Institute of FRP in Construction (IIFC) houses a working group on FRP-strengthened metallic structures. The working group membership consists of active researchers and engineers from around the world with an interest in the use of FRP composites for the rehabilitation of metallic structures. The working group maintains a comprehensive list of relevant journal and conference publications in this area, which is updated annually. The IIFC also sponsors two relevant international conference series: the *Composites in Civil Engineering (CICE)* conference series is held biannually on even years while the *Asia-Pacific Conference on FRP in Structures (APFIS)* is held biannually on odd years. Both conference series provide a venue for dissemination of research findings on the use of FRP composites in structural engineering applications, and both conference series typically host sessions on FRP strengthening and repair of metallic structures.

In North America, the Transportation Research Board (a division of the US National Research Council administered by the National Academies) hosts Standing Committee AFF80–Structural Fiber Reinforced Polymers. The committee activities focus on all aspects of the use of FRP materials in bridges and transportation infrastructure applications. The committee hosts a subcommittee on FRP-Strengthened Steel Bridge Girders. The committee meets annually at the TRB annual meeting in Washington, DC, and typically hosts presentation sessions that provide a venue for dissemination and discussion of research on the use of FRP composites in

transportation infrastructure applications, including the rehabilitation of metallic bridges.

Relevant research is published in a number of international journals including the *Journal of Bridge Engineering* and *Journal of Composites for Construction* (American Society of Civil Engineers), *Composite Structures*, *Composites Part B: Engineering* and *Construction and Building Materials* (Elsevier), and *Structural Engineering and Mechanics* (Techno Press) among others. The interested reader is also referred to documents that have been published in the UK (Cadei *et al*., 2004) and Italy (National Research Council, 2007), which provide guidance for the design of externally bonded FRP composite systems for the rehabilitation of metallic structures.

## 7.9 References


Adams R D (1989), 'Strength predictions for lap joints, especially with composite adherends. A review', *Journal of Adhesion*, 30, 219–242.

Adams R D, Comyn J and Wake W C (1997), *Structural Adhesive Joints in Engineering*, 2nd edn, London, Chapman & Hall.

Ageorges C and Ye L (2002), *Fusion Bonding of Polymer Composites*, London, Springer.

Albat A M and Romilly D P (1999), 'A direct linear-elastic analysis of double symmetric bonded joints and reinforcements', *Composites Science and Technology*, 59, 1127–1137.

Albrecht P (1987), 'Fatigue strength of adhesively bonded cover plates', *Journal of Structural Engineering*, 113, 1236–1250.

Albrecht P and Hall T T (2003), 'Atmospheric corrosion resistance of structural steels', *Journal of Materials in Civil Engineering*, 15, 2–24.

Al-Zubaidy H, Al-Mahaidi R and Zhao X-L (2013), 'Finite element modelling of CFRP/steel double strap joints subjected to dynamic tensile loadings', *Composite Structures*, 99, 48–61.

Arnott D, Rider A and Mazza J (2002), 'Surface treatment and repair bonding', in *Advances in the Bonded Composite Repair of Metallic Aircraft Structure*, Oxford, Elsevier, 41–86.

Arronche L, Gordon K, Ryu D, La Saponara V and Cheng L (2013), 'Investigation of galvanic corrosion between AISI 1018 carbon steel and CFRPs modified with multi-walled carbon nanotubes', *Journal of Materials Science*, 48, 1315–1323.

Aylor D M (1993), 'The effect of a seawater environment on the galvanic corrosion behaviour of graphite/epoxy composites coupled to metals', in *High Temperature and Environmental Effects on Polymeric Composites, ASTM STP 1174*, West Conshohocken, PA, American Society for Testing and Materials, 81–94.

Belingardi G, Goglio L and Tarditi A (2002), 'Investigating the effect of spew and chamfer size on the stresses in metal/plastics adhesive joints', *International Journal of Adhesion and Adhesives*, 22, 273–282.

Bellucci F (1991), 'Galvanic corrosion between nonmetallic composites and metals: I. Effect of metal and of temperature', *Corrosion*, 47, 808–819.

Bellucci F (1992), 'Galvanic corrosion between nonmetallic composites and metals: II. Effect of area ratio and environmental degradation', *Corrosion*, 48, 281–291.

Bonk R B, Ostendorf J F, Ambrosio A M, Pettenger B L and Froelich K A (1996), 'Evaluation of adhesives for adhering carbon/epoxy composites to various metallic substrates', *Proc. 41st International SAMPE Symposium and Exhibition*, Covina, CA, Society for the Advancement of Material and Process Engineering (SAMPE), 1472–1485.

Bourban P E, Karamuk E, Don R C and Gillespie J W Jr (1994), 'Induction heating for rehabilitation of steel structures using composites', *Proc. 3rd ASCE Materials Engineering Conference*, Reston, VA, American Association of Civil Engineers, 287–294.

Cadei J M C, Stratford T J, Hollaway L C and Duckett WG (2004), *Strengthening Metallic Structures Using Externally Bonded Fibre-reinforced Polymers*, London, CIRIA.

Campbell F C (2001), 'Secondary adhesive bonding of polymer-matrix composites', in *Composites*, ASM Handbook Vol. 21, Materials Park, OH, ASM International, 620–632.

Clifford S M and Manger C I C (2002), 'Characterisation of a glass-fibre reinforced vinylester to steel joint for use between a naval GRP superstructure and a steel hull', *Composite Structures*, 57, 59–66.

Colombi P and Poggi, C (2006), 'Strengthening of tensile steel members and bolted joints using adhesively bonded CFRP plates', *Construction and Building Materials*, 20, 22–33.

Colombi P, Bassetti A and Nussbaumer A (2003a), 'Analysis of cracked steel members reinforced by pre-stress composite patch', *Fatigue and Fracture of Engineering Materials and Structures*, 26, 59–66.

Colombi P, Bassetti A and Nussbaumer A (2003b), 'Delamination effects on cracked steel members reinforced by prestressed composite patch', *Theoretical and Applied Fracture Mechanics*, 39, 61–71.

Dawood M and Rizkalla, S (2010), 'Environmental durability of a CFRP system for strengthening steel structures', *Construction and Building Materials*, 24, 1682–1689.

Dawood M, Guddati M and Rizkalla S (2009), 'Effective splices for a carbon fiber–reinforced polymer: strengthening system for steel bridges and structures', *Transportation Research Record: Journal of the Transportation Research Board*, 2131, 125–133.

Faleh H, Al-Mahaidi R and Shen L (2012), 'Fabrication and characterization of nano-particles-enhanced epoxy', *Composites Part B: Engineering*, 43, 3076–3080.

Fam A, Witt S and Rizkalla S (2006), 'Repair of damaged aluminum truss joints of highway overhead sign structures using FRP', *Construction and Building Materials*, 20, 948–956.

Fisher J W (1984), *Fatigue and Fracture in Steel Bridges: Case Studies*, New York, Wiley.

Fontana M G (1986), *Corrosion engineering*, 3rd edn, New York, McGraw-Hill.

Gasparini D A, Nara H, Andreani J, Boggs C, Brewer D and Etitum P (1990), 'Steel-to-steel connections with adhesives', *Journal of Structural Engineering*, 116, 1165–1179.

Gettings M and Kinloch A J (1977), 'Surface analysis of polysiloxane/metal oxide interfaces', *Journal of Materials Science*, 12, 2511–2518.

Gleich D M, Van Tooren M J L and Beukers A (2001), 'Analysis and evaluation of bondline thickness effects on failure load in adhesively bonded structures', *Journal of Adhesion Science and Technology*, 15, 1091–1101.

Goland M and Reissner E (1944), 'The stresses in cemented joints', *Journal of Applied Mechanics*, 11, A17–A27.

Grabovac I (2003), 'Bonded composite solution to ship reinforcement', *Composites Part A: Applied Science and Manufacturing*, 34, 847–854.

Hart-Smith L J (1973a), *Adhesive-bonded Double-lap Joints*, NASA Langley Research Center Technical Report NASA-CR-112235, Washington, DC, National Aeronautics and Space Administration.

Hart-Smith L J (1973b), *Adhesive-bonded Single-lap joints*, NASA Langley Research Center Technical Report NASA-CR-112236, Washington, DC, National Aeronautics and Space Administration.

Hart-Smith L J (1974), 'Advances in the design and analysis of adhesive-bonded joints in composite aerospace structures', *Proc. 19th National SAMPE Symposium and Exhibition*, Azusa, CA, Society for the Advancement of Material and Process Engineering, 722–737.

Hart-Smith L J (2001), 'Bolted and bonded joints', in *Composites*, ASM Handbook Vol. 21, Materials Park, OH, ASM International, 271–289.

Hildebrand M (1994), 'Non-linear analysis and optimization of adhesively bonded single lap joints between fibre-reinforced plastics and metals', *International Journal of Adhesion and Adhesives*, 14, 261–267.

Jones S C and Civjan S A (2003), 'Application of fiber reinforced polymer overlays to extend steel fatigue life', *Journal of Composites for Construction*, 7, 331–338.

Karbhari V M and Shulley S B (1995), 'Use of composites for rehabilitation of steel structures – Determination of bond durability', *Journal of Materials in Civil Engineering*, 7, 239–245.

Kaye R H and Heller M (2002), 'Through-thickness shape optimisation of bonded repairs and lap-joints', *International Journal of Adhesion and Adhesives*, 22, 7–21.

Kim K S, Kim W T, Lee D G and Jun E J (1992), 'Optimal tubular adhesive-bonded lap joint of the carbon fiber epoxy composite shaft', *Composite Structures*, 21, 163–176.

Kim Y G, Oh J H and Lee D J (1999), 'Strength of adhesively-bonded tubular single lap carbon/epoxy composite-steel joints', *Journal of Composite Materials*, 33, 1897–1917.

Kinloch A J (1983), *Durability of Structural Adhesives*, London, Applied Science Publishers.

Klaiber F W, Dunker K F, Wipf T J and Sanders W W Jr (1987), *Methods of Strengthening Existing Highway Bridges*, NCHRP Report No. 293, Washington, DC, Transportation Research Board.

Krieger R B Jr (1988), 'Stress analysis concepts for adhesive bonding of aircraft primary structure', in Johnson W S (ed.), *Adhesively Bonded Joints: Testing, Analysis, and Design, ASTM STP 981*, West Conshohocken, PA, American Society for Testing and Materials, 264–275.

Lenwari A, Thepchatri T and Watanabe E (2002), 'Prediction of premature separation of bonded CFRP plates from strengthened steel beams using a fracture criterion', *Structural Engineering and Mechanics*, 14, 565–574.

Love C T and Karbhari V M (2006), 'High density polyethylene/reactive ethylene terpolymer composites for strengthening steel structures', *Proc. SAMPE '06*, Covina, CA, Society for the Advancement of Material and Process Engineering, 51, 10 p.

Luke S (2001), 'Strengthening structures with carbon fibre plates – Case histories for Hythe Bridge, Oxford and Qafco Prill Tower, Qatar', *Proc. NGCC First Annual Conference and AGM – Composites in Construction Through-Life Performance*, Chesterfield, Network Group for Composites in Construction.

Malvar L (1998), 'Durability of Composites in Reinforced Concrete', *Proc. 1st International Conference on Durability of Composites for Construction*, Sherbrooke, University of Sherbrooke, 361–372.

Marianos W N Jr, Chen G, Galati N and Matta F (2006), *Investigation of cause of cracked stringer on the blanchette bridge*, Report RI05-036 for the Missouri Department of Transportation, Rolla, MO, Center for Infrastructure Engineering Studies, University of Missouri-Rolla.

Matta F, Karbhari V M and Vitaliani R (2005), 'Tensile response of steel/CFRP adhesive bonds for the rehabilitation of civil structures', *Structural Engineering and Mechanics*, 20, 589–608.

Matta F, Rizzo P, Karbhari V M and Lanza di Scalea F (2006), 'Acoustic emission damage assessment of steel/CFRP bonds for rehabilitation', *Journal of Composites for Construction*, 10, 265–274.

Mazumdar S K (2001), *Composites Manufacturing – Materials, Product and Process Engineering*, Boca Raton, FL, CRC Press.

McKnight S H, Bourban P E, Gillespie J W Jr and Karbhari V M (1994), 'Surface preparation of steel for adhesive bonding in rehabilitation applications', *Proc. 3rd ASCE Materials Engineering Conference*, Reston, VA, American Association of Civil Engineers, 1148–1155.

Mertz D R and Gillespie J W Jr (1996), *Rehabilitation of Steel Bridge Girders Through the Application of Advanced Composite Materials*, IDEA Project Final Report, Contract NCHRP-93-ID011, Washington, DC, Transportation Research Board.

Miller T C, Chajes M J, Mertz D R and Hastings J N (2001), 'Strengthening of a steel bridge girder using CFRP plates', *Journal of Bridge Engineering*, 6, 514–522.

Moy S S J (2007), 'CFRP reinforcement of steel beams: adhesive cure under cyclic loading', *Proc. 1st Asia-Pacific Conference on FRP in Structures*, Hong Kong, China, 2, 1019–1024.

Naboulsi S and Mall S (1996), 'Modeling of a cracked metallic structure with bonded composite patch using the three layer technique', *Composite Structures*, 35, 295–308.

Nara H and Gasparini D A (1981), *Fatigue resistance of adhesively bonded connections*, Report No. FHWA-OH-81-011, Washington, DC, US Department of Transportation, Federal Highway Administration.

National Research Council (1991), *Life Prediction Methodologies for Composite Materials*, Washington, DC, National Materials Advisory Board.

National Research Council (2007), *Guidelines for the design and construction of externally bonded FRP systems for strengthening existing structures – Metallic structures*, Rome, NRC.

Nishikawa K, Murakoshi J and Matsuki T (1998), 'Study on the fatigue strength of steel highway bridges in Japan', *Construction and Building Materials*, 12, 133–141.

Photiou N K, Hollaway L C and Chryssanthopoulos M K (2006), 'Strengthening of an artificially degraded steel beam utilising a carbon/glass composite system', *Construction and Building Materials*, 20, 11–21.

Pitrone L R and Brown S R (1988), 'Environmental durability of adhesively bonded joints', in *Adhesively Bonded Joints: Testing, Analysis, and Design, ASTM STP 981*, West Conshohocken, PA, American Society for Testing and Materials, 289–303.

Poole P (2002), 'Graphite/epoxy patching efficiency studies', in *Advances in the Bonded Composite Repair of Metallic Aircraft Structure*, Oxford, Elsevier, 415–441.

Rajagopalan G, Immordino K I and Gillespie J W Jr (1996), 'Adhesive selection methodology for rehabilitation of steel bridges with composite materials', *Proc. American Society for Composites 11th Technical Conference*, Lancaster, PA, Technomic, 222–230.

Renton W J and Vinson J R (1973), *The analysis and design of composite material bonded joints under static and fatigue loadings*, Report No. AFOSR-TR-73-1627, Air Force Office of Scientific Research.

Roach D P and Scala C M (2002), 'Non-destructive evaluation and quality control for bonded composite repair of metallic aircraft structures', in *Advances in the Bonded Composite Repair of Metallic Aircraft Structure*, Oxford, Elsevier, 659–726.

Sen R, Liby L and Mullins G (2001), 'Strengthening steel bridge sections using CFRP laminates', *Composites Part B: Engineering*, 32, 309–322.

Sika (2009), *Sika CarboDur plates*, product data sheet, edition 25.02.2011.

Sika (2011), *Sikadur 30*, product data sheet, edition 5.5.2011.

Sumerak J E and Martin J D (2001), 'Pultrusion', in *Composites*, ASM Handbook Vol. 21, Materials Park, OH, ASM International, 550–564.

Tavakkolizadeh M and Saadatmanesh H (2001), 'Galvanic corrosion of carbon and steel in aggressive environment', *Journal of Composites for Construction*, 5, 200–210.

Teodosiadis R (1969), *Plastic analysis of bonded composite lap joints*, Report No. DAC-67836, Long Beach, CA, Douglas Aircraft Company.

Tsai M Y and Morton J (1995), 'The effect of a spew fillet on adhesive stress distributions in laminated composite single-lap joints', *Composite Structures*, 32, 123–131.

Volkersen O (1938), 'Die nietkraftverteilung in zugbeanspruchten nietverbindungen mit konstanten laschenquerschnitten' (The rivet-force distribution in tension-stressed rivet joints with constant adherends thickness), *Luftfahrtforschung*, 15, 41–47.

Walsh P J (2001), 'Carbon fibers', in *Composites*, ASM Handbook Vol. 21, Materials Park, OH, ASM International, 35–40.

Wang C H and Rose L R F (1997), 'Determination of triaxial stresses in bonded joints', *International Journal of Adhesion and Adhesives*, 17, 17–25.

Wang C H and Rose L R F (2000), 'Compact solutions for the corner singularity in bonded lap joints', *International Journal of Adhesion and Adhesives*, 20, 145–154.

West T D (2001), *Enhancements to the bond between advanced composite materials and steel for bridge rehabilitation*, MS thesis, Newark, DE, University of Delaware.

Wetzel E (1995), *Assessment of heating techniques for metal to composite bonding in infrastructure rehabilitation*, BS thesis, Newark, DE, University of Delaware.

Xiao Z-G, Zhao X-L and Tong L-W (2011), 'Tests on CFRP repaired welded thin-walled cross-beam connections', *Advances in FRP Composites in Civil Engineering, Proc. 5th International Conference on FRP Composites in Civil Engineering (CICE 2010)*, Berlin, Springer, 903–906.

Yamaguchi T, Kato Y, Nishimura T and Uomoto T (1997), 'Creep rupture of FRP rods made of aramid, carbon and glass fibers', *Proc. 3rd Int. Symposium on Non-Metallic (FRP) Reinforcement for Concrete Structures (FRPRCS-3)*, Tokyo, Japan Concrete Institute, 2, 179–186.

Zoccola J C (1976), *Eight year corrosion test report – Eight Mile Road Interchange*, Bethlehem, PA, Bethlehem Steel.

# 8

# Rehabilitation of cracked aluminum components using fiber-reinforced polymer (FRP) composites

C. P. PANTELIDES, University of Utah, USA

**DOI**: 10.1533/9780857096654.2.201

**Abstract**: Overhead signs are used to provide the traveling public with clear messages under a variety of conditions, directly over the roadway. In many cases, due to their location over vehicular traffic, a support failure on sign support structures poses a significant threat to the traveling public. A repair method of cracked aluminum welded connections of overhead sign structures is described. Results for both static and fatigue tests of K-tube-to-tube connections are presented. The successful research and the minimal traffic disruption required in field application make this method a good choice for repair and rehabilitation of aluminum overhead sign structures.

**Key words**: aluminum, fatigue, fiber-reinforced polymers, rehabilitation, sign supports.

## 8.1 Introduction

Overhead signs include signs over portions of the roadway requiring vertical clearance for vehicles to pass underneath. Overhead signs are used to provide the traveling public with clear messages under a variety of conditions, directly over the roadway. Sign support structures, such as the one shown in Fig. 8.1 are considered to be ancillary structures. Design requirements for these structures in the US are contained in the 'AASHTO Standard Specifications for Structural Supports for Highway Signs, Luminaires and Traffic Signals' (AASHTO, 2001). Most sign support structures are fabricated from structural steel or aluminum tubes, angles and plate.

Constant-amplitude fatigue thresholds for aluminum are quite low compared to the thresholds for steel. As a result, steel is the material of choice for many sign structures. Although weathering steel has some advantages and could be utilized in some circumstances, it is not appropriate for all states and locations. Galvanization is considered to be a long-term, low maintenance method of protecting steel from corrosion; therefore, galvanized steel is also specified.

Aluminum members are light weight and corrosion resistant and are commonly constructed using alloys 6061-T6 and 6063-T5. Aluminum is used

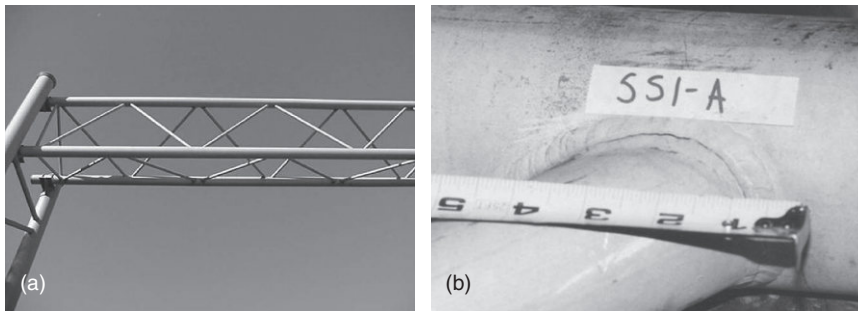


*8.1* Overhead sign structure truss (a) and cracked weld (b).

with other elements to increase strength, and the T series is heat treated. Allowable stresses of these alloys when welded are reduced because the heat from welding reduces the beneficial heat treatment. Design loads for sign support structures include dead and live loads, ice loads and wind loads. The primary loads applied to sign support structures are due to natural winds.

In many cases, due to their location over vehicular traffic, a support failure on sign support structures poses a significant threat to the traveling public. Sign support structures must not only have sufficient strength to withstand the maximum expected wind loads, normally a once in 50 year maximum, but also the fatigue effects of fluctuating winds, typically of lower force. Fatigue strength of aluminum is 40 % that of steel with comparable yield strength, and its modulus of elasticity is one-third that of steel, which increases member deflections. Wind-loading phenomena that lead to vibration and fatigue include natural wind gusts, truck-induced gusts, vortex shedding, and galloping. Sign support structures consisting of three-dimensional, three-chord or four-chord trusses are not susceptible to vortex shedding or galloping (FHWA, 2005).

Fatigue failure of a sign support structure occurs because the stress ranges resulting from wind or truck-induced gusts exceed fatigue thresholds at certain critical details and result in cracks between diagonals and chords, as shown in Fig. 8.1. Instances of similar cracks have been reported in many states in the US (Sharp *et al*., 1996). These failures cannot be blamed on weld defects; instead, they demonstrate that the structure is not adequately designed for fluctuating loads and is subjected to larger stress ranges. In the AASHTO Specifications, fatigue design provisions for support structures are similar to those in the bridge specifications. Fatigue design procedures are based on control of the nominal stress range and knowledge of the fatigue threshold of certain critical details. Each of these details is assigned a 'stress category', and the fatigue threshold stress range for each category

is given. Support structures should be designed so that stress ranges due to fatigue design loads are less than the fatigue thresholds for each detail, thus ensuring that fatigue will not occur even for a large number of applied load cycles.

The AASHTO Specifications require that cantilever sign structures be designed for fatigue loads, but simply supported trusses are not required to be designed for fatigue. A recent study evaluated fatigue effects for consideration by the Illinois DOT (Foutch *et al*., 2006). The stress ranges experienced by selected truss members were measured under wind loads and truck gusts. It was projected that stress ranges experienced by horizontal and diagonal members would occasionally exceed the constant amplitude fatigue limit (CAFL). This is most likely to occur under the simultaneous action of moderate wind in conjunction with larger truck gusts, a design loading condition not currently mandated by the Specifications which is rather conservative, since the peak response to wind and the peak response to truck gust would have to occur simultaneously to produce a significant stress range.

There are two conventional options of repair when it comes to damaged overhead sign structure (OSS) connections: (i) re-weld the connection or (ii) replace the whole OSS truss. Aluminum welded truss structures are very difficult to repair in the field. Even truss removal and repair is considered more difficult than a steel truss. Corrections to weld problems may include hammer peening, hole drilling to arrest the crack, or detail modification. Hammer peening introduces a compressive stress to the weld surface to reduce the tendency to crack and minimize crack propagation. Ultrasonic impact treatment, sometimes called ultrasonic peening, is a technique used to treat fillet welds to increase their fatigue strength. A drilled hole is used to arrest a crack that goes through the thickness of the weld material. For small cracks this may be sufficient to arrest the crack permanently, but it offers only a temporary fix for larger cracks. The other method which has been studied is the use of fiber-reinforced polymer (FRP) composites for aluminum sign truss bridges with cracked welds in the connections of diagonals to the chord (Pantelides *et al*., 2003; Fam *et al*., 2006; Nadauld and Pantelides, 2007).

## 8.2 Rehabilitation of connections in aluminum overhead sign structures (OSS)

Transportation departments have been using aluminum overhead sign structures since the 1950s. It is well documented that cracks develop in the welds between diagonal and chord members due to fatigue stresses from wind-induced vibration of the slender members. These cracks propagate to

complete failure of the members, which can cause collapse of the truss and inflict injuries. The original design of overhead sign structures did not consider fatigue as a limit state. In addition, field welding of aluminum structures for any possible repairs is prohibited. A repair method for the cracked aluminum welded connections between diagonals and chord members using glass fiber-reinforced polymer (GFRP) composites is described.

### 8.2.1 Surface preparation

A repair method for cracked aluminum welded connections of overhead sign structures using GFRP composite materials has been investigated (Pantelides *et al*., 2003). Several steps are recommended for surface preparation of aluminum surfaces, an extremely important step for providing an adequate bond between aluminum surface and GFRP composite:

1. Scrub the tube surface to remove road film and dirt using a high alkaline cleaner and rinse the surface with water and wipe dry.
2. Daub aluminum preparation liquid over all tubular surfaces and allow to set for at least three minutes and rinse with water.
3. Roughen the surface of the aluminum with 'no gray' sandpaper.
4. Drill holes at the two ends of the crack to prevent crack propagation.
5. Clean the tube surface for a second time as in step (2).
6. Apply epoxy putty to the joint to create a smooth transition from the large tube of the chord member to the smaller tubes of the diagonal members.
7. Apply a special compound which converts the aluminum surface to a new compound that provides a stronger bond to the GFRP composite.

### 8.2.2 Glass fiber-reinforced polymer (GFRP) architecture

Glass fabric pre-impregnated with a urethane resin has been used to implement the repair method described by Pantelides *et al*. (2003). Polymerization starts when water is added to the glass fabric. Four different GFRP composite materials were prepackaged in aluminum foil so they could be easily accessed and applied quickly in the field. Once water is added to the GFRP composite, it sets in approximately one hour. The following nine steps outline the method of application and the function of each layer of the GFRP composite. A schematic of the major GFRP application steps is given in Fig. 8.2:

1. A primer is brushed over the entire specimen and allowed to set; since the prepackaged composite is 67 % by weight fiber, the primer is necessary to achieve the desired bond strength (Step A1, not shown in Fig. 8.2).

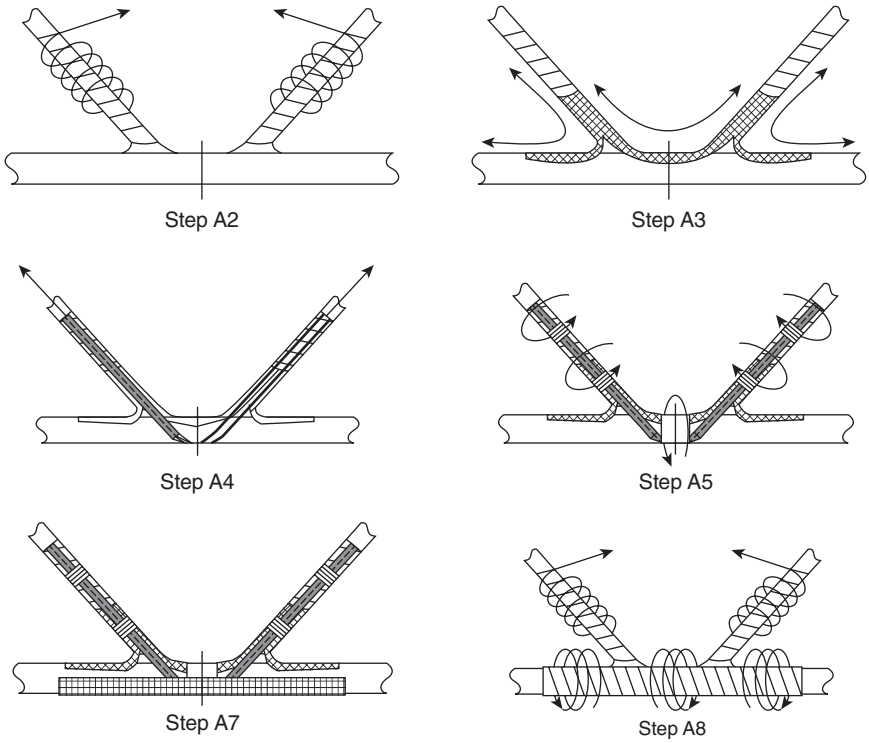


*8.2* GFRP composite application steps.

2. A bonding layer of fine weave tape GFRP composite is applied to the diagonal truss members such that no aluminum surface is left exposed (Step A2).
3. One layer of bare tubular braid weave is applied to the joint structure; the tubular braid consists of fibers orientated at ±45°, whose function is to connect the chord to the two diagonals (Step A3).
4. The unidirectional GFRP composite tendons are then applied; the tendon runs down the diagonal, under the main chord, and back up the other diagonal on the opposite side. The process is repeated with the second tendon on the other side of the second diagonal (Step A4).
5. Fine weave GFRP composite is used as bands at the following locations to hold the tendons in place: one 51 mm band near the top of each diagonal, one 51 mm band near the bottom of each diagonal, and one 102 mm band at the center of the main chord (Step A5).
6. A second layer of tubular braid is applied (Step A6, not shown in Fig. 8.2).
7. One layer of heavy woven roving GFRP composite is applied to the bottom half of the main chord, to add stiffness to the main chord and create a GFRP composite system with a uniform thickness (Step A7).

8. Apply a fine weave GFRP composite over the entire connection to consolidate the GFRP composite wrap and fit composite pieces around the joint to create a smooth transition (Step A8).
9. Wrap stricture banding, a high strength stretch film, tightly around the entire connection to constrain the GFRP composite (Step A9, not shown in Fig. 8.2).

## 8.3 Static tests of K-tube-to-tube connections

The test specimens consisted of two diagonal members attached to a main chord; the diagonals were oriented at 48° from the bottom chord. A monotonic static tensile load was applied to a diagonal of the specimen which was positioned vertically, directly under the hydraulic actuator as illustrated in Fig. 8.3, while the chord was being held down. The diagonal had an inside diameter of 50.8 mm and an outside diameter of 63.5 mm; the chord had an inside diameter of 88.9 mm and an outside diameter of 101.6 mm (Pantelides *et al.*, 2003). One test was carried out on a welded aluminum connection without any visible cracks (AS3). Four connections of diagonal to chord truss members obtained from actual structures in the field (SS1-A, SS1-B, SS2-A, and SS2-B) were retrofitted with GFRP composites. In addition, four tests were performed in which new aluminum specimens were fabricated with four tack welds that were used to assemble the connection, with GFRP composites being the only load resisting elements (TS1, TS2, TS4, and TS4-B); tack welds simulate the condition in which cracks develop along the length of the weld.

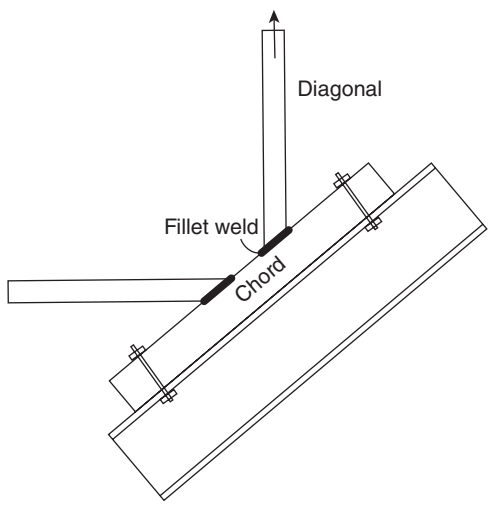


*8.3* Test set-up for static and fatigue tests.

### 8.3.1 Uncracked field specimens

Specimen AS3 was obtained from a truss that was taken out of service; the connection did not have any visible cracks, and was tested to determine the baseline load capacity of the welded aluminum connection; this load capacity was compared to the allowable stress for welded tubular members. Specimen AS3 had a load capacity of 110 kN, as shown in Fig. 8.4. Specimen SS1-B also had no visible cracks, but it was rehabilitated with GFRP composites as described earlier and reached the maximum load capacity of any specimen at 151 kN, as shown in Fig. 8.5.

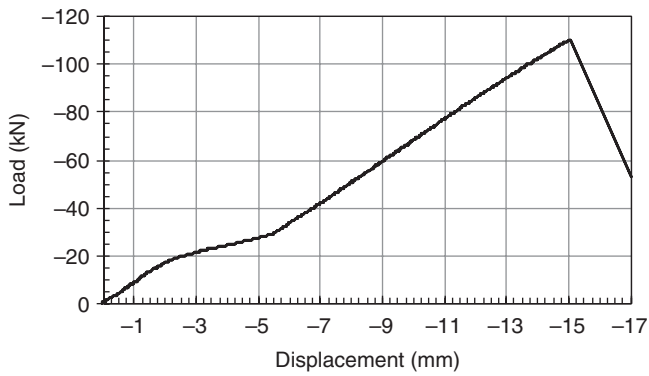


*8.4* Load versus displacement for welded connection without visible crack: specimen AS3.

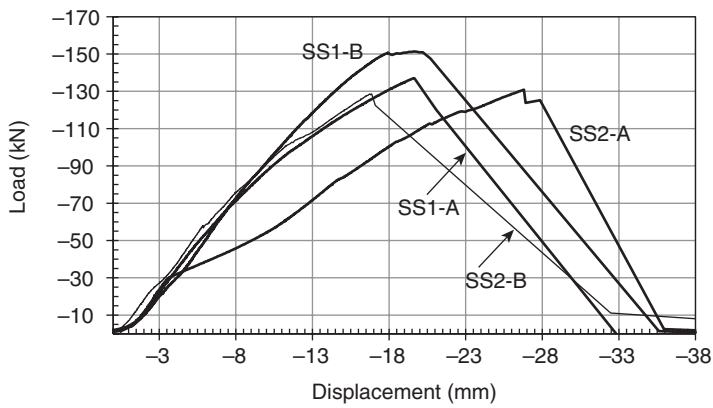


*8.5* Load versus displacement for tests SS1-A, SS1-B, SS2-A, and SS2-B rehabilitated with GFRP composites.

*Table 8.1* Test results of new fabricated and field specimens

| Specimen | Description | Peak load (kN) | Displacement at peak load (mm) |
|---|---|---|---|
| New: GFRP TS1 | 305 mm wrap | 71 | 8.7 |
| New: GFRP TS2 | 305 mm wrap | 76 | 7.7 |
| New: GFRP TS4 | 457 mm wrap | 109 | 18.8 |
| New: GFRP TS4-B | 457 mm wrap | 104 | 23.6 |
| Field: Welded AS3 | No crack in weld | 110 | 15.1 |
| Field: GFRP SS1-A | Crack 52% of weld | 137 | 19.6 |
| Field: GFRP SS1-B | No crack in weld | 151 | 20.2 |
| Field: GFRP SS2-A | Crack 24% of weld | 131 | 26.8 |
| Field: GFRP SS2-B | Crack 66% of weld | 129 | 16.9 |

### 8.3.2 Cracked field specimens repaired with GFRP

The retrofitted aluminum tube field specimens had cracks in the weld, induced by fatigue loading in the field, which went through the thickness of the weld, and varied in length as shown in Table 8.1. Specimen SS1-A had a crack that was 140 mm long which corresponds to 52 % of the weld length; specimen SS2-A had a 64 mm long crack or 24 % of the weld length; and specimen SS2-B had a 178 mm long crack or 66 % of the weld length. The GFRP composite retrofit design details were the same for all repaired specimens as outlined earlier. It is interesting to note from the results, shown in Fig. 8.5 and Table 8.1, that the retrofitted specimens with cracks in the weld (SS1-A, SS2-A, and SS2-B) failed at similar loads in the range 129–137 kN regardless of the crack length. This demonstrates the effectiveness of the GFRP composite retrofit regardless of the crack length. Before the weld completely failed, both the weld and the GFRP composite were carrying the load; however, after weld failure, the GFRP composite carried the load alone; this explains why the cracked weld specimens failed at similar loads – even though the original crack lengths in the weld differ significantly.

### 8.3.3 Newly fabricated specimens with GFRP

Four of the specimens tested (TS1, TS2, TS4, and TS4-B) were new fabricated specimens, built using the same aluminum alloy 6061-T6 material, dimensions, and configuration as the field specimens. However, the new specimens were not welded but were instead constructed by tack welding the diagonals in four spots to the main chord to hold them in place so that the GFRP composite retrofit could be applied. These specimens simulate the case when the weld is severed and the diagonals and chord

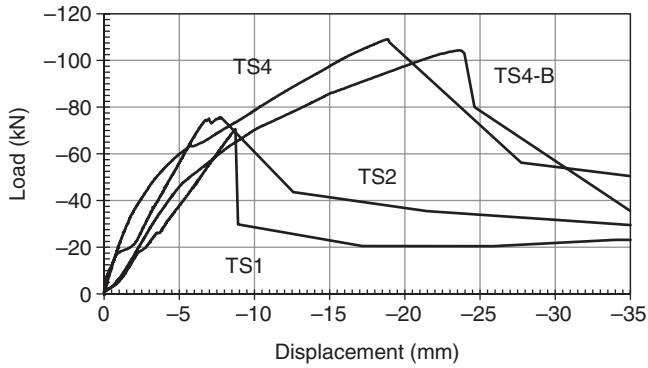


*8.6* Load versus displacement for new fabricated specimens wrapped with GFRP composites.

become two separate members. For specimens TS1 and TS2, the wrap extended up the diagonals 305 mm from the center of the chord; for TS4 and TS4-B the wrap extended 457 mm from the center of the chord. Specimens TS1 and TS2 also had inferior surface preparation and failed at a lower tensile load than TS4 and TS4-B as shown in Table 8.1 and Fig. 8.6.

## 8.4 Constant amplitude fatigue performance of K-tube-to-tube connections

The original design of existing aluminum overhead sign structures did not consider fatigue as a limit state. Cracks propagate in the welds of the connection between the main chord and diagonals due to fatigue stresses caused by wind-induced vibration, and they occasionally lead to complete fracture of the welds. A rehabilitation method for cracked aluminum welded connections using GFRP composites is investigated for its effectiveness under fatigue stresses. The results of constant amplitude fatigue tests for three types of aluminum connections from actual sign structures are presented:

1. connections with no known cracks;
2. cracked connections rehabilitated with GFRP composites;
3. connections with 90 % of the weld removed and subsequently repaired with GFRP composites.

The fatigue limits of the three connection types are established for the following stress ranges:

- a maximum stress of 82.8 MPa, which is 6.3 times the CAFL threshold for Detail Category E of the AASHTO Specifications (AASHTO, 2001);
- a stress of 58.6 MPa;

*Table 8.2* Experimental results of fatigue tests

| Test Unit | Size type* | Failure mode | Maximum stress (MPa) | Stress ratio | No. of cycles |
|---|---|---|---|---|---|
| AL1(a) | I | W | 82.8 | 0.19 | 5690 |
| AL1(b) | I | WB | 82.8 | 0.19 | 14448 |
| AL2(a) | II | WB | 58.6 | 0.27 | 28491 |
| AL2(b) | II | WB | 58.6 | 0.27 | 48096 |
| AL3 | II | WB | 39.3 | 0.20 | 320829 |
| AL4 | I | IL | 20.0 | 0.17 | 1000000 |
| R1 | II | WBF | 82.8 | 0.19 | 6763 |
| R2 | I | WBF | 58.6 | 0.27 | 69194 |
| R3 | II | IL | 39.3 | 0.20 | 1000000 |
| R4 | II | IL | 18.7 | 0.14 | 1000000 |
| WRR1 | II | F | 82.7 | 0.20 | 76 |
| WRR3(a) | II | A | 39.3 | 0.20 | 229503 |
| WRR3(b) | II | F | 39.3 | 0.20 | 371100 |
| WRR4 | II | IL | 23.5 | 0.16 | 1000000 |

*Type I = main chord and diagonals are 6.35 mm thick; Type II = main chord 6.35 mm thick and diagonals 4.76 mm thick.
*Note*: AL = test unit with no known cracks; R = repaired test unit with GFRP; WRR = test unit with 90% of weld removed repaired with GFRP; A = adhesive failure; F = GFRP failure; IL = infinite life; W = weld fracture; WB = weld and base fracture; WBF = weld, base and GFRP fracture.

- a stress of 39.3 MPa;
- a minimum stress of 18.7 MPa, which is 1.4 times the CAFL threshold for Detail Category E.

The frequency of the fatigue cycles used in the present tests was selected as 2 Hz, with a stress ratio equal to 0.2. In Table 8.2, there are two types of specimens: for Type I specimens, the diagonal had an inside diameter of 50.8 mm and an outside diameter of 63.5 mm; the chord had an inside diameter of 88.9 mm and an outside diameter of 101.6 mm. For Type II specimens, the diagonal had an inside diameter of 53.9 mm and an outside diameter of 63.5 mm; the chord had the same dimensions as Type I specimens (Nadauld and Pantelides, 2007).

### 8.4.1 Uncracked field specimens: series AL

Two failure modes were observed in Series AL: (i) fracture through the throat of the weld; and (ii) crack formation at the throat of the weld through the base metal that propagated to fracture of the chord. The cycles to failure varied depending on the stress range and are shown in Table 8.2.

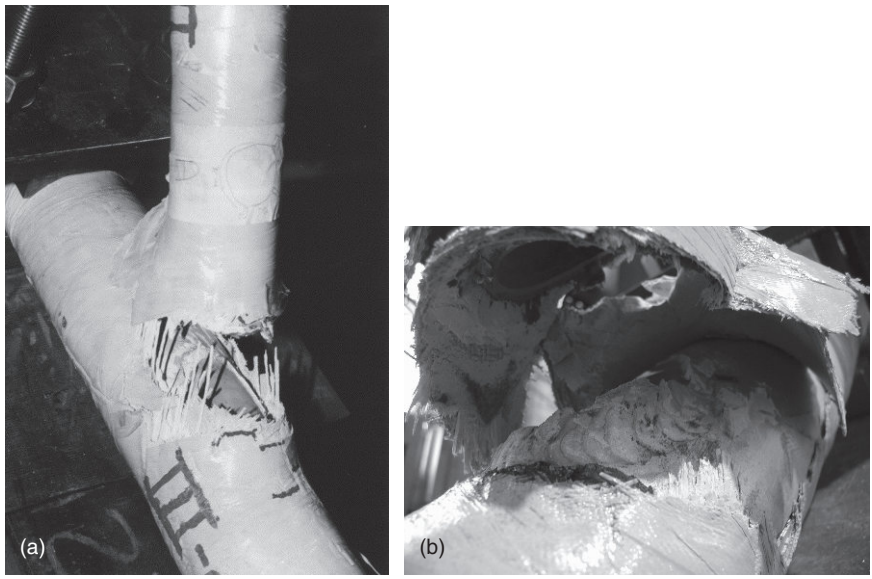


*8.7* Static test after fatigue cycles and failure of weld and GFRP composite: (a) cracking through the throat of the weld; (b) cracking through the toe of the weld.

### 8.4.2 Cracked field specimens repaired with GFRP: series R

Two failure modes were observed in Series R: (i) cracking through the throat of the weld and GFRP tensile failure; and (ii) cracking through the toe of the weld, followed by cracking through the throat of the weld and GFRP tensile failure. The first failure mode occurred for R1, as shown in Fig. 8.7a. A similar failure mode occurred in the static test of R4, which survived the one million fatigue cycles at the 18.7 MPa stress level, as shown in Table 8.2. This failure mode consisted of multiple cracks in the GFRP composite followed by fracture through the throat of the weld and tensile failure of the GFRP composite. The GFRP composite did not change the stiffness of the connection appreciably, but it improved the strength and displacement capacity. The second failure mode for Series R was observed for R2 and R3; cracking was seen in the GFRP composite first, directly above the initial crack at the toe of the weld. The crack at the toe of the weld propagated around the chord; next, the weld was slowly fatigued in the throat until it fractured, which was followed by tensile failure of the GFRP composite as shown in Fig. 8.7b. R3 reached the endurance limit of one million cycles without failure. The cycles to failure varied depending on the stress range and are shown in Table 8.2.

### 8.4.3 Cracked field specimens with majority of weld removed repaired with GFRP: series WRR

Two failure modes were observed in Series WRR: (i) adhesive failure with the GFRP composite tearing; and (ii) GFRP composite tensile failure. Adhesive failure with the GFRP composite tearing was observed for WRR3(a) as shown in Table 8.2, caused by insufficient bond length. A GFRP composite tensile failure mode was observed in the fatigue test for WRR1 due to the high maximum stress applied. WRR4 reached the one million cycle endurance limit and was, subsequently, tested to failure in static tension; the static load capacity for WRR4 after one million cycles was 113 kN, which is 0.85 times the average static capacity of GFRP repaired units with cracks in the welds without fatigue of 132 kN; this indicates that the GFRP composite retained its strength at this stress range. The cycles to failure varied depending on the stress range and are shown in Table 8.2.

### 8.4.4 *S–N* curves

Figure 8.8 shows the *S–N* curves for all fatigue tests. Series AL and the GFRP rehabilitated connections of Series R show similar behavior with Series R showing slightly better fatigue behavior for the lowest maximum stress level. Series WRR for the test units with the weld 90 % removed and repaired with GFRP composites did not perform as well as Series AL and Series R in the high maximum stress level; however, Series WRR performed as well as Series AL in the lowest maximum stress level. In Fig. 8.8, it should be noted that the lowest maximum stress level of 18.7 MPa is 1.4 times the

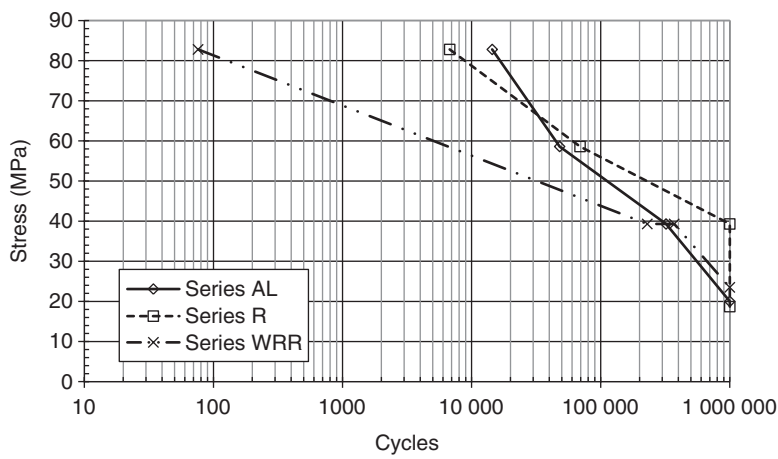


*8.8 S–N* curves for aluminum connections.

CAFL threshold specified by AASHTO (AASHTO, 2001) for Detail Category E. A fatigue reduction factor has been developed for the rehabilitation design of aluminum connections using GFRP composites (Nadauld and Pantelides, 2007).

## 8.5 Conclusion and future trends

A method for rehabilitation of cracked aluminum welded connections of overhead sign structures using GFRP composites has been presented. The retrofitted connections obtained from trusses used in the field with cracks in the welds, which ranged from 24 to 66 % of the total weld length, reached capacities from 1.17 to 1.25 times that of the welded aluminum connection with no visible cracks. By providing adequate surface preparation and GFRP composite bond length, the tack-welded connections with GFRP composite laminates reached capacities from 0.95 to 0.99 times that of the welded aluminum connection with no visible cracks. The lowest maximum stress level tested in the fatigue portion of the research was 1.4 times the CAFL threshold specified by AASHTO (AASHTO, 2001) for Detail Category E. Given the fact that the repaired specimens reached the endurance limit of one million cycles, it can be concluded that rehabilitation of the aluminum joints with GFRP composites concerning fatigue resistance was successful. The static and fatigue test results have shown that the GFRP-repaired aluminum connections behaved as well as the aluminum connections with no known cracks, for the range of loads expected in service; therefore, the repair technique with GFRP composites is successful and is recommended for construction.

Research conducted at the University of Utah for the Utah State DOT (UDOT) and New York State DOT (NYSDOT) has resulted in a fiber composite wrap that surrounds the deficient weld area and helps transfer the load past the area of damage. It is an attractive repair option since it can be installed *in situ* with materials that cost just a few hundred dollars (FHWA, 2005). The fiber composite wrap is actually a FRP. The FRP repair method is relatively quick and economical. It is accomplished by cleaning the damaged area of the sign support thoroughly and wrapping FRP around it. Repairs can be done in place, with only the lanes below the repair area blocked off. A typical repair takes three workers three hours to complete, at an estimated cost of $3000 per joint; more importantly, the repair technique costs less than full structural support replacement.

As a result of research (Pantelides *et al*., 2003; Nadauld and Pantelides, 2007), the New York State DOT has developed a specification for using FRP in overhead sign repair and has implemented such repairs. The specification covers restoration of the tensile capacity of secondary sign structural members, such as internal truss diagonals, and not main members,

such as longitudinal truss chords. The specification has been approved for a five-year lifespan with annual inspections of the repair. The repair of aluminum sign truss bridges with cracked welds in the connections of diagonals to the chord is a good example of using FRP composite materials to repair effectively conventional metallic materials. Several states in the US and several Canadian provinces have expressed interest in implementing the technology. Three demonstrations were held in 2007 and an additional one was held in 2008 as a product demonstration showcase. These repairs, initially thought to be just temporary for one year or less, are now being considered as a permanent repair solution.

## 8.6 Acknowledgments

The author would like to thank the NYSDOT and UDOT for financial support, and Air Logistics Corporation for in-kind support. The author would also like to thank Harry L. White of NYSDOT and Doug Anderson of UDOT for their assistance.

## 8.7 References

AASHTO (2001). *Standard Specifications for Structural Supports for Highway Signs, Luminaires and Traffic Signals* (4th edn), American Association of State Highway and Transportation Officials, Washington, DC.

Fam, A., Witt, S. and Rizkalla, S. (2006). 'Repair of damaged aluminum truss joints of highway overhead sign structures using FRP.' *Construction and Building Materials*, 20, 948–956.

FHWA (2005). *Guidelines for the Installation, Inspection, Maintenance and Repair of Structural Supports for Highway Sings, Luminaires, and Traffic Signals*. Publication No. FHWA NHI 05-036, March, Federal Highway Administration, Washington, DC.

Foutch, D. A., Rice, J. A., LaFave, J. M., Valdovinos, S. and Kim, T.-W. (2006). *Evaluation of Aluminum Highway Sign Truss Designs and Standards for Wind and Truck Gust Loadings*. Report No. FHWA/IL/PRR 153, Illinois DOT, Springfield, IL.

Nadauld, J. and Pantelides, C. P. (2007). 'Rehabilitation of cracked aluminum connections with GFRP composites for fatigue stresses.' *ASCE Journal of Composites for Construction*, 11(3), 328–335.

Pantelides, C. P., Nadauld, J. and Cercone, L. (2003). 'Repair of cracked aluminum overhead sign structures with glass fiber reinforced polymer composites.' *ASCE Journal of Composites for Construction*, 7(2), 118–126.

Sharp, M. L., Nordmark, G. E. and Menzemer, C. C. (1996). *Fatigue Design of Aluminum Components and Structures*. McGraw-Hill, New York.

# Part III

Fatigue performance

This page intentionally left blank

# 9

# Fatigue life of adhesive bonds joining carbon fibre-reinforced polymer (CFRP) composites to steel components

J. DENG, Guangdong University of Technology, China and
M. M. K. LEE, Curtin University Sarawak, Malaysia

**DOI**: 10.1533/9780857096654.3.217

**Abstract**: This chapter assesses the fatigue performance of the adhesive bond between the carbon fibre-reinforced polymer (CFRP) plate and the steel substrate, particularly in the regions where the CFRP plate terminates. It describes a fatigue test programme of CFRP plate-strengthened steel beams leading to the proposal of an *S*–*N* curve from which the fatigue life to crack propagation can be easily estimated. A simple analytical solution is presented to calculate the maximum interfacial stresses in the steel beams strengthened by a CFRP plate. Finally, design recommendations are presented for steel beams strengthened by bonded CFRP plates based on the research findings obtained.

**Key words**: carbon fibre-reinforced polymer (CFRP), steel, adhesive bonding, strengthening, fatigue.

## 9.1 Introduction

Highway bridges in the UK are designed for a lifetime of 120 years. Depending on the type of highway, components in decks can experience up to $7 \times 10^8$ stress cycles over the their design lives (Mays and Tilly, 1982). In the US, major highway bridges generally experience more than $1.5 \times 10^6$ truck passages per year, which can be translated to between $1 \times 10^8$ and $3 \times 10^8$ stress cycles during their 100 year service life (Moses *et al.*, 1987). Consequently, fatigue damage is one of the main problems that occur in old metallic bridges. It is therefore necessary to predict the fatigue behaviour of the updated bridge structures [BS5400-10 (BSI, 1980)]. Hollaway and Cadei (2002) pointed out that the adhesive bonding between the CFRP plate and the metallic substrate is the weakest link and its fatigue performance is of particular importance. Many studies have been carried out to investigate the fatigue behaviour of the adhesive bonding, but mainly in lap joints.

The extremely limited information on the fatigue behaviour of structures reinforced with carbon fiber-reinforced polymer (CFRP) means that much research is needed if this retrofitting and strengthening technique is to be widely promoted. Although there are some good static test data from

literature, these cannot be used to predict the fatigue behaviour of beams strengthened with CFRP plates. Previous research shows improved fatigue behaviour by bonded CFRP materials and the good fatigue resistance of the bond. However, direct relationship between the fatigue life, the interfacial stresses and the specimen characteristics is still yet to be established. Therefore, the results cannot be extrapolated for practical applications.

It has been demonstrated analytically that there is a stress concentration in the adhesive layer at the end of the CFRP plate, and this stress concentration may lead to interfacial debonding and eventually fatigue failure of retrofitted metallic beams. Consequently, to avoid fatigue crack initiating in the adhesive at the end of the plate, the maximum interfacial stresses must be limited. CIRIA Design Guide C595 (Cadei *et al*., 2004) indicates that no *S–N* curve is currently available to characterize the adhesive joint in an externally-bonded FRP strengthening system. Instead, the use of the *S–N* curve formulation for FRP from the tests carried out by the National Physical Laboratory on bonded joints is proposed. In this formulation, the peak shear stress in a fatigue cycle was limited to only 20–30 % of the ultimate static shear strength.

The principal aim of the current work is to investigate the fatigue performance of the adhesive bond between the CFRP plate and the steel substrate, particularly in the regions where the CFRP plate terminates. This was achieved through a fatigue test programme of CFRP plate-strengthened steel beams subjected to mechanical cyclic loading.

## 9.2 Previous research on the fatigue performance of adhesive bonding between carbon fibre-reinforced polymer (CFRP) plates and steel substrates

Hollaway and Head (2001) indicated that unidirectional continuous fibre composites, which essentially behave linearly up to failure when loaded parallel to the longitudinal fibres, generally have good fatigue properties. Tavakkolizadeh and Saadatmanesh (2003) reported that beams in aged metallic bridges can have their fatigue life extended more than three-fold through CFRP plate reinforcement. While the composite materials may behave well under fatigue loading, the adhesive bonding can be a source of weakness.

Adhesive properties that are based on the results of experiments on bulk adhesives cannot be used to predict fatigue performance, as the fracture behaviour depends strongly on the adhesive bond line thickness (Mostovoy *et al*., 1971; Kinloch and Shaw, 1981). Therefore, Althof (1984) suggested the

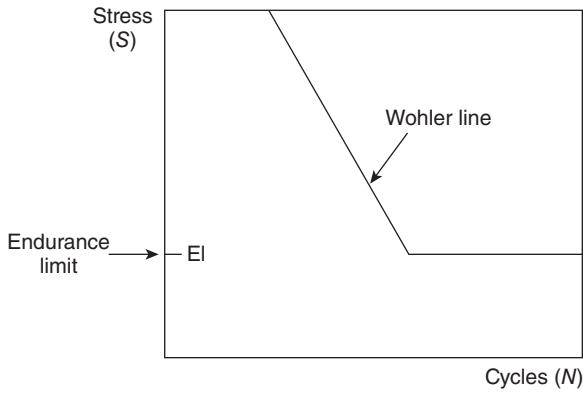


*9.1* Idealised Wohler diagram (Wake, 1982).

thick adherend shear joint specimen as a suitable configuration for evaluating the fatigue properties of adhesive. The fatigue results of Wohler's tests (Wake, 1982) are customarily presented as *S*–*N* curves, in which the stress as a percentage (*S*) of the ultimate strength determined in a 'static' test is plotted against the number of cycles (*N*) at that stress to failure, on a logarithmic scale, as shown on Fig. 9.1.

Whilst test methods for adhesive fatigue properties have been suggested by ISO 9664 (ISO, 1993) and ASTM D3166 (ASTM, 1999), de Geoij *et al*. (1999) indicated that predicting the fatigue properties of a complex joint in an actual structure would be difficult with data from simple test specimens. Fatigue life is strongly influenced by the profile of the edges of the joint. Harris and Fay (1992) indicated that the initiation of small cracks at the edges of the joint represents the major factor in fatigue life. Therefore, if the strain in the adhesive layer under full live loading at the serviceability limit state is kept below that at first cracking (corresponding to the first 'knee' in the loading–deflection curve), then fatigue failure without forewarning is relatively unlikely (Cadei *et al*., 2004). Experimental and numerical investigations to predict the fatigue life of bonded joints based on the fatigue crack initiation and growth mechanism have been conducted by Curley *et al*. (2000), and by Cheuk *et al*. (2002). Furthermore, Abdel Wahab *et al*. (2002, 2004) presented a generalised numerical procedure using finite element (FE) analysis for prediction of the fatigue lifetime of adhesively bonded structures.

The present authors have demonstrated analytically that there is a stress concentration in the adhesive layer at the end of the CFRP plate (Deng *et al*., 2004), and this stress concentration may lead to interfacial debonding and eventually to fatigue failure of the retrofitted metallic beams. The Concrete Society (2000) recommend that the sustained stress in the adhesive

should be kept below 25 % of the short-term strength, which equates to the recommended minimum materials partial factor of 4.0. CIRIA C595 (Cadei *et al*., 2004) reported that tests carried out by the National Physical Laboratory on bonded joints suggest that the *S–N* curve formulation for FRP is also applicable to adhesive joints. This *S–N* curve limits the peak shear stress in a fatigue cycle to 20–30 % of the ultimate static failure strength.

To assess the fatigue bond resistance of a steel bridge girder strengthened with CFRP plates, Miller *et al*. (2001) conducted two test programmes. First, they subjected seven small-scale, doubly reinforced specimens to cyclic loads at a stress range of 82.7 MPa for 2.55 million cycles. All CFRP plates were found to remain fully bonded to the steel substrate without deterioration based on the strain data taken before and after the cycling. Next, two full-scale bridge girders rehabilitated with CFRP plates were fatigued for 10 million cycles at a stress range of 34 MPa. Throughout the tests, the CFRP plates were monitored and inspected for debonding, but none was detected. The retrofit was therefore regarded as having good fatigue resistance.

Tavakkolizadeh and Saadatmanesh (2003) carried out fatigue tests on steel beams strengthened with CFRP. They tested 21 notched steel beams with CFRP patches for medium cycle fatigue loading. Unretrofitted beams were also tested as control specimens. Each steel beam, tested under four-point bending, had a span of 1.22 m, with a centrally located adhesively bonded CFRP plate, 300 mm long. The two central loading points were 200 mm apart. The CFRP plates were manufactured from unidirectional pultruded carbon sheets with a Young's modulus of 144.0 GPa. The steel beams were tested with different constant stress ranges of between 69 and 379 MPa, and between 5 and 10 Hz. The results showed that the CFRP patch not only tends to extend the fatigue life of a detail more than three-fold, but also decreases the crack growth rate significantly.

If a bridge is strengthened with CFRP plates, it is usually not economic to close it to traffic during the curing period, which can take up to 48 hours. During this period, the adhesive is subjected to cyclic loading from the traffic. The Concrete Society (2000) suggested that the change in the adhesive properties caused by the cyclic load during the curing period is likely to be small, perhaps a 10 % reduction in the strength of the fully cured materials. Nikouka *et al*. (2002) investigated the development of stiffness and strength in CFRP-reinforced steel beams subjected to cyclic loading during the early age cure of the adhesive. Five pairs of steel beams 127 × 76UB13, each 1.2 m long, were reinforced with a single carbon fibre composite plate, 0.98 m long, attached to the tension flange. The CFRP plates, each 7.6 mm thick and 76 mm wide were fabricated using K13710 ultra high-modulus carbon fibres with a Young's modulus of 310 GPa. A

sinusoidal load was applied to five specimens at a frequency of 0.25 Hz and this was continued for up to around 48 hours. The tests confirmed that cyclic loading while the adhesive is being cured would have an effect on the final stiffness and failure load of the reinforced beam if the maximum cyclic load were larger than 42 kN, and the bond would fail to develop if the shear deformation in the adhesive during cure is too large. They also suggested that it was prudent to limit the shear stress in the adhesive layer to a maximum of 1 MPa.

The very limited information on the fatigue behaviour of CFRP-reinforced metallic structures means that further research is needed if this retrofitting and strengthening technique is to be widely promoted. Although previous research shows the improved fatigue behaviour by bonded CFRP materials and the good fatigue resistance of the bond, no qualitative relationship has been established between the fatigue life, the interfacial stresses and the specimen characteristics. Therefore, the results cannot be extrapolated for practical applications.

## 9.3 Modelling and predicting fatigue of adhesive bonds

The maximum interfacial stresses at the plate ends are given in this section, together with an analytical expression for the longitudinal strain in the bottom of a plate. Furthermore, an empirical equation to predict fatigue life during crack propagation is developed based on Paris Law.

### 9.3.1 Maximum interfacial stresses

An analytical solution to calculate interfacial stresses has already been presented by the authors (Deng *et al*., 2004). Considering the prestressing force applied on the CFRP plate before bonding, this solution was further developed to give the expressions for the maximum shear stress $\tau_{max}$ and the maximum normal stress $\sigma_{max}$ at the end of the CFRP plate as:

$$\tau_{max} = \sqrt{\frac{G}{t_a b \bar{\lambda}}}\left[(\alpha_b - \alpha_p)\Delta T + \frac{F_f}{E_p A_p}\right] + \bar{g}\sqrt{\frac{G}{t_a b \bar{\lambda}}}M(0) + \frac{\bar{g}}{b\bar{\lambda}}V(0) \quad [9.1]$$

$$\sigma_{max} = -2\bar{\beta}Z_p\tau_{max} + \frac{t_p G}{2t_a}\left[(\alpha_b - \alpha_p)\Delta T + \frac{F_f}{E_p A_p} + \bar{g}M(0)\right] \quad [9.2]$$

where

$$\bar{g} = \frac{Z_b}{E_b I_b}, \bar{\lambda} = \frac{(Z_b + Z_p)Z_b}{E_b I_b} + \frac{1}{E_b A_b} + \frac{1}{E_p A_p}, \bar{\beta} = \sqrt[4]{\frac{E_a b}{4t_a E_p I_p}},$$

$V(0)$ and $M(0)$ are the applied shear force and the applied bending moment on the beam at the end of plate, respectively, $b$ is the width of the plate, $G$ is the shear modulus of the adhesive, $\alpha$ is the thermal expansion coefficient, $\Delta T$ is the temperature change, $F_f$ is the prestressing force applied on the CFRP plate before bonding, $t_a$, $Z_b$ and $Z_p$ are the thickness of adhesive, the distance from the neutral axis to the bottom of the beam and the distance from the neutral axis to the top of the CFRP plate, respectively, and $E$, $I$ and $A$ are the elastic modulus, the second moment of area and the area, respectively. The subscripts b, a and p denote the steel beam, the adhesive and the CFRP plate, respectively. Combining the maximum shear and normal stresses, the maximum principal stress $\sigma_{1max}$ can be written by:

$$\sigma_{1\max} = \frac{|\sigma_{\max}|}{2} + \sqrt{\left(\frac{\sigma_{\max}}{2}\right) + \tau_{\max}^2} \qquad [9.3]$$

## 9.3.2 Longitudinal strain in the bottom of the CFRP plate

The longitudinal strain $\varepsilon_{pb}$ in the bottom of the CFRP plate is given as (Deng and Lee, 2007b):

$$\varepsilon_{pb} = \frac{N_f}{E_p A_p} + \frac{1}{E_p}\frac{3\delta^2}{t_p^2}(-\sigma_{\max}) - \frac{1}{E_p}\frac{2\delta}{t_p}\tau_{\max} \qquad [9.4]$$

where $\delta$ is a small distance from the end of plate and $N_f$ is the longitudinal force applied at the end of plate by the spew fillet. $N_f$ increases with the size of the spew fillet.

From this equation, the strain $\varepsilon_{pb}$ will be more compressive as the effect of the spew fillet reduces and as the peel stress '$-\sigma_{max}$' reduces, but will be less compressive as the shear stress '$\tau_{max}$' reduces. With cracking, or debonding, initiating at the spew fillet, the effect of the spew fillet will lessen, and this occurs before any reduction of the peel and shear stresses in the adhesive layer. Cheuk *et al*. (2002) reported that crack initiates in Mode I earlier than in Mode II in composite–metal double-lap joints under fatigue loading. Hence the peel stress will deteriorate earlier than the shear stress in the adhesive layer.

## 9.3.3 Fatigue life prediction

In accordance with the FE analysis (Deng and Lee, 2008), the crack will initiate in the adhesive from the end of the plate and propagate along the interface between the steel beam and the adhesive. In accordance with Paris Law, the relationship between the crack propagation rate d$a$/d$N$ and the energy release rate $G$ can be expressed as:

$$\frac{\mathrm{d}a}{\mathrm{d}N} = D(G_{\max})^n \qquad [9.5]$$

where $G_{\max}$ is the maximum energy release rate during one fatigue cycle, $a$ is the crack length and $D$ and $n$ are empirical coefficients, which can be determined by experimental data. CIRIA C595 (Cadei *et al.*, 2004) provides an equation to calculate the energy release rate $G$ of strengthened beams:

$$G = \frac{M^2}{2b}\left[\frac{1}{(EI)_{\mathrm{S}}} - \frac{1}{(EI)_1}\right] \qquad [9.6]$$

where $M$ is the applied bending moment on the beam at the plate end or the crack front, $b$ is the width of adhesive layer and $(EI)_1$ and $(EI)_{\mathrm{S}}$ are the section bending stiffness of beam strengthened with the FRP plate and the plain beam, respectively. If the beam is under three-point bending, $M$ is given as:

$$M = \frac{1}{2}p(l_0 + a) \qquad [9.7]$$

where $p$ is the concentrated load and $l_0$ the distance from the supports to the plate end. Substituting Eqs (9.6) and (9.7) into Eq. (9.5) gives:

$$N = \frac{(-2n+1)^{-1}(l_0 + a)^{-2n+1} + C}{D\left[\frac{1}{4}p^2\left(\frac{1}{(EI)_{\mathrm{s}}} - \frac{1}{(EI)_1}\right)\right]^n} \qquad [9.8]$$

Considering the boundary condition $N = 0$ when $a = a_0$,

$$C = -(-2n+1)^{-1}(l_0 + a_0)^{-2n+1} \qquad [9.9]$$

In accordance with the energy release rate equation of infinite plate with a small crack, the initial crack length $a_0$ is given as:

$$a_0 = \frac{E_{\mathrm{a}}G_{\max}}{\pi\sigma_n^2} \qquad [9.10]$$

When the crack crosses the middle of the beam, i.e. $a = l_{\mathrm{p}}/2$, the fatigue crack propagation life $N_2$ can be obtained from Eq. (9.8).

### 9.3.4 End effect to reduce the stress concentration

The CIRIA guidance document C595 (Cadei *et al.*, 2004) proposes a variety of other options for reducing the interfacial stress concentration at plate

ends. These include a spew fillet covering the plate end, tapering the end of the plate (outside taper), a tapered plate with a matching counter taper in the adhesive thickness (inside taper), the use of lower modulus adhesive near the plate end, and some kinds of mechanical restraint at the plate end. Among these, spew fillets and tapers are the more practical and reliable options. In practice, surplus adhesive (spew fillet) is always squeezed out of the end of the bonded zone under pressure. The square-ended (without spew fillet) adhesive bonded joints are, perhaps, only of theoretical interest.

A simple numerical procedure for calculating the interfacial stresses of retrofitted beams bonded with a tapered CFRP plate has been proposed by Deng *et al*. (2004). The use of tapered plates was found to be able to reduce the interfacial stress concentrations that occur at the ends of the adhesively bonded plates. The test results show (i) the strength of the metallic beams reinforced with a bonded CFRP plate with spew fillets at the ends is about 5 % higher than that without spew fillets (Deng and Lee, 2007a), and (ii) a spew fillet can improve the fatigue performance of retrofitted metallic beams (Deng and Lee, 2007b).

FE analysis was employed to determine the effects of the spew fillet and the taper on interfacial adhesive stresses and the strains in the CFRP plate (Deng and Lee, 2008). A total of eight cases with different configurations of spew fillets and different tapers have been considered. The results show:

- The adhesive stresses, especially the normal stresses, on the steel and the CFRP interfaces are different due to the load transfer and the influence of the singularity at the adhesive corner.
- A spew fillet will reduce both the shear and the normal stress concentrations at the adhesive entry corner, and the stress distributions close to the adhesive end are smoother when a spew fillet is introduced. Therefore, cracking in the with-fillet cases may not initiate at the corner as in the without-fillet cases. But the crack will still progress along the steel surface in all cases.
- A small entry angle between the fillet edge and the steel beam is more beneficial for reducing the maximum stresses than the size of the spew fillet.
- A taper reduces the maximum stresses, but the stress concentration is still quite significant. The beneficial effect of an inside taper is larger than that of an outside taper.
- To reduce the normal stress, spew fillets are better than tapers, but the inside taper is more effective in reducing the shear stress than the fillet. Therefore, a combination of inside taper and spew fillet is the best way to reduce the maximum interfacial stresses.

## 9.4 Testing adhesive bonds

In order to investigate the fatigue behaviour of the adhesive layer in the retrofitted steel beam bonded with CFRP plate, ten small-scale steel beams strengthened with prepreg carbon fibre plates were tested. Due to the stress concentration in the adhesive layer at the ends of CFRP plate, the maximum interfacial stresses at the end of the CFRP plates, calculated by Eq. (9.3), are the fatigue stresses. Different principal stress ranges of 23.8–80.4 MPa were considered in the study.

### 9.4.1 Specimens

Ten small-scale steel beams strengthened with prepreg carbon fibre plates were tested. The steel beams used were 1.2 m long 127 × 76UB13. The steel had a design strength of 275 MPa and a Young's modulus of 205 GPa. The flange surface that received the CFRP plate was sand blasted to SA2½ industry standard and the plate was attached to it within four hours. The CFRP plates used were 3 mm thick and 400 mm long and fabricated from 0.3 mm thick unidirectional epoxy prepreg. The adhesive used was a two-part thixotropic epoxy resin epoxy adhesive (Sikadur®-31 Normal), with a Young's modulus of 8 GPa, a shear modulus of 2.6 GPa and a tensile strength of 29.7 MPa (data provided by the manufacturer). It was mixed with 1 % by weight 1 mm diameter ballotini to ensure a uniform bond thickness.

### 9.4.2 Test set-up and instrumentation

The fatigue tests were carried out in a servo-hydraulic Dennison test machine with a maximum capacity of 200 kN, using a three-point bending set-up. The clear span was 1.1 m and the loading point was in the middle. The specimens were supported on two rollers, which allowed the specimens to behave in a simply supported manner. Steel bars fixed by clamps were placed on either side of the rollers to prevent any side movements of the system. The loading block had two steel plates with counter seats and a roller in between to prevent its movement when the test was in progress. A photograph of the test set-up is shown in Fig. 9.2.

The first of the ten beams (specimen F135 in Table 9.1) was first tested under static load, by displacement control at a rate of 0.5 mm/second, to determine the failure load, which then governed the maximum load applied to the other nine beams under fatigue loading condition. The failure load obtained for this beam was 135 kN. This load was then used to obtain the maximum principal interfacial stress $\sigma_{1max}$ of 80.4 MPa, calculated using Eq. (9.3), at the end of CFRP plate. The stress concentrations caused by the discontinuity at the ends of CFRP plate mean that $\sigma_{1max}$ is the governing

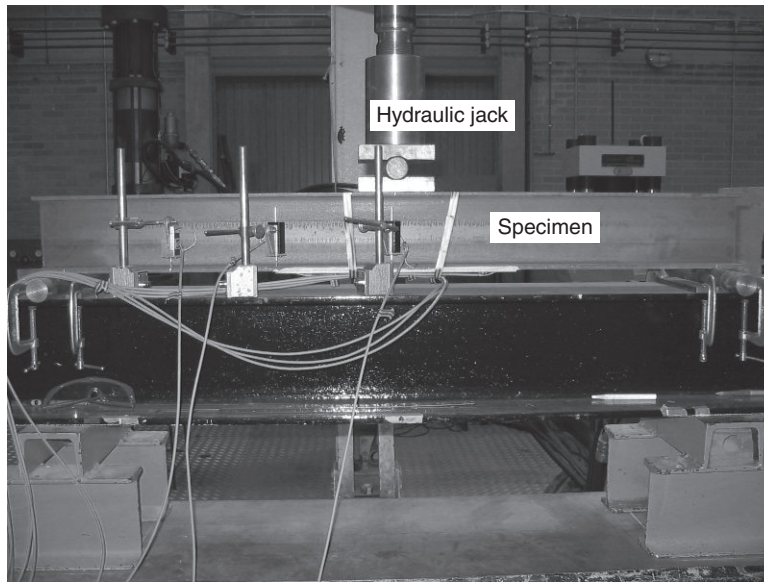


*9.2* Test set-up.

*Table 9.1* Specimen details and test results under fatigue loading

| Specimen | $P$ (kN) | $\sigma_{1max}$ (MPa) | $\sigma_{1max}/\sigma_{1max,u}$ (%) | Crack-free life $N_1$ | | Fatigue life $N_1 + N_2$ | |
|---|---|---|---|---|---|---|---|
| | | | | End A | End B | End A | End B |
| F135 | 135 | 80.4 | 100 | – | – | – | – |
| F125 | 125 | 74.4 | 92.6 | 3 | – | 30 | – |
| F90 | 90 | 53.6 | 66.7 | 700 | 600 | 5000 | 5000 |
| F70 | 70 | 41.7 | 51.2 | 3000 | 4000 | 25000 | 20000 |
| F55-1 | 55 | 32.8 | 40.7 | 17000 | 18000 | 130000 | 111000 |
| F55-2 | 55 | 32.8 | 40.7 | 16000 | 15000 | 100000 | 110000 |
| F50 | 50 | 29.8 | 37.0 | 300000 | 350000 | 965000 | 965000 |
| F40-1 | 40 | 23.8 | 29.6 | – | – | – | – |
| F40-2 | 40 | 23.8 | 29.6 | – | – | – | – |
| F70* | 70 | 41.7 | 51.2 | 6400 | 7000 | 28900 | 28900 |

*Note*:
1. F135 was tested under static loading.
2. $P$ is the maximum applied load.
3. $\sigma_{1max}$ is the maximum interfacial principal stress at the end of the plate under the maximum applied load.
4. $\sigma_{1max}/\sigma_{1max,u}$ is the normalised maximum interfacial principal stress.
5. A and B indicate the two different ends of adhesive joint in the same retrofitted beams.
6. The minimum applied load was 5 kN except for specimen F70*, which had a minimum load of 20 kN.

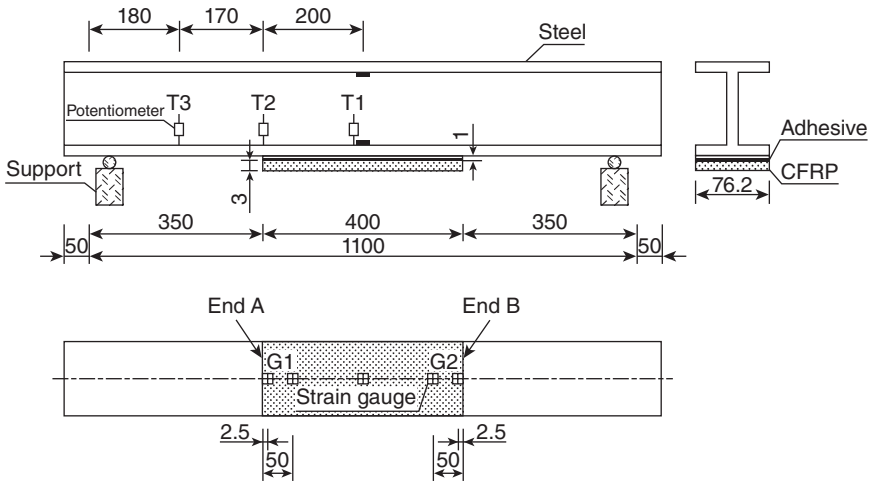


*9.3* Schematic of test specimens (dimensions in mm).

fatigue stress. The other nine beams were tested under fatigue loading with the maximum centrally applied load $P$ between 40 and 125 kN. These loads convert to a range for $\sigma_{1max}$ of 23.8–80.4 MPa, as shown in Table 9.1. In this table, $N_1$ and ($N_1$ + $N_2$) are the number of cycles up to crack initiation recorded by strain gauges (crack-free life) and up to specimen failure (fatigue life), respectively. End A and end B are two ends in the same specimens.

Referring to Fig. 9.3, deflections were measured at three locations using potentiometers, shown as T1, T2 and T3. To investigate the phenomenon of crack initiation, the backface-strain technique was employed. Two 2 mm long strain gauges were mounted on the face of the CFRP plate at the ends of the plate along the longitudinal centre line, shown as G1 to G2 in Fig. 9.3. All data, including the load values measured by the sensor in the hydraulic system, were automatically recorded by a data logging system.

## 9.4.3 Test procedure

A minimum load of 5 kN was applied to all the fatigue tested beams except for specimen F70* (which had a minimum load of 20 kN) so as to ensure firm contact between the beam and the supports. Loading was applied sinusoidally, with a frequency of 1 (for specimens F125, F90 and F70) to 2 Hz (for specimens F55, F50 and F40).

During the fatigue cyclic loading, the test was stopped at regular intervals, or when cracking was detected, and the specimen was then subjected to

three cycles of loading and unloading between 0 kN and the maximum applied load at a rate of 2 kN/second. This was done in order to measure the loads, the strain values at the CFRP plate ends and the deflections during the load cycle, since these data cannot be recorded accurately during the fatigue load cycles.

Apart from monitoring by strain gauges, the initiation and growth of cracks was also monitored visually using a magnifying glass, and the length of the crack with the associated number of cycles were noted. The test was stopped when crack propagation passed the middle of the specimen or when the crack stopped growing, which means that the CFRP plate had lost its strengthening effect and the specimen failed. In order to assess the performance of beams which showed no sign of debonding after undergoing the fatigue test, specimen F40-2 was tested to failure under static load by displacement control at a rate of 0.5 mm/second after it had endured 4 million cycles of fatigue loading.

## 9.5 Test results and analysis

### 9.5.1 Strain at the end of the plate

Figure 9.4 shows the strain range – the range between the minimum strain and the maximum strain in the same cycle – measured by gauge G1 (at one end of the CFRP plate) during the fatigue tests. The strain range, rather than the absolute strain, was used to eliminate the effect from temperature fluctuation. Specimen F125 is not included in the plot because of its very short fatigue life. All the curves except those for F40-1A and F40-2A display a trough of maximum compression before finally reducing to almost zero. Figure 9.4 clearly shows a delay in crack initiation as the load is reduced. For the two lightly loaded specimens – F40-1 and F40-2 – the curves in Fig. 9.4 show that the maximum compressive strain, once reached, was maintained until the test stopped. This shows no crack had initiated in these specimens, indicating that 40 kN was the threshold load for the fatigue tests.

With the theoretical analysis in Section 9.3, it is possible to divide each of the curves representing a specimen that failed in fatigue into four distinct phases, shown in Fig. 9.5 for specimen F70B. Phase A is from the start to $\varepsilon_s$. $\varepsilon_s$ is the strain range measured in a similar specimen without spew fillet under static loads between 70 and 5 kN (the maximum and minimum loads for specimen F70). In this phase, the spew fillet was effective but was losing its strength gradually. Phase B is from $\varepsilon_s$ to the maximum compressive strain. During this phase, the spew fillet no longer affects the strain, and the peel stress at the plate end reduced gradually. Phase C begins when the strain reaches maximum compression and ends when it is almost zero as a result of the gradual disappearing of the shear stress at the plate end. Phase

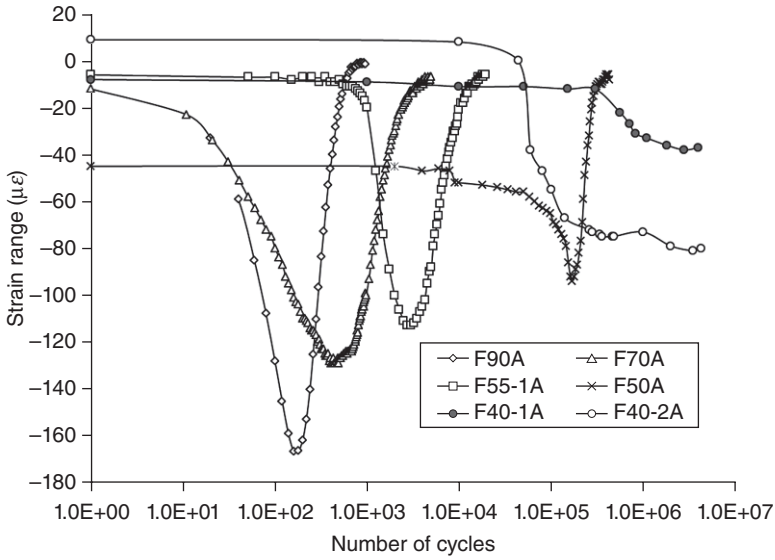


*9.4* Strain range measured during the fatigue test.

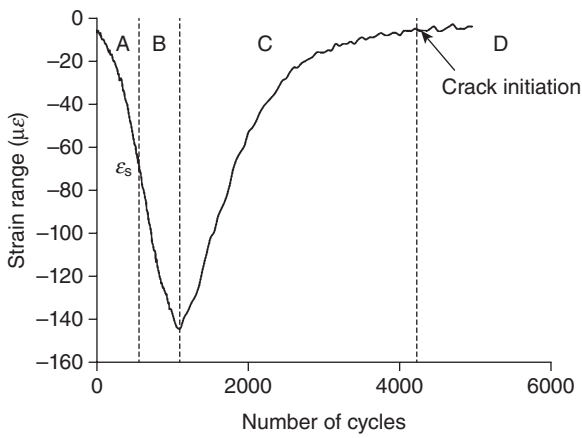


*9.5* Strain ranges measured in F70B.

D is the remaining part, when the adhesive close to the plate end has completely lost its strength, and cracking has started.

## 9.5.2 Stiffness change

Figure 9.6 shows the deflections measured from the three potentiometers during the fatigue test of specimen F70. It can be observed that:

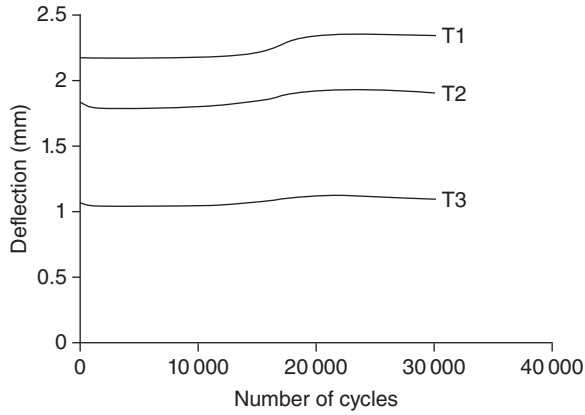


*9.6* Deflections of specimen F70 measured during the fatigue test.

- Before crack initiating, the stiffness of the beam had remained constant.
- With crack growth, the deflections obtained by the potentiometers increased in the order from T3 to T1, until the crack crossed the middle of the retrofitted beam.
- The increase in deflections was small because of the thinness of the plate compared to that of the steel beam.

Similar observations were made on the other specimens.

### 9.5.3 *S–N* curve and crack-free life

The maximum principal interfacial stresses ($\sigma_{1max}$) of all specimens are calculated using Eq. (9.3), and shown in Table 9.1. The curve for $\sigma_{1max}$ versus the log of the crack-free life $N_1$ is presented in Figure 9.7. $\sigma_{1max,\,u}$ (80.4 MPa) is the maximum principal interfacial stress of specimen F135 with a maximum applied load of 135 kN. The relationship is approximately linear, and regression analyses produce the following best-fit equation (with a correlation coefficient, $R^2 = 0.96$):

$$\sigma_{1max} = -4.19 \ln(N_1) + 78.62 \qquad [9.11]$$

It has been established by the authors that the bonded strength of retrofitted metallic beams is not influenced by the size and material properties of either the metallic beams or the CFRP plates (Deng and Lee, 2007a). Therefore, this *S–N* curve can be applied generally as long as the same adhesive is used.

Specimens F40-1 and F40-2 did not fail even after 4 million cycles. Furthermore, the variation of the strain at the end of plates is very small

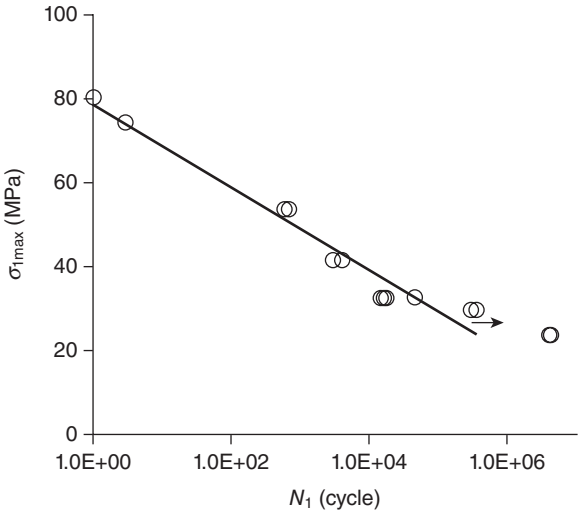


*9.7 S–N* curve.

after 3 million cycles in F40-1 and after 2 million cycles in F40-2 (Fig. 9.4), which indicates that the specimens are not likely to fail in fatigue. Therefore, the fatigue threshold for the tested beams is 40 kN, with a corresponding threshold stress 23.8 MPa for the adhesive. This threshold limit is about 30 % of the ultimate failure stress 80.4 MPa under static loading.

### 9.5.4 Crack propagation life

The crack initiation and propagation in all the specimens were similar except for specimen F125. The load range on this specimen was too high and caused it to debond suddenly from one end after only 30 cycles, similar to the phenomenon observed in the static tests. For all the plates that had debonded, cracking started from the middle of the spew fillet and then propagated to the interface between the steel beam and the adhesive at an angle of 45°. The crack then grew along the interface and stopped eventually. There was always a short length of adhesive remaining uncracked that bonded the plate to the beam. Figure 9.8 shows the typical crack in the failed specimens, except for F125.

Crack initiation, recorded by gauges G1 and G2, has been discussed in Section 9.5.1. Furthermore, crack initiation and growth were also observed visually using a magnifying glass. The crack lengths which developed on two sides at one plate end were not the same, because the load applied could be a little eccentric and the spew fillets might not be uniform along the edges. The longer ones were chosen as the crack length of the specimen.

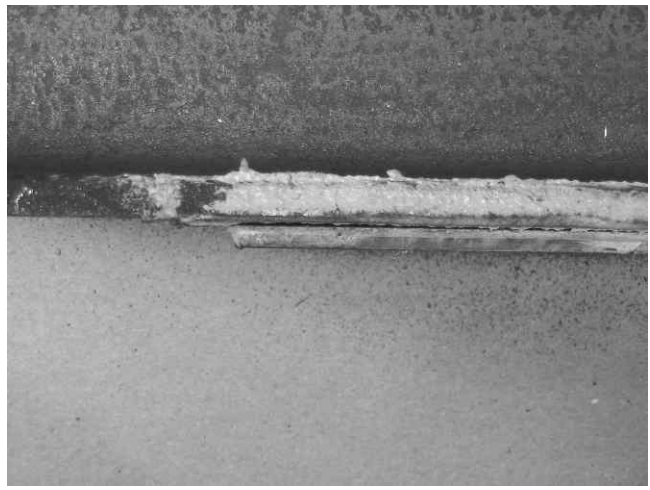

*9.8* The typical debonding.

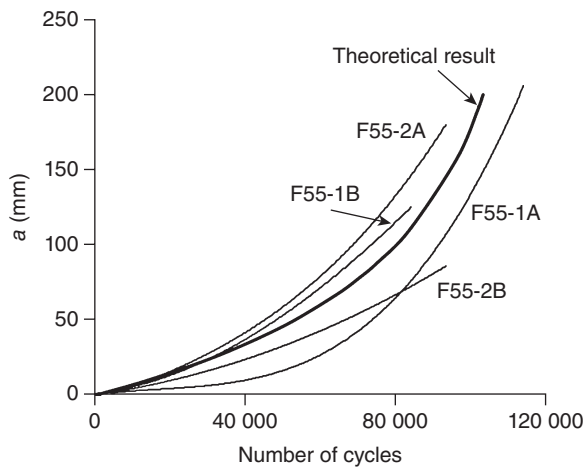


*9.9* *a–N* curves.

The curves of the crack length $a$ versus the number of cycles $N$ (not including the crack-free life) of specimens F55-1 and F55-2 are presented in Fig. 9.9. The crack propagation rate d$a$/d$N$ can be obtained from the curves. The energy release rate $G$ can be calculated from Eq. (9.6).

The curve for the log of the crack propagation rate d$a$/d$N$ versus the log of the energy release rate $G$ is presented in Fig. 9.10. The relationship is approximately linear and regression analyses produce the following best-fit equation (with a correlation coefficient, $R^2 = 0.7896$):

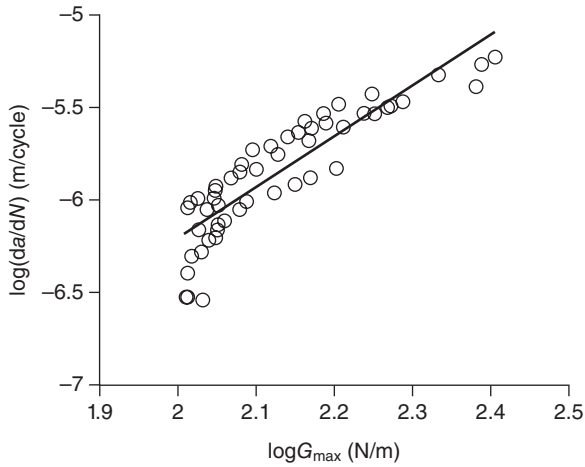


*9.10* $\log G_{max} \sim \log(da/dN)$.

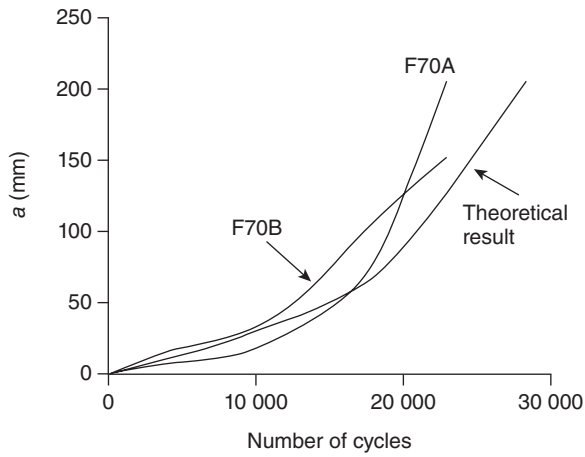


*9.11* *a–N* curves of F70.

$$\log(da/dN) = 2.753\log(G_{max}) - 11.718 \quad [9.12]$$

Therefore, the empirical coefficients $D$ and $n$ in Eq (9.6) are $10^{-11.7}$ and 2.75, respectively. Substituting $G_{max}$ and $\sigma_n$ into Eq. (9.10) gives $a_0 = 0.24$ mm.

To validate the prediction equation of the crack propagation life [Eq. (9.8)], the curves for the crack length $a$ and the number of cycles $N$ (not including the crack-free fatigue life) of specimen F70 obtained from the test are compared to the corresponding predicted results calculated by Eq. (9.8) in Fig. 9.11. This shows that the agreement is good.

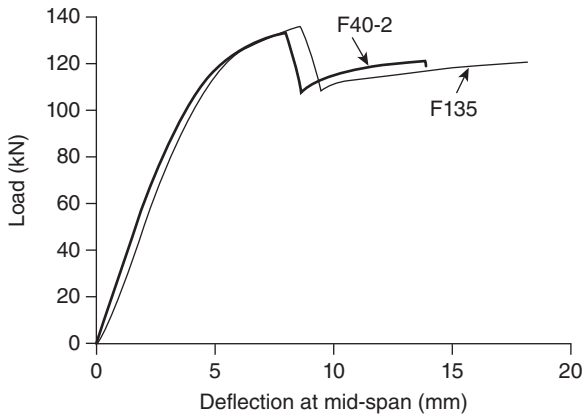


*9.12* Comparisons of load–deflection curves between specimens with fatigue test and without fatigue test.

### 9.5.5 Strength after fatigue testing

As detailed in Section 7.4, specimen F40-2 was tested to failure under static loading after the fatigue test. The failure load obtained was 133 kN, which was only marginally lower than 135 kN, the strength of the specimen F135. Figure 9.12 compares the load–deflection curves obtained from these two specimens, which indicate that the fatigue test had caused very little, if any, deterioration in the static performance.

The strains measured at the ends of the plates in specimen F40-2 under a static load superimposed onto the load–strain curves for specimen without spew fillets (specimen S304s) (Deng and Lee, 2007a) are shown in Fig. 9.13. It is observed that the strains for the current specimen are compressive and the descending segments of the curves are more linear than those for the beam without spew fillets. This indicates that the spew fillets were no longer affecting the strains and that the adhesive at the end of plate was less plastic after the fatigue test.

### 9.5.6 The effect of the load range

The minimum load on specimen F70* was 20 kN. Therefore, the load range for this beam was 50 kN, which was the same as the load range for specimen F55-1. The comparisons of the strain range versus cycle curves of F70, F70* and F55-1 are shown in Fig. 9.14. The curve for beam F70* can be seen to be closer to the F70 curve than to the F55-1 curve. Moreover, the numbers of cycles up to crack initiation recorded by strain gauges for F70* are 6400 and 7400, which is much closer to those for F70 (3000 and 4000) than those

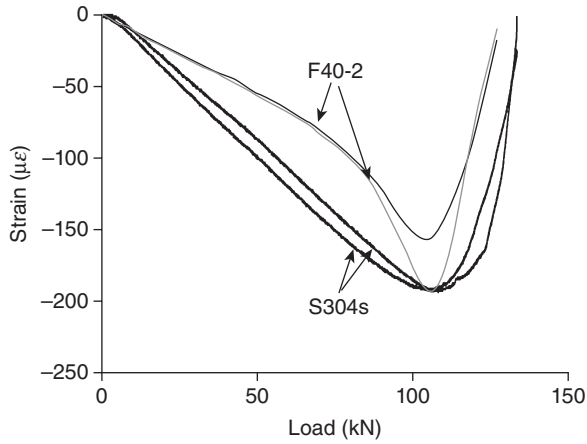


*9.13* Comparisons of strain at the plate ends between specimens F40-2 and S304s.

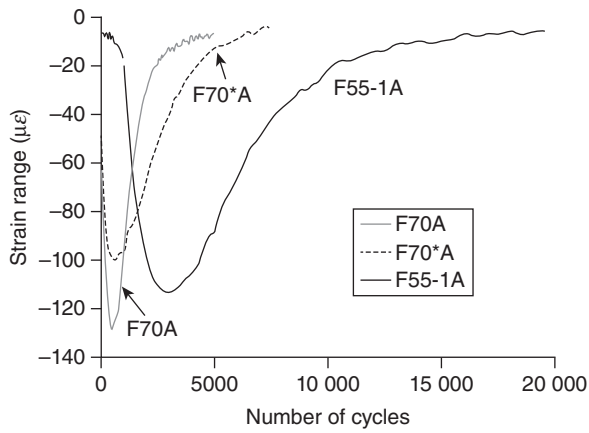


*9.14* Comparisons of the strain ranges obtained for specimens F70A, F70*A and F55-1A.

for F55-1 (17 000 and 18 000). Therefore, it can be concluded that while the load range affects the fatigue behaviour, it is less significant than the effect of the maximum load.

## 9.6 Conclusion and future trends

### 9.6.1 Conclusion

This chapter gives a theoretical and experimental analysis of the fatigue life of CFRP adhesively bonded to steel beams. The backface-strain technique

was applied to monitor crack initiation. The test results show that the debonding, which was the main failure mode of the retrofitted beams, occurs as a result of the maximum interfacial stresses. Taper and natural spew fillet are suggested to reduce the maximum interfacial stresses. Moreover, the stiffnesses of the retrofitted beams were found to deteriorate with crack growth, but the deterioration was insignificant due to the thin thickness of the plates used in the tests.

The fatigue life of the retrofitted beams is divided into two phases, crack-free life and crack propagation life. In accordance with the fatigue test results, an *S–N* curve based on the peak interfacial stresses is proposed to predict the crack-free life and an empirical equation based on Paris Law is proposed for the crack propagation life. The fatigue limit, i.e. threshold, of the *S–N* curve is about 30 % of the ultimate static failure stress, which validates the fatigue limit suggested by the CIRIA Design Guidance (Cadei *et al*., 2004).

The static performance of retrofitted beam is not affected in any significant way by fatigue loading under the threshold limit. The fatigue load range will affect the fatigue life, but its significance is much less than the magnitude of the maximum load in the load range.

### 9.6.2 Implications for design and use

1. *Proposed details to reduce the maximum adhesive stresses*. Adhesives with low elastic modulus are suggested to reduce the maximum adhesive stresses. Taper is also suggested to reduce the maximum adhesive stresses. The natural spew fillet at the end of plate is suggested to be retained in fabrication, but its effect on the reduction on stress concentration should not be included in design.
2. *Fatigue limit of the bonded joint in reinforced beams*. To avoid fatigue crack initiation in the adhesive at the end of the plate, the maximum adhesive stresses must be limited. The *S–N* curve investigated in this study shows that the fatigue limit is 30 % of the ultimate static failure stress.
3. *Curtailment of plate length*. The strength and the stiffness of reinforced beams are not influenced by the plate length. Therefore, the plate length is determined by the maximum allowable adhesive stresses. Except for the thermal effect, the maximum adhesive stresses are influenced by the applied bending moment and the applied shear force, especially the former. Therefore, to curtail the plate length, the plate ends should be located in an area of low applied bending moment.
4. *Monitor reinforced beams*. The backface-strain technique is suggested to be used to monitor the deterioration of the adhesive and crack initiation at the plate end, especially for beams under fatigue load.

## 9.7 Acknowledgements

This work is supported by the National Natural Science Foundation of China through grants 51278131 and 50808085 Program for New Century Excellent Talents in University through grant NCET-13-0739, and Fok Ying Tong Education Foundation through grant 131073.

## 9.8 References

Abdel Wahab M M, Ashcroft I A, Crocombe A D and Smith P A (2002), 'Numerical prediction of fatigue crack propagation lifetime in adhesively bonded structures,' *International Journal of Fatigue*, 24(6): 705–9.

Abdel Wahab M M, Ashcroft I A, Crocombe A D and Smith P A (2004), 'Finite element prediction of fatigue crack propagation lifetime in composite bonded joints,' *Composites Part A-Applied Science and Manufacturing*, 35(2): 213–22.

Althof W (1984), 'Effects on low cycle fatigue on shear stressed adhesive bondlines,' in Mittal K L (ed.), *Adhesive Joints: formation, characteristics, and testing*, vol. 1. New York City: Plenum Press, 659–77.

ASTM (1999), *ASTM D3166-99 Standard test method for fatigue properties of adhesives in shear by tension loading*. West Conshohocken, PA: ASTM International.

BSI (1980), *BS 5400-10 Steel, concrete and composite bridges – code of practice for fatigue*. London: British Standards Institute.

Cadei J M C, Stratford T J, Hollaway L C and Duckett W G (2004), *Strengthening Metallic Structures Using Externally Bonded Fibre-reinforced Polymers, C595*. London: CIRIA.

Cheuk P T, Tong L, Wang C H, Baker A and Chalkley P (2002), 'Fatigue crack growth in adhesively bonded composite-metal double-lap joints,' *Composite Structures*, 57(1–4): 109–15.

Concrete Society (2000), *Design guidance for strengthening concrete structures using fibre composite materials: report of a Concrete Society Committee*. Crowthorne.

Curley A J, Hadavinia H, Kinloch A J and Taylor A C (2000), 'Predicting the service-life of adhesively-bonded joints,' *International Journal of Fracture*, 103(1): 41–69.

de Goeij W C, van Tooren M J L and Beukers A (1999), 'Composite adhesive joints under cyclic loading,' *Materials & Design*, 20(5): 213–21.

Deng J and Lee M M K (2007a), 'Behaviour under static loading of metallic beams reinforced with a bonded CFRP plate,' *Composite Structures*, 78(2): 232–42.

Deng J and Lee M M K (2007b), 'Fatigue performance of metallic beams strengthened with a bonded CFRP plate,' *Composite Structures*, 78(2): 222–31.

Deng J and Lee M M K (2008), 'Effect of plate end and adhesive spew geometries on stresses in retrofitted beams bonded with a CFRP plate,' *Composites: Part B*, 39(4): 731–39.

Deng J, Lee M M K and Moy S S J (2004), 'Stress analysis of steel beams reinforced with a bonded CFRP plate,' *Composite Structures*, 65(2): 205–15.

Harris J A and Fay P A (1992), 'Fatigue life evaluation of structural adhesives for automotive applications,' *International Journal of Adhesion and Adhesives*, 12(1): 9–18.

Hollaway L C and Cadei J (2002), 'Progress in the technique of upgrading metallic structures with advanced polymer composites,' *Progress in Structural Engineering and Materials*, 4(2): 131–48.

Hollaway L C and Head P R (2001), *Advanced Polymer Composites and Polymers in the Civil Infrastructure* (1st edn). New York: Elsevier.

ISO (1993), *ISO 9664: 1993 Adhesives – test methods for fatigue properties of structural adhesives in tensile shear*. Geneva: International Organization for Standardization.

Kinloch A J and Shaw S J (1981), 'The fracture resistance of a toughened epoxy adhesive,' *Journal of Adhesion*, 12: 59–77.

Mays G C and Tilly G P (1982), 'Long endurance fatigue performance of bonded structural joints,' *International Journal of Adhesion and Adhesives*, 2(2): 109–13.

Miller T C, Chajes M J, Mertz D R and Hastings J N (2001), 'Strengthening of steel bridge girder using CFRP plates,' *Journal of Bridge Engineering*, 6(6): 514–22.

Moses F, Schilling C G and Raju K S (1987), *Fatigue evaluation procedures for steel bridges*, NCHRP Rep. No. 299. Washington, DC: Transportation Research Board.

Mostovoy S, Ripling E J and Bersch C F (1971), 'Fracture toughness of adhesive joints,' *Journal of Adhesion*, 3: 125–44.

Nikouka F, Lee M M K and Moy S (2002), 'Strengthening of metallic structures using carbon fibre composites', *IABSE Symposium, Melbourne 2002: Towards a Better Built Environment – Innovation, Sustainability, Information Technology*. Zurich: IABSE, 121–7.

Tavakkolizadeh M and Saadatmanesh H (2003), 'Fatigue strength of steel girders strengthened with carbon fiber reinforced polymer patch,' *Journal of Structural Engineering*, 129(2): 186–96.

Wake W C (1982), *Adhesion and the Formulation of Adhesives*. London: Applied Science Publishers.

# 10

# Fatigue life of steel components strengthened with fibre-reinforced polymer (FRP) composites

P. COLOMBI and G. FAVA, Technical University of Milan (Politecnico di Milano), Italy

**DOI**: 10.1533/9780857096654.3.239

**Abstract**: This chapter deals with fibre-reinforced polymer (FRP) strengthening of steel components under fatigue loading. Special attention is given to old riveted steel girders. The principles of fatigue reinforcement by FRP elements are illustrated with reference to small-scale specimens, and the advantages related to the use of pre-stressed FRP strips are highlighted. Analytical and numerical models for stress intensity factor evaluation are also introduced and discussed. Applications to full-scale steel girders and welded details are then outlined with particular reference to prestressed FRP strips. The chapter concludes with the design of FRP fatigue reinforcements of riveted steel girders.

**Key words**: fatigue strengthening, fibre-reinforced polymer (FRP) materials, adhesive bonding, prestressed carbon fibre-reinforced polymer (CFRP) plates, steel components.

## 10.1 Introduction

Fibre-reinforced polymer (FRP) materials are particularly recommended for reinforcing civil engineering structures such as bridges, buildings and other infrastructure, and they are widely used for the reinforcing of concrete structures. There has been extensive research on these applications. More recently, FRP materials have been also adopted for the reinforcement of timber, masonry and steel structures. Generally, carbon fibre-reinforced polymer (CFRP) materials are used to reinforce steel structures by bonding wraps or strips to the steel surface since they have an elastic modulus which is comparable to the elastic modulus of the steel substrate and high tensile strength. CFRP composites have been mainly used for flexural strengthening, using both non pre-stressed and pre-stressed wraps and strips. Strengthening by pre-stressed CFRP strips is particularly appealing since CFRP reinforcements respond to both permanent and live loads.

A particular feature of the FRP reinforcement of steel structures is that the adhesive layer is the weakest point of the system due to the very high strength of the steel substrate. Cohesive failure in the adhesive layer, interface failure (generally at the steel–adhesive interface) and FRP

delamination are the most common failure modes. Interface failure can be avoided by a proper steel surface preparation, while a proper selection of the adhesive type and bond length is required to prevent cohesive failure. A proper selection of the mechanical properties avoids FRP delamination. Finally, mechanical anchorage can also be used to prevent debonding in critical regions.

Research has been carried out on bond behaviour between steel and FRP, flexural strengthening of steel girders, local buckling and stability of compressed elements, dynamic and fatigue loading, and bond durability. These activities are well documented in recent state-of-the-art review articles (Hollaway and Cadei, 2002; Shaat *et al*., 2004; Zhao and Zhang, 2007; Teng *et al*., 2012). Several topics are covered in these contributions, such as selection of the appropriate adhesive type and surface preparation, bond behaviour and durability, flexural strengthening, fatigue improvement and strengthening against local buckling and stability. Design guidelines for the strengthening of steel structures by FRP materials are also available in the literature (Cadei *et al*., 2004; Schnerch *et al*., 2007). In Cadei *et al*. (2004), conceptual design, structural behaviour and analysis, design and detailing and installation and quality control are covered. In particular, detailed stress analyses in the adhesive layer are presented and different failure criteria are suggested (based on stress or fracture mechanics). The benefits of pre-stressing FRP strips are also highlighted. Worked examples finally illustrate the proposed design procedures. In Schnerch *et al*. (2007), special attention is devoted to the strengthening of typical steel–concrete composite bridge girders. In particular, a flexural design procedure based on moment–curvature analysis is proposed. Moreover, a bond model is described to evaluate the shear and peel stresses in the adhesive joint between FRP and steel. A worked example finally illustrates the proposed flexural design approach. A detailed analysis of the potential of FRP materials to reinforce steel structures is beyond the scope of this chapter since they are discussed in detail in other chapters of this book.

This chapter focuses on the use of FRP materials to improve the fatigue lifetime of steel girders. Special attention is dedicated to old riveted bridges since they exhibit fatigue problems in their connections. The fatigue behaviour of FRP bonded to steel or the fatigue behaviour of the adhesive joint is not covered since these topics are treated in detail in other chapters of this volume. A state-of-the-art review of FRP strengthening of metallic structures subjected to fatigue loading was recently presented in Zhao (2011), including the effect of fatigue loading on the bond between FRP and steel, the improvement of the fatigue lifetime and modelling of fatigue crack growth propagation. FRP materials have a great potential to reinforce fatigue-sensitive steel structures due to their unique properties, such as a very high strength-to-weight ratio and excellent resistance to corrosion and

environmental degradation. FRP reinforcements (at least wraps reinforcement) are also very flexible and they can be used to form different shapes. Finally, both FRP wraps and strips can be easy handled during construction. A comparative study of fatigue behaviour of standard reinforcing techniques (such as stop hole, welding and bolting) with FRP reinforcement is performed in Jiao *et al*. (2012).

FRP reinforcement does, however, suffer from several drawbacks generally associated with the long-term behaviour of adhesive joint between FRP and steel. In fact the adhesive layer is sensitive to high temperature, water and moisture exposure. In particular, due to the steel high thermal conductivity, the steel surface temperature produced by fire or sunlight exposure rapidly approaches the glass transition temperature of the adhesive layer. Galvanic corrosion is also a potential problem since, when the carbon fibres come in contact with the steel surface, they form a galvanic cell. Also, FRP reinforcement cannot be efficiently applied to a non-smooth surface. This is the case with riveted girders due to the high rivet density. In this case, pre-stress of the FRP strips prior to bonding provides an efficient way to improve the fatigue lifetime. Finally, for heritage structures, reversibility of the strengthening system is highly recommended and bonded FRP materials cannot be easily removed from the steel surface.

Section 10.2 discusses the use of FRP materials to improve the fatigue lifetime of riveted steel girders. The factors affecting fatigue lifetime are outlined and the principles of FRP strengthening are emphasised and documented through the results of experimental programs on cracked steel plates. In particular, the benefits of pre-stressing the FRP reinforcement prior to bonding are illustrated.

In Section 10.3, the concepts of the fracture mechanics approach to fatigue crack propagation are outlined. Factors affecting fatigue life are described together with the benefits of FRP strengthening with or without pre-stressing prior to bonding. Models (analytical and numerical) for the calculation of fracture mechanics parameters (stress intensity factor) involved in the fatigue crack growth law are described. Particular attention is dedicated to the evaluation of the crack growth rate for pre-stressed FRP strips in order to take into account the beneficial effect of FRP pre-stressing (crack closure effect).

Section 10.4 is dedicated to the fatigue strengthening of steel girders by FRP materials. Experimental evidence of the effectiveness of the proposed reinforcement technique is documented with special attention to the reinforcement of riveted steel girders. Models for the evaluation of fracture mechanics parameters for reinforced girders are also proposed and validated.

In Section 10.5 attention is directed at the fatigue strengthening of welded details of steel girders. Innovative techniques are described for the use of

FRP strips or wraps to reinforce non-load-carrying cruciform welded joints or welded connections of steel girders. In the final section, design procedures for the fatigue reinforcement of steel girders reinforced by pre-stressed or non-pre-stressed FRP strips are described.

## 10.2 Improvement of the fatigue life of steel components

Fatigue strengthening of steel elements for civil engineering applications has received research attention in the last decades (Hollaway and Cadei, 2002; Shaat *et al*., 2004; Zhao and Zhang, 2007; Teng *et al*., 2012). For a number of reasons (corrosion, fatigue cracks, increase of the traffic volume, etc.), steel structures for civil engineering applications, and in particular metallic girders of railway and highway bridges, all around the world are subjected to stresses greater than the design ones. Many of these bridges are constructed with riveted steel and they are more than 50 years old. Strengthening operations are then mandatory and FRP materials have the potential to reinforce steel railway and highway bridges.

Traditional reinforcing techniques are based on two general approaches. In the first approach stop holes, cold expansion of rivet holes or high strength bolts are used to modify the stress state around the crack or to eliminate the crack itself. In the second approach, steel plates are welded or bolted to the tension flange in order to restore the flexural capacity of the steel member. Unfortunately, the rehabilitation methods listed above are not always successful since the crack may reinitiate close to the reinforced area. Moreover, reinforcements performed by steel plates suffer from corrosion problems and they introduce additional stress concentrations due to welding or bolting.

The use of CFRP materials has several advantages, such as their light weight, good mechanical properties and durability. This results in easier handling and minimal maintenance costs. Moreover, the strengthening operations can be quickly realised, reducing the costs associated with the structure being out of service. This is particularly appealing for bridge applications since there is no need to close the bridge to traffic during rehabilitation. The higher material cost of the CFRP is then mitigated by the lower installation and maintenance costs resulting in a decrease in the global rehabilitation costs.

### 10.2.1 Experimental evidence

Several experimental programs assessing the effectiveness of fatigue reinforcement of steel elements by FRP materials are described in the literature. Many of these consider notched steel plates subjected to cycling

loading reinforced by FRP strips. In Jones and Civjan (2003), FRP strips were applied to extend the fatigue lifetime of both edge and central notched steel plate using different FRP system, bond length, bond area and one- or two-sided applications. A significant increment of the fatigue lifetime was observed, in particular when the reinforcement was applied directly to the potential crack trajectory. In Liu *et al*. (2009a), experimental tests were performed on central notch specimens reinforced by FRP strip and subjected to fatigue loading. The influence of patch thickness, patch length and patch configuration (single/double-sided repair) on fatigue performance was investigated. It was also found that high modulus CFRP strips were much more effective in crack repair and fatigue lifetime extension. In Liu *et al*. (2009b), the fatigue lifetime of CFRP-strengthened steel plate was taken into account. A fracture mechanics-based analytical model for estimating the fatigue crack growth of CFRP-repaired notched steel plates was presented and validated through experimental results.

In Wu *et al*. (2012), ultra-high modulus (UHM) CFRP strengthening was used to perform double-sided repair of central notched steel plates. Fatigue tests were performed and the experimental results compared to data from the literature. It was shown that use of UHM CFRP significantly increased the fatigue lifetime and that eventually the crack propagation was arrested if the crack was completely covered by UHM CFRP strips. Experimental results showed also that the location, width and length of the CFRP reinforcement had a considerable influence on the fatigue lifetime. Finally, the reinforcement by UHM CFRP strips exhibited fatigue performance much greater than normal modulus CFRP strips, even comparable to the CFRP pre-stressing technique.

Due to the high tensile strength of the CFRP strips, pre-stressing of CFRP double-sided reinforcement was proposed in Bassetti *et al*. (2000a) for the fatigue lifetime enhancement of central notched steel plates. With a pre-stressing level approximately equal to one-third of the tensile strength of the CFRP strips, the fatigue lifetime was increased by a factor of about 20. In Taljsten *et al*. (2009), both pre-stressed and non-pre-stressed low modulus CFRP strips were considered for strengthening steel plates with a central notch. Experimental results showed that pre-stressed strips are able to stop fatigue crack propagation. In Huawen *et al*. (2010), a parametric analysis was performed in order to investigate the effect of the applied stress range, CFRP elastic modulus and pre-stressing level on the fatigue performance of edge notched steel plate. The pre-stressing level was found to be the most important parameter, and the highest pre-stressing level extended the fatigue lifetime four times compared to the bare steel plates. Finally, in Colombi (2005), a semi-analytical model for predicting fatigue crack growth rate in central notched steel plate reinforced by both pre-stressed and non-pre-stressed CFRP strips was

proposed. The model results matched well the experimental data from Bassetti *et al*. (2000b).

### 10.2.2 Principles of crack repair by carbon fibre-reinforced polymer (CFRP) materials

The onset and growth of a fatigue crack in a steel element is a process mainly influenced by the phenomena acting around the crack tip. Denoting the crack length as $c$, around the crack tip, severe stress concentrations take place at the maximum stress $\sigma_{max}$, and a plastic zone of size $\rho$ is created when the stresses exceed the elastic limit (see Fig. 10.1). Cyclic plastic deformation produces local damage around the crack tip and, when local damage exceeds a critical level, fatigue crack propagation takes place. As the crack propagates, a zone of plastic deformations is left in the wake of the advancing crack tip. These permanent elongations are not recovered as the load is released to the minimum stress $\sigma_{min}$ where a reverse plastic zone of size $\omega$ is created and then premature contact (see Fig. 10.1) between crack lips occurs (crack closure) at a load level greater than $\sigma_{min}$. The concept of crack opening stress, $\sigma_{op}$ (i.e. the stress level at which the crack is fully opened), is then introduced to model the phenomenon. The plasticity-induced reduction of the cyclic deformations results in slower local damage to the material at the crack tip and leads then to a slower crack propagation.

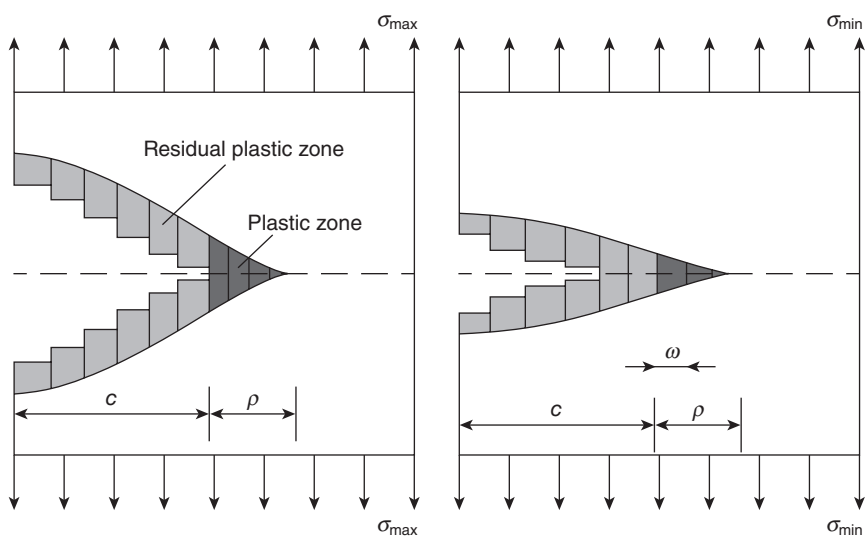


*10.1* Residual plastic zone at crack tip at minimum and maximum loading.

Fatigue crack propagation can be reduced in one of the following ways:

- *Reducing the stress range around the crack tip*; The high stiffness of the CFRP strips results in the reduction of the stress range around the crack tip.
- *Reducing the crack opening displacement*; CFRP strips bonded to the crack bridge the crack lips and reduce the crack opening displacement.
- *Promoting crack closure*;The reduction of the crack opening displacement produced by crack patching promotes crack closure.

Crack patching by pre-stressed CFRP strips produces additional benefits since the compressive stress introduced by the pre-stressing in the steel elements gives rise to an additional reduction of the crack opening displacement and emphasises the crack closure phenomenon. Pre-stressed CFRP strips then act on a cracked steel member in two different ways: a local effect is achieved by patching the crack (local reduction of the crack opening displacement and reduction of the stress level around the crack tip); and a global effect is induced by the compressive stresses applied to the whole element (additional reduction of the crack opening displacement). Note that such effect is also beneficial if the crack is not patched by the CFRP strips or if debonding of the CFRP reinforcement takes place. This is of particular relevance for riveted steel girders since, due to complex rivet geometry, it is not possible to efficiently patch the cracks emanating from the rivet holes. Pre-stressing of the CFRP strips is also effective for stopping small cracks under rivet holes which are not easily detected by conventional inspection techniques (Bassetti *et al.*, 2000a).

## 10.3 Fracture mechanics modelling

Evaluation of the fatigue lifetime is usually performed by Miner's rule, i.e. by assuming a linear damage accumulation:

$$d_i = \frac{1}{N_i} = \frac{1}{2 \cdot 10^6}\left(\frac{\Delta\sigma_i}{\Delta\sigma_c}\right)^m$$
$$D = \sum_{i=1}^{k} n_i d_i \leq 1 \qquad [10.1]$$

where $N_i$ is the number of cycles to failure for a given stress range $\Delta\sigma_i$, $\Delta\sigma_c$ is the detail fatigue class, $m$ is the slope of the relevant fatigue resistance curve and $n_i$ is the number of applied load cycles for the stress range $\Delta\sigma_i$. Experimental results (Bassetti, 2001) showed that the linear damage accumulation rule (Eq. 10.1) produces a very conservative fatigue lifetime estimation, in particular under variable amplitude loading. Alternatively, the fatigue lifetime can be evaluated by fracture mechanics concepts.

Stable fatigue crack growth is usually studied by Paris' law (Broek, 1986):

$$\frac{da}{dN} = C \cdot \left(\Delta K^m - \Delta K_{th}^m\right) \quad [10.2]$$

where $\Delta K$ is the stress intensity factor range, $C$, $m$ and $\Delta K_{th}$ (i.e. the threshold stress intensity factor range) are materials parameters. The stress intensity factor range is usually computed as:

$$\Delta K = Y \cdot \Delta\sigma\sqrt{\pi a} \quad [10.3]$$

where $Y$ is a correction factor depending on crack and element geometry and applied load, $\Delta\sigma = \sigma_{max} - \sigma_{min}$ is the stress range and $a$ is the crack length.

In order to introduce crack closure effects, the concept of effective stress intensity factor range, $\Delta K_{eff}$ and $\Delta K_{eff,th}$, must be established in Eq. (10.2) instead of $\Delta K$ and $\Delta K_{th}$, respectively:

$$\Delta K_{eff} = Y \cdot \Delta\sigma_{eff}\sqrt{\pi a} \quad [10.4]$$

where $\Delta\sigma_{eff}$ is the effective stress range:

$$\Delta\sigma_{eff} = \sigma_{max} - \sigma_{op} \quad [10.5]$$

Of course, if $\Delta K_{eff} < \Delta K_{eff,th}$ no crack propagation is observed (see Eq. 10.2). Different models are available in the literature to evaluate the 'opening stress' $\sigma_{op}$. For instance, considering the model proposed by Veers (1987):

$$\frac{\sigma_{op}}{\sigma_{max}} = \max\left[R; \frac{1}{1+\alpha}\left(1 + R \cdot \frac{\sigma_{max}}{\sigma_0}\right)\right] \quad [10.6]$$

or the well-known model proposed in (Schijve, 1988):

$$U = \frac{\Delta\sigma_{eff}}{\Delta\sigma} = \begin{cases} 1 & (R \geq 0.7) \\ 0.69 + 0.45R & (-0.5 \leq R < 0) \\ 0.465 & (R < -0.5) \end{cases} \quad [10.7]$$

where $U$ is the Elber ratio, $R = \sigma_{min} / \sigma_{max}$ is the stress ratio, $\alpha$ is the constraint factor and $\sigma_0$ is the mean value between the yield stress, $\sigma_y$, and the failure stress, $\sigma_t$, i.e. $\sigma_0 \approx \frac{1}{2}(\sigma_y + \sigma_t)$. The constraint factor $\alpha$ is function of the stress state at the crack tip and of the plastic zone size. In Broek (1986), it is proposed that $\alpha = 1.68$, while experimental results indicated that $\alpha = 1.5$ for plain stress and $\alpha = 2$ for plain strain. Equations (10.6) and (10.7) produce quite similar estimations of the effective stress range $\Delta\sigma_{eff}$ (see Fig. 10.2), but Eq. (10.6) takes explicitly into account the effect of $\sigma_{max}$ on the crack opening stress.

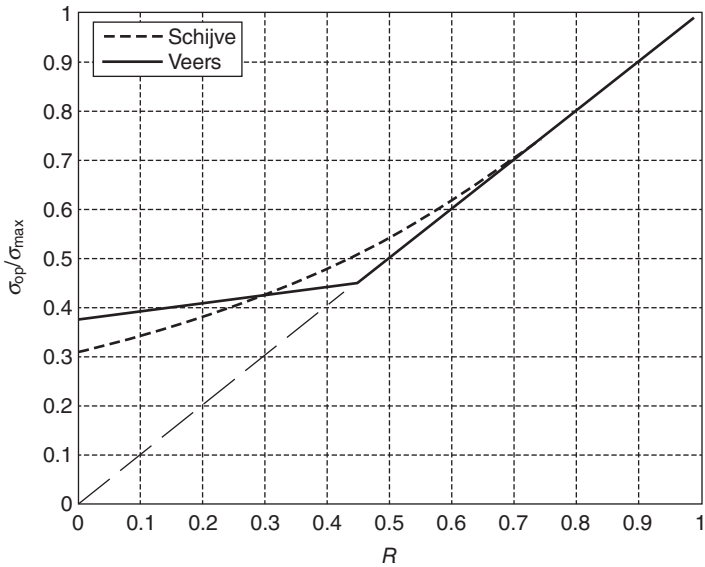


*10.2* Crack opening stress $\sigma_{op}$ as function of the stress ratio $R$ (Schijve and Veers models).

The fracture mechanics approach produces accurate estimation of the fatigue lifetime of old steel structures but requires the calibration of the fatigue crack growth material parameters ($C, m$ and $\Delta K_{th}$) and the evaluation of the stress intensity factor range.

## 10.3.1 Stress intensity factor evaluation

The application of the fracture mechanics approach to evaluate the fatigue lifetime of a structural element requires the integration of the fatigue crack propagation law (Eq. 10.2). The effective stress intensity factor range (see Eq. (10.4)) must then be evaluated in order to compute the relevant fatigue crack growth rate. To this end, in a general situation numerical methods, such as the finite element (FE) method, may be implemented (Colombi *et al.*, 2003a). In particular, the stress intensity factor $K$ of CFRP-reinforced central cracked steel plate was evaluated by the FE method. Figure 10.3 illustrates the main results with reference to both pre-stressed and non-pre-stressed patches.

Without pre-stressing, the effectiveness of the reinforcement is higher for long cracks compared to short cracks. In particular, for short cracks the reduction of the stress intensity factor is marginal and a pre-stress must be introduced in order to prevent crack propagation. In this case, the patch

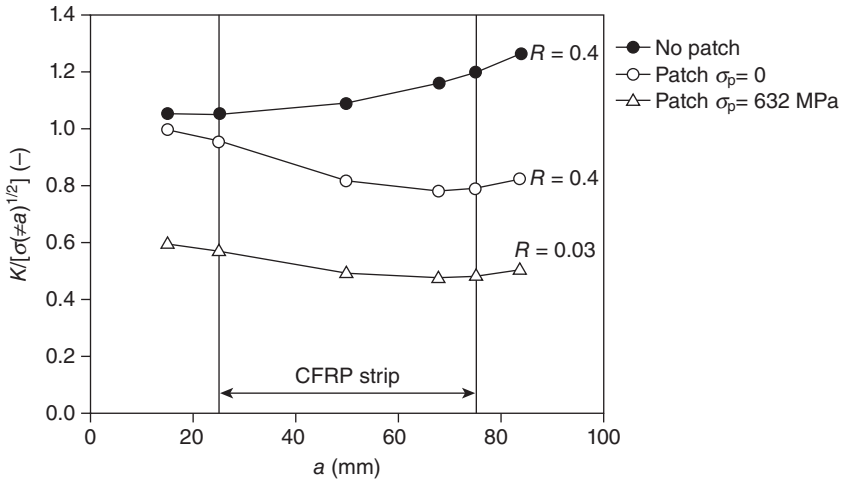


*10.3* Stress intensity factor of a centre cracked steel plate reinforced by CFRP strips (effect of pre-stressing level).

reinforcement simply reduces the stress range in the steel plate. Since the stiffness of the steel plate is much larger than that of the CFRP strips, a marginal reduction in the stress range is achieved. The effectiveness of the patch reinforcement is maximised for a long crack close to the external boundary of the strip. In this case, the patch covers a large amount of the crack and its plastic zone and then an additional significant reduction of the correction factor $Y(a)$ is achieved. Pre-stressing of the CFRP strips does not produce a reduction in the stress intensity factor range but a reduction in the stress ratio $R$ that promotes crack closure (see Fig. 10.2). As an example, the application of a pre-stress $\sigma_p = 632$ MPa reduces the stress ratio to 0.03. Finally, the effect of CFRP patch stiffness, adhesive thickness and pre-stressing level is also illustrated.

Few attempts to evaluate the stress intensity factor of CFRP reinforced centre-cracked tension (CCT) steel plates have been described in the literature. In Wu *et al*. (2013a), formulas for stress intensity factor evaluation were presented in order to take into account, by use of the appropriate correction factors, both the effect of CFRP strips in reducing the far field stress range and the effect of CFRP bond width. Reference is made in Wu *et al*. to a CFRP reinforcement symmetrically covering the crack, and the relevant correction factors were derived and validated from experimental results. In Wu *et al*. (2013b), the effect of bond location on the stress intensity factor of CFRP-reinforced CCT steel plates was investigated. As mentioned earlier, in some cases (riveted connections), the CFRP strip has to be bonded away from the crack and then the reinforcement

location plays a fundamental rule in the evaluation of the effectiveness of the strengthening scheme. In this case, reference is made to a CFRP reinforcement partially covering the crack. In addition to the effects listed above (far field stress reduction and CFRP strips width), a new correction factor taking into account the bond location is introduced and calibrated through FE analyses.

Alternatively, in Liu *et al*. (2009c), the boundary element method (BEM) was used to calculate the stress intensity factor of CCT steel plates reinforced by CFRP strips. The result was validated by experimental results and parametric analysis was performed in order to investigate the effect of CFRP patch and adhesive mechanical properties, bond length and width, reinforcement configuration and CFRP layer number. In Taljsten *et al*. (2009), a technique is proposed to evaluate the stress intensity factor of CCT steel plates reinforced by CFRP strips. The technique refers to a method developed for the design of steel sheets with stringers bolted or riveted as reinforcement (see Broek, 1986). Superposition of stress intensity factor due to far field stress and to the force in the CFRP laminates is performed. No experimental or numerical verification of the stress intensity evaluation was performed.

### 10.3.2 Effect of reinforcement debonding

As long as the fatigue crack approaches the interior border of the reinforcement strips, debonding takes place at the steel–adhesive interface due to the high stress concentration at the crack tip. Debonding between CFRP strips and the steel plate at the crack tip was investigated by Bassetti (2001) using the Optical Speckle Interferometry technique (see Fig. 10.4) with reference to CFRP-reinforced CCT steel plates. The selected reinforcement configuration represents the strengthening of a crack emanating from a rivet hole.

Optical techniques allow the observation of the whole displacement field on the specimen surface. By observing the interference fringes, it is possible to detect the relative displacement between steel and CFRP at the borders of the debonding zones (fringe discontinuities at the CFRP strip edges). As the crack in the steel plate propagates under the CFRP strips, relative displacements are present between the steel plate and the adhesive layer as shown in Fig. 10.4. Moreover, the deformation level in the CFRP patch is increased. The shape and dimension of the debonding zone were investigated by comparing the displacement field obtained by FE calculations with the experimental ones (in Fig. 10.4 each fringe represents a displacement of 1.3 $\mu$m in the longitudinal direction of the specimen). FE calculation showed that the debonding zone between CFRP and steel is well approximated by an ellipse with a diameter ratio *c/b* equal to 1:5. The

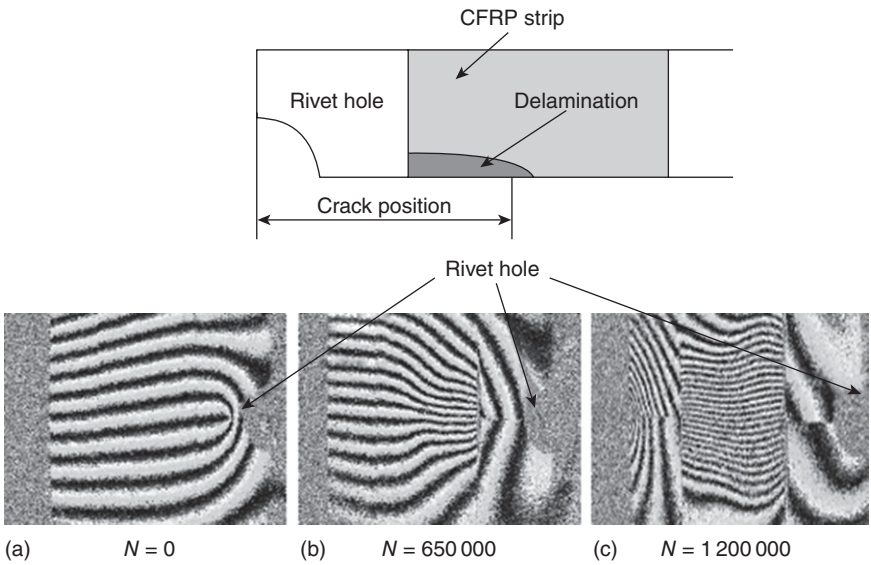


*10.4* Debonding field on specimen surface by optical speckle interferometry at different loading cycles.

delamination front was supposed (Bassetti, 2001) to be ahead of the crack tip at a distance equal to the plastic zone (see Fig. 10.4).

In Colombi *et al*. (2003b), a numerical FE model was implemented for the CFRP-reinforced CCT steel plate investigated in Bassetti (2001). Debonding was modelled as a crack located at the interface between the steel and the adhesive. The numerical model is based on the modified virtual crack closure technique (MVCCT) to evaluate the debonded crack energy release rate $G$ which is a measure of the interface driving force and hence characterises the crack tip-induced debonding. Numerical results indicated that the contribution of the debonded crack to the global strain energy release rate is marginal. As an example, the $G$ distribution along the arch length showed a maximum value of 0.4 N/mm while the corresponding strain energy release rate $G$ of the crack in the steel plate was equal to 8.9 N/mm. Parametric analysis was also performed, indicating that the $G$-values are sensitive to the adhesive thickness and the pre-stressing level. Figure 10.5 clearly shows that a thinner adhesive layer increases the debonded crack energy release rate and a larger debonded region is then expected.

The effect of the debonding shape was also investigated in Colombi *et al*. (2003b). Different aspect ratio $c/b$ values of the elliptical debonded region were considered as reported in Fig. 10.6.

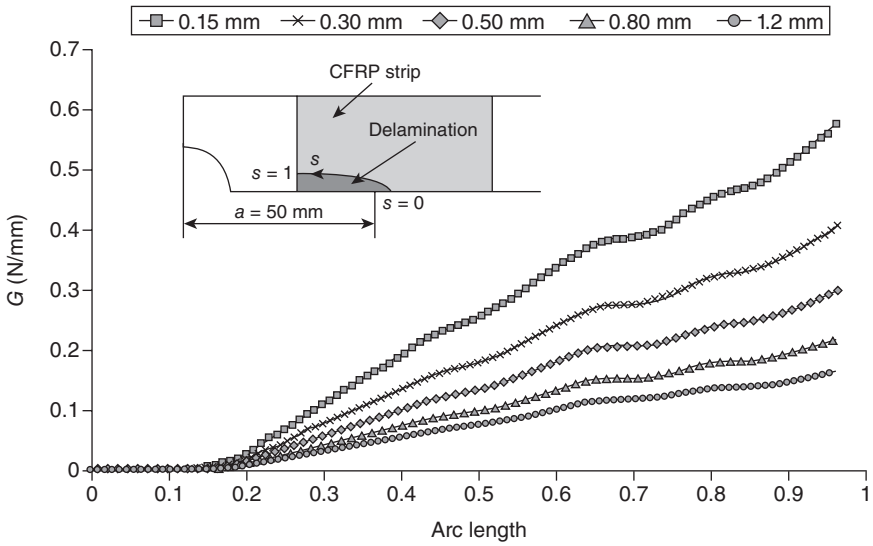


*10.5* Effect of adhesive thickness on the strain energy release rate for an elliptical adhesive crack.

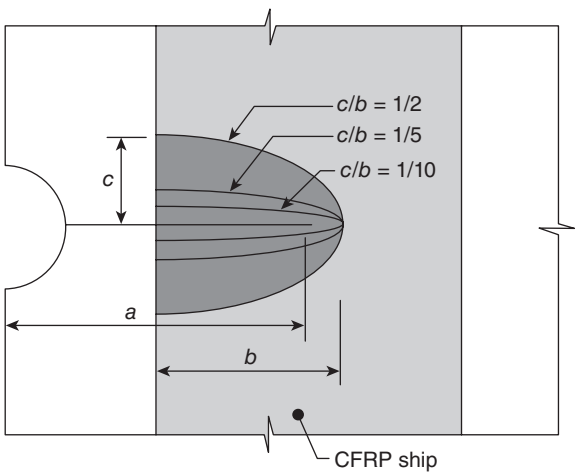


*10.6* Different elliptical adhesive cracks used in the FE analysis.

By increasing the debonded area, the *G*-value is significantly decreased (see Fig. 10.7), and this means that the debonded area is expected to be limited to a region close to the steel plate crack.

As clearly stated in Teng *et al.* (2012), debonding of the CFRP in the steel plate crack region has a significant effect on stress intensity factor evaluation

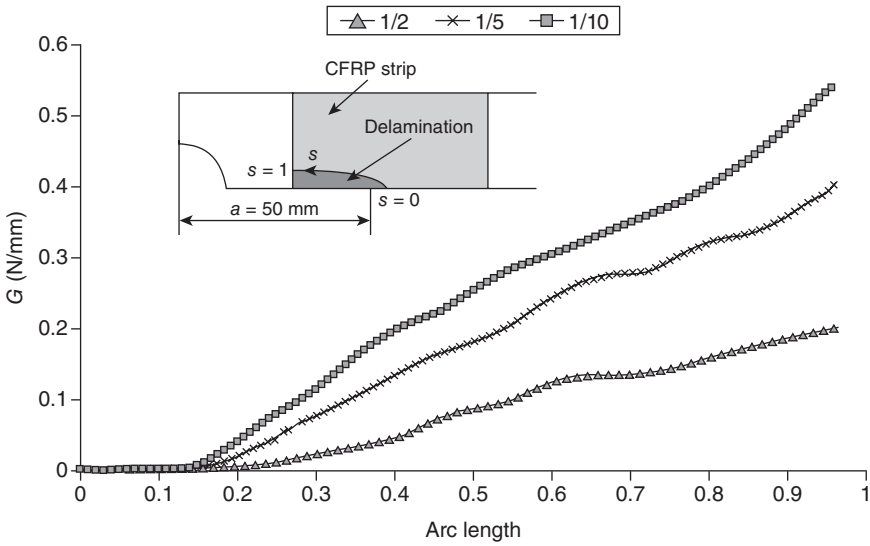


*10.7* Effect of different elliptical debonding on the strain energy release rate of the adhesive crack.

and then on fatigue crack growth rate. In Colombi *et al*. (2003a), the effect of the debonded region at the crack tip was quantified by FE analysis. Results indicate (Fig. 10.8) that the effect is more important for long cracks for which the crack bridging effect is reduced by the increment of the debonded area. In contrast, the size of the debonded region has no effect on short cracks since, in this case, the debonded region does not influence the stress field at the crack tip.

Recently, additional studies were performed in order to investigate the effect of debonding at the crack tip region on the fatigue reinforcement. In Huawen *et al*. (2010), a debonded area was detected at the end of the experimental tests, and it was shown that the area of the debonded region decreases as the pre-stressing level is increased. In Aggelopoulos *et al*. (2011), debonding of adhesively bonded CFRP patch repairs of cracked steel members was investigated from the numerical point of view. Debonding was modelled as a crack located at the interface between the steel and the adhesive in order to determine by FE analysis the strain energy release rate $G$. Two-dimensional plane strain FE analyses were performed so it was not possible to investigate the effect of debonding shape on the stress intensity factor of the steel crack and on the energy release rate $G$ at the debonded interface. Results showed that the effect on the stress intensity factor of the steel crack is more pronounced for deeply cracked members while for interface crack the $G$-values decrease with increasing debonding lengths.

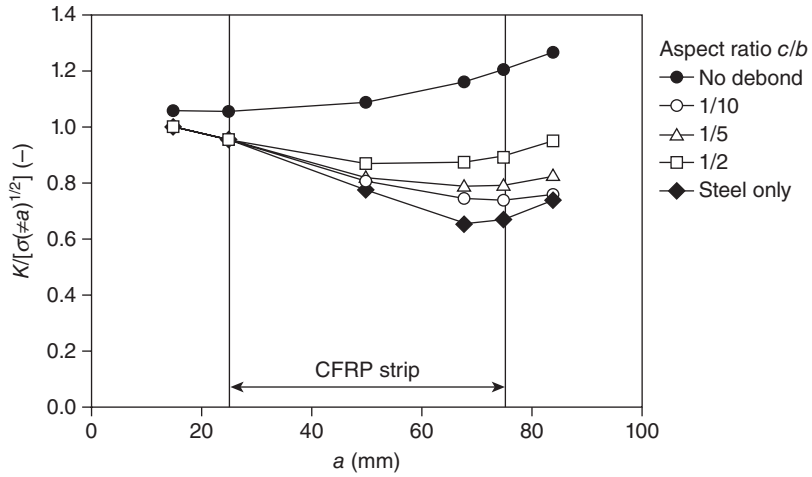


*10.8* Effect of different elliptical debonding on stress intensity factor of the steel crack.

Finally, in Wu *et al*. (2012), elliptical debonding was considered in order to explain the different observed failure modes.

### 10.3.3 Semi-analytical model for stress intensity factor evaluation

Consider a cracked plate reinforced with a CFRP patch (see Fig. 10.9). The stress intensity factor is reduced by crack patching in two different ways:

- by reducing the stress level at crack tip;
- by reducing the crack opening displacement.

While the patch stiffness reduces the stress level at the crack tip, the reinforcement stiffness reduces the crack opening displacement and then the stress intensity factor. The first is modelled by introducing a reinforcing parameter, $\rho$ ($\rho < 1$), given as the ratio between the elastic stiffness of the unreinforced specimen and that the reinforced one. The external load experienced by the steel plate is then given by $\rho \cdot \sigma$, where $\sigma$ is the applied stress. In order to model the second effect, note that the intact CFRP layers bridge the cracked metal and the stresses in the reinforced plate are called bridging stress, $\sigma_{br}$ (Fig. 10.9). The bridging stress must then be determined in order to compute the stress intensity factor and elastic compliance. The bridging stress is, in general, non-uniform (Bassetti, 2001) since it depends on many factors such as the delamination shape and size and the shear deformation of the adhesive.

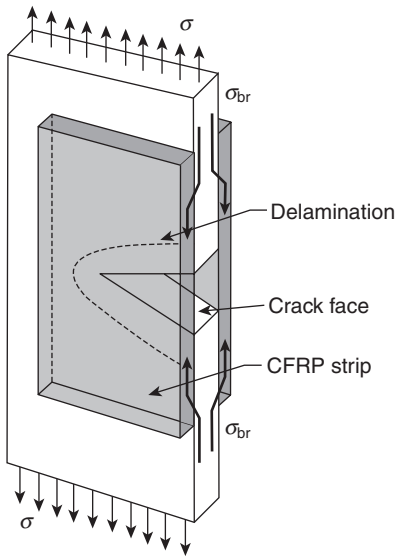


*10.9* Debonded steel crack patched by CFRP strips.

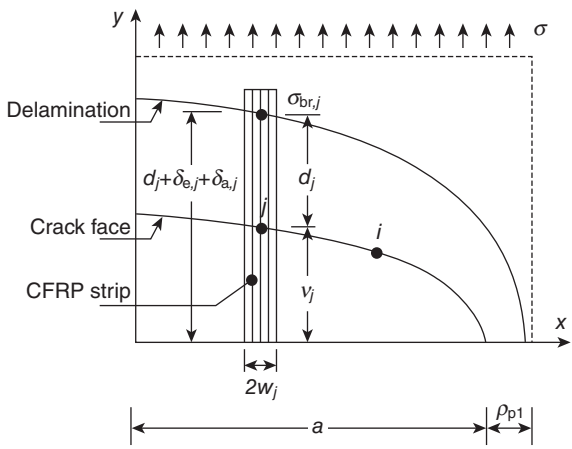


*10.10* Bridging stress and crack opening displacement of a steel crack patched by CFRP strips.

*Bridging stress evaluation*

The bridging stress must be computed for a given boundary condition, crack length and geometry. It is assumed that delamination occurs (Bassetti, 2001) at the interface between the metal and the CFRP–adhesive layers (Fig. 10.9). Referring to Fig. 10.10, the bridged area is divided into $N$ bar

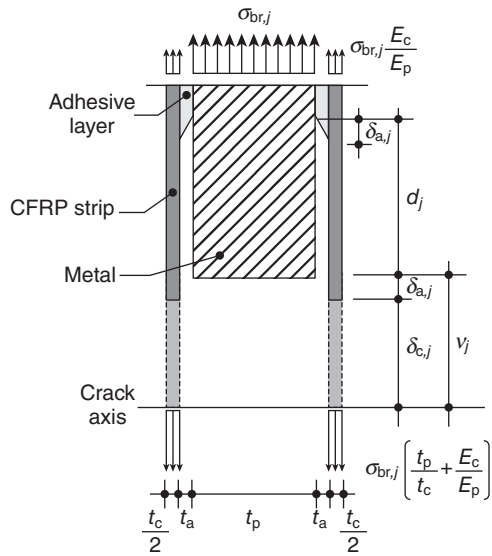


*10.11* Displacement and stress distribution in the strengthened section.

elements and the element width at a distance of $x_j$, is $2w_j$. Bridging stress acting on the boundary of the delaminated area arrests the crack (Fig. 10.9). In the following, subscripts c, a and p refer to the composite strips, the adhesive layer and the steel plate, respectively. The extension of the intact bridging fibers, $\delta_{c,j}$, plus the shear deformation, $\delta_{a,j}$, of the adhesive in the boundary of the delaminated area, should be equal to the crack opening displacement, $v_j$, produced by both the applied stress, $\sigma$, and the bridging stress, $\sigma_{br,j}$. At any point $x_j$ of the crack face, one then has (Bassetti, 2001):

$$v_j = \delta_{c,j} + \delta_{a,j} \qquad [10.8]$$

The extension of the bridging fibres at any point of the crack face (see Fig. 10.11) is equal to the product of the fibre length and the relevant strain, i.e. the delamination size, $d_j$, and the strain of the fibre $\varepsilon_{br,j}$:

$$\delta_{p,j} = \varepsilon_{br,j} \cdot d_j = \frac{\sigma_{br,j}\left(t_p + t_c \dfrac{E_c}{E_p}\right)}{E_c t_c} d_j \qquad [10.9]$$

where $t_c$ is the total thickness of the CFRP strips, $t_p$ is the steel plate thickness, $E_c$ is the Young's modulus of the bridging strips in the fibres direction and $E_p$ is the Young's modulus of the steel.

The shear deformation of the adhesive decreases the bridging efficiency of the fibres. An estimation of the shear deformation of the adhesive can be calculated from the interlaminar shear stress of a modified double cracked lap shear specimen (Bassetti, 2001). As a result, for the shear deformation $\gamma_j$ at a given point of the crack face one has:

$$\gamma_{a,j} = \frac{\sigma_{br,j}}{E_{la}} \sqrt{\frac{f_{la} f_p}{n_b f_c G_a t_a}} \qquad [10.10]$$

and then, for an adhesive thickness equal to $t_a$, the adhesive shear displacement is equal to:

$$\delta_{a,j} = \gamma_{a,j} \cdot t_a = \frac{\sigma_{br,j}}{E_{la}} \sqrt{\frac{f_{la} f_p}{n_b f_c f_a}} \qquad [10.11]$$

where $n_b$ is the number of bonded interfaces in the specimen and $E_{la} = f_{la} / (t_a + t_c)$, where subscript la refers to the laminate.

In Eqs (10.10) and (10.11) four stiffness parameters are defined:

$$\begin{aligned} &f_p = E_p t_p; \quad f_c = E_c t_c; \\ &f_{la} = f_p + f_c; \quad f_a = G_a / t_a \end{aligned} \qquad [10.12]$$

where $G_a$ is the shear modulus of the adhesive.

The evaluation of the crack opening displacement at any point $x_j$ of the crack face is performed as:

$$v_j = v_{\sigma,j} - v_{\sigma br,j} \qquad [10.13]$$

where $v_{\sigma,j}$ and $v_{\sigma br,j}$ are the crack opening displacement due to, respectively, the applied stress and the bridging stress. The crack opening displacement due to applied and bridging stress is computed as (Broek, 1986):

$$\begin{aligned} v_{\sigma,j} &= \sigma f(x_j) \\ v_{\sigma br,j} &= \sum_{i=1}^{N} v_{br,i}\, g(x_j, x_i)\, k(x_i) \end{aligned} \qquad [10.14]$$

where $f(x_j)$ is the crack surface displacement due to unit applied stress and $g(x_j,x_i)$ is the displacement at element $j$ due to unit stress acting on element $i$. In Eq. (10.14), $k(x_i)$ is a corrector factor taking into account the fact that the bridging stress does not act on the crack face, but on the delamination boundary (see Fig. 10.9). Numerical results showed that the effect of the correction factor $k$ can be neglected.

Making use of Eqs. (10.9), (10.11) and (10.14) the compatibility conditions, Eq. (10.8) are given by:

$$\sigma f(x_j) - \sum_i^N \sigma_{\mathrm{br},i} g(x_j, x_i) = \sigma_{\mathrm{br},j} \cdot (p d_j + q) \qquad [10.15]$$

where:

$$p = \frac{t_\mathrm{p} + t_\mathrm{c} \dfrac{E_\mathrm{c}}{E_\mathrm{p}}}{E_\mathrm{c} t_\mathrm{c}}; \quad q = \frac{1}{E_\mathrm{la}} \sqrt{\frac{f_\mathrm{la} f_\mathrm{p}}{n_\mathrm{b} f_\mathrm{c} f_\mathrm{a}}} \qquad [10.16]$$

and $d_j$ is the delamination size. The stress intensity factor in the cracked plate is eventually computed as (Colombi, 2004):

$$K = K_\sigma + \sum_j^N K_{\sigma,\mathrm{br},j} \qquad [10.17]$$

where $K_\sigma$ is the contribution due to the applied stress, $\sigma$, while $K_{\sigma\mathrm{br},j}$ is the contribution due to the bridging stress. Finally, the crack opening displacement of the cracked geometry is computed according to Eq. (10.13).

*Weight function*

The evaluation of the bridging stress distribution depends on the knowledge of the crack surface displacement $v_{\sigma,j}$ and $v_{\sigma\mathrm{br},j}$, i.e. from the knowledge of the influence functions $f(x_j)$ and $g(x_j,x_i)$. In a general situation, this problem can be solved by the weight function concept (Broek, 1986). If the stress intensity factor $K^{(1)}$ and the surface displacement $v^{(1)}(x,a)$ for a given load system (1) are known, the stress intensity factor $K^{(2)}$ for any other load system (2) acting on the same body can be calculated by:

$$K^{(2)} = \int_0^a \sigma^{(2)}(x) \cdot m(a, x)\,\mathrm{d}x \qquad [10.18]$$

where $m(a,x)$ is the weight function, $a$ is the crack length and $\sigma^{(2)}(x)$ is the crack surface stress distribution due to load system (2). For mode I problems, once the weight function $m(a,x)$ and the stress intensity factor $K_\sigma(a)$ due to applied stress are computed, the corresponding crack surface displacement $v_\sigma(x,a)$ can be obtained as:

$$v_\sigma(x, a) = \frac{1}{E} \int_x^a K_\sigma(a) m(a, x)\,\mathrm{d}a \qquad [10.19]$$

The stress intensity factor for the bridging stress, $\sigma_{\mathrm{br},j}$, i.e. a uniform stress acting on a segment $2w_j$ of the crack front with a centre at $x_j$ (see Fig. 10.10), can be computed as:

$$K_{\sigma \mathrm{br},j}(a, x_j) = \int_{x_j - w_j}^{x_j + w_j} \sigma_{\mathrm{br},j}(x) \cdot m(a, x)\,\mathrm{d}x \qquad [10.20]$$

The corresponding crack surface displacement can also be solved as:

$$v_{\sigma \mathrm{br},j}(a, x_j, x) = \frac{1}{E} \int_{a_1}^{a} K_{\sigma \mathrm{br},j}(a, x_j) m(a, x)\,\mathrm{d}a \qquad [10.21]$$

where $a_1 = \max(x, x_j)$. Therefore, the influence function $f(x_j)$ and $g(x_j, x_i)$ in Eq. (10.14) are computed as:

$$f(x_i) = \frac{v_\sigma}{\sigma}$$
$$g(x_j, x_i) = \frac{v_{\sigma \mathrm{br},j}(a, x_j, x_i)}{\sigma_{\mathrm{br},j}} \qquad [10.22]$$

## 10.4 Fibre-reinforced polymer (FRP) strengthening of steel girders

Few fatigue tests on full-scale steel girders reinforced by CFRP strips have been performed in the literature. Full-scale fatigue tests were performed in Bassetti (2001) and Bassetti *et al.*, (2000b) on three riveted cross girders taken from a dismantled 91-year-old bridge. The main dimensions of the riveted composite girders used in the fatigue tests are reported in Fig. 10.12. The basic material of the I-shape girders was mild steel.

The first cross girder was pre-cracked under constant amplitude loading with a stress range in the net steel section of 80 MPa and a stress ratio $R$ = 0.1. A total of four cracks were detected at the end of the test (3.5 millions of cycles) by standard non-destructive testing (NDT) techniques (magnetic particle examination). Crack length was measured between 4 and 10 mm

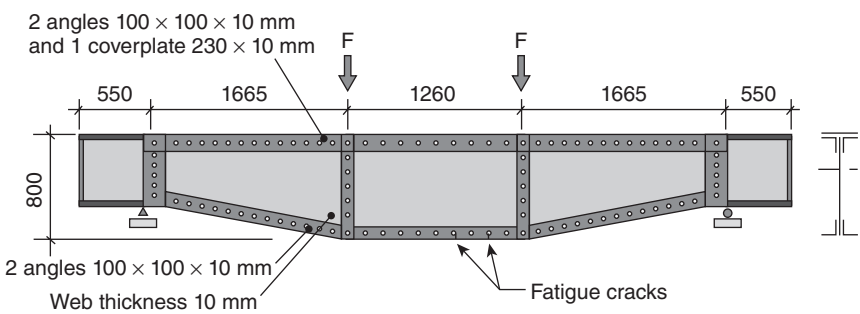


*10.12* Main dimensions of the riveted composite girders.

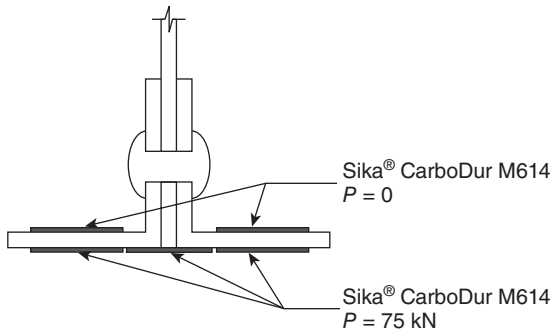


*10.13* Reinforcement configuration of the bottom tension flange.

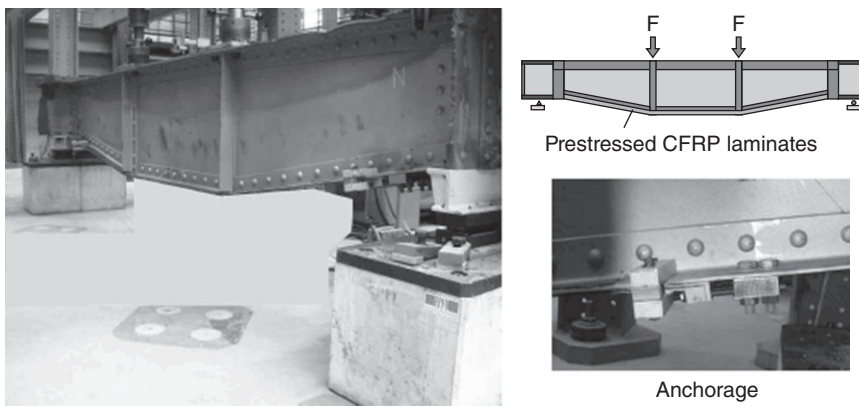


*10.14* Detail of the composite steel girder and the anchorage system.

from the rivet heads (the rivet head diameter was approximately 40 mm). The bottom flange of the cross girder was reinforced by bonding a total of five CFRP strips as in Fig. 10.13. In particular, two plates were positioned on the upper face of the bottom flange and they were not pre-stressed. The main function of these CFRP strips was to stop the crack propagation toward the bottom flange and to reduce the stress range in the cracked section. Three additional CFRP strips were positioned on the bottom face and pre-stressed with a force of 75 kN each. The pre-stressed CFRP strips produced a compressive stress in the bottom flange equal to –36 MPa.

The tested girder together with the the anchorage system of the pre-stressed CFRP strips is illustrated in Fig. 10.14. Additional details of the anchorage system are available in Bassetti (2001).

After strengthening, the fatigue test on the cross girder was continued by applying the same loading cycle used for the pre-cracking. The bonded CFRP strips produced a marginal reduction in the stress range in the

bottom flange (76 MPa compared to 80 MPa for the unreinforced steel section) while pre-stressing reduced significantly the stress ratio in the cracked section ($R = -0.5$ compared to $R = 0.1$ for the unreinforced steel section). This promoted crack closure, and the fatigue test was continued up to 20 million cycles without any additional crack growth. The pre-stressed CFRP reinforcement was then capable of stopping crack propagation in the steel girder. The other two composite steel girders were tested in the same way but, at the end of the pre-cracking phase, longer fatigue cracks were detected (between 72 and 200 mm). The same reinforcement configuration as for the first girder was used and the fatigue test was continued up to 10.4 million cycles and 2.4 million cycles without any additional crack growth. It can be concluded that fatigue tests showed that pre-stressed CFRP reinforcement is capable of stopping fatigue crack propagation of small cracks emanating from rivet holes of composite steel girders.

Other fatigue tests have been performed in the literature with reference to cracked steel beams. Fatigue tests were performed by Kim and Harries (2011) on steel beams initially damaged at the mid-span and reinforced by CFRP strips. The beams were loaded in a three point bending set-up and the interaction of the initial damage and the CFRP reinforcement was investigated. A model was proposed based on the strain-life method and cumulative damage theory to predict fatigue response of the repaired beams. The behaviour of steel beams strengthened by bonded CFRP strips under fatigue loading was also investigated by Tavakkolizadeh and Saadatmanesh (2003). They showed that the application of CFRP strips can increase the fatigue lifetime of a steel beam more than three-fold and also decreases the crack growth rate significantly. Pre-stressed bonded and unbonded CFRP reinforcement systems were investigated to improve the fatigue lifetime of steel beams by Ghafoori *et al*. (2012a). Unbonded systems represent an option when traditional bonded systems cannot be used due to the irregularities of the steel surface or when the adhesive performance is a concern due to high temperature, moisture, water, etc. A theoretical model was also proposed to estimate the required pre-stressing level to stop fatigue crack propagation. Finally, steel–concrete composite beams were investigated in Dawood *et al*. (2007). The feasibility of the strengthening techniques was investigated experimentally with reference to large-scale steel–concrete composite beams strengthened using pre-stressed CFRP strips. All the strengthened beams sustained three million cycles without exhibiting any indication of failure.

## 10.5 Strengthening of welded details

Strengthening of welded details of steel beams by CFRP patches has been recently investigated in the literature. Nakamura *et al*. (2009) presented

repair methods of fatigue cracks at welded web gusset joints using CFRP strips. Specimens were fabricated with gusset plates welded to both sides at the centre of the steel plate. When the crack in the specimens progressed to a length of approximately 12 % of the overall width, it was repaired using two systems. In the first, four single-layered CFRP strips bonded to both sides of the weld bead were used while, in the second, additional multilayered CFRP strips with a rectangular slit in the centre were bonded close to the weld bead. The number of laminations was one, three or five layers. Four-point bending tests were performed: the minimum stress was approximately 20 MPa and the stress range varied from 64 to 114 MPa. Fatigue life was found to be improved and the repair methods greatly contributed to the increase in joint strength and to the reduction in the opening displacement at the joint. Moreover, it was observed that multilayered CFRP strips were effective in preventing debonding and sharing axial force. Finally, it was confirmed that, as the number of laminations of CFRP strips increases, the post-repair fatigue life improved considerably.

Alemdar *et al*. (2012) and Kaan *et al*. (2012) presented experimental tests to evaluate the performance of different methods to prevent and repair fatigue damage in welded connections of steel bridge girders. The fatigue performance of cover plate specimens in which the welded connections were reinforced with CFRP strips was analysed. Different overlays were used in the testing program. Three-point bending tests under fatigue loading were performed to evaluate the effect of CFRP overlays on fatigue crack initiation and propagation. Test results showed that, when bond between the CFRP overlays and the steel was maintained, the application of CFRP strips increased the stiffness and reduced the stress demand at fatigue-vulnerable welds, improving the fatigue performance of the connections and inhibiting crack initiation. In fact, the reduction in stress demand was sufficient to extend the fatigue life of the welded connections to the infinite fatigue life range. Finite element simulations were developed to analyse the effects of bond layer thickness and length on the effectiveness of the CFRP reinforcement. Based on the stress fields, it was noticed that the reinforcement strips were successful in reducing the high stress demand occurring at the weld toe of the unreinforced specimen and in distributing those stresses over a much greater area. Finally, a parametric study was performed to determine the optimum CFRP overlay configuration.

Chen *et al*. (2012) reported an experimental study on the use of CFRP sheets to strengthen non-load-carrying cruciform welded joints subjected to fatigue loading. Failure modes and corresponding fatigue lives were recorded during tests. Then, a series of numerical analyses were performed to study the effects of material properties and geometric parameters such as the weld toe radius and the number of CFRP layers on local stress concentration at a weld toe. Fatigue life of welded connections can be

enhanced because of the reduction in stress concentration produced by CFRP strengthening. Parametric study indicates that the weld toe radius and the amount of CFRP are extremely important in influencing the stress concentration factors and stress ranges of the joint, while high elastic modulus of the strengthening materials is effective in reducing the stress concentration.

## 10.6 Design of FRP reinforcement

In the following, a design proposal for the fatigue reinforcement of steel girders is formulated. CFRP strips are intended to be adhesively bonded to the tension flange of the steel girders. In this case, as previously stated, the CFRP strips act in two different ways:

- by reducing the stress level at crack tip (global effect);
- by reducing the crack opening displacement (local effect).

On the one hand, the global effect is emphasised by the pre-stressing of the CFRP strips since a compressive stress is introduced into the steel section leading eventually to a reduction in the stress ratio, $R$, at the crack tip (the stress range is unchanged). Crack closure effects are augmented as $R$ is significantly reduced by the additional compressive stress (see Fig. 10.2). In this case, beneficial effects of CFRP reinforcement are also recognisable if the crack is not covered by the CFRP strips. On the other hand, the local effect is present only if the crack propagates under the CFRP strips, i.e. the crack is covered by the reinforcement. Generally, this condition is difficult to obtain due to the presence of irregularities on the steel surface, in particular for riveted composite steel girders. In this case, the crack emanating from a rivet hole can be at most only partially covered by the CFRP patches.

For reinforcement design, the stress intensity factor of the strengthened steel girders must first be evaluated. In order to take into account both the global and local effects, the semi-analytical model illustrated in Section 10.3.3 is proposed. If the local effect is negligible (the crack is not or is partially covered by the reinforcement), the evaluation of the stress intensity factor can be significantly simplified. First, the effect of the CFRP strip stiffness is considered introducing the reinforcement parameter $\rho$:

$$\rho = \frac{I_s \cdot z_{rein}}{I_{rein} \cdot z_s} \qquad [10.23]$$

where $I_s$ is the moment of inertia of the bare steel section, $z_{rein}$ denotes the position of the centroid of the strengthened steel section, $I_{rein}$ is the moment of inertia of the reinforced steel section and $z_s$ is the position of the centroid of the bare steel section. As long as $\rho$ is known, the stress intensity factor

range is evaluated by inserting $\rho \cdot \Delta\sigma$ in Eq. (10.3). Clearly, the definition of the stress intensity factor range requires knowledge of the correction factor, $Y$. Eventually, the pre-stressing of the CFRP strips does not reduce the stress range (it is modelled as an external stress) but produces a decrement of the stress ratio, $R$, thus promoting crack closure.

This is, in general, a difficult task for a steel girder, but a simplified method was suggested by Bassetti (2001) and Nussbaumer *et al*. (2004). In this way, the correction factor $Y$ is computed (see Fig. 10.15) by replacing the structural element by a cracked plate of appropriate dimensions. The equivalent cracked steel plate produces the same fracture mechanics parameters as in the real structural element and the relevant correction factor, $Y$, is generally available from the literature (Broek, 1986). As long as the correction factor, $Y$, is evaluated, the required compressive stress in the steel section to stop crack propagation is evaluated as in Bassetti (2001) and Nussbaumer *et al*. (2004).

The principles of the method, which accounts only for the global effect, are summarised in Fig. 10.16, where subscripts s and f refer to the steel section and the composite strip, respectively while subscripts sp and fp indicate the pre-stress level in the steel and composite, respectively.

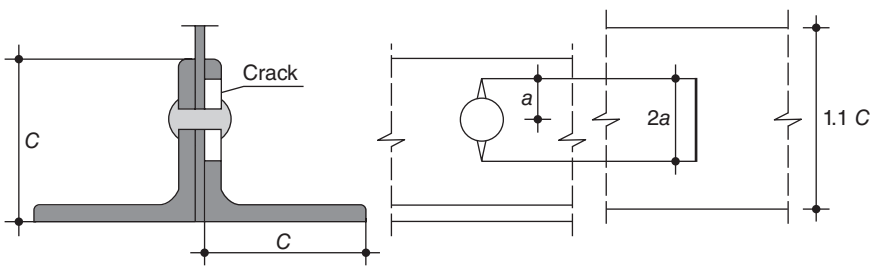


*10.15* Evaluation of the correction factor *Y*.

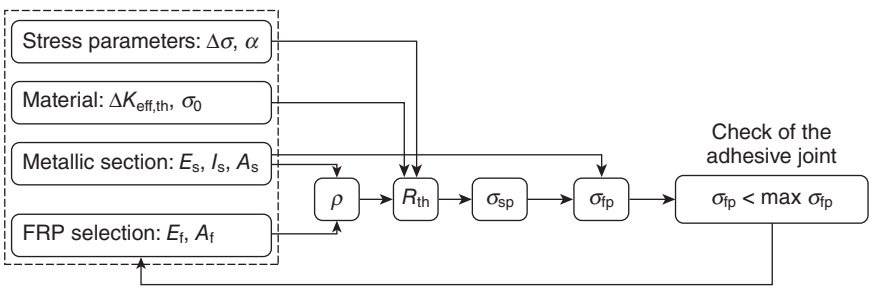


*10.16* Design procedure for the pre-stressed CFRP reinforcement.

At first, the stress parameters $\Delta\sigma$ (the stress range in the bare steel section) and $\rho$ are evaluated (see Eq. 10.23). As the material parameters $\Delta K_{\text{eff,th}}$ (see Eqs. (10.2) and (10.4)) and $\sigma_0$ (see Eq. (10.6)) together with the plastic constraint factor $\alpha$ (see Eq. 10.6) are known, the condition for crack stop is:

$$\Delta K_{\text{eff}} < \Delta K_{\text{eff,th}} \qquad [10.24]$$

This means that the crack does not propagate if the effective stress intensity factor range is lower than the effective threshold stress intensity factor range. Taking into account of Eq. (10.3), one has:

$$U \cdot Y \cdot \left(\rho \cdot \Delta\sigma\sqrt{\pi a}\right) < \Delta K_{\text{eff,th}} \qquad [10.25]$$

where $U$ is the Elber ratio, depending on the opening stress $\sigma_{\text{op}}$:

$$U = \frac{\sigma_{\max} - \sigma_{\text{op}}}{\sigma_{\max} - \sigma_{\min}} \qquad [10.26]$$

Inserting Eq. (10.6) into Eq. (10.26), gives for $R < 0.4$ (see also Fig. 10.2):

$$U = \frac{1}{1-R}\left[1 - \frac{1}{1+\alpha}\left(1 + \frac{R \cdot \Delta\sigma}{(1-R)\sigma_0}\right)\right] \qquad [10.27]$$

Note again that the application of a pre-stress to the CFRP strips prior to bonding does not produce any reduction in the applied stress range $\Delta\sigma$ while a decrement of the stress ratio $R$ is obtained. Inserting then Eq. (10.27) into Eq. (10.25), gives a relationship between the stress range $\Delta\sigma$ and the stress ratio $R_{\text{th}}$ to achieve crack stop:

$$\Delta\sigma = \frac{(1-R_{\text{th}}) \cdot \sigma_0 \cdot \alpha}{2 \cdot R_{\text{th}}}\left(1 - \sqrt{1 - \frac{4 \cdot R_{\text{th}} \cdot \Delta K_{\text{eff,th}} \cdot (1+\alpha)}{\alpha^2 \cdot \sigma_0 \cdot \rho \cdot \sqrt{\pi \cdot a}}}\right) \qquad [10.28]$$

Finally, solving Eq. (10.28) for a given stress range gives the threshold stress ratio $R_{\text{th}}$ for crack stop. Since the compressive stress is added to the effect of the external loading, $R_{\text{th}}$ is given by:

$$R_{\text{th}} = \frac{\rho \cdot \sigma_{\min} - \sigma_{\text{sp}}}{\rho \cdot \sigma_{\max} - \sigma_{\text{sp}}} \qquad [10.29]$$

The required compressive stress level in the steel section $\sigma_{sp}$ to stop crack propagation is then equal to:

$$\sigma_{\text{sp}} = \frac{\rho}{1-R_{\text{th}}}(\sigma_{\min} - R_{\text{th}}\sigma_{\max}) \qquad [10.30]$$

Eventually, the required pre-stressing level in the CFRP strips can be evaluated using classical strength of materials relationships.

In Ghafoori *et al*. (2012b), a procedure was proposed to determine the required pre-stressing level in the reinforcement strips to stop fatigue crack growth. However, the model does not take into account retardation effects and then the required pre-stressing level is over-estimated. Finally, Wang and Nussbaumer (2009) presented a fracture model for fatigue crack propagation of a repaired cracked steel member. According to strength of material relationships and fracture mechanics concepts, a stress reduction coefficient was first suggested. Finally, a new expression of the fatigue crack propagation rate for a repaired cracked steel member was proposed.

## 10.7 Conclusion and future trends

In this chapter, the fatigue performance of steel girders reinforced by CFRP materials was discussed. The benefits and the drawbacks of the fatigue reinforcement of steel girders using CFRP strips were first outlined. The fracture mechanics modelling of fatigue crack propagation was described and a simplified model was described for stress intensity factor evaluation of reinforced steel plates. The effect of reinforcement debonding at the crack tip was also considered and discussed. Finally, a design procedure was proposed to evaluate the required pre-stressing level of the CFRP strips for stopping fatigue crack growth in the steel section. Future research needs can be summarised as follows:

- Methods for an efficient estimation of the stress intensity factor of reinforced steel girders should be provided in order to include in the design procedure the local effect due to crack bridging.
- The effect of the CFRP reinforcement on fatigue crack growth retardation should be estimated. When the CFRP strips are bonded on the steel crack, an additional reduction of the crack opening displacement is observed. Such an effect can be quantified, for example, by the method proposed in Colombi (2005).
- Research is needed to better understand the interaction of crack tip debonding of the CFRP reinforcement and fatigue crack growth. This is required in order to predict the detrimental effect of debonding on fatigue lifetime estimation.

## 10.8 References

Aggelopoulos E S, Righiniotis T D, Chryssanthopoulos M K (2011), 'Debonding of adhesively bonded composite patch repairs of cracked steel members', *Composites Part B: Engineering*, 42(5), 1262–1270.

Alemdar F, Matamoros A, Bennet C, Barret-Gonzalez R and Rolfe S T (2012), 'Use of CFRP overlays to strengthen welded connections under fatigue loading', *Journal of Bridge Engineering (ASCE)*, 17(3), 420–431.

Bassetti A (2001), *Application de lamelles precontraintes en fibres de carbon pour le renforcement d'elements de pont rivetes endommages par fatigue* (in French). PhD Thesis n. 2440, Lausanne, Swiss Federal Institute of Technology (EPFL).

Bassetti A, Nussbaumer A and Hirt M A (2000a), 'Crack repair and fatigue life extension of riveted bridge member using composite material', *Proceedings of the International Bridge Engineering Conference*, Vol. I, ESE-IABSE-FIB, Sharm El Sheikh, 26–30 March, 227–238.

Bassetti A, Nussbaumer A and Hirt M A (2000b), 'Fatigue life extension of riveted bridges members using pre-stressed carbon fiber composites', *Proceedings of the International Conference Steel Structures of the 2000s*, ECCS, Istanbul, 11–13 September, 375–380.

Broek D (1986), *Elementary engineering fracture mechanics*, Dordrecht, Martinius Nijoff Publishers.

Cadei J M C, Stratford T J, Hollaway L C and Duckett W H (2004), *Strengthening Metallic Structures Using Externally Bonded Fibre-reinforced Composites*, C595, London, CIRIA.

Chen T, Yu Q Q, Gu X L and Zhao X L (2012), 'Study on fatigue behaviour of strengthened non-load carrying cruciform welded joints using carbon fibre sheets', *International Journal of Structural Stability and Dynamics*, 12(1), 179–194.

Colombi P (2004), 'On the evaluation of compliance information for common crack growth specimens reinforced by composite patch', *International Journal of Fracture*, 125, 73–87.

Colombi P (2005), 'Plasticity induced fatigue crack growth retardation model for steel elements reinforced by composite patch', *Theoretical and Applied Fracture Mechanics*, 43(1), 63–76.

Colombi P, Bassetti A and Nussbaumer A (2003a), 'Analysis of cracked steel members reinforced by pre-stress composite patch', *Fatigue and Fracture of Engineering Materials and Structures*, 26(1), 59–66.

Colombi P, Bassetti A and Nussbaumer A (2003b), 'Delamination effects on cracked steel members reinforced by prestressed composite patch', *Theoretical and Applied Fracture Mechanics*, 39, 61–71.

Dawood M, Rizkalla S and Sumner E (2007), 'Fatigue and overloading behaviour of steel-concrete composite flexural members strengthened with high modulus CFRP materials', *Journal of Composites for Construction*, 11(6), 659–669.

Ghafoori E, Motavalli M, Botsis J, Herwig A and Galli M (2012a), 'Fatigue strengthening of damaged metallic beams using prestressedunbonded and bonded CFRP plates', *International Journal of Fatigue*, 44, 303–315.

Ghafoori E, Schumacher A and Motavalli M (2012b), 'Fatigue behaviour of notched steel beams reinforced with bonded CFRP plates: determination of prestressing level for crack arrest', *Engineering Structures*, 45, 270–283.

Hollaway L C and Cadei J (2002), 'Progress in the technique of upgrading metallic structures with advanced polymer composites', *Progress in Structural Engineering and Materials*, 4(2), 131–148.

Huawen Y, Konig C, Ummenhofer T, Shizhong Q and Plum R (2010), 'Fatigue performance of tension steel plates strengthened with pre-stressed CFRP laminates', *Journal of Composites for Construction*, 14(5), 609–615.

Jiao H, Mashiri F R and Zhao X L (2012), 'A comparative study on fatigue behaviour of steel beams retrofitted with welding, pultruded CFRP plates and wet layup CFRP sheets', *Thin-Walled Structures*, 59, 144–152.

Jones S C and Civjan S A (2003), 'Application of fibre reinforced polymer overlays to extend steel fatigue life', *Journal of Composites for Construction*, 7(4), 331–338.

Kaan B N, Alemdar F, Bennet C, Matamoros A, Barret-Gonzalez R and Rolfe S T (2012), 'Fatigue enhancement of welded details in steel bridges using CFRP overlay elements', *Journal of Composites for Construction*, 16(2), 138–149.

Kim Y J and Harries K A (2011), 'Fatigue behaviour of damaged steel beams repaired with CFRP strips', *Engineering Structures*, 33(5), 1491–1502.

Liu H B, Al-Mahaidi R and Zhao X L (2009a), 'Experimental study of fatigue crack growth behaviour in adhesively reinforced steel structures', *Composites Structures*, 90(1), 12–20.

Liu H B, Xiao Z G, Zhao X L and Al-Mahaidi R (2009b), 'Prediction of fatigue life for CFRP strengthened steel plates', *Thin-Walled Structures*, 47(10), 1069–1077.

Liu H B, Zhao X L and Al-Mahaidi R (2009c), 'Boundary element analysis of CFRP reinforced steel plates', *Composite Structures*, 91(1), 74–83.

Nakamura H, Jiang W, Suzuki H, Maeda K and Irube T (2009), 'Experimental study on repair of fatigue cracks at welded web gusset joint using CFRP strips', *Thin-Walled Structures*, 47(10), 1059–1068.

Nussbaumer A, Bassetti A and Colombi P (2004), 'Elements en acier sous charges de fatigue renforces par des lamelles precontraintes en materiau composite' (in French), *Construction Metallique*, 3, 3–13.

Schijve J (1988), 'Fatigue crack closure: observation and technical significance', in Newman J C Jr and Alber W (eds), *Mechanics of Fatigue Crack Closure*, ASTM STP 982, West Conshohocken, PA, ASTM, 5–34.

Schnerch D, Dawood M, Rizkalla S and Sumner E (2007), 'Proposed design guidelines for strengthening of steel bridges with FRP materials', *Construction and Building Materials*, 21(5), 1001–1010.

Shaat A, Schnerch, D, Fam, A and Rizkalla S (2004), 'Retrofit of steel structures using fiber-reinforced polymers (FRP): state-of-the-art', *Transportation Research Board (TRB) 83rd Annual Meeting*, Washington, DC 11–15 January.

Taljsten B, Hansen C S and Schmidt J W (2009), 'Strengthening of old metallic structures in fatigue with prestressed and non-prestressed CFRP laminates', *Construction and Building Materials*, 23(4), 1665–1677 (P).

Tavakkolizadeh M and Saadatmanesh H (2003), 'Fatigue strength of steel girders strengthened with carbon fiber reinforced polymer patch', *Journal of Structural Engineering*, 129(2), 186–196.

Teng J G, Yu T and Fernando D (2012) 'Strengthening of steel structures with fiber-reinforced polymer composites', *Journal of Constructional Steel Research*, 78, 131–143.

Veers P J (1987), *Fatigue Crack Growth Due to Random Loading*, SAND87-2037, Sandia National Laboratories.

Wang R and Nussbaumer A (2009), 'Modelling fatigue crack propagation of a cracked metallic member reinforced by composite patch', *Engineering Fracture Mechanics*, 76, 1277–1287.

Wu C, Zhao X L, Al-Mahaidi R, Emdad M and Duan W H (2012), 'Fatigue tests of cracked steel plates strengthened with UHM CFRP plates', *Advances in Structural Engineering – An International Journal*, 15(10), 1801–1816.

Wu C, Zhao X L, Al-Mahaidi R and Duan W H (2013a), 'Mode I stress intensity factor of centre-cracked tensile steel plates with CFRP reinforcement', *International Journal of Structural Stability and Dynamics*, 13(1), 1350005.

Wu C, Zhao X L, Al-Mahaidi R and Duan W H (2013b), 'Effects of CFRP bond locations on the Mode I stress intensity factor of centre-cracked tensile steel plates', *Fatigue & Fracture of Engineering Materials & Structures*, 36(2), 154–167.

Zhao X L (2011), 'FRP strengthening of metallic structures subject to fatigue loading', *Seventh National Conference on FRP in Construction*, Hangzhou, 15–16 October.

Zhao X L and Zhang L (2007), 'State of the art review on FRP strengthened steel structures', *Engineering Structures*, 29(8), 1808–1823.

# 11

# Extending the fatigue life of steel bridges using fiber-reinforced polymer (FRP) composites

R. BARRETT-GONZALEZ, S. ROLFE, A. MATAMOROS and C. BENNETT,
University of Kansas, USA

**DOI**: 10.1533/9780857096654.3.269

**Abstract**: This chapter examines the use of fiber-reinforced polymeric doublers to repair fatigue damage in steel bridges. The use of composite materials to prevent and limit fatigue damage is discussed for various types of structural elements, loading conditions and geometric configurations. Fatigue damage in steel bridges is classified into two broad categories based on the type of driving force mechanism: in-plane and out-of-plane or distortion-induced fatigue damage. Methods of repair for both types of fatigue damage are presented. The chapter includes discussions on the use of composite materials to repair fatigue damage in plates subjected to tension, in welded connections and in cross-frame to girder web connections. The main parameters affecting the performance of each type of repair are presented and discussed, based on the results from computer simulations and experiments with components and systems subjected to cyclic loading.

**Key words**: fatigue, steel bridge, composite materials, repair, fatigue life.

## 11.1 Introduction

Composite materials have been used since the dawn of humankind in nearly every major class of civil structure. Fibrous composites have become ever more prevalent in recent times in some of the most demanding applications, most notably in high performance ground vehicles and aircraft. In addition to possessing outstanding strength-to-weight and toughness-to-weight ratios, fibrous composites are also well known for their ability to resist fatigue. While most isotropic and quasi-isotropic metals will experience crack initiation and essentially 'unzip' via rapid crack propagation mechanisms, fiber-reinforced composites possess countless millions of crack arresting microstructures. These microstructures force the crack to alter its path, often 90° to the direction of propagation to continue its formation. These right angle turns consume high levels of energy as fiber–matrix bonds are broken, overstressing other portions of the fibers and causing them to snap deep inside the otherwise intact matrix. As a result, fibers end up sliding within friction-bound holes. On a microscopic scale, direct contact,

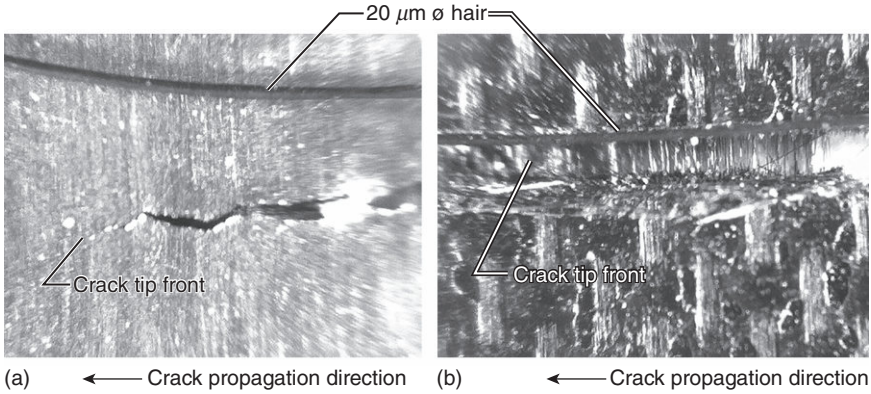


*11.1* Fundamental difference between isotropic metal (a) and composite (b) fatigue-crack formation and propagation.

debond and Coulomb friction mechanisms all combine to make for materials which inherently resist failure due to fatigue loading more readily than isotropic metals.

To illustrate this, Fig. 11.1a shows a micrograph of a fatigue-induced crack progressing along an isotropic metal sheet. Figure 11.1b shows a similar coupon made from a plain weave graphite–epoxy composite with a crack zone (no crack tip evident) progressing from right to left. The reader will note that the isotropic metal possesses a well-defined, very sharp crack tip which is splitting the specimen from right to left. The composite coupon is very much a different story. While the plain weave pattern of 5k tow elements is visible in Fig. 11.1b, the area just below the human hair shows a region which appears to be blurred with no warp-fill pattern. This is because as the crack in the specimen propagated from right to left, no single crack tip pried the specimen open like a wedge. Instead, thousands of fibers and the matrix around them failed successively, which in turn transferred the loads to the adjacent fibers via matrix shear.

Clearly, this crack propagation mechanism consumes significantly more energy per unit time and weight than an isotropic metal does. Figure 11.2 shows the details of several failure mechanisms which are observed in fibrous composites on the microscopic scale. Because the direction of crack propagation is often normal to many of the debonds and shear failures, the total crack path and surface can become quite large with respect to those of isotropic metals. Many fibers which have themselves failed in local tension actually carry loads as the hole formed by partial pull-out binds due to fibrous surface roughness. These bound fibers provide a high level of residual strength and stiffness even after the crack has propagated through the composite. If one examines the fracture surface of the hypothetical

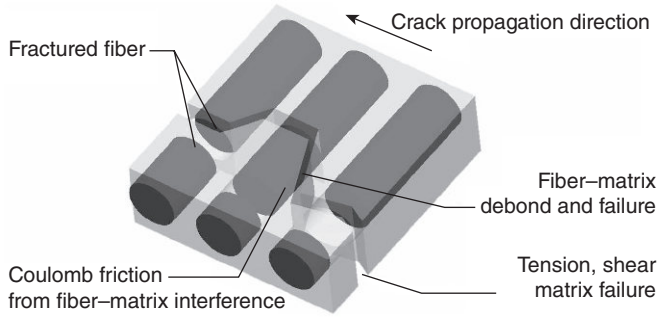


*11.2* Major failure mechanisms in fibrous composites under fatigue loading.

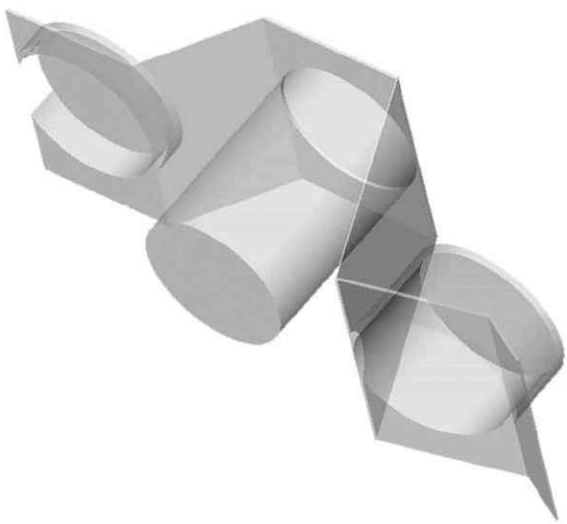

*11.3* Fracture surface of composite model of Fig. 11.2.

composite of Fig. 11.3, then one can see immediately that it is substantially larger than an equivalent crack that would be found in an isotropic metal.

## 11.2 The development of composite materials for the repair of fatigue damage

Although fibrous composites themselves have many favorable properties, they are not inherently amenable to use in civil infrastructure because they are often not as easily post-processed as isotropic metallic materials. To skirt these issues, a new material class was invented and patented by AkzoNobel

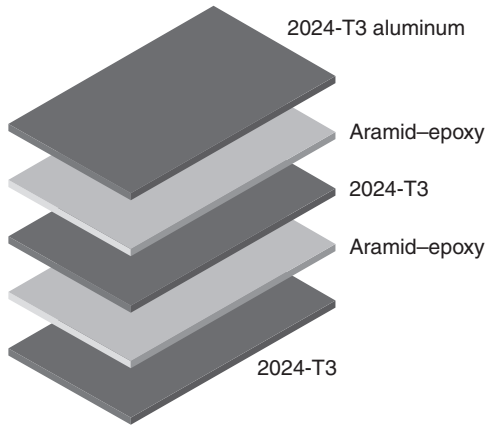


*11.4* ARALL metal–fibrous composite layup.

in 1987 which includes the most favorable aspects of both isotropic metals and fibrous composites.

Because large swings in humidity, temperature, pressure and loading are common on aeronautical structures, airplanes became flying testbeds for structural composites. Eventually, governmental standards were developed and structural composite materials reached the high level of maturity they are at today. One of the most highly evolved materials is a hybrid composite made with aramid fibers, epoxy resin and aluminum. These GLARE and ARALL composite materials are standard on many Airbus aircraft and often comprise five or more alternating layers of aluminum and aramid cloth as shown in Fig. 11.4. These new materials are Federal Aviation Administration (FAA) certified, have been tested both in the lab and in flight to hundreds of millions of cycles and clearly show that fibrous composites can be successfully integrated with isotropic metals. Figure 11.4 shows the high level of integration of both metal and composites.

This layup sequence imparts to the material some profound benefits, most importantly significant resilience against fatigue damage. Figure 11.5 shows the dramatic fatigue performance improvement over conventional aluminum. Clearly, an order of magnitude improvement in fatigue life indicates that the material configuration may be well suited to certain applications. In addition to conventional composite fatigue failure modes, metal–fibrous composite hybrids also possess outer matrix–inner metallic sheet failure surfaces which helps to further enhance resistance to fatigue as shown in Fig. 11.5.

For primary structures, certain classes of structural composites have been shown to be well suited to resisting fatigue damage. However, after a structure has suffered fatigue damage and is in need of repair, material

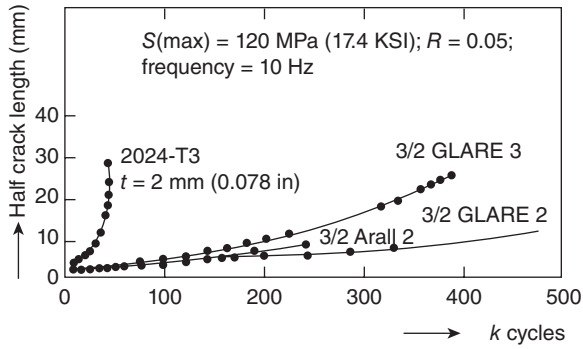


*11.5* Dramatic fatigue performance improvement available from integration of composite materials (Vlot *et al.,* 1999).

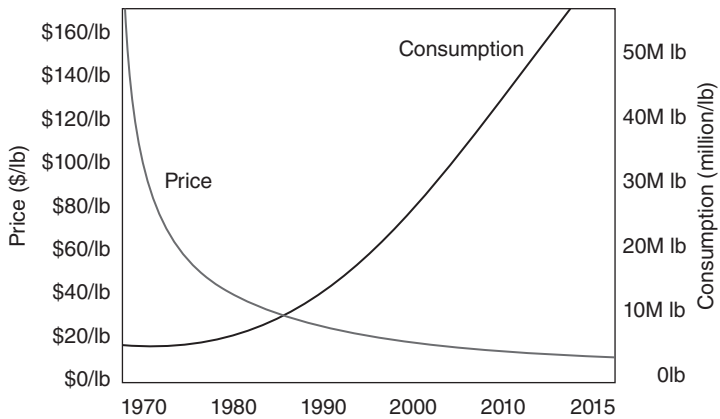


*11.6* Price and consumption trends for industrial graphite fiber material (Vakili, 2012).

selection can be significantly more challenging. Although the aerospace composite industry has settled on various classes of aramid fibers as being best suited for fatigue repair overlay construction (i.e. ARALL), this is not necessarily the case for all situations. One of the most important characteristics to recall when considering aerospace repair techniques applied to another discipline is that the majority of aerospace load-bearing structures are thin-walled and/or thin-skinned and often take the form of shear panels. This is dramatically different from structures that are formed as bending load-bearing I-shapes and built-up structures carrying torsion. Perhaps the most important considerations are associated with cost.

When one factors in the cost of material, labor, installation and inspection, it immediately becomes apparent that maintaining low costs is imperative. Figure 11.6 shows the trend of structural graphite fiber cost and consumption

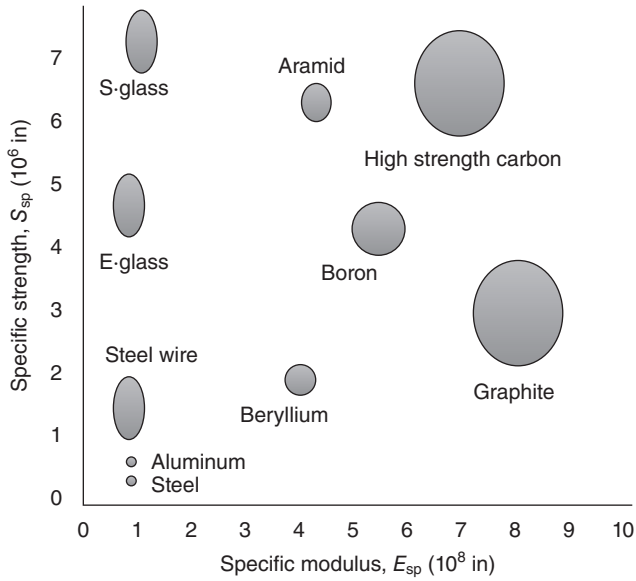


*11.7* Specific strength and modulus of common structural fibers and isotropic materials.

with time. Because the raw chemical foundations of graphite fiber are so readily available, the continued price decline is inevitable as is the increased consumption. If one examines polymeric fibers, the cost per unit of specific strength and specific stiffness is significantly higher. Accordingly, graphite fibers are most often the fiber of choice for many structural applications when considering cost alone. Of course, the other great metrics for comparison are the specific moduli and strength. If one looks at them beside each other, as shown in Fig. 11.7, graphite and high strength carbon fibers are highly competitive. Accordingly, for many structural applications, carbon and graphite fibrous composites are often seen as the materials of choice for reinforcement.

## 11.3 Understanding fatigue damage in steel bridges

Given the increasingly larger economic losses associated with traffic disruptions, there is great need for innovative fatigue retrofit measures in the realm of civil infrastructure, particularly for applications in steel bridges. Fatigue cracking is common in aging steel bridges, many of which are approaching or have already exceeded their design life. Fatigue damage in steel infrastructure is often divided into two overarching categories: in-plane fatigue damage and out-of-plane fatigue damage. The latter mode is often referred to as distortion-induced fatigue damage.

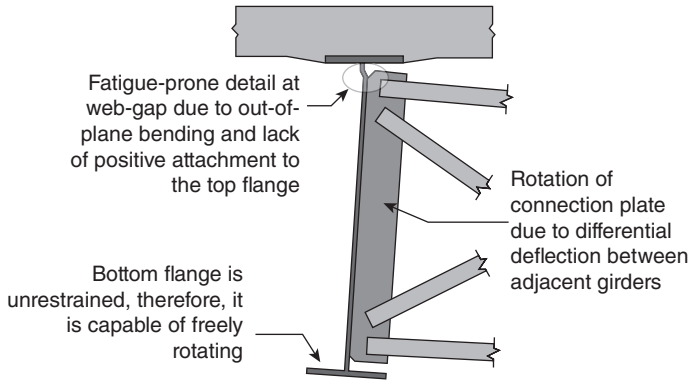


*11.8* Schematic of web-gap detail susceptible to distortion-induced fatigue.

In-plane fatigue damage occurs when repeated loading produces stress cycles that act in the longitudinal sense of bridge girders. Out-of-plane (distortion-induced) fatigue damage occurs when the stress cycles producing damage occur from secondary load paths, such as stresses transferred between girders via cross-frame or diaphragm elements. Distortion-induced fatigue cracks often initiate and propagate under relatively low stress magnitude, and can generally be prevented in the design phase through sound detailing practice. However, there exist a great number of bridges that contain details susceptible to distortion-induced fatigue damage, wherein the load path provided between the secondary and primary structural elements is likely to induce fatigue cracks. The classic example of a detail susceptible to distortion-induced fatigue damage is a web-gap within a bridge girder, as illustrated in Fig. 11.8.

Composite materials are an attractive retrofit measure and/or repair technique for fatigue-vulnerable connection details in steel bridges in part due to their high strength-to-weight ratio, but foremost because of their ability to be applied in completely customizable geometries. Cracking in bridge structures often occurs in geometrically 'congested' areas, making traditional steel repairs difficult to implement. Additional difficulty is encountered when connecting traditional steel repairs to the existing girder and components; bolting is generally the preferred method of connection and in many cases, access to both sides of a structural element (i.e., top flange) is not possible without some level of deconstruction (i.e., partial deck removal). For this reason, bonding of composite materials in such constrained regions is an attractive alternative to bolting steel components.

To describe how composite materials may be used to improve the fatigue life of steel bridge girders, it is useful at first to examine the components of

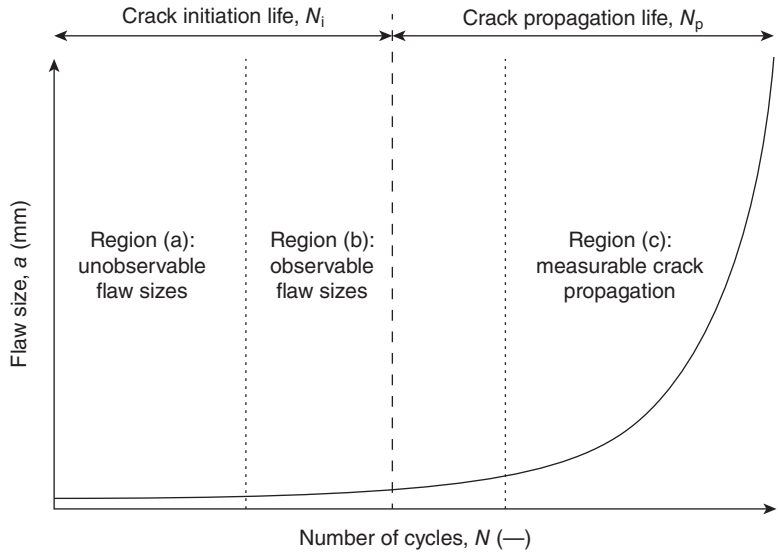


*11.9* Relationship between flaw size and fatigue life in steel substrate.

fatigue life. Fatigue life of structural components and connections can be divided into two primary components: fatigue initiation life $N_i$, and fatigue propagation life $N_p$. The total fatigue life $N_t$, can be expressed as:

$$N_t = N_i + N_p \quad [11.1]$$

Fatigue initiation life describes the number of cycles, under a specific constant-amplitude stress range $\Delta\sigma$ before an observable crack is detected in the structural element. Fatigue propagation life describes the number of cycles under constant amplitude cyclic stress while a crack is actively growing in the structural element. The fatigue propagation life describes the number of cycles from crack initiation to failure of the structural component.

Both fatigue initiation and propagation life are directly related to flaw (crack) size in the substrate material and stress range. For a single stress range, the relationship between flaw size $a$ and the number of applied cycles $N$ is as shown in Fig. 11.9.

Application of a composite retrofit to a fatigue-vulnerable connection detail effectively reduces the stress range that the steel substrate experiences, because a new load path is provided through the composite retrofit. Referring to the reduced stress range in the steel as $\Delta\sigma'$, this new stress range can be thought to produce a new relationship between flaw size and number of cycles, as illustrated in Fig. 11.10. Because the new relationship between $a$ and $N$ will fall below that of the original curve for the unretrofitted

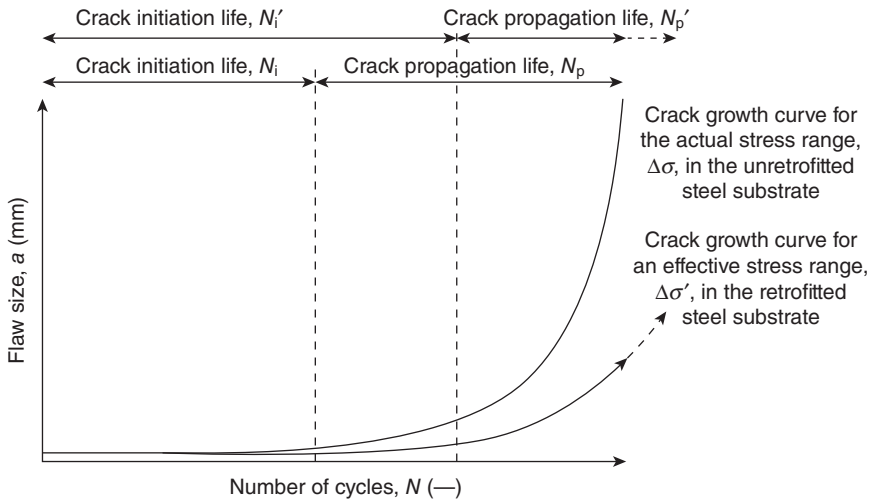


*11.10* Relationship between flaw size and fatigue life in steel substrate before and after a composite retrofit has been applied.

steel substrate, the point of crack initiation, $N_i'$ will be shifted to correspond with a greater number of fatigue cycles. Correspondingly, the propagation life $N_p'$ will also be expected to increase.

Thus, the increases in fatigue initiation and propagation life can be expected to be proportional to the decrease in stress range afforded to the metal substrate by the composite retrofit measure. Determination of the post-retrofit stress in the metal substrate $\Delta\sigma'$ can be approached in a number of manners. For axially loaded thin plates, one concept that is useful when considering that decrease is the stress ratio *SR* which normalizes the axial stiffness of the composite material to that of the steel substrate:

$$SR = E_{FRP}t_{FRP} / E_m t_m \qquad [11.2]$$

where *SR* is the stiffness ratio, $E_{FRP}$ is the modulus of elasticity of the FRP, $t_{FRP}$ is the thickness of the FRP patch, $E_m$ is the modulus of the metal and $t_m$ is the thickness of the metal plate. For situations in which the state of stress being resisted is complex, such as is the case for distortion-induced fatigue, either direct measurement or finite element (FE) analysis may be required to determine both $\Delta\sigma$ and $\Delta\sigma'$.

Determining the exact level of increase in $N_i$ as the stress range is reduced from $\Delta\sigma$ to $\Delta\sigma'$ is a difficult task, as is locating the exact position of $N_i$ or $N_p'$ in Fig. 11.9 or Fig. 11.10. The definition of crack initiation is somewhat subjective, as it is dependent upon tools used to inspect for crack formation and the definition of flaw size adopted as an initial crack. Determining

increases in propagation life can be approached in a more quantitative manner.

The relationship that governs the behavior of stable crack propagation for stress intensities greater than $\Delta K_{th}$ is, in general form (Barsom and Rolfe, 1999):

$$\frac{da}{dN} = A(\Delta K)^m \quad [11.3]$$

where $a$ is crack length, $N$ is the number of cycles experienced, $\Delta K$ is the range of stress intensity factor for the crack, $\Delta K_{th}$ is the stress intensity threshold for the material and $A$ and $m$ are constants. For a through-thickness crack of length $2a$ in an infinite plate subjected to uniform tension stress, $\sigma$, the stress intensity factor, $K$, can be calculated as:

$$K = \sigma\sqrt{\pi a} \quad [11.4]$$

Therefore, for a range of stress comprising maximum and minimum stresses, $\sigma_{max}$ and $\sigma_{min}$, the stress intensity factor range could be determined as:

$$\Delta K = (\sigma_{max} - \sigma_{min})\sqrt{\pi a} \quad [11.5]$$

Stress intensity factors for other crack geometries and loading conditions are well-documented (Barsom and Rolfe, 1999).

## 11.4 Repair of fatigue cracks in plates subjected to tension

A significant amount of research on the use of composite materials has been carried out in the field of aerospace engineering to address fatigue problems in the fuselages of airplanes (Naboulsi and Mall 1996; Schubbe and Mall 1999a, b; Umamaheswar and Singh 1999; Lee and Lee 2004; Liu *et al.*, 2009b; Mall and Conley 2009). The most recent research performed on this topic in the aerospace field has focused on the use of fiber-reinforced polymer (FRP) patches to repair fatigue damage in aluminum plates. These studies have shown that FRP plates can reduce the stress demand in a vulnerable element or connection significantly if properly proportioned and bonded to the steel substrate. An experimental study by Mall and Conley (2009) reported that bonding a boron FRP overlay to only one side of an aluminum specimen increased the fatigue-crack propagation life between four and 10 times compared to the propagation life of an untreated specimen.

One of the most important concerns when implementing this repair method is to achieve adequate bond between the steel and the composite

overlay. Voids or imperfections in the layer of resin used to attach the composite overlay to the underlying metal can lead to the formation and propagation of fatigue cracks within the resin. This can eventually cause debonding of the overlay, rendering the repair ineffective.

In the aerospace field, a commonly used parameter for proportioning composite patches for the purpose of repairing fatigue damage is the ratio of axial stiffness of the composite patch to the axial stiffness of the plate (Sabelkin *et al*., 2006), which is defined by Eq. (11.2). The *SR* parameter is used to determine thickness of FRP needed to repair fatigue-damaged steel plates by assuming that the driving force is redistributed in proportion to the relative axial stiffness of the two materials. For aerospace structures the recommended stiffness ratio is 1.0 (Schubbe and Mall, 1999a). Schubbe and Mall (1999a) performed experimental tests on aluminum plates that were repaired with a bonded composite patch and found that as the stiffness ratio between the repair and steel plate increased, so did the fatigue life of both thin and thick plates. Stiffness ratios of 1.0 and 1.3 were evaluated in that study.

Several studies have investigated the use of composite materials to repair fatigue-related damage in steel structures. Tavakkolizadeh and Saadatmanesh (2003) studied the effectiveness of unidirectional CFRP sheets to improve the fatigue strength of S127x4.5 steel girders with pre-existing notch cracks. The authors reported that the fatigue-crack propagation life of the specimens with CFRP sheets was extended by a factor of approximately three compared with that of control specimens. Liu *et al*. (2009a) studied the tensile fatigue behavior of notched steel plates strengthened with single-ply CFRP patches. Results showed that single-sided repair extended the fatigue-crack propagation life of the specimen by a factor ranging between 2.2 and 2.7, whereas a double-sided repair extended the fatigue-crack propagation life by a factor ranging between 4.7 and 7.9. Roy *et al*. (2009) performed a study using the same type of materials and procedure used by Liu *et al*. (2009a), but focused the study on the single-sided repair because of the inherent asymmetry. Roy *et al*. (2009) reported that the fatigue-crack propagation life was increased by a factor of 2.2 compared with that of the control specimens. Both Liu *et al*. (2009a) and Roy *et al*. (2009) showed similar increases in fatigue-crack propagation life of steel plates repaired with single-sided CFRP patches.

Several studies at the University of Kansas have explored the use of composite materials to repair fatigue damage in structural steel bridges. A significant number of aging steel bridge structures experience structural problems due to fatigue cracks in girder webs. Composite material overlays can be applied as a patch over the region where the fatigue crack occurs and would not need to extend over the full depth of the web. The main concern about this type of repair is that its effectiveness is highly dependent

on the bond between the steel and the CFRP overlay. If an adequate bond is not achieved, the overlay may eventually separate from the steel causing the repair to become ineffective. The optimal proportioning of the CFRP overlay is best determined by the stiffness ratio, as defined in Eq. (11.2).

Studies performed at the University of Kansas investigated the effectiveness of adhesively bonded CFRP overlays to repair fatigue damage in steel plates. The studies included both analytical and experimental components aimed at evaluating the effect of the axial stiffness ratio on fatigue-crack propagation life and effective stress range, identifying relationships between the stiffness of the CFRP overlays and the steel substrate to determine which proportions would be most effective in slowing or halting fatigue-crack propagation in the steel substrate, and determining the effect of both the bond layer thickness and CFRP overlay thickness on reduction in the hot spot stress (HSS).

### 11.4.1 Effect of composite overlays on the stress field of cracked plates

The computational studies carried out at Kansas focused on the development of FE models to investigate the effect of CFRP overlays on the stress demand in cracked steel plates. Comparisons were performed on the basis of HSS, which was shown to be an efficient indicator of potential for fatigue damage in other studies (Hartman *et al.*, 2010; Hassel, 2011; Kaan *et al.*, 2012). Simulations of steel specimens repaired with CFRP overlays were performed by Gangel (2011) to investigate the effect of varying the modulus of elasticity and thicknesses of the composite overlay on the stress demand of the repaired specimens. Simulations and experimental testing were performed on identical specimens, with dimensions shown in Fig. 11.11.

As Fig. 11.12 shows, Gangel (2011) found that the relationship between the modulus of elasticity of the CFRP overlay and HSS was parabolic and inversely proportional. This indicates that even CFRP overlays with a low modulus of elasticity would be effective in reducing HSS in a cracked steel plate. Figure 11.12 also shows that the factor of reduction in the HSS of the steel specimen reduced as modulus of elasticity was increased. This is an important consideration in determining optimal configuration of the overlay, because it implies that there is no economic incentive for using stiffer, more expensive fibers.

Gangel (2011) also found that the effect of varying thickness of the CFRP overlay was very similar to that of the effect of varying its modulus of elasticity. Figure 11.13 shows that the relationship between thickness of the CFRP and the HSS of the steel specimen was also inversely proportional and parabolic. In addition, as thickness of the CFRP was increased, the factor of reduction in the HSS of the steel specimen decreased. These

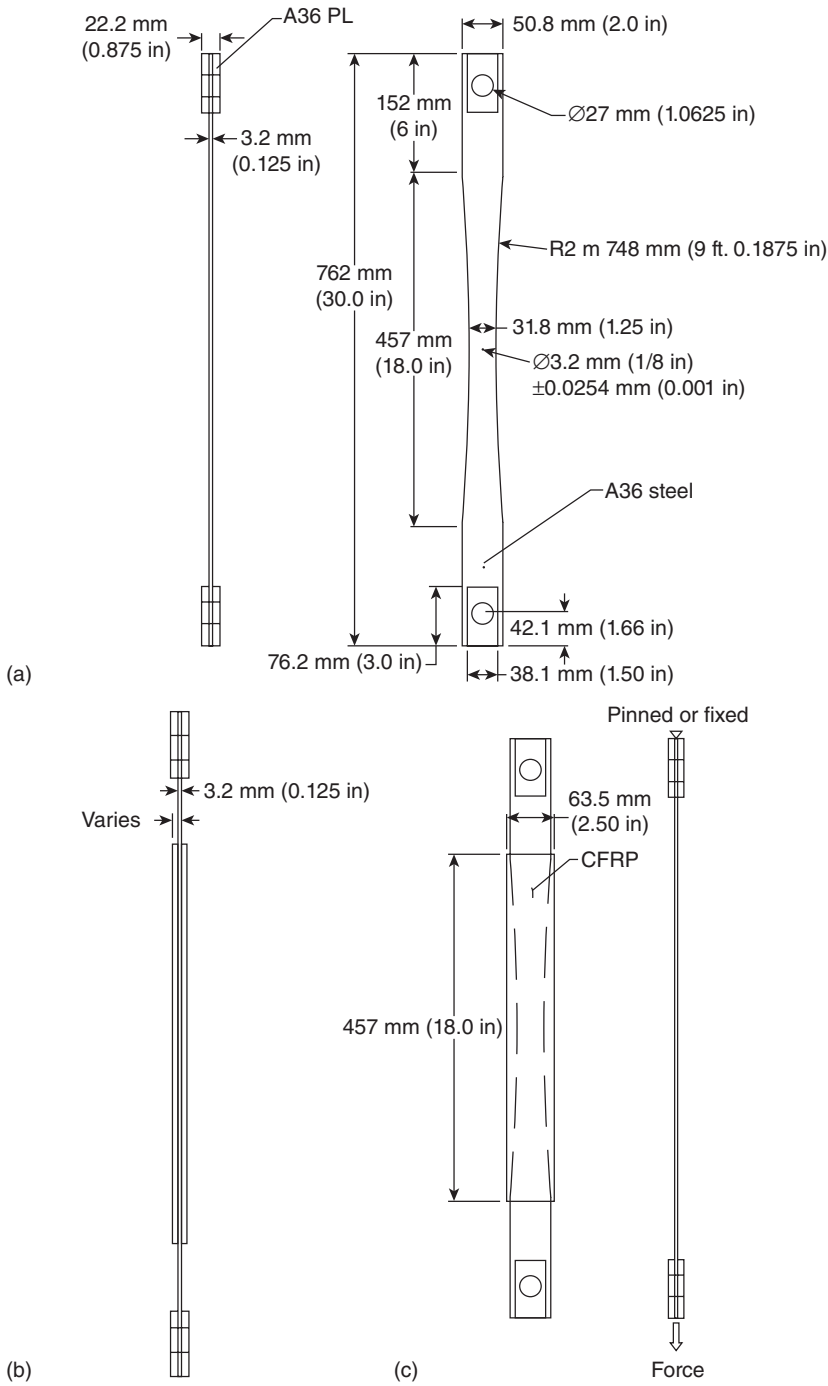


*11.11* Tension specimen: (a) 3 mm ($\frac{1}{8}$ in) bare steel; (b) specimen with CFRP overlay attached; (c) boundary and loading conditions imposed on the FE model and experimental test.

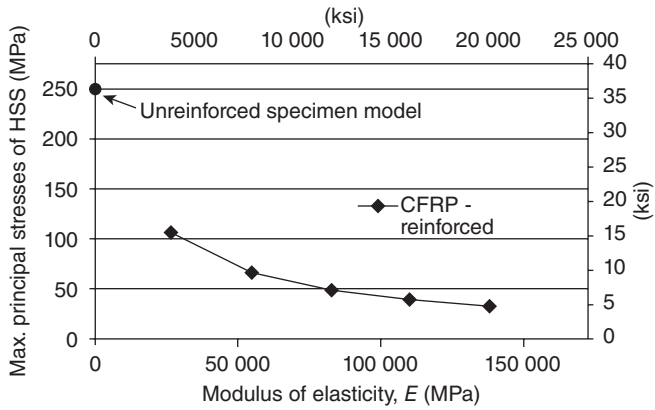


*11.12* Effect of stiffness of the CFRP overlays on maximum principal hot spot stresses in the steel specimen (Gangel, 2011).

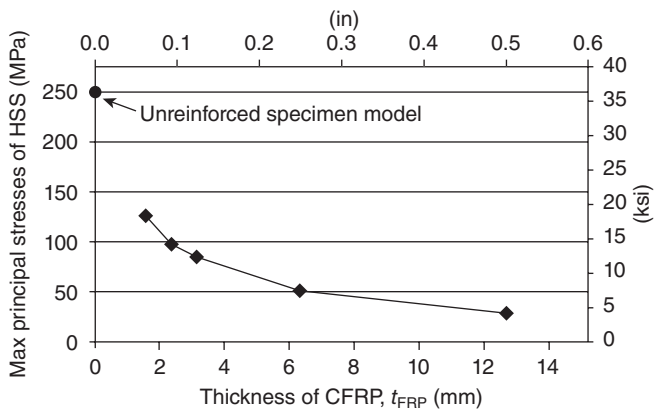


*11.13* Effect of CFRP overlay thickness on maximum principal hot spot stresses in the steel specimen (Gangel, 2011).

results are essential in determining an optimal design for the CFRP overlay, since thickness of the overlay is an important factor in the stiffness ratio of the system.

As previously shown in Eq. (11.2), the stiffness ratio can be modified by changing the modulus of elasticity of the CFRP, the thickness of the CFRP or both. In the study, the optimal stiffness ratio was determined by varying one of these two parameters while keeping the other at a constant value. Gangel (2011) showed that in terms of stress reduction, it did not matter whether modulus of elasticity of the CRFP or thickness of the CFRP was changed. Changing the stiffness ratio by modifying the modulus of elasticity

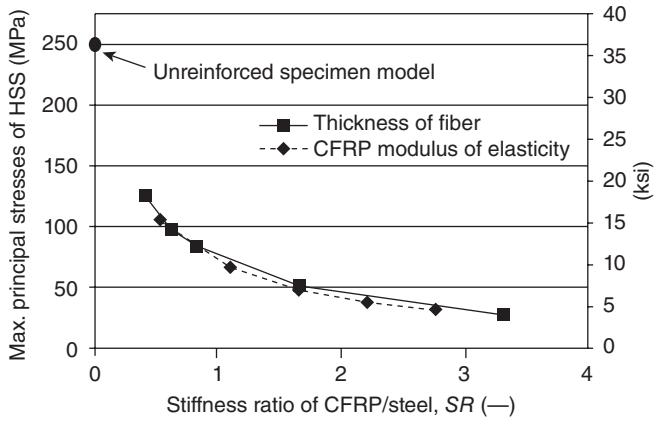


*11.14* Effect of stiffness ratio on maximum principal hot spot stresses in the steel (Gangel, 2011).

of the overlay had similar results to changing the stiffness ratio by modifying the thickness of the overlay, as shown in Fig. 11.14. Both resulted in similar reductions in the HSS. The factor that did affect the HSS was the stiffness ratio itself. As shown in Fig. 11.14, an optimal stiffness ratio seems to be 1.0 for specimens modeled at the 221 MPa (32 ksi) testing stress range. At stiffness ratios greater than 1.0, diminishing returns on reduction in HSS begin to occur.

## 11.4.2 Stress demands along the interface layer

A parameter often ignored in FE simulations of composite overlays is the inherent flexibility of the adhesive resin used to bond the composite overlay to the metal substrate. However, consideration of this interface layer is important because maintaining the bond between the composite and the steel is essential to the success of the CFRP retrofit. Explicit modeling of this interface layer can be used to gage the potential for debonding by providing the average shear demand on the resin and the tensile demand on the resin–steel interface. The higher these stress demands, the more the probability of fatigue failure at the interface increases. The shear and tensile demands are greatly affected by the thickness of the resin layer, thus making the thickness an important parameter to consider in developing an effective CFRP retrofit.

Results by Alemdar (2011) confirmed that, even though the thickness of the interface layer does not affect the maximum principal HSS, an important design consideration is the effect of the interface layer thickness on the stress demand at the interface layer itself. Figure 11.15 shows that shear and

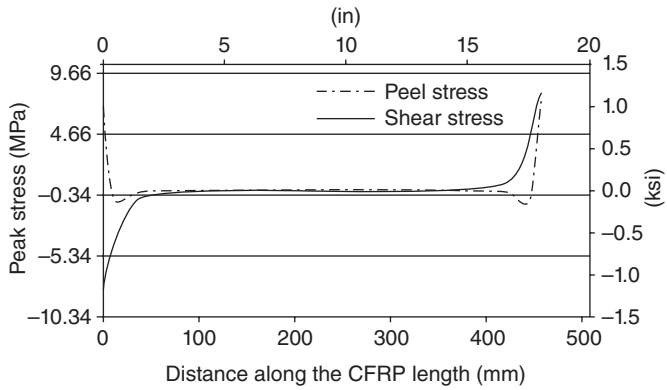


*11.15* Peak stresses along CFRP overlay on resin layer end of hole (Gangel, 2011).

peel stress (out-of-plane stress) were relatively low along most of the interface, with the greatest stress demand occurring at both ends of the interface. Thus, the ends of the interface were the locations most susceptible to fatigue failure.

As Fig. 11.16 shows, increasing the interface layer thickness from 0.6 mm (20 mil) to 50 mm (200 mil) led to a reduction in peak shear and peel stress demands by approximately 66 % and 40 %, respectively. The trends observed for the shear and peel stress differed in that, as the interface layer thickness increased, the shear stress continuously decreased while the peel stress decreased until an interface layer thickness of 2.5 mm (100 mil) and then began to increase. Together, Fig. 11.15 and Fig. 11.16 demonstrate that, while the interface layer has a negligible effect on the stress range of the CFRP retrofit, it is still an important parameter in terms of the bond performance of the interface layer under cyclic loading.

### 11.4.3 Configuration parameters most significant to fatigue performance

In the experimental program of the studies, steel specimens with pre-existing fatigue cracks were repaired with CFRP overlays and tested under cyclic loading to evaluate the effect of stiffness ratio on the fatigue-crack propagation life of steel specimens. Two parameters of Eq. (11.1), the thickness of the CFRP overlay and the thickness of the steel plate, were varied to alter the stiffness ratio. Also of interest in the experiment was the role that stress ranges have in determining an optimal stiffness ratio for CFRP overlay repair. In order to evaluate this, testing was performed at

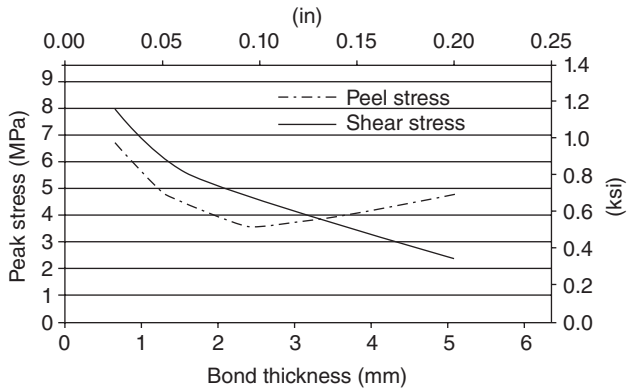


*11.16* Peak stresses demand on CFRP layer as a function of resin layer thickness (Gangel, 2011).

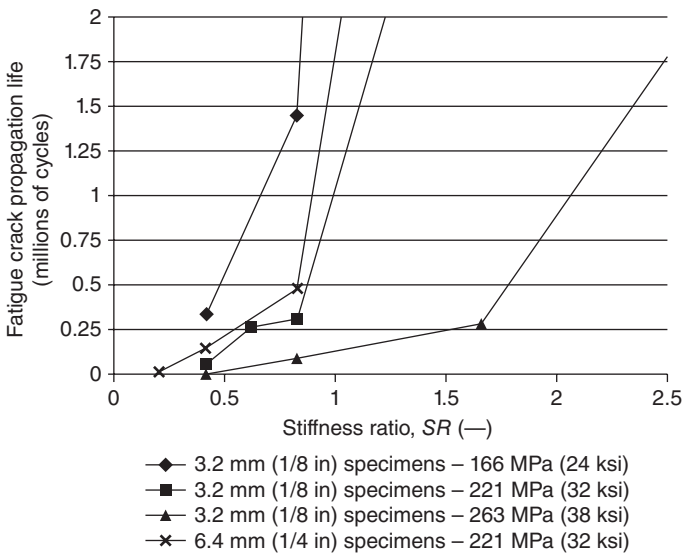


*11.17* Fatigue-crack propagation life for all specimens treated with CFRP overlays and an initial crack length of 7 mm (0.3 in) (Gangel, 2011).

varying stress ranges of 166 MPa (24 ksi), 221 MPa (32 ksi), and 263 MPa (38 ksi).

The fatigue-crack propagation lives of each steel specimen tested were compared on the basis of the stiffness ratio. Figure 11.17 shows that for all specimens, the fatigue-crack propagation life increased as the stiffness ratio increased. In addition, Fig. 11.17 illustrates that as the stress range at which

a specimen with a specific stiffness ratio was tested increased, the fatigue life decreased. This indicates that the effect of the stiffness ratio on fatigue-crack propagation life is dependent on the applied stress range. As shown in Fig. 11.17, the critical stiffness ratio at which each set of data trended towards infinity increased with stress range, indicating that the stiffness ratio must be increased as stress range increases in order to achieve infinite fatigue life.

Due to the large initial crack size used in the experiment relative to the remaining steel net section, unretrofitted control specimens were not tested since their fatigue life would have been quite low. Therefore, the experimental crack propagation lives of the retrofitted specimens were compared to the theoretical crack propagation lives of unretrofitted specimens. This comparison also showed that the applied stress range plays a critical role in the level of improvement on fatigue life provided by a CFRP retrofit. Overall, Gangel (2011) found that a CFRP overlay repair will be more effective at a lower stress range, but will still show promising improvements at higher stress ranges.

## 11.5 Repair of welded connections

Before the 1980s, it was common for bridge engineers to use welded cover plates to reinforce steel girder flanges in regions of high moment demand. Although seldom used in present practice, these welded connections can still be found in aging, existing steel bridges. This retrofit technique has been the major source of fatigue-crack initiation, especially for welds at the ends of thick steel cover plates. AASHTO has categorized this type of weld into the most critical fatigue grouping, Category E′ (AASHTO, 2007). Due to limitations caused by complex geometry, these welded connections are often difficult to reinforce/repair.

An emerging technique for lessening stresses at welded connections vulnerable to fatigue for aging bridge structures involves the use of FRPs. FRPs are ideal for strengthening theses welded connections for several reasons. In addition to having high strength, high stiffness and low weight, they have the ability to be molded into different geometries and to diffuse crack propagation (Meier, 1992). FRPs as an external overlay can reduce stress demand at the tip of an existing crack or previously uncracked welded connection by providing an alternate load path. This reduction in stress demand at the welded connections increases fatigue-crack initiation and propagation life.

In recent research at the University of Kansas, CFRP overlays, or doubler elements, were investigated to determine their use in enhancing fatigue performance in the fatigue-critical welded connections in steel bridge girders. The studies involved bonding CFRP overlays to welds categorized

as AASHTO Category E′ fatigue details to determine their effectiveness in providing an alternate load path and reducing stress demand at the weld. Initial study results effectively showed that the use of CFRP overlays led to an increase in crack-initiation life of the welded connection and that maintaining the bond between the CFRP overlay and the steel is a critical factor if infinite fatigue life is to be achieved (Kaan, 2008; Alemdar *et al.*, 2009; Alemdar, 2010).

After determining a solution for maintaining bond strength, the remaining question was whether the reduction in stress demand at the fatigue-critical weld created by the CFRP overlay would be sufficient to extend the fatigue life of welded connections to the infinite range. Alemdar (2010) performed a study focusing on the effectiveness of CFRP overlays with breather cloths in the interface layer as a fatigue-strengthening and repair method for welded connections. To meet the objectives of the study, three point bending welded cover plate specimens were tested in fatigue under a constant stress range. Experimental testing was performed on specimens with pre-existing fatigue cracks in the weld and on specimens without observed fatigue cracks in the weld. The experiment consisted of a series of welded cover plate specimens (Fig. 11.18) loaded in three point bending and subjected to cyclic loading under a constant stress range.

No fatigue cracks were detected in the welds upon final inspections of specimens tested under fatigue loading up to 3.29M cycles that did not have pre-existing fatigue cracks. Two other types of weld treatment were utilized to gage the effectiveness of composite overlays in comparison to other repair techniques. They included ultrasonic impact treatment (UIT) and a weld smoothing treatment. The weld treatment involved smoothing the weld using an angle grinder until the weld was approximately flat and formed a 45° angle with respect to the surface of the steel plates. This treatment was done to ensure that there was a smooth transition between the weld and the plate at the weld toe and to reduce the size of the weld flaws created during the initial welding process. Figure 11.19 shows the results of the comparison between treatments. Specimens treated by UIT are designated UIT, specimens treated by the weld smoothing process are designated GRND and control specimens are designated Control. As shown in Fig. 11.19, repairing the specimen with a CFRP overlay or treating the weld with UIT showed similarly effective results, as both techniques extended fatigue life to run-out. Thus, the experiment showed that composite overlays were not only successful in extending fatigue life to run-out, but that they were as effective as other well-established repair methods such as UIT.

No significant crack growth was found on a pre-cracked specimen tested under fatigue loading up to 2.88M cycles. Meaningful comparisons for this result came from theoretical fatigue life predictions. Theoretical crack

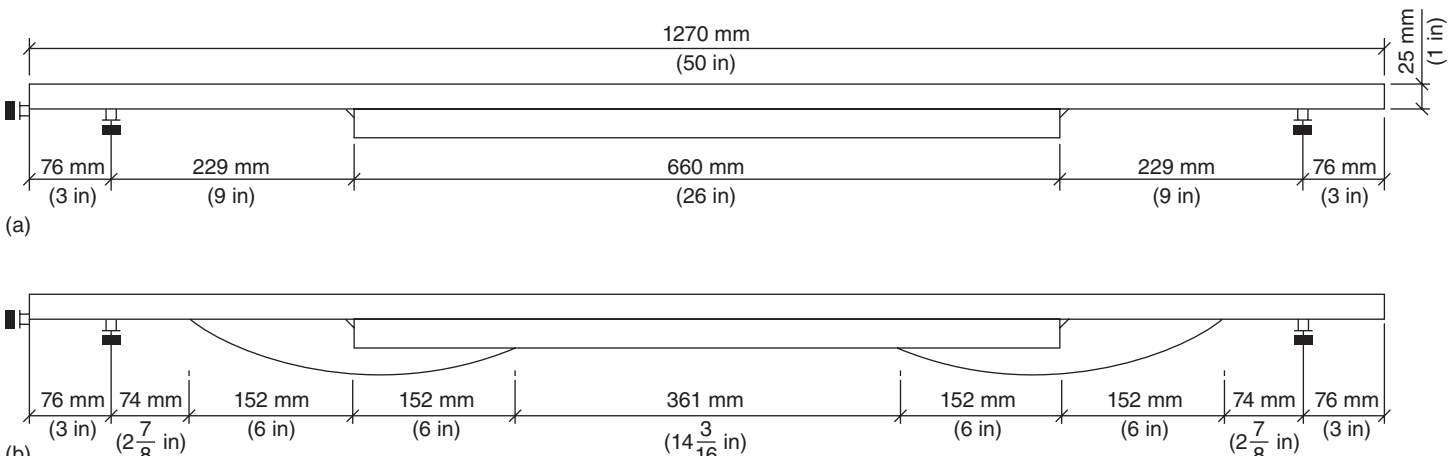


*11.18* Three point bending specimens: (a) without CFRP retrofit (Vilhauer, 2007); (b) with CFRP retrofit applied (Alemdar, 2010).

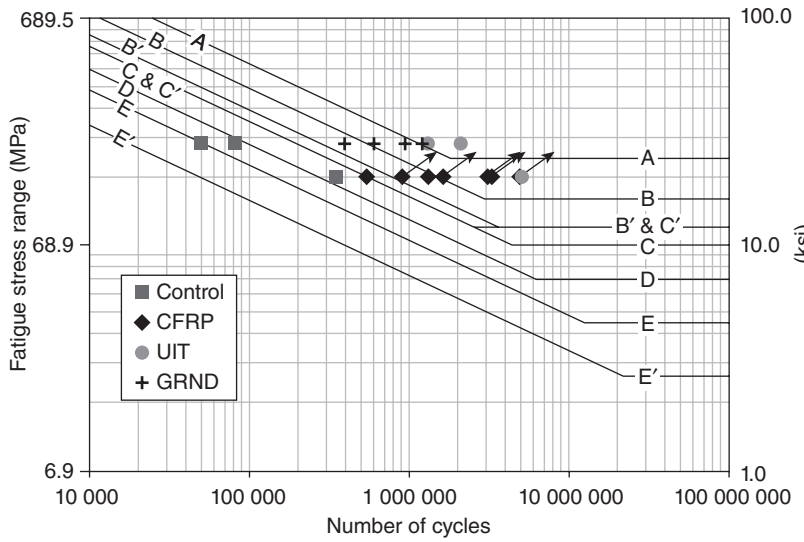


*11.19* Fatigue life of welded connections for various types of treatments (Alemdar, 2010).

propagation rates based on the assumption of an edge crack in a finite plate yielded the closest match to the experimental results of the control specimens. As shown in Fig. 11.20, experimental crack lengths measured in steel specimens retrofitted with CFRP overlays tested at 138 MPa (20 ksi) were in close agreement with the theoretical crack growth estimates for bare steel specimens subjected to a 34.5 MPa (5.0 ksi) stress range. This indicates that an AASHTO Category E′ specimen with CFRP overlays will see a reduction of 80 % in the stress demand at the welded connection.

## 11.5.1 Fabrication of resilient composite overlays

Laminar CFRP materials are assembled by subjecting layers (plies) of graphite fibers and bonding material (matrix) to heat and pressure. Typically, the heat is applied by an oven or heat press and the pressure is supplied by a vacuum bag. The applied heat activates the matrix material so that it can flow and encompass the graphite fibers while the applied pressure reduces air voids throughout the composite. The quality of a finished composite is categorized by its level of consolidation, which is defined by the fibers, matrix material and relative volume fractions of the voids in the composite. A higher level of consolidation corresponds to a composite with higher strength and stiffness characteristics along with a higher resistance to crack propagation (Mallick, 1993). A common matrix material used in the

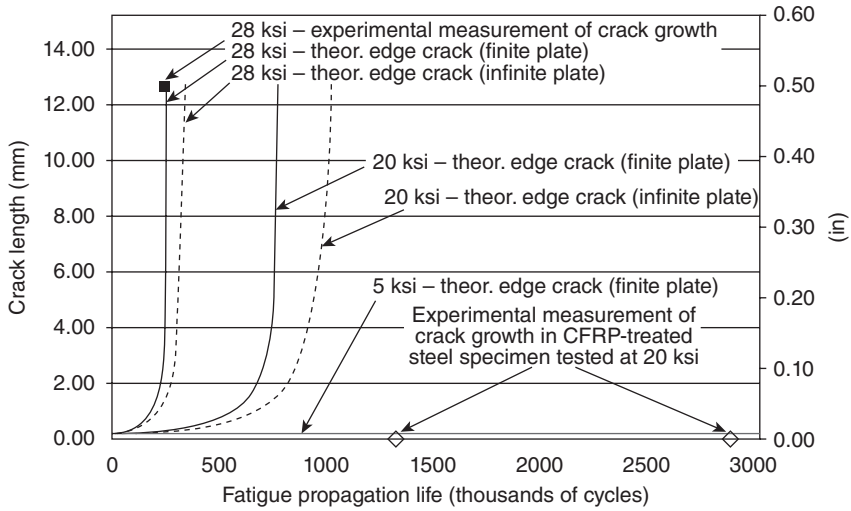


*11.20* Theoretical and experimental propagation life of untreated and CFRP retrofitted three point bending specimens (Alemdar, 2010).

development of CFRP materials is resin epoxy. During heat application, cross-linking of the polymer molecules of the resin cause the resin to form a solid structure. This type of resin is thermo-set, meaning that even if reheated to the original application temperature, the epoxy resin will no longer flow plastically after cross-linking occurs.

One study performed at the University of Kansas focused on the development of the composite doubler element. The objective of the study was to develop a CFRP overlay with sufficient strength and stiffness characteristics so that when bonded to a fatigue-critical detail, the CFRP overlay could efficiently carry out its purpose of creating an alternate load path and reducing stress demand at the weld. In the study, CFRP-stiffened steel specimens were fabricated by bonding CFRP overlays to two steel plates welded together to create an AASHTO Category E′ fatigue detail. The stiffened specimens were then subjected to fatigue loading in a three point bending test.

Initially, the focus of the CFRP overlay development was creating overlay elements with thicknesses that would have significant stiffening effects on the steel specimens. Thickness of the overlay element affects the overall bending moment of inertia of the specimen around the fatigue-critical welds. As the thickness of the overlay increases, the overall moment of inertia increases giving the specimen increased stiffness, smaller deflections and lower stress demands in the area around the welds. Thicker CFRP overlays were created using a larger number of plies than generally used in

conventional CFRP composites. However, increasing the number of plies made it difficult to achieve good consolidation using standard vacuum pressure. Despite poor consolidation, the composite overlays showed a significant increase in specimen stiffness when compared to unreinforced control specimens. Kaan (2008) found that lack of adequate consolidation did have detrimental effects, however, as failure occurred in the specimens due to interlaminar cracking and delamination of the CFRP overlay and not to degradation of the bond between the overlay and the steel.

The CFRP overlay was redesigned with the goal of creating a resilient CFRP overlay that would restrain fatigue failure within the composite material itself and make bond strength between the overlay and the steel the controlling failure element. The initial CFRP overlay was fabricated using 36 plies of bidirectional woven carbon fiber fabric impregnated with a cyanoacrylite resin. The overlay was consolidated under vacuum pressure and heat and had an average dimensional thickness of 25.4 mm (1.00 in). In the redesign of the CFRP overlay, the molding pressure was increased and a heat press was used to apply the pressure and heat during the consolidation process. The number of carbon fiber plies was increased to 40 and an additional five boron fiber layers were added to prevent the carbon fiber fabric from migrating too far out of plane during consolidation. In addition, a resin film was incorporated in the set-up to supply additional resin in areas where voids could not be eliminated during the molding process. The new design produced CFRP overlays that were uniform in shape with very high levels of consolidation and an average dimensional thickness of 12.7 mm (0.50 in). Throughout fatigue tests performed on the redesigned CFRP overlays, no damage to the composite material occurred, thus achieving a resilient design for the double element itself.

### 11.5.2 Effect of overlay configuration on fatigue life

Research at the University of Kansas included an analytical parametric study performed with the intention of determining the optimum configuration for the CFRP overlay. In the study, finite element models were analyzed to investigate the significance of the geometric profile and length of the overlay, the modulus of elasticity of the overlay, and the presence of a gap in the direct vicinity of the weld. Figure 11.21 shows the different CFRP overlay configurations that were evaluated in the parametric study.

Alemdar (2010) found that the geometric profile and length of the overlay were insignificant parameters. Figure 11.22 shows that the curved and rectilinear CFRP overlay configurations were equally effective in reducing the stress demand at the weld toe. What was a significant parameter in reducing stress at the weld toe, however, was the presence of a gap between the weld and the CFRP overlay. The presence of a gap, investigated to

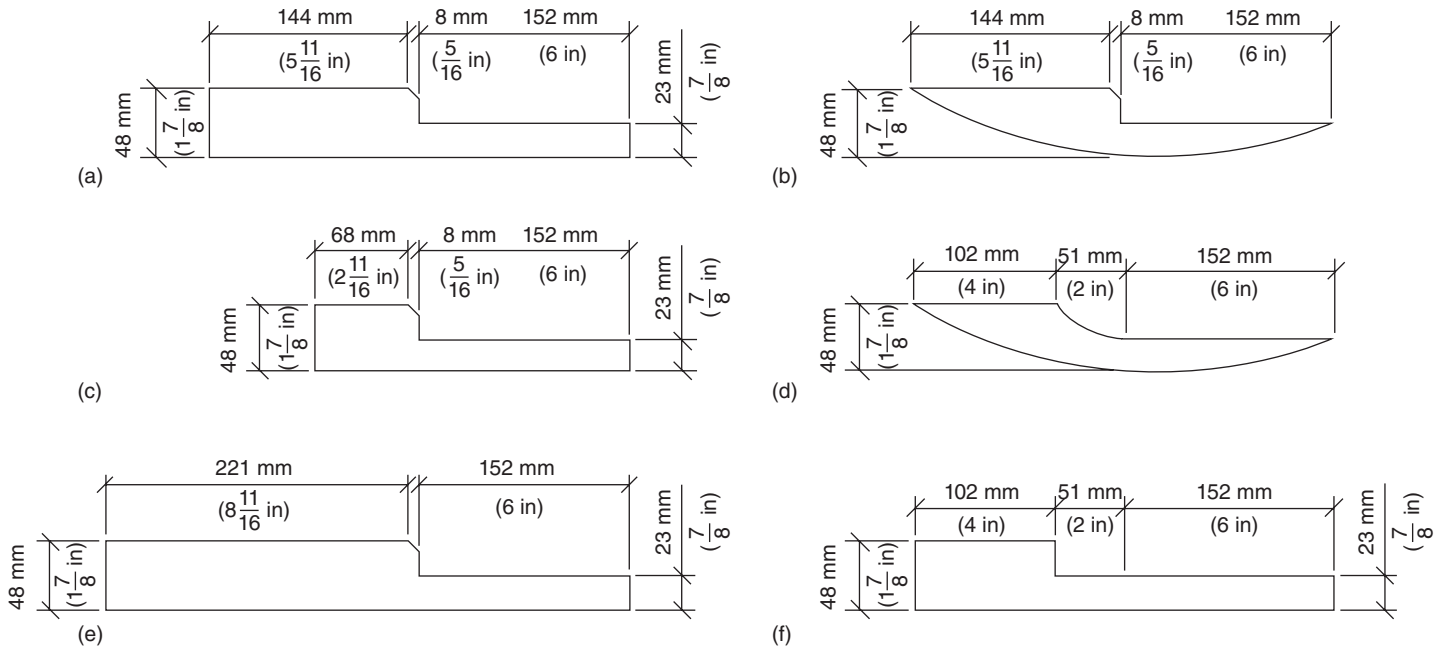


*11.21* Different configurations of CFRP overlay evaluated in the analytical model: (a) rectangular, standard; (b) curved without gap; (c) rectangular, short; (d) curved with gap; (e) rectangular, long; (f) rectangular with gap (Alemdar, 2010).

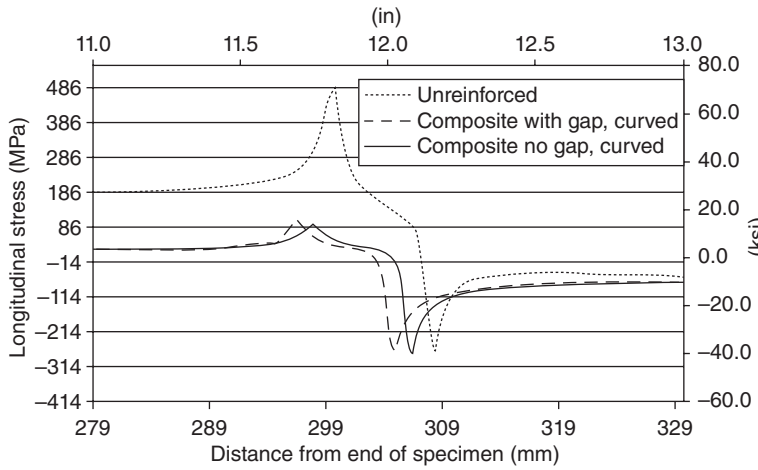


*11.22* Effect of composite overlay shape on longitudinal stresses in the area of the weld (Alemdar, 2010).

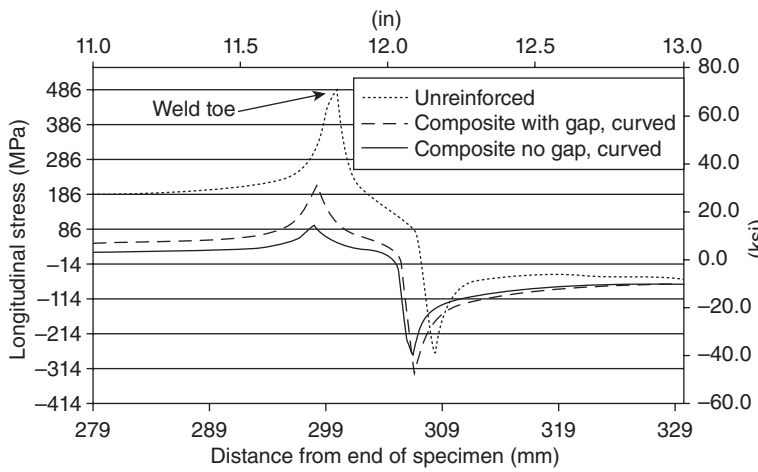


*11.23* Effect of the presence of a gap between the composite and the steel on longitudinal stresses in the area of the weld (Alemdar, 2010).

determine the effectiveness of the overlay and bond near the weld, negatively affected the reduction in peak stress at the weld toe. As shown in Fig. 11.23, the CFRP overlays with a gap had a significantly higher peak stress than did the overlays without a gap.

Figure 11.24 shows the results of a suite of FE analyses performed on the basis of studying the effect of the modulus of elasticity of the CFRP overlay. In the analyses, the modulus of elasticity of the CFRP overlay was varied

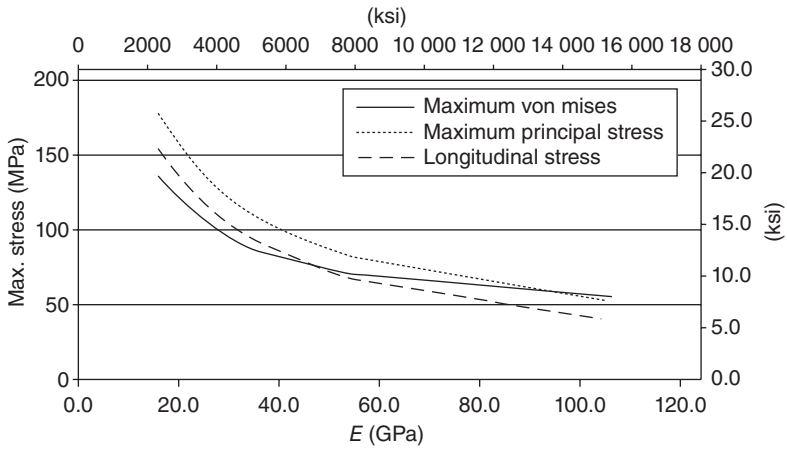


*11.24* Effect of composite overlay stiffness on maximum stress demand at the weld toe (Alemdar, 2010).

over a range of 60–400 % of the reference value, which was 26.6 GPa (3,860 ksi). As shown in Fig. 11.24, as the modulus of elasticity of the CFRP overlay was increased, diminishing returns on the reduction in stress occurred. This indicates that using stiffer, more expensive fibers may not be necessary to bring about a significant increase in fatigue life beyond that achievable by using conventional fibers.

### 11.5.3 Bond between composite overlays and metals

In the studies performed at the University of Kansas, the most critical factor in determining the level of effectiveness of CFRP overlays in enhancing the performance of welded connections was maintaining the bond between the overlay and the steel. Results by Alemdar (2010) and Kaan (2008) showed that effectiveness of the CFRP overlay was not governed by the configuration or fatigue life of the overlay, but by the bond between the overlay and the steel. Insufficiencies in the resin layer used to bond the CFRP to the steel led to debonding events during testing. Each time these debonding events occurred, the CFRP overlays had to be completely removed from the specimen and rebonded. Kaan (2008) showed through three point bend testing at a stress range of 137.9 MPa (20 ksi) that control steel specimens repaired with CFRP overlays were able to achieve 2.1 million cycles of loading without any observable fatigue crack. However, numerous debonding events occurred throughout testing after an average of 431 500 cycles. In addition to hindering greatly the number of loading cycles a CFRP repaired specimen can endure, these debonding events allowed the

specimens to cycle in an unreinforced state before being rebonded. In order to achieve infinite fatigue life, the issue of debonding needed to be addressed. For this reason, the University of Kansas performed a study focused on evaluating the effect of configuration parameters and fabrication techniques of the bond layer. The study included a combination of analytical studies of FE analysis models and experimental testing of three point bending specimens.

*Effect of the configuration of the interface layer*

The configuration of the bond layer was studied based on the following two parameters: the use of a breather cloth and the use of a resin pool. Breather cloth allows air and volatile gases to escape within the vacuum bag throughout the vacuum-bagging process. It is generally used to maintain a vacuum throughout the molding process of composite material. Breather cloth is also used for soaking up excess resin and reducing spillage and flow in the construction of composite materials. Initially, the breather cloth was used to keep the bonding resin in place while wet but, after improved performance of the bond with its addition, breather cloth was included in subsequent tests to investigate its effects on the interface layer.

FE analyses showed that peak tensile and shear stress demands occurred at the edge of the overlay. It was hypothesized that this location would be a trigger point for bond failure under fatigue loading. For this reason, experimental testing also included investigation of a resin pool that extended beyond the edge of the overlay.

Figure 11.25 shows the three point bending set-up used for the experimental program of the study. The assembly was subjected to cyclic loading until a crack initiated in the steel substrate, a bond failure occurred or a run-out threshold of 1.5 million cycles was met. This run-out threshold was chosen because it corresponded to expected infinite life for an AASHTO Category B detail subjected to a stress range of 138 MPa (20 ksi) (AASHTO, 2007). Hysol™ (Loctite™ 9412), a high grade resin epoxy, was used as the bonding agent. In the event of debonding, testing was stopped and the CFRP overlay was removed. The weld to which the overlay was bonded was inspected for cracks and, if none were present, the CFRP overlay was rebonded to the specimen and testing was resumed.

Figure 11.26 shows the effects of configuration of the interface layer on bond life. CPB0125 were specimens that included both a resin pool and a breather cloth, CP0125 were specimens that included a resin pool but not a breather cloth, and C0125 were specimens that had neither a resin pool nor a breather cloth. As Fig. 11.26 shows, the addition of a resin pool provided a significant improvement in bond life. While one C0125 specimen did outperform the CP0125 group, the average fatigue life for C0125

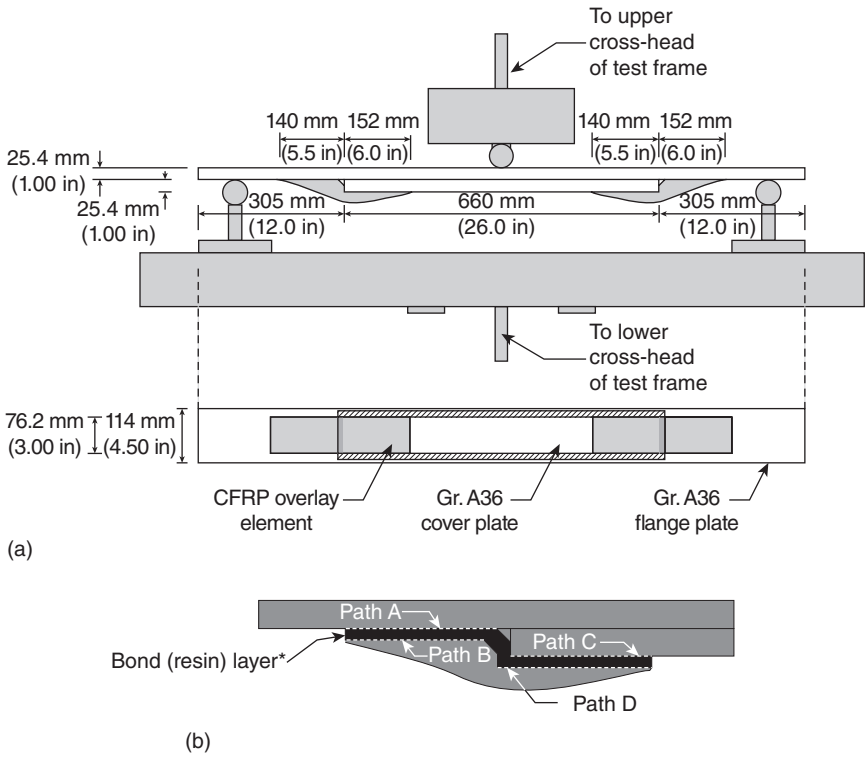


*11.25* (a) Schematic of three point bending fixture with CFRP-stiffened specimen. (b) Detail of CFRP–resin–steel bond interface. *Exaggerated scale to show detail in bond layer (Kaan *et al.*, 2012).

specimens was significantly less than CP0125 specimens. Additionally, Fig. 11.26 shows that the best performance resulted from specimens that included both a resin pool and a breather cloth.

*Effect of the thickness of the interface layer*

Six different bond layer thicknesses of 0.3 mm (0.01 in), 0.8 mm (0.03 in), 1.3 mm (0.05 in),1.7 mm (0.07 in), 2.5 mm (0.10 in) and 3.2 mm (0.13 in) were investigated analytically using FE analysis models. Stress demands between the steel and the interface layer and the CFRP overlay and the interface layer were evaluated by extracting the shear and tensile stresses along the paths in the interface shown in Fig. 11.25b. As Fig. 11.27 shows, increasing the thickness of the resin layer resulted in a small reduction on the maximum stress demand at the weld toe, which was located approximately 300 mm (11.8 in) from the end of the specimen. In addition, Fig. 11.27 shows that at the location of the weld, greater resin layer thicknesses produced higher

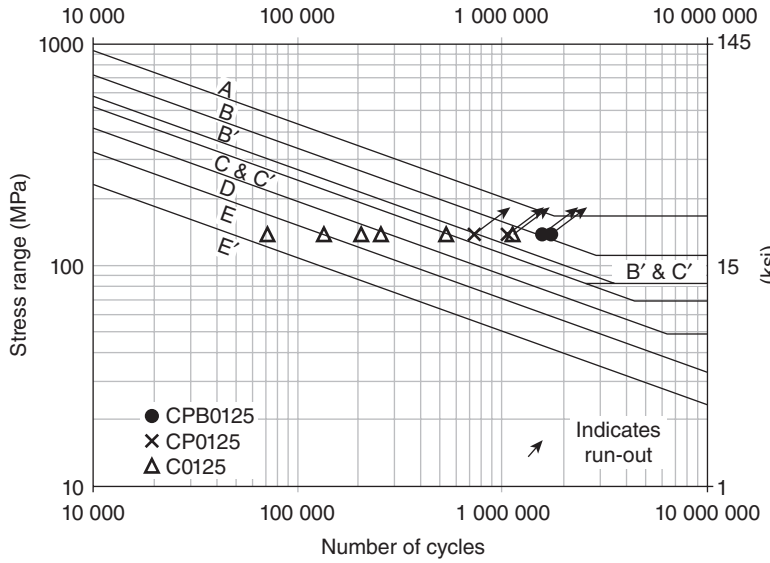


*11.26* *S–N* diagram of fatigue test results for test trials with a bond layer thickness of 3.2 mm ($\frac{1}{8}$ in) (Kaan *et al.*, 2012).

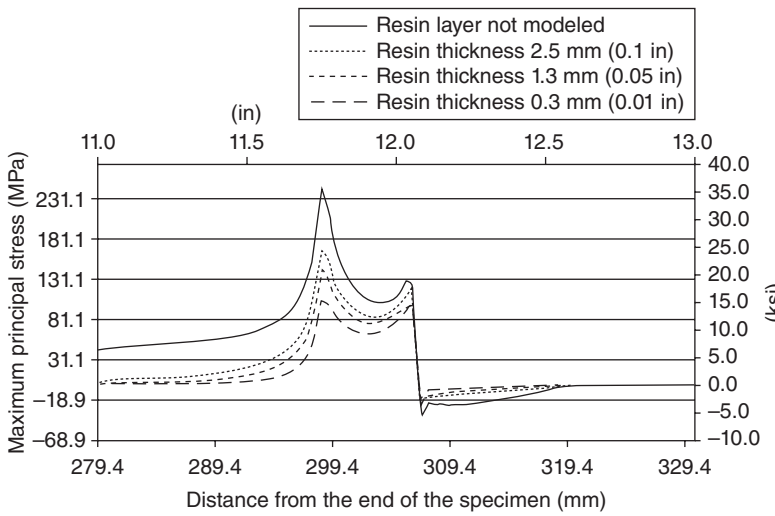


*11.27* Maximum principal stress on the steel plate in the area of the weld (Kaan *et al.*, 2012).

calculated stress demands, which indicated that the CFRP overlay becomes less effective in increasing fatigue life as the resin layer thickness increases.

Another important consideration developed from the FE analysis was the effect of resin layer thickness on peel and shear stresses at the interface. These stress demands provide useful information on the bond strength under fatigue loading. Results showed that for both shear and peel stress, the maximum stress demand in the bond layer decreased as the resin layer thickness increased. However, results also showed that stresses in the steel increased as the thickness of the resin layer increased. This indicated that, as the resin layer becomes thicker, more load is transferred through the steel. Thus, the findings of the FE analyses showed that increased resin layer thicknesses would increase bond tenacity, but that some stiffening capability would be sacrificed.

In light of the findings of the FE analyses, the goal of experimental testing of the thickness of the interface layer was to determine an optimal bond thickness. An optimal thickness would provide enough stiffness to the specimen to increase the life of fatigue-vulnerable welds while still minimizing shear stress at the interface layer to prevent debonding of the CFRP overlays from the steel substrate. Experimental results contradicted the analytical investigation; fatigue performance was not found to be affected by increasing bond layer thickness. During the experimental testing described previously, Kaan *et al*. (2012) found that for bond layers as thick as 6.4 mm (0.25 in), the effectiveness of the CFRP overlay was not reduced as long as breather cloth was incorporated into the resin bond.

Figure 11.28 shows the results from specimens tested with various bond layer thicknesses without a resin pool and without a breather cloth. The trials designated as C0030 and C0125 had bond layer thicknesses of 0.8 mm (0.03 in) and 3.2 mm (0.13 in), respectively. As shown in Fig. 11.28, there was no discernible effect of layer thickness on bond life. It is clear from Fig. 11.27 and Fig. 11.28 that the presence of a breather cloth or a resin pool had a much greater effect on the bond life of the resin layer than did the thickness of the resin layer. The experimental results showed that a resin layer with a thickness of 6.4 mm (0.25 in) and a breather cloth provided the best balance of stiffness and bond tenacity. Therefore, when breather cloths are present to maintain bonding, an optimal interface layer thickness can be based on fatigue performance without concern for how the resin thickness will affect the bond strength.

## 11.6 Repair of fatigue damage due to out-of-plane forces

For the successful use of composite materials to prevent or repair fatigue damage due to out-of-plane forces, two important challenges must be

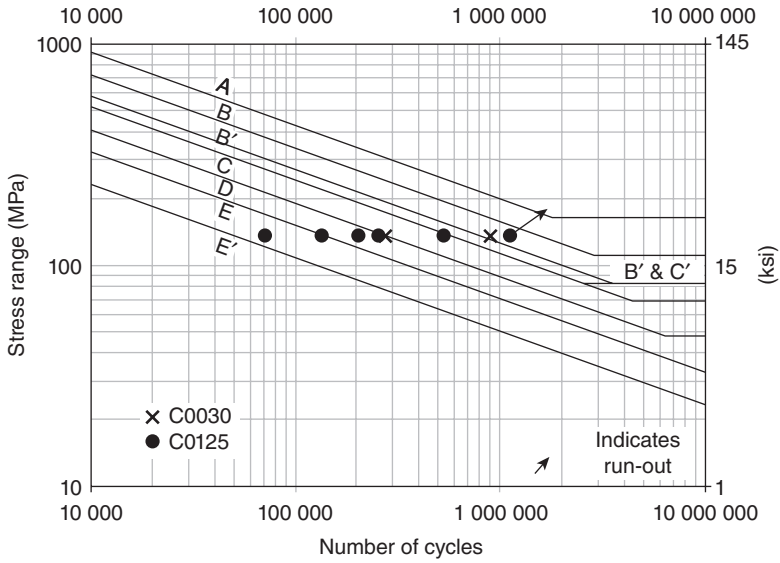


*11.28* *S–N* diagram of fatigue test results for specimens without a resin pool and without breather cloth.

overcome. The first is identifying a suitable configuration for the composite overlay that creates a significant reduction in the stress demand, and the second is to attach the composite overlay so that bond between the composite material and the damaged metal is maintained for infinite fatigue life.

The task of identifying a suitable overlay configuration is specific to the fatigue problem being addressed. A common problem in which fatigue damage is caused by out-of-plane forces is distortion-induced fatigue damage of plate girders in steel bridges. This problem, described in Section 11.1.3, is most often observed in girder webs, between transversely welded structural components (floor beams, diaphragms or cross-frames) and an adjacent flange (Fisher, 1984) of steel bridge plate girders. It is caused by out-of-plane forces imposed by cross-frame elements on bridge girders as a result of differential caused by passing trucks.

Fatigue damage occurs in the web-gap region of the girder, shown in Fig. 11.29 and Fig. 11.30, which is a flexible area of the plate girder subjected to significant out-of-plane deformations caused by the cross-frame forces. Studies (Gangel, 2011) have shown that within this web-gap region there are three types of cracks that are most commonly found. They are: (i) a horizontal crack oriented parallel to the web-to-flange weld along the weld toe, designated as Type 1; (ii) a horseshoe-shaped crack originating in the web-gap region and propagating outward into the web, designated as Type

*11.29* Fatigue crack in the bottom web-gap region of a steel bridge girder due to out-of-plane deformation induced by a cross-frame.

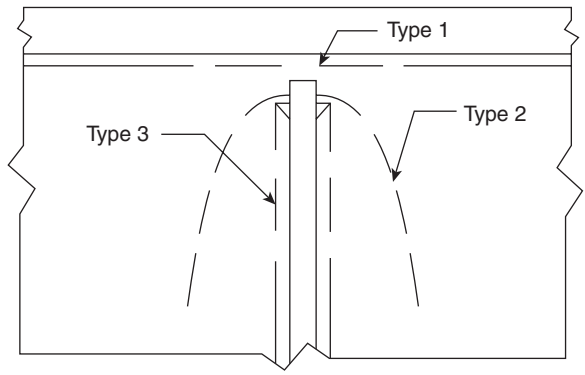


*11.30* Typical fatigue crack locations and types.

2; and (iii) a vertical crack originating in the web-gap region following the weld toe of the stiffener-to-web weld, designated as Type 3 (Fisher, 1984). The crack type designations, shown in Fig. 11.30, will be used throughout this chapter.

A case study of a Kansas Department of Transportation (KDOT) bridge constructed in 1977 found cracks of Type 1 and 2 in the web-gap adjacent to the top flange in positive and negative flexure (Roddis and Zhao, 2001). Cracking near the top flange was attributed to the composite action of the slab, which restrains rotation in the top flange of the girder but not in the bottom flange. The bridge studied was a two-girder non-skewed bridge (Roddis and Zhao, 2001). Two other non-skewed bridges evaluated for

fatigue damage, the Belle Fourche River Bridge and Chamberlin Bridge over the Missouri river (Fisher, 1984), also had the majority of fatigue damage occur in the positive moment region, in the web-gap adjacent to the compression flange. The fatigue cracks were recorded as through-thickness cracks (Fisher, 1984).

Type 2 cracks have also been found to propagate deep into the web of steel girder bridges, as was observed in a Maryland highway bridge investigated by Zhou and Biegalski (2010). This skewed continuous steel girder bridge had web fractures initiating near the tension flange and extending the entire depth of the web. Fatigue cracks of this magnitude are not common, but do occur and pose a serious threat to the structural integrity of a bridge. Because Type 1, 2 and 3 cracks experience openings due to out-of-plane motion of the connection stiffener, a successful repair must restrain the out-of-plane motion of the stiffener and provide an alternate load path between the connection stiffener and the flange of the girder.

### 11.6.1 Suitable configurations for repair of fatigue damage due to out-of-plane loading

A study by Adams (2009) evaluated the effectiveness of multiple CFRP overlay configurations in reducing the stress demand at the critical locations of the web-gap region. The initial concept for the retrofit configurations evaluated by Adams (2009) came from the combination of two established retrofits. The first retrofit provides new connectivity between the connection plate and the girder flange to decrease the stress demand. The second retrofit, developed at the University of Kansas by Kaan (2008), uses CFRP overlays to create an alternative load path to reduce the magnitude of stress at the weld toe of a partial length cover plate shown in Fig. 11.31. The combination of these two ideas led to the CFRP shapes shown in Figs 11.32 through 11.37. Adams (2009) performed a parametric study assuming perfect bond between the composite overlay, the connection plate, the girder web and the flange of the girder.

The first retrofit configuration (shown in Fig. 11.32) used CFRP (various elastic moduli were evaluated) on both sides of the connection plate. It is

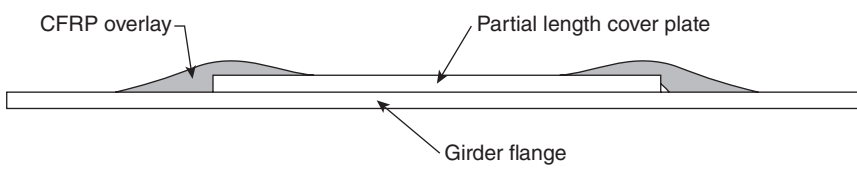


*11.31* Partial length cover plate retrofit – CFRP overlay (Kaan, 2008).

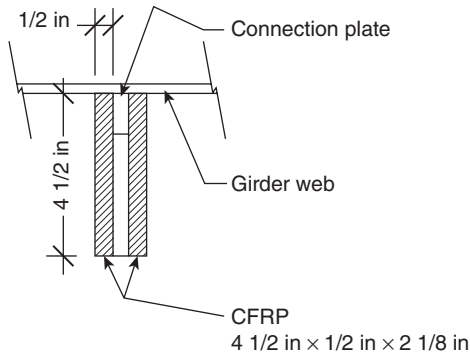


*11.32* CFRP retrofit A – 13 mm ($\frac{1}{2}$ in) thick composite overlays (plan view).

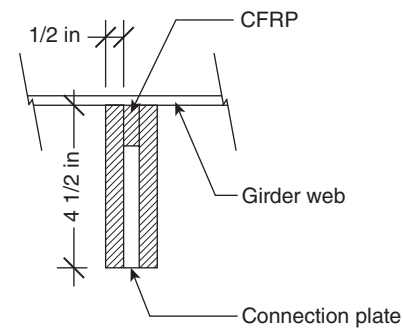


*11.33* CFRP retrofit A – 13 mm ($\frac{1}{2}$ in) thick composite gap filled (plan view).

important to note that this configuration did not include placement of composite material in the web-gap region above the connection plate.

The second retrofit configuration (shown in Fig. 11.33) is very similar to the configuration shown in Fig. 11.32. The only difference is that the second configuration utilized composite material above the connection plate in the web-gap region.

The third retrofit configuration (Fig. 11.34) was also a variation of the configuration shown in Fig. 11.32. This configuration, however, was twice as thick and also did not include composite material above the connection plate in the web-gap region.

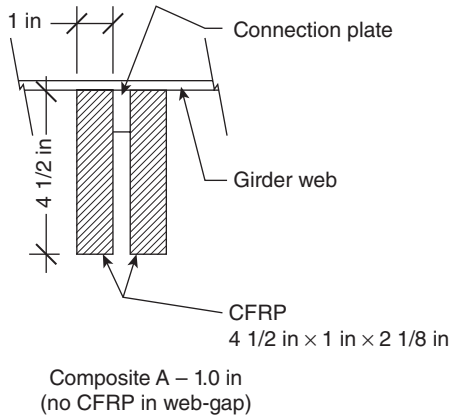


*11.34* CFRP retrofit A – 25 mm (1 in) thick composite (plan view).

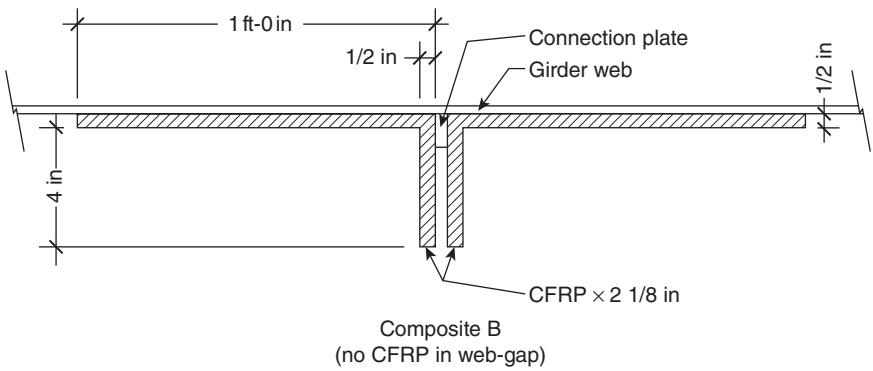


*11.35* CFRP L-shaped retrofit B (plan view).

The fourth retrofit configuration studied was also a variation of the first retrofit shown in Fig. 11.32. This retrofit involved using a 3.2 mm ($\frac{1}{8}$ in) resin layer between the composite and all contacted steel surfaces. The resin layer had material properties of a modulus of elasticity of 3450 mPa (500 ksi) with a Poisson's ratio of 0.1. It was important to model a resin layer to investigate whether a bond layer between the composite and the steel affected the results.

A different retrofit shape was used in the fifth configuration (Fig. 11.35), in which an L-shape was used to see if this has an effect on the magnitude of web-gap stress. This shape had a thickness of 13 mm ($\frac{1}{2}$ in) and extended for a length of 30.5 cm (1 ft) on each side of the connection plate. No composite materials were utilized above the connection plate in the web-gap region.

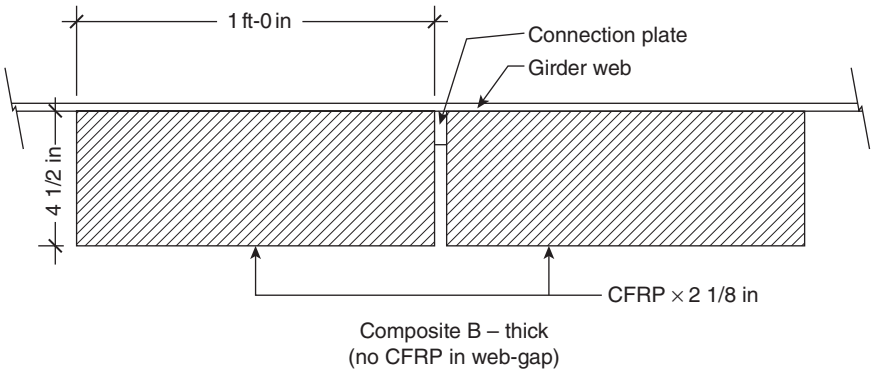


*11.36* CFRP retrofit B – thick (plan view).

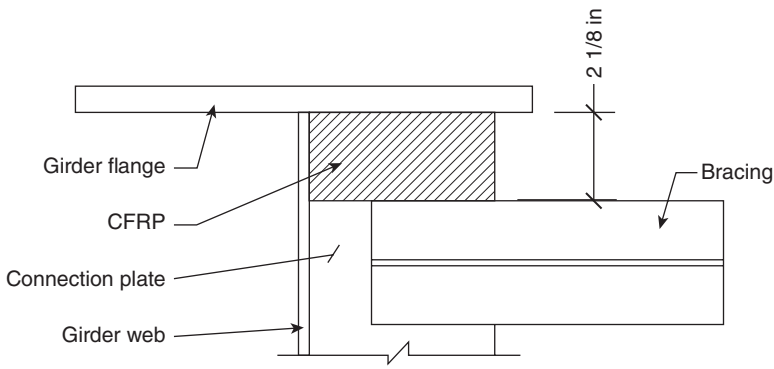


*11.37* Section view of all CFRP retrofits.

The sixth and final retrofit configuration (Fig. 11.36) was a modified version of the scheme shown in Fig. 11.35, except the L-shape was thickened so that a large piece of composite material existed on both sides of the connection plate. Again, composite material was not used above the connection plate in the web-gap region.

All of the above retrofitting schemes had the same length along the connection plate [54 mm ($2\frac{1}{8}$ in)]. The controlling factor on the length of these CFRP materials was the location of the cross-frames; the composite materials were discontinued at the location of the cross-frame as shown in Fig. 11.37.

Stress demands at the critical location of FE models with retrofit schemes using composite materials were compared with results from FE models of established retrofit methods (slot repair and positive attachment repair) and the non-retrofitted web-gap details. The path shown in Fig. 11.38 along with the non-retrofitted connection plate (Fig. 11.39) and retrofitted

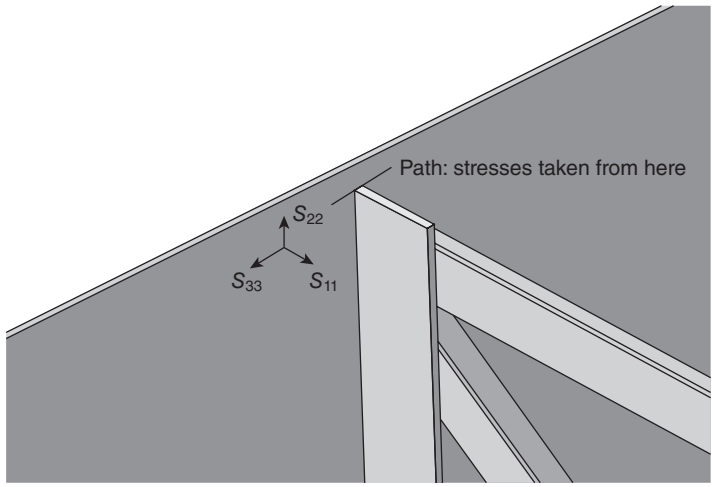


*11.38* Stress directions for analysis.

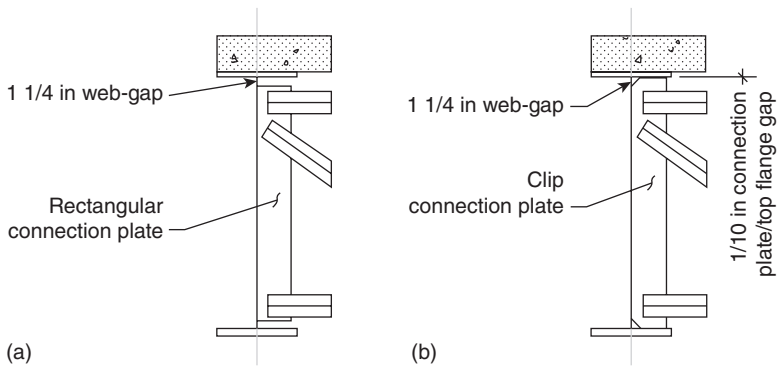


*11.39* As-is (non-retrofitted) connection plate geometry.

connection plate (Fig. 11.40) were modeled to asymptotic convergence. The maximum principal stress demand for the various configurations is shown in Fig. 11.41. The stress demands shown in Fig. 11.41 were extracted along the path shown in Fig. 11.38.

The following notation is used in Fig. 11.41 to describe the non-retrofitted and retrofitted transverse stiffener web-gap details.

- *Non-retrofitted – rect*: a rectangular connection plate was used with a 31.8 mm ($1\frac{1}{4}$ in) web-gap as shown in Fig. 11.39a.
- *Non-retrofitted – clip*: a clip connection plate with a 31.8 mm ($1\frac{1}{4}$ in) web-gap was used as shown in Fig. 11.39b.

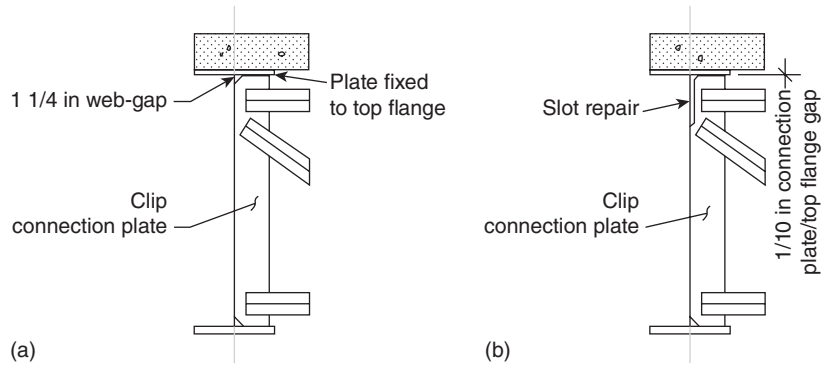


*11.40* Retrofitted schemes connection plate geometry.

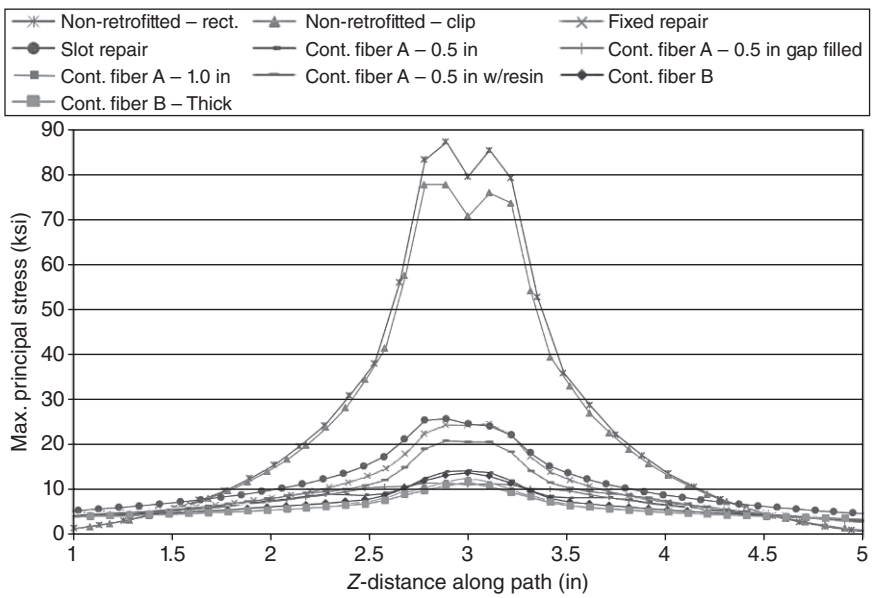


*11.41* Maximum principal stress – continuous fiber retrofit results.

- *Fixed repair*: the clip connection plate was rigidly connected to the top flange as shown in Fig. 11.40a.
- *Slot repair*: a slot was created in the clip connection plate to soften the connection as shown in Fig. 11.40b.
- *Carbon fiber A – 0.5 in*: FRP retrofits with a thickness of 12.7 mm ($\frac{1}{2}$ in) on both sides of the clip connection plate were used as shown in Fig. 11.32.

- *Carbon fiber A – 0.5 in gap filled*: FRP retrofits with a thickness of 12.7 mm ($\frac{1}{2}$ in ) on both sides of the clip connection plate were used. Also, the gap between the connection plate and top flange was filled with composite as shown in Fig. 11.33.
- *Carbon fiber A – 1.0 in*: FRP retrofits with a thickness of 25.4 mm (1 in) on both sides of the clip connection plate were used as shown in Fig. 11.34.
- *Cont. fiber A – 0.5 in w/ resin*: FRP retrofit with a thickness of 12.7 mm ($\frac{1}{2}$ in) including a 3.2 mm ($\frac{1}{8}$ in) resin layer between the composite and all steel surfaces was used.
- *Carbon fiber B*: FRP retrofits in an 'L' shape were used on both sides of the clip connection plate as shown in Fig. 11.35.
- *Carbon fiber B – thick*: FRP retrofits of the thickened 'L' shape were used on both sides of the clip connection plate as shown in Fig. 11.36.

From the stress paths shown in Fig. 11.41, it can be observed that the FRP retrofits reduced the magnitude of web-gap stress more than the slot and positive attachment repairs. The FRP retrofits reduced the magnitude of HSS from approximately 397 MPa (55 ksi) for the non-retrofitted detail to approximately 69 MPa (10 ksi). The analyses showed that the FRP configurations evaluated performed better than the slot and positive attachment repairs by approximately 41–69 MPa (6–10 ksi). The retrofit configuration with the resin layer performed slightly better than the slot and positive attachment repairs. Adams (2009) concluded that, based on his FE studies, the FRP overlay retrofits had the potential to be more effective than commonly-used methods to reduce the stress demand at the web-gap.

### 11.6.2 Preventing debonding of the composite overlay

While the analyses carried out by Adams (2009) showed that the use of composite overlays had the potential to be effective in the repair of fatigue damage, experimental studies by Kaan (2008), Kaan *et al*. (2012), Alemdar *et al.* (2009) showed that maintaining bond between the overlay and the metal is essential for this type of repair. Furthermore, the work by Kaan and Alemdar showed that preventing debonding is significantly more difficult when there are peel stresses at the interface between the composite and the metal than when the interface is loaded primarily in shear. Because of the nature of the loads, repairs to out-of-plane loading are likely to impose peel stresses along the composite–metal interface, making the bond between the composite and the metal a critical aspect for this type of application.

Two different alternatives to maintain bond for a number of cycles equal to infinite fatigue life were explored by researchers at the University of

Kansas. The first technique consisted of placing the composite overlay between the girder web and a steel plate, bolted together with tensioned bolts. This type of repair was evaluated using FE analyses by Gangel (2011) for girders with very severe fatigue damage, for configurations with and without composite overlay. The models evaluated by Gangel had pre-existing fatigue cracks simulated using the extended FE method (Simulia, 2011) and utilized a girder geometry as shown in Fig. 11.42.

The first repair evaluated by Gangel (2011) consisted of attaching 13 mm ($\frac{1}{2}$ in) thick steel splice plates along the full depth of the girder shown in Fig. 11.43. This retrofit did not include composite materials and was utilized

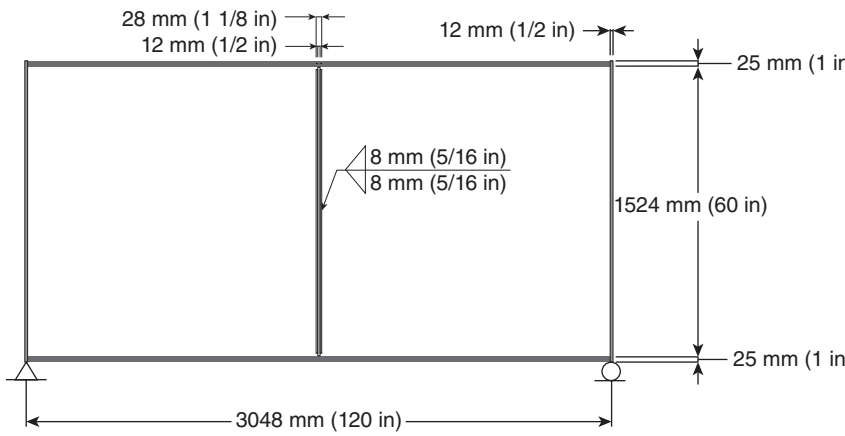


*11.42* Geometry of the girder section modeled by Gangel (2011).

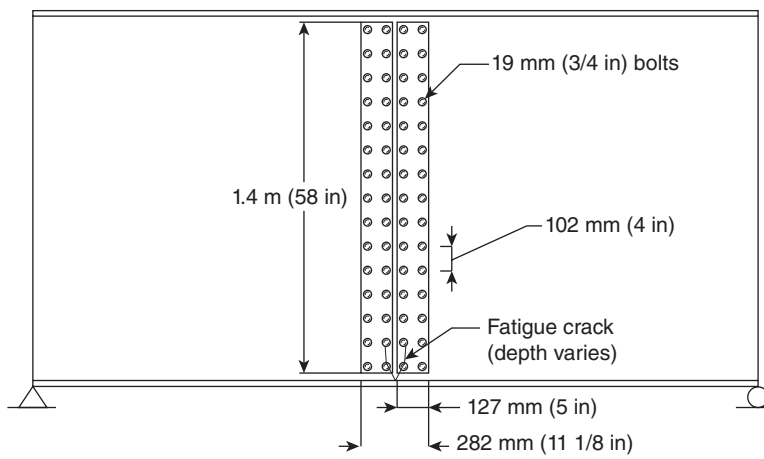


*11.43* Full-depth splice plate fatigue damage repair.

as a baseline. Because crack-stop holes are an accepted and widely used fatigue repair technique, the model included the simulation of a 19 mm ($\frac{3}{4}$ in) crack-stop hole in the web at each tip of the fatigue crack. Two splice plates measuring 127 × 1473 mm (5.0 by 58.0 in) were attached to the interior side of the web, one on each side of the stiffener.

Because there was no transverse stiffener on the opposite side of the web, a single splice plate measuring 283 × 1473 mm (11.1 × 58.0 in) was attached there. Each splice plate was terminated at a distance of 25 mm (1.0 in) from the adjacent flange to prevent the splice plate from restraining the motion of the flange. Splice plates were attached using high strength 19 mm ($\frac{3}{4}$ in) tensioned bolts spaced at 102 mm (4.0 in). Each bolt was tensioned to 125 kN (28 kip) following the stipulations in AASHTO Table 6.13.2.8-1 (AASHTO, 2010). When attached to the web, the steel splice plates completely covered all the fatigue damage, except for the initiation site. They also covered the area where any further crack propagation would occur, making inspection impossible without removal and reattachment of the repair.

The FRP repair assemblage evaluated in the study by Gangel was intended to be representative of fabrication methods under field conditions. As with the full-depth steel splice plate repair, the FRP repair system included the simulation of a 19 mm ($\frac{3}{4}$ in) crack-stop hole in the web at each tip of the fatigue crack. The assemblage then consisted of a 6 mm ($\frac{1}{4}$ in) thick FRP overlay adhesively bonded to the web. A 13 mm ($\frac{1}{4}$ in) steel cover plate covering the FRP overlay was bolted to the web to provide a uniform compression force on the overlay and prevent debonding under cyclic loading. 19 mm ($\frac{3}{4}$ in) bolts were used to bolt the steel cover plate. Each bolt was simulated to have a tension force of 125 kN (28 kip), following the stipulations in AASHTO Table 6.13.2.8-1 (AASHTO, 2010). A 13 mm ($\frac{1}{2}$ in) thick cover plate was chosen because it was considered sufficiently thick to evenly distribute the force from the tensioned bolts without damaging the FRP overlays. A very thin steel cover plate could result in an uneven distribution of the bolt force, damaging the FRP layer and greatly decreasing the effectiveness of the repair. The adhesive bond layer between the steel and FRP overlay was estimated to have a thickness of 0.6 mm (25 mil).

Dimensions of both the FRP overlay and steel cover plate (Figs 11.44–11.46) were chosen as 127 × 267 mm (5.0 × 10.5 in). A repair system of this size would cover a large portion of the damaged web and the region with the highest stress demand. If for any reason the repair would not perform adequately and allowed crack reinitiation to occur, this type of repair would allow increased fatigue damage to be detected during inspection. A repair of this size was placed on each side of the welded stiffener on the interior face of the web. On the opposite side of the web, the repair system consisted

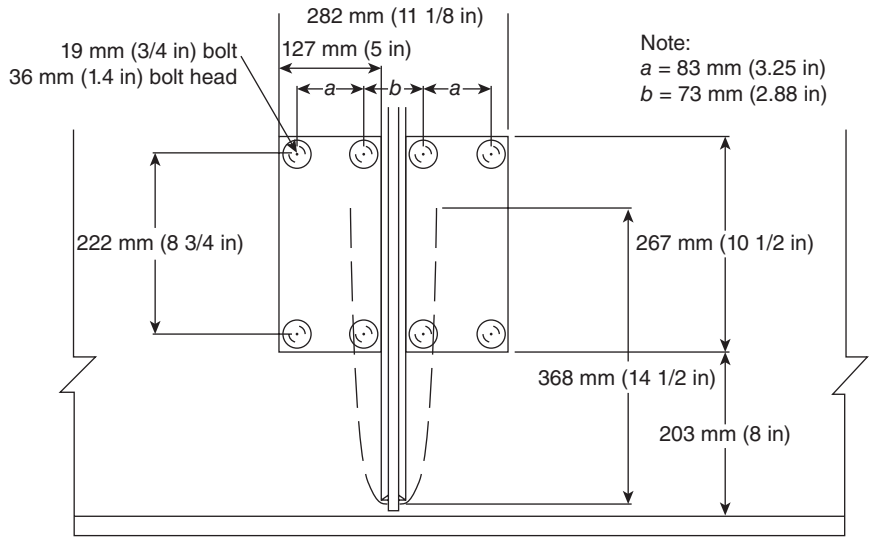


*11.44* Repair dimensions for crack length equal to 1/4 of the web depth.

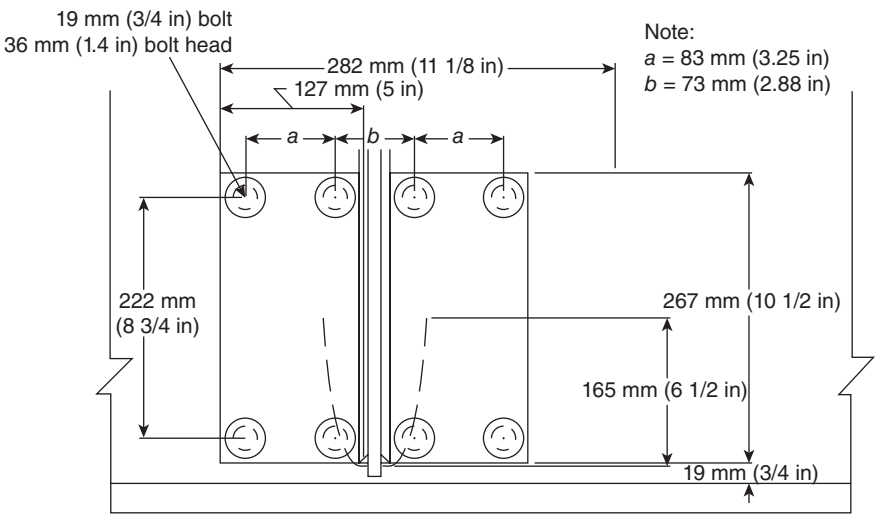


*11.45* Repair dimensions for crack length equal to 1/8 of the web depth.

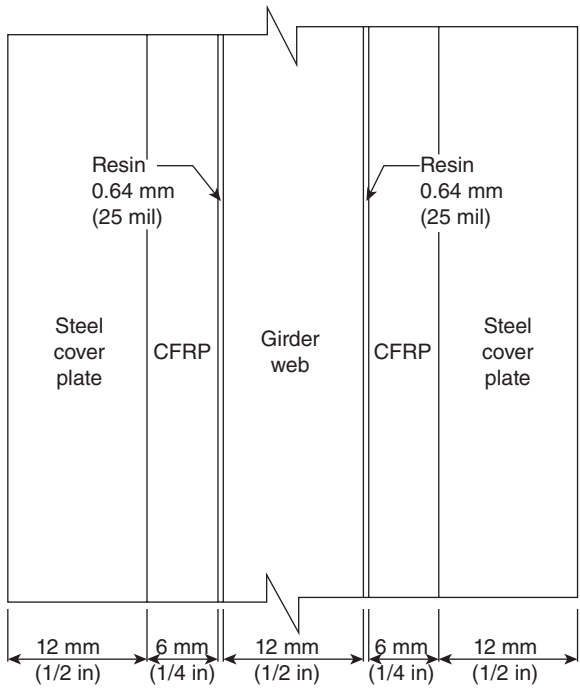


*11.46* Cross-section of CFRP repair.

of a single FRP overlay and cover plate with dimensions of 267 × 283 mm (10.5 × 11.1 in).

Repairing the girder web with full-depth steel splice plates was effective in reducing the stress demands on both sides of the web. Effectiveness of this repair method also increased as the crack length was increased from 1/8 of the depth of the web to 1/4 of the depth of the web. Reductions in stress demand for the model with the shorter crack length were 56 % and 78 % on the interior and fascia side of the web, respectively. When the crack length was increased to one-quarter of the depth of the web, larger reductions in stress demand of 77 % and 89 % on the interior and fascia side of the web, respectively, were observed. Reductions in stress demands of this magnitude are a positive indicator that the potential for crack reinitiation is greatly reduced if this repair method is implemented.

### 11.6.3 Evaluation of carbon fiber-reinforced polymer (CFRP) overlay and steel plate retrofit measure

The use of adhesively bonded CFRP overlays in combination with a 19 mm ($\frac{3}{4}$ in) crack-stop hole and bolted steel cover plates showed drastic reductions

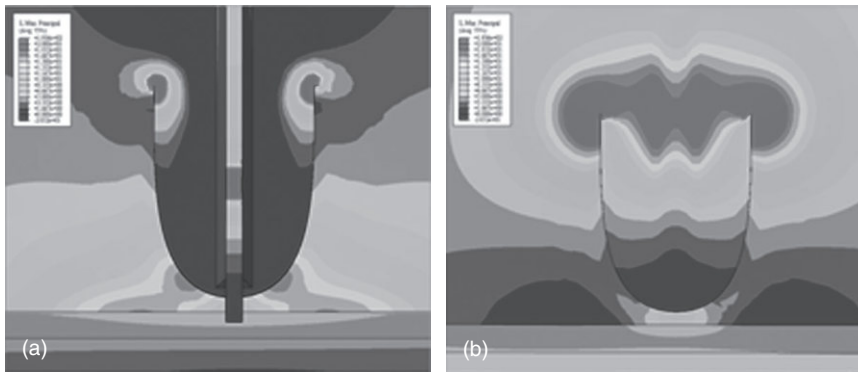


*11.47* Maximum principal tension stresses in unrepaired models: (i) no retrofit – interior; (b) no retrofit – fascia.

in stress in the cracked region of the web when compared with simulation results from unretrofitted models (Fig. 11.47), models repaired with crack-stop holes (Fig. 11.48) and models repaired with full-depth splice plates (Fig. 11.49).

With a crack length equal to 1/8 of the depth of the web, the introduction of the CFRP steel plate repair measure decreased the stress demand by 83 % and 92 % on the interior and fascia sides of the web, respectively (Fig. 11.50). Of all the repair methods evaluated, this was the only one that produced a significant decrease in the stress demand near the web-to-flange weld. Simulating the presence of a resin layer between the steel web and the CFRP layer was shown to be effective in transferring the high stress demands in the web-gap to the CFRP and the steel plate. Bonding the CFRP layer had the effect of distributing the stress over the entire area covered by the repair, eliminating the presence of small regions with highly concentrated stress demands. This smoothing effect is the main benefit of this retrofit measure with respect to the others discussed.

The FE model with a crack length 1/4 the depth of the web and the CFRP repair also showed positive results. The stress demand at near the tip of the web crack decreased by 95 % and 96 % on the interior and fascia side of the web, respectively. The reduction in the stress demand near the web-to-flange weld was not as significant as in the case of the shorter crack configuration because the CFRP overlay and steel plates only covered approximately 50 % of the length of the horseshoe-shaped crack. These results suggest that the effective crack length, defined as the length of crack not covered by the retrofit measure, seems to be a driving factor in the magnitude of the reduction in the stress near the flange. For this reason, an additional CFRP retrofit configuration was evaluated for the model with

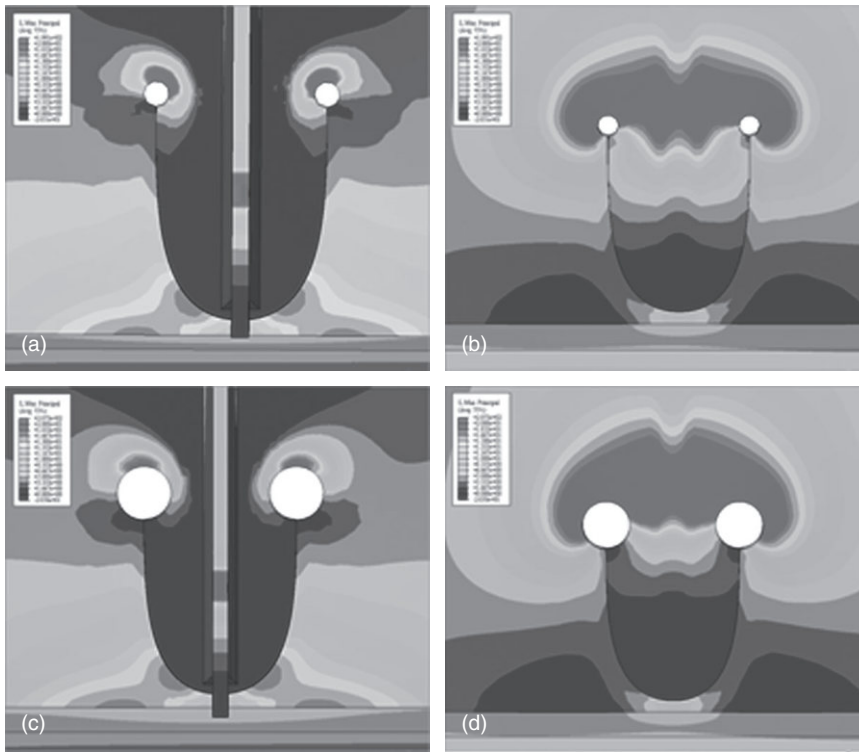


*11.48* Maximum principal tension stresses in models repaired with crack-stop holes (CSH) under combined loading conditions: (a) 19 mm (0.75 in) CSH – interior; (b) 19 mm (0.75 in) CSH – fascia; (c) 51 mm (2.0 in) CSH – interior; (d) 51 mm (2.0 in) CSH – fascia.

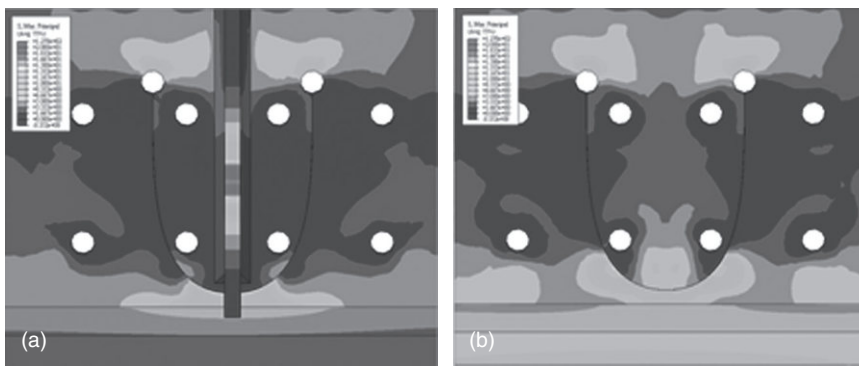


*11.49* Maximum principal tension stresses in models repaired with full-depth steel splice plate: (a) full-depth splice plate – interior; (b) full-depth splice plate – fascia.

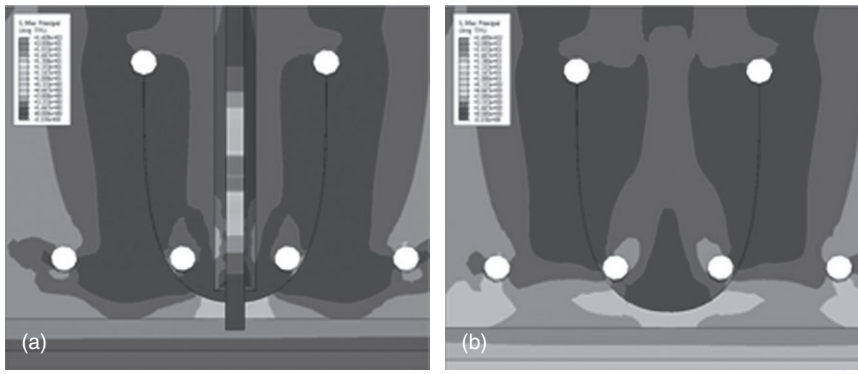


*11.50* Maximum principal tension stresses in model repaired with CFRP: (a) CFRP retrofit system – interior; (b) CFRP retrofit system – fascia.

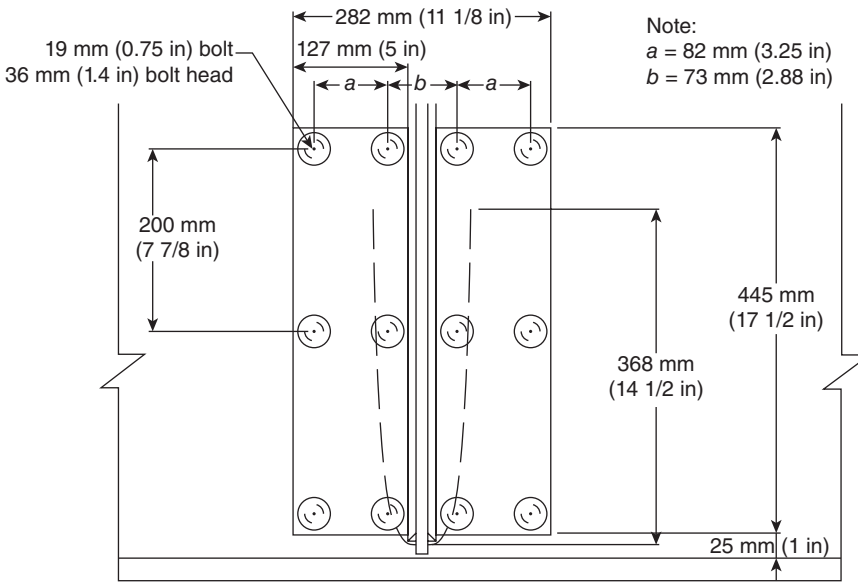


*11.51* CFRP repair measure with increased length of repair.

the longer crack (1/4 depth) so that the CFRP and steel plates covered the majority of the crack. In this extended configuration, shown in Fig. 11.51, the length of all layers of the retrofit assemblage was increased from 267 mm (10.5 in) to 444 mm (17.5 in).

The increased dimensions of this retrofit measure made the effective crack length approximately equal for the two crack configurations evaluated. A comparison between the calculated stress demands for the models with

a crack length equal to 1/4 of the depth of the girder showed that stress demand near the flange on the interior side of the web was 43 % lower for the configuration with the shorter overlays and 61 % lower for the configuration with the longer overlays. On the fascia of the web, the reductions in the stress demand near the flange were 7 % for the model with the shorter overlays and 33 % for the model with the longer overlays. These results are consistent with the results from the models with the full-depth splice plate repair in that if the effective crack length was kept approximately constant, the effectiveness of the repair increased as the crack length increased. The decrease in stress demand produced by each retrofit method is shown in Fig. 11.52.

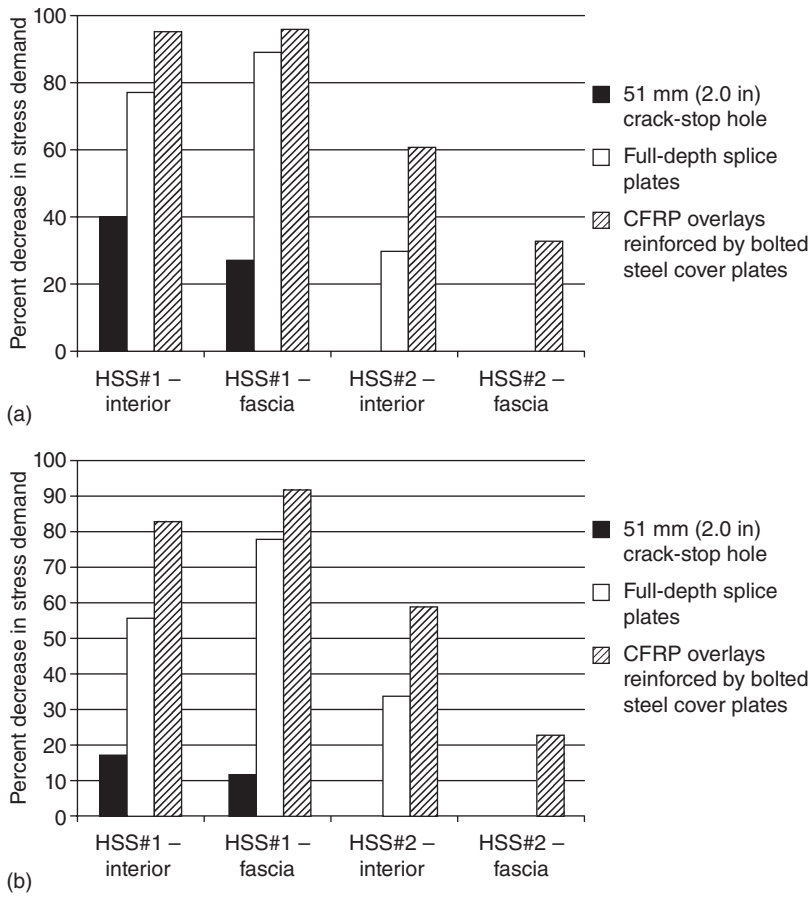


*11.52* Comparison of decrease in stress demand for model with crack length equal to (a) 1/4 the depth of the web and (b) 1/8 the depth of the web.

In the computational study carried out by Gangel (2011) the modulus of elasticity of the CFRP was varied as a parameter because previous research has shown that the stiffness of the CFRP may have a significant effect on the effectiveness of the repair (Alemdar, 2011). For the range of elastic moduli and overlay thickness evaluated in this study, it was found that changes in the modulus of elasticity of the CFRP did not have a significant effect on the stress demand. This behavior can be attributed to the fact that the layer of CFRP was relatively thin compared with the thickness of the web and the steel cover plates, causing the stiffness of the repair to be dominated by the steel.

The increased effectiveness of the CFRP repair with respect to the bolted splice plate repair can be attributed to the bond provided by the layer of resin used to attach the CFRP overlay to the web. This layer introduces an alternate load path which allows stresses to transfer between the two sides of the fatigue crack through shear. If bond is lost between the web and the CFRP overlay at localized areas of high peel or shear stress demand, the repair is designed to remain effective due to the effect of the tensioned bolts, which are intended to limit the amount of debonding. Although the compression force is likely to keep the overlay in place, it is also possible that the effectiveness of the repair could decrease as a consequence of partial debonding of the overlay. This type of behavior is very difficult to evaluate through computer simulations and should be quantified through physical simulations.

Within the resin layer, the highest shear stress demand in the vertical direction was found to take place at the corner adjacent to the bottom flange and opposite the connection stiffener, where the greatest geometric discontinuity occurs. In the horizontal direction, the largest shear stress demands were found to follow the path of the existing fatigue where the relative motion between the two faces of the fatigue crack is restrained by the repair. Further analytical and physical testing is needed to determine if the shear stress demand at the critical locations in the resin layer is high enough to cause debonding of the CFRP. As previously discussed, the compressive stress imposed by the bolts is intended to limit the potential for debonding of the CFRP overlay. Another measure that could reduce the potential for debonding is the fabrication of resin pools extending beyond the edges of the CFRP overlays, which would allow a more gradual transition of stresses by staggering the geometric discontinuities induced by the edge of the overlay and the edge of the resin layer. This technique was shown to drastically increase the number of cycles prior to debonding in three point bending tests (Kaan *et al.*, 2012).

A second method to prevent debonding of the composite overlay has been evaluated experimentally at the University of Kansas. In this case, bolts were pre-attached to the girder web and the connection stiffener, and

a composite block with glass fibers was cast in place. After casting of the composite block, the bolts were tightened so they would exert a compression force at the interfaces between the composite block and the girder web, and between the composite block and the connection stiffener. After the composite block was fastened in this manner to the web-gap region of the test girder, the specimen was loaded for 1.2 million cycles with a force range that caused severe damage to a similar but unrepaired specimen. This method of attachment proved to be effective in maintaining bond between the composite block and the damaged specimen. Not only was bond maintained for the entirety of the test, but removal of the composite overlay for final inspection of the girder web was extremely difficult.

## 11.7 Conclusion

The various studies described in this chapter illustrate that composite materials can be used effectively to prevent and repair fatigue damage for a wide range of loading conditions. The keys to make effective use of composite materials are to devise an overlay configuration that is effective in providing an alternate load path, and to maintain the bond between the composite material and the underlying metal. Experimental studies described in this chapter illustrated several techniques to maintain the bond between the composite material and the underlying metal for cyclic loading conditions. Taking proper measures to maintain the bond is essential to make this type of repair effective.

## 11.8 References

AASHTO (2007). *AASHTO LRFD Bridge Design Specifications* (4th edn). American Association of State Highway and Transportation Officials, Washington, DC.

AASHTO (2010). *AASHTO LRFD Bridge Design Specifications* (5th edn). American Association of State Highway and Transportation Officials, Washington DC.

Adams, C. (2009). *Finite Element Study on Bridge Details Susceptible to Distortion-Induced Fatigue*, thesis, presented to University of Kansas, at Lawrence, KS, in partial fulfillment of the requirements for the degree of Master of Science in Civil Engineering.

Alemdar, F. (2010). *Use of Composite Materials to Repair Steel Structures Vulnerable to Fatigue Damage*, thesis, presented to the University of Kansas at Lawrence, KS, in partial fulfillment of the requirements of the degree of Master of Science in Civil Engineering.

Alemdar, F. (2011). *Repair of Bridge Steel Girders Damaged by Distortion-induced Fatigue*, thesis, presented to University of Kansas, at Lawrence, KS, in partial fulfillment of the requirments for the degree of Doctor of Philosophy in Civil Engineering.

Alemdar, F., Kaan, B., Bennett, C., Matamoros, A., Barrett-Gonzalez, R. and Rolfe, S. (2009). 'Parameters affecting behavior of CFRP overlay elements as retrofit measure for fatigue vulnerable steel bridge girders,' *Proceedings of the Second International Conference on Fatigue and Fracture in the Infrastructure*, Philadelphia, PA, July 26–29.

Barsom, J.M. and Rolfe, S.T. (1999). 'Fatigue and fracture behavior of welded components,' *Fracture and Fatigue Control in Structures* (3rd edn), American Society for Testing and Materials, West Conshohocken, PA, 237–280.

Fisher, J.W. (1984). *Fatigue and Fracture in Steel Bridges: Case Studies*. Wiley, New York.

Gangel, R. (2011) *Use of CFRP Overlays to Repair Fatigue Damage in Steel Bridge Girders and Components*, thesis, presented to the University of Kansas, at Lawrence, KS, in partial fulfillment of the requirements for the degree of Master of Science in Civil Engineering.

Hartman, A., Hassel, H., Adams, C., Bennett, C., Matamoros, A. and Rolfe, S. (2010). 'Effects of lateral bracing placement and skew on distortion-induced fatigue in steel bridges,' *Transportation Research Record: The Journal of the Transportation Research Board*, No. 2200, Dec, 62–68.

Hassel, H.L. (2011). *An Analytical Evaluation of Distortion-induced Fatigue in Steel Bridges*, thesis, presented to University of Kansas, at Lawrence, KS, in partial fulfilment of the requirements for the degree of Master of Science in Civil Engineering.

Hysol™ Loctite™ 9412 Epoxy Adhesive, 2001, http://www.henkelna.com.

Kaan, B. (2008). *Fatigue Enhancement of Category E′ Details in Steel Bridge Girders Using CFRP Materials*, thesis presented to the University of Kansas at Lawrence, KS, in partial fulfillment of the requirements for the degree of Master of Science.

Kaan, B., Alemdar, F., Bennett, C., Matamoros, A., Barrett-Gonzalez, R. and Rolfe, S. (2012). 'Fatigue enhancement of welded details in steel bridges using CFRP overlay elements,' *Journal of Composites for Construction*, 16(2), 138–149.

Lee, W.Y. and Lee, J.J. (2004). 'Successive 3D FE analysis technique for characterization of fatigue crack growth behavior in composite-repaired aluminum plate,' *Composite Structures*, 66(1–4), 513–520.

Liu, H.B., Al-Mahaidi, R. and Zhao, X.L. (2009a). 'Experimental study of fatigue crack growth behaviour in adhesively reinforced steel structures,' *Composite Structures*, 90(1), 12–20.

Liu, H.B., Xiao, Z.G., Zhao, X.L. and Al-Mahaidi, R. (2009b). 'Prediction of fatigue life for CFRP-strengthened steel plate,' *Thin-Walled Structures*, 47(10), 1069–1077.

Mall, S. and Conley, D.S. (2009). 'Modeling and validation of composite patch repair to cracked thick and thin metallic panels,' *Composites Part A: Applied Science and Manufacturing*, 40(9), 1331–1339.

Mallick, P.K. (1993). *Fiber-Reinforced Composites: Materials, Manufacture, and Design* (2nd edn), Marcel Dekker, New York, NY.

Meier, U. (1992). 'Carbon fiber-reinforced polymers: modern materials in bridge engineering,' *Structural Engineering International*, 1(92), 7–12.

Naboulsi, S. and Mall, S. (1996). 'Modeling of a cracked metallic structure with bonded composite patch using the three layer technique,' *Composite Structures*, 35(3), 295–308.

Roddis, W.M. and Zhao, Y. (2001). 'Out-of-plane fatigue cracking in welded steel bridges: why it happened and how it will be reapired,' *Welding Innovation*, 27(2), 2–7.

Roy, M., Lang, C. and May, I. (2009). 'Modelling composite repairs to cracked metal structures,' *Proceedings of the Institution of Civil Engineers (ICE)-Structures and Buildings*, 162(2), 107–113.

Sabelkin, V., Mall, S. and Avram, J.B. (2006). 'Fatigue crack growth analysis of stiffened cracked panel repaired with bonded composite patch,' *Engineering Fracture Mechanics*, 73, 1553–1567.

Schubbe, J.J. and Mall, S. (1999a). 'Modeling of cracked thick metallic structure with bonded composite patch repair using three-layer technique,' *Composite Structures*, 45(3), 185–193.

Schubbe, J.J. and S. Mall. (1999b). 'Investigation of a cracked thick aluminum panel repaired with a bonded composite patch,' *Engineering Fracture Mechanics*, 63(3), 305–323.

Simulia (2011). ABAQUS FEA Version 6.8.2. Providence, RI. http://www.simulia.com.

Tavakkolizadeh, M., and Saadatmanesh H. (2003). 'Fatigue strength of steel girders strengthened with carbon fiber reinforced polymer patch.' *Journal of Structural Engineering*, 129(2), 186–196.

Umamaheswar, T.V.R.S. and Singh, R. (1999). 'Modelling of a patch repair to a thin cracked sheet,' *Engineering Fracture Mechanics*, 62(2), 267–289.

Vakili, A. (2012) *Carbon Fiber Production, University of Tennessee Space Institute*, Tullahoma, TN.

Vilhauer, B. (2007). *Fatigue Behavior of Welded Connections Enhanced by UIT and Bolting*, thesis, presented to the University of Kansas at Lawrence, KS, in partial fulfillment of the requirements of the degree of Master of Science in Civil Engineering.

Vlot, A., Vogelesang, L.B., and de Vries, T.J. (1999) 'Towards application of fibre metal laminates in large aircraft,' *Aircraft Engineering and Aerospace Technology*, 71(6), 558–570.

Zhou, Y.E. and Biegalski, A.E. (2010). 'Investigation of large web fractures of a welded steel plate girder bridge,' *Journal of Bridge Engineering*, 15 (4), 373–383.

This page intentionally left blank

# Part IV

Application to infrastructure systems

This page intentionally left blank

# 12

# Using fibre-reinforced polymer (FRP) composites to rehabilitate differing types of metallic infrastructure

L. C. HOLLAWAY, University of Surrey, UK

**DOI**: 10.1533/9780857096654.4.323

**Abstract**: This chapter discusses the field applications of advanced polymer composite materials for upgrading and for rehabilitating metallic structures in the UK. For a variety of reasons, metallic systems may be found to be structurally unsatisfactory, particularly the early cast iron, wrought iron and early steel materials. Discussions of some of the field applications of strengthening metallic structures in the UK will be given, and these will be divided into three groups depending upon the technique used: (i) the bonding of the fibre-reinforced polymer (FRP) composite directly on to the degraded structure; (ii) the partial prestressing of the FRP composite by temporarily jacking the structure, generally relevant to bridge structures; and (iii) prestressing the FRP composite plate before bonding on to the beam and anchoring the plate.

**Key words**: fibre-reinforced polymer (FRP) composites, rehabilitation, metallic structures.

## 12.1 Introduction

Metallic structures exist in a wide range of systems; these include bridges, metal-framed structures, pipes and vessels. In the UK, rail bridges count for the greater number of these structures. These systems have a variety of structural forms which reflect the development of metallic materials from cast iron, through to wrought iron, to early and then to modern steels. The use of metallic structural units commenced at the end of the 18th century when cast iron columns were first used in churches in the 1770s; from 1790 onwards, the material was used more widely, particularly in textile mills. The first iron-framed building, Ditherington Flax Mill, Shrewsbury, dates back to 1796. Cast iron was subsequently extensively used in the construction of large buildings, such as major public buildings in London, and textile mills in Northern England, but it is the expansion of the railways and hence bridges which progressed the use of the cast iron material.

The transport infrastructure of the UK contains some 22 000 iron and steel bridges, ranging from single- to multi-span systems constructed from cast iron, wrought iron, old and modern steels. The oldest surviving cast iron

bridge in the UK is Iron Bridge, in Shropshire. It was the first arch bridge in the world to be made using cast iron; it crosses the River Severn at the Iron Bridge George and was opened in 1781. At that time, there was no precedent for cast iron structural design and, consequently, the bridge was designed on the principle of a timber system. The reason for utilising this material for the bridge was due to the iron ore smelting works at Coalbrookedale, which at the beginning of the Industrial Revolution was one of the first to open. The coal was drawn from drift mines in the side of the valley and was of superior quality with fewer impurities compared to normal coal. At the other end of the period covered by this chapter, there are also a few modern steel bridges that have been built since 1960; these have been designed to modern standards but, nevertheless, some have required strengthening or widening to meet the increase in volume of traffic and in vehicle weight (see Section 12.8.2).

Network Rail Ltd (Network Rail is its trade name) has by far the greater number of bridges to maintain in the UK than any other authority. These structures are constructed from cast iron, wrought iron, steel, aluminium, concrete, masonry or timber, and the majority are between 60 and 100 years old, particularly the early metallic ones. Network Rail manages some 40 000 bridges of which approximately half are masonry arches, with the remaining half consisting of about 16 000 metallic structures and 4000 concrete decks. Of the 40 000 bridges, about 28 000 carry the railway over roads, rivers and valleys (underline bridges) and over 6000 bridges carry public highways over the railway (overline). The remainder (overline bridges) carry private roads, farm tracks and watercourses over the line.

Of the 16 000 rail bridges, some 12 000 were constructed before 1914 and therefore many have exceeded the notional design life of 120 years (BSI, 2007; British Standards Institute (2005)). With the increased traffic loadings and intensities, all require regular inspections and maintenance and some require strengthening. Some 12 000 of the 16 000 Network Rail bridges built before World War I (see Sections 12.5.3–12.5.9 on Network Rail Bridges) still carry vehicular traffic and indeed some with increased loadings in spite of the fact that their nominal design life is exceeded. The bridge stock has to be appropriately managed as they all require regular inspection and routine maintenance to verify their performance and structural integrity; those that are heritage listed, as they have special significance in industrial history, require special treatment bound by legislation. It is inevitable that some will require repair and strengthening or even complete superstructure renewal. To facilitate the maintenance of the rail bridges, the upgrade design should address the following requirements:

- Rain run-off – positive falls, camber, provision of drips, weather flats, avoidance of debris traps, etc.

- Durability requirements:
  - appropriate selection of materials;
  - protective treatment in accordance with the performance specification of Network Rail;
  - appropriate workmanship specification;
  - no debris traps.

## 12.2 Types of metallic materials and structures needing rehabilitation

The UK infrastructure, as stated above, includes a range of structures made from a series of metallic materials. The structural forms used in bridges and buildings have evolved taking advantage of the materials available at the time. A comprehensive review of these different metallic structures can be found in Bussell (1997). Many of the early metal bridges are currently still in use on the rail network, carrying loads far in excess of those for which they were designed; modern metal bridges are constructed almost exclusively in steel. The wrought iron and early steels were usually of riveted construction. Welded construction did not became established for UK bridges until after World War II while riveted construction, although becoming less common, did not finally become redundant until the 1960s.

The appropriate method of analysis and design for plate bonding of metallic structures will depend upon the material from which the beam is made and the geometry of the cross-section. The five metallic materials most used in the civil infrastructure over the last two centuries are:

- *Grey cast iron* was widely used in the UK in the period 1700–1880. The behaviour of cast iron is difficult to predict accurately and the properties of the material have large variations; it is weak in tension and brittle failure characteristics. The tensile and compressive strengths are typically 120–160 MPa and 500–650 MPa, respectively. The material displays non-linear behaviour in both tension and compression; its properties can vary widely according to the method of production and manufacturing defects.
- *Wrought iron* was manufactured by raising the iron to a high temperature and subjecting it to a strong blast of air to remove carbon and other impurities. It was then heated to a welding temperature and rolled to remove further slag. Depending upon the quality of wrought iron required, this latter process was repeated several times. The material produced was almost pure iron; it was softer than steel but less liable to corrode. The quality of the wrought iron depended upon where it was made, and its characteristic strength could vary considerably. The

strength values of wrought iron are directional and vary between 310 and 360 MPa in the direction of rolling and, at 90° to this direction, the strength values are about two-thirds of these values.

- *Ductile cast iron* has similar properties to those of carbon steels and is used in structures where the formability or thickness is essential.
- *Early steel* replaced wrought iron in about 1860, but it was not until 1890s that it was used to manufacture structures and, by that date, it had largely replaced wrought iron. The rapid growth of carbon steel was due to the invention of the Bessemer manufacturing process; this made the production inexpensive and the material has since been prevalent in all forms of structures, such as bridges, building frames, pipes, steel–concrete composite floors, piles, etc., and since that time steel is being developed continually. The pre-1950 early steel has many similarities with wrought iron where large sections were fabricated by riveting together smaller sections; steel plates were often laminar in nature.
- *Modern steel* (post-1950s) is ductile, available in a variety of quality-controlled grades, and can be joined by welding or high strength friction-grip bolts.

Tilly *et al*. (2008) describes the physical/chemical properties and manufacture of iron and steels.

During the 18th century when cast iron was mainly used for bridge building, the dimensions of the structures were governed by the properties of the material. For instance, for spans less than 15 m, cast iron longitudinal girders were combined with transverse secondary girders, or with a timber deck. For span values up to 35 m, cast iron beams were bolted together and trussed with wrought iron rods. For spans greater than 35 m, cast iron arched bridges were used. Arched bridges of up to 60 m are still in use; one of the longest cast iron bridges of span 73 m constructed was the old Southwark Bridge (also known as Queen Street Bridge) over the Thames in London, it opened in 1819. It was replaced in 1921 by the new Southwark Bridge of total length 245 m. This latter has five spans and was constructed using early steel plate girder ribs; it has not had an update to this author's knowledge. Jack arch construction was widely used to form road decks and for the sub-surface of London Underground lines; this type of construction remained in use until about 1870. The collapse of the cast iron Dee Bridge in 1847 led to the setting up of a Royal Commission into the failure of the bridge which reported in 1849. The Commission condemned the design and the use of trussed cast iron in railway bridges; however, there were a number of other bridge failures, which did not use wrought iron trusses, viz. the Staplehurst rail crash, the Inverythan crash and the Norwood Junction crash; these structures generally failed from blowholes or other casting defects within the bulk material.

The capacity of a metallic structure may be governed by the strength of connections between members. Cast iron structures were generally connected by direct bearing or mechanical interlock; the latter method was based upon that used in timber or masonry connections such as a spigot and socket or a wedge connection. The cast iron beams were supported on the capitols at the upper part of cast iron columns.

Between 1830 and 1850, combinations of cast iron and wrought iron were used in efforts to overcome the shortcomings of cast iron in tension and its brittle failure characteristics. There were three principal methods used to 'reinforce' cast iron with wrought iron:

1. To use the wrought iron compositely in a similar way to that of steel in reinforced concrete.
2. The second method was not a true composite structure *per se*. Various people showed that the strength of cast iron could be appreciably increased by adding molten wrought iron scrap to the molten cast iron up to a value of about 40 %, in effect simply lowering the carbon content, which improved the iron's mechanical properties.
3. The cast iron girder was reinforced by using wrought iron as a truss. Such structures incorporated wrought iron bars or rods that were fitted to the cast iron girders in such a way that the cast iron should resist only compression stresses and the wrought iron only tension stresses.

In the 1850s, wrought iron gradually superseded cast iron as a higher performing structural material. Initially it was common to use the more expensive wrought iron in tension or bending members with cast iron being used for the compression members. Two early examples of this combination are (i) the Paxton's Crystal Palace that housed the Great Exhibition of 1851 in Hyde park, London and (ii) the great lenticular spans (135 m span) of the Royal Albert Bridge, Saltash, England (1859) over the Tamar River. The bridge was designed having two main spans manufactured from wrought iron, these lenticular trusses with the upper chord of each truss consisting of a heavy tubular arch in compression and a curved bottom chord of linked eyebar chains connected by open truss bracing. This bridge has been strengthened on various occasions throughout its long history, and currently corroded elements on the bridge are being repaired and extra efforts are being made to restore Brunel's original design by using special bolts that are similar in design to the Victorian rivets. No parts of this strengthening procedure have used fibre-reinforced polymer (FRP) composites.

Research on the repair and strengthening of wrought iron is limited, notwithstanding the fact that it has been used in other rail infrastructure and there are many wrought iron structures in the UK that are in need of structural upgrading and strengthening. The assessment and design of wrought iron relies on limited test information which has been summarised

by Bussell (1997). BD 21/01 (Department for Transport/Highways Agency, 2001) provides some guidance when assessing wrought iron structures, although it is not comprehensive; Morgan (1999) provides some information on the strength of Victorian wrought iron. Beagles (1993) has discussed the research work that has been undertaken to determine the static and fatigue strength of wrought iron. Assessment of Victorian wrought iron and its engineering properties has been given by Moy *et al*. (2004) and Moy *et al*. (2009). The latter publication has stressed the need for great care to be exercised in choosing the characteristic values for wrought iron material properties when strengthening wrought iron structures; it also discusses the damage that environmental exposure can cause.

## 12.3 Structural deficiencies in metallic structures

All structures deteriorate with time, due to the service conditions to which they are subjected. In some cases, this deterioration might be reduced or rectified by maintenance; however, if the deterioration is unchecked, the structure will not be able to perform the function for which it was originally designed. The reasons for deficiencies in structures placed in the civil infrastructure can be split into two broad groups

- *Group 1 Changes in the use of a structure*: It is required to carry different loads from those originally specified.
- *Group 2 Degradation of a structure*: It is not able to carry the loads for which it was originally intended.

For metallic structures, the first group may be subdivided into four areas:

- *Increased live load*: An increase in traffic load on a bridge, a change in the use of a structure resulting in greater imposed loads on it.
- *Increased dead load*: An additional load on underground structures due to new construction above ground.
- *Increased dead and live load*: A widening of a bridge by adding an extra lane of traffic.
- *Modern design practice*: An existing structure may not satisfy modern design requirements; for example, due to development of modern design methods, or due to changes in design codes.

The second group may be subdivided into four areas:

- *Corrosion* is the most common mechanism of structural degradation, particularly where a member is exposed to an aggressive environment, such as relative humidity and temperature, atmospheric pollutants (e.g. $SO_2$) and high airborne salinity. Corrosion is discussed in more detail below.

- *Fatigue* is a cause of structural degradation, which can govern the remaining life of a structure. The fatigue life may be controlled by crack propagation from the stress concentration around a particular detail, such as openings, welded connections or rivet and bolt holes. Many wrought iron and early steel structures contain a large number of stress raisers and therefore in order to extend the fatigue life of a structure, crack propagation must be arrested at all fatigue-critical positions.
- *Structural degradation* is the result of an impact (for example, 'bridge bashing' by over-height vehicles), vandalism, fire, blast loading or inappropriate structural alterations during maintenance. A single event may not be structurally significant, but multiple events could cause significant cumulative degradation to a structure.
- *Design or construction errors* are the result of poor construction workmanship and management. The use of inferior materials and inadequate design results in deficient structures that cannot carry the intended loads.

Corrosion can lead to a loss of member cross-section and, consequently, a reduction in the capacity of the member. This reduction is often in regions that are:

- difficult to paint;
- around connection details;
- in members that trap water;
- in a member that is subjected to frequent water flow.

Material corrosion is most likely to be significant in modern thin-walled steel members, but it can cause delamination of wrought iron and early rolled steels. Cast iron is generally more corrosion resistant than steel. This is due to the silica-rich outer surface left by sand mould used in casting but, once this outer layer wears off or is damaged, the cast iron will corrode rapidly. If external surfaces of pipes require renovating because of corrosion attack from acids in the environment, generally, polyester or vinylester polymers are suitable for their rehabilitation due to their excellent acid resistance. In most cases, isophthalic or terephthalic resin can be used but, for high concentrations or high temperatures, premium resins should be used.

Acidic attack on metal pipes can come from the soil in which the pipe is buried, especially from anerobic sulphate-reducing bateria which form hydrogen sulphide ($H_2S$) and ferrous ion ($Fe^{2+}$). FRP composites are used extensively to protect underground pipes as well as fuel tanks. Polyester is not resistant to basic or alkaline environments; consequently, isophthalic and terephthalic resins should not be used to upgrade metallic systems where the pH value exceeds 10.5. However, polyester resins based on

alkoxylates adducts of bisphenol-A have good alkaline resistance. General resin selection data are presented in the manufacturers' corrosion resistance guides.

## 12.4 Strengthening metallic structures using fibre-reinforced polymer (FRP) composites

### 12.4.1 Introduction

It was seen in Section 12.3 that metallic beams commonly require strengthening in flexure, shear or bearing capacities due to deficiencies in the material, particularly cast iron and early steels. This is generally undertaken by either bonding (or bolting) plate sections of the parent material of the steel or by bonding FRP composites onto the defective members of the metallic structure. Air voids and other defects found in the material are typical of finished cast iron products used in the 19th century. Consequently, the material can fail in an unpredictable brittle manner at relatively low tensile stresses, compared to modern metals. In addition, crack propagation from defects is exacerbated by cyclic loading from vehicle passage. Furthermore, the key technology for the effectiveness of FRP rehabilitating and retrofitting metallic members largely depends upon the adhesion between the FRP composite and the substrate of the structure; the variables which influence this adhesion include the resin used in the repair system, the surface preparation procedure of both materials and the application procedure that allows the resin to fill all voids.

### 12.4.2 Practical applications of FRP composites to metallic structures

The largest number of applications worldwide utilising FRP composites to strengthen metallic structures have been in the UK, and the experience gained on these projects has led to three comprehensive guidance documents being published: (i) Moy (2001), (ii) Cadei *et al*. (2004) and (iii) Tilly *et al*. (2008). Hollaway and Cadei (2002) have written a state-of-the-art review on the progress in the technique of upgrading metallic structures with advanced polymer composites, Luke and Canning (2004) wrote a case study on strengthening engineering structures, and Zhao and Zhang (2007) wrote a case study in advanced polymer composite for structural applications in construction.

The advantages of using FRP composites compared to steel plate bonding have been discussed in Hollaway (2003) and can be stated as:

- The fibres can be introduced in a certain position, volume fraction and direction in the matrix to obtain maximum efficiency allowing the composites to be tailor made to suit the required shape and specification.
- The resulting materials have high strength and stiffness in the fibre direction at a fraction of the weight of steel.
- The material has good durability characteristics.
- The material is easy to transport and handle – as the plates are lightweight there is not the requirement for heavy support equipment during the period of polymerisation of the adhesive, thus requiring less false work than for steel plates.
- The material can be used in areas of difficult access.
- Traffic disruption is kept to a minimum.

In addition, carbon and aramid fibre-reinforced polymer (CFRP and AFRP) composites exhibit excellent fatigue and creep properties and require less energy per kg to produce and to transport to site than for steel.

There are, however, some drawbacks to the use of FRP:

- It is intolerant to uneven substrate surfaces, which may cause peeling of the FRP plate away from the metallic material and give rise to the possibility of brittle failure modes (Swamy and Mukhopadhyaya, 1995).
- CFRP strengthening systems are being used mostly in bridge structures, in which fire resistance is not usually a primary design consideration. In buildings, CFRP systems also present great potential, but the widespread application of its use is being hindered due to concerns regarding its performance at elevated temperatures; several researchers have identified the fire behaviour of FRPs as one of the top priorities in terms of critical research needs (Harries *et al*., 2003; Kharbari *et al*., 2003).
- Material cost, can be between four and 20 times those of steel in terms of unit volume, but it should be considered that:
  - 2 kg of FRP material could replace 47 kg of steel on an equal strength basis (Peshkam and Leeming, 1994).
  - In a rehabilitation project, the installation savings can offset the higher material costs, which rarely exceed 20 % of the overall project (Meier, 1992). The exception to this percentage value is the ultra-high modulus carbon fibre for which case the percentage value could be as high as 50 %.
  - When traffic management, traffic delays and maintenance costs are included, the use of FRP provides a cost saving in the region of 17.5 % over steel.
  - Peshkam and Leeming (1994) presented a cost comparison of bridge replacement against strengthening with FRP, and demonstrated a possible saving of 40 %.

At the beginning of the 2000s, only a limited amount of research had been conducted on the application of FRP materials to metallic structures, but this situation has now changed (Mosallam *et al*., 1999; Tavakkolizadeh and Saadatmanesh, 2003; Cadei *et al*., 2004; Luke and Canning, 2004, 2005; Hollaway *et al*., 2006; Zhang *et al*., 2006; Photiou *et al*., 2006; Schnerch and Rizkalla, 2008; Hollaway, 2009). Bell (2009) has discussed a series of high level requirements relating to the use of FRP composites in bridge strengthening developed by Network Rail UK. Between 2001 and 2007 over 25 bridges were shortlisted for FRP strengthening; other bridges considered but, following a preliminary site visit, these were rejected either on the basis of condition or because the capacity increase required was considered to be excessive.

The upgrading or retrofitting of metallic structures poses a different and more difficult set of problems compared to that of reinforced concrete structures; these problems have been discussed by Mertz and Gillespie (1996) and by Mertz *et al*. (2001). The first problem to consider is the likelihood of lateral buckling which makes it necessary to fabricate composite metallic sections where the compression flange is continuously supported by a reinforced concrete slab. The second problem is the high strength and stiffness of metals, which makes it a more difficult material to strengthen, particularly as the high modulus CFRP composites have the same order of stiffness as the material to be strengthened. In this case, the main load transfer will only take place after the metallic material has yielded. However, if the ultra-high modulus (UHM) carbon fibre is used, where its stiffness is up to 900 GPa, load transfer will take place when the metallic material is within its linear region; the thickness of the composite will be typically 5–6 mm. In the case of cast iron, the low remaining strain to failure results in an inefficient use of the strengthening material unless it is pre-stressed before being bonded to the substrate. It is noted that the UHM CFRP composite will have a low strain to failure of the order of 0.4 % strain and, with a modulus of elasticity value of about 30 GPa, the system will fail with a small inelastic characteristic. The high modulus (HM) CFRP composites have a value of ultimate strain of the order of 1.6 % strain for a modulus of elasticity of 22 GPa. This implies that the material is ductile and is unlikely to fail in a rehabilitation situation by ultimate strain but, rather, by some other criteria (Photiou, 2005).

Considering the above points, there are three main requirements for a FRP composite strengthening system. These are that:

- The system should contain high strength and stiffness fibres such as carbon or aramid; the latter fibre might be considered when the upgrade is in the near vicinity of overhead electrical cables. The modular ratio of CFRP (high modulus fibres) to cast iron is higher than that for CFRP

(high modulus fibres) to steel, making the former rehabilitation more effective.
- The polymer matrix has good in-service properties, particularly durability.
- The adhesive must provide a good bond between the composite material and the adherent. This implies that the adhesive connection allows distributed load transfer between the FRP and the cast iron, unlike conventional mechanical connections (such as bolts or clamps) which cause stress concentrations that can cause brittle failure of the cast iron.

The FRP composite plate material used for the bonding operation is either the UHM (European definition) or the HM (European definition) CFRP composite, and the methods of manufacture and installation of the CFRP composite onto the site structure would be by one of the following methods:

- The pultrusion technique – the fully cured composite plate produced is bonded on to the site structure with an ambient cured adhesive. The surface of the plate to be bonded, or sometimes both surfaces, are generally given a textured finish by applying a peel-ply sheet at the beginning of travel into the heated die of the pultrusion machine; the peel-ply is removed immediately before application of the adhesive to the composite's surface.
- The prepreg sheets are preformed into a plate in the factory, cured at an elevated temperature, delivered to site and bonded onto the structure with an ambient cured adhesive in a similar way to the above item.
- A factory-made low temperature-cured epoxy resin with carbon fibre laminates and compatible film adhesive is wrapped onto the bridge structure and cured under an elevated temperature (by heat blanket) of 60 °C for 16 hours or 80 °C for 4 hours under a 1 bar pressure.
- Vacuum infusion, namely, the resin infusion under flexible tooling (RIFT) process.
- Dry mats are placed on the structure and impregnated with polymer and heat assisted (wet layup) followed by post-cure at an elevated temperature; in this case, the polymer acts as the matrix material of the composite as well as the adhesive.

These manufacturing procedures have been discussed in Hollaway (2008).

Both CIRIA Report C595 (Cadei *et al*., 2004) and CIRIA Report C664 (Tilly *et al*., 2008) provide the mechanical and in-service properties of CFRP. These property values will not be included in this chapter, but it is noted that there are three types of carbon fibres which can be used. These are:

- *The high stiffness fibre*: The modulus of elasticity and tensile strength are up to 390 GPa and up to 2900 MPa, respectively, suitable for cast iron, wrought iron and early steels.
- *The high strength fibre*: The modulus of elasticity and tensile strength are up to 230 GPa and up to 3400 MPa, respectively, suitable for cast iron, wrought iron and early steels.
- *The ultra-high stiffness fibre*: The modulus of elasticity and tensile strength are up to 900 GPa and up to 3700 MPa, respectively, suitable for the modern steels and also cast iron and pre-1950 steel materials. It should be noted that the strain to failure is low for this fibre composite.

The appropriate method of analysis and design for FRP composite plate bonding of metallic structures is dependent upon the material of the bridges and their geometric cross-sections. The material is likely to be one of the following: (i) grey cast iron, (ii) wrought iron, (iii) ductile cast iron and (iv) carbon steel (Cadei *et al*., 2004; Hollaway and Teng, 2008).

Case studies are a convenient way of illustrating the advantages and possible pitfalls of upgrading/strengthening metallic structures. From the experience that has been gained by analysing case studies of FRP strengthening schemes in the civil engineering infrastructure, designers have observed a number of factors that are clearly favourable to the use of FRP composites in rehabilitating/retrofitting of civil engineering structures. These are:

- *Mechanical and physical properties*: FRP composites offer high strength and stiffness and improved durability compared to other forms of rehabilitation of degraded structures that are available; composites may also minimise aesthetic impact. The most important characteristic of FRP composites in repair and strengthening is the speed and ease of installation. Reduced labour and shut-down costs and site constraints usually offset the material costs of FRP composites.
- *Requirements for the continuous flow of traffic in the case of bridge upgrades*: The strengthening scheme is able to be undertaken when only one lane of a bridge is closed for a short length of time. Often with other forms of upgrading the road over the bridge is closed for periods of days.
- *Possession length*: FRP strengthening has lesser requirement for long possession times compared with other strengthening systems.
- *Presence of services*: When the rehabilitation is close to services, non-invasive work is preferable compared with the reconstruction option; this type of work prevents any risk of damage to services or possible costs of diverting services.
- *Cast iron substrate*: It is generally not recommended to drill into cast iron, but bonding is acceptable.

- *Cost-effective rehabilitation*: FRP strengthening methods generally minimise disruption to both railway and highway networks compared with other forms of strengthening systems.
- *Benefits include*: (i) control of risk by allowing FRP strengthening where there is sufficient knowledge and design guidance, design checks and critical review after each installation; (ii) the business case for FRP composite.

### 12.4.3 Techniques for pre-stressing FRP composites to strengthen metallic structures

The bonding technique for upgrading a structural system is undertaken by bonding the composite plate directly onto the degraded member. However, when a FRP plate is bonded in the longitudinal direction onto a loaded metallic specimen, the FRP plate carries only a portion of the superimposed and dead load on the beam and, at the final stages of loading, the plate is stressed only to about 25–30 % of its ultimate tensile strength. It has been suggested that pre-stressing a FRP plate before bonding it to the beam is a more economical alternative; the technique is not straightforward.

There are basically two methods for applying the pre-stress to a site structure:

1. *Prestressing the FRP plate before anchoring and bonding it to the structural beam*: The pre-stressing operation is generally reacted against the beam and the free end of the plate is anchored to that beam. A key problem is forming the anchorage at the jack end of the FRP plate after it has been pre-stressed. During the ROBUST project (Hollaway and Leeming, 1999), a jacking system was developed for this research project and the system was further modified by Mouchel for prestressing CFRP plates against site metallic beams. Stocklin and Meier (2003) developed at EMPA, Switzerland, another method for transferring the prestressed force in the plate on to the beam. This method is described by Canning and Luke (2008).
2. *To jack out dead load deflection of the metallic element using hydraulic jacks prior to the application of the unstressed FRP composite*: This operation effectively cambers the degraded structural member thus reducing the stresses in the tensile region. The FRP plate is then bonded onto the tensile face of the member. After polymerisation of the adhesive and removal of the jacks, the dead load tensile stress that was taken by the jacks is transferred to the FRP plate as the member deflects in the direction of the tensile face.

There are some concerns with strengthening cast iron, wrought iron and early steel:

- There are difficulties with investigating the strengthening of wrought and cast iron systems due to the lack of available representative 19th century wrought and cast iron test samples for laboratory testing, although Network Rail is now making available samples from cast iron bridges built in the 19th century that have recently been replaced.
- The variation of material properties of field-manufactured FRP composites (the wet layup composites) is not addressed in any field applications of FRP composite. Therefore, the issue of durability and its effects on the performance of some of the FRP-strengthened structures are unresolved.

The following sections include case studies of rehabilitation of cast iron and older steel structures. There is no rehabilitation of wrought iron structures using CFRP composite plates in the UK known to the author.

## 12.5 Rehabilitating cast iron bridges and other structures: case studies

All bridges in Europe were required to carry 40 tonne vehicles by 1st January 1999 and, following a highway structures assessment, many bridges in the UK built before the 1950s were found to be in need of strengthening or replacement because they failed to reach the 40 tonne requirement. Bridges constructed before 1922 were required to be assessed in accordance with Department of Transport Standard BD2/84 to determine their local carrying capacity. This led to weight restrictions being imposed on many metallic UK bridges, mainly ones which were built pre-1950s using cast iron, wrought iron and early steels. Upgrading these bridges utilising composite materials offer advantages such as low weight, high strength and availability in long lengths (thus avoiding overlapping), and good fatigue and creep characteristics. Furthermore, CFRP composite plates are light enough to be able to pre-stress them on site.

It will be shown that the strengthening of cast iron bridges is notoriously difficult. Air voids and other defects found in the material are typical of finished cast iron products used in the 19th century. Consequently, the material can fail in an unpredictable brittle manner at relatively low tensile stresses, in comparison to modern metals. In addition, crack propagation from defects is exacerbated by cyclic loading from vehicle passage.

The majority of strengthening schemes which will be discussed in the following sections are the rehabilitation of cast iron bridges (incorporating jack arches) with CFRP composite plate material which is invariably used

for strengthening. The general procedure for cast iron commences with removing the flaked and corroded parts of the beam progresses through the various stages before finally bonding the CFRP plate to the beam. As an illustrative example, the various stages for the rehabilitation of a degraded metallic beam are shown during the upgrading of Streatham Station Bridge (South London), (see Section 12.5.5). Figure 12.1a emphasises the condition of some cast iron beams which are required to be upgraded. Figure 12.1b illustrates a method of cleaning the beam before applying a paint to its surface (Fig. 12.1c). Figure 12.1d shows the preparation for bonding the CFRP plate with the adhesive on it before raising it to the beam. The plate in position with temporary supports (these are removed after about one week) to hold the composite in position during polymerisation is presented in Fig. 12.1e.

The repair, strengthening and upgrading methods used for modern steel structures (post-1950s), generally come under one or more of the following categories (these are not discussed in this chapter):

- waterproofing the deck to stop inadequate or faulty drainage;
- appropriate repair of welds, fatigue cracks and rivets;
- reducing corrosion (e.g. using paint systems);
- plating or member replacement using bolted or adhesively bonded steel or FRP plates;
- encasement in concrete;
- strengthening individual steelwork connections by additional bolts, welding or additional steel or FRP plates;
- strengthening by altering the load path (load relieving).

The rehabilitation of one modern steel structure is given in Section 12.6.2.

### 12.5.1 Iron Bridge

**Iron Bridge** at Ironbridge, Shropshire (1779) was the first arch bridge in the world to be constructed of cast iron and was built by Abraham Darby III. It crosses the River Severn at Ironbridge, which is recognised as the birthplace of the Industrial Revolution. It carried vehicular traffic up to 1934 when it was designated an Ancient Monument and became a pedestrian only bridge. Some of the present-day cracks which are visible in the cast iron structure may date from the time it was first constructed, whilst others are probably casting cracks from defects such as blow holes; no attempt has been made to repair these cracks. The cast iron railings were showing signs of distress.

The original cast iron railings of Iron Bridge were strengthened in 2000 with 3.8 mm thick HM CFRP composite plates bonded to the inside faces of parapet posts. The work involved shotblasting the internal faces of the

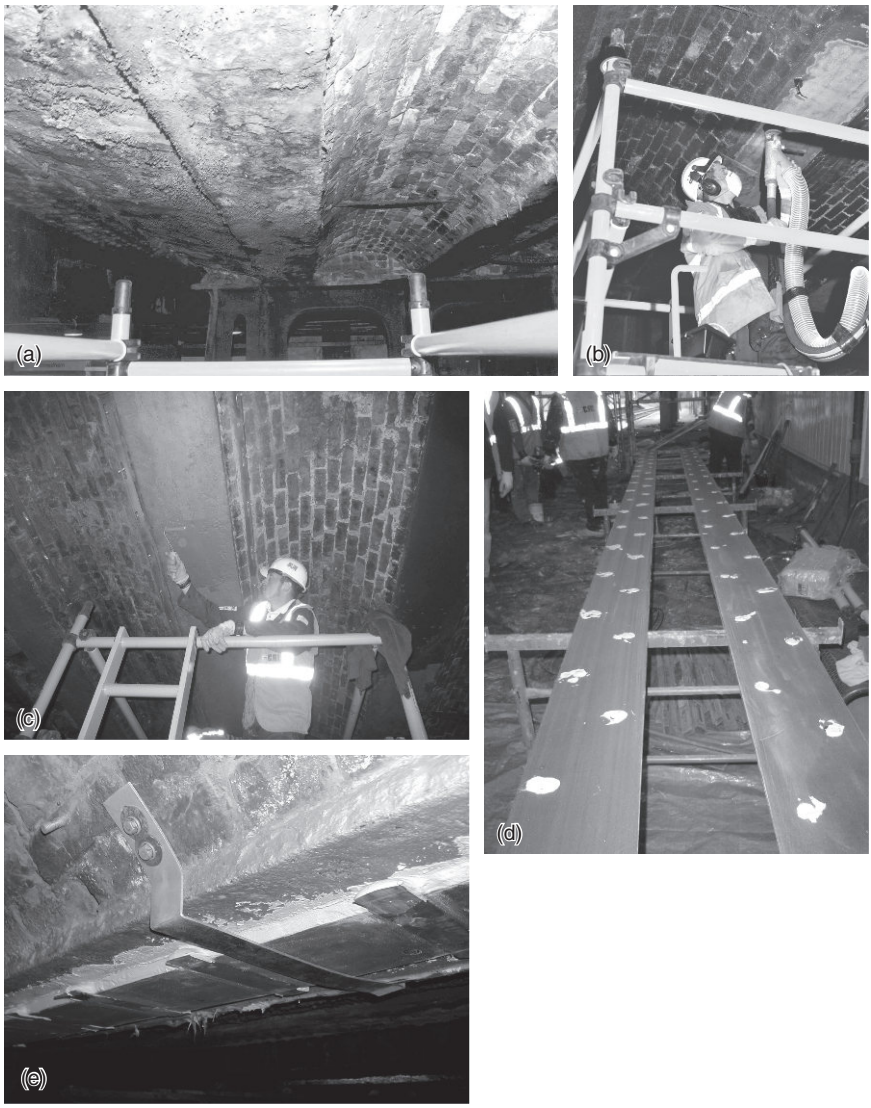


*12.1* The various stages for the rehabilitation of a degraded metallic beam are illustrated during the upgrading of Streatham Station Bridge (courtesy of Concrete Repairs Ltd). (a) Condition of the cast iron beam before upgrading. (b) Cleaning the cast iron beam. (c) Applying a primer to the cast iron beam before bonding the CFRP plate. (d) Applying the adhesive to the CFRP plate. (e) Temporary supports to the CFRP plate during polymerisation of the adhesive.

posts, applying carbon fibre to the cast iron surface and finally repainting the posts with aesthetically pleasing surface finish to mirror aged cast iron in texture (Oliver, 2002).

### 12.5.2 Tickford Bridge

**Tickford Bridge**, Northamptonshire is the oldest operational highway cast iron bridge in the world; it was erected in 1810 over the River Ouzel at Newport Pagnell. Designed by Thomas Wilson and built by Walkers of Rotherham, it is a Scheduled Ancient Monument. The bridge is an elegant structure, made up of six girders with spans of 18.29 m supporting a deck with six arches having spans of 7.2 m. In 1998, Maunsell (now AECOM), Beckenham, Kent, UK was appointed to suggest the most appropriate strengthening strategy. They recommended that the full highway loading could be achieved by strengthening the structure with CFRP; at this stage there was a 3 tonne gross weight restriction placed on the bridge.

Tickford Bridge was strengthened in 1999 and the selected strengthening system used was the Japanese Replark® repair system. It was chosen for its partially pre-impregnated sheets of carbon fibre cloth which were flexible and readily fixed to the curved arch surfaces. An insulating 'veil' of a layer of polyester fabric was placed between the iron and the carbon fibre to prevent any possibility of galvanic action taking place. The whole intervention used a pigmented polymer which matched that of the existing structure. The many layers of paint were grit-blasted off and a total area of 120 $m^2$ of the carbon fibre dry prepreg sheets was laminated in 14 layers to the three largest spandrel rings and to the lower main chord; the final thickness of CFRP composite was up to 10 mm. The bridge was then repainted and it was difficult to detect any change in appearance from the original.

The Replark® composite technique was chosen as it offered an advantage over other composite systems; it could be readily applied around the curved surfaces and small circumference sections. In some critical areas, the composite was cured at a temperature of between 50 and 60 °C with hot air blowers; this is higher than the normally applied ambient temperature cure for a wet layup composite. The final thickness demonstrates that this system of strengthening can be achieved with negligible visible effect on the appearance of the bridge, and the work was completed within 10 weeks. Final tests on the bridge confirmed that the strengthening had been successful and has upgraded the capacity of the bridge to 40 tonne vehicles. Lane and Ward (2000) have discussed the restoration of Tickford Bridge. Figure 12.2 shows Tickford Bridge after being strengthened.

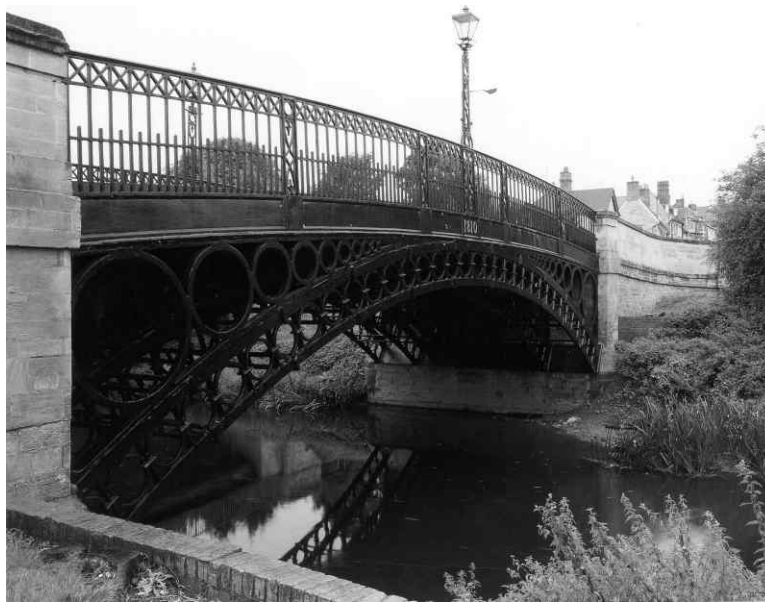

*12.2* Tickford Bridge, Newport Pagnell, Northamptonshire, UK (courtesy of AECOM, UK).

### 12.5.3 Bow Road Bridge

**Bow Road Bridge**, East London, built in 1850, is the oldest cast iron bridge in the UK to be strengthened using *unstressed* CFRP composite plates. The bridge carries the A11 over Docklands Light Railway and is constructed from seven cast iron beams supporting a combination of brick jack arches and steel plates. In 1999, the seven cast iron beams of Bow Road Bridge were strengthened by installing 11 custom-design tapered 170 mm wide, 20 mm thick and 5 m long *unstressed* UHM CFRP plates; these were bonded to the underside of the cast iron beams which then support 40 tonne vehicles.

All seven beams were prepared by grit-blasting prior to the bonding operation and were heated to an ambient temperature above 5 °C, before painting. Concrete Repairs Ltd (CRL), Hull, England, who were the contractor for the upgrading of the bridge, managed a 24-hour shift pattern to complete the job with 2 hours to spare and within budget. Docklands Railway Management Ltd approved the CFRP system as the most cost-effective, practicable and least disruptive strengthening option because of the high tensile capacity and lightweight nature of the composite plating, together with its ease of application to the existing substrate. Crouch Waterfall and Partners Ltd were the designers for the scheme.

### 12.5.4 Hammersmith Road overbridge

**Hammersmith Road overbridge**, West London, was constructed in around 1860–1880 (no accurate record is known), and is located on the A315, near Olympia; it is a three-span structure over two Network Rail lines and a London Underground track. The bridge is owned by two London Boroughs (Hammersmith and Fulham and the Royal Borough of Kensington and Chelsea), excepting those sections that pass over the railway lines. Each span is made up of 13 simply supported longitudinal hog back symmetrical cast iron beams (totalling 39 longitudinal beams) spaced approximately 1.8 m apart and two outer simply supported asymmetric cast iron beams; they are supported on brick abutments and piers. Between the beams, there are transversely spanning shallow masonry jack arches in all but two bays of each span; the two bays are formed by cast iron deck plates accommodating large service pipes. The fill in the jack arch bays is saturated ballast and within the deck plate bays is a lean concrete mix. The lean concrete mix also forms a 200 mm slab over the beams and below the running course of the road. The abutments and pier are constructed of masonry with hard padstones. The parapets are approximately 2 m high and constructed of masonry and hard stone.

During the assessment investigation stage, a large number of services were identified, from small traffic power cables through to banks of communication fibre optics to large-diameter high pressure water and gas mains. In 2004, the bridge was shown to be well below the required capacity for accommodating 40 tonne vehicles with a deck plate resistance of 3 tonnes and a beam capacity of 17 tonnes. As a result, the number of lanes on the deck was limited and a weight restriction was applied. This was not a long-term solution due to the busy nature of that area serving Earls Court and Olympia exhibition venues and the bustling area of Kensington High Street.

Figure 12.3 shows the working conditions at Hammersmith Road overbridge. Several options were examined to improve the load resistance of the bridge; these had to be lightweight schemes. Replacing the bridge was not an option due to the busy nature of the area. The options considered included replacing the existing concrete and fill with a lightweight concrete or foam concrete, but the final recommendation was to use an unstressed CFRP composite strengthening system with some dead load reduction. A bespoke design was produced by Mouchel Consulting Advanced Engineering Group (now SKM) and was independently checked by Tony Gee and Partners (TGP); the specialist contractor was CRL.

Some of the fill material was removed and replaced with a lightweight concrete. The CFRP plates were bonded to the soffit of each beam using a two-part cold cure epoxy adhesive; no additional fastening was employed.

*12.3* Hammersmith Road overbridge (courtesy of CRL).

The upgrading of the bridge was undertaken over various possession periods. During the first 52 hours possession at Christmas and New Year 2004/2005, the girders and part of the deck plate over the London Underground District line were strengthened. A further 52 hours possession in July 2005 was required to complete strengthening of the deck plates. Strengthening of the main span on the Network Rail West London Line was undertaken in 2009 during a suitable possession time. The design engineers are confident that the bridge should not require any major work for a further 40 years.

### 12.5.5 Streatham Station Bridge

**Streatham Station Bridge**, South London, was constructed in 1850 and is owned by Network Rail. It has been modified on several occasions during its history. Each time the materials used were of the period, and this resulted in an unusual and complex structure. It was originally built as two-span simply supported cast iron beams with masonry jack arches. It was modified in the early 20$^{th}$ century to accommodate trams, and the original cast iron and jack arches which supported the trafficked highway were replaced with steel beams encased in concrete; the remaining 10 cast iron beams supported the footpaths. These cast iron beams had low live load capacity and, to overcome this problem, railings were installed to ensure that vehicle

loadings were confined to the steel beams. Since its first upgrading, the bridge has been further extended on both sides to accommodate offices, shop units and some station buildings. This has required considerable upgrading of the footpath area with longitudinal and transverse reinforced concrete beams with spans varying between 1.9 and 11.7 m. In 2004, the bridge was again modified to take bus lanes. An assessment was then undertaken on the strength of the original 10 cast iron beams to take these extra loads; it was found necessary to strengthen them. This was undertaken by utilising unstressed UHM CFRP composite, with modulus of elasticity and strength values of 350 GPa and 1000 MPa, respectively.

In 2005, work was commenced to strengthen the cast iron beams and, after the grit blasting by a combination of vacuum blasting where the grit was recovered within a sealed system and open blasting to suit the requirements of the programme and the need to contain lead-paint contaminated grit, the beams were then cleaned and primed. Following this operation, adhesive was applied to the beams and to the CFRP plates; the latter were lifted to the soffit of the beams. The plates were strapped temporally to the cast iron beams during polymerisation of the adhesive, and this minimised disruption to the rail services. As no secondary heating was used for the polymerisation of the adhesive and as the upgrading procedure had to be completed within the closure period, the works on site had to be stopped over the winter period when the temperatures and moisture levels were likely to prove unsatisfactory. The design work was carried out by TGP and the specialist site contractor was CRL. The adhesive used to bond the composite plates was tested in tension during the installation of the plates. More information may be obtained from Smith (2006).

### 12.5.6 Bid Road Bridge

**Bid Road Bridge** (1876), Hildenborough, Kent, was strengthened in 1999 with tapered UHM CFRP plates bonded to the beams to allow continued use by all permitted traffic including the 40 tonne, five axle vehicles allowed on UK roads since January 1999. The bridge construction was of similar design to other bridges built at that time with cast iron beams supporting brick jack arches; there were nine cast iron beams. The installation is the first commercial project to adopt the *partially prestressed* CFRP composite system of strengthening cast iron beams on a *highway* bridge using tapered CFRP plates.

Bid Bridge crosses the Bid Stream on the B2027 at Hildenborough, Kent, and consists of brick jack arches supported on nine cast iron beams. The bridge had been temporarily propped, but the props had to be removed before the onset of winter floods; thus the bridge beams had to be

strengthened. Twelve 6 m length prepreg UHM CFRP composite plates of thickness 0.5 mm were adhesively bonded to seven of the nine cast iron beams to provide the required additional strength; Devonport Management Ltd, (now Babcock), Devonshire manufactured the composite plates. The inclusion of tapers and the localised reinforcement reduced stress concentrations in the adhesive at the ends of the plates and improved durability. Following the polymerisation of the adhesive, the prop struts were removed, thus providing a small amount of pre-stress to the CFRP composite plates. The work in progress during strengthening of Bid Bridge is shown in Figure 12.4.

The deployment of carbon fibre strengthening offered a quick and cost-effective alternative to demolition and reconstruction, albeit without some

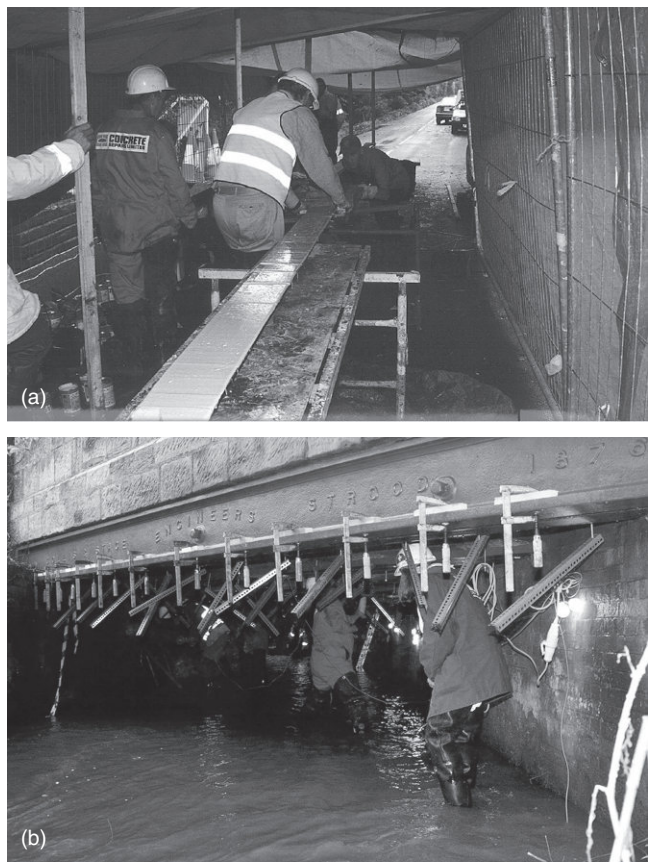


*12.4* Strengthening of Bid Bridge: (a) the application of the adhesive to the CFRP plate under cover. (b) Supporting the CFRP beam during the polymerisation of the adhesive (courtesy of CRL).

of the benefits of local widening that replacement would have provided. Consulting Engineers, TGP, undertook the strengthening design and CRL carried out the site work.

### 12.5.7 King Street Railway Bridge

**King Street Railway Bridge**, Mold, Flintshire, was constructed in 1870 on behalf of the Railway Board. The bridge carries the B544 over the railway which originally had two tracks but, in the 1960s, one track was removed and a support system was installed beneath the near centre of the bridge reducing the girders' span from 8.9 m to 5.9 m. In the 1980s, the Borough Council acquired the disused railway line to provide access between two car parks and took over responsibility for the bridge. In 1999, an assessment of the bridge capacity indicated that it was suitable to carry only vehicles up to 17 tonnes gross weight and in 2000 it was strengthened to allow 40 tonne vehicles to use it. It is the first highway skewed bridge built in the UK to be constructed of brick arches spanning between cast iron girders and one of the first to use a propping system to apply a *partially prestressed* CFRP composite system to the upgrading material (Farmer and Smith, 2001).

The masonry jack arches of the King Street Railway Bridge span a distance of 1.99 m between six cast iron girders; the arches are supported on the lower flanges of the girders which have ties, and these resist the lateral thrust; the cast iron girders span 8.93 m and are supported on brick abutments; the girders are skewed at approximately 28°. A number of designs for upgrading the bridge were proposed, but the one selected was to install temporary preloaded struts to support the deck, then to remove the existing props and to apply bonded strengthening materials; following the curing of the adhesive, the temporary pre-loaded struts were removed. This operation effectively applied a pre-stress to the composite, thereby transferring some of the permanent load into the CFRP strengthening material.

The carbon fibres utilised in this upgrade were the UHM, unidirectional, carbon fibre and glass fibre laminate reinforcement; this hybrid composite had a mean elastic modulus of elasticity of 360 GPa and a tensile strength of 1.1 GPa. The glass fibres were used to give the laminates transverse strength and to prevent galvanic action from taking place. The four internal girders were upgraded using two 170 mm wide and 33 mm thick laminates which were positioned 153 mm apart in the longitudinal direction to allow sufficient room to accommodate the heads of the hydraulic jacks which were used to apply a pre-load to the temporary struts. The CFRP composite plates had a small camber and were tapered at their ends to a length of 2.5 m to reduce to a minimum the longitudinal shear stresses and end peel

stresses. As the edge girders had a different cross-section to the internal girders, the thickness of the edge laminates was limited to 10 mm, but the longitudinal space between them remained at 153 mm. The surfaces of the cast iron girders were prepared by grit-blasting to achieve a specified texture and to remove any corrosion; if it was thought necessary, localised repairs were made using a filled epoxy resin.

The thickness of the adhesive was between 2 and 10 mm, and it was applied to both the cast iron substrate and to the CFRP composite. To maintain the plate in its final position, a series of small clamping forces was applied along the length of the beams during the polymerisation of the adhesive layer. In addition, a weatherproof enclosure surrounded the plate to enable a temperature of at least 5 °C to be maintained at all times. Furthermore, to ensure that the designed strains were not exceeded and to monitor the performance of the bridge over a number of years, strain gauges were bonded, at specific points, to the FRP plates and to the cast iron girders. Figure 12.5 shows the King Street Railway Bridge; the linear variable differential transformers (LVDT) are clearly visible.

The advantages of using carbon fibre to upgrade this structure over other more conventional materials are:

*12.5* The upgrading of King Street Railway Bridge (courtesy of Tony Gee and Partners).

- the superior durability of the material;
- the minimal loss of head room under the bridge due to the application of the layer of composite;
- the simplification of the erection procedure.

The design for the strengthening system of King Street Railway Bridge was undertaken by TGP and the specialist contractors for the site work were CRL.

### 12.5.8 Maunders Road Bridge

**Maunders Road Bridge** was built in 1870 and is located in the Milton area of Stoke-on-Trent, Staffordshire; it is owned by Network Rail. It carries an unclassified road over a cutting on the now disused Stoke to Caldon Quarry railway line. The effective span of the bridge is 7.84 m with a carriageway width of 5.1 m and a 1.1 m wide footway on one side of the carriageway. The bridge construction has six primary cast iron girders, the inside beams being spaced at approximately 1.43 m centres and the edge girders at 1.23 m. The masonry jack arches support the road base and asphalt pavement. During a structural assessment in the late 1990s, it was identified that the main girders had a capacity of only 7.5 tonnes and the edge beams only 3 tonnes. One of the cast iron edge beams had been propped by the addition of a brick wall with a steel beam capping the wall and supporting the cast iron beam, but this steel beam was severely corroded and was assessed as providing no support to the bridge girder. The unclassified road was within a residential area and a small industrial area; it was regularly trafficked by 40 tonne heavy goods vehicles. The highway authority required the bridge to carry 40 tonne vehicles and 30 units of abnormal HB type loading.

Several bridge strengthening options, as well as its replacement, were considered in 2001 and the cheapest one chosen was to jack the bridge girders at mid-span, thereby relieving some of the superimposed and dead loads, thus applying a *prestressed* composite system to the beam. Bespoke Sika/DML UH-M CFRP composite plates were tailored to the particular requirements of each project, with smoothly tapered composites which would minimise anchorage and end-effect stresses whilst also minimising the quantity of material used. These plates were then bonded to the soffit of the bridge on either side of the temporary props before the beams were de-stressed. The adhesive adopted was a trowelled epoxy adhesive, recommended by Sika/DML for the composite plates. The glass transition temperature $T_g$ value of the adhesive was in the range 54–56 °C; the acceptance criterion was that the value should lie within 5 °C of the manufacturer's quoted mean value. The design was carried out by TGP

based upon linear-elastic analysis adopting conventional assumptions (such as plane sections remaining plane) in a manner compatible with BD21/97. Limiting stresses were taken from BD21/01 (Department for Transport/Highways Agency, 2001). An independent check of the design was carried out by MouchelParkman (now SKM) and the site contractor was CRL.

Following completion of the works, the information from this upgrade was compared with the designer's theoretical predictions and with the contractor's records of environmental conditions. The correlations were very good; for instance, the measured stiffness of the strengthened beams was approximately 2.5 times that of the unstrengthened beams and the theoretical prediction was between 2.4 and 3.2 times (this limit was within the likely range of properties for the existing materials). Canning *et al*. (2006) have given a full description of the strengthening scheme.

### 12.5.9 New Moss Road Bridge

**New Moss Road Bridge**, Greater Manchester, is a cast iron beam/brick jack arch carrying a public road over the railway in Irlam; the bridge is owned by Network Rail. The original bridge, constructed in 1873, was a single-span structure comprising six simply supported cast iron beams with brick masonry jack arches spanning between the beams. In 1956, the bridge was extended to the south by the provision of a second span of reinforced concrete construction; the track under this span has now been removed. The spans are named north (cast iron) span and south (reinforced concrete) span. The north span has a clear span of 7.89 m and is supported by dressed sandstone sills on a massive brick masonry abutment and central pier. The transverse tie-rods in the structure had corroded in a number of locations in the external bays, reducing the lateral stability of the jack arches. The structure was assessed to DB 21/97 which showed the internal beams of cast iron to have an assessment live load rating of 17 tonnes. The reinforced concrete span was also under-strength in flexure. The bridge was the only suitable access for HGVs to an industrial estate and therefore had to upgraded to a capacity of full HA loading and 30 units of HB to enable it to carry the industrial vehicles.

To increase the flexural capacity of the north (cast iron) span, several options were considered including complete deck reconstruction and infill replacement. This proved too expensive and the most appropriate solution was to strengthen the bridge with externally bonded FRP composite reinforcement. However, the headroom clearance from the rail was only 4.18 m. As the minimum headroom clearance for straight track as set out in Railway (now Network Rail) Group Standard (GC/RT5204) Issue 2

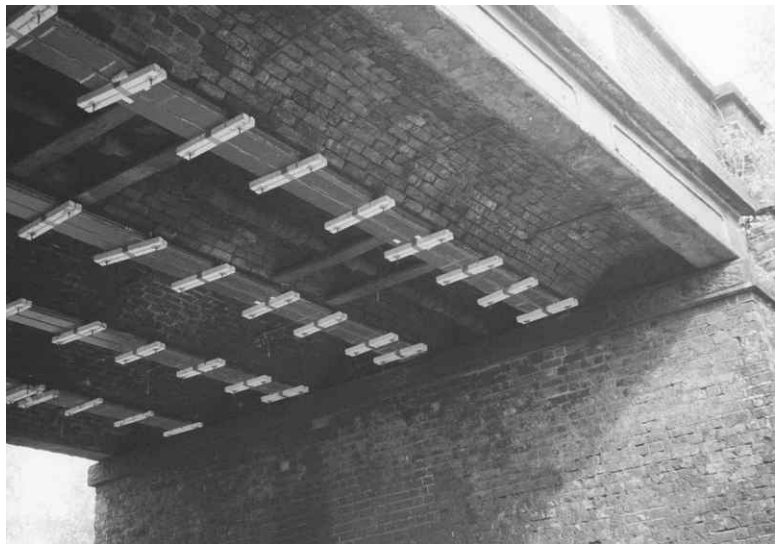

*12.6* New Moss Road, Greater Manchester (overline bridge) – the temporary supports to hold the FRP composites in position (courtesy of SKM, UK).

(1995) (now withdrawn) was 4.64 m, this reduction had to be referred to a Network Rail gauging engineer. UHM CFRP composite plates (tensile modulus in excess of 320 GPa) plates were selected for the upgrade and the site work had to be undertaken within the available possession time which in the case of New Moss bridge was less than 6 hours. A similar upgrade was performed on the south span (reinforced concrete) except here the HM CFRP composite plates were used. The upgrades strengthen the structure to the 40 tonne assessment load; the pultrusion technique was used to manufacture the plates (Luke, 2001a). Figure 12.6 shows the strengthening of the bridge with the temporary supports holding the CFRP composite plates in position whilst the adhesive polymerised: these supports were removed after about one week when full polymerisation had been achieved. The manufacturer of the FRP laminates recommended that the adhesive used for bonding the CFRP composite plates to the cast iron beams should be a thixotropic epoxy adhesive, and it was required to have a $T_g$ value in excess of 55 °C and an initial curing time of at least 45 minutes; in addition, it had to be suitable for site use in a temperature ranging from –10 to 45 °C. A maintenance manual was produced, with inspections scheduled at regular intervals after the installation of the laminates.

### 12.5.10 Hythe Bridge

**Hythe Bridge**, Oxford, Oxfordshire, is an historic cast iron structure which was constructed in 1874 over the River Thames, where it currently services a major arterial route into Oxford. It is a two-span bridge, each with a clear span of 7.8 m. Both spans were constructed with eight cast iron girders on which are built on the lower flange transversal masonry jack arches that sustain the traffic loading. In 1999, the bridge was weak in mid-span bending and capable of carrying only 7.5 tonnes, but it was able to support the full 40 tonnes assessment in shear; therefore, it was required to be strengthened to the EC requirement of 40 tonnes. A feasibility study was undertaken to evaluate possible options for strengthening the bridge, including reconstruction. It showed that it was possible to strengthen the structure with steel plate bonding, unstressed CFRP composite plates or stressed CFRP composite plates. Each of the three methods involved a degree of uncertainty because they extended practical limits in ways that threatened technical or economic viability. The most cost-effective way of strengthening the bridge was to use pre-stressed CFRP plates. It was necessary to stress the plates to mobilise the full load capacity of the composite and thus to take some of the dead load stresses in the cast iron beams to enable them to carry live loads.

Hythe Bridge was strengthened in 1999 utilising four pre-stressed CFRP plates bonded to each of 16 girders to increase load capacity on the bridge to 40 tonne vehicles. A proprietary jacking system for pre-stressing the CFRP composite plates against steel beams was developed for research purposes during the ROBUST project (Hollaway and Leeming, 1999; Luke, 2001b), and this system was further modified by Mouchel Consulting (now SKM) for pre-stressing CFRP plates for the strengthening of Hythe Bridge. The technique allowed end anchorages to be clamped at the extremities of the bottom flanges of the cast iron beams, thus eliminating the need for drilling into the brittle cast iron. End tab plates were bonded to each end of the carbon fibre-reinforced composite plates to provide a means of attaching jacking equipment and anchoring the plates when extended to the final working strain. The anchorage was surrounded by a protective casing and fully grouted. A total of 500 m of pultruded CFRP plates, manufactured by Fibreforce Ltd, were used and the bonding adhesive was supplied by Exchem Ltd. Before the upgrading commenced, extensive pre-stressing trials were undertaken by the specialist contractor. The scheme which cost £160 k in 1999 was estimated to be £100 k cheaper than the nearest strengthening alternative. Figure 12.7 shows an image of the soffit of the bridge and a section through the bridge. This was the first known metal structure in the world where *pre-stressed* CFRP plates have been used. Mouchel Cousulting (now SKM) undertook the design work on behalf of Oxfordshire County Council.

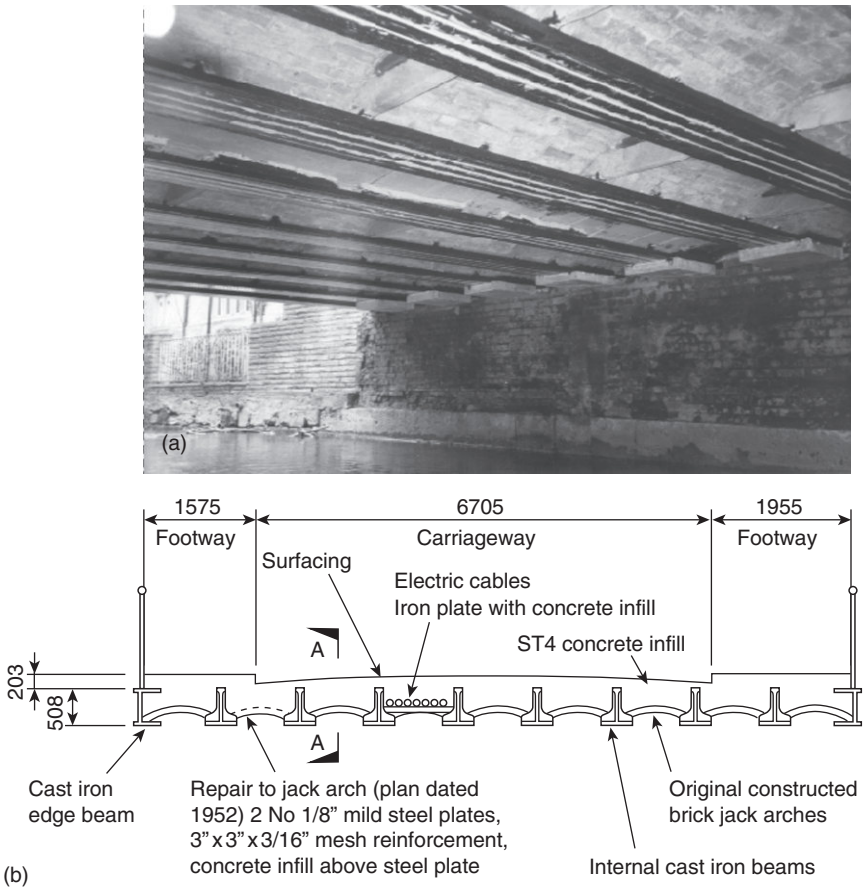


*12.7* Details of Hythe Bridge, Oxford: (a) the CFRP pre-preg applied to the soffit of the CI bridge beam; (b) typical section through the existing deck (courtesy of SKM, UK). (Parts of this figure have been published in Hollaway and Cadei, 2002).

## 12.5.11 The London Underground railway system

Certain sections of the London Underground railway system, such as the Circle and the District lines, were constructed mainly during the second half of the nineteenth century. The method used was the cut-and-cover technique with the tunnel being excavated from the surface; the walls and inverts of the tunnel were lined with brickwork. The general construction detail involved cast iron beams spaced typically at 2.4 m, positioned and supported on the side walls. Brick jack arches were then constructed

between the cast iron beams and were supported on the flanges of the beams. The tunnel was then covered with fill material. Current buildings and roads constructed above these tunnels are designed to carry much heavier loads and thus have resulted in significant increase in the loading on the tunnel support structure; furthermore, the cast iron would have aged over the years and now would have a weakened structure or indeed may have significant casting inclusions all of which will reduce the strength of the beams.

Throughout the manufacturing and installation process of the CFRP composite plates, a number of small experimental tests were undertaken – namely, (i) tensile and stiffness tests of CFRP samples made at the same time as the main site plates, (ii) flexural tests on prism samples of site-mixed adhesive polymer and *in situ* pull-off tests to check the adhesive bond to the prepared steel surfaces – to ensure the materials used and the workmanship involved met the design parameters. The following two examples will illustrate the strengthening procedures that have been used to upgrade two cast iron bridges on the London Underground railway system; the first illustrates the strengthening of a compressive member and the second the upgrading of the cast iron beams which were strengthened using a maximum thickness of 35 mm CFRP plates bonded to the bottom flange of the beams.

The first example relates to the second phase of the East London Railway construction, north of Brunel's brick tunnel below the Thames which was completed in 1876. This project included the construction of large shafts just to the north and to the south of Shadwell Station, London Underground; the shafts provided ventilation to the deep sections of the steam operated railway. The brick retaining walls forming the sides of the shafts were braced by two tiers of cruciform section cast iron struts. In 1980, the struts bracing the south shafts were removed when the new station was built. After a detailed study it was revealed that the cast iron struts in the upper tier were over-stressed, but the more substantial lower tier struts were found to be relatively lightly loaded.

The strengthening of the upper struts or their removal to be replaced by modern steel sections was considered. Several options were also examined, and the one eventually adopted was the FRP composite strengthening system which, in addition, incorporated secondary steel struts positioned above the upper tier of the cast iron struts. In 2000, a total of 18 cruciform section cast iron struts in the upper layer of the brick ventilation shaft were strengthened using up to 26 plies of UHM and HS CFRP on each strut; the technique used to fabricate the composite was the vacuum infusion technique. At Shadwell, the struts are subjected to solar heating and, as the coefficient of thermal expansion of the FRP composites is zero or slightly

negative, this will reduce the tendency for the extension of the heated cast iron struts to push the retaining walls apart. The results highlighted that the FRP strengthening would increase the load-bearing capacity of the structure by approximately 40 %. Further information on this project may be obtained from Leonard (2002).

The second example relates to the two parallel covered ways (known as Covered Ways 12 and 58) at Kelso Place, London, each being 110 m long with interconnecting cross passages; they carry the two tracks of the District Line and the Circle Line, London Underground, respectively. The covered ways were constructed in 1867 by the cut-and-cover method and support the highway of the predominantly residential area of the twin-ended cul-de-sac at Kelso Place. The two covered roofs are each supported by 45 'hog back' cast iron beams with jack arches spanning between them; the jack arches are concrete filled and waterproofed with asphalt. During an assessment in the late 1990s, the cast iron beams were found to be over-stressed and a load restriction of 13 tonnes was placed on vehicles using the two cul-de-sacs; furthermore, the buildings also significantly over-stressed the cast iron beams. There were problems with the foundations of the abutments and the central pier; although they were stable, the factors of safety were lower than those required by London Underground's Engineering Standards (LUES) for resistance against failure. (LUES are a primary risk control mechanism that has evolved over time to become highly prescriptive.) Furthermore, the vertical clearance between the highest rail level and the soffit of the cast iron beams was less than that required by LUES. In addition, there was also a history of concerns by local residents relating to noise caused by the passage of trains through the covered ways. The rehabilitation of the cast iron beams required that the track had to be lowered; the main issue, viz. the rehabilitation of the cast iron beams to prevent sudden failure of the system, will be discussed.

Strengthening of the structural work commenced in 1999. The initial operation was to increase the strength of the jack arches and, to implement this, 'aerofoil' semi-circular steel beams were erected within the jack arches. To obtain composite action between the jack arch intrados and the curved top steel plate, a pressure grout was used between the two structural components. The cast iron beams were strengthened using a maximum thickness of 35 mm CFRP plates bonded to the bottom flange of the beams; this was carried out during engineering hours. By limiting the thickness of the composite plates, it was possible to prevent encroaching on the track/beam headroom after it had been lowered; a new ballasted track bed was installed on a noise reduction mat. Church and Silva (2002) has discussed this project.

## 12.6 Rehabilitating steel structures: case studies

### 12.6.1 An early steel structure: Slattocks Canal Bridge

**Slattocks Canal Bridge**, Rochdale, Greater Manchester, which is on the A664 road between Middleton and Rochdale, was built in 1936 over the Rochdale canal at a 44° skew; it is a riveted historical *early steel beam* construction with a reinforced concrete deck. The square-spanning rolled-steel joists (RSJs) are 510 mm deep with 191 mm wide flanges, supporting the reinforced concrete deck slab below their top flanges. An assessment of the structure showed that the bridge required strengthening to take 40 tonne vehicles. The design involved an elastoplastic design, whereby the plastic capacity of the steel RSJs was mobilised with CFRP plates working well within their elastic range. It was the first early steel highway bridge to be strengthened with CFRP composite plates in Europe. Various strengthening options were considered and rejected such as (i) closing the bridge to traffic or (ii) supports being placed underneath the bridge, but an objection to this latter idea was the possibility that these members could be damaged by barges when the canal was restored and reopened. The main reasons for using CFRP composites over conventional methods were the ease of placing and bonding the unstressed CFRP composite plates and that it was a cost-effective alternative to steel plate bonding or other traditional methods of strengthening.

The historic Slattocks (highway) Canal Bridge was constructed from early steel and was strengthened in 2000 to increase its loading capacity from 17 tonnes to 40 tonnes; the bridge had been restricted to 17 tonnes load since 1996. The 7.6 m single-span bridge was strengthened by bonding 8 mm thick 100 mm wide *unstressed* CFRP composite plates to each of the 12 innermost RSJ beams. The bond stresses in the adhesive were limited to values which ensured that no peak stress effects were encountered. The strengthening solution involved using an elastoplastic design whereby the plastic capacity of the steel RSJs was mobilised, but the CFRP plates were working well within their elastic range. The upgrading maintained the navigable clearance required for the canal and preserved the historic nature of the bridge with minimal changes to the overall appearance of the structure and its surroundings; there was no traffic disruption during the site works. Figure 12.8 illustrates the installation of the CFRP plates.

Mouchel Consulting (now SKM) undertook the design work and the specialist contractor Balvac undertook the site work for Rochdale Metropolitan Borough Council. The contract value was £70 000 in 2000 and the programme lasted eight weeks. The bridge upgrading has been discussed in Luke (2001a); it received a Historic Bridge Awards commendation in the year 2000.

*12.8* Installation and temporary clamping of CFRP plate at Slattocks Canal Bridge. (Courtesy of SKM, UK)

### 12.6.2 A modern steel structure: the bridge at North Harrow, North West London

Carbon fibre composites were used to strengthen bridge (MR46A) on the Amersham Branch of the Metropolitan Line of the London Underground that carries twin rail tracks over Station Road, Harrow, adjacent to North Harrow Station. It was constructed in 1960 and is an all-welded modern steel half-through construction (a half-through bridge configuration is one in which the level of the track or road surface is below the top flanges or top chords [usually below mid-span of the beams] and there is no cross bracing between the upper flanges or chords). It has a clear span of 26.6 m and a clear width of 8.31 m. The bridge design consists of two simply supported fabricated steel edge girders of depth 2.45 m. Fabricated steel cross beams of about 690 mm depth (and spacing 2.25 m centres) are connected to the main girders' bottom flanges. These beams support longitudinal members of depth 250 mm and at 760 mm centres; the top flanges of these beams are at the same level as those of the cross beams. Pre-cast concrete deck soffit panels are supported by the longitudinal beams and *in situ* concrete surrounds the longitudinal beams to the top flange level and partly surrounds the transverse beams to their top flange. In 1997, a loading capacity evaluation of the bridge was undertaken, it was found to be under-strength in bending and the main girders were found to have a deficiency in shear strength.

Two remedial methods were considered to strengthen the bridge: the first was to weld steel cover plates to the main girders and transverse beams; and the second was to bond CFRP composites to the flanges of the beams. The second technique was chosen due to the material's high stiffness and high strength values, lightness and ease of installation. This method did not require the closure of the bridge. The main girders were upgraded by bonding UHM CFRP composite plates to both the top and bottom flanges; the plates were manufactured by DML Devonport Composites (now

Babcock International Group, plc.). The cross girders were strengthened by bonding UHM composite plates to their lower flange only, as bonding plates to the top flange would have required removing some of the track and a section of the ballast and waterproofing material; this procedure would have caused considerable disruption to train services. The composites were manufactured using pre-pregs consisting of epoxy impregnation of carbon fibre fabrics with a vacuum consolidation. The modulus of elasticity and the tensile strength of the composite were 360 GPa and 1030 MPa, respectively, and the maximum stresses were limited to 40 % of those values.

In the majority of cases, CFRP composite plates are bonded in one thickness throughout the length of the girder but, in the case of bridge MR46A, the plates were tapered in thickness to follow the moment envelope. This was more economic in material usage and it reduced the peeling forces at the end of the plates. They were also fabricated and bonded as two strips, each strip having a width of slightly less than half the width of the girder; this was to overcome concerns of handling and ensuring a uniform contact of the adhesive. Furthermore, in the design of this rehabilitation project, consideration was given to high temperatures that may occur on the surfaces of the steel members due to direct sunlight; this was considered necessary due to the relatively low glass transition temperature ($T_g$) of the adhesive. The maximum design temperature for an all-steel structure in the UK exposed to direct sunlight is 74 °C; this value was above the $T_g$ of the adhesive. To overcome this heating problem, a lightweight metal cladding with insulating and venting facilities was fixed to the top flange; this ensured a temperature below 50 °C. Sikadur® 30 was used for bonding the plates on to the members, and it had a $T_g$ value of 62 °C. In addition, glass fibre layers were incorporated between the steel surface and the CFRP plate to prevent possible galvanic corrosion between the carbon fibres and the steel substrate. The above information is based on the publication by Dodds (2003) and also Sika publicity phamplet. Figure 12.9 shows the various stages of upgrading bridge MR46A at North Harrow, North West London.

Gleeson MCL was appointed by London Underground Ltd to develop, design and implement the strengthening work for bridge MR46A. Gleeson MCL appointed Scott-White and Hookins to develop and design the work and the specialist subcontractor was CRL. A Category 3 check was undertaken by TGP.

## 12.7 Rehabilitating an aluminium beam structure: a case study

The **Boots Building**, Nottingham, is a Grade II listed building and was designed as a skeletal-framed structure which was constructed in two


*12.9* The various stages of upgrading bridge MR46A that carries twin rail tracks over Station Road, Harrow, adjacent to North Harrow Station (courtesy of Sika Ltd and CRL). (a) The bridge clad in polythene sheeting to give a weatherproof enclosure. (b) The adhesive being applied to the CFRP composite half plates. (c) The CFRP composite half plate being lifted into position. (d) The half plate being temporally supported during the polymerisation of the adhesive. (This support is removed after about one week.)

phases, the first completed in 1903 and the second in 1921. The earlier section was constructed as a frame consisting of cast iron columns and wrought iron beams, whilst the latter section was designed as a steel (early steel) frame. At the end of the 1990s, the section of the façade was showing signs of distress typical of early steel frame corrosion; this coincided with a change-in-use of the structure. During a subsequent investigation, it

was confirmed that two principal steel beams, which support the floors at second and third storey levels, had suffered a 30 % loss of flange and web section due to electrochemical corrosion. To return the beams to full strength and to fulfil the change-in-use requirements necessitated the beams to be reinstated with enhanced flexural capacity. The options were either to replace them or strengthen them; the latter option was adopted. In 2001, Taywood Engineering Leighton Buzzard, Bedfordshire (now Vinci Construction, UK) was appointed the specialist contractor for the work, and it was decided to use a strengthening system consisting of a Low Temperature Moulding (LTM®) advanced polymer composite material, manufactured by Advanced Composite Group (ACG), Heanor, Derbyshire, UK.

The purpose of the strengthening scheme was to restore the flexural and torsional capacity of the beam to above its original uncorroded level so that an anticipated increase in floor loading could be accommodated. However, the beam sizes were unknown until the Terra Cotta facia of the building was removed. Furthermore, the beams were curved in plan and connected to two straight members at their extremities at the corner of the building; due to the geometry of the structure the manufacture of replacement beams would have been impracticable because of the long lead times. There were also issues of access to the site associated with full replacement in a congested city centre location.

The LTM® composite pre-preg was supplied to the site in rolls of flexible material which was readily moulded to complex shapes, but the material had a limited outlife of only 3–4 days as it was not stored at a temperature of –20 °C. If the pre-preg had been stored at a temperature of –20 °C after manufacture it would have had an outlife of some two months. The thickness of the composite strengthening layer, which comprised unidirectional, 0°/90° and +/–45° fibre orientation, was 2 mm. The unidirectional fibres were aligned along the direction of the length of the beam for flexural strengthening. The 0°/90° fibre directions were used to resist shear and torsional loading; this latter was due to the curvature of the beam. The pre-preg composite layers were based upon glass and carbon fibres and a low temperature curing epoxy resin developed by ACG. The surface preparation for the steel adherent and the installation procedure was undertaken by grit blasting and cleaning with acetone or equivalent; in addition, after cleaning, the steel beam was kept in a dry condition by placing silica gel packs on to it and enclosing the packs and beam in polythene. An ambient-cured compatible epoxy adhesive was painted on to the clean and dry steel surfaces. The installation procedure for the LTM® composite pre-preg was under vacuum of 1 bar and polymerisation temperature of 65 °C for 16 hours; the latter was supplied by a heating blanket. Garden (2001) has described this strengthening project. The


*12.10* Strengthening the Boots Building, Nottingham: (a) final placement of the CFRP pre-preg around the flange and web of the aluminium beam; (b) CFRP pre-preg has been placed over the original bolted connections of the aluminium beam (courtesy of Vinci Construction, UK, and ACG, Derbyshire, UK). (First published in Hollaway and Cadei, 2002.)

composite pre-preg is an ideal way of navigating rivets as may be seen in Fig. 12.10 which illustrates the final placement of the carbon fibre pre-preg layers around the flanges and web of the steel beam; it also shows the CFRP composite covering of the bolted joint between the curved and straight sections of the aluminium.

## 12.8 Rehabilitation of onshore and offshore pipe work and other infrastructure

### 12.8.1 Onshore pipelines

Carbon fibre and epoxy resin liners have been used for a full structural repair, strengthening and rehabilitation of onshore steel pipelines. The main users of these pipeline structures are water utilities, power plants and industrial facilities. The composite layers do not change the internal diameter of the pipe significantly, and thus they result in a rapid installation process that is fully structural. The repair process for internal strengthening does not require a trench to be dug, therefore, the FRP composite lining becomes a trenchless structural rehabilitation. This technique has been successfully utilised for international pipes for more than a decade to rehabilitate many miles of pipelines ranging in diameter from 1 m through to 6 m. Pipeline rehabilitation can also be performed externally on any diameter pipeline without requiring dewatering of the line.

For smaller diameter pipework, from 0.1 m to 1.5 m, a resin-saturated felt tube manufactured from a polyester polymer is inverted or pulled into a damaged pipe from the upstream access point (manhole or excavation). The polymer is cured by hot water, by UV light or by ambient temperature to form a tight-fitting, jointless and corrosion-resistant replacement pipe. For the rehabilitation of the external surfaces of metallic pipes which have suffered corrosion due to (i) acid attack from the environment or from acidic soils in which the pipe is buried or (ii) alkaline environments when the pH value exceeds 10.5, reference should be made to Section 12.3 of this chapter.

### 12.8.2 Offshore pipelines

Providing protection from the elements for pipework located on the topside of offshore platforms around the coastal regions of the UK is extremely difficult in the highly saliferous marine environment of the North Sea. The probability of external corrosion damage is high. Consequently, the problem of corroded steel structures, especially pipework, is extensive on rigs in the offshore oil and gas industry and, as a result, there is considerable interest in temporary and permanent rehabilitation of such structures (Gibson, 2000, 2001; Mableson *et al*. 2000). When corrosion problems become severe on a pipeline, an alternative solution to replacement is to rehabilitate the pipe by adding CFRP composite wraps to its exterior surface. It is notable that the reasons for the interest in offshore CFRP composite technology and the advantages of this class of material for strengthening/repair applications were given by MSL Engineering Ltd (2004) as follows:

> On a technical level, these materials can be designed to be immensely strong and stiff. Coupled with their low weight compared to steel and other metallic alloys, this leads to high strength/weight and modulus/weight ratios, both of which are important in strengthening and repair situations. The materials are durable and this in turn leads to low life cycle costs. Laminates can be formed in-situ and the raw materials (fibres and resins) can be easily manhandled into confined spaces. There is minimal disruption of platform activities: no hot work, low labour requirements, no requirement for cranage, minimal amount of process equipment required and fast implementation.

Alexander and Bedoya (2011) have reported that a large volume of research and applications publications exist in the area of using composite materials to reinforce offshore pipelines.

A number of systems have been developed to address the problem of corrosion in pipework; these systems allow repair to take place without shutting down gas flow, purging the pipeline or cutting into the pipe. Composite wrap is a permanent, cost-effective pipeline repair technology, suitable for non-leaking defects such as pits, dents, gouges and external corrosion. There are many variations of composite wraps available for the energy industries to use in rehabilitation of pipework systems, including The Clock Spring®, The StrongBack and The Armour Plate®. The 'Clock Spring' system, developed in the USA by the Gas Research Institute, will be used to illustrate the general technique. This wrap consists of three parts:

- a high strength unidirectional composite structure of glass fibres and a polyester base;
- a fast curing high performance two-part epoxy methyl methacrylate adhesive system;
- a high compressive strength, load-transferring filler.

Composite wrap systems comprise a unidirectional glass fibre laminate, supplied in the form of a spiral helix or multidirectional fibre orientation to permit rehabilitation of both axial and hoop stress-bearing capability. They transfer the hoop stress from the defect through a high compressive strength filler to the composite. Application involves first cleaning the surface and filling external pits of damage to allow a uniform stress to be transmitted from pipe to the repair. The designed numbers of layers of composite sleeve are wound around the pipe with the adhesive applied between the layers. The composite wrap sleeve is tightened around the pipe with a tension strap and the adhesive is allowed to cure for about 2 hours; if the pipe is not buried after the repair it is coated with an anti-UV polymer. Geraghty *et al.* (2011) have presented general guidelines for the design and installation of CFRP composite wrap strengthening systems for steel pipelines; they have followed these discussions with some case histories. As a result of the widespread use of pipeline monitoring and assessment,

pipeline systems are now often able to be repaired prior to a rupture of the system by the application of FRP to the inside or outside of a pipe structure, but the proper design and implementation of these fibre wrap systems is paramount.

As with bridge and building structures, the following combination of materials is most commonly used in commercially supplied composite repair systems for the rehabilitation of corroded or damaged onshore and offshore pipework and structures for the oil and gas industries:

- *Fibre type*: Glass, carbon or aramid in various woven cloth architectures.
- *Matrix or resin type*: Epoxy (with various curing agents), polyurethane or esters (both poly and vinyl ester).

There are two common generic installation methodologies:

- the wet lay-up system;
- plates, shells or rolls manufactured off site and then bonded onto the pipework component on site.

The advantages of the use of composite repairs are:

- No hot work permit is required.
- They can be applied to the pipe whilst it is in operation.
- They are corrosion resistant and they also protect the pipework material underlying the repair.
- Minimal facilities are required on site.

The defective types in pipework that can be repaired include:

- internal defects, e.g. corrosion pits, general wall thickness loss;
- external defects, e.g. dents, corrosion under insulation;
- through-wall defects, e.g. leaks.

To decide whether a composite repair solution is possible, there are several issues that need to be resolved prior to performing a detailed repair design:

- Lifetime of the repair – (i) the maximum lifetime of a composite repair is 20 years according to ISO/TS 24817 (2006); (ii) short lifetimes (less than 2 years) are intended where the repair is required to survive until the next shutdown when the damaged component will be replaced.
- The chemical compatibility of the repair with either the internal or external service conditions. The resin systems used in composite repair must have good chemical resistance to hydrocarbons (e.g. alkanes, cyclo-alkanes), but generally these resins would not have resistance to strong acids (pH < 3) or strong alkalis (pH > 10). Reference should be made to resin manufacturers to determine the most suitable polymers to use.
- Whether fire performance is important.

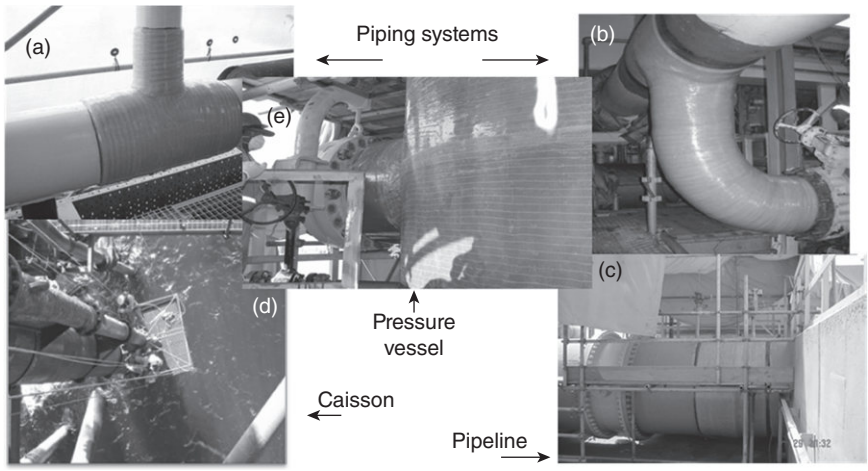


*12.11* Typical applications of composite repairs on a North Sea Oil rig (courtesy of Dr Simon Frost of Walker Technical Resources (WTR), Aberdeen). (a) Repair of tees in a gas receiving terminal; (b) a repair to a branch and elbow on an offshore platform; (c) a repair to a large-diameter pipeline; (d) a repair to a caisson above the splash-zone; (e) a repair to a large-diameter vessel.

These issues act as a guide as they give rise to further questions about the specific compatibility of the service conditions with composite repair. It is noted that chemical resistance is a function of temperature and the concentration of the chemicals in the pipe's environment and, consequently, the issue of chemical compatibility can only be assessed on individual cases.

Figure 12.11 illustrates applications of composite repairs associated with on- and offshore structures typical of those in the North Sea or on land in the vicinity of Aberdeen, Scotland. Presented in Fig. 12.12 are further examples of tanks, an external repair to a roof and structural repairs to a strut and a vessel. Figure 12.13 shows the repair to a submarine pipework.

### 12.8.3 Offshore infrastructure: steel blast wall at Mobil Beryl platform

Blast and firewall panels and three-dimensional mouldings comprising sandwich structures of composite materials with a thermal insulating core are manufactured for passive fire and blast restraint systems for jet fire and

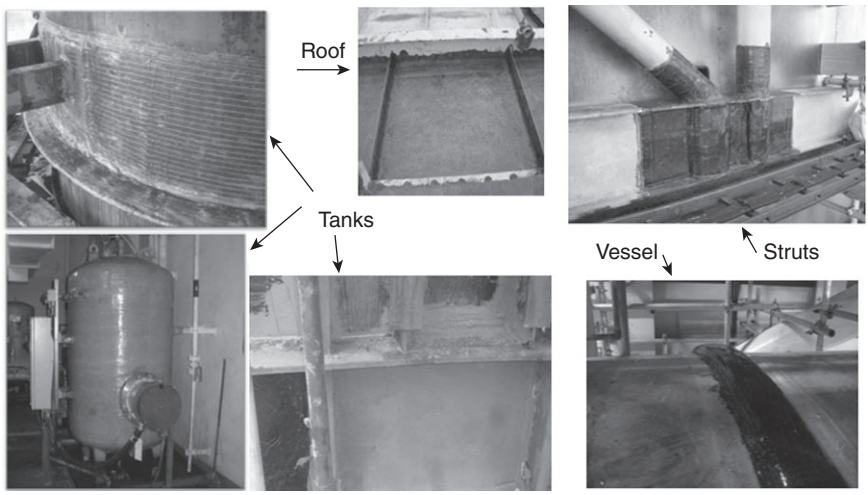


*12.12* Further typical applications of composite repairs on a North Sea oil rig (courtesy of Dr Simon Frost of WTR, Aberdeen).

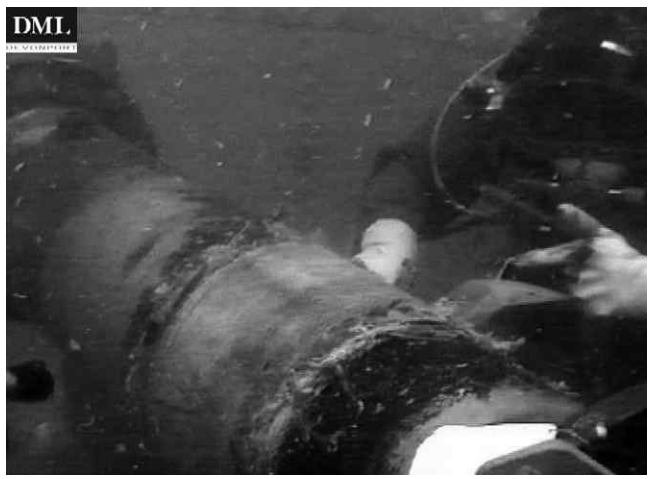


*12.13* Repair of a submarine pipe (first published in Hollaway and Cadei, 2002).

blast protection in the offshore oil and gas industries. Manufactured blast panels require the approval of authorities such as Lloyd's Register.

In the early 1990s, Mobil North Sea Limited (MNSL) prepared a Safety Case for their Beryl Bravo oil production platform in the northern part of the North Sea. This followed the Piper Alpha disaster in 1988 when the oil and gas production platform experienced a gas leak with the subsequent

fire and explosion reducing the platform to a wreck and causing the loss of many lives. An inquiry into this incident was initiated by Cullen (1990).

Groenenboom *et al.* (1995) and Galbraith and Barnes (1995) reported on a study to convert two 40 m by 8 m high non-structural firewalls to blast walls on the Mobil Beryl Bravo platform, thus enabling the walls to withstand over-pressures from hydrocarbon explosions. This study examined four options, and the one finally chosen led to the first application of the utilisation of CFRP composites to retrofit offshore oil and gas structures. Although the cost of the carbon fibre composite was high, this was offset by the savings in labour costs as the work was achieved in 500 man-days compared with 2500 man-days for the next alternative. Cost savings of over 50 % were made using the composite method and, in addition, the work was completed without having to shut down production.

In the early 1990s, there was considerable debate about the effectiveness of external repair systems, and this resulted in the preparation of a guideline document by AEA Technology (2001). This document deals with important issues such as the effectiveness of repair systems against internal corrosion and criteria for determining whether repairs should be regarded as temporary or permanent. Although this guideline is somewhat dated, it still provides a useful reference.

The upgrading of the blast walls on the Mobil Beryl Bravo platform used CFRP composite which was fabricated by the resin infusion under flexible tooling (RIFT) technique; it had been developed at Devonport Management Ltd (DML) (now Babcock). This process allowed high quality composites to be formed *in situ* and to be bonded to the existing structure. In this technique, dry fibres were pre-formed (fibre stack) in the workshop, and the necessary process materials were attached to the pre-form before packaging. The pre-form was placed onto the area of the structure to be upgraded and was infused with resin under a vacuum; the flexibility of the pre-form allowed it to conform well to any uneven surface. As the resin flowed into the dry fibre pre-form, it formed both the matrix of the composite material and the adhesive bond between the composite material and the adherent. As the dry fibre pre-forms are manufactured to the final dimensions of the system to be upgraded, it was possible to readily strengthen or repair three-dimensional systems such as Tee joints; this process provides a fibre volume fraction of about 55 % with thicknesses between 12 mm and 30 mm. As hot cured resins are not allowed to be used on offshore platforms because of the risk of fire, a suitable substitute was used to cope with curing the resin as well as functioning at 5 °C ambient temperature. Before being used on the Mobil Beryl B platform, strength and stiffness tests were performed on the high strength carbon fibre composites to provide mechanical property values close to those of the steel; the less costly standard modulus of elasticity glass fibres were used in secondary directions.

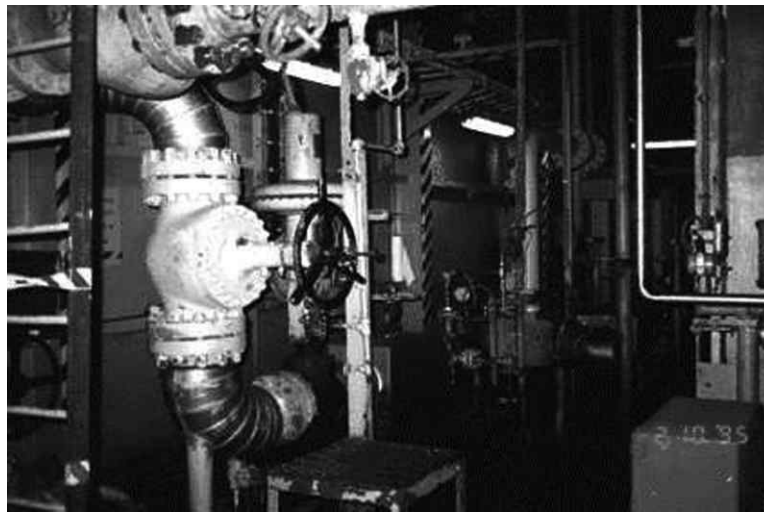

*12.14* Blast strengthening of a universal column supporting a steel blast wall; strengthening material UHM carbon. (First published in Hollaway and Cadei, 2002.) (The columns are highlighted by chevrons to warn welders not to strike an arc on them.)

Figure 12.14 shows blast strengthening of a universal column supporting a steel blast wall.

## 12.9 Conclusion: the use of FRP composites to strengthen metallic structures

The strengthening method of FRP plate bonding to metallic structural members is attractive to Network Rail, Highway Authorities and most consultants in the UK who are responsible for the maintenance of metallic bridges, buildings and pipework, particularly as the method allows the working life of structures to be extended by a factor of 1.5 and beyond.

The chapter has concentrated its discussions on problems associated with metallic structural systems which have deteriorated due to their long service life and/or being environmentally attacked; the latter causes corrosion to their surfaces. It has been stated that metallic materials first entered the construction industry as structural elements in late 18$^{th}$ and throughout the 19$^{th}$ centuries. During this time, mainly cast iron and wrought iron materials were used; examples of strengthening structures constructed from the first named material have been given. In the first half of 20$^{th}$ century, early steel was utilised to build structures; one example of early steel rehabilitation is given. During the second half of the 20$^{th}$ century and into the 21$^{st}$ century,

modern carbon steels and alloy steels were/are used; one strengthening example, namely, the bridge MR46A on the Amersham Branch of the Metropolitan Line of the London Underground, is discussed. When designing carbon steel structures, it is usual to apply to the system a corrosion allowance by adding an extra thickness to the steel member to account for gradual oxidation; an alternative would be to use thinner sheets of the more resistant but expensive stainless steel. To the author's knowledge, duplex steels and weathering steels in UK usage have not required to be rehabilitated to date.

In the degrading civil engineering environments, all materials have a finite life due to their decreasing durability, ductility, strength and stiffness, but it was noted that in many cases metallic structures built in the 19th century are carrying loads far in excess of their design loads; they are still in service because of their conservative design by modern standards. It was observed that, in spite of the deficiencies in the material and the design of the early metallic structures (namely, cast iron, wrought iron and early steel), the upgrading of these structures is advantageously undertaken by bonding CFRP composites on to the defective members; but it was recognised that the strengthening of cast iron is notoriously difficult. The reason given for this difficulty was air voids that had formed on the surface of the material during its manufacture and other defects typical of cast iron produced in the 19th century. It is known that the weakest link in rehabilitating metallic structures is the joining of CFRP composites to a metallic adherent; the adhesive is cured on site at ambient temperature, very rarely at an elevated temperature for further cure. It was stressed that special care must be taken when preparing the surfaces of the two adherents.

The manual operations of field applications for the strengthening of 'onshore' metallic structures in the UK may be divided into three groups depending upon the technique used: (i) the bonding of the fibres of the composite laminate directly on to the structure (the wet layup process) where the matrix of the composite is also the adhesive; (ii) pultrusion plates and pre-preg sheets, both of which required cold cure adhesives; and (iii) the vacuum infusion manufacturing method. Bridges, building, pressures vessels or pipework could be upgraded by any of these fabrication techniques. In all these cases, only a small part of the strength of the composite plate is utilised. Partially pre-stressing the FRP composite plate allows it to take a greater share of the load on the degraded member. This is achieved by forcing the member into a bending position by jacking, thereby releasing some of the tension stress on it. The FRP composite is then bonded on to the tensile side of the member and the jacking force is removed after polymerisation of the adhesive. An even greater percentage of the ultimate strength of the composite is utilised by pre-stressing the

FRP composite plate, before bonding and anchoring it to the degraded beam; this system is used mainly on bridges (the pultrusion technique or the pre-preg method are possible composite manufacturing systems for the pre-stressing technique). A pre-stressing force of about 35–40 % of the ultimate strength of the composite plate is applied. The alternatives to strengthening degrading bridge structures are to replace them, to change their structural form by inserting permanent props within the span, to add more beams or to reduce live loads by imposing lane, track closures or weight restrictions.

In the offshore industry, the use of composite materials for repair and rehabilitation of corroded steelwork, including pipes, decks, structural members and caissons, is now an established practice. The technique used for the rehabilitation of pipes on offshore platforms generally is to wrap a fibre mat of glass or carbon around the affected area; the type of fibre will depend upon the pressure requirements of the pipe. The resin may be a polyester, a vinylester or an epoxy which are usually applied as a vacuum infusion and cured using a heat source such as a thermal blanket. Patrick (2011) has reported that the durability examination of samples which were removed from previously strengthened pipework has proved the technology. It has been mentioned in the chapter that the important aspects of composite repairs are:

- Surface preparation which, for a carbon steel pipe, is normally possible with mechanical abrasion as the sole surface preparation, but it is important that the nature of the abrasion technique is fully specified. It has, however, been demonstrated that added durability can be achieved through the use of silane coupling agent.
- The cure of the repair composite, which is strongly influenced by temperature and the correct mixing of the resin constituents.

Finally, examples have been given of upgrading pipework for onshore and offshore oil installations and upgrading blast walls on oil rigs in the North Sea.

## 12.10 Acknowledgements

The author would like to express his thanks to the many engineers in the field of rehabilitating, retrofitting and upgrading metallic structures using advanced polymer composites for supplying technical information and images of structures discussed and shown in this chapter; their help is greatly appreciated. These firms include: Network Rail, London, UK; SKM, Manchester, UK; Tony Gee and Partners, Surrey, UK; Concrete Repairs Ltd, Hull, UK; AECOM, Beckenham, Kent, UK and Walker, Technical Resources, Aberdeen, UK.

## 12.11 References

AEA Technology (2001) *Temporary/permanent pipe repair – Guidelines*, prepared by AEA Technology Consulting for the Health and Safety Executive, AEA Technology Consulting, Abingdon.

Alexander, C. and Bedoya, J. (2011) 'An updated perspective on using composite materials to reinforce offshore pipelines and risers', *Proceedings of the 6th International Offshore Pipeline Forum* (IOPF), 19–20 October, Houston, TX.

BD21/97 (1997) *Design Manual for Roads and Bridges (DMRB)*. [This standard superseded by BD 21/01 (Department for Transport/Highways Agency, 2001).]

Beagles, M. (1993) *Static and Fatigue Properties of Wrought Irons and Early Steels*, BR Research Report LR MF 115, November.

Bell, B. (2009) 'Fiber-reinforced polymer in railway civil engineering', *Proceedings of the ICE – Engineering and Computational Mechanics*, 162(3), pp. 119–126.

British Standards Institute (2005) *BS 5400-5: Steel, concrete and composite bridges – Code of practice for design of composite bridges*, London, BSI. [This standard superseded by BS EN 1994-2: 2005 *Eurocode 4. Design of steel and composite structures – General rules and rules for bridges*.]

BSI (2007) *ISO/IS 24817:2006 Petroleum, petrochemical – Inspecton*, British Standards Institute, London.

Bussell, M.N. (1997) *Appraisal of Existing Iron and Steel Structures*, P138, Steel Construction Institute, Ascot.

Cadei, J., Stratford, T.J., Hollaway, L.C. and Duckett, W.G. (2004) *Strengthening Metallic Structures Using Externally Bonded Fibre-reinforced Polymers*, Report C645, Construction Industry Research and Information Association (CIRIA), London.

Canning, L. and Luke, S. (2008) 'Application of unstressed and prestressed composite flexural plates', in Hollaway, L.C. and Teng, J.G. (eds), *Strengthening and Rehabilitation of Civil Infrastructures Using Fibre-reinforced Polymer (FRP) Composites'*, Woodhead Publishing, Cambridge, Chapter 10.

Canning, L., Farmer, N., Luke, S. and Smith, I. (2006) 'Recent developments in strengthening technology and the strengthening/reconstruction decision', Paper 14 in *Conference on Railway Bridges Today and Tomorrow*, sponsored by Network Rail held at Marriott Hotel, 22–23 November, Bristol, pp. 107–113.

Church, D.G. and Silva, T.M.D. (2002) 'Application of carbon fibre composites at covered ways 12 and 58 and bridge E1', in Shenoi, R.A., Moy, S.S.J. and Hollaway, L.C. (eds), *Advanced Polymer Composites for Structural Applications in Construction*, Thomas Telford, London, 491–500.

Cullen, The Hon. Lord (1990) *The Public Inquiry into the Piper Alpha Disaster*, Vols I and II, CM 1310, HMSO, London.

Department for Transport/Highways Agency (2001) *Design Manual for Roads and Bridges*, Volume 3, Section 4, Part 3: BD21/01 The assessment of highway bridges and structures, TSO, London.

Dodds, N. (2003) 'Strengthening a bridge using carbon fibre reinforced plates', *The structural Engineer*, 4th March, pp. 17–19.

Farmer, N. and Smith, I. (2001) 'King Street Railway Bridge – strengthening of cast iron girders with FRP composites', *Proceedings of the 9th International Conference on Structural Faults and Repairs*, 4–6 July, London.

Galbraith, D.N. and Barnes, F. (1995) 'Beryl Bravo – blast walls conversion: development and testing of steel/carbon fibre composite', *Proceedings of the Fifth International Off-shore and Polar Engineering Conference*, 11–16 June, The Hague, pp. 229–236.

Garden, H.N. (2001) 'Use of composites in civil engineering infrastructure', *Reinforced Plastics*, 45(7/8), pp. 44–50.

Geraghty, M., Pridmore, A. and Julio Sanchez (2011) 'Transitioning from leak detection to leak prevention: proactive repair of steel pipelines using fiber reinforced polymer (FRP) composites', in Jeong, H.S. and Pecha, D.L. (eds), *Pipelines 2011: A sound conduit for sharing solutions*, American Society of Civil Engineers, Reston, VA, 100–107.

Gibson, A.G. (ed.) (2000) *Proceedings of Offshore and Marine Composites*, 5–6 April, University of Newcastle upon Tyne.

Gibson, A.G. (ed.) (2001) *Proceedings of Piping and Infrastructure*, 10–11 April, University of Newcastle upon Tyne.

Groenenboom, P.H.L., Galbraith, D.N., Jay, P.G. and Van der Weijde, P.J. (1995) 'Beryl Bravo – blast walls conversion: explicit dynamic FE analysis of steel/carbon fibre composite wall', in Chung, J.S., Das, B.M., Natvig, B.J. and Olagnon, M. (eds), *Proceedings of the Fifth International Off-shore and Polar Engineering Conference*, International Society of Offshore and Polar Engineers, Golden, CO, pp. 237–242.

Harries, K.A., Porter, M.L. and Busel, J.P. (2003) 'FRP materials and concrete – research needs', *Concrete International*, 25(10), pp. 69–74

Hollaway L.C. (2003) 'The evolution of and the way forward for adanced polymer composites in the civil infrastructure', *Construction and Building Materials*, 17(6–7), pp. 365–378.

Hollaway, L.C. (2008) 'Advanced polymer composite structural systems used in bridge engineering', in *Manual of Bridge Engineering*, G.A.R. Parke and Hewson, N. (eds), Thomas Telford, London, pp. 503–529.

Hollaway, L.C. (2009) 'Advanced polymer composites', in Hollaway, L.C. and Chen, J.F. (eds), *ICE Manual of Construction Materials*, (Ed. M. Forde), Thomas Telford, London, Chapter 52.

Hollaway, L.C. and Cadei, J. (2002) 'Progress in the technique of upgrading metallic structures with advanced polymer composites', *Progress in Structural Engineering and Materials*, 4(2), pp. 131–148.

Hollaway, L.C. and Leeming, M.B. (1999) *Strengthening of Reinforced Concrete Structures using Externally-bonded FRP Composites in Structural and Civil Engineering*, Woodhead Publishing, Cambridge.

Hollaway, L.C. and Teng, J.G. (eds) (2008) *Strengthening and Rehabilitation of Civil Infrastructures Using Fibre-reinforced Polymer (FRP) Composites*, Woodhead Publishing, Cambridge.

Hollaway, L.C., Zhang L., Photiou, N.K., Teng, J.G. and Zhang, S.S. (2006) 'Advances in adhesive joining of carbon fibre/polymer composites to steel members for repair and rehabilitation of bridge structures', *Advances in Structural Engineering*, 9(6), pp. 791–803.

Kharbari, V.M., Chin, J.W., Hunston, D., Benmokrane, B., Juska, T. and Morgan, M. (2003) 'Durability gap analysis for fiber-reinforced polymer composites in civil infrastructure', *Journal of Composites for Construction*, 7(3), pp. 238–247.

Lane, I.R. and Ward, J.A. (2000) *Restoring Britain's Bridge Heritage*, Institution of Civil Engineers (South Wales Association) Transport Engineering Group Award 2000.

Leonard, A.R. (2002) 'The design of carbon fibre composite (CFC) strengthening for cast iron struts at Shadwell Station vent shaft', in Shenoi, R.A., Moy, S.S.J. and Hollaway, L.C. (eds), *Advanced Polymer Composites for Structural Applications in Construction*, Thomas Telford, London, pp. 219–227.

Luke, S. (2001a) 'The use of carbon fibre plates for the strengthening of two metallic bridges of an historic nature in the UK', in Teng, J.G. (ed.), *Proceedings of the CICE 2001, FRP Composites in Civil Engineering*, Elsevier, Oxford, pp. 975–983.

Luke, S. (2001b) 'Strengthening structures with carbon fibre plates case histories for Hythe bridge, Oxford and Qafco Prill tower, Qatar', NGCC *First Annual Conference and AGM – Composites in Construction, Through Life Performance*, 30–31 October, Watford.

Luke, S. and Canning, L. (2004) 'Strengthening highway and railway bridge structures with FRP composites', in *Advanced Polymer Composites for Structural Applications in Construction: ACIC 2004*, L.C. Hollaway (ed.), Woodhead Publishing, Cambridge, pp. 747–754.

Luke, S. and Canning, L. (2005) 'Strengthening and repair of railway bridges using FRP composites', in Parke, G.A.R. and Disney, P. (eds), *Proceedings of the 5th International Conference on Bridge Management*, Thomas Telford, London, pp. 549–556.

Mableson, A.R., Dunn, K.R. and Gibson, A.G. (2000) 'Refurbishment of steel tubular pipes using composite materials', *Plastics, Rubber and Composites*, 29(10), pp. 558–565.

Meier, U. (1992) 'Carbon fiber-reinforced polymers: modern materials in bridge engineering', *Structural Engineering International*, 1, pp. 7–12.

Mertz, D.R. and Gillespie, J.W. (1996) *Rehabilitation of Steel Bridge Girders Through the Application of Advanced Composite Materials*', IDEA Project Final Report: Contract NCHRP-93-ID11, Transportation Research Board, Washington, DC.

Mertz, D.R., Gillespie, J.W., Chajes, M.J. and Sabol, S.A. (2001) *The Rehabilitation of Steel Bridge Girders Using Advanced Composite Materials*', Final Report, NCHRP-IDEA Project 51, Transportation Research Board, Washington, DC.

Morgan, J. (1999) 'The strength of Victorian wrought iron', *Proceedings of the Institution of Civil Engineers – Structures and Buildings*, 134(4), pp. 295–300.

Mosallam, A.S., Chakrabarti, P.R. and Arnold, M. (1999) 'Making the connections', *Civil Engineering, ASCE*, 69(4), pp. 56–59.

Moy, S.S.J. (ed.) (2001) *FRP Composites: Life Extension and Strengthening Metallic Structures: ICE Design and Practice Guide*, Thomas Telford, London.

Moy, S.S.J., Clark, J. and Clarke, H. (2004) 'The strengthening of wrought iron using carbon fibre reinforced polymer coposites', in Hollaway, L.C. (ed.), *Advanced Polymer Composites for Structural Applications in Construction: ACIC 04*, Woodhead Publishing, Cambridge, pp. 258–265.

Moy, S.S.J., Clarke, H.W.J. and Bright, S.R. (2009) 'The engineering properties of Victorian structural wrought iron', *Proceedings of the ICE – Construction Materials*, 162(1), pp. 1–10.

MSL Engineering Ltd (2004) *Assessment of repair techniques for ageing or damaged structures*, Contract Number 1435-01-04-CT-35320, December 2004. Study funded by the U.S. Department of the Interior, Washington, DC.

Network Rail Group Standard (GC/RT8029) (2000) *Management of Clearances and Gauges*, Safety& Standards Directorate Railtrack PLC, London.

Oliver, A. (2002) 'Strengthening of original hand cast iron railings on Ironbridge, Shropshire, England', *New Civil Engineer*, London, 14 February.

Patrick, A.J. (2011) 'Recent removals and examinations prove long term durability of technology', *PetroMin Pipeliner magazine*, Singapore, April–June 2011.

Peshkam, V. and Leeming, M. (1994) 'Application of composites to strengthening of bridges: Project ROBUST', *Proceedings 19th British Plastics Federation Composites Congress*, 22–23 Nov Birmingham, British Plastics Federation.

Photiou, N.K. (2005) *Rehabilitation of Steel Members Utilising Hybrid FRP Composite Material Systems*, PhD Thesis, University of Surrey, Guildford.

Photiou, N.K., Hollaway, L.C. and Chryssanthopoulos, M.K. (2006) 'Selection of carbon-fibre-reinforced polymer systems for steelwork upgrading', *Journal of Materials in Civil Engineering*, 18(5), pp. 641–649.

Schnerch, D. and Rizkalla, S. (2008) 'Flexural strengthening of steel bridges with high modulus CFRP strips', *ASCE Journal of Bridge Engineering*, 13(2), pp. 192–201.

Smith, I. (2006) 'Bridging solution', *Highways Magazine*, August/September, pp. 26–27.

Stöcklin, I. and Meier, U. (2003) 'Strengthening of concrete structures with prestressed and gradually anchored CFRP strips', Tan, K.H. (ed.), *6th International Symposium on Fibre-Reinforced Polymer (FRP), Reinforcement for Concrete Structures (FRPRCS-6)*, Singapore, World Scientific, Singapore, pp. 1321–1330.

Swamy, R.N. and Mukhopadhyaya, P. (1995) 'Role and effectiveness of non-metallic plates in strengthening and upgrading concrete structures', in Taerwe, L. (ed.), *Non-Metallic (FRP) Reinforcement for Concrete Structures*, E & FN Spon, London, pp. 473–481.

Tavakkolizadeh, M. and Saadatmanesh, H. (2003) 'Strengthening of steel-concrete composite girders using carbon fibre reinforced polymers sheets', *Journal of Structural Engineering (ASCE)*, 129(1), pp. 30–40.

Tilly, T.P., Matthews, S.J., Deacon, D., De Voy, J. and Jackson, P.A. (2008) *Iron and Steel Bridges: Condition Appraisal and Remedial Treatment*, Report C664, CIRIA, London.

Zhang, L. Hollaway, L.C. Teng, J.-G. and Zhang, S.S. (2006) 'Strengthening of steel bridges under low frequency vibrations', *Proceedings of the 3rd International Conference on FRP Composites in Civil Engineering (CICE 2006)*, 13–15 December, Miami, FL, pp. 643–648.

Zhao, X.L. and Zhang, L. (2007) 'State-of-the-art review on FRP strengthened steel structures', *Engineering Structures*, 29(8), pp. 1808–1823.

# 13

# Assessment and rehabilitation of steel railway bridges using fibre-reinforced polymer (FRP) composites

A. PIPINATO, University of Padova, Italy

**DOI**: 10.1533/9780857096654.4.373

**Abstract**: This chapter deals with the assessment and rehabilitation procedures related to steel railway bridges. The study considers first the main causes of in-service failures, then analyses step-level assessment procedures, also considering real-scale applications. The last section deals with FRP rehabilitation and strengthening, and traditional techniques of rehabilitation and strengthening. Each section describes both the theoretical and literature references and real-case applications.

**Key words**: steel bridges, railways, FRP, rehabilitation and strengthening.

## 13.1 Introduction

Bridges are strategic structures that form part of the transport infrastructure. Because of the age of most bridges and the traffic loads they face, they require retrofitting work, as proper functioning of transportation networks is essential for the socio-economic welfare of the population. Metal bridges in particular were widely used in transport infrastructure from the second half of the 19th century up to the middle of the 20th century. Most of these wrought-iron or older steel bridges are still in use around Europe. They were not designed explicitly to cope with fatigue or exceptional conditions such as seismic events. The lack of a comprehensive assessment methodology for such bridges, combined with some uncertainty about their reliability, has led to a number of research initiatives investigating their behaviour.

At the beginning of the 19th century, engineering design rules became more scientific with the development of the basis of modern static calculations. This did not happen without problems: several dramatic collapses occurred, for example the sudden collapse of the one-year-old bridge over the Albert Canal near Hasselt in Belgium due to brittle fracture in 1938, or the Quebec Bridge in Canada that collapsed due to buckling during construction on 29th August 1907. Steel structures were not exempt from serious failures. However, in many cases setbacks contributed to research and advances in better understanding of structural behaviour and

the development of new theories. This included the work of the Committee on Fatigue and Fracture Reliability of ASCE (1982), which reported that 80 % of failures in steel structures were related to fatigue and fracture. The factors behind these failures have been discussed by a number of researchers, including Brühwiler *et al*. (1990), Kulak (1992), Åkesson and Edlund (1995), Di Battista *et al*. (1997), Bursi *et al*. (2002), Matar and Greiner (2006), Boulent *et al*. (2008), Pipinato (2012) and Pipinato *et al*. (2012a–c, 2013) and Albrecht and Lenwari (2008, 2009).

Looking at steel structures, Oehme (1989) reviewed 448 damaged structures and their causes of damage. Approximately 98 % were damaged in the period between 1955 and 1984, and 62 % less than 30 years after erection. Cases of damage can be assigned, according to this study, to the type of structure as follows: buildings (including industrial buildings and crane supporting structures) 45.1 %; railway bridges 16.1 %; cranes 15.0 %; road bridges 8.7 %; plant and big machinery used in surface mining 8.0 %; masts and towers 5.8 %; other steel structures 1.3 %. As one can see, bridges (combining railway and roadway) are among the structures most often damaged. Another way of analysing the study is by looking at the cause for each incidence of damage, as presented in Tables 13.1 and 13.2. From these tables, one can see that fatigue is the third most common cause of damage among all observed cases and, for bridges, fatigue ranks first.

Looking specifically at railway steel bridges, the dead load versus live load ratio is usually about 15–20 %, implying that they are subjected to large variations of live load-induced stresses. Moreover, geometric imperfections,

*Table 13.1* Main causes of damage of steel structures

| Damage causes | Total | | Buildings | | Bridges | | Conveyors | |
|---|---|---|---|---|---|---|---|---|
| | No. | (%) | No. | (%) | No. | (%) | No. | (%) |
| Static strength | 161 | 29.7 | 102 | 33.6 | 19 | 14.8 | 40 | 36.0 |
| Stability (local or global) | 87 | 16.0 | 62 | 20.3 | 11 | 8.6 | 14 | 12.7 |
| Fatigue | 92 | 16.9 | 8 | 2.6 | 49 | 38.3 | 35 | 31.5 |
| Rigid body movement | 44 | 8.1 | 25 | 8.2 | 2 | 1.6 | 17 | 15.3 |
| Elastic deformation | 15 | 2.8 | 14 | 4.6 | 1 | 0.8 | 0 | 0 |
| Brittle fracture | 15 | 2.8 | 9 | 3.0 | 5 | 3.9 | 1 | 0.9 |
| Environment | 101 | 18.6 | 59 | 19.4 | 41 | 32.0 | 1 | 0.9 |
| Thermal loads | 23 | 4.2 | 23 | 7.6 | 0 | 0 | 0 | 0 |
| Others | 5 | 0.9 | 2 | 0.7 | 0 | 0 | 3 | 2.7 |
| Total | 543 | 100 | 304 | 100 | 128 | 100 | 111 | 100 |

*Sources*: Oehme (1989), Kuhn *et al*. (2008).

*Table 13.2* Analyses of common collapse damage on bridges

| No. | Collapse details | Number of collapses | |
|---|---|---|---|
| | | With detailed information | Without detailed information |
| 1 | During erection | 93 | 20 |
| 2 | In service, without external influence | 86 | 35 |
| 3 | Ship impact | 48 | 4 |
| 4 | Due to influence of traffic under the bridge | 16 | 0 |
| 5 | Due to influence of traffic on the bridge | 18 | 5 |
| 6 | Due to high water level or ice | 32 | 10 |
| 7 | Caused by fire, explosion, etc. | 15 | 2 |
| 8 | Of the supporting framework | 48 | 14 |
| Total | | 356 | 90 |

*Source*: Kuhn *et al.* (2008).

such as the inclination and/or deflection of structural elements, entail secondary stresses that are not usually taken into account in assessments. Vibrations, transverse horizontal forces, internal constraints and localised and diffused defects such as corrosion damages are concurrent causes of damage (Byers *et al.*, 1997). In addition, the use of different joint techniques may entail variable clamping force levels and load-carrying capacities in members and joints, and the presence of several joints, detail sizes and different materials in the same bridge induces different types of fatigue endurance. The most critical details in railway bridges are the floor–beam tension hanger and stringer-to-floor connections for medium and long span girder bridges (Al-Emrani, 2005) and the short shear diaphragm for small span bridges (Pipinato *et al.*, 2011a,b; Pipinato, 2011). These represent hot spot details in which alternating stresses decrease the fatigue strength of the whole structure. *In situ* and laboratory procedures, which are often not mentioned in code assessment procedures, increase our knowledge of material properties where they are not known (Farhey *et al.*, 1997; Ermopoulos and Spyrakos, 2006) and their effect on fatigue life evaluation.

## 13.2 Assessment procedures for damaged bridges

The assessment of an existing bridge aims at producing evidence to demonstrate that it will function safely over a specified residual service life, taking into account a specific code reference. It is mainly based on the results of assessing hazards and load effects to be anticipated in the future, and of assessing material properties, the geometry and the structural state

of the bridge. Guidelines for assessment of existing structures have been developed in many countries; however, it is rare for bridge assessment guidelines to be based on codes or standards. More frequently, such guidelines are prepared at a detailed level by scientific groups or research organisations. Whatever the source, the first issue deals with fixing risk acceptance criteria, which is quite difficult since these must be compatible with the code for new structures (limit state analysis, safety factor format, etc.). The second issue deals with the assessment procedure, which is commonly separated into phases, starting from preliminary evaluation, through to detailed investigation, expert and finally advanced assessment, depending on the condition of the investigated structure (Pipinato, 2010).

### 13.2.1 First level: preliminary evaluation

The first level of investigation is the preliminary evaluation aimed at removing existing doubts about the safety of existing structures, adopting fairly simple methods and identifying critical parts or members in the structure. In order to identify critical members, it is necessary to carry out an intensive study of the available original design documents, along with a visual inspection of the structure and a photographic survey. The inspection procedure is often set out in the infrastructural surveyors' own manuals; however, at a minimum the following points must be checked:

- Conformance of the bridge construction to the original drawings and/or differences between as-built and drawings.
- Bridge modification during service (rehabilitation, strengthening, changes in the static system, etc.).
- Presence of any visual evidence of degradation (damaged expansion joints, supports, corrosion, cracks, vibration or loose rivets, collision, lack of structural members, etc.).

Moreover, if available, previous inspection and maintenance reports can be used, and reference should be made to any existing evaluation report. The preliminary evaluation should take into account any codes and recommended analysis procedures where these are available, and conservative assumptions where information is lacking or doubtful. In this way, critical construction details can be identified.

### 13.2.2 Second level: detailed investigation

The aim of the detailed investigation is to update the information obtained in other analysis by carrying out a refined assessment, especially for those members for which adequate safety was not confirmed by preliminary evaluation. At this stage, a specialist consultant should assist. In this phase,

a finite element method (FEM) numeric model of the entire structure is developed. Based on the current code provisions, the structure should be recalculated and the results compared with verification tables in order to assess the safety of the structural members. Concerning specific issues, such as the fatigue and seismic behaviour of the bridge, detailed code provisions should be referred to. From this step-level investigation, non-destructive testing (NDT) could be used in order to characterise the basic material properties of the structure. The final report of the investigation should establish whether the structure is verified against specific standards and has sufficient static strength against actual loadings.

### 13.2.3 Third level: expert investigation

In the case of key structures which have major consequences in terms of risks or costs related to a decision, a team of experts should carefully check the conclusions and proposals reached in the last phase. Discussions and further assessments using specific tools can also be carried out to help reach decisions. At this level, on-site testing could be adopted in order to provide the dynamic identification of the structure, as reported in the following example.

### 13.2.4 Fourth level: advanced testing

This advanced level of investigation should be reserved for recurrent bridges along infrastructural nets, in which a rational procedure of analysis and intervention could help in determining if retrofitting interventions could be adopted, or if large-scale dismantling operations are, in fact, required. The procedure comprises a detailed survey of the existing bridge, a FEM analysis, a code verification procedure, NDT diffused sampling and, based on these data, real scale testing of one case study structure, with the aim of understanding the real static and cyclic behaviour of the bridge.

If appropriate, on-site dynamic identification could be carried out. Linear elastic fracture mechanics (LEFM) investigation is required for fatigue assessment and non-linear techniques for seismic analysis. Materials testing analysis suitable for the specific case under consideration should be performed. The advanced testing result should report on the various analyses performed, and should clearly state verification results indicating the specific retrofit needed for recurrent interventions. An advanced testing operation is reported in the following section, dealing with a recurrent existing bridge type in service along the railway lines.

A series of experiments and code comparisons have been carried out on the Meschio Bridge – an old railway riveted metal bridge taken out of service and transported to a testing laboratory. The focus of the study was on the short-diaphragm shear-riveted connections that carried the rails. In

the second phase, a material characterisation of the aged constitutive materials was carried out. The factors that could influence fatigue endurance were observed since they are not explicitly taken into account in codes (e.g. material composition and degradation). In the third and last phase, four high-cycle shear fatigue tests on short-diaphragm shear-riveted connections were realised at full scale, and the results compared with the appropriate fatigue category sections of Eurocode 3-1-9 (2005) (Figs 13.1, 13.2 and 13.3).

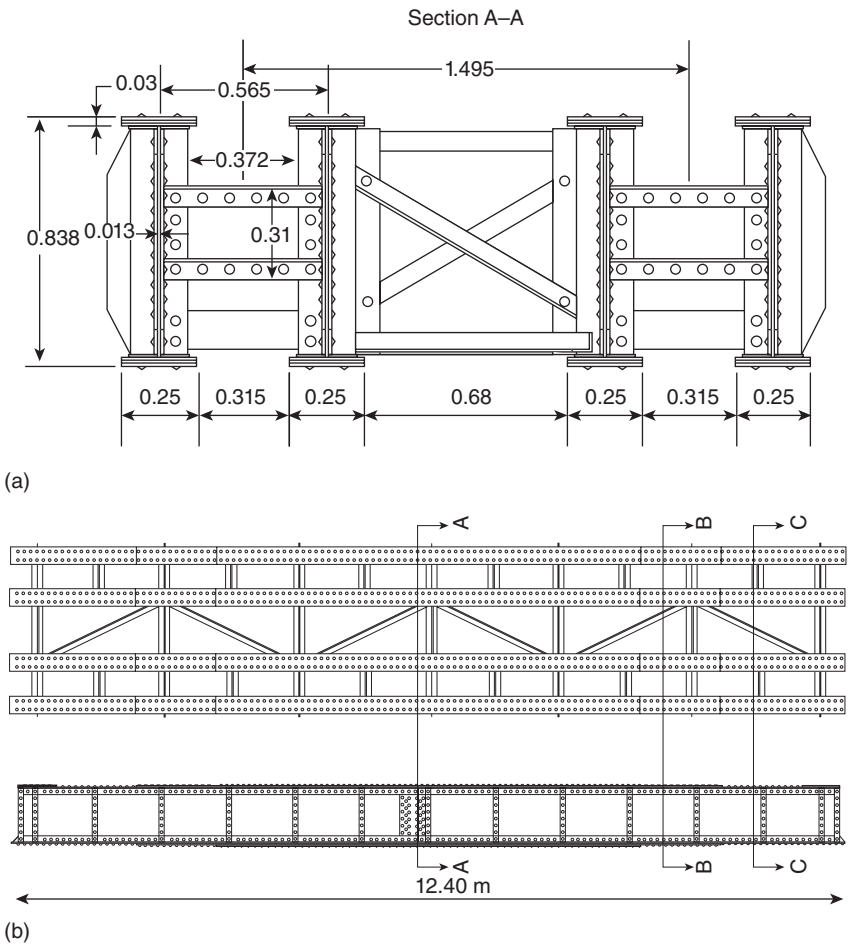


*13.1* Twinned girder structure of the Meschio Bridge: (a) midspan section A–A of one lane; (b) plan and lateral view of one lane. Dimensions in m (Pipinato *et al.*, 2009).

*13.2* The Meschio Bridge, out of service, Italy (Pipinato *et al.*, 2009).

The bridge has a single span of 12.30 m, with coupled-beams and independent lanes for each direction: every twinned-beam was 85 cm wide and 95 cm high. The thickness of the web is constant along the beam and measures 11 mm, while the flanges have different thickness along the axis, increasing towards the half span of the structure from 11 to 33 mm. The bridge has been completely dismantled and subdivided into its component parts, in order to perform static and high cycle fatigue testing, both in bending and in shear. The results of the research performed are extensively reported, for example in Pipinato *et al*. (2011a) and Pipinato *et al*. (2009).

## 13.3 Rehabilitation and strengthening of bridges with fibre-reinforced polymer (FRP) composites

An alternative technique for strengthening steel structures consists of the application of externally bonded fiber-reinforced polymer (FRP) sheets, used mainly to increase the tensile and/or flexural capacity of the structural element. FRP materials have a high strength-to-weight ratio, do not give rise to problems due to corrosion and are manageable. Some examples of guidelines for the design and construction of externally bonded FRP systems for strengthening existing metal structures include the ICE design

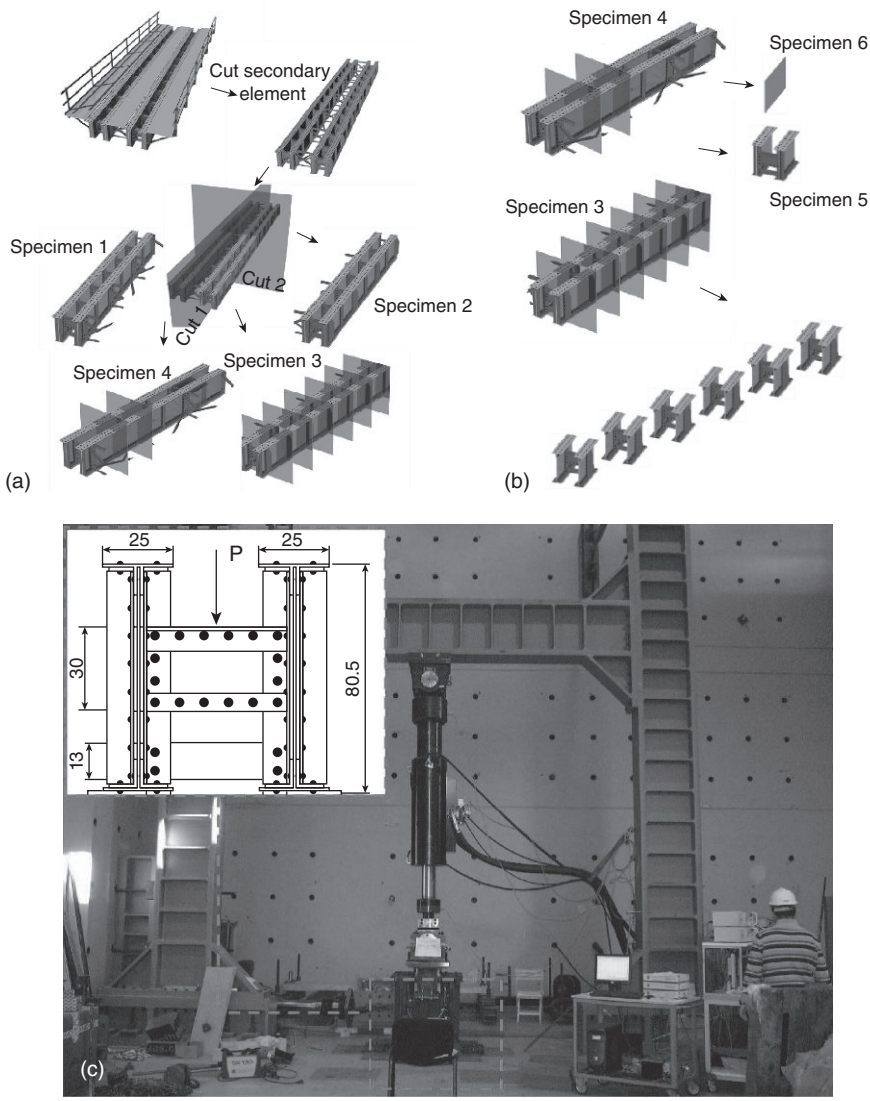


*13.3* The Meschio Bridge, divided into specimens for the testing phase (a, b) and full-scale testing of shear diaphragm specimens (c) (Pipinato *et al.*, 2009).

and practice guide (Moy, 2001), CIRIA Design Guide (Cadei *et al.*, 2004), US Design Guide (Schnerch *et al.*, 2007) and CNR-DT 202/2005 document (Italian Research Council, 2005).

The benefits of composite strengthening have been applied, for example, in a steel bridge on the London Underground (Moy and Bloodworth, 2007).

The benefits of strengthening large cast-iron struts with carbon FRP (CFRP) composites in the London Underground are illustrated in Moy and Lillistone (2006). A state-of-the-art review on FRP-strengthened steel structures was recently developed by Zhao and Zheng (2007). Apart from the well-known e-glass, high strength CFRP (HS CFRP) and aramid, high modulus CFRP (HM CFRP) materials, which have been developed with a tensile modulus approximately twice that of steel, are becoming widely used. Diverse applications reported in the literature concerning this type of material are discussed below.

Among the most common techniques of FRP strengthening systems in bridge engineering, three should be cited. The first is the wet layup system, which consists of dry unidirectional or multidirectional fibre sheets or fabrics that are impregnated on-site with a saturating resin. The saturating resin is used to provide a binding matrix for the fibre and bond the sheets to the concrete surface. Three common types of wet layup systems are:

- dry unidirectional fibre sheets with the fibre running predominantly in one planar direction;
- dry multidirectional fibre sheets or fabrics with fibres oriented in at least two planar directions; and
- dry fibre tows that are wound or otherwise mechanically applied to the concrete surface. The dry fibre tows are impregnated with resin during the winding operation.

The second technique is pre-cured FRP systems consisting of a wide variety of composite shapes manufactured in the system supplier's facility and shipped to the job site. Typically, an adhesive is used to bond the pre-cured flat sheets, rods or shapes to the surface. The adhesive must be specified by the system manufacturer. Common types of pre-cured systems are:

- pre-cured unidirectional laminate sheets in the form of large flat plate stock or as thin ribbon strips coiled on a roll;
- pre-cured multidirectional grids coiled on a roll or pre-cut in sheet form; and
- pre-cured shells in the form of shell segments cut so they can be opened and fitted around columns or other elements – multiple shell layers are bonded to the concrete and to each other to provide seismic confinement or strengthening.

Concerning the bond between FRP and steel, the use of epoxy FRP sheets bonded to the tension face of structural elements has been widely accepted; however, monitoring of the structure is required and durability needs to be extended by further applications over time.

### 13.3.1 Case studies

Among the studies available in the literature, some are relevant for their content and applicability. For example, as reported in a recent work by Schnerch and Rizkalla (2008), the use of externally bonded HM CFRP materials can strengthen steel bridges and structures: this study proposes guidelines and installation techniques based on best practice reported in the literature and on extensive practical experience in bonding of composite materials. The surface preparation of the materials, the application of the adhesive and the specifics of the strengthening are provided in detail. The design guidelines include the structural design criteria for the use of HM CFRP materials as a flexural strengthening system for typical steel–concrete composite bridge girders. The flexural design procedure is based on a moment–curvature analysis and a specified increase in the live load carried by the bridge to satisfy specific serviceability requirements. A bond model is also described in order to calculate the shear and peel stresses within the adhesive thickness. To prevent a premature debonding failure of the strengthening system, the criteria specify a maximum principal stress in the adhesive that cannot be exceeded for a given characteristic strength of an adhesive.

The research findings conclude that HM CFRP materials provide a promising alternative for strengthening steel bridges that can be easily designed and installed to increase their strength and stiffness. Stiffness increases between 10 and 34 % were found for the strengthened steel–concrete composite beams. Ultimate strength increases of up to 46 % were possible for the strengthening configurations studied. The beam using the pre-stressed CFRP strips was shown to make economical use of the CFRP material in providing a significant stiffness increase while maintaining the ductility of the original section. A wide range of research and real scale testing is available in the literature, the most relevant of which is reported in Table 13.3.

An interesting study in the area of bridge rehabilitation and research has been developed by Mertz *et al*. (2002). The project was performed in two stages. The first consisted of the selection of a steel bridge in collaboration with the Illinois Department of Transportation (IDoT) and developing site-specific design, installation and monitoring requirements for retrofitting in-service girders. This was followed by laboratory-scale preparatory tests representing site-specific conditions and, finally, a detailed field testing plan was developed for evaluating in-service performance. The second stage focused on the in-field installation and monitoring of the performance and durability of the retrofitted system under actual highway traffic and environmental conditions, followed by a review of the results and preparation of a guidance report for applying the system to steel

*Table 13.3* Fatigue test research results

| Reference | Details | Test type |
|---|---|---|
| Bocciarelli *et al.*, 2009 | S275 specimens reinforced on each side with Sika® CarboDur® M614 | Normal tension |
| Iwashita *et al.*, 2007 | Single-lap shear steel specimens | Normal tension |
| Jones and Civjan, 2003 | 5 steel specimens not reinforced and 24 specimens reinforced on each side | Normal tension |
| Monfared *et al.*, 2008 | 15 plates of steel reinforcing or not the specimens with FRP, with surface treatments, and applying the reinforcements on one or both sides | Normal tension |
| Zheng *et al.*, 2006 | 6 steel specimens with a hollow at the centre and provided with 2 cracks reinforced with CFRP on one or both sides | Normal tension |
| Colombi *et al.*, 2003 | Perforated steel specimens with 2 cracks, reinforced with 2 CFRP straps on each side | Normal tension |
| Taljsten *et al.*, 2009 | 5 historical steel specimens perforated, with 2 cracks | Normal tension |
| Liu *et al.*, 2005 | 12 steel joints comprising 2 steel plates CFRP reinforced, with normal or HM on each side | Normal tension |
| Tavakkolizadeh and Saadatmanesh, 2003 | 5 steel beams hollowed in the flanges and CFRP reinforced on the lower and midspan flange | Bending |
| Deng and Lee Marcus, 2007 | Steel beams CFRP reinforced on the lower and midspan flange | Bending |
| Bassetti *et al.*, 1999 | Truss riveted beams with I section, traditionally reinforced | Bending |
| Bassetti, 2001 | Truss riveted beams traditionally reinforced | Bending |
| | Truss riveted beams reinforced with 2 CFRP laminates and 3 CFRP post-tensioned laminates on the lower flange | Bending |
| Pipinato *et al.*, 2009 | Twinned riveted beams, not reinforced | Bending |
| Pipinato *et al.*, 2011a | Shear diaphragm | Shear |
| Pipinato *et al.*, 2012c | Literature database | Bending/shear |

bridge members. In addition, long-term monitoring was put into place in collaboration with the Delaware Department of Transportation (DelDoT). Load tests performed prior to and after the rehabilitation indicate a reduction in tension flange strains of 11 %. Monitoring has continued for an indefinite period of time to enable the durability of the CFRP–steel bond to be assessed. An analytical approach to FRP strengthening of steel and steel–concrete composite structures is presented in Pellegrino *et al*. (2009).

FRP decks have been used on increasingly significant projects throughout the world. Designers have become more familiar with the characteristics that FRP offers and have begun to apply FRP to projects that would most benefit – cases where low weight, corrosion resistance or rapid installation is critical. FRP decks are often suitable for historic, movable or high-traffic bridges. In the following sections, relevant case studies are presented which, even if not strictly related to railway bridges, are relevant because they involve the use of FRP for entire substructures.

### *Broadway Bridge*

The Broadway Bridge carries an average daily volume of 30 000 vehicles in four lanes of traffic (Figs 13.4 and 13.5). An FRP deck application could be

*13.4* The Broadway Bridge, Portland, OR, USA.

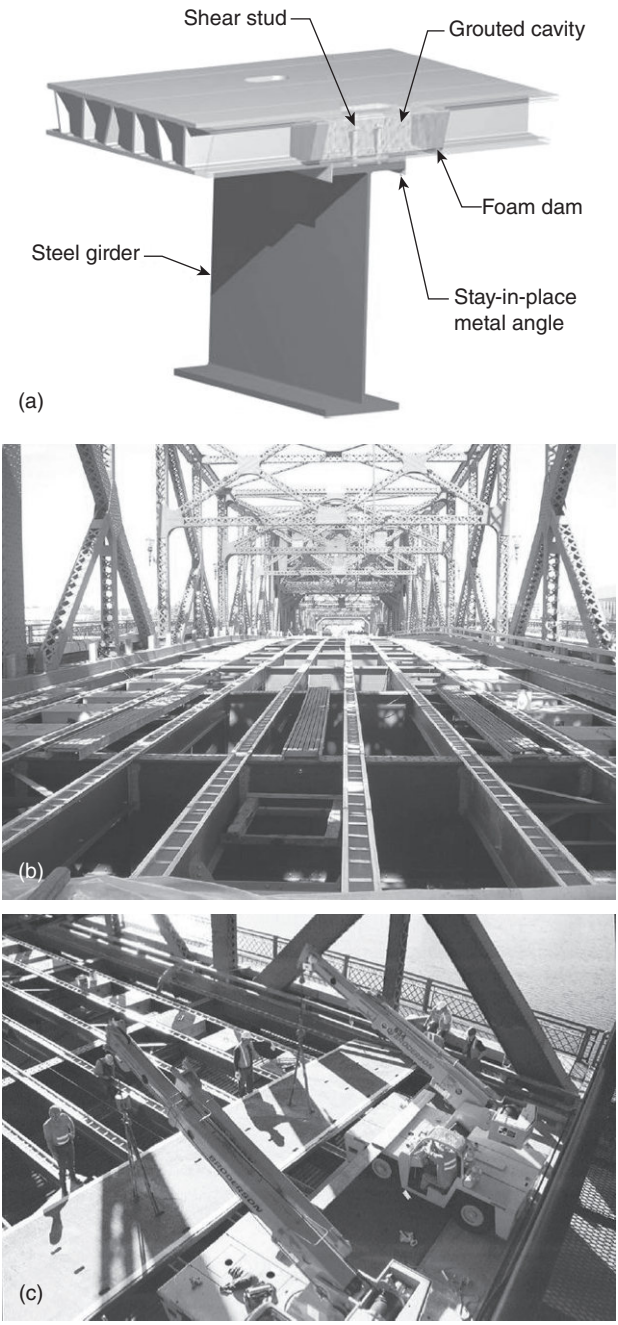


*13.5* The Broadway Bridge, Portland, OR, USA: the new FRP deck connection to the longitudinal steel girders (a); the steel grid deck without the old secondary structures (b); FRP deck panels setting in place with fork-lifts (c).

observed in this bascule bridge in Portland, Oregon. As reported by Sams (2005) the project deals with the requirement of a new deck that matched the weight of the bridge's existing steel grating, offering improved skid resistance, which could be installed quickly. Many of the FRP deck details were designed as conventional materials, particularly as precast concrete panels. The deck-to-beam connections are similar to conventional shear studs and grout-filled cavities to connect the new deck to the bridge's longitudinal beams. Grout was poured through the deck into a cavity formed by stay-in-place metal angles, providing a variable haunch along each longitudinal beam.

This attachment method had a proven track record in static testing, fatigue testing and in-place performance, and similar connections have allowed FRP decks and steel beams to perform together in composite action. Because of this connection's inherent ability to transfer shear, Broadway Bridge's beam–deck system likely exhibits some level of composite behaviour. However, the beams were sized to carry loads without consideration of the composite action. The prefabricated FRP panels arrived at the yard in $8 \times 46$ ft modules ($2.44 \times 14$ m), ready for installation on the beam's variable haunches. The length of each panel (46 ft/14 m) matched the width of the bridge deck, because the FRP panels span perpendicular to the bridge's longitudinal beams.

Shop workers had predrilled all holes to accommodate the connections to the bridge's longitudinal beams. At the heel of each bascule leaf, the FRP deck interfaced with a concrete transition deck, which was designed to accommodate dynamic vehicular forces. At the bridge's centre open joint (2 in/5.1 cm), the deck interfaced with heavy steel angles to accommodate dynamic forces. At the side edges, workers bonded an FRP curb to the deck along its full length. By their own weight, the pultruded panels matched the parabolic crown (2.25 in/5.7 cm) on the bridge's approach spans, so cambering was analysed in the shop, and panels arrived at the job site in their 'curved' state. Another key geometric feature of the existing bridge was its vertical alignment. In the portions of the bridge where the longitudinal stringers were vertically curved, each panel was placed on the stringers and conformed to the existing profile with a 'chord' effect. Each panel was straight, whereas the field joints accommodated incremental, extremely slight, rotations before adhesive curing.

Both accommodations facilitated the use of FRP on the unique structure and are expected to have minimal negative effects on the integrity of the deck system. At the time of construction, no AASHTO design criteria were established for FRP decks, so the supplier took full responsibility for the design and performance of this system.

*Morrison Bridge*

On the Morrison Bridge (Portland) (Fig. 13.6), the steel-grating on the bascule deck has been retrofitted using pultruded FRP decking. The FRP alternative to steel grating was chosen with a view to roadway safety (by providing improved traction for vehicles) and for its environmental protection and weight to strength characteristics. A prior experimental evaluation was conducted with the objective of evaluating the structural

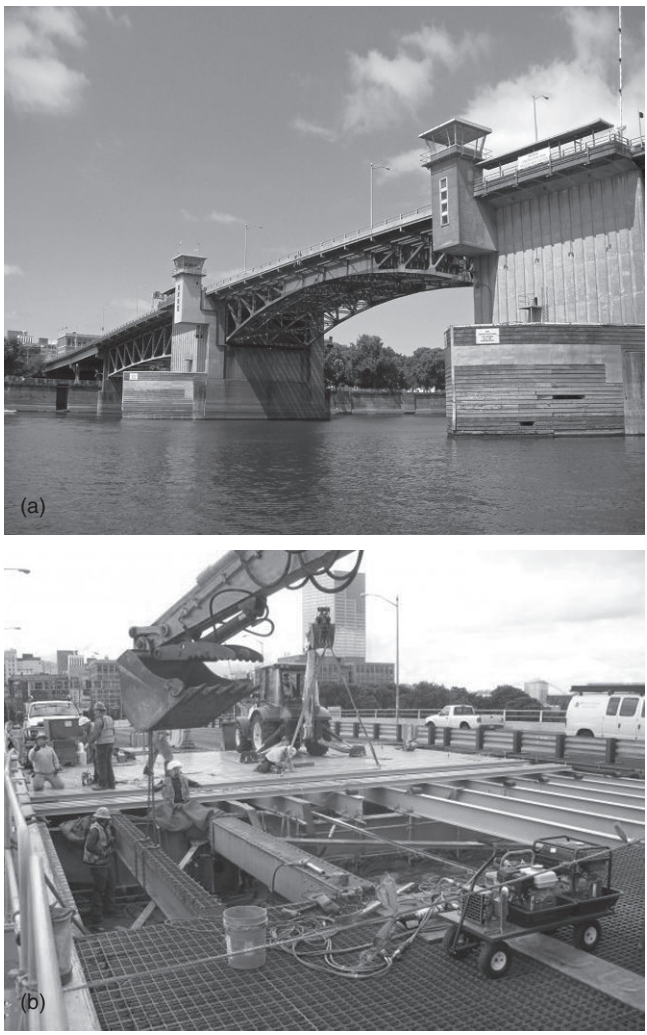


*13.6* The Morrison Bridge, Portland, OR, USA: actual state of the bridge (a); FRP deck panels setting in place (b).

performance of the FRP decking and the deck-to- stringer connections. The open steel grating on the double-leaf Chicago-type bascule span was replaced with a prefabricated, pre-engineered FRP composite bridge deck. The bridge, with over 50,000 vehicles crossing daily, is a major gateway in Portland. The work was completed in quads: for each quad, after the new stringers had been installed, the base section of the FRP deck was installed. Holes could then be drilled through both the FRP and the steel stringers. Once the two had been bolted together, the FRP top sheet of the FRP deck was attached with mechanical fasteners. After that, a wear surface was applied. On-site structural adhesives or resins were not adopted. Even if FRP decks can be attached to stringers with either shear studs and grout or structural bolts and neoprene, in this case the managing authority decided to proceed with bolting and neoprene for the connection system, because of weight constraints with the bascule spans.

## 13.4 Rehabilitation and strengthening against corrosion

Retrofitting procedures are needed to strengthen structural and non-structural members of bridges. The phenomenon most commonly affecting metal railway bridges is corrosion, which could have occurred on the bridge due to harsh environmental conditions and the loss of design accuracy to avoid water stagnation. Because corrosion is such a widespread damage issue, it is worth mentioning which structural details are most frequently affected:

- lacing bars;
- pinned/riveted connections, where small relative movements might trap moisture;
- bottom flanges of members due to debris build-up; and
- top flange of floor or girder beams due to deck leakage.

Fatigue capacity is related to corrosion damage and, if the corrosion loss was less than 50 % of the initial resisting area, notch effects rather than section loss governed fatigue capacity (Thiel *et al.*, 2001). Members to be investigated have to be chosen as shown in Fig. 13.7 according to ESDEP (2007) stepwise procedure.

Possible solutions to the problem of corrosion are as follows:

- *Do nothing solution*: If section loss is under 15 %, only NDT is necessary in order to investigate the ultimate strength of the structural element; a simplified FEM model could be performed to check the corroded structure in the critical details. If corrosion is diffused to the main structures of the bridge, even if section loss is under 15 %, a prevention

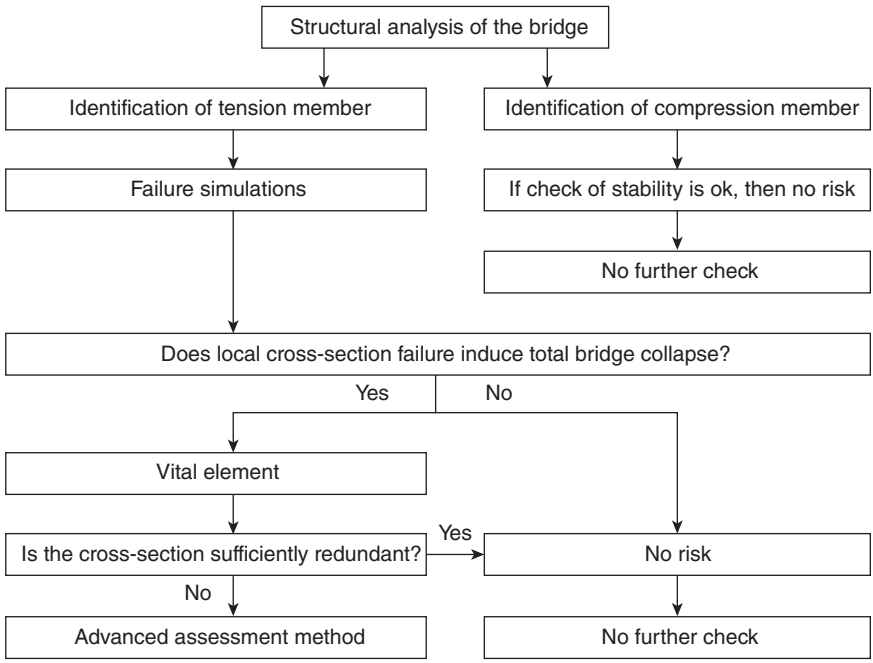


*13.7* Procedure for identification of vital elements.

of corrosion through painting works is needed. In this case, the precise intervention decision could be quantitatively assessed considering chloride contamination according to Chong (2004).

- *Repair member solution*: If section loss is under 40 % of the initial resisting area, the corroded member is moderately deteriorated and a repair of the member might be warranted. The rehabilitation technique is strictly related to the type of member: for example, a corroded tension member could be strengthened by adding new steel plates or a compression member could be reinforced using cover-plates or by post-tensioning. As a reference, some cover-plated and bolted repairs for members of the Eads St Louis Bridge (Luis Silano, 1992), whose floor system had been badly deteriorated by corrosion, are reported in Fig. 13.8: the weakened area is reinforced by cover-plating and bolting, or only by bolting in cases of rivet failure.
- *Replace member*: If section loss is over 40 %, the corroded member is severely deteriorated. Removing and replacing a member includes the following stages: (i) support structural system before removing member; (ii) remove damaged member; (iii) add replacement member; (iv) remove supporting system. Figure 13.9 shows the outlines of the

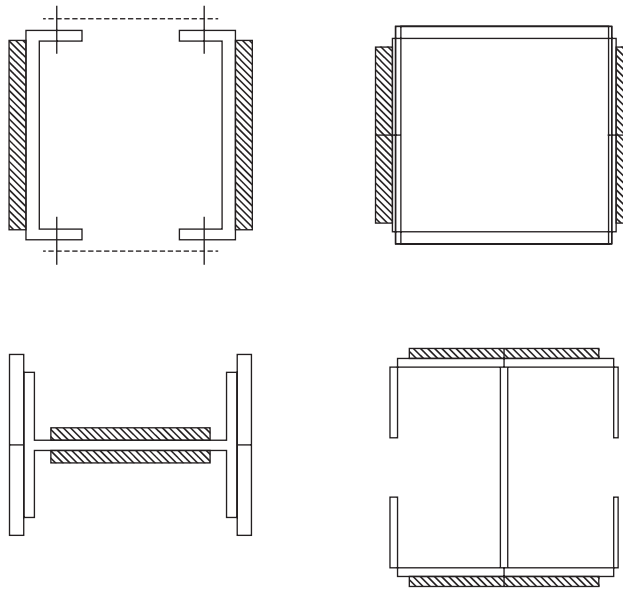

*13.8* Bolted repairs for corroded members: bolted reinforcement plates are designated by dashed lines areas.

replacement of a diagonal tension member of a truss bridge similar to the one investigated by Luis Silano (1992).

- *Replace the entire structure*: This choice has to be adopted in situations where member replacing or repairing is not affordable in terms of time, traffic delay or cost isssues.

A detailed procedure for retrofit or structure replacement can be found in Kuhn *et al*. (2008), while a global cost analysis should be performed according to BRIME (Woodward *et al*., 2001) in order to choose the most suitable intervention.

## 13.5 Strengthening of structural members

Historic bridges are often under-strength or have to be retrofitted to carry increasing loads or to improve fatigue resistance. These bridges were often built before the development of national standards, or designed using past loading models. If the entire structure is inadequate, it should be replaced. On the other hand, if one or a few members are under-strength, then rehabilitation might address only those members. Herein structural member-strengthening techniques are presented as possible guidelines for common design situations, in particular for floor beams, girders and

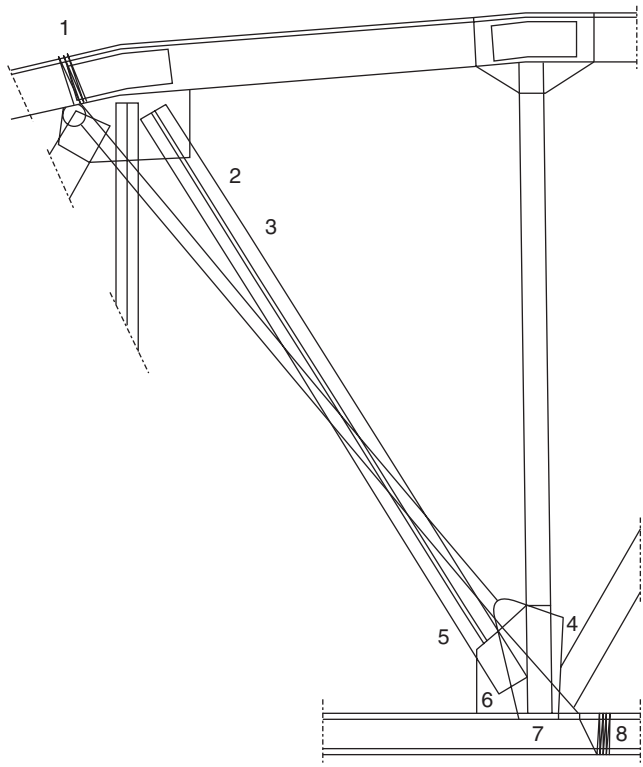


*13.9* Replacement of a diagonal tension member: (1) cable with minimum of four wraps; (2) upper diagonal to be replaced; (3) one loop cable and one turnbuckle; (4) blocking for cable to clear flange of floor-beam; (5) cable with minimum of four wraps; (6) burn holes in lateral plate for cable; (7) half round wood block or similar steel specimens; (8) cable with minimum of four wraps.

stringers, tension member, compression member, pinned connections and riveted connections:

- *Coverplating*: Coverplates are either bolted or welded to the existing member to increase its rigidity, thereby decreasing the stresses present in the member. Again, welding of old metals should be adopted with caution. Welding might cause delamination of wrought iron or fatigue cracking at the ends of cover plates.
- *Post-tensioning*: This technique relies on a supplementary element, for example to apply a negative moment, thereby reducing the flexural stresses in the member. Post-tensioning bars or pre-stressing tendons can often be used to apply equivalent external forces to the system. These systems increase the allowable service loads in the member.

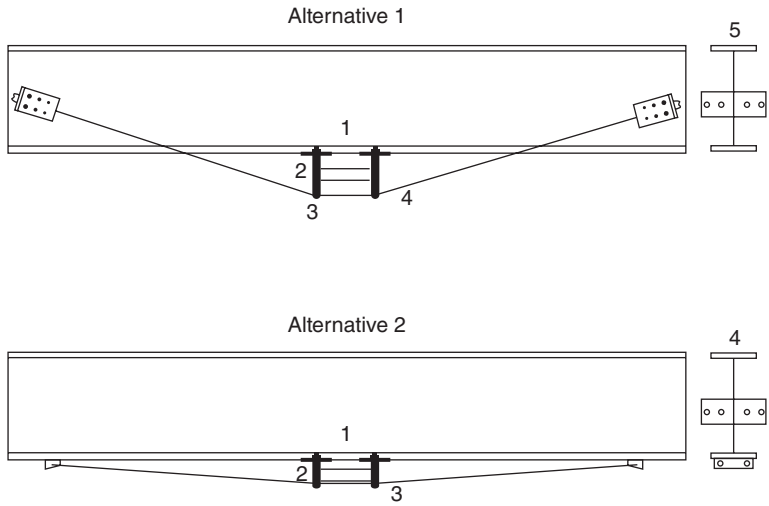


*13.10* King post-strengthened beam technique intervention, two alternatives. Alternative 1: existing beam (1), king post support (2), rounded edges on the bottom of the webs (3), post-tensioning truss rods (4), current section (5). Alternative 2: existing beam (1), king post support (2), post-tensioning truss rods (3), current section (4).

- *King post*: The principles of post-tensioning are utilised, but applied with a different geometry. King posts form a triangular shape stemming from a bracket located at mid-span of the beam separating the tendon from the flexural member. The primary benefit of the king post is the small axial force in the tendon, relative to the high negative moment applied to the beam. An example of a king post is given in Fig. 13.10 (Luis Silano, 1992).
- *Composite action*: This provides strengthening by adopting a composite deck solution, in which shear is transferred between concrete slab and steel beams.
- *Additional members*: The new members may redistribute the forces to other bridge elements. The addition of new members is most commonly undertaken during a deck replacement (see for example Fig. 13.11 according to Klaiber *et al.*, 1987).

For truss railway bridges, critical structural members to be strengthened could be:

- the main compressive members, that are generally repaired through cover plating, as reported in Fig. 13.12 according to Bondi (1985); and/or

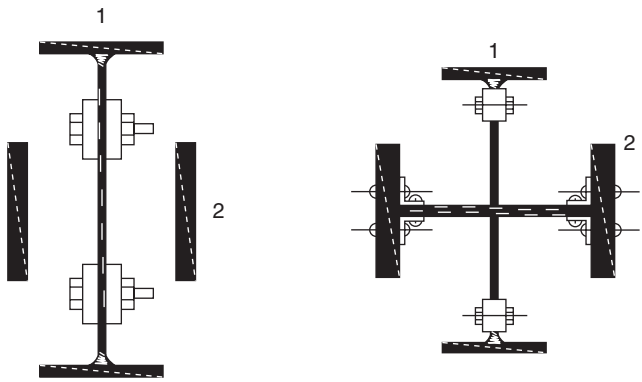


*13.11* New member added to existing tension members: new member (1), existing eyebar (2).

- the riveted connections, which are often susceptible to debris and corrosion due to the built-up nature of the elements.

Furthermore, it has to be considered that during the original design operation, fatigue may not have been considered, whereas a connection repair should address fatigue and be designed accordingly (Brühwiler *et al.*, 1990). High strength bolts should be used to replace rivets: this intervention introduces an higher clamping force imposed by the new bolts, acting as an increase in shear capacity and fatigue life. If corrosion or cracking propagate on the main parts of the member investigated, member replacing should be the most suitable intervention. Further specifications on bridge strengthening and repairing are presented in Table 13.4.

### 13.5.1 Case study: Adige Bridge

Simple truss spans are simply supported on the shoulders and on the central piles in the riverbed. The historic Adige Bridge was built in 1866 and, after 40 years, the second parallel track was added (Pipinato *et al.*, 2012a). These bridges were both destroyed during World War II. The configuration of the bridge structure is presented in Fig. 13.13: the even-track was built in 1946 and the other in 1949. The bridge studied is the oldest in service (from 1946). The superstructure consists of riveted built-up truss members. The bridge consists of a double three-span (50.16 m–60.648 m–50.160 m ≈ 161 m) two-way truss girder, 5.06 m wide (from the centre of mass of the lower chords) and 7.2 m high (from lower chord to upper).

Each bridge consists of two longitudinal truss girders with transverse frames at the deck. The longitudinal truss beam is made up of 32 different

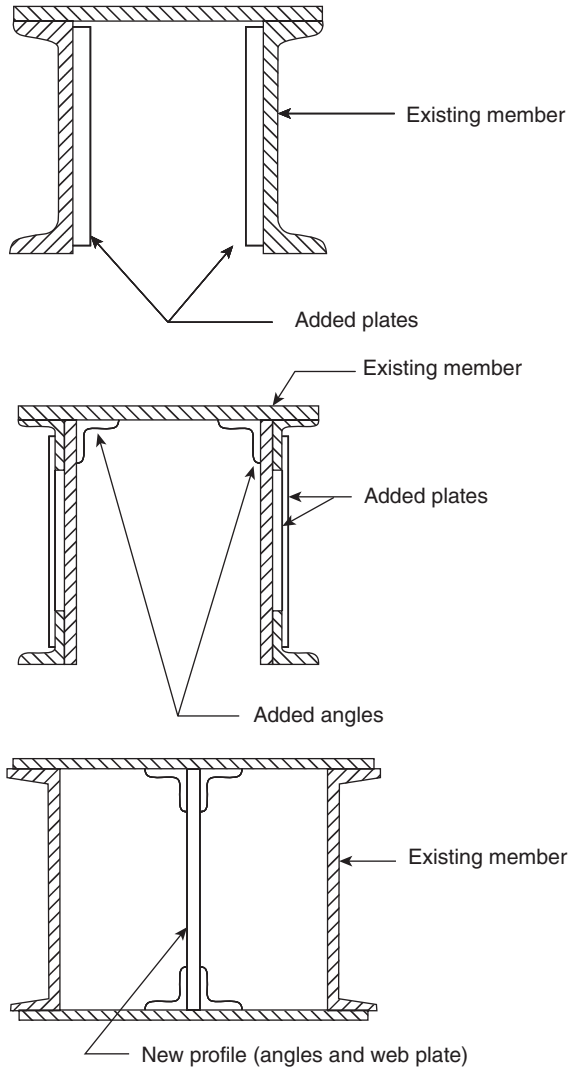


*13.12* Cover plate options for compressive members (Bondi 1985).

cross-sections having slightly variable geometric dimensions. Lower and upper chords are composed of U-shaped sections. The deck comprises longitudinal stringers and transverse floor beams. Wooden transverse beams have in fact been totally replaced along the national railway lines with concrete ones, except in metal bridges in which they remain in order to avoid induced failure or cracking related to vibrations. All structural elements are built-up members, connected by hot riveting. With regard to

*Table 13.4* Intervention techniques: case studies

| Failure | Repair | Strengthening | Structure mainly affected (W = welded; RB = riveted or bolted) |
|---|---|---|---|
| Fatigue cracks on the upper flange at the cross bracing connection detail | • stop holes<br>• full penetration welding and surface treatment | • improve the weld detail<br>• surface treatments such as grinding and/or peening<br>• use symmetrical connections | W |
| Cracks at the coped end of deck plate girders | • stop holes<br>• full penetration welding and surface treatment<br>• reinforcement by splice plates | • adding bolt connection with rib plates<br>• adding plates or FRP | W |
| Cracks in welded gusset plate joint on flanges | • stop holes<br>• improving of weld detail | • improving of weld detail<br>• surface treatments | W |
| Cracks at transverse front welds at cover plate end | Depending on the surface crack length:<br>• long cracks $L <$ 40 mm: stop holes and splicing with bolts<br>• short cracks $L <$ 10 mm: surface treatments such as TIG dressing or hammer peening | • improving the weld toe detail<br>• surface treatments such as grinding and/or peening<br>• adding filler plate or FRP<br>• shear splices using bolts or injection bolts | W |
| Cracks in the butt connection groove weld of tension-side longitudinal stiffener or flanges | • adding a filler plate or FRP<br>• splicing by using bolts<br>• re-welding and surface treatments if cracks are small and have not reached the web | • adding filler plate or FRP<br>• splicing by using bolts<br>• re-welding | W |

(*Continued*)

*Table 13.4* Continued

| Failure | Repair | Strengthening | Structure mainly affected (W = welded; RB = riveted or bolted) |
|---|---|---|---|
| Fatigue crack in sole plate connection detail at support | • adding plates or ribs to the web of the supported girder<br>• reinforcement by bolted splices<br>• stop holes | • adding plates or ribs to the web of the supported girder<br>• reinforcement by bolted splices<br>• modification of connection detail | W |
| Fatigue crack in the web or flange, initiated at the fillet weld toe of the cut out web | • stop holes (w-g) when crack in the web<br>• adding filler plate or FRP | • adding filler plate or FRP<br>• increasing the curvature ratios of the cut outs<br>• full penetration welding and surface treatment | W |
| Orthotropic steel bridge deck, different details with low fatigue strength | • stop holes<br>• adding filler plate or FRP | • preventive stop holes<br>• strengthening deck plate by thicker steel deck or thicker pavement<br>• adding steel plates or FRP strips | W |
| Cracks induced by vibration, e.g. by wind or traffic, mainly in hanger and pinned connections | re-welding of small cracks followed by surface treatment | • change of the static system or connection detail<br>• improvement of weld quality by surface treatment methods<br>• increase curvature ratios | W |

(*Continued*)

*Table 13.4* Continued

| Failure | Repair | Strengthening | Structure mainly affected (W = welded; RB = riveted or bolted) |
|---|---|---|---|
| Cracks near the end of a vertical web stiffener | • stop holes<br>• weld toe finishing by TIG-dressing or grinding | • prevention of out-of-plane distortion of the girder web<br>• increase flexibility of the connection | W |
| Fatigue crack occurred in the coped web of the end floor beam | • stop holes<br>• gouging and re-welding | • adding filler plate<br>• splicing by using HT bolts | RB |
| Cracks initiating at the holes in net cross section at the end of cover plates due to overload and due to changes of geometry | • remove cracked member, add longer cover and filler plate in the tension flange with bolts | • high strength bolts in the last connection of the upper cover plate<br>• adding filler plate and longer cover plate by bolts<br>• adding FRP or steel plates | RB |
| Cracks in the flange of the net cross section due to changes of geometry | • remove cracked member, add longer cover and filler plate in the tension flange with bolts | • high strength bolts in the last connection of the upper cover plate<br>• adding filler plate and longer cover plate by bolts<br>• adding FRP or steel plates | RB |
| Cracks in gusset plates due to insufficient thickness | • short cracks: HT-bolts<br>• long cracks: exchange of the gusset plate | • use bolts in the last 3–4 rivets of the connected truss members<br>• drilling of rivet holes to remove micro cracks, caused by riveting process | RB |

(*Continued*)

*Table 13.4* Continued

| Failure | Repair | Strengthening | Structure mainly affected (W = welded; RB = riveted or bolted) |
|---|---|---|---|
| Cracks in barrel shaped ballast sheets | • stop holes as temporary measure<br>• change of the static system by applying the load directly into the cross beams by means of stiff load transfer beams | • unload the barrel shaped ballast sheets without horizontal stiffeners by stiff load transfer beams | RB |
| Cracks in a connection between cross beam and longitudinal roadway beam | • reduce stiffness by means of large hole drilling<br>• exchange of structural member | • reduce stiffness by means of large hole drilling<br>• exchange of structural member | RB |
| Cracks due to frozen bearings or joints, because of corrosion or temperature differences | • stop holes<br>• exchange of the cracked member<br>• function control of the bearings | • control corrosion protection<br>• control of moveability of bearings and joints | RB |
| Fatigue failure of rivet heads due to local bending | • high strength bolts in the last connection of the connected member or angle of the stringer | • exchange rivets by high strength bolts<br>• adding additional members<br>• change static system | RB |

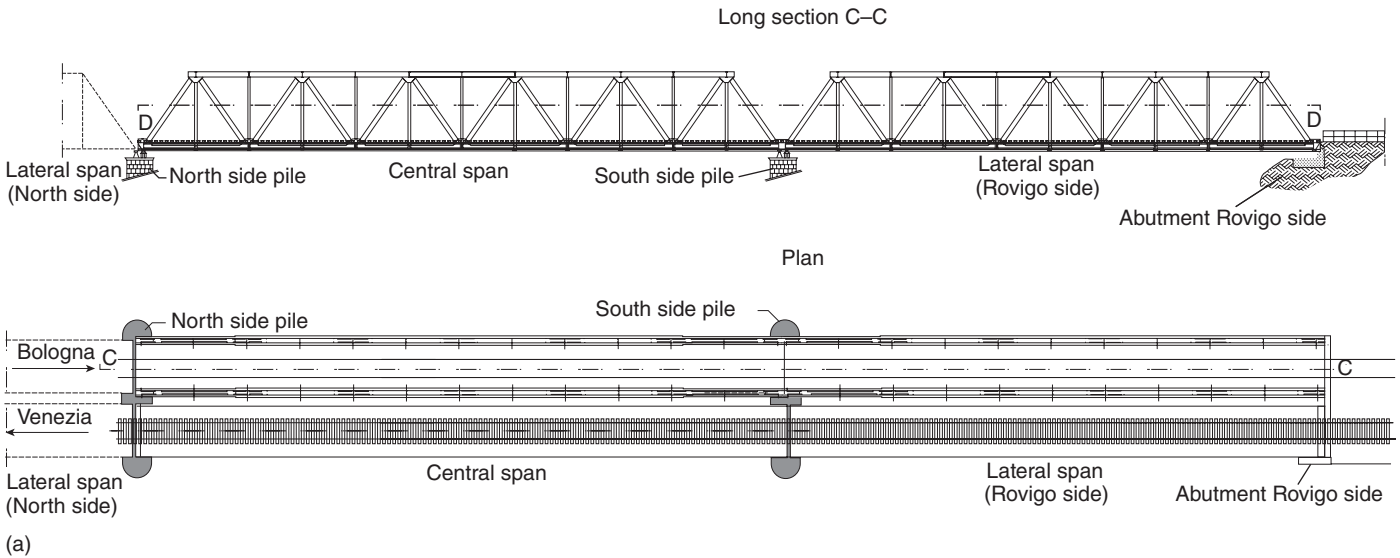


(a)

*13.13* Adige Bridge: (a) plan and long section of the central and south span; (b) long section and plan of the central span; (c) boundary conditions (Pipinato *et al.* 2012a).

(*Continued*)

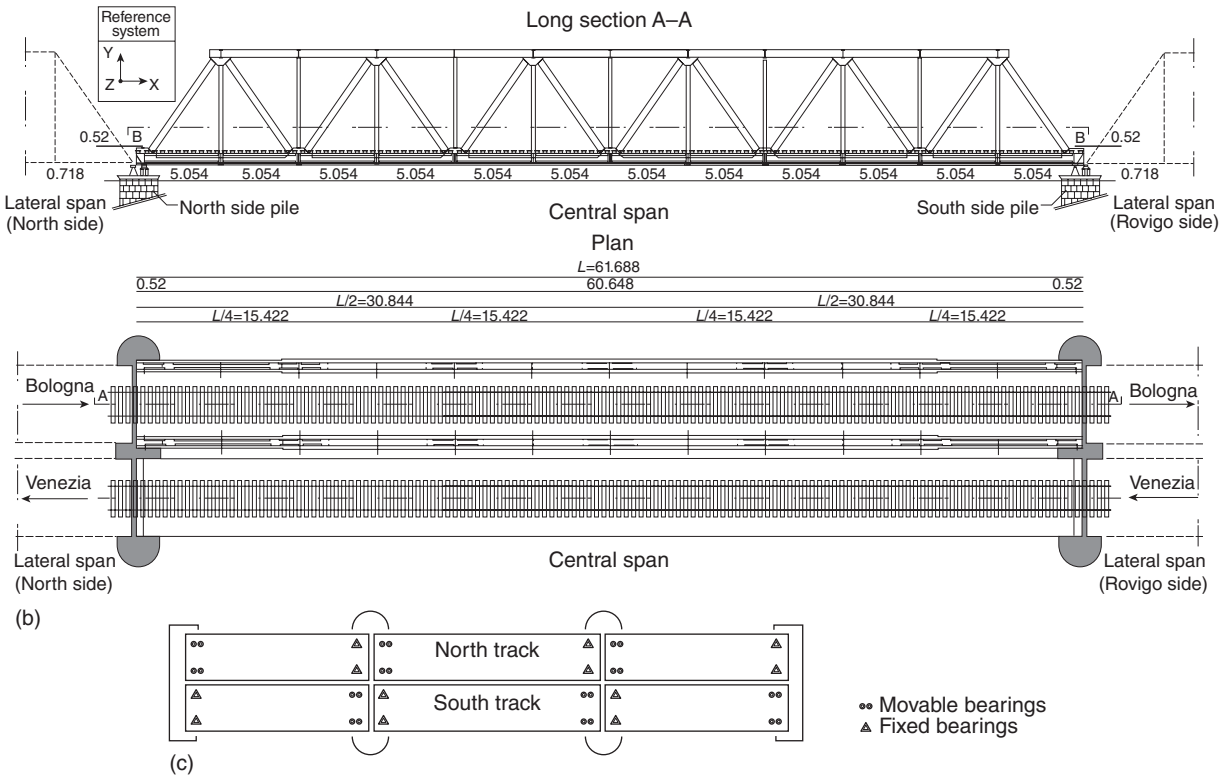


*13.13* Continued

boundary conditions, double fixed and movable bearings stand alternately on each side span as shown.

The application of an assessment procedure to the Adige Bridge outlined some relevant issues. The materials used in this railway bridge have shown mechanical and chemical properties (strength, chemical composition) comparable to those provided by actual Eurocodes; corrosion is a local phenomenon that does not necessarily play a relevant role in the global response of the bridge if section loss is less than 15 %; fatigue cracks have not been discovered in this first-phase assessment; fatigue assessment concerning the remaining life has been performed using the linear damage approach of the Palmgren–Miner procedure, accounting for the possible traffic increase for the estimation of its residual lifetime.

The result of this assessment has given a reasonable and detailed estimation of safe practice; monitoring has been considered to be an option when the calculated fatigue safety will be doubtful or insufficient. A dynamic evaluation has been carried out looking at ambient excitation and at the effects of external actions associated with low and high speed trains, etc. However, the behaviour of the structures remains satisfactory. The application of such a comprehensive procedure to the Adige Bridge, a common truss scheme in Italy for railway bridges, showed that a detailed analysis and assessment can result in limiting the economical effort for retrofitting works to a small fraction of the costs needed for replacing the bridge (Pipinato and Modena, 2010; Pipinato *et al.*, 2012a).

## 13.6 Conclusion

Bridges form an essential component in the transport infrastructure, and many steel railway bridges dating back to the 19$^{th}$ and early 20$^{th}$ centuries remain in use around the world. This chapter has focused on research initiatives in this area aimed at understanding the behavior of such bridges and, specifically, on procedures for their assessment and rehabilitation in order to prevent dangerous damage. A four-level assessment procedure has been described and case studies presented. Step-level assessment has been demonstrated to be the most useful and diffused way to prevent damage and to program the assessment and repair of single bridges and their network. Further studies are needed in this field: first, in the framework of real-scale testing in order to optimise interventions; second, in the optimisation of materials used to rehabilitate these old structures; finally, in the context of managing the risk of larger and larger amounts of ancient and damaged bridge networks, without appropriate funding to rebuild all infrastructures.

## 13.7 References

Albrecht, P. and Lenwari, A. (2008). Design of prestressing tendons for strengthening steel truss bridges. *Journal of Bridge Engineering*, 13(5), 449–454.

Albrecht, P. and Lenwari, A. (2009). Variable-amplitude fatigue strength of structural steel bridge details: Review and simplified model. *Journal of Bridge Engineering*, 14(4), 226–237.

Al-Emrani, M. (2005). Fatigue performance of stringer-to-floor-beam connections in riveted railway bridges. *Journal of Bridge Engineering*, 10(2), 179–185.

Åkesson, B. and Edlund, B. (1995). Fatigue life or riveted railway bridges. *IABSE Symposium (San Francisco): Extending the Lifespan of Structures*, Report 7311, Zurich IABSE, 1079–1084.

ASCE (1982). Committee on fatigue and fracture reliability of the committee on structural safety and reliability of the structural division. Fatigue reliability 1–4. *Journal of Structural Division, ASCE*, 108(ST1), 3–88.

Bassetti, A. (2001). *Lamelles Precontraintes en Fibres Carbonepour le Renforcement de Ponts Rivet es Endomma es par Fatigue*. Ph.D. Thesis no. 2440, Swiss Federal Institute of Technology (EPFL), Lausanne.

Bassetti, A., Liechti, P. and Nussbaumer, A. (1999). Fatigue resistance and repairs of bridge riveted members. *Fatigue Design and Reliability*, 23, 207–218.

Bocciarelli, M., Colombi, P., Fava, G.E. and Poggi, C. (2009). Fatigue performance of tensile steel members strengthned with CFRP plates. *Composite Structures*, 87, 334–343.

Bondi, R.W. (1985). Adding redundancy to fracture critical eyebar members in a cantilever truss bridge. In: *Proceedings of the 2nd Annual International Bridge Conference*, 17–19 June, Pittsburgh, PA, Engineer's Society of Western Pennsylvania, 47–53.

Boulent, M.I., Righiniotis, T. and Chryssanthopoulos, M.K. (2008). Probabilistic fatigue evaluation of riveted railway bridges. *Journal of Bridge Engineering*, 13, 237–244.

Bursi, O.S., Ferrario, F. and Fontanari, V. (2002). Non-linear analysis of the low-cycle fracture behavior of isolated Tee stub connections. *Computers and Structures*, 80(27–30), 2333–2360.

Brühwiler, E., Smith, I.F.C. and Hirt, M. (1990). Fatigue and fracture of riveted bridge members. *Journal of Structural Engineering*, 116(1), 198–213.

Byers, W.G., Marley, M.J., Mohammadi, J., Nielsen, R.J. and Sarkani, S. (1997). Fatigue reliability reassessment applications: State-of-the-art paper. *Journal of Structural Engineering*, 123(3), 277–285.

Cadei, J.M.C., Stratford, T.J., Hollaway, L.C. and Duckett, W.G. (2004). *Strengthening Metallic Structures Using Externally Bonded Fibre-reinforced Polymers*, C595. London: CIRIA.

Chong, S.L. (2004). *Preventing corrosion in steel bridges*, Technical Report. Washington, DC: United States Department of Transportation, Federal Highway Administration (FHWA), Paint and Corrosion Laboratory (PCL).

Colombi, P., Bassetti, A. and Nussbaumer, A. (2003). Delamination effects on cracked steel members reinforced by prestressed composite patch. *Theoretical and Applied Fracture Mechanics*, 39(1), 61–71.

Deng, J. and Lee Marcus, M.K. (2007). Fatigue performance of metallic beam strengthened with a bonded CFRP plate. *Composite Structures*, 78, 222–231.

Di Battista, J.D., Adamson, D.E. and Kulak, G.L. (1997). Fatigue strength of riveted connections. *Journal of Structural Engineering*, 124(7), 792–797.

Ermopoulos, J. and Spyrakos, C.C. (2006). Validated analysis and strengthening of a 19th century railway bridge. *Engineering Structures*, 28, 783–792.

EN 1993-1-9 (2005). *Eurocode 3: Design of steel structures – Part 1–9: Fatigue*. Brussels: CEN.

ESDEP (2007). *European Steel Design Education Programme*. Ascot: Steel Construction Institute.

Farhey, D.N., Thakur, A.M. and Buchanan, R.C. (1997). Structural deterioration assessment for steel bridges. *Journal of Bridge Engineering*, 2(3), 116–124.

Italian Research Council (2005). *Guidelines for the design and construction of externally bonded FRP systems for strengthening existing structures. Preliminary study. Metallic structures*, CNR–DT 202/2005. Rome: Italian Research Council, Italian Advisory Committee on Technical Recommendations for Construction.

Iwashita, K., Wu, Z., Ishikawa, T., Hamaguchi, Y. and Suzuki, T. (2007). Bonding and debonding behavior of FRP sheets under fatigue loading. *Advanced Composite Materials*, 16(1), 31–44.

Jones, S.C. and Civjan, S.A. (2003). Application of fibre reinforced polymer overlays to extend steel fatigue life. *Journal of Composites in Construction* 7(4), 331–338.

Klaiber, F.W., Dunker, K.F., Wipf, T.J. and Sanders, W.W. (1987). *Methods of strengthening existing highway bridges*, Highway Research Program 293. Washington DC: Transportation Research Board, National Cooperative.

Kulak, G.L. (1992). Discussion of 'Fatigue strength of riveted bridge members' by John W. Fisher, Ben T. Yen and Dayi Wang. *Journal of Structural Engineering*, 116(11), 2968–2981.

Kuhn, B., Lukic, M., Nussbaumer, A., Gunther, H.-P., Helmerich, R., Herion, S., Kolstein, M.H., Walbridge, S., Androic, B., Dijkstra, O. and Bucak, Ö. (2008). *Assessment of existing steel structures: Recommendations for estimation of remaining fatigue life*, EUR 23252 EN. Luxembourg: Office for Official Publications for the European Community.

Liu, H.B., Zhao, X.L. and Al-Mahaidi, R. (2005). The effect of fatigue loading on bond strength of CFRP bonded steel plate joints. In Chen, J.F. and Teng, J.G. (eds), *International symposium on bond behaviour of FRP in structures*. Hong Kong, 11FC Secretariat, 459–464.

Luis Silano, G. (1992). *Bridge Inspection and Rehabilitation: A practical guide*. Canada: Wiley-IEEE.

Matar, E.B. and Greiner, R. (2006). Fatigue test for a riveted steel railway bridge in Salzburg. *Structural Engineering International*, 16(3), 252–260.

Mertz, D.R., Gillespie, J.W., Chajes, M.J. and Sabol, S.A. (2002). *The Rehabilitation of Steel Bridge Girders Using Advanced Composite Materials*, Final Report NCHRP-IDEA Project 51. Washington, DC: Transportation Research Board.

Monfared, A., Soudki, K. and Walbridge, S. (2008). CFRP reinforcing to extend the fatigue lives of steel structures. In Motavelli, M. (ed.), *Fourth International Conference on FRP Composites in Civil Engineering* (CICE2008), Zurich, 22–24 July, 5.E.2.

Moy, S.S.J. (ed.) (2001). *FRP composites: Life extension and strengthening of metallic structures. ICE design and practice guide*. London: Thomas Telford.

Moy, S.S.J. and Bloodworth, A.G. (2007). Strengthening a steel bridge with CFRP composites. *Proceedings of the Institution of Civil Engineers (ICE), Structures and Buildings*, 160, 81–93.

Moy, S.S.J. and Lillistone, D. (2006). Strengthening cast iron using FRP composites. *Proceedings of the Institution of Civil Engineers (ICE), Structures and Buildings*, 159(6), 309–318.

Oehme, P. (1989). Schäden an Stahltragwerken – eine Analyse [Damage analysis of steel structures], *IABSE Proceedings* P-139/89, November.

Pellegrino, C., Maiorana, E. and Modena, C. (2009). FRP strengthening of steel and steel-concrete composite structures: an analytical approach. *Materials and Structures*, 42(3), 353–363.

Pipinato, A. (2010). Step level procedure for remaining fatigue life evaluation of one railway bridge. *Baltic Journal of Road and Bridge Engineering*, 5(1), 28–37.

Pipinato, A. (2011). Assessment of existing bridges: Safety and security issues [Problemi di sicurezza nelle valutazioni strutturali di ponti esistenti]. *Ingegneria Ferroviaria*, 66(4), 355–371.

Pipinato, A. (2012). Coupled safety assessment of cable stay bridges. *Modern Applied Science*, 6(7), 64.

Pipinato, A. and Modena, C. (2010). Structural analysis and fatigue reliability assessment of the Paderno bridge. *Practice Periodical on Structural Design and Construction*, 15(2), 109–124.

Pipinato, A., Pellegrino, C., Bursi, O.S. and Modena, C. (2009). High-cycle fatigue behavior of riveted connections for railway metal bridges. *Journal of Constructional Steel Research*, 65(12), 2167–2175.

Pipinato, A., Molinari, M., Pellegrino, C., Bursi, O.S. and Modena, C. (2011a). Fatigue tests on riveted steel elements taken from a railway bridge. *Structure and Infrastructure Engineering*, 7(12), 907–920.

Pipinato, A., Pellegrino, C. and Modena, C. (2011b). Fatigue assessment of highway steel bridges in presence of seismic loading. *Engineering Structures*, 33(1), 202–209.

Pipinato, A., Pellegrino, C. and Modena, C. (2012a). Assessment procedure and rehabilitation criteria for the riveted railway Adige Bridge. *Structure and Infrastructure Engineering*, 8(8), 747–764.

Pipinato, A., Pellegrino, C., Fregno, G. and Modena, C. (2012b). Influence of fatigue on cable arrangement in cable-stayed bridges. *International Journal of Steel Structures*, 12(1), 107–123.

Pipinato, A., Pellegrino, C. and Modena, C. (2012c). Fatigue behavior of steel bridge joints strenghtened with FRP laminates. *Modern Applied Science*, 6(9), 1–14.

Pipinato, A., Pellegrino, C. and Modena, C. (2013). Residual life of historic riveted steel bridges: an analytical approach. *Proceedings of the ICE–Bridge Engineering*, DOI: 10/1680/bren.11.00014.

Sams, M. (2005). Bridge deck application of fiber-reinforced polymer. *Transportation Research Record: Journal of the Transportation Research Board*, CD 11-S. Washington, DC: Transportation Research Board of the National Academies, 175–178.

Schnerch, D. and Rizkalla, S. (2008). Flexural strengthening of steel bridges with high modulus CFRP strips. *Journal of Bridge Engineering*, 13(2), 192–201.

Schnerch, D., Dawood, M. and Rizkalla, S. (2007). Proposed design guidelines for strengthening of steel bridges with FRP materials. *Construction and Building Materials*, 21, 1001–1010.

Taljsten, B., Hansen, C.S. and Schmidt, J.W. (2009). Strengthening of old metallic structures in fatigue with prestressed and non-prestressed CFRP laminates. *Construction and Building Materials*, 23, 1665–1667.

Tavakkolizadeh, M. and Saadatmanesh, H. (2003). Fatigue strength of steel girders strengthened with carbon fiber reinforced polymer patch. *Journal of Structural Engineering, ASCE*, 129(2), 186–196.

Thiel, M.E., Zulfiqar, K. and Engelhardt, M.D. (2001). *Evaluation and rehabilitation of historic metal truss bridges: Survey of literature and current practices*, Research Report 1741–10 Austin, TX: Center for Transportation Research, The University of Texas at Austin.

Woodward, R. (*et al.*) (2001). *Bridge Management in Europe. Final Report D14*. European research project under the EU 4th framework programme. Available at: http://www.trl.co.uk/brime/d14.pdf (accessed October 2013).

Zhao, X.L. and Zheng, L. (2007). State-of-the-art review on FRP strengthened steel structures. *Engineering Structures*, 29, 1808–1923.

Zheng, Y., Ye, L. and Lu, X. (2006). Experimental study on fatigue behaviour of tensile plates strengthened with CFRP plates. In Mirmirian, A. and Wanni, A. (eds) *Third International Conference on FRP Composites in Civil Engineering* (CICE2006), Miami, FL, 13–15 December, 733–736.

# 14

# Strengthening of historic metallic structures using fibre-reinforced polymer (FRP) composites

S. MOY, formerly University of Southampton, UK

**DOI**: 10.1533/9780857096654.4.406

**Abstract**: This chapter looks at strengthening cast and wrought iron structures using fibre-reinforced polymer (FRP) composites. These historic metals are still common in railway infrastructure and have metallurgical characteristics that influence any approach to strengthening. The chapter discusses their metallurgy, how it influenced the original structural forms and how it affects FRP strengthening. The chapter shows that examination of the causes of corrosion and then careful surface preparation are key and that manufacturing imperfections and riveted connections drive the method of FRP application.

**Key words**: cast and wrought iron, metallurgy of historic ferrous metals, interlaminar shear, vacuum infusion, FRP around rivets.

## 14.1 Introduction

Whilst other chapters deal with strengthening of steel structures using fibre-reinforced polymer (FRP) composites, this chapter considers the other ferrous metals, cast iron and wrought iron, which were used to create superb structures in the 18th and 19th centuries. Many of these historic structures are worth preserving in their own right, but many are still in use today particularly in railway infrastructure. Often they are so important strategically that they cannot be demolished because to do so would cause too much disruption to the railway system. Such structures need to have their effective life extended or need to be strengthened to meet new loadings or new design requirements. FRP has already been used for such remedial schemes, and the aim of this chapter is to show the possibilities of using FRP with the historic ferrous metals.

Cast and wrought iron, although alloys of iron and carbon like steel, are very different structural materials. Both have interesting metallurgy which influences their mechanical behaviour and the means by which FRP strengthening can be carried out. For this reason, a section of the chapter is devoted to their metallurgy. The author of this chapter is based in the

UK, where much of the research on the use of FRP with historic metals has been carried out. Consequently, the contents of the chapter have a UK focus. The author wishes to make clear that there are structures of cast and wrought iron throughout the world so the contents of this chapter have relevance for engineers everywhere.

## 14.2 Brief history of the use of cast iron and wrought iron

As explained in reference 1, the Industrial Revolution in the UK was driven by the production of ferrous metal on an industrial scale, and the key factor was the rapid expansion of various transport systems, particularly the railways. At first the metal used was cast iron, followed by wrought iron and finally steel. The use of structural cast iron developed towards the end of the 18th century. Cast iron columns were used in churches in the 1770s and in textile mills from the 1790s onwards. The well known Ironbridge, built in 1779, was the first cast iron bridge. Ditherington Flax Mill, Shrewsbury, UK dating from 1796 was the first iron-framed building. However, historic cast iron had serious limitations as a structural material, in particular, its weakness in tension and brittle failure characteristics.

Wrought iron has been produced since biblical times, but Henry Cort's 1783 patent for the puddling furnace is widely accepted as the start of wrought iron production on an industrial scale. Wrought iron manufacture became one of the great Victorian industries with hundreds of manufacturing companies throughout the UK. From the late 1840s, wrought iron gradually took over from cast iron as a higher performance material. It had high strength in both tension and compression and also, in the right circumstances, significant ductility. It was common to use the more expensive wrought iron in tensile or flexural members with cast iron for the compression members. The best example of this combination was Paxton's Crystal Palace that housed the Great Exhibition of 1851 in Hyde Park, London. Following the collapse of the cast iron Dee Bridge in 1847, wrought iron almost completely replaced cast iron in railway bridges.

Steel was produced commercially by the Bessemer process from the 1860s but was rarely used in structures completed before 1890. However, by 1900 steel was the only ferrous metal used in new construction in the UK. The cast iron developmental period largely bypassed the rest of Europe and the USA, although there are some notable examples of cast iron bridges. There is, however, a considerable legacy of wrought iron bridges in the USA, Europe and the rest of the world.

Structural forms used were governed by the properties of the materials available. Cast iron primary girders up to 15 m (50 ft) span were combined with transverse secondary girders or a timber deck. Jack arch construction was widely used until about 1870 to form the floors of industrial buildings and in the cut and cover construction used extensively on the sub-surface lines of the London Underground. Structurally efficient cast iron girders typically had large tensile flanges to reduce tensile stress and compact compression flanges designed to resist local buckling. Cast iron columns in buildings were usually circular, but the very large struts used to brace vent shafts on the London Underground had an efficient cruciform section to maximise resistance to local and overall buckling. Connections were generally made by direct bearing or mechanical interlock (often copying details from timber or masonry construction).

The manufacturing process meant that wrought iron had to be produced in thin plates or sections such as angles or channels. Larger sections were created by connecting together these basic pieces using rivets. Large wrought iron trusses have been used extensively for railway bridges, often with sophisticated details for the diagonal members. Early steel structures were fabricated in a similar manner, joining sheet and plate material using rivets or black bolts. Smaller wrought iron railway bridges typically comprise fabricated plate girders for main and secondary beams with a timber deck, on which the ballast and track is directly laid. Dead load is small compared to the fatigue loading from passing trains so these structures can be particularly susceptible to fatigue.

The legacy of structures fabricated from cast and wrought iron is part of the modern industrial landscape. In the UK, much of the infrastructure of the London Underground was constructed over 100 years ago; indeed, the earliest parts are 160 years old and many of the older structures are cast iron. There are several thousand wrought iron bridges in the UK railway infrastructure; they are all over 100 years old and most are still in continuous use. Many of these structures carry loads much greater than those for which they were originally intended and are only able to do so because of the conservative design criteria of the time. However, increased loading and/or fatigue requirements are still being demanded of these structures due to change of use or design philosophy.

The strengthening of railway or London Underground infrastructure can cause considerable disruption to services and any extended closures would be very difficult strategically. Consequently, FRP strengthening techniques that can be applied in a minimum amount of time and with little disruption to services can be of significant benefit. However, the metallurgy of cast and wrought iron needs to be understood when considering FRP strengthening because it determined the form of the original structures and influences both the design and the implementation of any strengthening schemes.

## 14.3 Production, metallurgy and properties of historic irons

Ferrous structural metals, cast iron, wrought iron and steel, are alloys of iron, carbon and other impurities, the most common of which is silicon. Pure iron is soft and weak and has no commercial application. During the Industrial Revolution, iron was extracted from iron ore (usually an iron oxide) by smelting. The ore was mixed with coal in a furnace and the oxygen was driven off as carbon dioxide or monoxide. The molten iron was poured into a sand mould where it solidified into ingots. The shape of this mould was such that the cooling ingots resembled piglets feeding from a sow and consequently the metal was called pig-iron. Pig-iron had high carbon content (about 4.5 %) and also had no structural application. When it was re-melted, many of the impurities floated to the top and could be scraped off. The resulting alloy had a carbon content of 2.5–4 %. Reference to the iron–carbon phase diagram (Fig. 14.1) shows that the melting point of the metal was in the range 1150–1200 °C (2102 °F–2192 °F), about 300 °C (540 °F) lower than that of pure iron, so that the free-flowing molten metal could be cast relatively easily into useful structural members using complicated sand moulds, hence the name cast iron.

Large items required several ladles of iron so there were potential problems at the pour interfaces. Also the items produced would have had geometric imperfections from the inaccuracies in the mould and differential

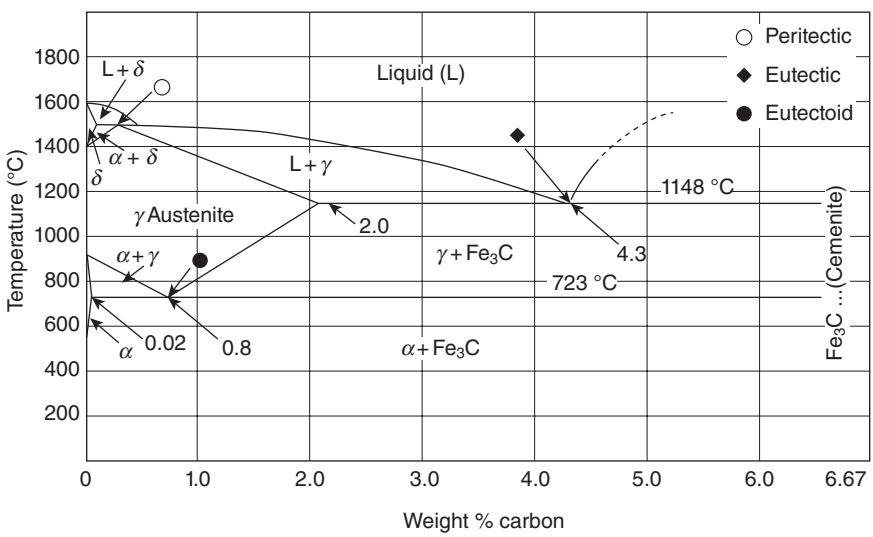


*14.1* Iron–carbon phase diagram. $\alpha$ = ferrite (BCC); $\gamma$ = austenite (FCC); $\delta$ = ferrite (BCC); $Fe_3C$ = cementite (6.67 % C).

*Table 14.1* Mechanical properties of historic cast iron

| Property | Tension | Compression |
|---|---|---|
| Strength (N/mm$^2$) | 188 | 699 |
| Modulus (kN/mm$^2$) | 132 | 133 |
| Elongation (%) | 0.7 | 2.6 |

cooling. The top surface of the casting had a relatively rough finish, sometimes with blowholes where trapped gases had escaped from the molten metal. On cooling, much of the carbon separated from the iron solution producing a mixture of $\alpha$-iron and graphite flakes. The $\alpha$-iron had a relatively coarse granular structure with the graphite flakes dispersed throughout the metal matrix. Under tensile load, the graphite flakes and other slag inclusions (impurities up to several millimetres in size) act as stress raisers resulting in brittle rupturing of the bond between the grains (tensile failure) at a low stress compared to the compressive strength of the material. The slag inclusions also formed localised very hard areas in the metal. Typical mechanical properties of Victorian cast iron are given in Table 14.1.

Wrought iron consists of very pure iron (0.02–0.05 % carbon) and siliceous slag (mainly a silicate of iron, $Fe_2SiO_4$). It was produced from cast iron in stages. In the first, cast iron was melted and puddled (stirred or agitated) to expose it to oxygen. This oxidised and removed many of the impurities, such as carbon, silicon and manganese, and cooled the mass until it became a semi-molten, pasty, iron and slag mixture which was split into balls weighing about 50 kg (one hundredweight in old units). These were hammered and rolled into bars, sometimes called bloom, about 25 mm (1 in) square. This so-called No.1 bar was only the starting point for the manufacture of better quality material and had no engineering application.

The bar was cut into suitable lengths and placed in orthogonal layers to form a cube of 'piled' bars. Typically, a 0.5 m (20 in) cube was used. This was reheated to 'welding heat', around 1300 °C (note higher than the melting point of cast iron), hammered into a solid mass and then rolled into bar. This No. 2, or merchant, bar was the lowest quality of bar considered suitable for general blacksmith use. Starting with No. 2 bar and repeating the piling, heating, hammering and rolling process produced No. 3 or 'best' bar which was often used for general structural applications. Repeating the process starting with No. 3 bar produced 'best-best' bar which was often used for chains, anchors and rivets. The repeated hammering and rolling improved the uniformity of the material and its properties, squeezed out excess slag and drew out the remainder into long thin fibres in the direction

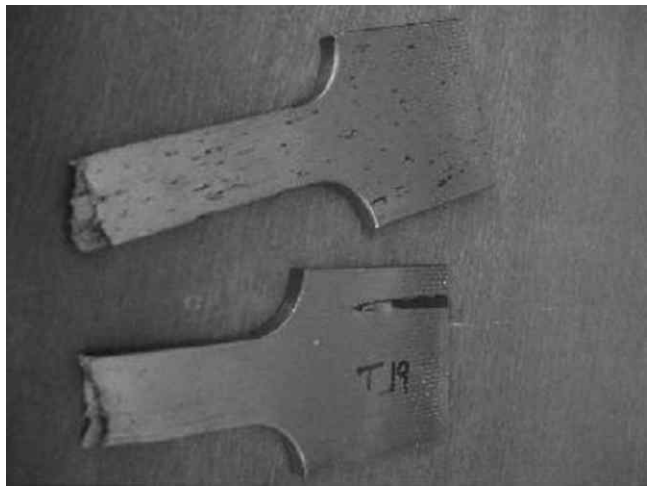

*14.2* With-grain tensile specimen showing slag fibres and laminar failure surface.

*Table 14.2* Typical mechanical properties of historic wrought iron – University of Southampton specimens[3]

| | Property | With-grain | Cross-grain | Web |
|---|---|---|---|---|
| Tension | Strength (N/mm$^2$) | 343 | 285 | 286 |
| | 0.2% proof (N/mm$^2$) | 257 | 270 | 228 |
| | Modulus (kN/mm$^2$) | 215 | 241 | 190 |
| | Elongation (%) | 8.6 | 1.7 | 6.8 |
| Compression | 0.2% proof (N/mm$^2$) | 206 | – | – |
| | Modulus (kN/mm$^2$) | 171 | – | – |

of rolling (called the with-grain direction as opposed to the cross-grain direction). Six repetitions generally achieved the best quality material as shown by Kirkaldy;[2] further working removed so much slag that the iron became brittle.

The slag fibres in the iron matrix, shown clearly in Fig. 14.2, gave the wrought iron highly directional mechanical properties as shown in Table 14.2, and the repeated hammering and rolling gave the metal a distinctive laminar structure as can be seen at the failure surface of the specimen shown in Fig. 14.2 and in the delamination of the compression specimen shown in Fig. 14.3. The manufacturing process produced relatively thin material; the test results in Table 14.2 came from 160-year-old 6–13 mm ($\frac{1}{4}$ in–$\frac{1}{2}$ in) thick plates which formed the piece of girder shown in Fig. 14.4.

*14.3* Delamination of compression specimen during testing.

*14.4* Wrought iron girder (2 m long) removed from demolished bridge.

This girder came from a demolished railway bridge located at Llangammarch Wells, Wales. The web plates (6 mm ($\frac{1}{4}$ in) thick) were rolled alternately in two perpendicular directions to achieve more even properties. Wrought iron is a very variable material, both within a single plate and especially when comparing material from different sources; the properties in Table 14.2 were obtained from between 22 and 28 specimens. A survey of test results from 33 sources[3] gave an average with-grain ultimate tensile strength of 348 N/mm$^2$ with a standard deviation of 36 N/mm$^2$ and an elongation of 15 % with a standard deviation of 7 % elongation. The latter values in particular show the variability of the material.

The unusual laminar structure of wrought iron is potentially a problem when considering FRP strengthening, since delamination under interlaminar shear would be a similar phenomenon to debonding of FRP at a metal/FRP interface. Research[4] at University of Southampton, UK, addressed interlaminar shear strength using the unique specimens shown in Fig. 14.5 (note that the shaded region is the test surface). The results are summarised in Table 14.3. There was considerable variability in the results and the averages presented were obtained from several specimens. It was found that abnormally low test results were due to large slag inclusions within the test surface as shown in Fig. 14.6. The main conclusion was that minimum interlaminar shear strength was at least double the shear strength of existing structural adhesives so that delamination of the wrought iron would occur after failure of the FRP strengthening.

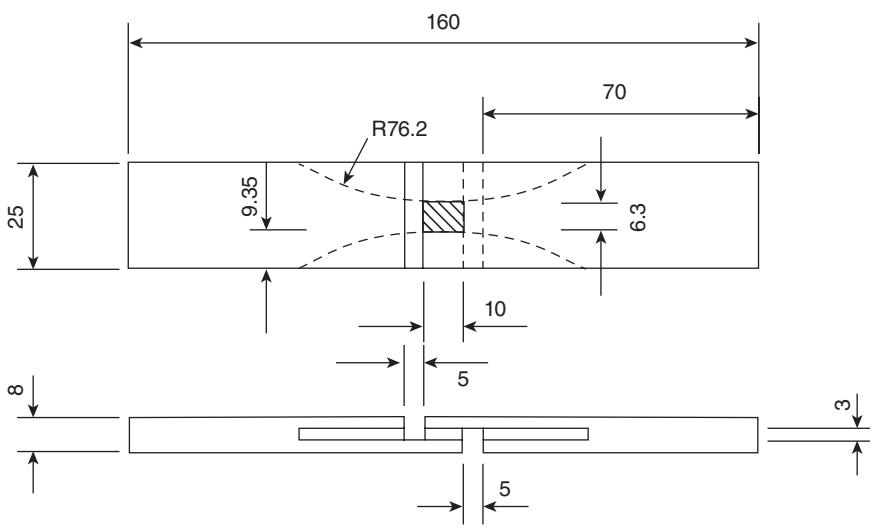


*14.5* Interlaminar shear specimens (all dimensions in mm).

*Table 14.3* Interlaminar shear test results, 10 mm thick tension flange plate

| Specimen preparation | Mean shear strength ($N/mm^2$) | Maximum shear strength ($N/mm^2$) | Minimum shear strength ($N/mm^2$) |
|---|---|---|---|
| *Cross-grain interlaminar shear specimens* | | | |
| None | 71.4 | 87.3 | 45.6 |
| *With-grain interlaminar shear specimens* | | | |
| None | 83.4 | 90.9 | 64.3 |
| 75% UCS* pre-load | 69.5 | 98.9 | 16.6† |
| Simulated seawater | 68.1 | 74.1 | 60.8 |
| pH4 room temp. | 47.3 | 64.3 | 21.6† |

* Uniaxial compressive strength.
† Specimen with slag inclusion.

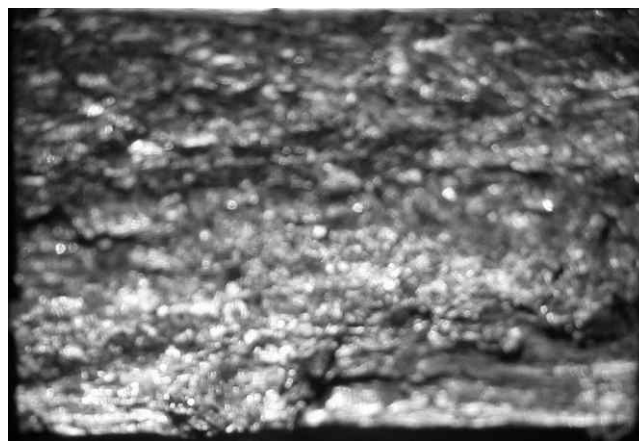

*14.6* Failure surface of interlaminar shear specimen with slag inclusion bottom right.

Both cast and wrought iron have, in the right circumstances, very good durability. Cast iron frequently has a thin oxide layer but no major corrosion damage. Wrought iron also lasts very well (Fig. 14.7) except when it is permanently wet. When it does corrode there is often delamination since the corrosion products in the interlaminar layer expand and split the metal (Fig. 14.8).

*14.7* Wrought iron girders erected 1886 to replace a Brunel designed wooden viaduct, Largin, Cornwall, UK. Note general good condition.

*14.8* Heavy corrosion of wrought iron with delamination, also from Largin Viaduct, Cornwall, UK.

*14.9* Cast iron struts at Shadwell Station, London Underground. Note upper and lower layers, cruciform section and elaborate end brackets.

## 14.4 Structures in cast and wrought iron

The production limitations and the mechanical properties drove the structural forms that are typical of cast and wrought iron. Generally cast iron was produced in relatively massive shapes. In struts, the section shapes were influenced by buckling considerations. Frequently circular shapes were used in building columns. Struts in deep tunnel vent shafts had spans up to 13 m (43 ft) and were produced in cruciform shapes as shown in Figs 14.9 and 14.10. This shape was a compromise between buckling and bending resistance. The struts were expected to bend under load so some regions could go into tension, but the regions in compression could buckle locally. The bulbs at top and bottom gave local buckling resistance. Overall buckling was resisted by the relatively efficient cruciform shape and also by the chunky cross-section. Bending girders often had an inverted 'T' shape, with a large tension flange and a relatively small compression flange, often with a bulb for local buckling resistance. Figure 14.11 is a view of a jack arch tunnel support structure showing the cast iron girders with bricks between.

Wrought iron was manufactured in thin sections, plates, angles and channels. In order to create large structures, these sections had to be

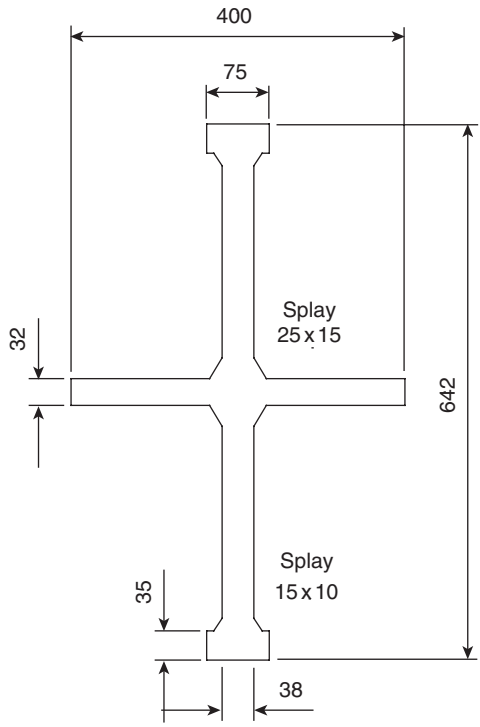


*14.10* Cross-section of lower layer of struts at Shadwell, UK (all dimensions in mm).

connected using rivets. Figures 14.12 and 14.13 show common details, while Figs 14.14 and 14.15 show typical examples of wrought iron bridges. Notice in Fig. 14.15b the lines of rivets connecting the girder plates.

## 14.5 Fibre-reinforced polymer (FRP) composite strengthening of cast and wrought iron structures

In some ways the title of this section is misleading because it is often necessary to increase stiffness and reduce stress levels rather than just strengthen the structure. However, the approach is the same whether stiffening or strengthening is required. Since cast and wrought iron are ferrous metals, the basic approach is identical to that for steel. Because of the relatively high elastic modulus of ferrous metal, the FRP of choice is carbon fibre-reinforced polymer composite (CFRP) using ultra-high modulus fibres and an epoxy resin. With an effective modulus of about

*14.11* Cut and cover tunnel showing cast iron girders with brick arches between.

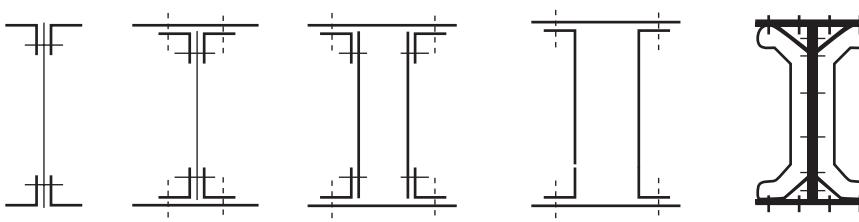

*14.12* Typical wrought iron cross-sections.

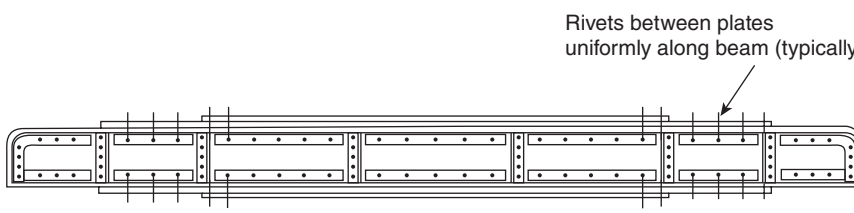


*14.13* Typical wrought iron girder, longitudinal view.


*14.14* Horseshoe Bridge, Southampton, UK, a wrought iron truss bridge. Note the varying sizes of the diagonal members.

305 kN/mm$^2$, the composite is at least 50 % stiffer than the metal. The design approach has been laid down in various design guides.[5,6,7] It is essential that interlaminar stresses, between CFRP and metal and within the wrought iron, are checked carefully. Flexural strengthening will usually involve the application of CFRP to the tension flange of the existing structure although there is an argument for also applying CFRP to the compression flange of wrought iron girders to prevent excessive compressive stresses in the wrought iron which could lead to delamination (see Fig. 14.3).


*14.15* Views of a typical riveted wrought iron plate girder railway bridge, Romsey, Hampshire, UK.

### 14.5.1 Cast iron

Complications arise when the practicalities of the CFRP strengthening are considered. In cast iron structures, the aim of the strengthening is to reinforce the cast iron in tension, and bonding CFRP strips to the tension flange is an obvious approach, as shown in Fig. 14.16.[8] However, in some situations it is impossible to determine which parts of the section are in tension. The vent shaft struts shown in Figs 14.9 and 14.10 were originally designed for axial compression only. However, development above ground and ground movement had increased the strut loads and this, combined


*14.16* King Street Bridge, Mold, Wales, UK: (a) general view of bridge; (b) CFRP on tension flanges of cast iron girder. Courtesy of Tong Gee and Partners.

with imperfections, non-homogeneous metal and the impossibility of having truly axial load, had caused the struts to bend. The sudden failure of a similar strut at Rotherhithe station had shown that significant tensile stresses were building up in the struts.[9] However, the imperfections were unique to each strut so it was impossible to determine *in situ* the direction of bending. The result was that CFRP had to be applied to the whole cross-section of the strut. An additional problem was that it was impossible to relieve the existing load in the struts before strengthening.

Tests were carried out on model scale struts[10] to investigate whether there would be any benefit from strengthening under existing load and whether early failure of the CFRP in compression (the compressive strength of

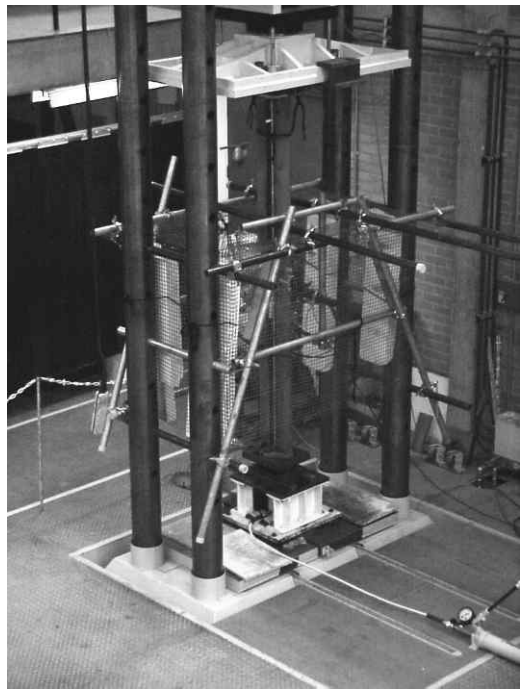

*14.17* Reinforced cast iron strut under test.

CFRP being less than the tensile strength) would prove catastrophic. Figure 14.17 shows a 2.4 m long strut under test. A preload of 50 % of the predicted strength of the cast iron was applied during application and curing of the CFRP strengthening using the hand pumped hydraulic jack that can be seen at the bottom of the photo. The tests confirmed that significant benefits would be gained. When the CFRP in compression failed during the loading process, the reinforced struts were still able to carry significant extra load before complete failure. Complete failure was catastrophic due to the rapid release of energy as the cast iron failed in tension. Figure 14.18 compares typical load–deflection graphs for reinforced and unreinforced struts and Fig. 14.19 shows how strains redistributed without overall collapse when the CFRP failed in compression.

The usual approach with steel structures is to fix 'pre-preg' (pre-impregnated) CFRP plates to the steel using an epoxy adhesive. If this approach had been used on the cast iron struts, unacceptably thick glue lines would have been required. As a result, the CFRP was applied by the vacuum infusion technique using the adhesive property of the epoxy resin to ensure a sound bond. As with any material, surface preparation is the

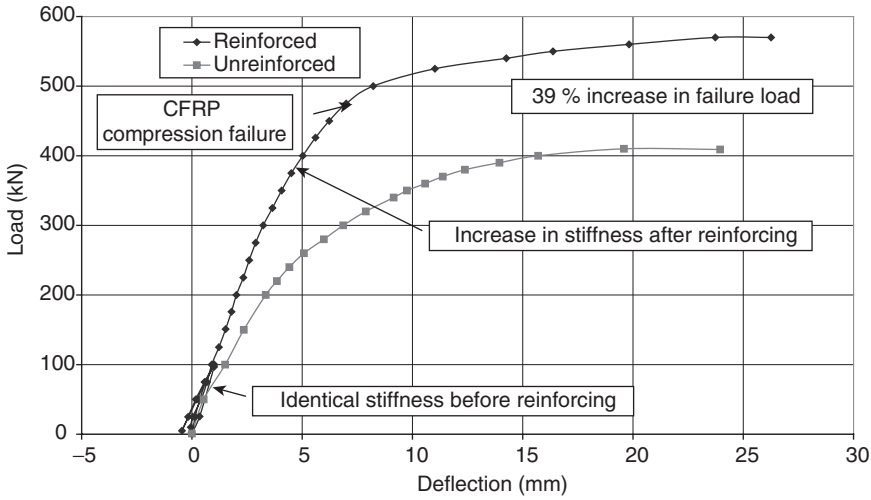


*14.18* Load–deflection graphs comparing reinforced and unreinforced struts.

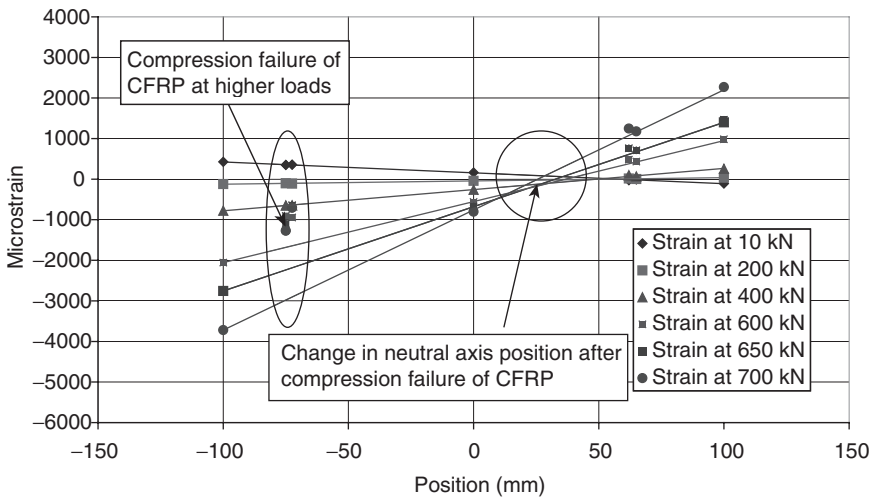


*14.19* Strain across reinforced strut at various loads.

key to achieving the desired bond. In cast iron this can be problematic. It is usual for the original structure to be coated in a lead-based paint so special safety precautions must be taken when grit blasting the metal surface. Once the surface has been cleaned, it is necessary to grind off large blemishes protruding from the metal surface and to fill blowholes with epoxy putty. Since the infusion process is time-consuming, the exposed

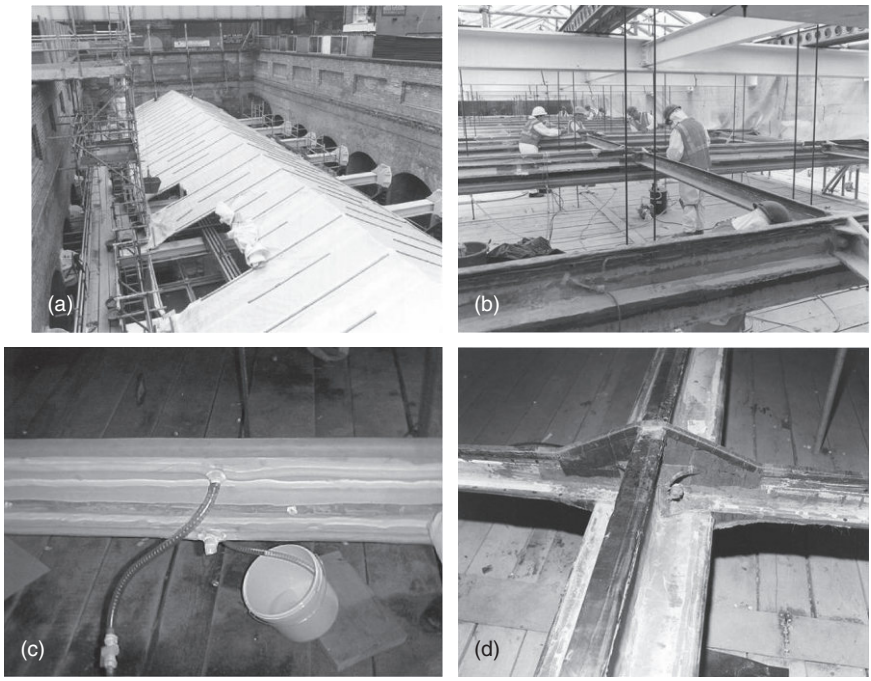


*14.20* Vacuum infusion of CFRP at Shadwell, London, UK: (a) overall view of vent shaft strengthening; (b) clean working conditions; (c) resin infusion; (d) completed strengthening. Courtesy of DML Composites.

surface has to be sealed with a suitable primer. In contrast to most construction site activities, vacuum infusion requires clean working conditions and very close control, as can be seen in Fig. 14.20.

### 14.5.2 Wrought iron

As with cast iron, it is the practicalities of CFRP strengthening that need careful consideration. Careful inspection of the existing structure is essential, and corrosion in particular must be examined. If it is only surface corrosion, as shown in Fig. 14.7, the usual surface preparation before CFRP application will be adequate. If the corrosion is heavy with delamination as in Fig. 14.8, it is essential to first address the cause of the corrosion. If the wrought iron is effectively continuously wet this must be remedied; if not, corrosion will continue. Also, the loss of effective cross-section must be assessed to ensure that sufficient strengthening is applied.

The present UK Design Guide for CFRP strengthening of metallic structures[5] specifically excludes strengthening of wrought iron due to

concerns about possible delamination of the wrought iron. However, as reported in Section 14.3, research has now shown that those fears are unfounded, since the interlaminar strength of wrought iron is at least double the bond strength of existing adhesives. Consequently, the exclusion of wrought iron will be removed in the next edition but, at present, there has been very little CFRP strengthening of full scale wrought iron structures by CFRP bonding, although research[8] has shown that the potential benefits are the same as those for steel and cast iron structures.

A practical problem that must be overcome is how to apply the CFRP around the rivets. Vacuum infusion is an obvious possibility since the application of the vacuum to the dry fibres will compress them around the rivet heads. Another possibility is to use 'prepreg' plates with glass fibres laid along the rivet lines. Holes could then be formed to an adequate depth in the glass fibres to fit over the rivets. Perhaps the easiest approach would be to use narrow strips of CFRP plate between the rivet lines and then bond full width plate across the flange. It would be advisable to fill the gaps with resin to prevent condensation and possible corrosion around the rivet heads. Adhesive stresses would need to be checked and, if necessary, mechanical clamps used to guarantee bond between the CFRP and the wrought iron.

### 14.5.3 General issues with FRP schemes

As with any FRP strengthening scheme for metallic structures certain general precautions are essential. The strengthening needs to be inspected regularly to ensure that it is functioning as required. Vandalism, including accidental vandalism from other contractors working on the structure, is a potential problem and the risk must be minimised.

As with all metallic structures, heat effects need to be carefully considered. The cast iron vent shaft struts[9] can experience daily temperature changes of over 40 °C (72 °F). To reduce the impact of this, the CFRP was painted white after installation to reflect heat. Suitable resin and adhesives need to be chosen so that their glass transition temperature is well above the anticipated maximum service temperature. Fire protection is probably not required on external structures but can be provided where necessary by intumescent paint.

### 14.5.4 Some alternative approaches to strengthening

It may sometimes be necessary to reduce some of the existing loading on the historic structure. Prestressed CFRP has been used to achieve this, for example on the cast iron Hythe Bridge, Oxford, UK[11] (see Fig. 14.21). A wrought iron through truss bridge in Valley Forge National Park, Chester

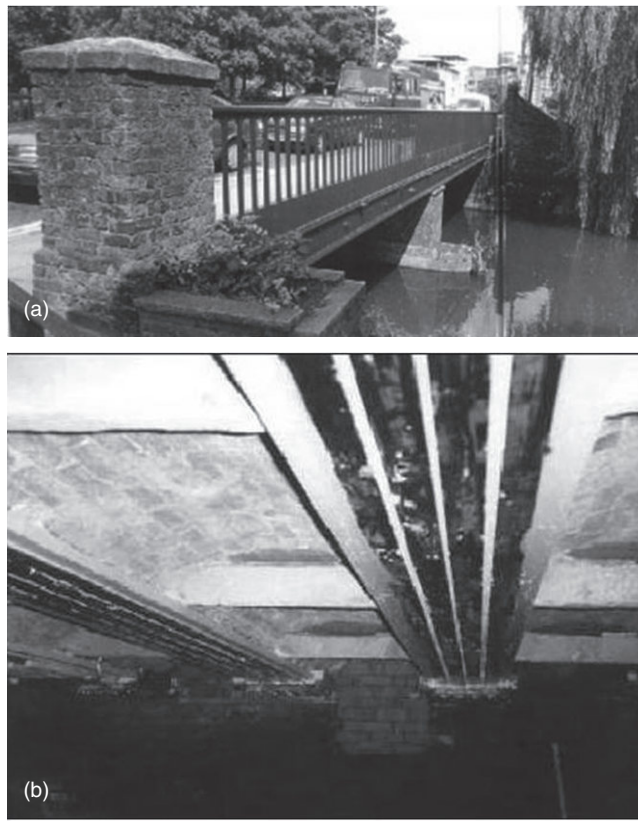


*14.21* Strengthening of Hythe Bridge, Oxford, UK: (a) general view; (b) mechanical anchors for prestressed CFRP plates.

County, Pennsylvania, USA was rehabilitated by replacing the existing timber and stringer deck[12] with a glass fibre-reinforced polymer (GFRP) deck. Since the new deck was only half the weight of the original, this was effectively a means of strengthening the wrought iron.

Unusual solutions can, however, present themselves, such as one proposed for the tunnel support structure shown in Fig. 14.11. The use of an all CFRP beam, 13 m long, that would fit within the brick arch was investigated.[13] A schematic of the system is shown in Fig. 14.22, and it can be seen that the strengthening does not reduce the headroom in the tunnel. Once the CFRP beam had been installed, grout would be pumped under pressure into the gap between the bricks and the CFRP, relieving load on the arch by stressing up the CFRP. A two-third scale prototype was fabricated using vacuum infusion and was shown under test to perform as predicted by finite element analysis. In the event, the strengthening was

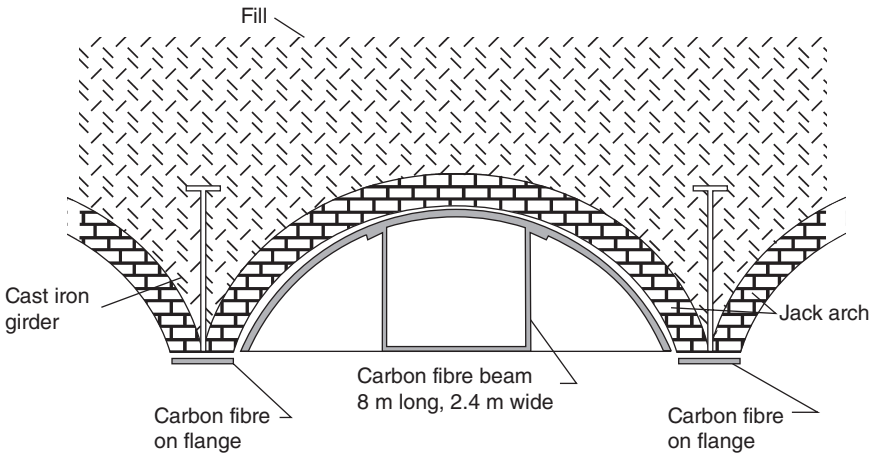


*14.22* CFRP strengthening scheme for brick jack arches and cast iron girders.

carried out using formed steel girders, but the potential of CFRP was clearly demonstrated.

## 14.6 Conclusion

The design of FRP reinforcing systems for historic structures fabricated from cast or wrought iron is not greatly different from that for steel structures. However, it has been shown that the metallurgy of these metals and their resulting mechanical properties need to be considered at the design stage. Although cast iron generally needs to be strengthened when in tension, it is not always possible to identify the regions of the structure or individual members that are in tension. In such cases, the whole section needs to have FRP attached to it. Also it is usually not possible to relieve existing load on the original structure so the strengthening scheme must also be designed to account for that situation. The good news is that testing has shown that, despite preload, strengthening still provides many benefits to the existing structure. Testing has also shown that an initial failure of FRP under compression does not lead to instantaneous failure of the whole structure.

What singles out FRP strengthening of historic structures is the practical details. Surface preparation is as important as ever, but more factors need to be addressed. The surface of cast iron has various imperfections. Protruding lumps of metal need to be ground off, blowholes need to be filled with epoxy putty. When casting imperfections are significant, it will not be possible to attach a preformed FRP plate to the surface because the

glue line will be unacceptably thick. Instead, it is better to use the vacuum infusion process to form the FRP, relying on the adhesive properties of the resin to achieve bond. With wrought iron, the problems are more to do with the lines of rivets connecting plates and sections together. Practical solutions to applying the FRP around the rivets are given in the main text above. Various cast iron structures have been strengthened using CFRP and, now that the reservations about FRP strengthening of wrought iron have been put to rest, it is likely that wrought iron structures will also be strengthened in the same way.

## 14.7 References


1. Moy S.S.J., Clarke H.W.J. Strengthening wrought iron structures using CFRP. *Proceedings of the Institution of Civil Engineers – Structures and Buildings*, 162, 251–261, 2009.
2. Kirkaldy D. *Results of an Experimental Enquiry into the Tensile Strength and Other Properties of Various Kinds of Wrought Iron and Steel.* Transactions of the Institution of Engineers in Scotland, Glasgow, 1863.
3. Moy S.S.J., Clarke H., Bright S.R. The engineering properties of Victorian structural wrought iron. *Proceedings of the Institution of Civil Engineers – Construction Materials*, 162, 1–10, 2009.
4. Clarke H.W.J. *Reinforcing Wrought Iron with Carbon Fibre Reinforced Polymers.* PhD thesis, University of Southampton, Southampton, 2006.
5. Cadei J.M.C., Stratford T.J., Hollaway L.C., Duckett W.G. *Strengthening Metallic Structures Using Externally Bonded Fibre-reinforced Polymers.* C595,
6. Schnerch D., Dawood M., Rizkalla S. *Design Guidelines for the Use of HM Strips: Strengthening of Steel Concrete Composite Bridges with High Modulus Carbon Fiber Reinforced Polymer (CFRP) Strips.* Technical Report: IS-06-02, North Carolina State University (NCSU), Constructed Facilities Lab (CFL), Raleigh, NC, June 2007.
7. Consiglio Nazionale delle Richerche (CNR) (2007). *Guidelines for the design and construction of externally bonded FRP systems for strengthening existing structures. Metallic structures.* Italian National Research Council Rep. CNR-DT 202/2005, Rome.
8. Farmer N., Smith I. King Street Railway Bridge – strengthening of cast iron girders with FRP composites. *Proceedings of the 9th International Conference on Structural Faults and Repairs*, London, 4th–6th July, 2001.
9. Moy S.S.J., Barnes F., Moriarty J., Dier A.F., Kenchington A., Iverson B. Structural upgrade and life extension of cast iron struts using carbon fibre reinforced composites. Gibson A.A. (ed.), *Proceedings of 8th International Conference on Fibre-reinforced Composites*, *FRC2000*, Newcastle-upon-Tyne, 13–15 September, pp. 3–10, 2000.
10. Moy S.S.J., Lillistone D. Strengthening cast iron using FRP composites. *Proceedings of the Institution of Civil Engineers – Structures and Buildings*, 159(6), 309–318, 2006.
11. Luke S. Strengthening structures with carbon fibre plates case histories for Hythe bridge, Oxford and Qafco prill tower, Qatar. *NGCC First Annual*

*Conference and AGM – Composites in Construction, Through Life Performance.* Watford, 30–31, October, 2001.
12. Shenton H.W.III., Chajes M.J., Finch W.W. Jr., Hemphill S., Craig R. Performance of a historic 19th century wrought-iron through-truss bridge rehabilitated using advanced composites. *Proceedings of ASCE 2000 Structural Congress and Exposition*, ASCE, Philadelphia, PA, pp 1–7, 2000.
13. Moy S.S.J., Hill P., Moriarty J., Dier A.F., Kenchington A., Iverson B. Strengthening of tunnel supports using carbon fibre composites. *Proceedings of the Institution of Mechanical Engineers Part L–Journal of Materials, Design and Applications*, 215(L), 235–243, 2001.

This page intentionally left blank

# Index

This page intentionally left blank

This page intentionally left blank